ACS SYMPOSIUM SERIES 1118

Fire and Polymers VI: New Advances in Flame Retardant Chemistry and Science

EDITED BY

Alexander B. Morgan, Charles A. Wilkie, and Gordon L. Nelson

Downloaded by DALHOUSIE UNIV on December 19, 2012 | http://pubs.acs.org
Publication Date (Web): December 18, 2012 | doi: 10.1021/bk-2012-1118.fw001

Fire and Polymers VI: New Advances in Flame Retardant Chemistry and Science

In Fire and Polymers VI: New Advances in Flame Retardant Chemistry and Science; Morgan, A., et al.;
ACS Symposium Series; American Chemical Society: Washington, DC, 2012.

Downloaded by DALHOUSIE UNIV on December 19, 2012 | http://pubs.acs.org
Publication Date (Web): December 18, 2012 | doi: 10.1021/bk-2012-1118.fw001

Downloaded by DALHOUSIE UNIV on December 19, 2012 | http://pubs.acs.org
Publication Date (Web): December 18, 2012 | doi: 10.1021/bk-2012-1118.fw001

ACS SYMPOSIUM SERIES **1118**

Fire and Polymers VI: New Advances in Flame Retardant Chemistry and Science

Alexander B. Morgan, Editor
University of Dayton Research Institute
Dayton, Ohio

Charles A. Wilkie, Editor
Marquette University
Milwaukee, Wisconsin

Gordon L. Nelson, Editor
Florida Institute of Technology
Melbourne, Florida

Sponsored by the
ACS Division of Polymeric Materials: Science and Engineering

American Chemical Society, Washington, DC

Distributed in print by Oxford University Press, Inc.

Downloaded by DALHOUSIE UNIV on December 19, 2012 | http://pubs.acs.org
Publication Date (Web): December 18, 2012 | doi: 10.1021/bk-2012-1118.fw001

Library of Congress Cataloging-in-Publication Data

Fire and Polymers (Conference) (6th : 2012 : San Diego, Calif.)
Fire and Polymers VI : new advances in flame retardant chemistry and science / Alexander B. Morgan, editor, University of Dayton Research Institute, Dayton, Ohio, Charles A. Wilkie, editor, Marquette University, Milwaukee, Wisconsin, Gordon L. Nelson, editor, Florida Institute of Technology, Melbourne, Florida ; sponsored by the ACS Division of Polymeric Materials:Science and Engineering.
pages cm. -- (ACS symposium series ; 1118)
Papers from the conference held San Diego, California, March 25-29, 2012.
Includes bibliographical references and index.
ISBN 978-0-8412-2780-4 (alk. paper)
1. Polymers--Fire testing--Congresses. 2. Fire resistant polymers--Congresses.
I. Morgan, Alexander B. II. Wilkie, C. A. (Charles A.) III. Nelson, Gordon L., 1943-
IV. American Chemical Society. Division of Polymeric Materials: Science and Engineering.
V. Title.
TH9446.5.P65F555 2012
628.9′222--dc23
2012042603

The paper used in this publication meets the minimum requirements of American National Standard for Information Sciences—Permanence of Paper for Printed Library Materials, ANSI Z39.48n1984.

Copyright © 2012 American Chemical Society

Distributed in print by Oxford University Press, Inc.

All Rights Reserved. Reprographic copying beyond that permitted by Sections 107 or 108 of the U.S. Copyright Act is allowed for internal use only, provided that a per-chapter fee of $40.25 plus $0.75 per page is paid to the Copyright Clearance Center, Inc., 222 Rosewood Drive, Danvers, MA 01923, USA. Republication or reproduction for sale of pages in this book is permitted only under license from ACS. Direct these and other permission requests to ACS Copyright Office, Publications Division, 1155 16th Street, N.W., Washington, DC 20036.

The citation of trade names and/or names of manufacturers in this publication is not to be construed as an endorsement or as approval by ACS of the commercial products or services referenced herein; nor should the mere reference herein to any drawing, specification, chemical process, or other data be regarded as a license or as a conveyance of any right or permission to the holder, reader, or any other person or corporation, to manufacture, reproduce, use, or sell any patented invention or copyrighted work that may in any way be related thereto. Registered names, trademarks, etc., used in this publication, even without specific indication thereof, are not to be considered unprotected by law.

PRINTED IN THE UNITED STATES OF AMERICA

Downloaded by DALHOUSIE UNIV on December 19, 2012 | http://pubs.acs.org
Publication Date (Web): December 18, 2012 | doi: 10.1021/bk-2012-1118.fw001

Foreword

The ACS Symposium Series was first published in 1974 to provide a mechanism for publishing symposia quickly in book form. The purpose of the series is to publish timely, comprehensive books developed from the ACS sponsored symposia based on current scientific research. Occasionally, books are developed from symposia sponsored by other organizations when the topic is of keen interest to the chemistry audience.

Before agreeing to publish a book, the proposed table of contents is reviewed for appropriate and comprehensive coverage and for interest to the audience. Some papers may be excluded to better focus the book; others may be added to provide comprehensiveness. When appropriate, overview or introductory chapters are added. Drafts of chapters are peer-reviewed prior to final acceptance or rejection, and manuscripts are prepared in camera-ready format.

As a rule, only original research papers and original review papers are included in the volumes. Verbatim reproductions of previous published papers are not accepted.

ACS Books Department

Downloaded by DALHOUSIE UNIV on December 19, 2012 | http://pubs.acs.org
Publication Date (Web): December 18, 2012 | doi: 10.1021/bk-2012-1118.pr001

Preface

There is always the possibility that a material may catch fire, potentially leading to the loss of property and, on occasion, life. Fire risk is not a new problem but, as new polymeric materials are developed and used, the potential for fire risk may increase. There are huge benefits to these new polymeric materials, including weight savings and resource (energy, durability) economy. In order to protect these materials against fire, there is a real need for effective fire retardants. Fire retardants are a large section of the world-wide polymer economy and the need continues to grow as more polymers are used in more applications where fire risk is present. Due to this ever-increasing need, as well as due to new regulations, there is a clear need for a peer-reviewed book delineating the latest advances in fire retardant chemistry and approaches to the study of fire and polymers.

A symposium was held at the 243rd American Chemical Society Meeting, held in San Diego, CA, in March of 2012. This symposium featured 59 presentations which covered the complete range of fire retardant activity, regulations, and material flammability testing. U.S. and international speakers were well represented, showing the global nature of this research field. This was the sixth symposium in a series dating back to 1989. From these presentations, a total of 32 were selected for inclusion in this book. We believe you will find them to be a good snapshot of flame retardant technology today should you, the reader, be a newcomer to the field or an experienced fire scientist.

Acknowledgments

We gratefully acknowledge the ACS Division of Polymeric Materials Science and Engineering for providing the venue for the symposium. We also acknowledge support from Albemarle Corporation, Ashland Chemical, BASF, Clariant, JM Huber, Great Lakes Solutions, WL Gore & Associates, Israel Chemicals Limited, Nanocyl, Samsung – Chiel Industries, PINFA, Saint Gobain, Specialty Products Inc., and Southern Clay Products. We wish to acknowledge support from our institutions, University of Dayton Research Institute, Florida Institute of Technology, and Marquette University.

Alexander B. Morgan
Microscale Composites and Polymer Division
University of Dayton Research Institute
300 College Park
Dayton, OH 45369-0160

In Fire and Polymers VI: New Advances in Flame Retardant Chemistry and Science; Morgan, A., et al.;
ACS Symposium Series; American Chemical Society: Washington, DC, 2012.

Charles A. Wilkie
Department of Chemistry and Fire Retardant Research Facility
Marquette University
P.O. Box 1881
Milwaukee, WI 53201-1881

Gordon L. Nelson
Department of Chemistry
Florida Institute of Technology
150 West University Boulevard
Melbourne, FL 32901-6975

Downloaded by DALHOUSIE UNIV on December 19, 2012 | http://pubs.acs.org
Publication Date (Web): December 18, 2012 | doi: 10.1021/bk-2012-1118.pr001

Editors' Biographies

Alexander B. Morgan

Alexander B. Morgan received his B.S in Chemistry from Virginia Military Institute in 1994 and his Ph.D. in Organic Chemistry from the University of South Carolina in 1998. He has worked as a National Research Council postdoctoral fellow at the National Institute of Standards and Technology, and as a research chemist at the Dow Chemical Company. He is currently a Distinguished Research Scientist and Group Leader at the University of Dayton Research Institute where he works on a variety of material science and material flammability projects. He is on the editorial review boards of *Fire and Materials* and the *Journal of Fire Science*, and is a member of the American Chemical Society, American Society for Testing and Materials, and Sigma Xi. Dr. Morgan has been in the flame retardant chemistry field for over 17 years and is the co-editor on four books on this topic with Prof. Charles Wilkie.

Charles A. Wilkie

Charles A. Wilkie received his undergraduate degree in Chemistry from the University of Detroit and his Ph.D. from Wayne State University in Inorganic Chemistry. He immediately joined Marquette University as Assistant Professor, rising through the ranks until he retired as the Pfletschinger-Habermann Professor of Chemistry in 2009. He is currently Professor Emeritus. He was a Fulbright-Hays Scholar in 1991–1992, received the Milwaukee Section (ACS) Award in 1992, and the Marquette University Haggerty Award for Excellence in Research in 2007.

Gordon L. Nelson

Gordon L. Nelson received his B.S. in Chemistry from the University of Nevada, Reno, in 1965 and his M.S. and Ph.D. from Yale University in 1967 and 1970, respectively (working with Dr. Kenneth B. Wiberg). Dr. Nelson is currently University Professor of Chemistry at Florida Institute of Technology. He previously served as Vice President for Academic Affairs (2011) and Dean of the College of Science (1989–2010). Before joining Florida Tech, Dr. Nelson was Professor and Chair of the Department of Polymer Science at the University of Southern Mississippi, Vice President of Springborn Laboratories, and a manager

In Fire and Polymers VI: New Advances in Flame Retardant Chemistry and Science; Morgan, A., et al.;
ACS Symposium Series; American Chemical Society: Washington, DC, 2012.

at GE Plastics. Dr. Nelson was 1992 Chair of the Council of Scientific Society Presidents (59 societies, 1.4 million members). He was 1988 President of the American Chemical Society and a member of its Board of Directors for fifteen years. He was the Charles Holmes Herty Medalist of the ACS Georgia Section in 1998. Dr. Nelson is editor/co-editor of 24 books, the author/coauthor of 33 book chapters and 165 papers, primarily in the areas of nanocomposites, polymer flammability, and smoke and toxicity studies.

Chapter 1

Fire Retardancy in 2012

Gordon L. Nelson,*,[1] Alexander B. Morgan,[2] and Charles A. Wilkie[3]

**[1]Department of Chemistry, Florida Institute of Technology,
Melbourne, Florida 32901
[2]Multiscale Composites and Polymers Division, University of Dayton
Research Institute, Dayton, Ohio 45469
[3]Department of Chemistry, Marquette University,
Milwaukee, Wisconsin 53201
*E-mail: nelson@fit.edu**

Downloaded by FORDHAM UNIV on December 19, 2012 | http://pubs.acs.org
Publication Date (Web): December 18, 2012 | doi: 10.1021/bk-2012-1118.ch001

Fire continues to be a worldwide problem as it has been since the "discovery" of fire. It claims thousands of lives and causes tens of billions of dollars in loss of property each year. In this 6th volume of Fire and Polymers, current fire-related problems are discussed and solutions discussing new technologies and approaches are delineated. This peer-reviewed volume is designed to be representative of the current state-of-the-art and places that recent work in perspective.

An Introduction

In the United States every 24 seconds a fire department responds to a fire somewhere in the country. A fire occurs in a structure at the rate of one in every 65 seconds. A vehicle fire occurs every 146 seconds. There is one civilian injury every 30 minutes. The result is 1.3 million fires per year (2010) responded to by fire departments. In 2010 those fires (urban and outdoor/wildfire) accounted for $11.6 billion in property damage. Those fires caused 3,120 civilian deaths and 17,720 civilian injuries. In 2010 there were 72 firefighter deaths and 78,150 firefighter injuries. In 2010 home structure fires caused 85% of the civilian fire deaths and 75% of the civilian injuries. Cooking is the primary cause of fires in

In Fire and Polymers VI: New Advances in Flame Retardant Chemistry and Science; Morgan, A., et al.;
ACS Symposium Series; American Chemical Society: Washington, DC, 2012.

home structures (42%), and smoking (25%) and heating equipment (21%) are the prime causes of death. Structural fires have declined over the period 1977 to 2010 from 1,098,000 to 482,000; structural fire deaths declined from 6,015 in 1978 to 2,755 in 2010. While those declines are progress, recent years have been fairly static (2007 2,865 deaths), and the United States still maintains one of the higher rates of fire in the world. Just as the U.S. has a high fire rate, the fire death rates in the U.S. vary by almost a factor of ten by state (2009), from 33.4 per million in the District of Columbia to 3.9 in Hawaii. California, the nation's largest state, is fourth best with a death rate of 5.5. Texas is 10.6 (versus an average of 11.0), New York 9.9, and Florida 8.8, of the remaining top four in population. While most U.S. homes have at least one smoke alarm, 62% of home fire deaths result from fires in homes without working smoke alarms. Fire kills the old, the young, the drunk (*1–3*).

Of western countries, the U.S. has an above average fire death rate (12.4 per million in 2007, versus an average of 10.7) (Figure 1). Since 1979 the U. S. has made a marked improvement (a reduction of 66.1%, from a rate of 34.4 to 12.4) (Figure 2). Interestingly, Austria which is at a rate of one-third of the average rate of the 24 countries presented in Figure 1, had a reduction of 50.9%, Germany a reduction of 52.6% and Spain a reduction of 54.6%. Clearly fire risk reduction measures work. But other countries have substantially higher fire risk. Russia with a population of 143 million had 13,000 fire deaths in 2010, versus 3120 in the U.S. (313 million population). Europe had some 4,400 deaths (27 countries) with a population of 502 million (*4–6*).

Downloaded by FORDHAM UNIV on December 19, 2012 | http://pubs.acs.org
Publication Date (Web): December 18, 2012 | doi: 10.1021/bk-2012-1118.ch001

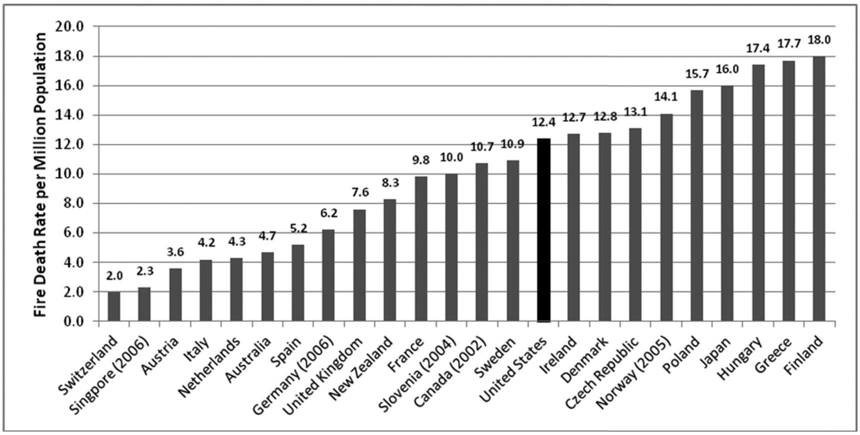

Figure 1. 2007 International Fire Death Rates per Million Population (4). Sources: World Fire Statistics Centre fire death and the United Nations (U.N.) Demographic Yearbook population estimate data.

Downloaded by FORDHAM UNIV on December 19, 2012 | http://pubs.acs.org
Publication Date (Web): December 18, 2012 | doi: 10.1021/bk-2012-1118.ch001

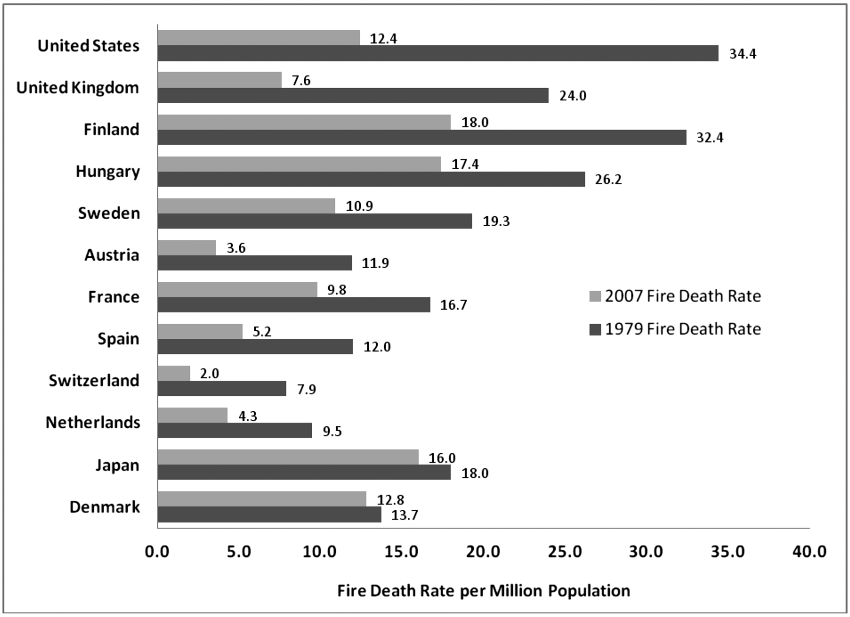

Figure 2. Comparison of Fire Death Rates per Million Population, 2007 versus 1979 (4). Sources: World Fire Statistics Centre fire death and the U.N. Demographic Yearbook population estimate data.

In the U.S. a person has a 1/3rd probability of having the fire department respond to a fire involving them in their lifetime. That high rate is probably a product of five factors: (1) the U.S. commits fewer resources to fire prevention activities; (2) there is a greater tolerance in the U.S. for "accidental" fires (no one is at fault); (3) Americans practice riskier and more careless behavior than people in other countries (example, the use of space heaters); (4) homes in the U.S. are not built with the same degree of fire resistance and compartmentalization as in some countries; and (5) most importantly, people in the U.S. have more contents or "stuff" than those in other countries (i.e., a higher fuel load) as well as a higher number of ignition sources (as measured by a higher use of energy). Therefore, fire risk in the U.S. remains high even as technologies and engineering solutions have advanced.

This volume is being written at a time when flame retardant chemicals have become controversial. In a series of articles the Chicago Tribune (*7*) expounded on the thesis that (1) flame retardants don't work, (2) that they are toxic, and (3) that regulations were developed following a cabal by the Tobacco Institute, chemical companies, and the newly formed National Association of State Fire Marshalls (in 1989), which forced standards requiring the use of hazardous flame retardants. But the first item (flame retardants do not work) flies in the face of five decades of work by thousands of fire scientists, chemists, and others, reported in thousands of peer reviewed papers, showing that from laboratory to full scale tests that flame retardants and flame retardant materials are effective. Further, no one would add additional cost to their product through the use of any additive (anti-oxidant, UV stabilizer, flame retardant) if they did not work to address fire risks found by regulators and fire safety engineers. The notion that flame retardants do not work is offensive to the scientists and engineers involved, and to the thousands of regulators at the local, state, and national level, and those who have participated in the voluntary consensus standards process (ASTM, NFPA, FAA, UL, etc.) establishing tests and standards based on research results. This notion effectively states that decades of peer reviewed work confirmed by thousands of scientists in multiple countries is worthless and that opinion trumps data. Finally, flame retardancy as a concept has been in place as long as mankind has realized that materials can catch fire and additives or other protections are needed to retard the spread of flame. One example of the decades of proven flame retardant value is in the area of televisions. One of us (GLN) was involved in burning some of the first televisions fabricated from UL-94 (Underwriter's Laboratories Test Standard 94) V-0 rated polystyrene at the General Electric Co. TV's had been determined by the U.S. CPSC to be of unreasonable risk in 1972, with 200 deaths, 800 life threatening fires , and 20,000 fires annually out of 120 million units. GE TV engineers indicated that fires were random, that they had fixed everything they knew how to fix. CPSC allowed Underwriters Laboratories to develop a voluntary national standard (UL 1410) requiring TV enclosures to be increasingly ignition resistant (Bunsen burner test) effective July 1, 1975; July 1, 1977; and July 1, 1979. GE TV was going to comply but was concerned if it really made a difference. At the time every component inside the TV was flame retardant except the antenna bracket and the tuner bracket. Working with the engineers, test workers decided to hot wire ignite the tuner bracket to simulate an internal fire since it was above the on-off switch. The testing was done in a 10 x 10 foot room. The result was a room flashover fire at five minutes with temperatures in the air duct coming from the room over 500 degrees F. Researchers then tested TV's with the enclosure, antenna bracket and tuner bracket made with decabromodiphenylether (Deca) in polystyrene which would meet the 1979 standard (UL 94-V0). There was no fire! Additional external trash fire ignitions were done. The plastic of the TV melted with minimal involvement. GE TV moved immediately to use FR antenna and tuner brackets and to use Deca/polystyrene for enclosures at the level required for July 1, 1979 prior to the 1975 date. With the adoption of the standard (UL 1410) CPSC found that TV fire deaths dropped to near zero, a more than one order of magnitude improvement. Other work at GE involved over 500 large scale tests involving a variety of applications of flame retardant materials with comparatively similar results. While this is just one in-depth example, clearly fire retardant materials and fire retardants work.

Regarding the toxicity assumption by the Chicago Tribune article, there are many factors driving the concern over flame retardants ranging from scientific illiteracy to new scientific findings showing problems with the chemistries in use today. The primary driver which results in concern about flame retardants in use

Downloaded by FORDHAM UNIV on December 19, 2012 | http://pubs.acs.org
Publication Date (Web): December 18, 2012 | doi: 10.1021/bk-2012-1118.ch001

Downloaded by FORDHAM UNIV on December 19, 2012 | http://pubs.acs.org
Publication Date (Web): December 18, 2012 | doi: 10.1021/bk-2012-1118.ch001

today is toxicity when said flame retardant enters into the environment and later into humans through environmental exposure. The issue of toxicity is complex. Are environmental issues of fires changed by the presence of flame retardants? Is there high health risk because of flame retardants which may migrate at low levels into the environment and onto contents of structures? To the first, workers at SP (Swedish National Research and Testing Institute) pioneered life cycle analysis (LCA) for products in fire. They looked at all environmental issues from manufacture on. Their studies have involved TVs, electrical cables, and upholstered furniture (*8–12*). In the last case, fire statistics from the UK were used to access the changes in the number and extent of fires resulting from the 1988 regulations requiring flame retardant materials. Fire environmental data were based on full scale testing of three different sofas based on a standard commercially available European model. Polycyclic aromatic hydrocarbons (PAH) were found to be most significant toxicologically. In terms of cancer risk, greater risk was found due to PAH (plus dioxins and furans) from the non-FR sofa, than from either of the FR treated sofas largely due to the fact that a non-FR sofa is expected to be involved in more and larger fires. Fires of any type (with or without flame retardants present) are highly toxic. Reducing the number of fires and reducing the size and speed of other fires are the key elements in reducing fire toxicity.

In the U.S. 60% of fire deaths are post-flashover outside of the room of origin. A large fire scenario maximizes the impact of carbon monoxide, which is the primary toxic gas in fires. Thus eliminating flashover or delaying flashover is key to eliminating fire death from both heat (burns) and toxic fire emissions (suffocation, CO poisoning). All organic polymers are combustible. They decompose when exposed to heat, their decomposition products burn, smoke is generated, and the products of combustion are highly toxic. The prime toxic product is carbon monoxide (CO) in concert with CO_2. While at times the heat from a fire can kill far sooner than toxic combustion gases, the preponderance of fire victims die in post-flashover fires in a room outside the room of origin, from toxic gases in smoke. Some 10-50,000 ppm CO has been found in smoke plumes coming out of a room in flashover, a very toxic level indeed. That toxicity is made more complex by the pervasive presence of alcohol on the part of fire victims, 52% of young adult fire victims and 74% of middle-aged fire victims have significant blood alcohol. Alcohol got them into the incident. Fire kills young children, the old and infirm, the drunk, not healthy unimpaired adults. And being poor adds to risky behaviors, such as the use of space heaters (*13*, *14*).

From laboratory toxicology papers one finds words like: suspected, linked, suggested. There are now some 7000 papers studying the effects of pentabromodiphenylether (Penta). Yet penta was withdrawn from sale in 2004 in part based on negative risk assessment data developed in Europe. U. S. suppliers of Deca have committed to U.S. EPA to its phase out by December 31, 2012 for most applications except military and transportation (*15*). This latter is in spite of a positive risk assessment report developed under REACH as published in the Official Journal of the European Union on May 29, 2008. Analytical chemistry now allows testing at very low levels. Reports of flame retardants at levels of parts per billion (PPB) have been reported for household dust and

Downloaded by FORDHAM UNIV on December 19, 2012 | http://pubs.acs.org
Publication Date (Web): December 18, 2012 | doi: 10.1021/bk-2012-1118.ch001

blood (*16*). The highest is 90 ppb for household dust reported by a prominent activist. In June 2004 blood samples were taken from fourteen ministers from the European Parliament, from 13 countries and others (*17*, *18*). Tests were run for 101 chemicals from seven different chemical families, including flame retardants, PCBs, pesticides, perfluorinated chemicals, phthalates, synthetic musks, and anti-bacterials, plus pharmaceuticals and heavy metals. 70 or more were frequently found. Thus knowing one class and not looking for or knowing the levels of the others can give misleading human health attribution. Interestingly halogen flame retardants receive considerable criticism, yet some 5000 different organohalogens are found in nature, 1500 organobromine compounds, and 3500 organochlorine compounds, some with substantial halogen percentages (*19–21*). Such compounds are frequently found in the marine environment. Indeed, as analytical techniques advance to the point where we can detect single molecules (truly amazing science) we continue to see how little we really know about our own environment and everything we have been utilizing for centuries. Flame retardants encompass a host of different chemistries: organo-halogens, phosphorus compounds, inorganics like hydrated alumina, hydrated magnesium hydroxide, borates, etc. A number of flame retardants have undergone extensive risk assessment in Europe under REACH. Some like Penta and Octa have been withdrawn as a result. Others have passed. Risk assessment is the key as eliminating all risk is impossible. Even compounds essential for life (water, table salt, potassium salts) can be lethal in the right circumstances and therefore one must always live with some risk. The "Green Chemistry" initiative enacted in California for example, and being implemented by its administration is a clear forum for discussion of complex chemicals, their potential risk, and potential alternatives. As new discoveries are made which identify new risks, chemistry rises to the occasion to come up with new solutions. Just because one chemical is found to be problematic does not mean that all chemicals are problematic. Rather it means that industry, academia, and government must work together to develop new solutions which solve the old problem while building the new solution upon current knowledge. For flame retardants a key issue is migration from the flame retarded object. One approach is flame retardants which are chemically bound in or the use of polymeric flame retardants. Indeed, new approaches exist, discussion of which is one purpose of this volume.

The third issue of the Chicago Tribune article relates to the cabal of the Tobacco Institute, the chemical industry, and NASFM. The date of the founding of NASFM is 1989. Incidentally the first of these volumes resulted from a symposium in April, 1989. California established its upholstered furniture regulations in 1975. The above TV requirements were also in 1975, the Flammable Fabrics Act was 1953 and 1967. Tests like Oxygen Index (ASTM D2863) were first published in 1970, D635 in 1941, E662 on smoke in 1979. All are well before whatever (if anything) may have happened at NASFM in 1989. Therefore it seems highly unlikely that the Tobacco Institute drove these regulations at all. They may have commented on it later on in resistance to having to change their products, but it seems quite clear they were not involved in the original regulatory issues which mandated the use of flame retardants for fire safety.

Table 1. U. S. PRODUCTION, SALES & CAPTIVE USE (*22*) (millions of pounds, dry weight basis)(1)

Resin	*Production*
	2011
Epoxy (2)	613
Other Thermosets (5)	13,187
Total Thermosets	**13,800**
LDPE (2)(3)	6,706
LLDPE (2)(3)	13,424
HDPE (2)(3)	17,117
PP (2)(4)	16,418
PS (2)(3)(4*)	5,472
Nylon (2)(4)	1,106
PVC (3)	14,434
Other Thermoplastics	14,732
Total Thermoplastics	**89,408**
GRAND TOTAL PLASTICS	**103,208**

(1) Except Phenolic resins, which are reported on a gross weight basis. (2) Sales & Captive Use data include imports. (3) Canadian production and sales data included. (4) Canadian and Mexican production and sales data included. (5) Includes: polyurethanes (TDI, MDI and polyols), phenolic, urea, melamine, unsaturated polyester (6) Includes: PET, ABS, engineering resins, SB Latex, and other thermoplastics.

Downloaded by FORDHAM UNIV on December 19, 2012 | http://pubs.acs.org
Publication Date (Web): December 18, 2012 | doi: 10.1021/bk-2012-1118.ch001

Flame retardant materials work when properly used. This is a key point for any chemical technology. If you take a chemical outside the application it was originally designed for, one should not be surprised that either (a) it doesn't work, or (b) it will cause unexpected problems. Polymers form a major part of our modern built environment. Fire safety depends upon those materials. Polymers are "enabling technology" for almost all of modern society as we know it today and indeed are seen as a major enabling technology to remove greenhouse gas emissions as lighter weight plastics are inserted into vehicles for energy savings. Advances in numerous technologies depend on appropriate advances in polymers for success. While polymers are both natural and synthetic, this book focuses entirely on the fire safety aspects of synthetic polymers. Production of synthetic plastics totaled over 103 billion pounds in the U.S. in 2011. In terms of consumption the U.S. is slightly less than a third of the world. Table 1 presents U.S. production by resin, and Table 2 presents thermoplastic sales by market segment.

Table 2. THERMOPLASTIC RESIN SALES BY MAJOR MARKET 2011 (*23*) (millions of pounds, dry weight basis)

Major Market	*2011*
Transportation	2,649
Packaging	25,302
Building and Construction	11,036
Electrical/Electronic	1,618
Furniture and Furnishings	1,818
Consumer and Institutional	14,743
Industrial/Machinery	781
Adhesives/Inks/Coatings	801
All Other	1,206
Exports	14,858
Total	**74,811**

ACC data were collected for the following thermoplastic resins only:
Low-Density Polyethylene (LDPE)
Linear-Low-Density Polyethylene (LLDPE)
High-Density Polyethylene (HDPE)
Polypropylene (PP)
Polyvinyl Chloride (PVC)
Styrene-Butadiene Latex

Downloaded by FORDHAM UNIV on December 19, 2012 | http://pubs.acs.org
Publication Date (Web): December 18, 2012 | doi: 10.1021/bk-2012-1118.ch001

Fire is not a single material property but is regulated by many material parameters. Fire behavior from a material combines ease of thermal degradation, ease of ignition, flame spread, rate of heat release, ease of extinction, complicated by smoke generation, toxic potency, and other properties.

Since fire risk has been around for a very long time, the field of fire safety science looks at specific scenarios where fires can occur, and works with government through codes and standards to minimize fire events and subsequent losses should the fire blaze out of control. These codes and standards use specific tests covering the properties of material flammability described above. The results of these tests are combined with engineering assessments for materials and systems as deemed appropriate for a particular application. Thus, for example, it is appropriate for small appliances to only worry about ignitability by a Bunsen burner flame or a needle flame, since in that application, from an

Downloaded by FORDHAM UNIV on December 19, 2012 | http://pubs.acs.org
Publication Date (Web): December 18, 2012 | doi: 10.1021/bk-2012-1118.ch001

internal perspective, that is the size of a fire source (from an electrical short) that is possible in real appliance failures. For wall linings one assumes a fire and is interested in the rapidity of flame spread given a fire, since that will determine if and when flashover will result. A layered approach is frequently used. Electronic equipment may have a fuse and use flame retardant components as well. When flame retardants are used to address these fire risks, they are specifically tailored to meet that fire risk scenario; they are not necessarily appropriate for all fire risk scenarios and so one must apply that chemistry with care through paying attention to the specific fire risk scenario and how the flame retardant chemistry works to address that scenario.

Some polymers are themselves difficult to ignite or be consumed by flame. Other polymers require flame retardant additives to pass the regulatory tests required for safe use. The total market for flame retardants in the U.S., Europe, and Asia in 2007 amounted to about 1.8 million metric tons and was valued at \$4.2 billion (in 2011 \$4.8 billion). Figure 3 shows the breakdown of the flame retardant market by value and Figure 4 by volume. On that basis halogen and antimony oxide constitutes 57% of the market (versus 38% by volume) because of the extensive use of brominated flame retardants in Asia (Figure 5). Figure 6 provides the consumption of flame retardants by region by volume. The market is projected to grow at 6.9% per year to \$7.1 billion in 2017. Different flame retardants are prominent in different world regions. China and India are focusing on increased fire safety, particularly in the area of electronics. It should be noted though that a significant portion of electronic parts or products manufactured in China and India and are exported to Europe and the US, and so demands there will affect flame retardant use worldwide. Asia/Pacific is expected to account for 50% of the world demand by 2014 as measured by value (*24–27*).

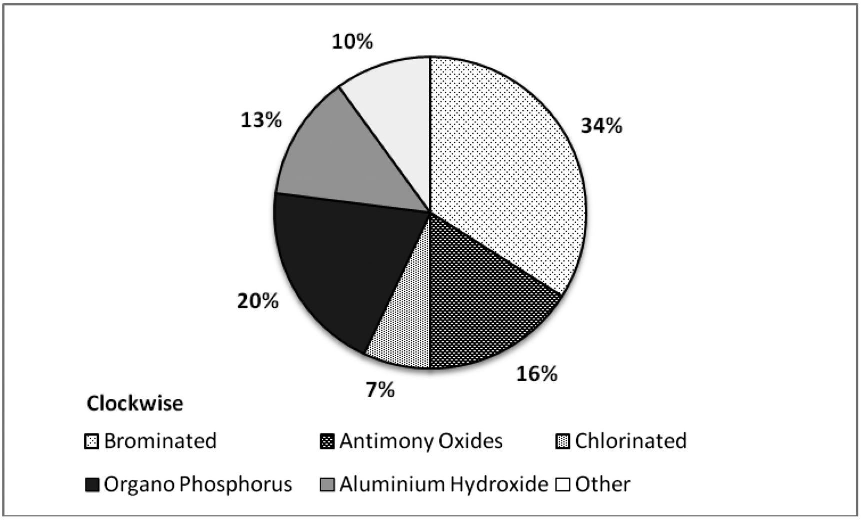

Figure 3. Global market of flame retardants. The Flame Retardants Market by value. Representing a total of 4.2 billion US\$, data for 2007 (24).

Downloaded by FORDHAM UNIV on December 19, 2012 | http://pubs.acs.org
Publication Date (Web): December 18, 2012 | doi: 10.1021/bk-2012-1118.ch001

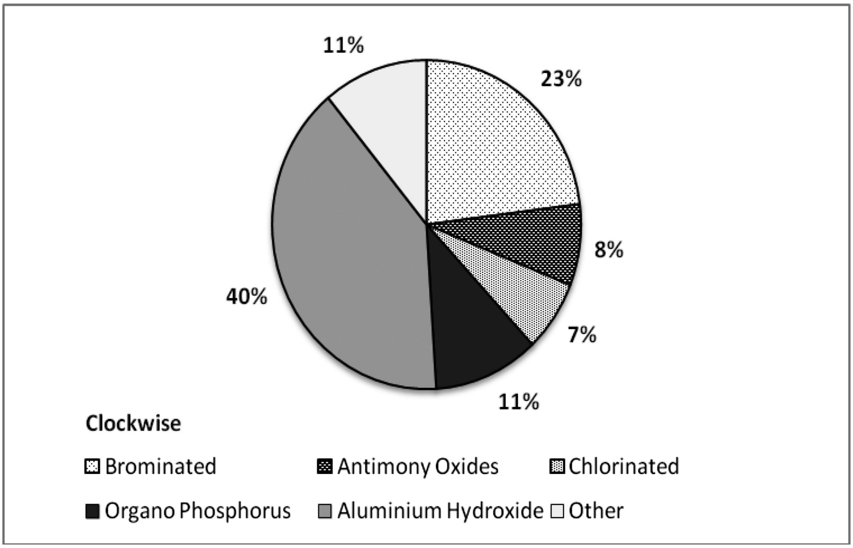

Figure 4. Global market of flame retardants. The Flame Retardants Market by Quantity. The total amount is 1.8 million metric tons, data for 2007 (25).

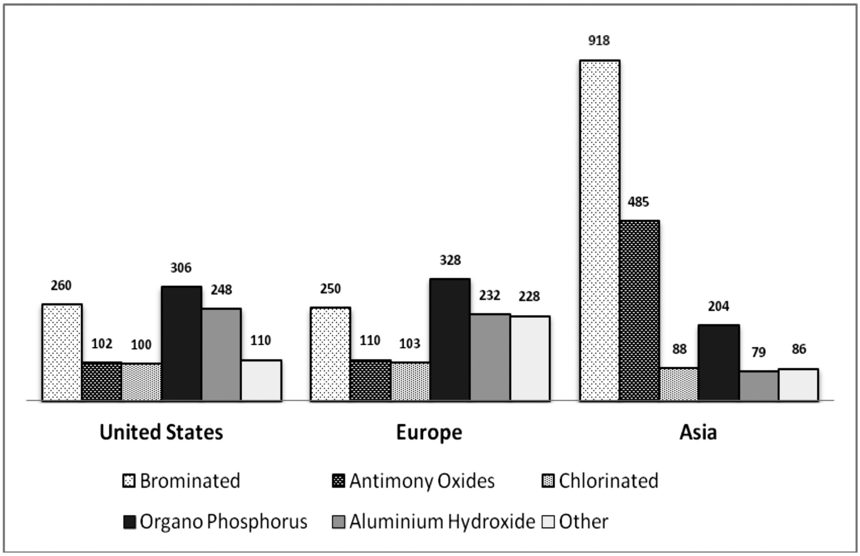

Figure 5. Global market of flame retardants. Sales of Flame Retardants by Region. Figures are in million $US, with a total of 4.2 billion $US, data for 2007 (24).

Downloaded by FORDHAM UNIV on December 19, 2012 | http://pubs.acs.org
Publication Date (Web): December 18, 2012 | doi: 10.1021/bk-2012-1118.ch001

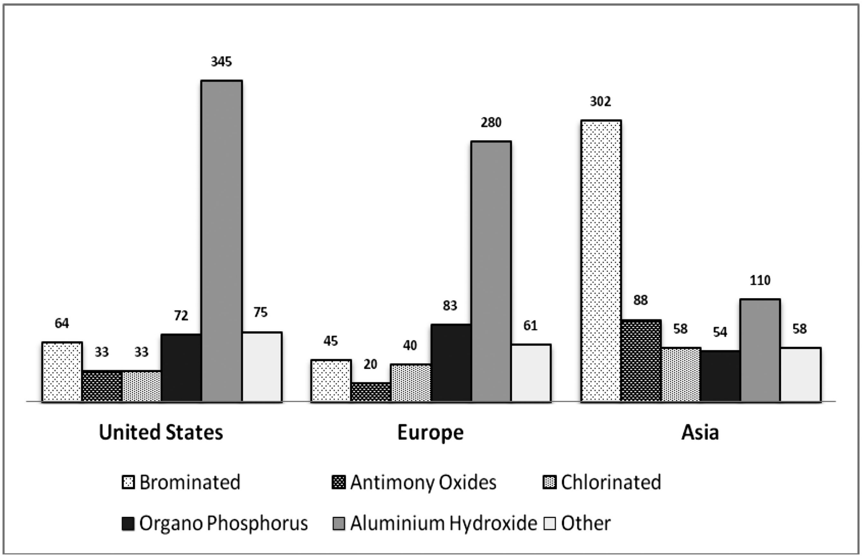

Figure 6. Global market of flame retardants. Consumption of Flame Retardants by Region, based on volume. Figures are 1000 tons, with a total of 1.8 million metric tons, data for 2007 (25).

With this background, one can see that research on Fire and Polymers has an important role to play in modern society. This includes its discussion in the political arena as fire affects our lives and any technology or phenomena which has wide-reaching consequences should be discussed at the political level to ensure protection is done in a way that society accepts. This volume is about the latest research at the intersection of the fields of Fire and Polymers with a strong focus on materials chemistry. With this volume, work is focused on improving the fire performance of polymers through a detailed understanding of polymer degradation chemistry. New and refined analytical techniques facilitate that analysis. Creative chemists continue to develop new approaches, new and more stable flame retardant and polymeric structures, including polymeric flame retardants. Mathematical fire models continue to become more sophisticated and fire tests themselves are becoming better understood.

There are many diverse approaches to enhancing the fire stability of polymer structures. In the past, the most common approach involved the use of simple additives via melt compounding. Twenty years ago halogenated flame retardants (with antimony oxide) were the additives of choice (e.g., the TV story above). Over the past 10 years there has been a strong emphasis on non-halogenated flame retardants, and of nano-scale additives in particular. In the electrical/electronic industry, halogen-free fire retardants are also demanded by end users such as Apple and Hewlett Packard. Also, computer server farms become more common, non-halogenated flame retardants are demanded for the wire and cable jackets inside those room to limit damage to vital electronics from smoke during accidental fires.

As one looks at previous Fire and Polymers volumes, topics have clearly changed over the years. In 1990 fire toxicity was the first section with six papers. In 1995 there again was a section on fire toxicity with seven chapters. In 2001 there was but one paper, in 2006, three, in 2009 one, and in this volume none. In 1990 there was a section on cellulosics, in 2001 only one chapter, and in 2006, 2009 and in this volume, none. In the 1995 volume there were twelve chapters on tests and regulations, in 2001, two, and in 2006, 2009, none and this volume two. In the 2006 volume, half of the papers were on nanocomposites and only two papers had a focus on halogen materials. In 2009 the majority of the papers were concerned with nanocomposites and their effects on flammability, but there were nine papers dealing with either conventional or novel flame retardant systems. This year (2012) nanocomposites are still a major topic of research at 5 papers. The 2012 volume of this book series is dominated by flame retardant chemistry ranging from traditional systems (brominated) to intumescent to phosphorus-based, to new chemistries for a total of 19 papers. Fire science and metrology papers are also represented with a total of 4 papers. What is most notable about the 2012 volume is the total number of papers, which is 31, a new record for total number of papers submitted to this ACS symposium series. Indeed, the conference that occurred in 2012 at San Diego had record attendance over 3 full days with a large number of US and international speakers and attendees. While funding for new flame retardant material science and chemistry remains low, the interest and demand in the phenomena remains high, especially in light of the issues brought up at the beginning of this chapter.

To conclude, this peer-reviewed volume is designed to be a snapshot in time, representing the state of the art in new approaches to flame retardant chemistry, material science, and new understanding of flammability phenomena and the regulations which drive our field of research. We believe that this work represents some of the best work from the key researchers in the field and hope that you, the reader, find this book of value as you develop new materials.

Downloaded by FORDHAM UNIV on December 19, 2012 | http://pubs.acs.org
Publication Date (Web): December 18, 2012 | doi: 10.1021/bk-2012-1118.ch001

References

1. Karter, M. J., Jr. *Five Loss in the United States During 2010*; National Fire Protection Association: Quincy, MA, September, 2011.
2. Karter, M. J., Jr. *Five Loss in the United States During 2007*; National Fire Protection Association: Quincy, MA, August, 2008.
3. State Fire Death Rates, FEMA, http://www.usfa.fema.gov/statistics/estimates/states.shtm.
4. *Fire Death Rate Trend: An International Perspective*, Topical Fire Report Series, FEMA, 12 (8), July, 2011.
5. *Statistics and New Fire Protection Activities in Russia*, http://www.flameretardants-online.com/web/en/news/index.htm?showid=303,5/7/12.
6. *Vladimir Putin Blasts Fire Safety in Russia*, http://en.rian.ru/russia/20091208/157148520.html,8/12/2009.
7. *Playing with Fire*, http://media.apps.chicagotribune.com/flames/index.html.

8. Anderson, P.; Simonson, M.; Stripple, H. *Fire Safety of Upholstered Furniture, A Life-Cycle Assessment Summary Report*; SP Swedish National Testing and Research Institute, http://www.sp.se./sv/units/fire/Documents/Rappporter/LCA_Summary.pdf.
9. *Fire LCA*, http://www.sp.se./en/index/services/fire/co/sider/default.aspx.
10. McNamee, M. S. *Life Cycle Assessment of Fire Retardants*, http://www.nist.gov/el/five_research/upload/3-McNamee.pdf.
11. Simonson, M.; Blomqvist, P.; Boldizar, A.; Möller, K.; Rosell L.; Tullin, C.; Stripple, H.; Sundquist, S. *Fire-LCA Model: TV Case Study SP Swedish National Testing and Research Institute SP Report*; Swedish National Testing and Research Institute, SP Report 2000:13.
12. Simonson, M.; Tullin, C.; Stripple, H. *Chemosphere* **2002**, *46*, 737–744.
13. Nelson, G. L. Toxicological Issues in Fire: Carbon Monoxide or Additives. The Tenth International Conference: Additives 2001: Plastics for the New Millennium; Executive Conference Management, Hilton Head, SC, March 18–21, 2001.
14. Hirscher, M. M.; Delamore, S. M.; Larsen, J. B.; Nelson, G. L. *Carbon Monoxide and Human Lethality: Fire and Non-Fire Studies*; Elsevier Applied Science; London, 1993; 425 pp.
15. Letter for Albemarle, Chemtura, ICL Industrial Products dated December 15−17, 2009.
16. Johnson, P. I.; Stapleton, H. M.; Sjodin, A.; Meeker, J. D. Relationships between Polybrominated Diphenyl Ether Concentrations in House Dust and Serum. *Environ. Sci. Technol.* **2010**, *44*, 5627–5632.
17. *Tests reveal presence of toxic chemicals in MEPs' blood*; http://www.euractiv.com/climate-environment/tests-reveal-presence-toxic-chemicals-meps-blood/article-117957, April 22, 2004.
18. Peters, R. *Man-made Chemicals in Human Blood*; TNO Report R2004/493, http://www.greenpeace.org/international/PageFiles/24502/man-made-chemicals-in-human-bl.pdf, November 2004.
19. Gribble, G. W. *Environ. Sci. Pollut. Res.* **2000**, *7*, 37–49.
20. Gribble, G. W. *Chemosphere* **2003**, *52*, 289–297.
21. Gribble, G. W. *Heterocycles* **2012**, *84*, 157–207.
22. http://www.americanchemistry.com/Jobs/EconomicStatistics/Productions-and-Sales-Data-by-Resin.pdf.
23. http://www.americanchemistry.com/Jobs/EconomicStatistics/Plastics-Statistics/Total-Sales-Captive-Use-by-Major-Market.pdf.
24. http://www.flameretardants-online.com/web/en/106/114.htm.
25. http://www.flameretardants-online.com/web/en/106/113.htm.
26. http://www.marketsandmarkets.com/PressReleases/flame-retardants-chemicals.asp.
27. http://www.marketresearch.com/Freedonia-Group-Inc-v-1247/Flame-Retardants-6049966/.

Downloaded by FORDHAM UNIV on December 19, 2012 | http://pubs.acs.org
Publication Date (Web): December 18, 2012 | doi: 10.1021/bk-2012-1118.ch001

Chapter 2

Synergistic Use of Talc in Halogen-Free Flame Retarded Polycarbonate/Acrylonitrile-Butadiene-Styrene Blends

Bernhard Schartel,* Kristin H. Richter, and Martin Böhning

BAM Federal Institute for Material Research and Testing,
Unter den Eichen 87, 12205 Berlin, Germany
***E-mail: bernhard.schartel@bam.de**

Pyrolysis, flammability, fire behavior, melt viscosity, and gas diffusion of bisphenol A polycarbonate/acrylonitrile-butadiene-styrene (PC/ABS) were investigated, with bisphenol A bis(diphenyl phosphate) (BDP), with 10 wt.% talc and with BDP in combination with 5, 10 and 20 wt.% talc, respectively. Compared to PC/ABS, PC/ABS + BDP results in an increased decomposition temperature of PC, a higher char yield, a significantly increased LOI, a V-0 classification in UL 94, a reduced peak heat release rate (pHRR), and a reduced total heat release (THR) in the cone calorimeter. This efficient flame retardancy is due to mechanisms in both the gas and condensed phases. PC/ABS + 10 wt.% talc shows a decrease in the PC decomposition temperature. The fire behavior is improved in part compared to PC/ABS, with an increased LOI and reduced pHRR. PC/ABS + BDP + 10 wt.% talc shows a strong synergism in LOI, a V-0 classification, and a decrease in pHRR, whereas THR is slightly increased compared to PC/ABS + BDP. Talc decreases the gas diffusion and enhances the flow limit for low shear rates, both of which influence the pyrolysis and flammability results. Further, talc improves the protection properties of the fire residues. Nevertheless it also partly suppresses flame inhibition and the charring effect of BDP. The synergism between BDP and talc in LOI is obtained even for low talc loadings in PC/ABS + BDP + talc, whereas for higher loadings saturation is observed.

In Fire and Polymers VI: New Advances in Flame Retardant Chemistry and Science; Morgan, A., et al.;
ACS Symposium Series; American Chemical Society: Washington, DC, 2012.

Introduction

Bisphenol A polycarbonate/acrylonitrile-butadiene-styrene (PC/ABS) is an engineering polymer blend which is also used in electronical engineering, in transportation and in construction. These applications have high demands on fire safety and thus flame retardants are needed. Aryl phosphates, like bisphenol A bis(diphenyl phosphate) (BDP), have become the common halogen-free flame retardants used in PC/ABS (*1–3*). Combining BDP with other synergistic or adjuvant additives results in especially efficient flame retardancy, but also tailored or multifunctional materials (*3–7*).

The flame retardancy mechanisms of aryl phosphates in PC/ABS were investigated by Levchik et al. (*8*, *9*). In a previous paper we, too, discussed in detail the pyrolysis and fire behavior of PC/ABS flame retarded by arylphosphates (*10*). BDP acts in both the condensed and gas phases. The flame inhibition in the gas phase is caused by the release of phosphorous species (*11–13*). The condensed-phase mechanism results mainly from reaction of the decomposition products of PC and BDP (*14*). An additional charring is observed caused by induced crosslinking, whereby BDP acts as an acid precursor, and what is more, a change in the composition and properties of the char due to the incorporation of phosphate groups into the network.

The combination of BDP with nano-dispersed boehmite, as reported in an earlier study (*15*), yielded synergism with regard to LOI, but had antagonistic effects on the charring of PC and BDP. The combination of BDP and zinc borate in PC/ABS (*16*) led to a reaction of both additives. The almost complete consumption of BDP through reaction with zinc borate clearly reduces both phosphorus-inducing crosslinking in the condensed phase and phosphorus released to inhibit flames in the gas phase. Instead the reaction products, metal phosphates and borophosphates have an effect on the barrier properties of the residue. An increase in flame retardancy effectiveness occurs for LOI and low heat fluxes in the cone calorimeter, whereas efficiency decreases for high external heat fluxes. It becomes clear that the flame retardancy mechanism and efficiency of BDP in PC/ABS is very sensitive to the presence of other additives with which BDP can react. This conclusion is confirmed by investigations on PC/silicon rubber/BDP (*17*), where all components show chemical reactions with each other.

Therefore in this study the combination of BDP with the rather inert filler talc was examined in PC/ABS. Talc is hydrated magnesium silicate and commonly used as an inert filler in plastics. In thermoplastics, talc is a reinforcing mineral that is often used to improve mechanical properties. In some studies it was supposed that talc, because of its lamellar character, forms a protective layer during combustion, acting as a mass diffusion barrier for volatile decomposition products (*18*, *19*). Effects on flame retardancy were also reported, *e.g.* when stabilization of the char occurred mechanically (*20*). Further the influence of talc in intumescent systems was examined (*21–23*), which may be related to the investigated PC/ABS system that also shows pronounced deformation during combustion. The influence of talc in intumescent systems can be beneficial or deleterious (*24*, *25*). Actually its effect on such systems is complex and quite different from system to system, since intumescence is sensitive to pyrolysing melt viscosity, char structure and char stability, all of which are influenced by adding talc. Thus the question arises as to how talc influences the fire behavior of PC/ABS, which also shows both significant char formation and deformation during fire testing, somewhat analogous to intumescent systems.

In particular, the flame retardant effect of BDP with 10 wt.% talc in PC/ABS and 10 wt.% talc in PC/ABS was studied. The focus was on the combination of BDP with talc and its influence on the flame retardancy mechanisms, to reveal synergisms or antagonisms. Further different concentrations of talc in PC/ABS + BDP + talc were examined, to reveal the dependence of the results on the talc loading.

Experimental

Table 1. Investigated materials: composition in wt.% (additional < 1 wt.% belong to other additives)

PC/ABS +	*-*	*BDP*	*10 wt.% talc*	*BDP + 10 wt.% talc*	*BDP + 5 wt.% talc*	*BDP + 20 wt.% talc*
PC	81.2	71.0	73.0	62.7	66.8	54.4
ABS	17.3	15.0	15.5	13.3	14.2	11.6
PTFE+SAN	0.9	0.9	0.9	0.9	0.9	0.9
BDP		12.5		12.5	12.5	12.5
talc			10	10	5	20

Four different PC/ABS blends with polytetrafluoroethylene (PTFE) were investigated, with and without BDP, 10 wt.% talc and the combination of BDP and 10 wt.% talc, and then compared to systems of PC/ABS + BDP with 5 and 20 wt.% talc, respectively. The A:B:S ratio of ABS was 21:13:66. A PC:ABS ratio of 4.7:1 was maintained at all times. All systems included 0.9 wt.% master batch of PTFE mixed 1:1 with styrene acrylonitrile (SAN). The molecular weight of BDP (n = 1) is 692.6 gmol^{-1}. The BDP used had an averaged repeating unit of n = 1.1 and contained about 2.5 wt.% TPP (triphenyl phosphate). Talc had the molecular formula $Mg_3Si_4O_{10}(OH)_2$ and a molecular weight of M_w(talc) = 379.3 gmol^{-1}. The samples were compounded and provided as granulate and test specimen by Bayer MaterialScience AG (Dormagen, Germany). Test specimens were produced by injection molding. The compositions of the investigated materials and the corresponding abbreviations used in the following are shown in Table 1. Note that in the abbreviations the component PTFE+SAN is not longer indicated.

The morphologies of PC/ABS + 10 wt.% talc and PC/ABS + BDP + 10 wt.% talc were characterized by TEM bright field investigations; corresponding images are shown in Figure 1. The talc is quite well and homogenously dispersed. The size of the talc particles is between several hundred nanometers and a few micrometers.

In Fire and Polymers VI: New Advances in Flame Retardant Chemistry and Science; Morgan, A., et al.;
ACS Symposium Series; American Chemical Society: Washington, DC, 2012.

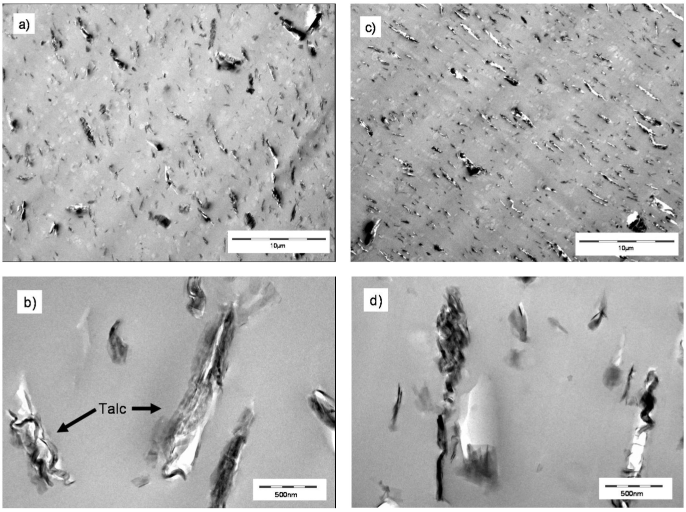

Figure 1. TEM bright field images of thin sections (cut in flow direction of the middle of a UL 94 sample, source: Bayer MaterialScience. a) and b) PC/ABS + BDP + 10 wt.% talc, c) and d) PC/ABS + 10 wt.% talc.

The anisotropic particles show a clear orientation in the investigated PC/ABS + 10 wt.% talc samples and some in PC/ABS + BDP + 10 wt.% talc. The relaxation times needed for the reorientation of the talc particles in the polymer melt are much longer than the relaxation times for the polymer chain segments. Thus the high orientation occurring during the injection molding is frozen in for the talc particles. Adding BDP in PC/ABS + BDP significantly decreases the melt viscosity due to the BDP plasticing effect (*10*, *26*), increasing the reorientation relaxation. Thus the PC/ABS + BDP + 10 wt.% talc clearly shows less orientation remaining after processing than PC/ABS + 10 wt.% talc.

Thermal decomposition was investigated by thermogravimetry (TG) (TGA/SDTA 851, Mettler Toledo, Germany). A Fourier transform infrared spectrometer (TG-FTIR, Nexus 470, Nicolet, Germany) coupled with the TG was used to analyze the evolved gases (*27*). The TG measurements were performed under nitrogen with a heating rate of 10 Kmin^{-1} and a sample weight of 10 mg. Decomposition kinetics were based on measurements using heating rates of 2, 5 and 10 Kmin^{-1}. The residue was determined at the end of the main decomposition step. The standard deviation for TG was about 1 wt.%, including the contribution of buoyant forces.

Diffusion coefficients for oxygen were determined from gravimetric gas sorption measurements, using an electronic high-pressure microbalance Sartorius M25D-P (Sartorius GmbH, Göttingen, Germany). The temperature of the setup was held constant by an air bath at 308.2 ± 0.1 K. Film samples with a well-defined thickness ranging from 266 to 390 µm and an initial weight of between 91.8 and 99.5 mg were used and evacuated in the cell at $p < 10^{-5}$ mbar for at least 48 h until any significant weight change ceased. The gas pressure was increased in a series of step-by-step increments and the resulting weight gain of the sample was observed for at least 24 hours at each step. After starting measurement, the signal of the microbalance was recorded at a rate of 0.5 s^{-1}. Diffusion coefficients were obtained by fitting Fickian diffusion kinetics to the time-dependent mass uptake data. Oxygen of purity 5.0 was used (Air Liquide Deutschland GmbH).

Melt rheology was done with an Anton Paar Physica MCR301 rheometer, plate-plate geometry (plate gap of 1 mm, plate diameter of 25 mm). Isothermal measurements were conducted at four temperatures (488 K, 498 K, 543 K and 588 K) using a small deformation ($\gamma = 0.5\%$) in the frequency sweep mode (100 Hz - 0.1 Hz). The used temperatures are clearly below the decomposition temperature and thus the measurements were performed under air. The results were summarized in master curves for 498 K.

The forced-flaming behavior was characterized by a cone calorimeter (*28–30*) (FTT, UK) according to ISO 5660. The samples (100 mm x 100 mm x 3 mm) were measured horizontally in a frame, applying different external heat fluxes (35, 50 and 70 kWm^{-2}). The total heat release (THR) for the whole burning was taken at the time to flame-out. Due to extensive deformation the materials show an uncertainty in time to ignition (t_{ign}), heat release rate (HRR) and peak HRR (pHRR) that is larger than that usual in cone calorimeter tests. The flammability (reaction to small flame) was determined by UL 94 tests following IEC 60695-11-10 (sample size: 120 mm x 12.5 mm x 3 mm) and the oxygen index (LOI) following ISO 4589 (sample size: 80 mm x 10 mm x 4 mm).

Results and Discussion

Thermal Decomposition of PC/ABS, PC/ABS + BDP, PC/ABS + 10 wt.% Talc and PC/ABS + BDP + 10 wt.% Talc

The TG results of PC/ABS, PC/ABS + BDP, PC/ABS + 10 wt.% talc and PC/ABS + BDP + 10 wt.% talc are shown in Figure 2 and summarized in Table 2. PC/ABS, PC/ABS + BDP and PC/ABS + BDP + 10 wt.% talc clearly decompose in two main steps, whereas for PC/ABS + 10 wt.% talc a strong overlap of the two different decomposition steps is observed. For PC/ABS + 10 wt.% talc the mass versus temperature pattern comes close to a one-step decomposition and the mass loss rate indicates the first decomposition only as a shoulder.

The decomposition of PC/ABS and PC/ABS + BDP was discussed in detail in an earlier paper (*10*). The most important results are that the first decomposition step is related to the ABS decomposition and the second to PC. This was concluded based on the results of the characteristic decomposition temperatures, activation energies, mass losses and volatile pyrolysis products (Table 2, Figure 2, Figure 3). Adding BDP results in a shift in the temperature of PC's maximum weight loss to temperatures 24 K higher. Especially this shift in the decomposition temperature of PC causes increased separation of both decomposition steps, as seen in Figure 2. Further, the residue increases for PC/ABS + BDP compared to PC/ABS. BDP interacted with PC. Taking into account the PC content, the char yield of PC is calculated assuming that no char was produced by ABS and BDP. It increases by a third (Table 2). It was proposed that BDP acts as an acid precursor, inducing additional charring and performing crosslinking by itself, probably through a reaction with decomposition products of PC such as phenolic groups arising from Fries rearrangements (*10*, *14*).

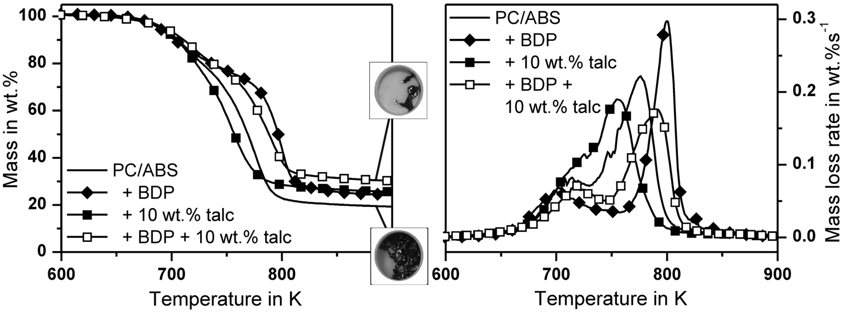

Figure 2. Mass loss (left) and mass loss rates (right) of PC/ABS, PC/ABS + BDP, PC/ABS + 10 wt.% talc and PC/ABS + BDP + 10 wt.% talc measured in nitrogen atmosphere with a heating rate of 10 Kmin^{-1}*. The TG residues of PC/ABS + BDP and PC/ABS + BDP + 10 wt.% talc are shown as inserts.*

Adding 10 wt.% talc to PC/ABS produces no change in the onset temperature of decomposition (Table 2). However the temperature of the maximum mass loss rate of the first decomposition step (ABS decomposition) increases by 11 K; the one for the second decomposition step (PC decomposition) decreases by 21 K compared to PC/ABS. Both decomposition steps overlap very strongly (Figure 2). The strong overlapping of both steps also explains the slight change in the evaluated mass losses for ABS and PC. A significant amount of ABS and PC decomposes at the same time, influencing the mass loss assignment. The residue for PC/ABS + 10 wt.% talc is 29.8 wt.%, which corresponds to what is calculated based on the reduced PC content and talc (resulting in 9.9 wt.% residue at those temperatures). Subtracting the inorganic residue and calculating the char yield per PC content proves that the char yield of PC in PC/ABS + 10 wt.% talc did not change compared to PC/ABS. Combining BDP with talc in PC/ABS + BDP + 10 wt.% talc, the onset temperature is higher (+ 11 K) than for PC/ABS + BDP and thus similar to PC/ABS and PC/ABS + 10 wt.% talc. The increase in the PC decomposition temperature because of BDP was counteracted to some extent by the presence of talc, but still increased compared to PC/ABS (+ 16 K). The mass loss for the second decomposition step was reduced for PC/ABS + BDP + 10 wt.% talc compared to PC/ABS + BDP; mainly because of the lower polymer content. The char yield due to PC may be slightly decreased, but this result was not clear.

Table 2. **Thermal decomposition of PC/ABS, PC/ABS + BDP, PC/ABS + 10 wt.% talc, and PC/ABS + BDP + 10 wt.% talc under nitrogen with a heating rate of 10 Kmin^{-1} (onset temperature = T_{onset}; temperature of maximum mass loss rate = T_{max}; calculated = cal.)**

PC/ABS + ...	*/*	*BDP*	*10 wt.% talc*	*BDP+10 wt.% talc*	*Error*
T_{onset} (K)	681	673	683	684	±2
		Mass loss I (decomposition of ABS)			
Weight loss (wt.%)	20.9	24.7	23.5	22.2	±1
T_{max} (K)	715	699	726	720	±2
		Mass loss II (decomposition of PC)			
Weight loss (wt.%)	56.4	46.6	43.9	43.4	±1
T_{max} (K)	776	800	755	792	±2
Residue (wt.%)	22.7	28.7	29.8	33.8	±1
Cal. char yield of PC	0.28	0.40	0.27	0.38	±0.01

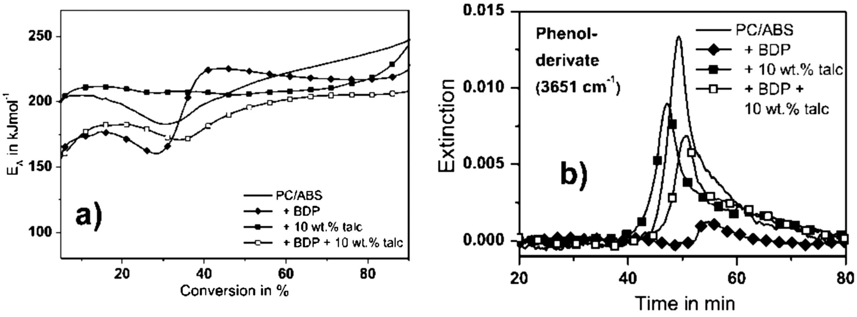

Figure 3. a) Activation energy (E_A) versus conversion and b) pyrolysis product release rates determined by TG-FTIR for phenol derivatives for PC/ABS, PC/ABS + BDP, PC/ABS + 10 wt.% talc and PC/ABS + BDP + 10 wt.% talc.

Reaction kinetics revealed at least two main activation energies for PC/ABS (Figure 3a), the first at around 180-210 kJmol^{-1} and the second at around 220-240 kJmol^{-1}. These values were related to decomposition dominated by ABS and PC, respectively. The activation energy pattern indicates overlapping processes for PC/ABS so that no distinct plateau values for the activation energy are observed versus conversion. For PC/ABS + BDP the activation energy of ABS and for PC decomposition decrease. A plateau, and thus more distinct values, are observed around 180 kJmol^{-1} for the ABS decomposition, and around 220 kJmol^{-1} for the PC decomposition, since the processes are clearly separated. For PC/ABS + 10 wt.% talc almost no separation at all into two different decomposition steps is observed up to conversion of 80%, but only a single, rather constant activation energy of around 210 kJmol^{-1}, characteristic of the nearly completely overlapping decomposition of ABS and PC. For PC/ABS + BDP + 10 wt.% talc the activation energy pattern is similar to PC/ABS + BDP, but the separation was less significant. The separation characteristics of all blends correspond to the overlapping of the decomposition steps of ABS and PC monitored in terms of mass and mass loss rate. Further the activation energy of PC decreased for the blends with talc.

TG-FTIR measurements (no figure shown here for the straightforward product identification reported before in (*10*)) show styrene as the main decomposition product for the first decomposition step, which indicates the decomposition of ABS. For the second decomposition step, CO_2 is observed as a major decomposition product, along with methane and phenol derivatives, such as methyl phenol, ethyl phenol, traces of bisphenol A and phenol. The identified volatile pyrolysis products are in agreement with other reports on the decomposition of PC (*31*, *32*). Adding BDP to PC/ABS leads to an increase in the amount of CO_2 released and to a decrease in the amount of phenol derivatives (Figure 3b). The change in the evolved gases corresponds to an increase in char, because fewer large volatiles, like phenol derivatives, were produced during decomposition. In an earlier paper it was assumed that P-O-C bonds of BDP reacted via transesterification with phenolic groups from PC, generated through Fries rearrangements (*10*, *14*). For PC/ABS + 10 wt.% talc the release of CO_2 is identical and the release of phenol derivatives is reduced slightly compared to the release rates of PC/ABS. PC/ABS + BDP + 10 wt.% talc shows the same CO_2 release as PC/ABS and PC/ABS + 10 wt.% talc and clearly smaller than PC/ABS + BDP. The release of phenol derivatives was rather similar to that of PC/ABS + 10 wt.% talc. Combining BDP with talc in PC/ABS + BDP + 10 wt.% talc clearly counteracts the effect of BDP on the release of CO_2 and phenol derivatives, and thus the increase in charring by BDP.

By analogy, a possible explanation for the effect of talc has been described in the literature (*33*). At high temperatures PC chains start to crosslink with each other, resulting in a thermally stable carbonaceous char. However, this crosslinking is only effective when volatile decomposition products are released and thus do not disturb the crosslinking through alternative reactions. This model is sketched in Figure 4a.

The presence of 10 wt.% talc (Figure 4b) is proposed to somehow hinder the decomposition products from being released sufficiently and therefore to enable reactions of PC with the decomposition products that compete with crosslinking. Reactions with these smaller decomposition products result only in the formation of side chains, which are much less beneficial for charring, if at all. With increasing temperature they decompose again into phenol derivatives, the typical decomposition products of PC.

This proposal for talc exerting such a physical-chemical influence on the PC decomposition is reasonable. Basically, corresponding effects were observed in this investigation. At room temperature the hindered transport of the decomposition products is confirmed by a change in the gas diffusion of small molecules. PC/ABS + BDP + 10 wt.% talc showed a reduction in O_2

diffusion of around 37% for 1 bar O_2 and room temperature. Talc particles work as microscopic barriers for diffusion embedded in the polymer matrix. Further, adding talc reinforces the pyrolysing polymer melt (*19*, *34*). This phenomenological effect was observed for the thermogravimetry residues (insert in Figure 2). PC/ABS + BDP forms a thin film during heating and decomposition, favoring the easy release of volatiles, whereas PC/ABS + BDP + 10 wt.% talc granules maintain some of their original structure and did not form a thin film. The increase in melt viscosity also influences the reactivity and diffusion of pyrolysis products.

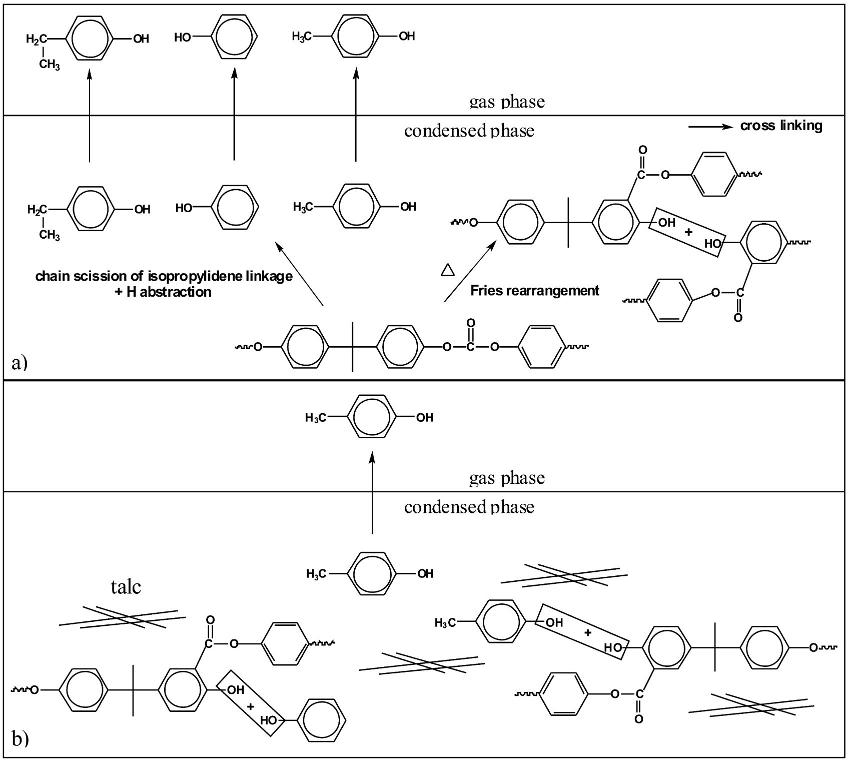

Figure 4. Decomposition scheme of PC (a) without and (b) with talc in PC/ABS + BDP + talc.

Figure 5 illuminates the different melt viscosity characteristics of PC/ABS, PC/ABS + BDP, PC/ABS 10 wt.% talc, and PC/ABS + BDP + 10 wt.% talc by plotting the master curve of shear stress against frequency. BDP functions as a plasticizer, decreasing the viscosity for all frequencies. The incorporated PTFE fibers function as anti-dripping agents, introducing a flow limit at low frequencies, whereas the viscosity for high frequencies is not changed (*26*, *35*). The processing properties of PC/ABS and the improved processing properties of PC/ABS + BDP are not deteriorated by adding PTFE. Adding talc strongly reinforces the flow limit at low frequencies without influencing the viscosity and thus processing properties at higher shear rates. The difference the addition of talc makes is nearly one order of magnitude at low frequencies, and is thus believed to significantly reduce melt flow, dripping, and the release of pyrolysis products. This physical effect corresponds well to the delayed release of products at the beginning of decomposition and the delayed release of ABS decomposition products.

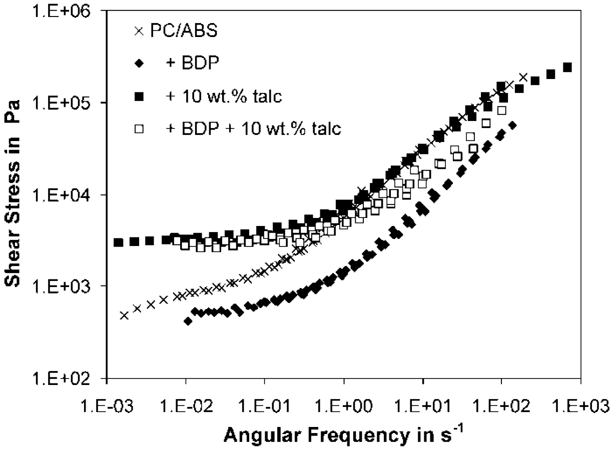

Figure 5. Characteristics of the melt viscosity (shear stress is plotted against angular frequency) of PC/ABS, PC/ABS + BDP, PC/ABS + 10 wt.% talc and PC/ABS + BDP + 10 wt.% talc.

Fire Behavior of PC/ABS, PC/ABS + BDP, PC/ABS + 10 wt.% Talc and PC/ABS + BDP + 10 wt.% Talc

The results for time to ignition (t_{ign}, cone calorimeter with an irradiation of 35 kWm^{-2}), flammability (reaction to a small flame: LOI and UL 94) and for forced-flaming fire behavior (cone calorimeter, applying three different irradiations) are summarized in Table 3. The HRR and the THR are shown in Figure 6. Adding BDP to PC/ABS led to an increase of 13 s in the t_{ign}. PC/ABS + 10 wt.% talc showed a t_{ign} reduction of 7 s, and PC/ABS + BDP + 10 wt.% talc showed a t_{ign} similar to PC/ABS. The effects of BDP and 10 wt.% talc balance each other out. The t_{ign} in the cone calorimeter experiments correlates with the T_{max} of the PC decomposition for all materials described before by thermal analysis. This is quite reasonable since the decomposition temperature of the main component PC determines the pyrolysis temperature of PC/ABS and thus the surface temperature that must be reached for sustained ignition.

Adding BDP to PC/ABS led to an increase in the LOI by 4.5%, from 23.6% for PC/ABS to 28.1% for PC/ABAS + BDP. Adding 10 wt.% talc to PC/ABS also improved the LOI of PC/ABS by 4.6%. This effect on the LOI of adding talc is astonishing for an inert filler. The effect of adding 10 wt.% of the inert filler talc equaled the effect of adding the flame retardant BDP to PC/ABS. Combining BDP + 10 wt.% talc in PC/ABS gave a strong (+ 15.4% to 39%) and synergistic (+ 15.4% > 4.5% + 4.6%) effect in terms of LOI. The cause of the LOI increase through talc is surprising. Maybe an advantageous effect is exerted on the properties of the residue based on its inorganic-carbonaceous character. This flame retardancy effect was somewhat specific to LOI. PC/ABS + 10 wt.% talc achieves only an HB classification in UL 94, like the unfilled PC/ABS, whereas PC/ABS + BDP yields a V-0. The combination of BDP and 10 wt.% talc in PC/ABS + BDP + 10 wt.% talc also achieves V-0.

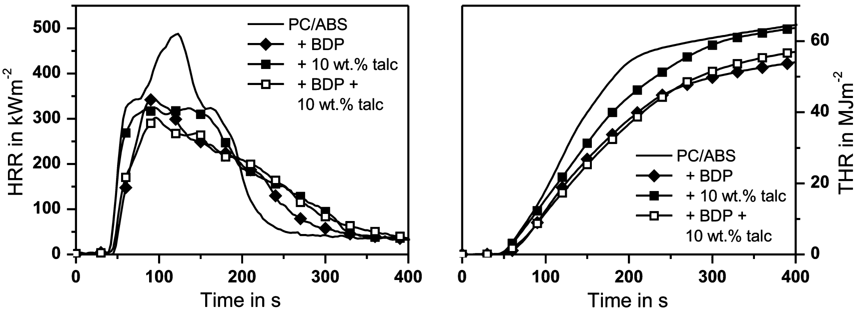

Figure 6. Heat release rate (HRR) and total heat release (THR) for PC/ABS, PC/ABS + BDP, PC/ABS + 10 wt.% talc and PC/ABS + BDP + 10 wt.% talc, applying an irradiance of 50 kWm^{-2}.

For forced-flaming behavior, the heat release of PC/ABS was controlled mainly by three distinct characteristics (Figure 6). The heat release rate (HRR) versus time follows the basic pattern for a char-forming material, with the peak heat release rate (pHRR) occurring at the beginning of burning after a protective layer had formed and followed by a decreasing HRR. The samples also showed a large deformation, decreasing the distance to the cone heater and thus resulting in an additional increase in HRR or even an additional pHRR (*29*). The deformation of the residue and the intensive afterglow of the carbonaceous char resulted in a rather continuous change from burning to afterglowing behavior. Extremely larger amounts of residues at 35 kWm^{-2} indicate that for lower irradiations the protection by the char is sufficient to result in extinction before all of the combustible material was consumed. This effect is much more pronounced for PC/ABS than for the other materials investigated. This effect competes somewhat with the mechanisms discussed for adding BDP and talc in the following.

The total heat release (THR) decreases when BDP was added to PC/ABS + BDP. The residue increases for high heat fluxes and the pHRR decreased compared to PC/ABS. The reduced THR/mass loss (THR/ML) indicated an effective flame inhibition, especially for high heat fluxes.

Table 3. Fire behavior of PC/ABS, PC/ABS + BDP, PC/ABS + 10 wt.% talc, and PC/ABS + BDP +10 wt.% talc; peak heat release rate = pHRR, total heat release/mass loss = THR/ML

PC/ABS + ...	*/*	*BDP*	*10 wt.% talc*	*BDP + 10 wt.% talc*	*Error*
Ignition/flammability (reaction to small flame)					
t_{ign}, 35 kWm^{-2} (s)	83	96	76	81	±5
LOI (%)	23.6	28.1	28.2	39.0	±1.0
UL 94 (1.5 mm)	HB	V-0	HB	V-0	
UL 94 (3 mm)	HB	V-0	HB	V-0	
Flaming combustion (cone calorimeter); irradiation: 35 kWm^{-2}					
THR (MJm^{-2})	43.6	46.1	58.1	47.0	±7.0
pHRR (kWm^{-2})	366	323	271	243	±25
Residue (wt.%)	46.9	41.0	36.7	41.6	±3.0
THR/ML (MJm^{-2}g^{-1})	2.33	2.20	2.47	2.32	±0.1
Flaming combustion (cone calorimeter); irradiation: 50 kWm^{-2}					
THR (MJm^{-2})	59.9	45.3	62.1	49.9	±7.0
pHRR (kWm^{-2})	555	357	327	273	±25
Residue (wt.%)	29.0	35.1	33.8	38.9	±3.0
THR/ML (MJm^{-2}g^{-1})	2.38	1.95	2.47	2.33	±0.1
Flaming combustion (cone calorimeter); irradiation: 70 kWm^{-2}					
THR (MJm^{-2})	63.7	44.7	65.5	50.0	±7.0
pHRR (kWm^{-2})	616	412	525	275	±25
Residue (wt.%)	25.2	31.6	31.5	40.1	±3.0
THR/ML (MJm^{-2}g^{-1})	2.38	1.81	2.45	2.17	±0.1

PC/ABS + 10 wt.% talc had the same THR as PC/ABS, except for the irradiation at 35 kWm^{-2}, where different deformation processes dominate the results. Considering the fact that the blend with talc contains less combustible polymer, the THR per unit polymer is increased compared to PC/ABS. This worsening of the fire behavior was clearly monitored by THR/ML. The THR/ML for PC/ABS + 10 wt.% talc had a consistently higher and therefore poorer value than for PC/ABS. This high THR/ML also indicated the absence of any gas-phase mechanism when talc is added in PC/ABS + 10 wt.% talc. The residue increased by about 5 wt.% for PC/ABS + 10 wt.% talc, which was less than expected for the addition of 10 wt.% talc. Either additional PC was pyrolysed or less charring occurred. This result corresponds with the changes in evolved gas analysis presented above in the thermal analysis discussion. The pHRR was reduced by adding talc to PC/ABS for all three heat fluxes (Table 3). It was proposed that

In Fire and Polymers VI: New Advances in Flame Retardant Chemistry and Science; Morgan, A., et al.;
ACS Symposium Series; American Chemical Society: Washington, DC, 2012.

such a decrease is a characteristic of protection surface layers during burning (*36*). Further, because neither flame inhibition in the gas phase nor an additional charring in the condensed phase was caused by talc in PC/ABS + 10 wt.% talc, it was concluded that the reduction of the pHHR was based on talc's effect on the properties of the char, which improve the protection function of the fire residue. Such a significant reduction in pHRR accompanied by a negligible effect on the THR was reported in the literature to be typical of flame retardancy in layered silicate nanocomposites (*37*, *38*) whenever no flame inhibition or relevant additional charring occur, but only a protective layer is formed.

The fire properties of PC/ABS + BDP + 10 wt.% talc are very similar to those for PC/ABS + BDP. However the THR is decreased slightly less than for PC/ABS + BDP; the residue, especially for 35 kWm^{-2}, was increased less than expected. The THR/ML was reduced by about 10% compared to PC/ABS, indicating a clear gas-phase mechanism due to flame inhibition. However, the gas-phase mechanism was not as pronounced for PC/ABS + BDP + 10 wt.% talc as for PC/ABS + BDP. Talc somehow suppresses part of the gas-phase activity of BDP, especially for higher heat fluxes. Phosphorus analysis of the cone calorimeter fire residues of PC/ABS + BDP + 10 wt.% talc showed that about 80% of the phosphorus used remained in residue (for all three different heat fluxes). This confirmed the reduced gas-phase activity for BDP, because in PC/ABS + BDP the phosphorus content in the cone calorimeter residues was between 35 and 50%. The reason for the higher maintenance of phosphorus in PC/ABS + BDP + 10 wt.% talc was probably that the released phosphorus radicals remained in the pyrolysis zone longer and recombined and reacted to residue rather than being released and acting in the gas phase (see thermal decomposition). For the pHRR of PC/ABS + BDP + 10 wt.% talc a superposition of the effects of talc and BDP was observed.

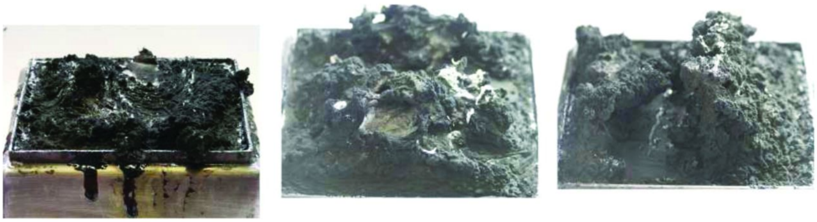

Figure 7. Cone calorimeter residues for PC/ABS + BDP (left), PC/ABS + 10 wt.% talc (middle) and PC/ABS + BDP + 10 wt.% talc (right) at a heat flux of 35 kWm^{-2}.

The cone calorimeter fire residues of PC/ABS + 10 wt.% talc and PC/ABS + BDP + 10 wt.% talc (Figure 7) showed a kind of intumescent behavior in addition to the deformation characteristic observed for PC/ABS and PC/ABS + BDP. It is believed that fire residues with an intact cellular structure are ideal for fire retardancy (*39*). For this to happen, the pyrolysis gas bubbles must become frozen in the expanding and thickening charring polymer melt to produce the honeycomb structure. This prevents the flow of volatile liquids or vapors into the flame and provides sufficient thermal insulation to keep the remaining polymer or polymer melt below its decomposition temperature. Talc improves the char morphology of PC/ABS and PC/ABS + BDP, resulting in improved protection by the fire residue during the fire, particularly with respect to pHRR. However, when BDP is combined with talc, the partial loss of the gas-phase mechanism and the reduced condensed phase mechanism of BDP increase fire hazards during forced-flaming behavior, particularly the THR.

PC/ABS + BDP + Talc with Various Talc Concentrations

PC/ABS + BDP + talc was investigated with different talc content. Apart from 10 wt.% talc, 5 and 20 wt.% talc were examined in PC/ABS + BDP + talc. The results of thermal analysis are shown in Figure 8 and listed in Table 4.

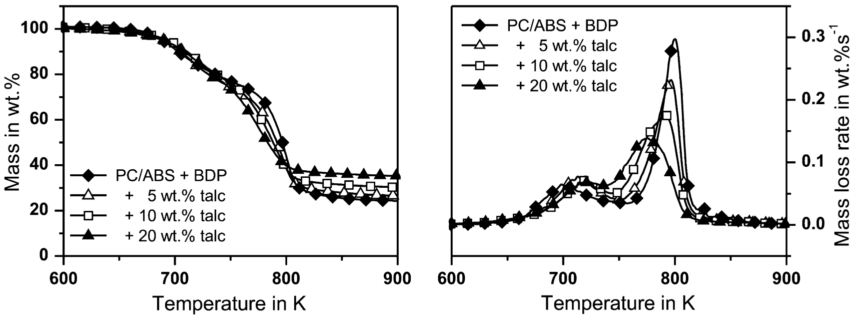

Figure 8. Mass loss and mass loss rate of PC/ABS + BDP, PC/ABS + BDP + 5 wt.% talc, PC/ABS + BDP + 10 wt.% talc, PC/ABS + BDP + 20 wt.% talc (under N_2; heating rate of 10 $Kmin^{-1}$).

PC/ABS + BDP + 5 wt.% talc and PC/ABS + BDP + 20 wt.% talc showed no change in onset temperature compared to PC/ABS + BDP + 10 wt.% talc. The temperature of the maximum weight loss rate for the first ABS-related decomposition step was in the order: PC/ABS + BDP < PC/ABS + BDP + 5 wt.% talc < PC/ABS + BDP + 10 wt.% talc < PC/ABS + BDP + 20 wt.% talc. The mass loss of the first decomposition step decreased with increasing talc content. Although this decrease in mass loss is expected, considering that polymer is replaced by talc, it did not exactly correlate to the concentration of talc. The more talc was added, the lower was the thermal decomposition temperature of PC decomposition. Further, for this second decomposition step a decrease in maximum mass loss rate and mass loss was observed with increased talc content. Consistently the residues increased by increasing the amount of talc. However, the residues did not increase by the amount expected for the amount of talc added. The char yield of PC decreases with increasing talc content. The characteristic effects of talc on the pyrolysis was confirmed when the talc content was varied.

Table 4. Thermal decomposition of PC/ABS + BDP, PC/ABS + BDP + 5 wt.% talc, PC/ABS + BDP + 10 wt.% talc and PC/ABS + BDP + 20 wt.% talc (under N_2; heating rate of 10 $Kmin^{-1}$)

PC/ABS + ...	*BDP*	*BDP + 5 wt.% talc*	*BDP + 10 wt.% talc*	*BDP + 20 wt.% talc*	*Error*
T_{onset} (K)	673	683	684	684	±2
Mass loss I (decomposition of ABS)					
Weight loss (wt.%)	24.7	25.3	22.2	20.8	±1
T_{max} (K)	699	713	720	726	±2
Mass loss II (decomposition of PC)					
Weight loss (wt.%)	46.6	44.2	43.4	40.7	±1
T_{max} (K)	800	796	792	773	±2
Residue (wt.%)	28.7	30.5	33.8	38.5	±1
Cal. char yield of PC	0.40	0.38	0.38	0.34	±0.01

Table 5. Diffusion coefficients for PC/ABS + BDP, PC/ABS + BDP +5 wt.% talc, PC/ABS + BDP +10 wt.% talc and PC/ABS + BDP + 20 wt.% talc at 1 and 5 bar

PC/ABS + BDP + ...	*/*	*10 wt.% talc*	*5 wt.% talc*	*20 wt.% talc*
Diffusion coefficient in 10^{-8} cm^2s^{-1}				
1 bar (O_2)	3.96	2.49	2.46	2.03
5 bar (O_2)	5.32	3.99	4.00	3.15

Non-linear dependency on the talc content was indicated for the diffusion coefficients (Table 5). Within the margins of uncertainty no difference between PC/ABS + BDP + 5 wt.% talc, and PC/ABS + BDP + 10 wt.% talc was observed and the decrease for PC/ABS + BDP + 20 wt.% talc was less than expected for a linear dependency on the concentration, indicating that it levels off with higher talc concentrations.

The rheological properties changed nicely with increasing talc content (Figure 9). The shear stress and thus viscosity at low frequencies increased. The log of viscosity at low frequencies came close to a linear dependency on the talc content. The decrease in diffusion coefficient as well as the change in the viscosity are caused by physical effects, which are highly sensitive to the concentration and distribution of the talc particles. A correlation with the delayed beginning of the pyrolysis product release as well as with the increasing temperature for the release of ABS pyrolysis products is proposed. The increasing deterioration of the PC decomposition with increasing viscosity at low frequencies seems to be obvious and thus supports the hypothesis of the physical effect of talc on pyrolysis.

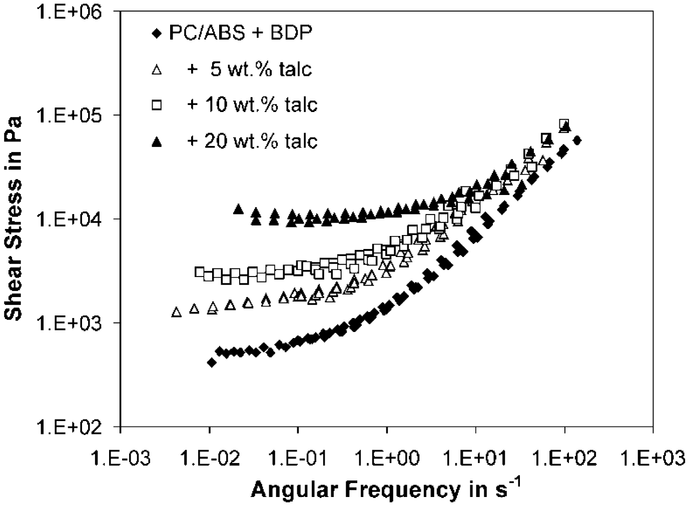

Figure 9. Characteristics of the melt viscosity (shear stress is plotted against angular frequency) of PC/ABS + BDP, PC/ABS + BDP + 5 wt.% talc , PC/ABS + BDP + 10 wt.% talc, and PC/ABS + BDP + 20 wt.% talc .

The t_{ign} of PC/ABS + BDP + 5 wt.% talc was similar to that for PC/ABS + BDP + 10 wt.% talc (Table 6). For a loading of 20 wt% talc in PC/ABS + BDP + 20 wt% talc, the t_{ign} increased significantly, by 26 s compared to PC/ABS + BDP + 10 wt.% talc. The t_{ign} was also longer than for PC/ABS, which is surprising and most probably a synergistic effect due to different effects competing with each other when the talc concentration is changed.

Table 6. Fire behavior of PC/ABS + BDP, PC/ABS + BDP+5 wt.% talc, PC/ABS + BDP +10 wt.% talc and PC/ABS + BDP + 20 wt.% talc

PC/ABS+BDP+ ...	*/*	*5 wt.% talc*	*10 wt.% talc*	*20 wt.% talc*	*Error*
Ignition/flammability (reaction to small flame)					
t_{ign}, 35 kWm^{-2} (s)	96	82	81	108	±5
LOI (%)	28.1	37.5	39.0	41.1	±1.0
UL 94 (1.5 mm)	V-0	V-0	V-0	V-0	
UL 94 (3 mm)	V-0	V-0	V-0	V-0	
Flaming combustion (cone calorimeter); irradiation: 35 kWm^{-2}					
THR (MJm^{-2})	46.1	39.5	47.0	46.9	±7.0
pHRR (kWm^{-2})	323	225	243	222	±25
Residue (wt.%)	41.0	49.7	41.6	47.2	±3.0
Cal. char yield of PC	0.58	0.67	0.51	0.50	±0.3
THR/ML (MJm^{-2}g^{-1})	2.20	2.10	2.32	2.16	±0.1
Flaming combustion (cone calorimeter); irradiation: 50 kWm^{-2}					
THR (MJm^{-2})	45.3	46.6	49.9	50.1	±7.0
pHRR (kWm^{-2})	357	238	273	274	±25
Residue (wt.%)	35.1	36.9	38.9	42.2	±3.0
Cal. char yield of PC	0.49	0.48	0.46	0.41	±0.3
THR/ML (MJm^{-2}g^{-1})	1.95	1.97	2.33	2.13	±0.1
Flaming combustion (cone calorimeter); irradiation: 70 kWm^{-2}					
THR (MJm^{-2})	44.7	45.7	50.0	54.2	±7.0
pHRR (kWm^{-2})	412	350.	275	312	±25
Residue (wt.%)	31.6	39.1	40.1	37.4	±3.0
Cal. char yield of PC	0.46	0.51	0.48	0.32	±0.3
THR/ML (MJm^{-2}g^{-1})	1.81	2.00	2.17	2.12	±0.1

PC/ABS + BDP, PC/ABS + BDP + 5 wt.% talc, PC/ABS + BDP + 10 wt.% talc and PC/ABS + BDP + 20 wt.% talc showed V-0 in UL 94 (Table 6). The observed large and synergistic effect of 10 wt.% talc in PC/ABS + BDP + 10 wt.% talc on the LOI occurred even for 5 wt.% talc used in PC/ABS + BDP + 5 wt.% talc (Figure 10). The increased talc concentration in PC/ABS + BDP + 20 wt.% talc showed only a small improvement in LOI compared to PC/ABS + BDP + 10 wt.% talc, revealing some kind of saturation with talc concentration.

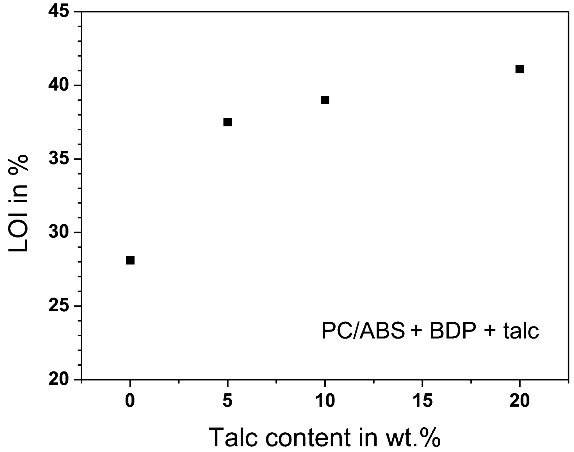

Figure 10. LOI plotted against talc content for PC/ABS + BDP, PC/ABS + BDP +5 wt.% talc, PC/ABS + BDP +10 wt.% talc and PC/ABS + BDP + 20 wt.% talc.

Discussing the cone calorimeter results (Figure 11, Table 6), the distinct dependencies on the addition of talc became obvious. The THR increased rather linearly with increasing talc concentration. This observation contrasted with the expectation that talc acts as inert filler to replace pyrolyzable polymer and thus normally decreases THR rather than increasing it. The fire residue actually increased with increasing talc addition, but the increase did not correspond to the amount of talc. Adding 5 wt.% talc in PC/ABS + BDP + 5 wt.% talc resulted in an increase in residue slightly larger than 5 wt.%. Larger talc loadings result in an increase clearly below the talc amount added. The char yield due to PC decreases as more talc is added (Table 6) and so counteracts the increase in residue due to the addition of inert filler. The release of fuel and thus the THR increase. Further the reduced charring of PC also results in an increase in effective heat of combustion of the released volatiles, since the ratio of aromatic carbon to less combustible decomposition products increases. The THR/ML increases with increasing talc concentration. This effect competes with the flame inhibition of BDP. The results for varying the talc content clearly confirm the interpretation of the results obtained for PC/ABS + BDP + 10 wt.% talc. The pHRR is reduced with increasing talc concentration, but not linearly. Again, the same characteristic dependence of the talc concentration was observed as reported before for the physical property diffusivity and the inverse dependency of the LOI. This is of course consistent, since the pHRR is extremely sensitive to the protection properties of the fire residue built during combustion, whereas no additional carbonaceous charring or flame inhibition occurs in the investigated samples. An analogous non-linear decrease in pHRR with increasing filler content, a large reduction for even low filler content and leveling off of the reduction for increasing the filler load above 8-10 wt.% was reported for layered silicate in the literature (*37*, *38*).

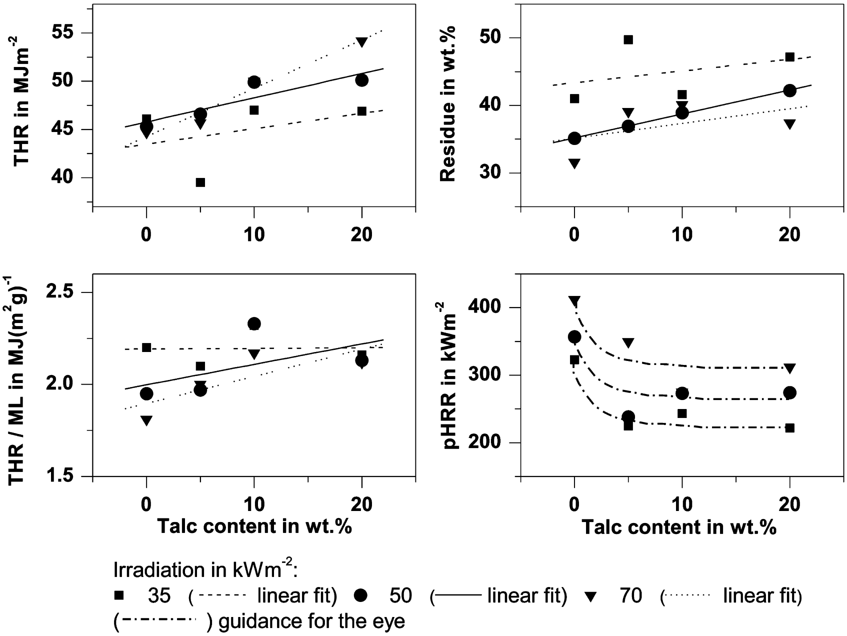

Figure 11. Cone calorimeter results with irradiation of 35, 50 and 70 kWm^{-2} applied: total heat release (THR), residue, effective heat of combustion for cone calorimeter (THE/ML) and peak of heat release rate (pHRR) for PC/ABS + BDP, PC/ABS + BDP + 5 wt.% talc, PC/ABS + BDP + 10 wt.% talc and PC/ABS + BDP + 20 wt.% talc.

Conclusion

The addition of 10 wt.% talc in PC/ABS + 10 wt.% talc resulted in a surprisingly large increase in LOI, but no change in UL 94 classification. Under forced-flaming behavior a decreased pHRR was obtained, caused by talc improving the morphology and protection properties of the fire residue.

PC/ABS + BDP showed an increase in LOI compared to PC/ABS and a V-0 in UL 94 classification. Under forced-flaming behavior a decreased THR and pHRR was obtained, caused by flame retardancy mechanisms in both the gas phase and condensed phase. The flame inhibition is more pronounced for high irradiations. In the condensed phase BDP increases the char yield of PC and phosphates are incorporated in the fire residue.

Combining BDP with 10 wt.% talc in PC/ABS + BDP + 10 wt.% talc resulted in a synergistic and thus a surprisingly strong increase in LOI, a V-0 classification in UL 94 and a decrease of the pHRR. Talc decreases the gas diffusion and enhances the flow limit for low shear rates, both of which influence the pyrolysis and flammability results. It was also concluded that talc improves the protection properties of the fire residue. However, this change in fire residue also has antagonistic effects regarding the flame retardancy mechanisms of BDP. The crosslinking due to PC was hindered, probably due to a longer maintenance of the released decomposition products, enhancing competitive reactions. Less residue is formed than expected for the amount of filler added. The char yield of PC decreases compared to PC/ABS + BDP. Further, the gas-phase activity of BDP was reduced. A higher THR/ML and THR occurred, especially for high irradiations. Therefore the effectiveness of the combination of BDP and talc in PC/ABS was better than PC/ABS + BDP only for the requirements of LOI and UL 94.

Investigating the materials with different talc content, PC/ABS + BDP, PC/ABS + BDP + 5 wt.% talc, PC/ABS + BDP + 10 wt.% talc and PC/ABS + BDP + 20 wt.% talc, confirms the interpretation and conclusions drawn from the data of PC/ABS + BDP + 10 wt.% talc. The synergistic effect in LOI and the clear reduction in pHRR were already obtained for low loadings of talc. For higher loadings up to 20 wt.% talc saturation in the flame retardancy efficiency was observed, meaning that more talc did not yield significantly more improvement. Instead higher loadings of talc in PC/ABS + BDP + talc worsened the forced-flaming behavior by reducing the charring of PC and thus increasing the THR.

Apart from the detailed insight in the complex behavior, contributing mechanisms and sensitive interactions of multicomponent PC/ABS blends the paper indicates a promising route towards multifunctional or tailored halogen-free flame retarded materials.

Acknowledgments

We gratefully acknowledge the support received from the Bayer MaterialScience AG, and thank in particular Dr. V. Taschner, Dr. T. Eckel and Dr. D. Wittmann. Thanks to T. Himmel and Prof. Dr.-Ing. M. Wagner (TU Berlin) and F. Kempel for their help with the rheological investigations.

References

1. Levchik, S. V.; Weil, E. D. *J. Fire Sci.* **2006**, *24*, 137–151.
2. Levchik, S. V.; Weil, E. D. *Polym. Int.* **2005**, *54*, 981–998.
3. Eckel, T. In *Plastic Flammability Handbook*, 3rd ed.; Troitzsch, J., Ed.; Hanser Publishers: Munich, 2004; pp 158−172.
4. Bödinger, M.; Eckel, T.; Wittmann, D.; Alberts, H. German Patent DE 19530200 A1, 1997.
5. Eckel, T.; Wittmann, D.; Keller, B.; Alberts, H. German Patent DE 19734666 A1, 1999.
6. Wenz, E.; Eckel, T.; Buchholz, V.; Wittmann, D.; Thuermer, B. U.S. Patent US 2007/0225441, 2007.
7. Seidel, A.; Wagner, M.; Endtner, J.; Ebeneck, W.; Eckel, T.; Wittmann, D. European Patent EP 1570002 B1, 2008.
8. Levchik, S. V.; Bright, D. A.; Moy, P.; Dashevsky, S. *J. Vinyl Addit. Technol.* **2000**, *6*, 123–128.

9. Levchik, S. V.; Bright, D. A.; Alessio, G. R.; Dashevsky, S. *J. Vinyl Addit. Technol.* **2001**, *7*, 98–103.
10. Pawlowski, K. H.; Schartel, B. *Polym. Int.* **2007**, *56*, 1404–1414.
11. Green, J. *J. Fire Sci.* **1996**, *14*, 353–366.
12. Hastie, J. W. *J. Res. Natl. Bur. Stand., Sect. A* **1973**, *77A*, 733–754.
13. Fenimore, C. P.; Jones, G. W. *Combust. Flame* **1964**, *8*, 133–137.
14. Perret, B.; Pawlowski, K. H.; Schartel, B. *J. Therm. Anal. Calorim.* **2009**, *97*, 949–958.
15. Pawlowski, K. H.; Schartel, B. *Polym. Degrad. Stab.* **2008**, *93*, 657–667.
16. Pawlowski, K. H.; Schartel, B.; Fichera, M. A.; Jäger, C. *Thermochim. Act.* **2010**, *498*, 92–99.
17. Wawrzyn, E.; Schartel, B.; Seefeldt, H.; Karrasch, A.; Jäger, C. *Ind. Eng. Chem. Res.* **2012**, *51*, 1244–1255.
18. Longerey, M.; Lopez-Cuesta, J.-M.; Gaudon, P.; Crespy, A. *Polym. Degrad. Stab.* **1999**, *64*, 489–496.
19. Durin-France, A.; Ferry, L.; Lopez-Cuesta, J.-M.; Crespy, A. *Polym. Int.* **2000**, *49*, 1101–1105.
20. Laoutid, F.; Ferry, L.; Lopez-Cuesta, J.-M.; Crespy, A. *Fire Mater.* **2006**, *30*, 343–358.
21. Duquesne, S.; Samyn, F.; Bourbigot, S.; Amigouet, P.; Jouffret, F.; Shen, K. *Polym. Adv. Technol.* **2008**, *19*, 620–627.
22. Ameras, X.; Le Bras, M.; Hornsby, P.; Bourbigot, S.; Marosi, G.; Keszei, S.; Poutch, F. *Polym. Degrad. Stab.* **2003**, *82*, 325–331.
23. Clerc, L.; Ferry, L.; Leroy, E.; Lopez-Cuesta, J.-M. *Polym. Degrad. Stab.* **2005**, *88*, 504–511.
24. Bertelli, G.; Marchetti, E.; Camino, G.; Costa, L.; Locatelli, R. *Angew. Makromol. Chem.* **1989**, *172*, 153–163.
25. Bourbigot, S.; Le Bras, M.; Duquesne, S.; Rochery, M. *Macromol. Mater. Eng.* **2004**, *289*, 499–511.
26. Wawrzyn, E.; Schartel, B.; Ciesielski, M.; Kretzschmar, B.; Braun, U.; Döring, M. *Eur. Polym. J.* **2012**, *48*, 1561–1574.
27. Kunze, R.; Schartel, B.; Bartholmai, M.; Neubert, D.; Schriever, R. *J. Thermal Anal. Calorim.* **2002**, *70*, 897–909.
28. Babrauskas, V. *Fire Mater.* **1984**, *8*, 81–95.
29. Schartel, B.; Hull, T. R. *Fire Mater.* **2007**, *31*, 327–354.
30. Schartel, B.; Bartholmai, M.; Knoll, U. *Polym. Degrad. Stab.* **2005**, *88*, 540–547.
31. Davis, A.; Golden, J. H. *J. Macromol. Sci., Rev. Macromol. Chem.* **1969**, *3*, 49–68.
32. Jang, B. N.; Wilkie, C. A. *Polym. Degrad. Stab.* **2004**, *86*, 419–430.
33. Davis, A.; Golden, J. H. *Nature* **1965**, *206*, 397.
34. Levchik, S. V.; Levchik, G. F.; Camino, G.; Costa, L. *J. Fire Sci.* **1995**, *13*, 43–58.
35. Kempel, F.; Schartel, B.; Marti, J. M.; Butler, K. M.; Rossi, R.; Idelsohn, S. R.; Oñate, E.; Hofmann, A. *Fire Mater.* **2012** submitted for publication.
36. Schartel, B.; Braun, U. *e-Polymers* **2003** *art. 13*.

37. Schartel, B.; Bartholmai, M.; Knoll, U. *Polym. Adv. Technol.* **2006**, *17*, 772–777.
38. Bartholmai, M.; Schartel, B. *Polym. Adv. Technol.* **2004**, *157*, 355–364.
39. *Fire Retardant Materials*; Horrocks, A. R.; Price, D.; Eds.; Woodhead Publishing: Cambridge, UK, 2000; p 19.

Chapter 3

Mechanistic Aspects of Flame Retardation by Phosphorus-Containing Groups in Some Chain Growth Polymers

Paul Joseph* and Svetlana Tretsiakova-McNally

School of the Built Environment and the Built Environment
Research Institute, University of Ulster, Newtownabbey BT37 0QB,
County Antrim, Northern Ireland, U.K.
***E-mail: p.joseph@ulster.ac.uk**

Elemental phosphorus and its various compounds have been widely used to flame retard a variety of polymers for several decades. They can be used either as *reactives* or as components in *additive* systems, and are believed to be active in the condensed phase, in the vapor phase and, perhaps to a lesser degree, at the interface. Generally, phosphorus-based flame retardants tend to decrease the ignition propensities of polymeric materials. However, the actual mechanistic pathway(s) in achieving this, believed to be suppressing the combustion efficiency, greatly depends on the structural features of the polymeric substrate as well as on the chemical environment of the phosphorus-containing compound(s) in question. In the present chapter, the mechanistic aspects of flame retardation by *reactive* phosphorus compounds in some commercially important chain growth polymers are discussed.

Introduction

The release of energy, mainly in the form of heat, from the embedded chemical energy within the bonds of a molecule is quite often achieved through combustion processes, *i.e.* the fuel is combined with oxygen, or oxidized, resulting in thermodynamically more stable gaseous products. Such reactions are

In Fire and Polymers VI: New Advances in Flame Retardant Chemistry and Science; Morgan, A., et al.;
ACS Symposium Series; American Chemical Society: Washington, DC, 2012.

exothermic without any exceptions, and with the added advantage of an increase in the entropy of the system, naturally leading to a decrease in the Gibbs's free energy. Therefore, the overall process is thermodynamically feasible. Mankind from pre-historical times relied on various combustion processes as means of deriving energy, often from burning complex cellulosic materials and other fuels, which were carbon rich.

Fire, on the other hand, is a phenomenon where *uncontrolled* combustion occurs. Unwanted fires are a huge drain on our society and economy. In most cases, some sort of a synthetic polymeric material is implicated. Needless to say, most of the organic polymers easily degrade to give volatile combustible material when they are heated above certain critical temperatures, which in turn depend on their chemical structures. If the gaseous mixture resulting from the mixing of degradation volatiles with air is within the flammability limits, and the temperature is above the ignition temperature, then combustion begins. The combustion of a polymeric material is a highly complex process involving a series of interrelated and/or independent stages occurring in the condensed phase and in the gaseous phase, and at the interfaces between the two phases (*1*).

Successful strategies to reduce the flammability of a polymeric material involve interrupting the complex stages of the combustion process at one or more points so as to reduce the rate and/or to change the mechanism of combustion at that point. From a practical point of view, this is achieved either by the mechanical blending of a suitable flame retardant compound with the polymer substrate (*i.e.* by introducing an *additive*) or by chemical incorporation of the retardant into the polymer molecule by simple copolymerization or by the chemical modification of the preformed polymer (i.e. using a *reactive* component). The method of flame retarding a polymer, namely by chemical modification, has several potential advantages such as: (a) low levels of modification may suffice; (b) the modifying groups are chemically attached and therefore less likely to be lost during the subsequent service; and (c) the modifying groups can more readily be molecularly dispersed throughout the polymer (*2*).

However, reactive incorporation of flame retarding groups can also bring with it problems, not least the relative difficulty and expense of reactively modifying polymers for which commercially well established methods for manufacturing the unmodified variants already exist. Furthermore, extensive reactive modification of a partly crystalline polymer is likely to lead to a significant loss of crystallinity, whereas if an additive is introduced to a partly crystalline polymer, it will most probably end up in the amorphous phase and has little impact upon crystallinity (although it may plasticize the amorphous regions).

In general, reactive modification of chain growth polymers is less readily accomplished than for step growth polymers, unless the reactive modification is applied after manufacture of the primary chain, say, through a post polymerization grafting reaction. Grafting reactions may also be useful for covalently attaching flame retardant groups to the surfaces of polymer based plastics moldings, films and fibers, where they will be particularly effective at the point of first impingement of any flame. In the following sections, the mechanistic aspects of flame retardation by reactive phosphorus compounds in some commercially important chain growth polymers are discussed.

Flame Retardation by Phosphorus Compounds: General Considerations

Elemental phosphorus and its various compounds have been used to flame retard a wide variety of polymer based materials for several decades. The first evidence of the use of a phosphorus compound was documented by Gay Lussac in 1821. He impregnated theatre curtains with ammonium phosphate solution to render them with the required degree of flame retardance (*3*). Environmental considerations, especially concerning the use of halogen based systems, have paved the way, in recent years, for the increased use of phosphorus based flame retardants as alternatives to the halogen containing compounds. Furthermore, this has generated active research in identifying novel flame retardants based on phosphorus, as well as synergistic combinations with compounds of other flame retardant elements (such as nitrogen and the halogens) and with several inorganic nanoscopic fillers (for example, phyllosilicates and carbon nano-tubes). This research on halogen alternatives has resulted, especially in recent years, in a wealth of literature (including patents) and in the market acceptance of several phosphorus based flame retardants (*4*).

Although phosphorus compounds can be highly effective flame retardants, they are not effective in some major classes of polymers such as styrenic resins and polyolefins (*5*). Furthermore, the basic mode of intervention of phosphorus compounds, regardless of the phase in which they are active, is to suppress the efficiency of combustion reactions which are mostly radical in nature and occurr in the gas phase. This invariably involves less oxidation of a carbonaceous substrate to carbon dioxide, and thus leads to the production of more soot/smoke and to a comparatively higher value of the CO/CO_2 ratio (*6*). The increased production of smoke and toxic vapors (mainly CO) is a major concern, especially in real fire scenarios, where materials passively protected with phosphorus flame retardants are involved. However, from an ignitability point of view, albeit only a low level indicator of the overall flammability hazard associated with a material, the use of phosphorus-containing flame retardants has proved to be of great value in that they generally increase the ignition resistance of materials very significantly (*7*).

Phosphorus-containing fire retardants can be active in the condensed phase or in the vapor phase (Figure 1), or in both phases (*9*). The salient features of the vapor phase mechanism include reactions that promote hydrogen recombination and the scavenging of oxygen radicals by molecular phosphorus. This in turn will reduce the number of effective flame propagating radical species below the level at which the flame can be sustained.

The relative predominance of the different mechanisms actually operating in a particular system depends on the structural features of the base polymer as well as on the chemical environment of the phosphorus, i.e. whether phosphorus is in the elemental state or, if present as a compound, on the valency and the nature of the chemical moieties surrounding the phosphorus atom. Physical and chemical actions have also been implicated in both phases. These could involve flame inhibition, heat loss owing to melt flow, surface protection by phosphorus-containing acids, acid catalyzed char accumulation, char enhancement

In Fire and Polymers VI: New Advances in Flame Retardant Chemistry and Science; Morgan, A., et al.;
ACS Symposium Series; American Chemical Society: Washington, DC, 2012.

and protection of char from oxidation. Flame retardant mechanism(s) can also be influenced by the presence of other additives, *e.g.* synergistic combinations of co-additives such as compounds of nitrogen or halogens.

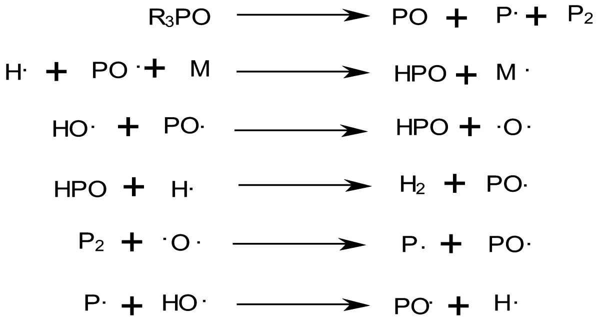

Figure 1. Elementary steps involved in vapor phase flame retardation.

A classical and thoroughly investigated example, which amply illustrates the condensed phase activity of phosphorus flame retardant, is the flame retardation of cellulosic substrates with phosphoric acid and/or its organic/inorganic esters (*9*). In the presence of phosphoric acid and/or its organic and inorganic esters, or compounds having P-O-C bonds, phosphorylation of cellulose occurs predominantly at the C-6 hydroxyls. This in turn alters the degradation pathway of cellulose so that, instead of depolymerization reactions, dehydration of the cellulose substrate occurs leading to enhanced char production. Similar explanations can be given for P-N synergism in cellulosics. The polar nature of P-N bond, as compared with P-C and P-O bonds, would result in enhanced rates of phosphorylation at the cellulose hydroxyls. Thus, the formation of P-N bonds *in situ* increases the reactivity of the phosphorus compound towards the cellulose hydroxyls, leading to a reduction in volatiles and a corresponding increase in char formation.

Another mode of action in which phosphorus is important as a char promoter is in intumescent fire retardant paints and mastics (*8*). These typically have phosphorus compound, such as ammonium polyphosphate, a char forming polyol, such as pentaerythritol, a blowing agent, such as melamine, and a binder. On decomposition, the phosphorus compound provides the phosphorylating agent, which in turn reacts with the pentaerythritol to form polyol phosphates, which then break down to char through a series of elimination steps. The spumific agent will endothermally decompose to form gaseous products, which will expand the char already formed.

Physical effects such as those involving increased heat capacity, heat of vaporization, and endothermic dissociation in the vapor phase, may make a nominal, but recognizable, contribution to the overall efficacies of various phosphorus based flame retardant systems (*9*). These types of mode of action, especially in the vapor phase, become more important in the case of readily volatile additives.

Polyolefins and Some Related Polymers

The reactive modification of polyolefins *via* copolymerization with phosphorus-containing monomers is not straight forward given the stringent conditions that pertain during the polymerization of olefin monomers, especially using organo-metallic coordination catalysts. However, both polyethylene (PE) and polypropylene (PP) can be chemically modified after polymerization so as to introduce phosphorus-containing side groups. For example, PE has been oxidatively phosphonylated to give a polymer containing about 5 wt. % P as $-P(O)(OH)_2$ side groups. This polymer has limiting oxygen index (LOI) significantly greater than that of unmodified PE but unfortunately the crystallinity is greatly reduced leading to inferior physical and mechanical properties (*10*).

A comparison of the thermograms of PE and phosphonylated PE revealed that, whilst PE degraded in a single stage, the phosphonylated analogue degraded in two stages. The first stage in the case of phosphonylated PE could be attributed to the loss of water, owing to the formation of cross-linking reactions between the phosphonic acid groups, while the second stage could be due to the main chain depolymerization reactions. The less pronounced decomposition of the phosphonylated PE, together with the reduction in the formation of some residue, may be the reason for the increased flame retardation brought about by phosphonylation. The flame retardance of the modified PE is also believed to arise, at least in part, through a vapor phase mechanism

PP is commercially modified by free radical grafting with maleic anhydride to give maleated PPs used as compatibilizers for additives such as nanoscopic clays (Figure 2). Similar strategies can be used to graft phosphorus-containing monomers to PPs. These copolymers, when blended with virgin PP also allow compatibilization with nanoscopic clays, but in addition, they work synergistically with the clays to improve flame-retardance (*11*). The grafts also included maleimide, *N*-ethyl maleimide, diethyl maleate, diethyl-*p*-vinylbenzyl phosphonate (Figure 4, structure I) and acrylic acid-2-[(diethoxyphosphoryl) methylamino]ethyl ester (Figure 4, structure IV).

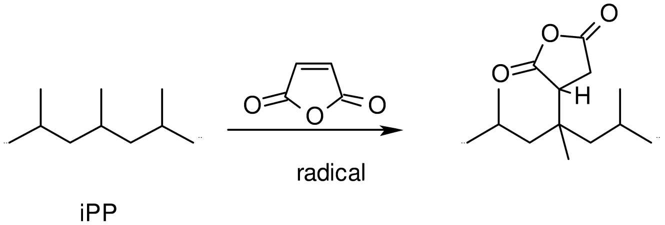

Figure 2. Radical induced grafting of maleic anhydride on to PP.

In addition to improving the dispersion of nanoscopic clay minerals in these systems with the blending of grafted PP with virgin PP, some degree of exfoliation was observed with diethyl-*p*-vinylbenzyl phosphonate as the grafting agent. It was also observed that the grafting groups had minimal effects on the melting point of the parent polymer matrix. However, the grafting reactions led to slight increases in the thermal stability of the modified PP, as revealed by thermogravimetric runs in different atmospheres. Also, as compared to the unmodified PP, the grafted analogs show improvements in flame retardation. This effect was particularly noticeable in the case of PP grafted with diethyl-*p*-vinylbenzyl phosphonate.

Phosphorylated poly(vinyl alcohol) and ethylene-vinyl alcohol copolymers were found to be significantly flame retarded as compared to their unmodified parent polymers (*10*) (Figure 3). The flame retardance in these systems is shown to arise primarily from a condensed phase mechanism involving dehydration, cross-linking and char formation. The degree of flame retardance of the modified polymers, as gauged by the LOI measurements, showed a strong correlation with their phosphorus contents. Also, as the LOI values increased the weights of char residues obtained through thermogravimetric runs increased. This essentially shows that, in these modified polymers, the phosphorus-containing groups are functioning as flame retardants by char formation, *i.e.* through a condensed phase mechanism.

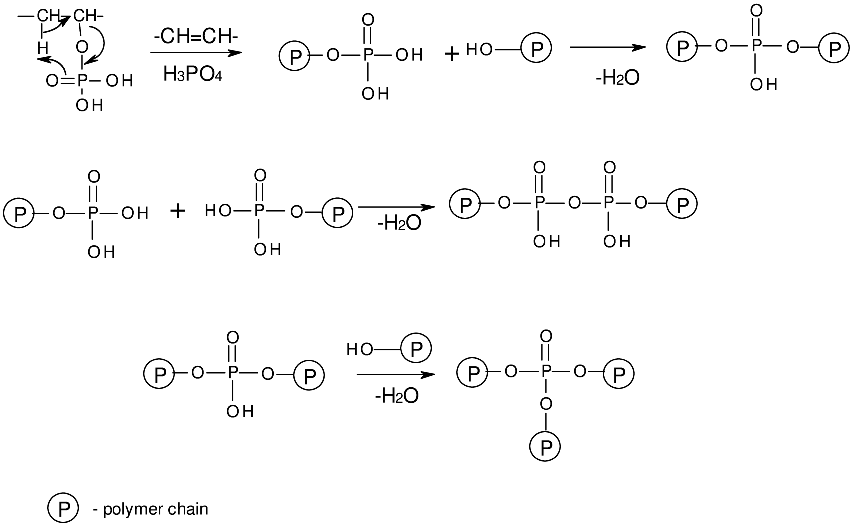

Figure 3. Formation of phosphorus anhydride cross links in phosphorylated PVA.

In the case of phosphorylated ethylene-co-vinyl alcohol samples, there was a strong linear correlation between the phosphorus content of the char residues obtained on burning in air and the phosphorus content of the copolymers. Therefore, this can be considered as a strong evidence for a condensed phase mechanism of flame retardation operating in these systems. In both cases of the phosphorylated materials, as the phosphorus content increased, the values for heats of combustion, as measured by oxygen bomb calorimetry, decreased. This is to be expected given that the amount of material combusted decreases as the amount of char residue from the polymer increases.

Acrylic Polymers

Generally, the *reactive* route to flame retardance offers various advantages over the alternative route of using analogous phosphorus-containing compounds as *additives*, in that additives tend to plasticize a polymer significantly and to give rise only to vapor phase modes of flame retardance. However, the vapor phase mechanism alone cannot account for the very high flame retardant efficiencies observed in some acrylic polymers.

A systematic exploration of the effects of incorporating various phosphorus-containing comonomer units on the flame retardance, particularly on poly(methyl methacrylate) (PMMA) and polyacrylonitrile (PAN), has been widely reported (*7*, *12*, *13*). It was found that the introduction of phosphorus, irrespective of its chemical environment within the comonomer unit, increases flame retardance to a significant degree and also leads to enhanced production of char. Phosphorus retention in char residues of the modified polymer systems was also found to be high, thus indicating a predominant element of condensed phase activity by the phosphorus-containing groups. In addition, copolymers of acrylamide with phosphorus-containing comonomers appeared to display considerable N-P synergism (*14*).

A variety of phosphorus-containing acrylates, methacrylates and styrene derivatives, structures of which are shown on Figure 4, have been copolymerized, using free radical initiators, with acrylonitrile (AN) and methyl methacrylate (MMA).

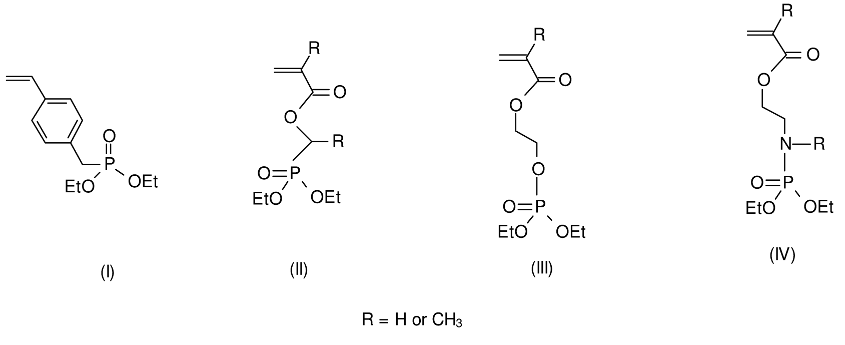

Figure 4. Structures of comonomers based on styrenic (I) or acrylic/methacrylic phosphonates and phosphates (II-IV).

For example, copolymers of MMA with diethyl(methacryloyloxy)methyl phosphonate (DEMMP) (Figure 4, structure II with R=CH_3) had higher LOIs, lower rates of heat release, lower overall heats of combustion, and gave a V0 rating in a UL-94 test (*15*). Moreover, the transparencies of these copolymers are comparable with that of PMMA. Also, their physical and mechanical properties are not significantly inferior to those of pristine PMMA. Other phosphorus-containing comonomers led to similar improvements. Studies of the thermal degradation and combustion behavior of some of these reactively modified PMMAs suggest that flame retardance mechanism involves both vapor phase and condensed phase activity, with the latter leading to significant char production. Char production probably involves trans-esterification reactions and inter-chain cyclizations catalyzed by phosphoric acid groups liberated during combustion (see for instance, in Figure 9).

Chemical incorporation of phosphorus-containing comonomers such as diethyl-*p*-vinylbenzyl phosphonate (DEpVBP) (Figure 4, structure I) and acrylic or methacrylic phosphates and/or phosphonates into PAN chains greatly increases char production during combustion (*16*, *17*). The condensed phase activity of the modifying phosphorus-containing groups in PAN is also reflected in the significant increase in the flame retardance of these modified systems as gauged by the LOIs and by the values of heats of combustion. In this case, the phosphorus-containing comonomer appears to act by promoting the intra-molecular cyclization of -C≡N groups located along the PAN chain, leading to the well known precursor structures to a graphitic char, which is a relatively poorly combustible material (*17*).

The condensed phase activity of phosphorus-containing covalently bound groups is predominant for modified PANs. Usually, upon heating PAN undergoes thermal degradation, and a range of volatile compounds such as acrylonitrile, ammonia, organic and inorganic nitriles are produced (*17*). In addition, depending on the mode and/or rate of heating, intra-molecular cyclization of the pendent nitrile groups occur to form cyclic structures, 'locking' nitrogen atoms onto conjugated polyene sequences. This well characterized cyclization scheme is the basis for a route to carbon fibers (*18*, *19*).

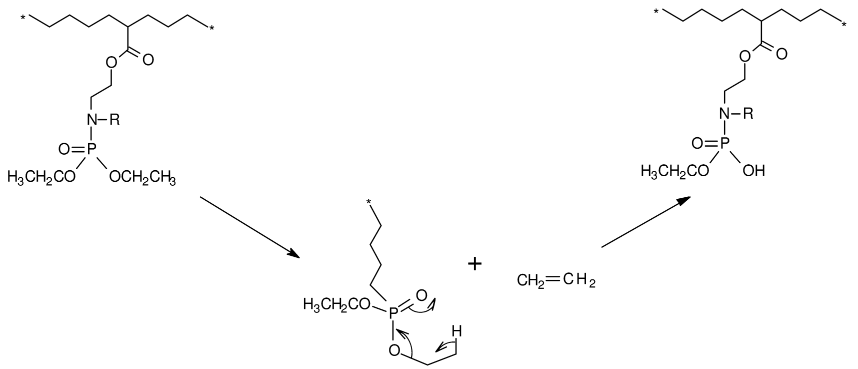

Figure 5. Thermal/base catalyzed cracking of phosphonate ester group and formation of acidic nucleophilic species.

At lower temperatures, an early thermal cracking of the phosphonate ester groups occurs according to the scheme shown in Figure 5. The formation of the cyclic intermediate is entropically favored owing to the elimination of olefin molecules, in this case, ethene. The phosphoric acid species produced can act

In Fire and Polymers VI: New Advances in Flame Retardant Chemistry and Science; Morgan, A., et al.; ACS Symposium Series; American Chemical Society: Washington, DC, 2012.

as nucleophilic centers that promote intra-molecular cyclization of the nitrile groups in the AN sequences (Figure 6). Thus, the condensed phase activity of the phosphorus-containing modifying groups in PAN chains, in enhancing the extent of intra-molecular cyclization, leads to increased production of char (*16*).

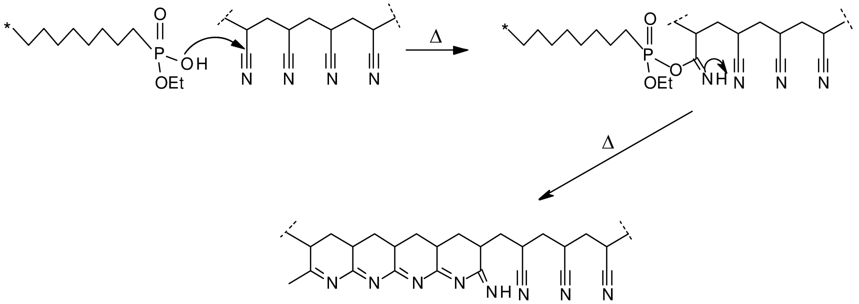

Figure 6. Cyclization initiated by nucleophilic species (in this case, an intra- or inter-molecular attack by a phosphonate monoester).

As mentioned above, PAN initially undergoes side chain cyclization, resulting ultimately in carbonaceous char formation with a concomitant loss of combustible compounds, whereas polystyrene (PSt) usually undergoes random chain scission followed by volatilization of styrene monomer and oligomers. Wyman *et al.* (*16*) compared thermal degradation and combustion behavior of AN copolymers with St and with various dialkyl-*p*-vinylbenzyl phosphonates. The reduced amount of char produced for the copolymer of AN with St was explained by the 'blocking' effects of St units, which shortened the available propagation distance for cyclization along the polymer chain (Figure 7). As the amount of St moieties increases, the probability of AN unit having an adjacent St unit increases as well, and hence with it the possibility of homolytic chain cleavage into smaller oligomers and other less readily combustible material (*16*).

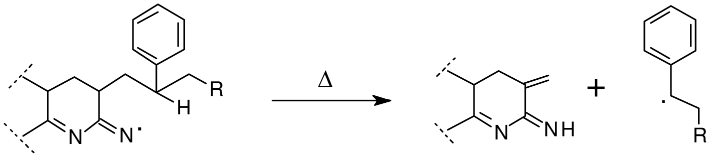

Figure 7. Possible radical mechanism for the interruption of intra-molecular cyclization in the copolymer of AN with St.

The initial weight losses of AN copolymers with dialkyl-*p*-vinylbenzyl phosphonates upon thermal degradation can be attributed to volatilization of the alkene side groups attached to phosphorus atom as shown on Figure 8. Although the presence of a styrenic entity inhibits the propagation of the cyclization step, the nucleophilic and/or acidic nature of the phosphorus acids produced by the elimination of alkenes from the phosphonate comonomer units offsets this deficiency, and leads to char yields comparable to, or greater than, those of PAN. The strongly condensed phase mode of flame retardant action of DEpVBP moieties incorporated into PAN chains is supported by the dependency of LOI *vs.* char yield. High LOI values along with high char yields are significant indicators of condensed phase component of flame retardance, while high LOIs coupled with little char formation point towards predominantly vapor phase mode of action (*16*).

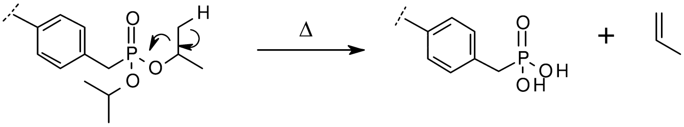
O
P
O
O
H
Δ
O
P
OH
OH
+

Figure 8. Elimination of alkyl side-groups from the phosphonate unit.

Mechanistic studies of thermal degradation and flame retardance in some copolymers of MMA containing organophosphorus groups were performed using analysis of gaseous products of degradation and through the spectroscopic examinations of solid residues (*20*). Flame retardance in these systems is believed to occur by a combination of vapor phase processes and condensed phase activity, i.e. char formation. The condensed phase mechanism is believed to involve generation of phosphonic acid species and their subsequent reaction with MMA units to give methacrylic anhydride units, which then decarboxylate *en route* to form char (Figure 9).

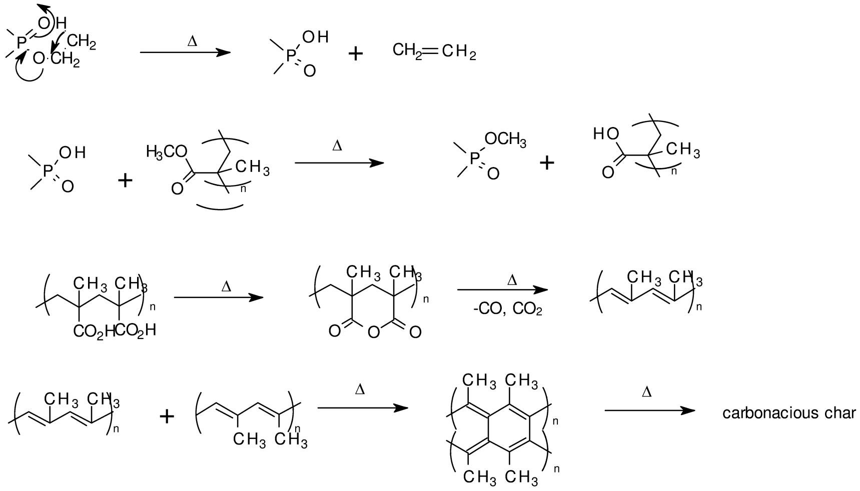
OH
P
O
CH2
CH2
Δ
OH
P
O
+
CH2=CH2
OH
P
O
+
H3CO
O
CH3
n
Δ
OCH3
P
O
+
HO
O
CH3
n
CH3 CH3
CO2H CO2H
n
Δ
CH3 CH3
O O O
n
Δ
-CO, CO2
CH3 CH3
n
CH3 CH3
n
+
CH3 CH3
n
Δ
CH3 CH3
CH3 CH3
n
n
Δ
carbonacious char

Figure 9. Condensed phase mechanism of flame retardance in copolymer of MMA with DEMMP.

In this mechanism the phosphonate ester group, after elimination of ethene and formation of phosphonic acid groups, trans-esterify with MMA fragments to give methacrylic acid units. Methacrylic acid fragments dehydrate, and also react with other MMA units (by alcoholysis) to form anhydride links (mainly intra-molecular but also inter-molecular). Such anhydride links, in turn, can interrupt the thermally induced chain depolymerization of MMA sequences leading to the evolution of less MMA monomer (the principle fuel source in any fire involving PMMA). Eventually, the anhydride sequences lose CO and/or CO_2. Presumably, these decarboxylated sequences are the main precursors to the aromatic components of the chars (*7*, *20*).

In addition to the condensed phase component to flame retardance in PMMAs modified with phosphorus-containing groups, there must also be a significant vapor phase component in which the combustion of the fuel (mainly MMA monomer) is impeded, giving rise to the characteristic products of partial combustion, CO and smoke. It is suggested the mixture of volatile phosphorus-containing species or fragments is responsible for the flame-retardation (*20*).

Styrenic Polymers

Monomers with structures I-IV, shown in Figure 4, can copolymerize, free radically as readily with styrene as they do with MMA and AN, and give rise to products that are also significantly flame retarded. Flame retardance here too involves both vapor phase and condensed phase action. Char formation and flame retardance in the phosphorus-containing styrene copolymers occur by mechanisms somewhat different from those for AN and MMA based copolymers. In this case, char production is probably initiated by Friedel-Crafts type condensation of phenyl groups, catalyzed by phosphorus acids liberated during combustion. It is possible that phosphorus acids act as protonic initiators of carbcationic cross-linking reactions (*7*).

The St based copolymers that incorporate phosphorus all show an increase in time to ignition and greater LOI values than did PSt (*7*). Phosphorus species were observed in the laser pyrolysis and microfurnace experiments for all samples that contained phosphorus. These findings are consistent with vapor phase flame retardant action. In all the copolymers the phosphorus content of the char was substantial, which is characteristic of the condensed phase mode of action.

Although phosphorus-containing moieties usually promote char production in the condensed phase *via* formation of dehydrating phosphoric acid, it is likely that in case of St based copolymers a further interaction takes place. The phosphorus-containing compounds could enhance cross-linking reactions in polystyrene during its decomposition. The strong phosphoric and phosphonic acids produced in the non-polar environment during the copolymer decomposition would most likely catalyze Friedel-Crafts cross-linking of aromatic rings. The phosphonate would form the weaker phosphonic acid, which would be less able to promote cross-linking. As cross-linking increases the stability of a polymer, the polymer degradation and the release of volatile products may be less inhibited in the case of the phosphonate containing copolymers compared to phosphate containing copolymers. There is also evidence for some potential phosphorus vapor phase flame retardant action as phosphorus-containing species were identified among pyrolysis products (*21*).

In conclusion, one could say with a fair degree of confidence that in the case of chemically modified St based systems, the flame retardant action due to the modifying groups acts, in almost equal extents, in both gas phase and in the condensed phase. This directly follows from the fact that several definite species containing phosphorus were identified in the vapor phase and that concurrently the char residues had a significant phosphorus content. Regardless of the chemical nature of the phosphorus-containing moieties in the starting materials, upon combustion, they produce the same species in the flame region. However, the exact timing of the release of these species into the vapor phase does influence the overall flame retardant effects of the phosphorus-containing compound in question. For the maximum effectiveness, the phosphorus species need to be present concurrently in the volatile polymer degradation products. Due to this, low molecular weight and readily volatile additive compounds may not be effective enough compared to covalently bound groups, as in the former case a premature release of the flame retardant species into the vapor phase is more likely (*21*).

Concluding Remarks

The use of phosphorus based flame retardants in combination with other, better established, flame-retardants is most effective in situations in which the combination proves synergistic. However, as yet our understanding of such synergistic effects is far from complete and more fundamental work is required in this area, work in which the gaseous and solid products of combustion, with and without flame retardants present, are carefully analyzed. Such analyses can now be undertaken more readily than in the past, owing to the relatively recent development of techniques such as gas phase FT-infrared spectroscopy and laser pyrolysis time-of-flight mass spectrometry for the identification of volatiles, and solid state NMR spectroscopy and x-ray photoelectron spectroscopy for the analysis of chars.

Given that pyrolysis, ignition and combustion first affect the surface of a polymeric material, it is sensible to ask whether or not flame retardant treatments might optimally be applied to the surfaces of materials, especially in cases where surface to volume ratios are high, e.g. films, fibers and textiles. A number of interesting studies have been reported in this regard in which, for example, free radical graft copolymerizations have been used to attach phosphorus-containing monomer units to the surfaces of cotton fabrics to impart flame retardancy (*22*). Cotton surfaces have also been grafted with phosphorus-containing monomers by plasma polymerization as have the surfaces of PAN fabrics (*23*).

It has been seen that a wide variety of phosphorus compounds have been explored, both as additives and reactive components, for the flame retardation of a wide range of polymers, both thermoplastics and thermosets. As yet, however, commercial exploitation of phosphorus based flame retardant systems is still somewhat in its infancy, with halogen containing flame retardants still dominating the market. Largely this is a consequence of the generally higher cost of phosphorus based materials, especially organophosphorus compounds, and the lower flame retardant efficiency of many. As environmental pressures to reduce the use of halogenated organic flame retardants increase, it is likely that the commercial exploitation of phosphorus-containing alternatives will increase, bringing with it economies of scale and reduced costs. In the interim period, the use of phosphorus compounds in combination with established halogenated flame retardants is likely to increase, leading at least to some reductions in overall use of the latter.

Perhaps the most exciting developments are likely to be in the increasing use of various nanoscopic additives, such nanoscopic clays and carbon nano-tubes, in combination with both halogenated and phosphorus-containing flame retardants. Also, we are likely to see increased emphasis on topical treatments of polymeric materials with flame retardant chemicals. Such treatments, involving conventional chemical or physical processes, are already well established in the textiles but will be augmented by more technologically advanced processes, such as those involving plasma polymerizations. Surface treatments in which a flame retardant barrier layer is laid down by plasma polymerization could be particularly effective for polymeric materials having high surface to volume ratios, such as fibers and films.

Acknowledgments

The authors wish to thank their colleagues, past and present, especially, Professor John Ebdon, and Drs. Barry Hunt, Paul Wyman and Vincent Crook. One of us, STM, is grateful to the Engineering and Physical Sciences Research Council (EPSRC), U.K., for the provision of Research Associateship (Grant: EP/F068867/1).

References

1. Cullis, C. F.; Hirschler, M. M. *The Combustion of Organic Polymers*; Clarendron Press: Oxford, 1981.
2. Ebdon, J. R.; Joseph, P.; Hunt, B. J.; Konkel, C. S. In *Speciality Polymer Additives: Principles and Applications*; Al-Malaika, S., Golovoyn, A., Wilkie, C. A., Eds.; Blackwell Science: Oxford, 2001; Vol. 2, pp 231−257.
3. Granzow, A. *Acc. Chem. Res.* **1978**, *11*, 177–183.
4. Levchik, S. V.; Weil, E. D. *J. Fire Sci.* **2006**, *24*, 345–364.
5. Lewin, M; Weil, E. D. In *Fire Retardant Materials*; Horrocks, A. R., Price, D., Eds.; Woodhead Publishing Limited: Cambridge, 2000; pp 31−68.
6. Price, D.; Bullett, K. J.; Cunliffe, L. K.; Hull, T. R.; Milnes, G. J.; Ebdon, J. R.; Hunt, B. J.; Joseph, P. *Polym. Degrad. Stab.* **2005**, *88*, 74–79.
7. Ebdon, J. R.; Price, D.; Hunt, B. J.; Joseph, P.; Gao, F. G.; Milnes, G. J.; Cunliffe, L. K. *Polym. Degrad. Stab.* **2000**, *69*, 267–277.

8. Ebdon, J. R.; Jones, M. S. In *Polymeric Materials Encyclopaedia*; Salamone, J. C., Ed.; CRC Press: Boca Raton, 1995; pp 2397−2411.
9. Joseph, P.; Ebdon, J. R. In *Fire Retardancy of Polymeric Materials*, 2nd ed.; Wilkie, C. A., Morgan, A. B., Ed.; CRC Press: Boca Raton, 2012; pp 107−127.
10. Banks, M.; Ebdon, J. R.; Johnson, M. *Polymer* **1993**, *34*, 4547–4556.
11. Kandola, B. K.; Smart, G.; Horrocks, A. R.; Joseph, P.; Zhang, S.; Hull, T. R.; Ebdon, J.; Hunt, B.; Cook, A. *J. Appl. Polym. Sci.* **2008**, *108*, 816–824.
12. Cochez, M.; Ferriol, M.; Weber, J. V.; Chaudron, P.; Oget, N.; Mieloszynski, J. L. *Polym. Degrad. Stab.* **2000**, *70*, 455–462.
13. Gentilhomme, A.; Cochez, M.; Ferriol, M.; Oget, N.; Mieloszynski, J. L. *Polym. Degrad. Stab.* **2003**, *82*, 347–355.
14. Banks, M.; Ebdon, J. R.; Johnson, M. *Polymer* **1994**, *34*, 3470–3473.
15. Price, D.; Pyrah, K.; Hull, T. R.; Milnes, G. J.; Ebdon, J. R.; Hunt, B. J.; Joseph, P.; Konkel, C. S. *Polym. Degrad. Stab.* **2001**, *74*, 441–447.
16. Wyman, P.; Crook, V.; Ebdon, J.; Hunt, B.; Joseph, P. *Polym. Int.* **2006**, *55*, 764–771.
17. Ebdon, J. R.; Hunt, B. J.; Joseph, P.; Wilkie T. K. In *Fire Retardancy of Polymers: New Strategies and Mechanisms*; Hull, T. R., Kandola, B. K., Ed.; Royal Society of Chemistry: Cambridge, 2009; pp 331−364.
18. Xue, T. J.; McKinney, M. A.; Wilkie, C. A. *Polym. Degrad. Stab.* **1997**, *58*, 193–202.
19. Martin, C. S.; Liggat, J. J.; Snape, C. E. *Polym. Degrad. Stab.* **2001**, *74*, 407–412.
20. Ebdon, J. R.; Hunt, B. J.; Joseph, P.; Konkel, C. S.; Price, D.; Pyrah, K.; Hull, T. R.; Milnes, G. J.; Hill, S. B.; Lindsay, C. I.; McCluskey, J.; Robinson, I. *Polym. Degrad. Stab.* **2000**, *70*, 425–436.
21. Price, D.; Cunliffe, L. K.; Bullett, K. J.; Hull, T. R.; Milnes, G. J.; Ebdon, J. R.; Hunt, B. J.; Joseph, P. *Polym. Degrad. Stab.* **2007**, *92*, 1101–1114.
22. Abdel-Mohdy, F. A. *J. Appl. Polym. Sci.* **2003**, *89*, 2573–2578.
23. Tsafack, M. J.; Levalois-Grutzmacher, J. L. *Surf. Coat. Technol.* **2006**, *200*, 3503–3510.

Chapter 4

Synergistic Effects of Ni^{2+}-Fe^{3+} Layered Double Hydroxide on Intumescent Flame-Retarded Polypropylene Composites Containing Melamine Phosphate and Pentaerythritol Phosphate

Yongchun Kan, Shun Zhou, and Yuan Hu*

State Key Laboratory of Fire Science, University of Science and Technology of China, 96 Jinzai Road, Hefei, Anhui 230026, PR China
***E-mail: yuanhu@ustc.edu.cn**

The effects of Ni^{2+}-Fe^{3+} layered double hydroxide (LDH) as a synergistic agent on the flame retardancy of intumescent flame retardant (IFR) polypropylene composites were studied; the IFR system mainly consisted of melamine phosphate (MP) and pentaerythritol phosphate (PEPA). The flame retardancy was studied by the limiting oxygen index (LOI), UL-94 test, cone calorimetry (CONE) and microscale combustion calorimetry (MCC). Thermal decomposition analysis was investigated via thermogravimetric analysis (TGA), real time Fourier transform infrared spectroscopy (RTFTIR) and thermogravimetric analysis/infrared spectroscopy (TG-IR). The crystallization behavior was tested by the differential scanning calorimetry (DSC). Char residues were analyzed by scanning electron microscopy (SEM) and Raman diffusion spectroscopy. Results demonstrated that a little addition (0.2%) of Ni^{2+}-Fe^{3+} LDH could improve the flame retardancy of PP/MP/PEPA composites, and affect the P-O-C degradation of MP/PEPA in PP. The crystallinity of the composites is lowered by Ni^{2+}-Fe^{3+} LDH. It also has an influence on the structure of char residual, which may benefit the flame retardancy and thermal stability of materials.

In Fire and Polymers VI: New Advances in Flame Retardant Chemistry and Science; Morgan, A., et al.;
ACS Symposium Series; American Chemical Society: Washington, DC, 2012.

1. Introduction

Polypropylene (PP) has been widely used in many fields, for example, housing, wire and cables, automobiles, electronic and electric industry, and so on. However, its applications are restricted due to its flammability. Generally, halogen-containing flame retardants produce large amounts of smoke and corrosive and irritating gases on burning, and this limits their use (*1*).

In the search for halogen-free retardants, increasing attention has been given to intumescent systems. A typical intumescent system consists of an acid source - a dehydration catalyst for char formation - , a carbon source - a carbonization agent - and a gas source - a blowing agent (*2*). It has been shown that intumescent flame retardant (IFR) PP composites release relatively lower smoke and toxic gases during burning, and are anti-dripping (*3*). However, the classic IFR systems, like ammonium polyphosphate(APP)/pentaerythritol(PER) and MP/PER series, also have some drawbacks, such as low flame retardant efficiency and low thermal stability. As a result, it is necessary and forward-looking to find new intumescent flame retardant systems (*4*, *5*). Pentaerythritol phosphate (PEPA), synthesized by the reaction between PER and $POCl_3$, can be used as carbonization agent and acid source in the IFR system, which has been shown to be more effective than PER series (*6–9*). In our previous papers, it has been found that the combination of MP and PEPA could greatly improve the flame retardancy of PP (*10–12*).

Recently, in order to further improve the flame retardant efficiency, synergistic agents have been used in IFR systems, such as zeolites, rare earth oxides, and some transitional metal oxides and metal compounds (*13–19*). Research has shown that synergistic agents can effectively increase the strength and stability of the char formed during the combustion process. Layered double hydroxides (LDH), as a new class of synthetic inorganic/organic anionic clays, have been studied for many years (*20*, *21*). The ideal formula of LDH can be described as $[M^{2+}_{1-x}M^{3+}_{x}(OH)2]^{x}[(A^{m-})_{x/m}.nH_2O]^{x-}$, where M^{2+} and M^{3+} are metal cations, such as Mg^{2+}, Zn^{2+}, Mn^{2+}, Al^{3+}, Fe^{3+} and so on. A^{m-} is charge balancing interlayer anion. According to the literature (*22*, *23*), LDHs, as synergistic agents, have been used to improve flame retardancy of APP in polyvinyl alcohol matrix. Moreover, it has been found that LDHs can act as flame retardant synergist and apparently increase the LOI values and improve the elongation at break of ethylene-vinyl acetate/hyperfine magnesium hydroxide/LDH nanocomposites. However, little attention has been paid to the study of the synergistic effect of LDH with IFR system in PP matrix.

In the present study, Ni^{2+}-Fe^{3+} LDH as a synergistic agent was used to improve flame retardancy of MP/PEPA IFR system in PP matrix. The flame retardant properties and thermal stability of the samples were evaluated by LOI, UL-94, cone calorimetry, MCC, TG, TG-IR and RTFTIR. DSC was used to investigate the crystallization behavior. Moreover, the characterization of the intumescent char was studied by SEM and Raman.

2. Experimental

2.1. Materials

Polypropylene (F401, MFI = 2.0 g/10min, density = 0.9 g/cm^3) was provided by Yangzi Petroleum Chemical Company, China. Melamine phosphate (1:1 salt) was supplied by Hefei Jinhui Institute of Chemical Engineering, China. PEPA, an article of commerce, i.e. Great Lakes (now Chemtura) NH-1197, was provided by Balin Petroleum Chemical Company, China. Ni^{2+}-Fe^{3+} layered double hydroxide was prepared following a literature hydrothermal method (*24*).

2.2. Preparation of Samples

The flame retardant PP composites were prepared on a Brabender-like apparatus at about 175 °C for 15 min. After melt-mixing, the samples were hot-pressed at about 180 °C under 10 MPa for 5 min into sheets of suitable thickness and size for analysis. MP and PEPA were dried in oven at 100 °C for 24 h before use. It is necessary to note that the total loading of flame retardants is 25%, the weight ratio of MP/PEPA is always 1:1 and the loading of Ni^{2+}-Fe^{3+} LDH is 0.2%, 0.6% and 1%.

2.3. Measurements

2.3.1. Cone Calorimetry (CONE)

The cone calorimetry (Stanton Redcroft, UK) test was performed according to ISO 5660 standard procedures. Each specimen of dimensions 100×100×3 mm was wrapped in aluminum foil and exposed horizontally to an external heat flux of 35 kW/m^2.

2.3.2. Microscale Combustion Calorimetry (MCC)

GOVMARK MCC-2 Microscale Combustion Calorimetry was used to investigate the combustion of the UV-cured film. In this system, about 5 mg samples of UV-cured film were heated to 700 °C at a heating rate of 1 °C/s in a stream of nitrogen flowing at 80 cm^3/min.

2.3.3. Thermogravimetric Analysis (TGA)

The thermogravimetric analysis (TGA) was carried out on the TGA Q5000 IR thermogravimetric analyzer (TA instruments) using a heating rate of 20 °C/min in air and nitrogen atmosphere.

2.3.4. *Differential Scanning Calorimetry (DSC)*

The crystallization behaviour of PP/MP/PEPA and PP/MP/PEPA/Ni^{2+}-Fe^{3+} LDH was studied by DSC analyzer (Perkin-elmer Pyris 1). Samples of about 4-6mg were encapsulated in hermetically sealed pans. The samples were first heated to 200°C at 10 °C/min, maintained at the temperature for 5 min, and then cooled to 40°C at 10 °C/min. All DSC tests were performed under a nitrogen purge (20 ml/min).

2.3.5. *Thermogravimetric Analysis-Infrared Spectrometry (TG-IR)*

Thermogravimetric analysis/infrared spectrometry (TG-IR) of the sample was performed using the TGA Q5000 IR thermogravimetric analyzer that was interfaced to the Nicolet 6700 FTIR spectrophotometer. About 5.0 mg of the sample was put in an alumina crucible and heated from 30 to 600 °C. The heating rate was set as 20 °C /min (nitrogen atmosphere, flow rate of 60 mL/min).

2.3.6. *Real-Time Fourier Transform Infrared (RTFTIR)*

Real time FTIR spectra were recorded using Nicolet MAGNA-IR 750 spectrophotometer equipped with a ventilated oven having a heating device. The temperature of the oven was raised at a heating rate of about 10 °C/min. Samples were mixed with KBr powder, and the mixture was pressed into a tablet. Real time FTIR spectra were obtained *in situ* during the thermal oxidative degradation of the samples.

2.3.7. *Scanning Electron Microscopy*

The char formed after combustion was first sputter-coated with a conductive layer, and then its morphologic structures were observed by scanning electron microscopy AMRAY1000B.

2.3.8. *Raman Spectrometry*

Laser Raman spectroscopy measurements were carried out at a room temperature with a SPEX-1403 laser Raman spectrometer (SPEX Co., USA) with excitation provided in back-scattering geometry by a 514.5 nm argon laser line.

3. Results and Discussions

3.1. Flame Retardancy

From table 1, it can be seen that the LOI value of PP/MP/PEPA nanocomposites (MP/PEPA=1:1. total addition 25 wt.%) is 32, and its UL-94 rating can reach V-0. By adding 0.2wt.% Ni^{2+}-Fe^{3+} LDH into the composite as synergistic agent, the LOI value is raised to 35. Along with the change in LOI value, the UL-94 rating of PMPN remains V-0 level. But when the loading of Ni^{2+}-Fe^{3+} LDH in PMPN1 is increased to 0.6wt.%, the LOI value and the UL-94 rating are reduced to 31 and V-1, respectively. And when the addition of the Ni^{2+}-Fe^{3+} LDH is further raised to 1%, the sample PMPN2 has a lower LOI value (30.5), and it is unclassified in the UL-94. Hence, the sample PMPN containing 0.2wt.% Ni^{2+}-Fe^{3+} LDH is chosen for investigation of the synergistic effect of Ni^{2+}-Fe^{3+} LDH in the PP/MP/PEPA system.

Table 1. LOI values and UL-94 testing results of sample PMP and PMPN

Sample	*Component (wt.%)*				*Flame retardancy*	
	PP	*MP*	*PEPA*	*Ni^{2+}-Fe^{3+}-LDH*	*LOI (%)*	*UL-94 rating*
PMP	75	12.5	12.5	0	32	V-0
PMPN	75	12.4	12.4	0.2	35	V-0
PMPN1	75	12.2	12.2	0.6	31	V-1
PMPN2	75	12.0	12.0	1	30.5	No-rating

Figure 1 and 2 show the cone test results of PP/MP/PEPA and PP/MP/PEPA/Ni^{2+}-Fe^{3+} LDH composite, and the related data are given in Table 2. A comparison of heat release rate curves between sample PMP and PMPN is shown in Figure 1. It can be seen that, the heat release rate of PP/MP/PEPA/Ni^{2+}-Fe^{3+} LDH composite is lower than that of PP/MP/PEPA even though the loading of Ni^{2+}-Fe^{3+} LDH in PP/MP/PEPA is only 0.2 wt.%. The peak heat release rate of PMPN declines by more than 20%, from 207 to 164 kW/m^2. From Figure 1 it also can be observed that both curves consist of two peaks. A small peak appears in 80s, which is typical of the intumescent flame-retardant system. This is due to the formation of intumescent char layer at the early stage of combustion. Adding Ni^{2+}-Fe^{3+} LDH makes the PHRR of the first peak lower and it appears earlier than the composite without synergist; the char layer of flame-retarded nanocomposite containing Ni^{2+}-Fe^{3+} LDH forms more rapidly and effectively.

Table 2. Cone calorimetry data of sample PMP and PMPN at 35 kW/m²

Sample	*Time to ignition (s)*	*Peak HRR (kW/m²)*	*THR(MJ/m²)*	*FPI*
PMP	30	207	84	0.14
PMPN	29	164	52	0.18

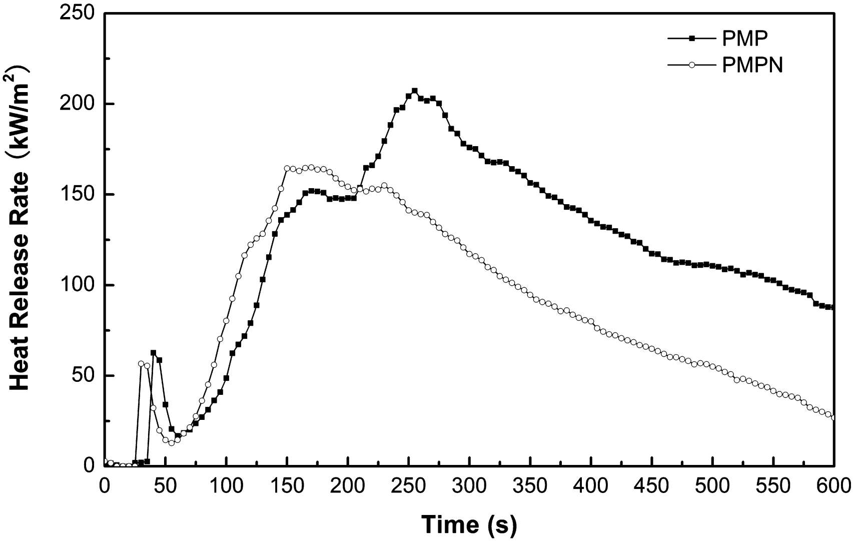

Figure 1. HRR curves of sample PMP and PMPN.

The time to ignition (TTI) and the Fire Propagation Index (FPI) calculated from TTI and PHRR are listed in table 2. In PP/MP/PEPA no significant reduction is observed for TTI in the presence of Ni^{2+}-Fe^{3+} LDH. The FPI value of Ni^{2+}-Fe^{3+} LDH synergistic flame-retarded PP/IFR composites is higher than that without synergist. It suggests that the fire safety of the materials upon addition of Ni^{2+}-Fe^{3+} LDH is improved.

The difference in the total heat release between PMP and PMPN is shown in Figure 2. At the end of burning, the PP/MP/PEPA composite has released a total heat of 84 MJ/m². When the composite is synergized by Ni^{2+}-Fe^{3+} LDH, the total heat release is decreased to 52 MJ/m². The remarkable reduction (38%) in total heat release indicates that a little Ni^{2+}-Fe^{3+} LDH has a significant synergistic effect on the MP/PEPA intumescent flame retardant system. The effect can be due to the layer structure and/or the transition metal ions Ni^{2+} and Fe^{3+}.

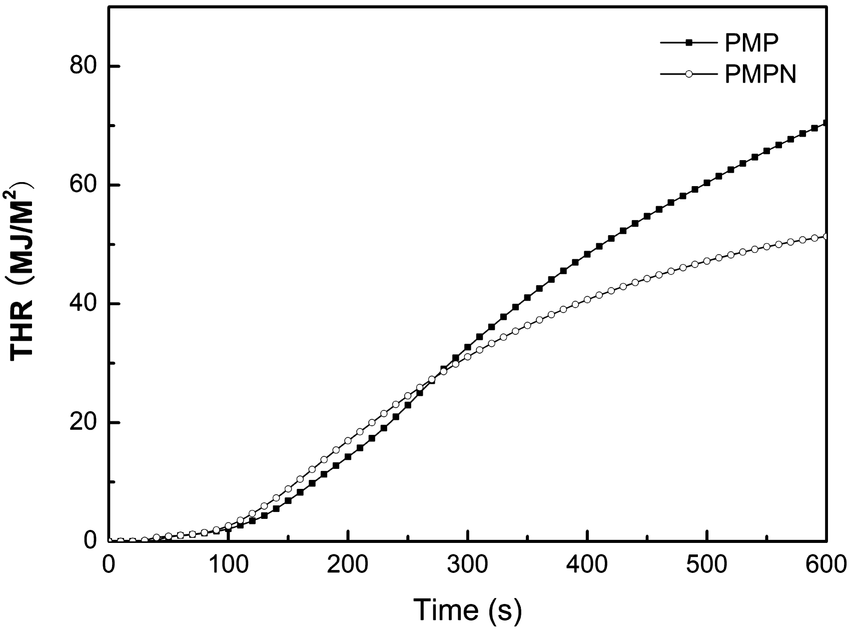

Figure 2. Total heat release curves of sample PMP and PMPN at 35 kW/m^2.

Microscale combustion calorimetry (MCC) is a technique that uses thermal analysis methods to measure chemical properties related to fire. From just a few milligrams of specimen a wealth of information on material combustibility and fire hazard is obtained in minutes. Figure 3 shows the specific heat release rate curves, and the related date is listed in table 3. Associated data for PP/MP/PEPA are peak HRR = 862.9 W/g, heat release capacity (HRC) = 868 J/g·K. Incorporation of 0.2% Ni^{2+}-Fe^{3+} LDH into PP/MP/PEPA reduce the PHRR and HRC to 704.5 W/g and 709 J/g·K respectively. By comparing the results of MCC and CONE, there is a consistent change in HRR, but the HRR curve in MCC test has one peak while that in cone test consists of two peaks. This is due to the difference between the testing principles of MCC and CONE, even though the heat release rate in both is calculated from the measured oxygen consumption rate. In CONE testing, the surface of material forms an intumescent char layer quickly at the beginning of burning, so the first peak appears. Then the char layer starts to degrade and be destroyed, leading to the material combusting again, the second peak appears. In contrast, controlled pyrolysis of material takes place under nitrogen atmosphere in MCC testing, which produces fuel gas. The combustion of the fuel gas leads to the appearance of HRR curve and peak. The value of PHRR depends on the pyrolysis process of material. It can be concluded that the remarkable reduction (18%) in HRC and PHRR is due to that the addition of Ni^{2+}-Fe^{3+} LDH which limits the formation of the thermal degradation products. On the other hand, the ignition temperature of sample PMPN is earlier than that of sample PMP, which indicates that the Ni^{2+}-Fe^{3+} LDH quickens the thermal degradation of composite.

Table 3. Microscale combustion calorimetry data of sample PMP and PMPN

Sample	*HRC (J/g K)*	*PHRR(W/g)*	*IT (°C)*
PMP	868	862.9	479.3
PMPN	709	704.5	475.0

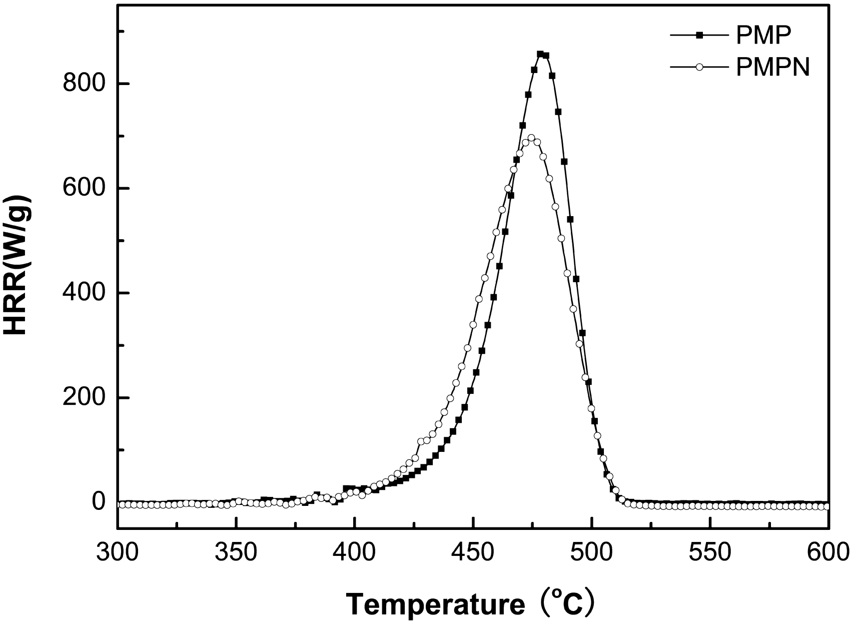

Figure 3. HRR curves of sample PMP and PMPN from microscale combustion calorimetry testing.

3.2. Thermal Stability

TG and DTG curves of Ni^{2+}-Fe^{3+} LDH, PP/MP/PEPA and PP/MP/PEPA/Ni^{2+}-Fe^{3+} LDH in air are shown in Figure 4 and the data are summarized in Table 4. The degradation of Ni^{2+}-Fe^{3+} LDH in air consists of two stages of weight loss: the first stage below 200 °C is due to the loss of physisorbed and interlayer water, and the second stage in the temperature range 200-350 °C is assigned to removal of water molecules from condensation of hydroxyl groups and CO_2 from the interlayer carbonate anions (*25*). The thermo-oxidative degradation of PMP starts at about 200 °C, and begins to slow after 400 °C, with the maximum rate of weight loss occurring at 308 °C. In comparison, PMPN degrades more rapidly, between 200 °C and 350 °C, which is similar to the second weight loss stage of Ni^{2+}-Fe^{3+} LDH, and the temperature of maximum rate of weight loss is shifted to 284 °C. According to the data in table 4, the onset degradation temperature (temperature at 10% mass loss, $T_{-10\%}$) of PMPN is decreased by 7 °C, while the mid-point temperature (temperature at 50% mass loss, $T_{-50\%}$) is reduced by 20 °C. On the other hand, the residue at 650 °C of PMPN is increased from 9.5% to 10.5%, suggesting that Ni^{2+}-Fe^{3+} LDH promotes the thermo-oxidative degradation of PP/MP/PEPA and char formation.

Table 4. TG and DTG data of Ni^{2+}-Fe^{3+} LDH, PMP and PMPN

Sample	*T_{peak} (°C)*	*$T_{-10\%}$ (°C)*	*$T_{-50\%}$ (°C)*	*Residue at 650°C*
PMP	308	264	305	9.5%
PMPN	284	257	285	10.5%
NiFe-LDH	107, 274			

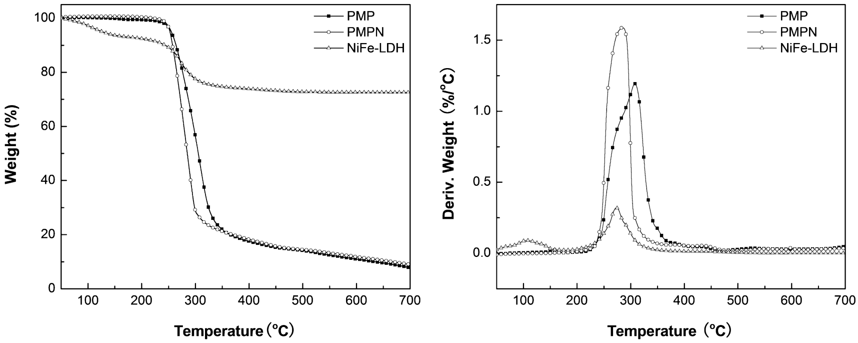

Figure 4. TG and DTG curves of Ni^{2+}-Fe^{3+} LDH, PMP and PMPN in air.

3.3. Crystallization Behavior

DSC is commonly used to study the crystallization behavior of polymers. From DSC exotherms, T_O(the temperature at the crossing point of the tangents of the baseline and the high-temperature side of the exotherm), T_P(the peak temperature of the exotherm) and X_c(the crystallinity degree) can be obtained

(*26*). Figure 5 shows the DSC exotherms of PMP and PMPN, and the relative data is listed in table 5. It can be seen that the T_O and T_P show almost no difference between PMP and PMPN, indicating that Ni^{2+}-Fe^{3+} LDH has no effect on the crystallization temperature of the material. Remarkably, enthalpy of crystallization ($\triangle H_C$) of PMPN is much lower than that of PMP. Because the crystallinity content X_c is proportional to $\triangle H_C$, the transformation means that PMPN has lower crystallinity. This result may be due to the layer structure of Ni^{2+}-Fe^{3+} LDH, which can restrain the tropism of the chain segment of PP and restrict the spherulitic growth.

Table 5. Onset temperature, peak temperature and enthalpy of crystallization of sample PMP and PMPN

Sample	*T_O (°C)*	*T_P (°C)*	*$\triangle H_C$ (J/g)*
PMP	120.7	116.6	-95.8
PMPN	120.6	116.3	-57.6

3.4. The Volatilized Products Analysis

TG-FTIR is an effective measurement for volatilized products analysis during thermal degradation. The 3D TG-FTIR spectra of the gases during the thermal degradation of PMP and PMPN are shown in Figure 6. In this figure FTIR spectrum of all the volatile pyrolysis products evolved at different time is shown, and the characteristic spectra obtained at the maximum decomposition rate can be seen in Figure 7. The characteristic absorbance at 3080, 2960, 2916, 1462, 1377 cm^{-1} indicate that the major volatilized pyrolysis products for PMP and PMPN both consist of alkane and alkene. However, the gas phase in the thermal degradation of PMP has a peak at 2360 cm^{-1} which does not appear in the thermal degradation of PMPN. This can be ascribed to the C≡N bond stretching vibration. Therefore, the addition of Ni^{2+}-Fe^{3+} LDH reduces the production of cyanide in the thermal degradation process of PP/MP/PEPA composite. Figure 8 presents the total intensity of the pyrolysis products for PMP and PMPN. The peak of the total intensity for PMPN is 10 min later than that of PMP; the release of the pyrolysis products for PMPN is much later than for PMP. By calculating the ratio of the peak area to the weight of test samples, it may be concluded that the volatilized products of PMPN are fewer than from PMP, which is in agreement with the MCC results. The amount of the volatilized pyrolysis products for PMP and PMPN is similar, so fewer products mean lower heat release rate and fewer heat release capacity.

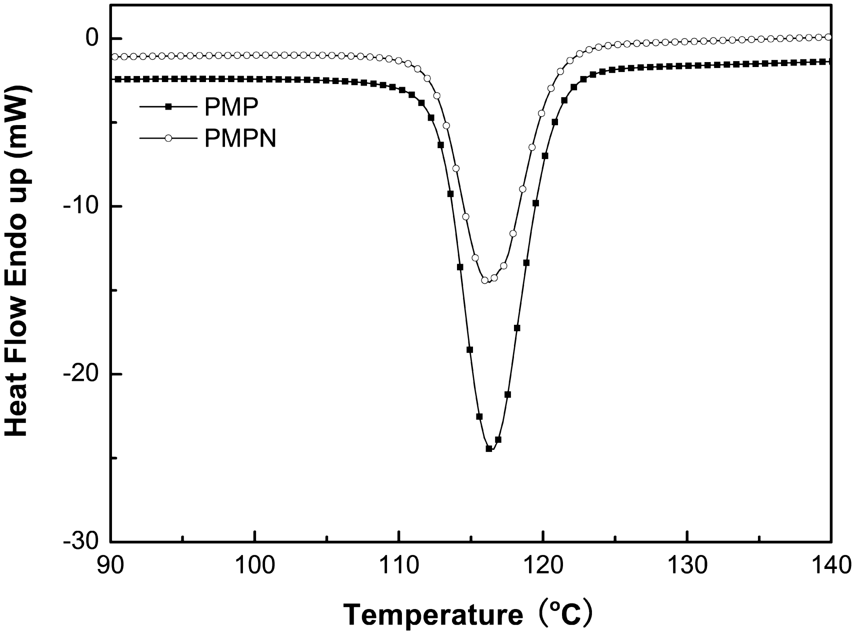

Figure 5. DSC exotherms of sample PMP and PMPN.

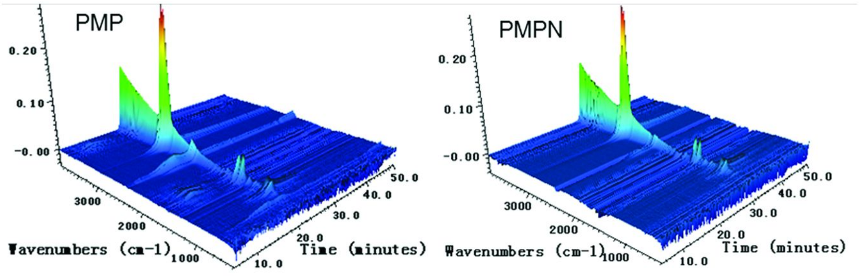

Figure 6. 3D TG/FTIR spectrum of gas phase in the thermal degradation of PMP and PMPN.

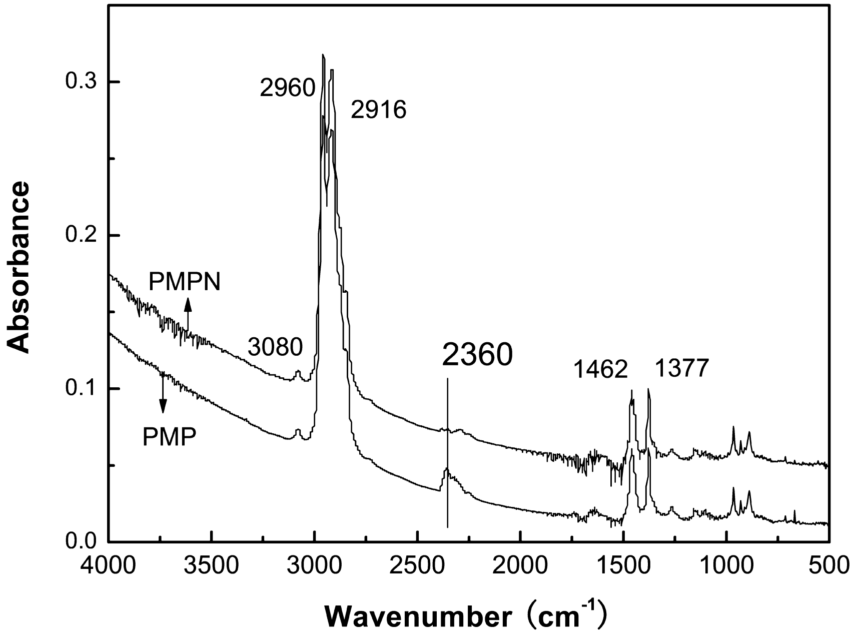

Figure 7. FTIR spectrums of volatilized pyrolysis products for PMP and PMPN at the maximum decomposition rate.

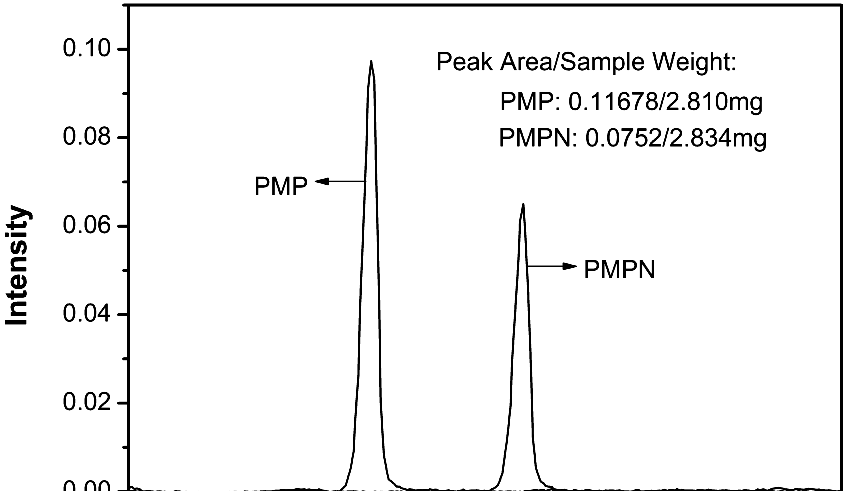

Figure 8. Total intensity of the pyrolysis product for PMP and PMPN.

3.5. Thermal Oxidative Degradation

The thermal oxidative degradation of PMP and PMPN were investigated using RT-FTIR spectroscopy. Figure 9 shows the changes in the absorption bands of PMP and PMPN during heating. The peaks at 3422 and 1148 cm^{-1} are attributed to OH absorptions of PEPA, while the peaks at 3394 and 956 cm^{-1} are ascribed to MP. All the intensities of these OH stretching and deformation absorptions are reduced from 200 °C, caused by the dehydration of PEPA and MP, leading to the formation of pyrophosphate. The absorption peaks of N-H stretching and deformation at 3159 and 1676 cm^{-1} decrease from 200 °C and disappear completely at 450 °C, which may be due to the progressive condensation of the melamine group with the evolution of NH_3 and the evaporation of melamine itself. The three peaks at 1612, 1562, 1519 cm^{-1}, ascribed to the characteristic absorbance of the triazine ring structure of MP, have disappeared at 250 °C, which is in agreement with the condensation of the melamine. In the region of 3000-2800 cm^{-1}, the peaks refer to the C-H absorptions of PP and PEPA. By comparing the peaks at 1298 cm^{-1}(P=O of PEPA) and 1256 cm^{-1} (O=P(OH) of MP), the change of the intensities indicates the degradation of the cyclic structure of PEPA, resulting in the transformation from P=O into O=P(OH). This corresponds to changes of the peaks at 856 and 671 cm^{-1} which are the characteristic cyclic absorption of PEPA. The disappearance of the peaks at 1298, 856 and 671 cm^{-1} suggests that the degradation has finished at 250 °C. Besides, with an increase of temperature, the 1256 cm^{-1} peak is gradually shifted to higher wavenumber, and moves to 1284 cm^{-1} at 400 °C, assigned to the formation of pyrophosphate. The characteristic absorption at 1028 cm^{-1} is attributed to the stretching of P-O-C; the intensity decreases during heating. At 500 °C, the peaks at 1284 cm^{-1}(P=O), 1085 and 878 cm^{-1}(P-O-P) indicate that the residue is mainly composed of P=O and P-O-P groups.

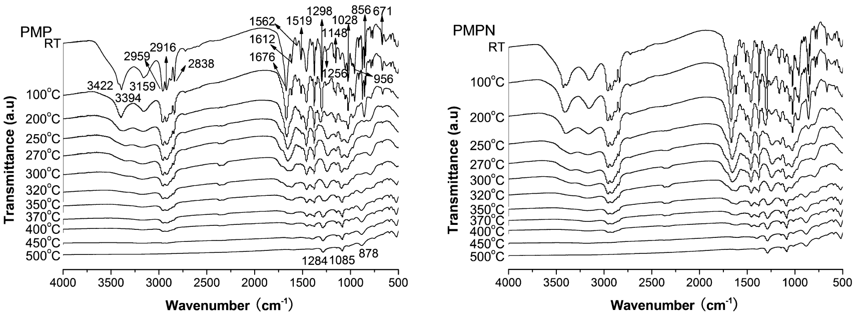

Figure 9. RT-FTIR spectra of PMP and PMPN with different pyrolysis temperatures.

The RT-FTIR spectra of PMP and PMPN are similar. For further comparison, the FTIR spectra of PMPN and PMPN at 250, 270, 300, 320 °C are shown in figure 10. It is noted that, the change of the 1028 cm^{-1} peak (P-O-C) for PMPN in this temperature range is different with that for PMP. While the P-O-C of PMP has almost completely degraded at 300 °C, the PMPN needs to reach 320 °C. Thus, Ni^{2+}-Fe^{3+} LDH has an effect on the degradation of P-O-C, making it slower.

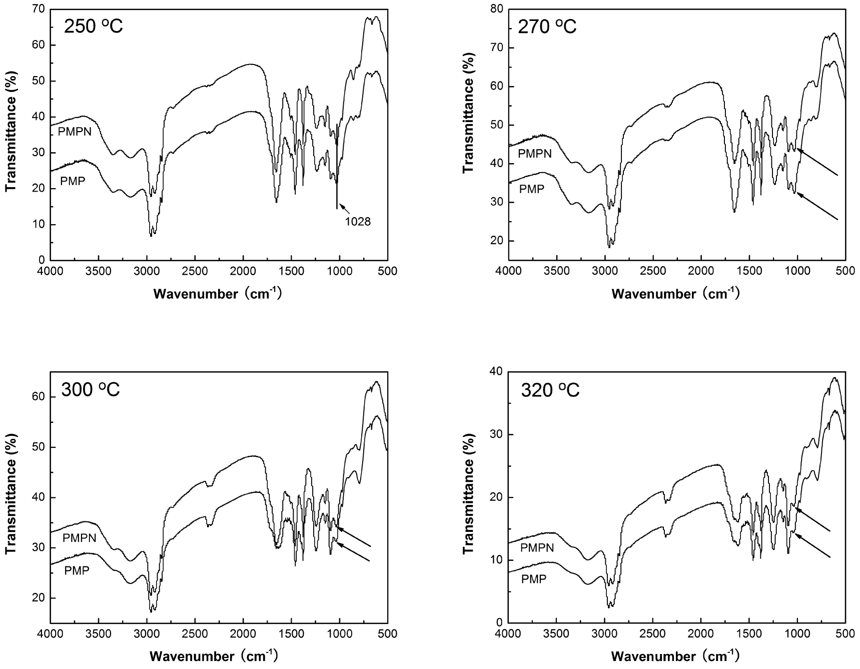

Figure 10. FTIR spectra of PMP and PMPN at different temperatures.

3.6. Characterization of the Intumescent Char

SEM micrographs in figure 11 and 12 show the microstructure of the residual char of PMP and PMPN formed after the cone calorimetry experiment. Figure 11 presents the SEM micrographs of outer char layer formed after the cone test. It can be seen that, the outer char is continuous, smooth and dense. As the structure can store gas, especially noncombustible gas produced in combustion, the heat flux is retarded. As oxygen penetrates the outer char layer into the interior to accelerate combustion, it needs to go further, so the outer char provides a good flame shield for the underlying material. Interestingly, there are lots of micron sized tubes on the surface of the char residue of PMPN while none on PMP. At 6000 times magnification, the netlike structure of the tube wall is observed clearly, which is more compact than the outer char. This kind of structure can permit more gas and heat to be stored in the micron sized tubes, leading to better flame retardancy.

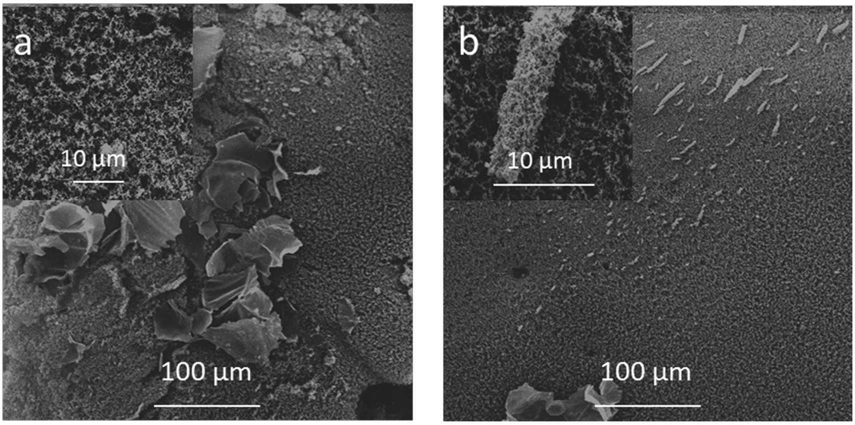

Figure 11. SEM micrographs of outer char layer formed after cone test of (a) PMP and (b) PMPN.

Figure 12a and 12b present the SEM micrographs of the inner char layer of PMP and PMPN formed after cone test. Some small globular particles can be observed, which may ascribed to the flame retardant that has not decomposed completely. There are fewer small particles in the char of PMPN than that of PMP, indicating that Ni^{2+}-Fe^{3+} LDH promotes the degradation of flame retardant. Another difference of inner char between PMP and PMPN is that there are some big bubbles in the char of PMPN. Perhaps the Ni^{2+}-Fe^{3+} LDH can prevent the caving of the char layer.

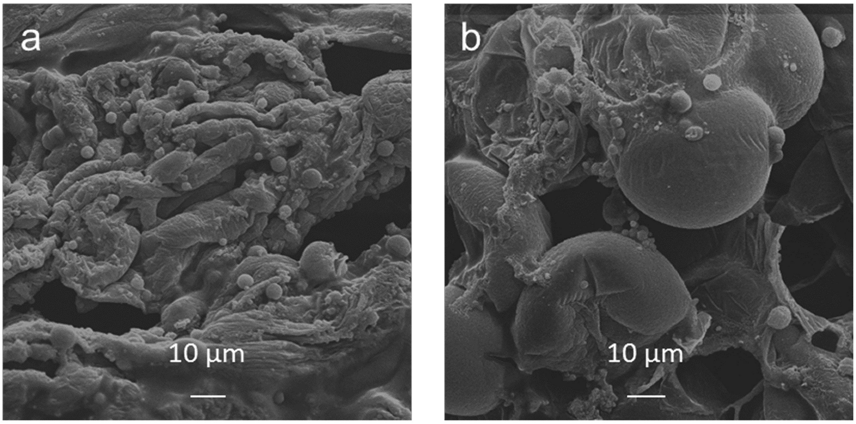

Figure 12. SEM micrographs (magnified 1000 times) of inter char layer of (a) PMP and (b) PMPN.

Raman spectroscopy is a powerful tool for the characterization of an intumescent carbonaceous material. As shown in figure 13, both the spectra of outer char of PMP and PMPN have two peaks at 1590 cm^{-1} (G-band) and 1360 cm^{-1} (D-band). The G-band is ascribed to the E_{2g} vibrational mode, indicating the existence of graphitic carbon. The D-band reflects the A_{1g} breathing mode of the disordered carbons (or rings). The intensities of the peaks in the curve of the char of PMPN are much weaker than those in PMP. As the two bands change as a function of the structural organization level of the carbon, the addition of Ni^{2+}-Fe^{3+} LDH affects the structural regularity of outer char layer visibly.

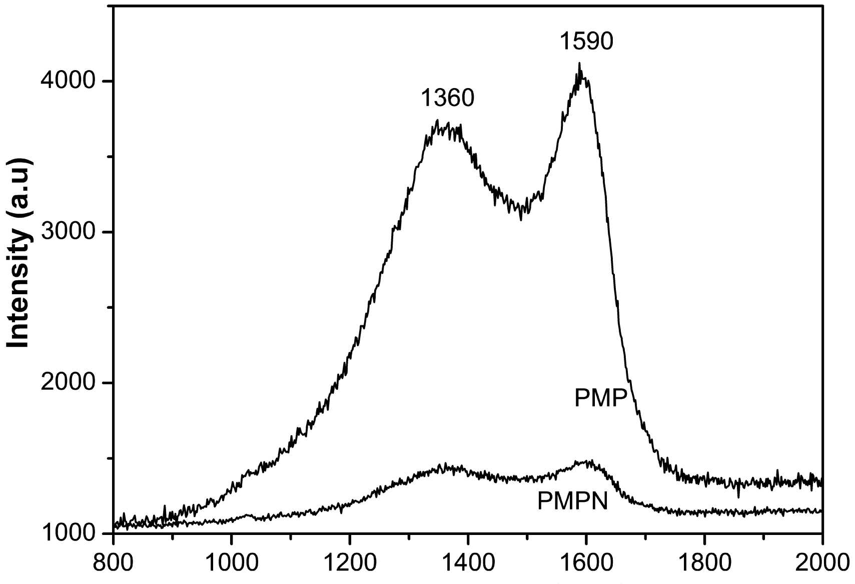

Figure 13. Raman curves of the outer residual char of sample PMP and PMPN.

From the fitted Raman curves in figure 14, the intensity ratio of G to D can be calculated by the peak area ratio, illustrating the purity of graphitic carbon. Basically, the larger is I_G/I_D ratio, the better is the purity of the graphite. The data listed in Table 6 shows that the addition of Ni^{2+}-Fe^{3+} LDH can increase the percentage of the graphitic carbon in the outer char residue.

Table 6. the relative intensity ratio of two peaks around 1360 and 1590 cm^{-1}

Sample	*Intensity ratio*
PMP	$I_{1579/1398}=0.22$
PMPN	$I_{1601/1397}=0.50$

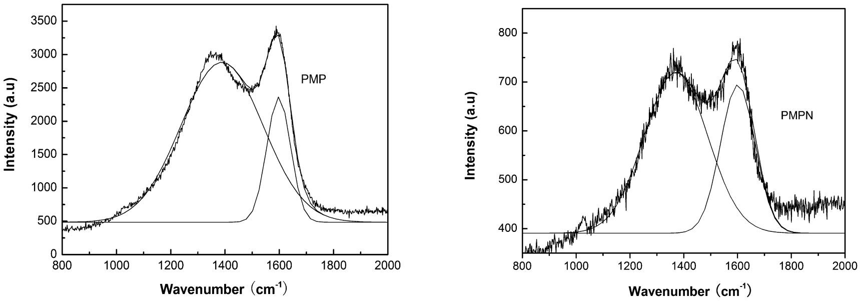

Figure 14. the fitted Raman curves of the outer residual char of sample PMP and PMPN.

4. Conclusion

The effects of Ni^{2+}-Fe^{3+} LDH on the flame retardancy of the PP/MP/PEPA composite are remarkable. The LOI value of the composite containing 0.2 wt.% Ni^{2+}-Fe^{3+} LDH is increased, and the UL-94 rating still can reach V-0 level. The cone calorimetry experiment shows that the addition of Ni^{2+}-Fe^{3+} LDH can decrease the PHRR and HRR of the composite remarkably and promote char formation. The TGA results indicate that the Ni^{2+}-Fe^{3+} LDH promotes thermo-oxidative degradation of the composite, and the RTFTIR results show the effect is mainly on the P-O-C degradation. As seen in the results of MCC and TG-FTIR, the Ni^{2+}-Fe^{3+} LDH can reduce the volume of the volatilized pyrolysis products and change the components. From DSC, the crystallinity of the material is lowered by Ni^{2+}-Fe^{3+} LDH. Also the Ni^{2+}-Fe^{3+} LDH can affect the structure and composition of char residue. The micron sized tubes on the surface of char residue after the addition of Ni^{2+}-Fe^{3+} LDH can provide better protection for the underlying material.

Acknowledgments

The work was financially supported by National Natural Science Foundation of China (No. 51036007), the joint fund of NSFC and Guangdong Province (No. U1074001) and specialized research fund for the doctoral program of higher education (20103402110006).

References

1. Sen, A. K.; Mukherjee, B.; Bhattacharya, A. S.; Sanghi, L. K.; De, P. P.; Bhowmick, K. *J. Appl. Polym. Sci.* **1991**, *43* (9), 1674–1684.
2. Camino, G.; Costa, L. *Polym. Degrad. Stab.* **1989**, *23* (4), 359–376.
3. Lv, P.; Wang, Z. Z.; Hu, K. L.; Fan, W. C. *Polym. Degrad. Stab.* **2005**, *90*, 523–534.
4. Li, B.; Xu, M. J. *Polym. Degrad. Stab.* **2006**, *91*, 1380e6.
5. Allen David, W.; Edwyn, C. *Polym. Degrad. Stab.* **1994**, *45*, 399–408.
6. Hills, W. A. U.S. Patent 3873496, 1975.
7. Tamura, Y.; Tanaka, R. U.S. Patent 4584331, 1983.
8. Li, X.; Ou, Y.; Shi, Y. *Polym. Degrad. Stab.* **2002**, *77* (3), 383–390.
9. Balabanovich, A. I.; Levchik, G. F.; Gruber, F. In *Polymer Composites, Coatings, Films*, Proceedings of the IV International Scientific Conference, Gomel, Belarus, July 22–24, 2003; pp 186–187.
10. Zhou, S.; Wang, Z.; Gui, Z.; Hu, Y. *Fire Mater.* **2008**, *32*, 307–319.
11. Zhou, S.; Song, L.; Wang, Z.; Hu, Y. *Polym. Degrad. Stab.* **2008**, *93*, 1799–1806.
12. Zhou, S.; Wang, Z.; Gui, Z.; Hu, Y. *J. Appl. Polym. Sci.* **2008**, *110*, 3804–3811.
13. Demir, H.; Arkıs, X. E.; Ulku, S. *Polym. Degrad. Stab.* **2005**, *89*, 478–83.
14. Bourbigot, S.; Le Bras, M.; Delobel, R.; Bre´ant, P.; Tremillon, J.-M. *Polym. Degrad. Stab.* **1996**, *54*, 275–87.
15. Ravadits, I.; Toth, A.; Marosi, G.; Marton, A.; Szep, A. *Polym. Degrad. Stab.* **2001**, *74*, 419–22.
16. Wu, Q.; Qu, B. *Polym. Degrad. Stab.* **2001**, *74*, 255–61.
17. Yuan, L.; Qi, W. *Polym. Degrad. Stab.* **2006**, *91*, 2513–9.
18. Shibin, N; Yuan, H; Lei, S; Shuqing, H; Dandan, Y *Polym. Adv. Technol.* **2008**, *19*, 489–495.
19. Shibin, N; Lei, S; Jing, Z; Yuan, H; Qilong, T; Lijuan, C. *J. Macromol. Sci., Pure Appl. Chem.* accepted.
20. Khan, A. I.; O'Hare, D. *J. Mater. Chem.* **2002**, *12*, 3191–3198.
21. Carlino, S. *Solid State Ionics* **1997**, *98*, 73–84.
22. Zhang, G.; Ding, P.; Zhang, M.; Qu, B. *Polym. Degrad. Stab.* **2007**, *92*, 1715–1720.
23. Zhao, C.-X.; Liu, Y.; Wang, D.-Y.; Wang, D.-L.; Wang, Y.-Z. *Polym. Degrad. Stab.* **2008**, *93*, 1323–1331.
24. Han, Y.; Liu, Z.-H.; Yang, Z.; et al. *Chem. Mater.* **2008**, *20*, 360–363.
25. Boukraa, F.; Saiaha, D.; Sub, B.-L.; Bettahara, N. *J. Hazard. Mater.* **2009**, *165*, 206–217.
26. Yu, J.; He, J. *Polymer* **2000**, *41*, 891.

Chapter 5

Cucurbit[6]uril as a Fire Retardant Material

Guipeng Cai, Zvonimir Matusinovic, Deqi Yi, Thirumal Mariappan, Ruchi Shukla, Richa Rathore, and Charles A. Wilkie*

Department of Chemistry and Fire Retardant Research Facility,
Marquette University, P.O. Box 1881, Milwaukee, WI 53201
***E-mail: Charles.wilkie@marquette.edu**

Cucurbit[6]uril (CB[6]) was modified with dimethyldioctadecylammonium chloride (Cloisite 20A surfactant) then assembled with montmorillonite (MMT) to obtain CB[6]/Cloisite 20A-MMT. Both CB[6] and the MMT-modified CB[6] were evaluated as potential fire retardants in polystyrene, poly(methyl methacrylate) and polyurea. The morphologies of the composites were evaluated using X-ray diffraction; thermogravimetric analysis and cone calorimetry were used to study thermal stability and fire performance of the composites.

Introduction

CB[6] is an exceptionally robust macrocyclic host molecule that has a rigid cavity capable of binding small guests, including amines, under variety of conditions (*1*–*5*). CB[6] was first synthesized in 1905 by Behrend et al. (*6*) from acidic condensation of glycoluril with an excess of formaldehyde. Although this reaction was discovered more than one century ago, the unique molecular structure of cucurbituril was not determined until 1981 by Mock and Freeman (*7*). They found that it consists of a highly ordered and symmetrical macrocyclic structure of six glycoluril units linked by twelve methylene bridges and has enough room to host a variety of molecules. The fundamental binding properties of CB[6] - high affinity, highly selective and constrictive binding interactions - have been delineated by the pioneering work of the research groups of Mock and Freeman (*7*), Kim (*2*, *3*, *8*) and Buschmann (*1*, *4*, *5*), which has led to applications in waste-water remediation, as artificial enzymes and as molecular switches. In recent years, the cucurbit[n]uril family has grown to

In Fire and Polymers VI: New Advances in Flame Retardant Chemistry and Science; Morgan, A., et al.;
ACS Symposium Series; American Chemical Society: Washington, DC, 2012.

include homologues (CB[5]-CB[10]), prepared by the research groups of Kim and Day (*8–10*). There were a number of issues with the supramolecular chemistry of CB[6] early on, including poor solubility in aqueous and organic media, a lack of a homologous series of different sized hosts (CB[n]) and an inability to access CB[n] derivatives and analogues by tailor-made synthetic procedures. The CB[n] family has overcome all of these early issues and is now emerging as an outstanding platform for fundamental and applied molecular recognition and self-assembly studies. They possess a variety of properties (*11*) and show high potential in nanotechnology. These properties now include commercial availability in four different sizes, binding interactions of high affinity, high selectivity of binding, synthetic control over size, shape and functional-group placement, high structural integrity, solubility in both organic and aqueous solution, association and dissociation with controlled kinetics and control of the molecular recognition processes by suitable electrochemical, photochemical and chemical stimuli (*12*, *13*).

For the purposes of this work, the unique feature of the CB[n] family is their ability to bind amines. This potentially means that one can bind an ammonium salt within the CB cage and then use that to organically-modify clay. One of the great limitations in the world of polymer-clay nanocomposites is the compatibility between the organophilic polymer and the hydrophilic clay. By binding the ammonium salt that modifies the clay within the CB cage, it is anticipated that the clay will become less hydrophilic and thus more compatible with the polymer. Thus the initial premise of this work was that one might be able to obtain a more organophilic surfactant to organically-modify a montmorillonite-type clay and obtain better dispersed nanocomposites and hence systems with enhanced fire retardancy. Of course, the pristine CB[6] must be compared to these CB[6]-modified clays as well.

In this work CB[6] was assembled with different polymer matrices in order to investigate its fire retardant potential. CB[6] was used both as pristine material, as a control, and as the cage for the surfactant in a clay. The polymers selected for investigation include polystyrene (PS), poly(methyl methacrylate) (PMMA) and polyurea (PU), as representatives of the many possible classes of polymers that are available.

Experimental

Materials

The following materials were used as received: glycoluril (Sigma-Aldrich); paraformaldehyde, reagent grade (Sigma-Aldrich); 36% hydrochloric acid (EMD Chemicals); methanol, gradient grade for HPLC (Sigma-Aldrich); polystyrene (reagent grade), M_W=192,000; poly(methyl methacrylate), M_W=120,000; poly (tetramethylene oxide-di-p-amino benzoate) (Versalink P1000, Air Products); polycarbodiimide modified diphenyl methane diisocyanate (Isonate 143L, Dow Chemical); dimethyldioctadecylammonium chloride (Spectrum Chemical); sodium montmorillonite, Cloisite 20A (C20A, Southern Clay Products) and DMSO-D6 (Cambridge Isotope Lab. Inc.).

Preparation of CB[6]

CB[6] was prepared by the modification of one of the literature procedures (*10*). A 14 g portion of powdered glycoluril and 6 g of paraformaldehyde were mixed in a flask, then 90 mL of ice-cold 36% HCl was added with intensive stirring. After the solid material gradually dissolved, the solution, appearing as a clear gel, was heated to 100 °C in an oil bath overnight, producing a homogeneous solution. The solution was then poured into methanol and the resultant precipitate was collected by filtration and washed with portions of methanol, water, and again, methanol repetitively, three times. The precipitate was air-dried, and then overnight in vacuum oven at 80 °C. ^{1}H NMR: DMSO-D6 δ4.13 (d, 2H, *J*=15.5 Hz, CH_2), δ5.36 (s, 2H, CH), δ5.60 (d, 2H, *J*=15.5 Hz, CH_2).

Preparation of Complex of CB[6]/20A

A 10g portion of CB[6] (0.01mol) was suspended in 500 ml deionized water, then reacted with 5g dimethyldioctadecyl-ammonium chloride (0.01mol) at 50 °C for 24 h. The CB[6]/20A complex was filtered and washed with deionized water. This complex was first air-dried and afterwards overnight in vacuum oven at 50 °C.

Preparation of CB[6]/20A–MMT

5 g Cloisite Na^+ (NaMMT) was suspended in 500 ml deionized water, then reacted with 10 g of the CB[6]/20A complex (about 150% CEC value of NaMMT) at 50 °C for 24h. The CB[6]/20A modified MMT (CB-C20A) was filtered and washed with deionized water, dried at room temperature and then dried in vacuum oven at 50 °C.

Preparation of Polymer/CB[6]/20A-MMT

A 50 g mixture of PS or PMMA, fillers (either C20A, CB[6] at 3% loading or CB-C20A-MMT at 6% loading) was placed in a vacuum oven at 60 °C overnight prior to mixing. Then the mixtures were melt-blended in a Brabender Plasti-Cord at 200 °C for PS and 190 °C for PMMA at high rotor speed (60 rpm) for 30 min.

For polyurea, the fillers (1% C20A, 5% CB[6] or 1% CB-C20A) were stirred in the diamine for a few minutes, then the diisocyanate was added to the diamine and stirred once, finally the mixture was poured into a mold and allowed to set up following the normal protocol for this material (*14*).

Instrumentation

X-ray diffraction measurements (XRD) were performed on a Rigaku, Miniflex II desktop X-ray diffractometer with CuKα radiation (λ=1.54 Å) at a generator voltage of 30 kV and a current of 15 mA. Data acquisition was performed using a scan speed of 2°/min, at a step size of 0.05° from 2° to 40° (2θ).

Thermogravimetric analysis (TGA) was carried out on a TA instruments SDT Q600. Samples were heated from 30−700 °C at a scan rate of 10 K/min under an inert nitrogen atmosphere with a flow rate of 100 mL/min.

Cone calorimeter measurements were conducted on an Atlas CONE-2 instrument according to ASTM E 1354 at an incident flux of 35 kW/m^2(for PS and PMMA) and 50 kW/m^2 (for polyurea) using a cone shaped heater. The exhaust flow was set at 24 L/sec. Based on thousands of samples that have been run; the day-to-day error bars are ±10%. The specimens of PMMA and PS for cone calorimetry were prepared by compression molding of the sample (approximately 30 g) into 10 cm × 10 cm square plaques with thickness of 3 mm. PU cone plaques were prepared as described above.

NMR spectra were recorded on a Varian 400 MHz spectrometer.

Results and Discussion

Preparation of CB[6]

CB[6] has a robust cage structure (Figure 1) with high nitrogen content (33.7%) and a high degree of unsaturation (Ω=36 for CB[6]). It is almost insoluble in water but shows solubility in acidic solutions and in solvents containing salts. The ^{1}H NMR spectrum clearly shows that it has been synthesized. Likewise the incorporation of the surfactant is shown by NMR (Figure 2). The chemical shifts of the methyl groups on the nitrogen in the surfactant shift upfield while the other protons are unaffected by the CB[6]. This is a good indication that the methyl groups are contained within the CB[6] cage and the long chains extend outside of the cage (*15*, *16*).

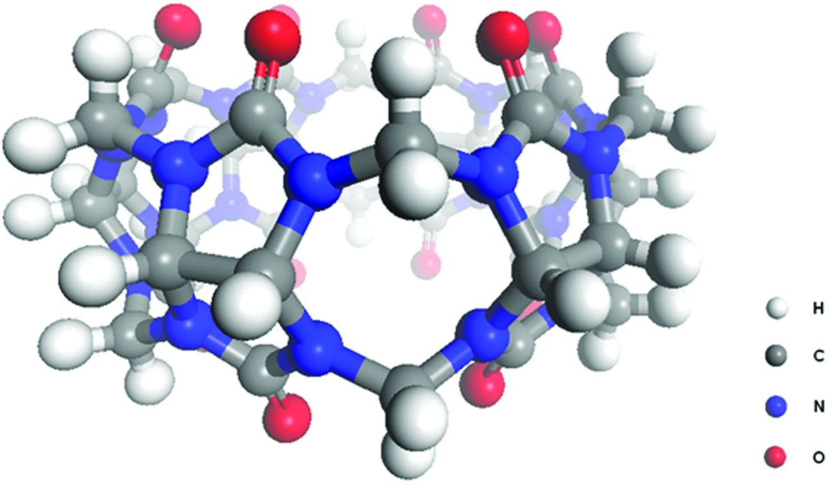

Figure 1. Structure of Cucurbit[6]uril (CB[6]).

PS- and PMMA Composites with CB[6]

XRD Results

The XRD traces for PMMA and PS combined with CB[6] are shown in Figure 3. Peaks are only seen for PMMA with the pristine clay, C20A, and with the CB-modified clay, CB-C20A. The d-spacing in pristine C20A is 2.42nm while in PMMA-C20A the d-spacing increases to 3.20 nm (2θ~2.7°). The XRD peak for PMMA-CB-C20A is at 2.49°, indicating an increase in the d-spacing. In CB-C20A the peak is smaller and broader than with the pristine C20A clay which likely indicates some increased disorder. The PS system, shown in Figure 1b, behaves similarly with strong indications of disorder.

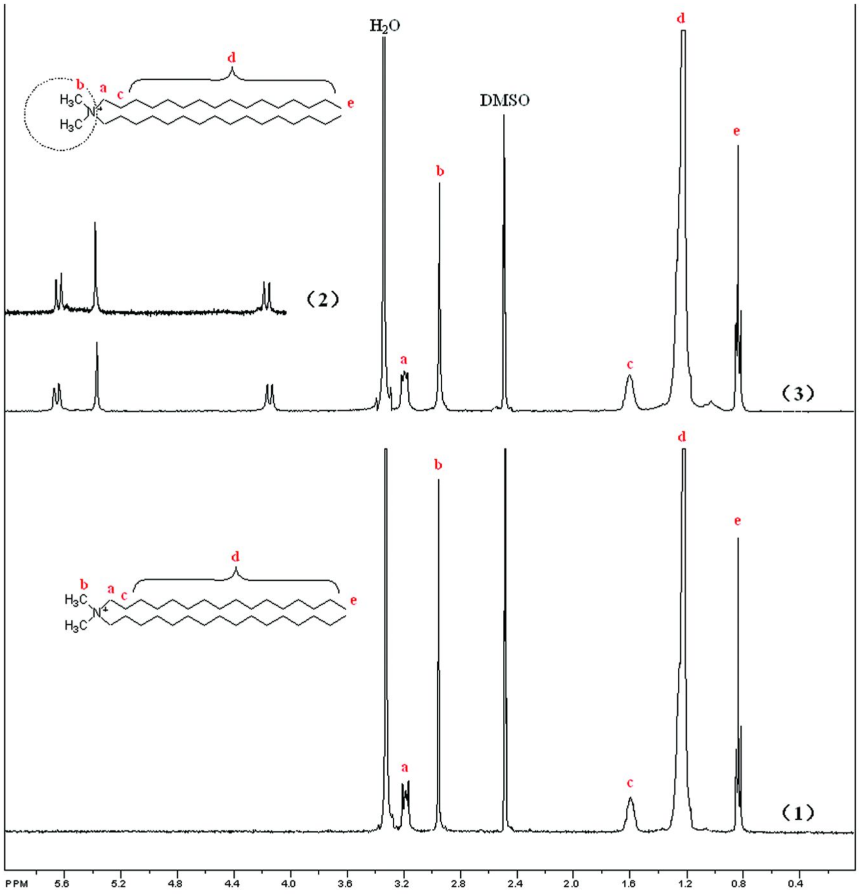

Figure 2. Comparison of ^{1}H NMR spectra in DMSO-D6 (1) 20A, (2) CB[6], (3) complex of CB[6]/20A.

Thermal Stability

It is regularly found that the thermal stability of a polymer-clay nanocomposite increases compared to that of the polymer and the results from this study are in accord with this statement (*17*, *18*).

The onset degradation temperatures for neat PMMA, PMMA/CB-C20A-6%, PMMA/CB[6]-3% and PMMA-C20A-3% are: 284, 297, 291 and 300 °C, respectively. The addition of pristine CB[6] brings about an increase in the onset degradation temperature of 7 °C and the clays, whether the surfactant is encased in the cage or not, give a larger increase. The 50% weight loss temperature follows the same trend but there is less difference (Figure 4a). For the PS system, there is not much change in the onset temperature but both C20A and CB-C20A bring about an increase in the 50%degradation temperature (Figure 4b).

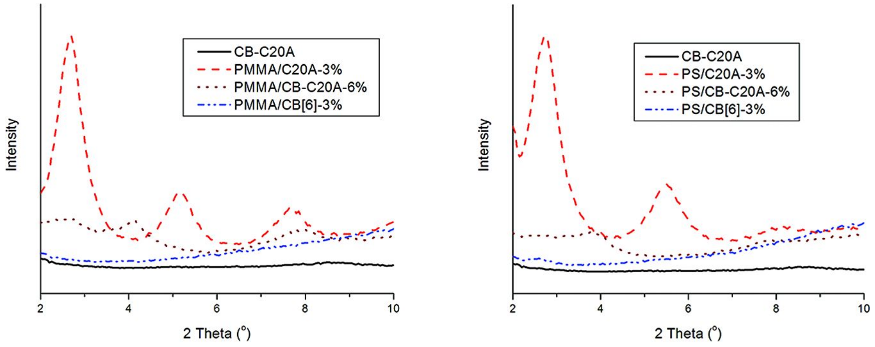

a b

Figure 3. X-ray diffraction patterns taken on the compression-molded surfaces of PMMA (a) and PS (b) series.

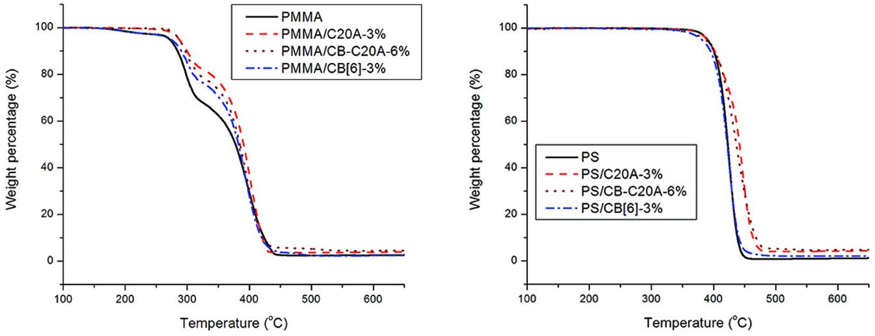

a b

Figure 4. TGA plots of PMMA (a) and PS (b) series.

Table I. Cone Calorimetry at 35 kW/m^2 for PMMA and PS

Sample	*t_{ig} (s)*	*PHRR(kW/m^2) (% red)*	*THR (MJ/m^2)*	*MLR (g/m2s)*	*ASEA (m^2/kg)*
PMMA	20±1	971±12 (--)	93±1	31±1	138±8
PMMA/CB-C20A-6%	19±1	854±16 (12)	91±2	27±1	142±7
PMMA/ C20A-3%	21±1	726±10 (25)	91±1	23±0	181±14
PMMA/ CB[6]-3%	8±1	762±14 (21)	82±2	26±1	146±7
PS	38±1	1389±47 (--)	100±1	35±2	1166±22
PS/CB-C20A-6%	28±1	1189±11 (14)	92±2	29±1	1199±12
PS/C20A-3%	39±2	946±37 (32)	89±1	28±1	1221±26
PS/CB[6]-3%	19±1	1204±77 (13)	96±1	30±1	1284±37

Cone Calorimetry Results

Cone calorimetry is generally considered to be the most effective laboratory method to evaluate the fire properties of polymers. Using this technique, one can evaluate the time to ignition (t_{ig}); the rate of heat release (*i.e.*, the size of the fire), and especially its peak value (PHRR); the total heat released (THR), the average mass loss rate (AMLR); and the specific extinction area (ASEA), a measure of the amount of smoke released. With polymer-clay nanocomposites, the usual observations are that the time to ignition is decreased while the PHRR is reduced and the reduction is roughly proportional to the change in the mass loss rate and the total heat released, *i.e.*, how much polymer is burned, is unchanged. The data for this system is shown in Table I and the heat release rate curves are displayed in Figure 5. For PMMA, there is a significant reduction in the PHRR upon the addition of CB[6] and Cloisite 20A separately but a rather poor reduction when CB-C20A, the caged surfactant clay, is used. It is rather surprising that CB-C20A is not effective since it is as effective as C20A in enhancing thermal stability. It is equally surprising that pristine CB[6] has an effect which is quite similar to that of the C20A clay. One also observes that with CB[6] the total heat released also falls. From the mass loss rate data, one may conclude that CB[6] does not function in the same way as does a clay, which is by reducing the mass loss rate. The time to ignition appears to be relatively unaffected by the two clays while when only CB[6] is added, t_{ig} shows a large reduction, which is typical of many additives (*19*).

The results for PS are similar, but here neither pristine CB[6] nor the CB[6] caged MMT is effective.

Photographic images of the chars after cone calorimetric analysis are shown in Figure 6. The greatest amount of char is seen with Cloisite 20A and the least is seen for CB[6] alone in PS. One might expect that a similar amount of char would be seen for both clays but this is not the case. The inorganic fraction is smaller with the CB-caged surfactant clay and therefore this shows less residue.

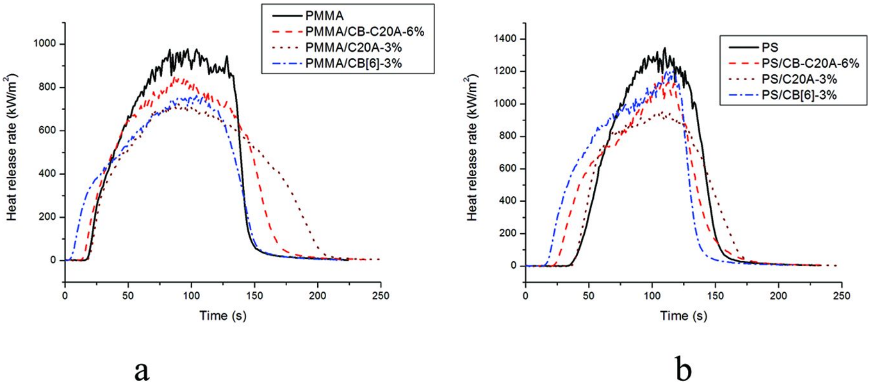

Figure 5. Heat release rate curves for melt blended PMMA (a) and PS (b) series at 35 kW/ m^2.

Polyurea Composites with CB[6]

In previous work from these laboratories, it has been shown that a suitable fire retardant package for polyurea must contain several components; the most useful of these components appear to be ammonium polyphosphate (APP) and expandable graphite (EG) (*14*). Thus in this study, CB[6] has been combined with APP in order to evaluate the performance. Both pristine CB[6] and the CB-C20A clay have been used.

Thermal Stability

Thermal stability has been evaluated through thermogravimetric analysis and the TGA curves of the pristine CB[6] in PU are shown in Figure 7 with the data in Table II. Both CB[6] and APP filled samples shows earlier degradation with a more pronounced two-step degradation process and the thermal stability of PU is decreased in both cases. The CB[6] filled sample shows slightly higher thermal stability between 350 and 450 °C and the amount of char retained at high temperature is quite close to that in the APP filled sample. There is no change in onset temperature ($T_{10\%}$) of PU filled with either CB[6] or APP and its mixture, while the maximum degradation temperature (T_{max}) of the CB[6] filled sample is higher than that of the APP filled and mixed sample. There is no change in the amount of char residue at higher temperature when combined with CB[6] and APP, which indicates that there is no interaction with CB[6] and APP.

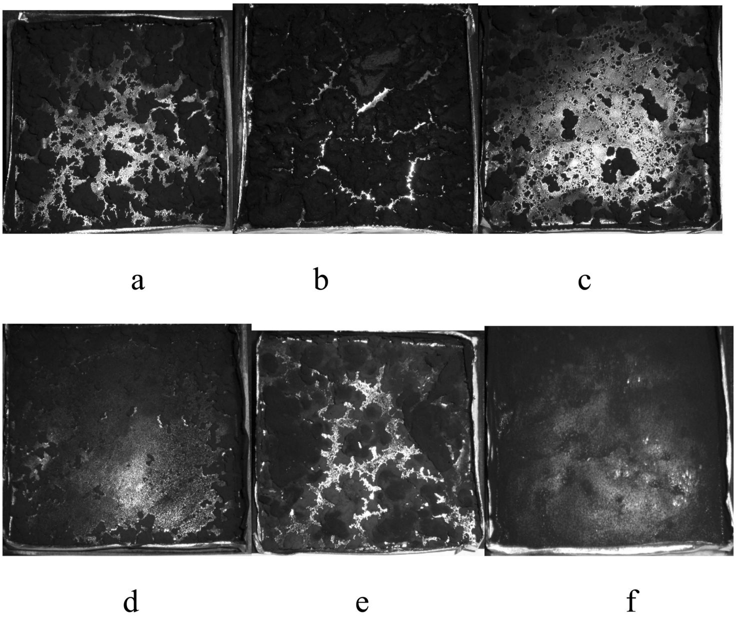

Figure 6. Char morphology of PMMA and PS series after cone tests: (a) PMMA/CB-C20A-6%, (b) PMMA/C20A-3%, (c) PMMA/CB[6]-3%, (d) PS/CB-C20A-6%, (e) PS/C20A-3%, (f)PS/CB[6]-3%.

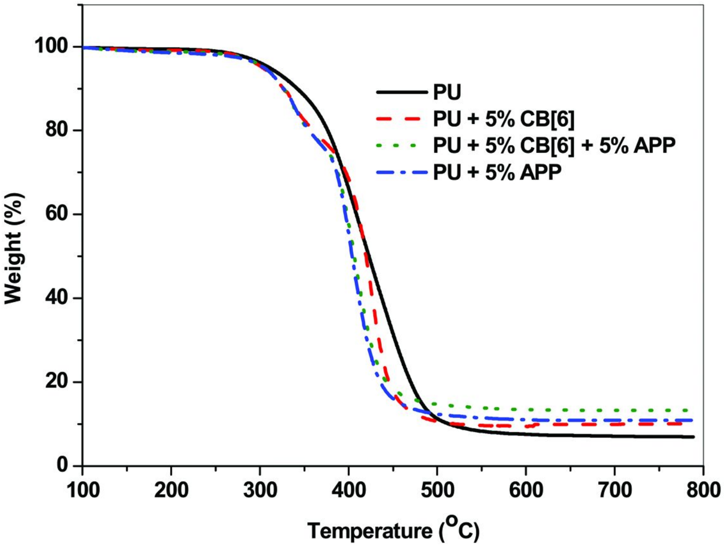

Figure 7. TGA of polyurea filled with CB[6] + APP.

Figure 8 shows the TGA curves for PU filled with CB-C20A modified clay and its blend with APP and EG. There is no change in degradation pattern of PU upon the addition of either CB-C20A clay or the clay with APP and/or EG and no significant changes in the onset temperature and T_{max} (Table III). The small changes in residue can be attributed to the presence of the various additives.

Table II. Effect of CB[6] + APP on the thermal properties of polyurea

Sample	*$T_{10\%}$ (°C)*	*T_{max} (°C)*	*% Char at 700 °C*
Polyurea (PU)	333	426	7.6
PU + CB[6] (5%)	326	426	10.0
PU + CB[6] (5%) + APP (5%)	327	407	13.3
PU + APP (5%)	327	403	10.9

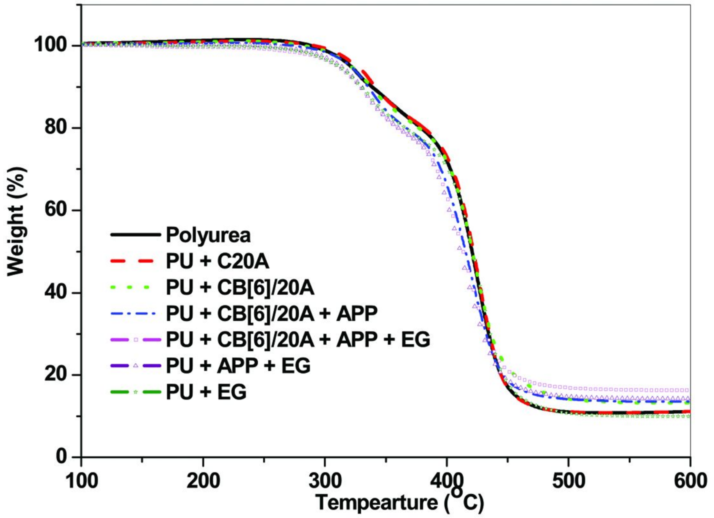

Figure 8. TGA of polyurea filled with CB-C20A modified clay + FR.

Cone Calorimetry

The influence of CB[6] on the flammability of PU has been investigated using cone calorimetry at 50 kW/m^2 external heat flux. The cone calorimetric data is given in Table IV and the heat release rate curves are in Figure 9. There is a strong reduction in the peak heat release rate curves when CB[6], APP or the combination of APP and CB[6] are present. For pristine PU, a two-step process is seen with the second step, the degradation of the soft segments (*14*), much more pronounced. When the additives are present, the two steps are somewhat smeared together. The time to ignition shows a small decrease but this is not as large as seen with the thermoplastics above. It is surprising that the total heat released shows a significant decrease when CB[6] is added to PU.

Table III. Effect of CB-C20A on the thermal properties of FR filled PU

Sample	*$T_{10\%}$ (°C)*	*T_{max} (°C)*	*% Char at 700 °C*
Polyurea (PU)	339	425	12.0
PU + 1% C20A	341	427	11.9
PU + 1% CB[6]-C20A	338	422	13.8
PU + 1% CB[6]-C20A + 5% APP	335	420	14.1
PU + 1% CB[6]-C20A + 5% APP + 2% EG	329	418	16.9
PU + 5% APP + 2% EG	330	411	14.7
PU + 2% EG	330	427	10.3

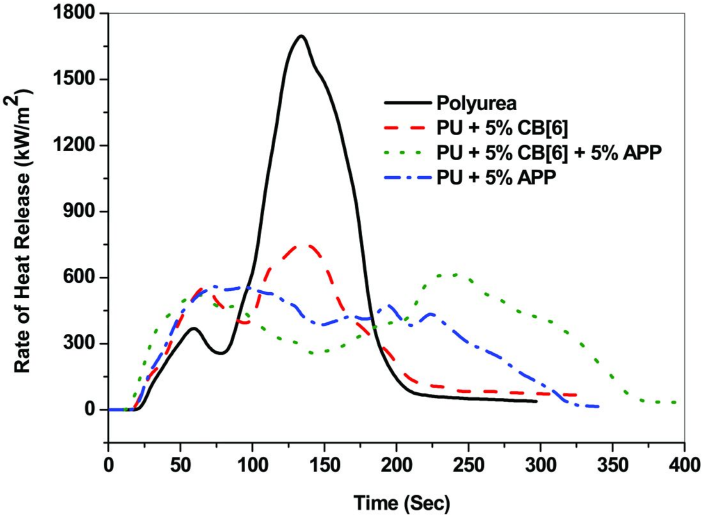

Figure 9. HRR curves of PU filled with CB[6] + APP.

The cone results for the samples containing the CB-C20A are presented in Table V with the heat release rate curves in Figure 10. It is clear that there is no advantage to the utilization of the CB-C20A compared to either C20A or the other additives. One may summarize this data by saying that the use of APP and EG in polyurea gives a good reduction in the PHRR with the expected changes in other properties and that the addition of the CB-C20A clay has no effect.

Table IV. Cone calorimetric data for PU filled with CB[6] + APP

Sample	*t_{ig} (s)*	*P_{HRR} (kW/m^2) (% red)*	*THR (MJ/m^2)*	*AMLR (g/m^{2}s)*	*ASEA (m^2/kg)*
Polyurea (PU)	21 ± 1	1689 ± 122	140 ± 7	30 ± 3	481 ± 26
PU +CB[6](5%)	16 ± 1	776 ± 161 (54)	95 ± 10	20 ± 3	577 ± 15
PU + CB[6](5%) + APP(5%)	13 ± 1	766 ± 148 (55)	125 ± 26	16 ± 1	660 ± 53
PU + APP (5%)	15 ± 3	598 ± 53 (65)	120 ± 13	17 ± 2	626 ± 20

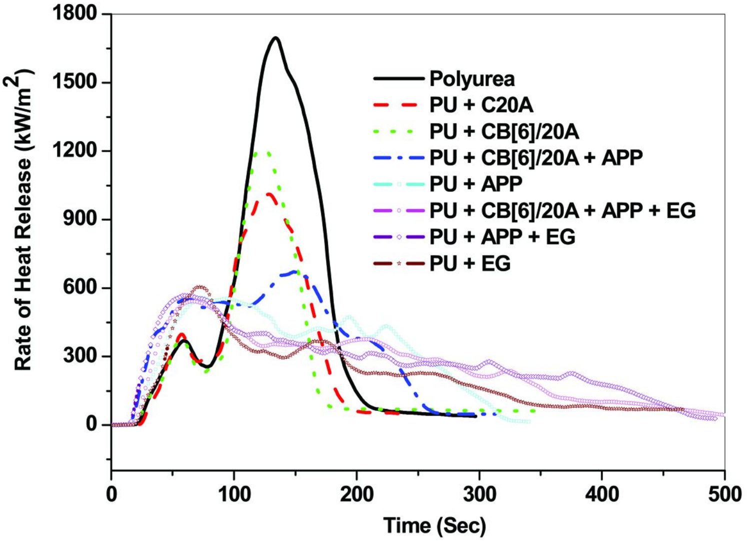

Figure 10. HRR curves of PU filled with CB[6]-20A + FR.

The dispersion of the clays in the various polymers has not been evaluated. It is well-known that with montmorillonite-type clays, there is no reduction in the PHRR unless the clay is well-dispersed and in this work it is clear that the CB[6]-C20A clays are not well-dispersed.

Table V. Cone data of PU filled with CB-C20A modified clay and FR

Sample	*t_{ign} (s)*	*P_{HRR} (kW/m^2) (% reduction)*	*THR (MJ/m^2)*	*AMLR (g/m^{2}s)*	*ASEA (m^2/kg)*
Polyurea (PU)	21 ± 1	1689 ± 122	140 ± 7	30 ± 3	481 ± 26
PU + 1% C20A	24 ± 3	1015 ± 34 (40)	105 ± 8	20 ± 4	476 ± 67
PU + 1% CB[6]-C20A	19 ± 2	1153 ± 62 (32)	99 ± 14	22 ± 6	576 ± 55
PU + 1% CB[6]-C20A + 5% APP	16 ± 1	581 ± 92 (66)	112 ± 12	17 ± 2	632 ± 42
PU + 5% APP	15 ± 3	598 ± 53 (65)	120 ± 13	17 ± 2	626 ± 20
PU + 1% CB[6]-C20A + 5% APP + 2% EG	16 ± 2	545 ± 6 (68)	127 ± 3	15 ± 2	542 ± 64
PU + 5% APP + 2% EG	14 ± 1	561 ± 14 (67)	133 ± 3	13 ± 1	731 ± 13
PU + 2% EG	18 ± 2	594 ± 46 (65)	122 ± 20	11 ± 2	573 ± 53

Conclusions

The initial premise of this work was that one might be able to make the gallery space of a clay more organophilic and increase the size of this gallery space by caging the surfactant used to modify the clay within a CB[n] cage. This premise was not realized and while the d-spacing may have slightly increased, there is no evidence to suggest that this clay is better than conventional organically-modified clays, such as the Cloisite family of modified clays. It is most unlikely that the CB[6]-modified clays are well-dispersed in any of the polymers herein studied.

On the other hand, it appears that the use of CB[6] alone as an additive with both PMMA and polyurea has an effect on the fire properties of the polymers. Thus the idea which led to this work is not realized but it seems that there is some benefit from CB[6]. It is unlikely that CB[6] can be used alone as a suitable fire retardant for a polymer but it may be a component of a fire retardant package. Further work is required on this topic.

Acknowledgments

This work has been partially supported by The U.S. Air Force under Grant No. FA8650-07-1-5901 and by the U.S. Department of Commerce, National Institute of Standards and Technology under Grant No. 70NANB10H224, and this support is gratefully acknowledged.

References

1. Buschmann, H. J.; Jansen, K.; Schollmeyer, E. *Thermochim. Acta* **1998**, *317*, 95–98.
2. Jeon, Y. M.; Kim, J.; Whang, D.; Kim, K. *J. Am. Chem. Soc.* **1996**, *118*, 9790–9791.
3. Jeon, Y. M.; Whang, D.; Kim, J.; Kim, K. *Chem. Lett.* **1996**, 503–504.
4. Meschke, C.; Buschmann, H. J.; Schollmeyer, E. *Polymer* **1998**, *40*, 945–949.
5. Meschke, C.; Buschmann, H. J.; Schollmeyer, E. *Thermochim. Acta* **1997**, *297*, 43–48.
6. Behrend, R.; Meyer, E.; Rusche, F. *Liebigs Ann. Chem.* **1905**, *339*, 1–37.
7. Freeman, W. A.; Mock, W. L.; Shih, N. Y. *J. Am. Chem. Soc.* **1981**, *103*, 7367–7368.
8. Kim, J.; Jung, I. S.; Kim, E.; Lee, J. K.; Kang, S.; Sakamoto, K.; Yamaguchi, K.; Kim, K. *J. Am. Chem. Soc.* **2000**, *122*, 540–541.
9. Day, A. I.; Blanch, R. J.; Arnold, A. P.; Lorenzo, S.; Lewis, G. R.; Dance, I. *Angew. Chem.* **2002**, *114*, 285–287.
10. Day, A. I.; Arnold, A. P.; Blanch, R. J.; Snushall, B. *J. Org. Chem.* **2001**, *66*, 8094–8100.
11. Lagona, J.; Mukhopadhyay, P.; Chakrabarti, S.; Isaacs, L. *Angew. Chem.* **2005**, *44*, 4844–4870.
12. Karcher, S.; Kornmuller, A.; Jekel, M. *Water. Res.* **2001**, *14*, 3309–3316.
13. El Haouaj, M.; Luhmer, M; Ho, Y.; Kim, K.; Bartik, K. *J. Chem Soc., Perkin Trans.* **2001**, *35*, 3309–3316.
14. Awad, W.; Wilkie, C. A. *Polymer* **2010**, *51*, 2277–2285.
15. Montes-Navajas, P.; Garcia, H. *J. Phys. Chem. C* **2010**, *114*, 2034–2038.
16. Kim, S.; Lee, J. W.; Han, S. C.; Kim, K. *Bull. Korean Chem. Soc.* **2005**, *26*, 1265–1268.
17. Gilman, J. W. *Appl. Clay Sci.* **1999**, *15*, 31–49.
18. Zhu, J.; Uhl, F. M.; Morgan, A. B.; Wilkie, C. A. *Chem. Mater.* **2001**, *13*, 4649–4654.
19. Morgan, A. B.; Bundy, M. *Fire Mater.* **2007**, *31*, 257–283.

In Fire and Polymers VI: New Advances in Flame Retardant Chemistry and Science; Morgan, A., et al.;
ACS Symposium Series; American Chemical Society: Washington, DC, 2012.

Chapter 6

A Comparative Study of the Fire Retardant Effect of Several Metal-Based Compounds Added to an Epoxy-Amine Thermoset

Charles Manzi-Nshuti, Yingji Wu, and Sergei Nazarenko*

School of Polymers and High Performance Materials,
University of Southern Mississippi, 118 College Drive,
Hattiesburg, Mississippi 39406
***E-mail: sergei.nazarenko@usm.edu**

Several metal containing compounds such as layered double hydroxide of cobalt aluminum dodecanoate, cobalt (II, III) oxide, zinc acetate dihydrate, and cobalt acetate tetrahydrate have been evaluated as fire-retardant additives for a standard epoxy-amine thermoset polymer system. A cone calorimeter was used to evaluate the fire behavior properties of the composites at an external heat irradiation of 50 kW/m^2. The layered double hydroxide and the metal oxide were found to be rather ineffective fire retardant additives for the epoxy-amine thermoset. In contrast, both hydrated salts performed surprisingly well. The efficacies of metal salts of zinc acetate and cobalt acetate were correlated with the formation of a metal oxide inorganic layer that covered the surface of the underlying polymer under fire conditions. This morphology slowed the release of any flammable volatiles and reduced the heat transfer to the degrading polymer.

Introduction

Epoxy-based resins are commonly used for applications including adhesives, coatings and advanced composites in the aerospace and electronics industries (*1*–*4*). However, the poor fire resistance properties of epoxy-based polymers is a crucial technical disadvantage. Consequently, multiple efforts have been undertaken to enhance the fire properties of these polymer systems. Epoxy systems

In Fire and Polymers VI: New Advances in Flame Retardant Chemistry and Science; Morgan, A., et al.;
ACS Symposium Series; American Chemical Society: Washington, DC, 2012.

can be rendered fire retardant either by incorporation of fire retardant additives (e.g. triphenyl phosphate (*5*), 9,10-dihydro-9-oxa-10-phosphaphenanthrene 10-oxide (DOPO) (*6*), decabromo diphenylether (*7*), aluminum ethyl phosphinate (*8*)) or by copolymerization with reactive fire retardants (e.g. diglycidylether of tetrabromobisphenol A) (*9*). Due to recent ecological and health concerns, however, a general tendency towards banning halogen based fire-retardants has been observed. This gives rise to extensive research activities that are aimed at replacing these substances.

An analysis of the wealth of relevant scientific publications shows that metal-based compounds have the potential to become the next generation of effective flame retardant additives for polymers (*10–12*). However, if a substance contains metal atoms, it is impossible to state a priori, whether or not it will exhibit the desired flame retardancy effect in a particular polymer system. Many factors control the effect of these compounds in polymer combustion including the nature of the metal, degree of oxidation, type of compound, manner of introduction into the polymer, concentration level, dispersion state, conditions of combustion and pyrolysis and the nature of the polymer (*13*). This field is still in its embryonic stage but recent studies have shown that an understanding of the mechanisms of action of these materials will facilitate the production of materials with enhanced fire performance.

Recently, Morgan (*10*) in his review article summarized the recent findings on fire retardancy effectiveness of metal oxides, metal salts and metal complexes. He highlighted that there appeared to be a lot of promise in this diverse group of flame retardant additives which utilize a wide range of chemistries and solid state structures to induce either char formation or highly effective vapor phase free radical inhibition for the burning plastic. In particular, he pointed out a study by Yang *et al.* (*14*) that showed that small concentrations of nickel phosphate (2 wt.%) can allow for the replacement of 7 wt.% of the intumescent FR system while maintaining a UL-94 V-0 result. Prior to that study, Lewin and Endo (*15*) observed that small concentrations of several divalent and multivalent metallic compounds in the range of 0.1-2.5 wt.% catalyzed intumescent flame retardancy of polypropylene. In that study, it was noted that the extent of the observed catalytic effect varied with the metal ion applied.

Another type of metal-based additives, the layered double hydroxides (LDHs), have also been investigated as potentially novel and effective fire retardant additives for polymers (*16*, *17*). The LDH structure is described with the ideal formula $[M^{II}_{1-x}M^{III}_{x}(OH)_2]_{intra}[A^{m-}_{x/m}.nH_2O]_{inter}$, where M^{II} and M^{III} are metal cations, A^{m-} is the anion of charge m-, and intra and inter denote the intralayer domain and the interlayer space, respectively (*18*). With poly(methyl methacrylate) (PMMA), in which the LDH is well-dispersed, a peak heat release rate (PHRR) reduction of 50% over the pristine polymer was obtained in cone calorimeter studies (*19*). A correlation between PHRR reduction and the morphology of the char residues was observed. This char formed a compact residue that covered the entire surface of the aluminum foil holding the sample. It is likely that this char layer serves as a barrier for the heat transfer and slows the transport of combustible volatiles thus leading to considerable enhancement of the fire resistance.

The common theme in the relevant literature reports on the fire retardancy properties of polymeric systems modified with metal-based compounds is the lack of complete understanding of the mechanisms of actions of these additives. However, all authors recognize the great deal of potential associated with the use of metallic compounds due to the numerous chemical compounds commercially available or obtainable through chemical synthesis. The goal of this study was to evaluate a potential use of several metal-containing compounds such as cobalt oxide, cobalt aluminum layered double hydroxide, and hydrated metal salts of zinc and cobalt as fire retardant additives for a standard epoxy-amine thermoset polymer.

Experimental

Zinc acetate dihydrate [$Zn(C_2H_3O_2)_2.2H_2O$] (ZnAc), cobalt acetate tetrahydrate [$Co(C_2H_3O_2)_2.4H_2O$] (CoAc) and cobalt (II,III) oxide nanopowder (CoOnano) with a reported characteristic particle size smaller than 50 nm, were purchased from Aldrich Chemical Company and used as received. Layered double hydroxide of cobalt aluminum dodecanoate (CoAl) was synthesized via coprecipitation as reported elsewhere (*20*). The ratio of the metals, cobalt to aluminum, was maintained at 2 to 1. The structure and composition of the synthesized CoAl was confirmed by powder X-ray diffraction (XRD), Fourier transform infrared spectroscopy (FTIR) and thermogravimetric analysis (TGA).

EPON 826, a low viscosity liquid epoxy resin often used in coatings and composite applications with an epoxy equivalent weight of 178-186 grams was supplied by Hexion and used as received. The hardener, Jeffamine D230, with an amine equivalent weight of 60 grams, was supplied by the Huntsman Corporation and also used as received.

The composites were prepared as follows: the additives were mixed directly in bisphenol A epoxy resin for several minutes at 60 °C. The additives were dispersed with a mechanical stirrer. The hardener was added to the mixture in a stoichiometric amount and stirring continued for an additional 30 minutes at room temperature before the contents were poured into a mold. The samples were cured at 80 °C for 12 hours and post cured at 135 °C for an additional 3 hours. Prior to curing, the mold containing the mixed reactants was degassed in vacuum to remove any trapped air. The prepared compositions are listed in Table 1.

The glass transition temperature values for various epoxy/amine composites were obtained using a TA instruments Q1000 DSC at a heating rate of 10 °C/min. The sample size was maintained between 7 and 10 mg. Tg value was taken as the midpoints of the inflection from DSC scans. The additives exhibited no effect on the extent curing as confirmed by the fact that the glass transition of the composites was the same as of the epoxy-amine control. In addition, the consecutive DSC runs of the composites showed no difference in Tg from scan to scan. A TA instruments Q500 thermogravimetric analyzer (TGA) was used to evaluate the thermal stability of the networks and the additives. The samples (~10 mg) were tested in air or nitrogen environments at a heating ramp rate of 10 °C/min from 25 to 600 °C.

In Fire and Polymers VI: New Advances in Flame Retardant Chemistry and Science; Morgan, A., et al.;
ACS Symposium Series; American Chemical Society: Washington, DC, 2012.

Cone calorimeter measurements were performed with the Govmark cone instrument according to ASTM E 1354 using a cone shaped heater with an incident flux set at 50 kW/m^2. The exhaust flow was set at 24 L/s and the spark was turned on continuously until the sample was ignited. Typically the data generated by a cone are quite reproducible with an uncertainty which does not exceed ± 10% (*21*). A set of fire-relevant parameters can be obtained using the cone calorimeter including the peak heat release rate (PHRR), average mass loss rate (AMLR), average specific extinction area (ASEA), time to ignition (t_{ig}), carbon monoxide yield, and specific heat of combustion.

Table 1. Studied Compositions

Formulation	*Additive (wt.%)*
Epoxy/amine control	0
Epoxy/amine/a% CoAl	a = 4 , 7
Epoxy/amine/b% CoOnano	b = 4 , 7
Epoxy/amine/c% CoAc	b = 4 , 7
Epoxy/amine/d% ZnAc	c = 4 , 7 , 13 , 18 , 27

Results and Discussion

This section begins with a report on the flame retardant potential of a layered double hydroxide and a metal oxide additive in an epoxy/amine thermoset polymer. The efficacy of hydrated metal salts of zinc acetate and cobalt acetate dispersed in the same polymer is discussed next. This work enables a comparative study on the flame retardant potential of the different metal-containing additives in an epoxy/amine system.

Layered Double Hydroxide and Metal Oxide

Cobalt–aluminum dodecanoate LDH (CoAl) was added to an epoxy/amine thermoset, as described in the experimental section, and the samples were tested in the cone. Figure 1 shows the heat release rate curves for the pristine epoxy/amine and its LDH composites containing 4% and 7% wt/wt of the mineral phase. The reduction in the PHRR, as compared to the pure polymer, was only 22% with 7% wt/wt of LDH. Figure 2 shows the char remaining after epoxy/amine and epoxy/amine/7%CoAl samples were burned in the cone. Adding LDH apparently did not enhance the char formation. The virgin epoxy/amine sample yielded a rather small amount of residue accounting for only 1 wt.% of the original sample mass. In addition to the carbonaceous residue, one can also clearly see traces of an inorganic phase, the residue of the LDH. Very modest enhancement of the fire retardant properties of the epoxy/amine/CoAl systems was attributed to the rather poor LDH dispersion in the polymer matrix. The epoxy/amine composites of CoAl were opaque even at low concentration while the pure epoxy/amine control sample was transparent. LDH exhibited a pronounced sedimentation caused by gravity leading to a rather heterogeneous dispersion state when top and bottom of samples are compared. The samples though were consistently tested with the same side oriented towards the heat flow. Poor LDH phase dispersion was related to low viscosity of the original epoxy resin which prevented the dispersion of the layered stacks beyond the primarily particle size. It is clear based upon these observations that one can anticipate further enhancement in fire properties once the improvement in the dispersion state of the LDH additive in this polymer can be achieved.

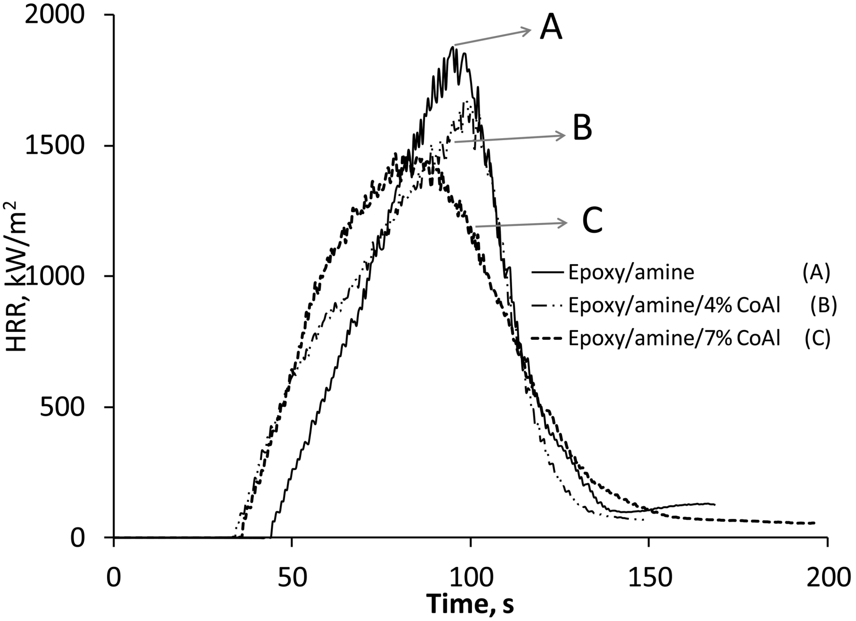

Figure 1. Heat release rate curves for the pristine epoxy/amine thermoset and the resin modified with different amounts of CoAl layered double hydroxide conducted at an external irradiation 50 kW/m².

Cobalt oxide has also been added to the epoxy/amine system and the fire behavior properties of the corresponding composites evaluated in the cone. Figure 3 displays the corresponding heat release rate curves for epoxy/amine control and also the resins containing different amounts of CoOnano. From the cone data, one can see only a minimal, less than 10% at best, improvement of PHRR. Thermal degradation studies are required to further understand how this additive interacts with the polymer matrix and help explain the poor performance observed for this set of samples.

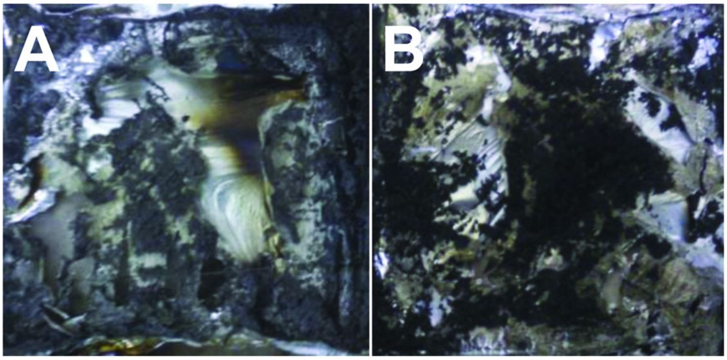

Figure 2. Images of the residues for (A) epoxy/amine and (B) epoxy/amine/7%CoAl samples after cone testing.

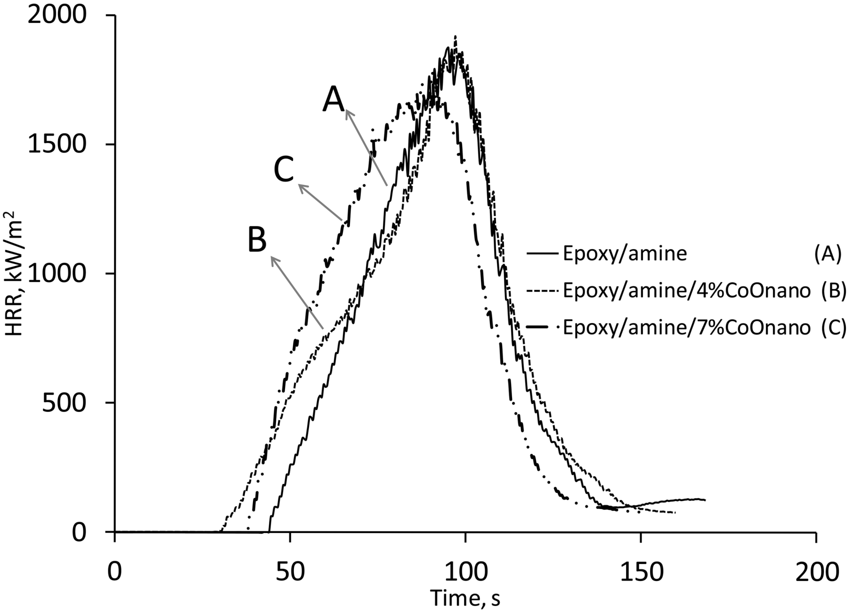

Figure 3. Heat release rate curves for epoxy/amine control and resins modified with CoO nanopowder conducted at an external irradiation of 50 kW/m².

Table 2. Cone data summary for epoxy/amine systems containg ZnAc

Matrix	t_{ig} *[s] ± 4*	*PHRR [kW/m^2] ± 70*	*THR [MJ/kg] ± 1*	*AMLR [g/m^2.s] ± 1.6*	*EHC [MJ/kg] ± 0.5*	*Residue [%] ± 0.7*	*ASEA [m^2/kg] ± 23*
Epoxy/amine	42	1861	93	45.5	31.0	1.2	759
Epoxy/amine/7 %ZnAc	38	1015	81	28.2	29.9	11.3	635
Epoxy/amine/13%ZnAc	36	846	77	24.3	30.1	14.4	631
Epoxy/amine/18%ZnAc	29	853	73	24.8	29.3	15.9	623
Epoxy/amine/27%ZnAc	20	607	73	17.0	29.5	17.9	608

Note: t_{ig}, time to sustained ignition; PHRR, peak heat release rate; THR, total heat released; AMLR, average mass loss rate; EHC, Average effective heat of combustion; ASEA, average specific extension area.

Hydrated Metal Salts

The use of metal salts to enhance the fire retardant properties of polymers has only recently caught researchers' attention. Kashiwagi *et al.* prepared clay-based SAN nanocomposites with zinc chloride as the catalyst (*11*). They observed a large improvement in the PHRR relative to the control polymer, but their results indicated that the two additives (clay and zinc chloride) were contributing independently. In our work, a question was posed of whether the fire retardancy properties of an epoxy-amine thermoset can be enhanced by only adding a halogen-free metal containing salt.

Therefore, zinc acetate dihydrate (ZnAc) was added to the epoxy/amine thermoset polymer. ZnAc formed a microdispersion in the epoxy-amine thermoset. With a naked eye, small, microscopic inclusions could be observed near the surface. The fire behavior properties of the epoxy/amine composites of ZnAc were evaluated in the cone calorimeter at an external heat flux of 50 kW/m^2. The cone data are summarized in Table 2. Epoxy/amine resins containing different amounts of ZnAc revealed significant reductions of the PHRR values. The fire retardant effect of ZnAc additives is fairly strong. Adding only 4% wt. of ZnAc led to 36% of PHRR reduction. Adding 7 wt.%, 13 wt.%, 18 wt.% and 27 wt.% resulted in 46%, 55%, 54% and 67% reductions of PHRR values as compared to the unmodified control respectively. The time to ignition however gradually decreased with increasing ZnAc content. The reduction of the time to ignition showed a correlation with the thermal stability data. The TGA experiments revealed that the thermoset polymer containing ZnAc starts decomposing at lower temperature as compared to the pure epoxy-amine control. It should be noted here that ZnAc melts and decomposes at considerably lower temperatures than the polymer in the composites. Somehow ZnAc or the products of its degradation promote earlier degradation of the epoxy-amine polymer.

The heat release rate curves of both the unfilled polymer and the various epoxy/amine composites of ZnAc are provided in Figure 4. The HRR curve for the pure epoxy/amine sample showed a sharp, narrow peak, indicative that the sample was pyrolyzed fairly rapidly. This cone behavior was in accord with the classical patterns typical of weakly charring samples (*22*). With addition of ZnAc, the shape of HRR curves for the composites changed towards the behavior associated with the formation of a very resistant char barrier layer on the surface of the burning polymer. Figure 5 shows images of the cone test residues for the epoxy-amine control and the sample containing 7% of ZnAc. Adding ZnAc led to the formation of a char layer upon ignition that is enriched on the surface with crystalline ZnO, an inorganic product of the thermal decomposition of ZnAc, making the whitish surface appearance of the composites after burning. Formation of crystalline ZnO was confirmed by WAXD, and it is generally known that zinc oxide is a white substance. With the addition of more ZnAc, the whitish surface layer became much denser, with lesser vent holes observed on the char surface. Apparently this whitish zinc oxide char layer formation on the top of the degrading polymer matrix contributes to the fire resistance as it prevents the entry of flammable gases into the gas phase and insulates the underlying polymer from the flame (*23*). A question can be posed as to how ZnO micro particulates reach the surface and concentrate there. Inspecting the char residue bulk morphology suggests the presence of small bubbles which form a cellular structure within the char residues. It is quite possible that these small bubbles formed by the products of degradation or water released upon melting of zinc acetate dihydrate in the cone experiment lead to the convectional flow which carries the zinc oxide particles to the surface of the burning polymer.

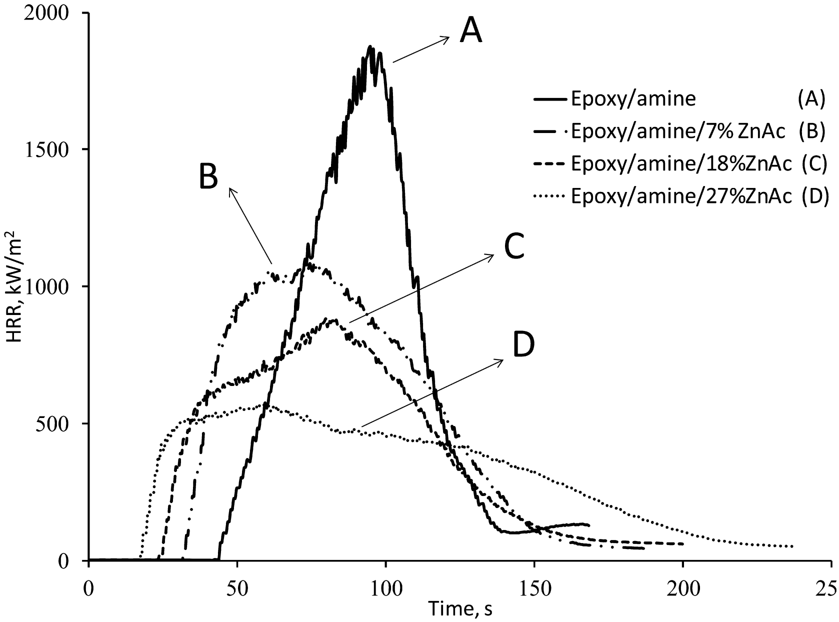

Figure 4. Heat release rate curves of epoxy/amine thermoset containing different amounts of ZnAc.

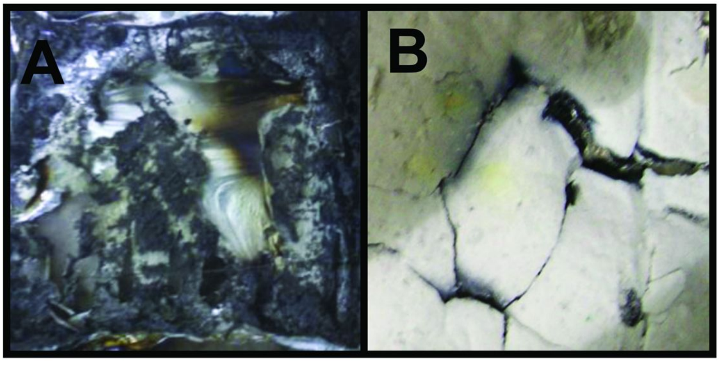

Figure 5. Images of the char residues for: (A) epoxy/amine and (B) epoxy/amine/7%ZnAc.

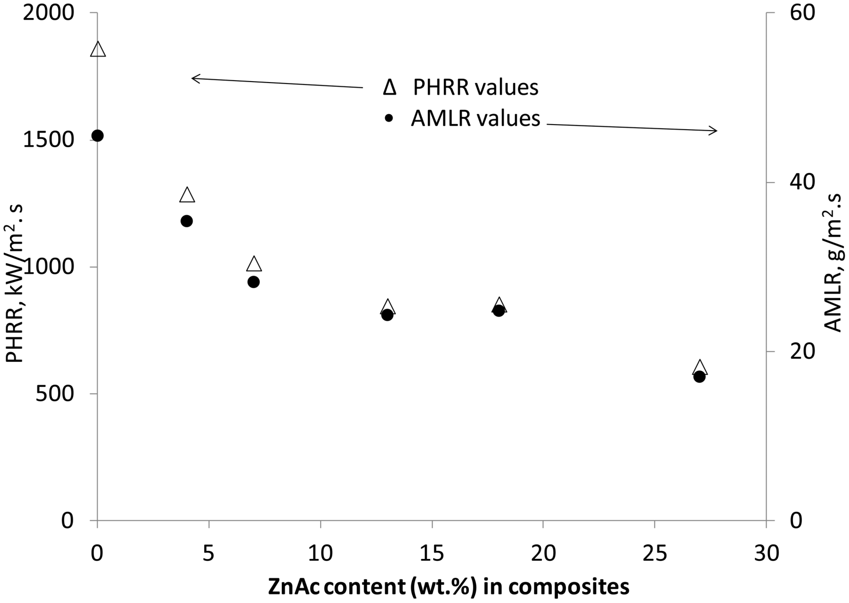

Figure 6. Peak heat release rate (PHRR) and Average mass loss rate (AMLR) values for the composites of ZnAc.

A correlation was found between the reduction in the average mass loss rate (AMLR) and the PHRR values which are graphically shown in Figure 6. Slow release of the fuel or a delay in mass loss has been typically correlated to a combination of physical and chemical phenomena (*24*, *25*). Three possible reasons are put forward to explain the fire retardant action of ZnAc in the epoxy-amine thermoset. Perhaps the primary cause is that under fire conditions most of the ZnAc additive is converted into zinc oxide. Crystalline zinc oxide forms an inorganic layer that covers the surface of the underlying polymer and thus slows the release of any flammable fragments from the burning polymer and also reduces the heat transfer to the degrading polymer. Also ZnAc may participate in the pyrolysis reactions within the condensed phase by promoting a carbonization process which reduces the yield of volatile and combustible products. Finally ZnAc may also act as a heat sink since when it is heated to higher temperatures it releases water molecules that may cool the flame.

An interesting feature of the fire retardant effect of ZnAc discovered here is that in addition to a considerable reduction of PHRR, the epoxy/amine composites of ZnAc do not produce extra smoke upon ignition. In fact smoke generation was even slightly suppressed in the presence of this metal salt as compared to the epoxy-amine control as one can see from the comparison of average specific extension areas shown in Table 2.

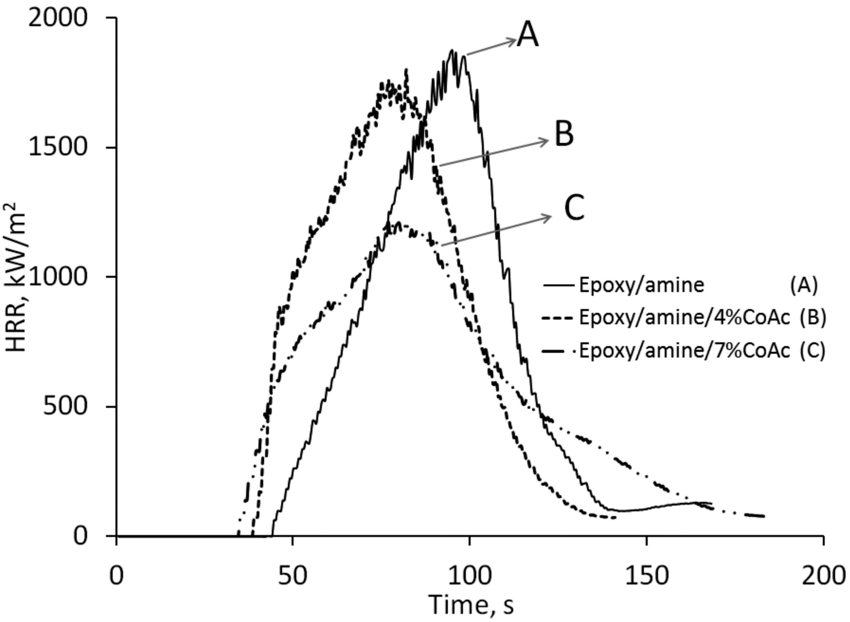

Figure 7. Heat release rate curves conducted at an external irradiation of 50 kW/m² for the pristine epoxy/amine thermoset and the resin modified with different amounts of CoAc.

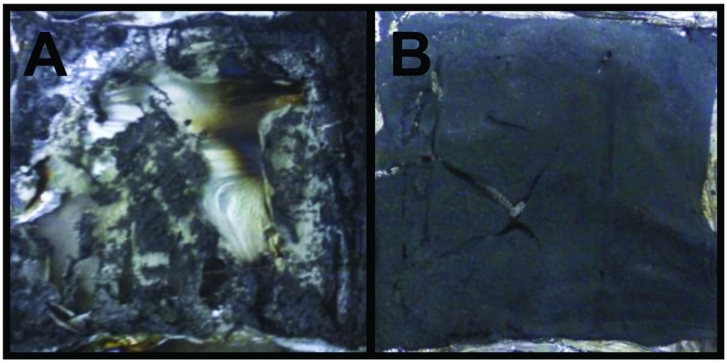

Figure 8. Images of the char residues for: (A) epoxy/amine and (B) epoxy/amine/7%CoAc.

A question was posed if the nature of the metal in the salt plays any role. To explore this fact, cobalt acetate (CoAc) was also added to the epoxy-amine thermoset and the fire properties of its composites were evaluated using a cone calorimeter at an external heat flux of 50 kW/m². The HHR curves for epoxy-amine control and also those containing 4% and 7% (wt/wt) CoAc are shown in

Figure 7. Qualitatively, the HRR behavior of epoxy-amine thermoset containing CoAc was comparable to that with ZnAc. Quantitatively, the fire retardant effect of adding cobalt based salt was found to be slightly smaller than that of adding zinc salt as preliminary measurements showed. When 7 wt.% of CoAc was added, the reduction in PHRR was 38% as compared to 46% with the addition of ZnAc.

The photographs of the char residues after completion of the cone tests for the epoxy-amine control and the 7% wt of CoAc composite are shown in Figure 8. As compared to the ZnAc containing epoxy-amine thermosets, adding CoAc did not lead to the whitish surface appearance. The surface was greenish-black. It should be noted that cobalt oxide color may vary broadly depending on the valence of the Co atom but a green-blackish color is rather common. Therefore, we believe that the mechanism of CoAc action is similar to that of ZnAc. A protective layer of cobalt oxide forms on the surface of the burning polymer which helps with improving the fire retardant properties. Interestingly, adding pure cobalt oxide to an epoxy-amine thermoset as described previously did not lead to a considerable improvement of fire retardant properties. At the same time, the oxide protective surface layer did not form in this case upon burning. We speculate here that the melting of crystalline $[Co(C_2H_3O_2)_2.4H_2O]$ and subsequent release of water plays a predominant role in the formation of bubbles which carry the oxide to the surface of the burning polymer. Naturally the same idea can be applied for ZnAc $[Zn(C_2H_3O_2)_2.2H_2O]$ salt. New experiments will focus on investigating the efficacy of anhydrous forms of zinc and cobalt acetate as well as the salts with longer organic tails, which are not hydrates, to investigate whether water release plays such as important role.

Conclusions

When fire retardant nano-additives LDH of cobalt aluminum dodecanoate and cobalt oxide were added to an epoxy/amine thermoset polymer, only modest improvement of fire properties was discovered. The poor dispersion of these nano-additives achieved at the primary microparticle level was suggested to be the main reason why these fire retardant additives did not perform well in the epoxy-amine thermoset polymer as compared to many other polymers. However, if the dispersion state of these additives is improved and reaches a nano-level, greater enhancement of the fire retardancy properties for these systems can be anticipated.

In contrast, metal salt hydrates of zinc acetate and cobalt acetate have been found to be very effective in imparting flame retardancy of epoxy/amine thermoset despite the micro-dispersion state for these additives as well. PHRR values have been reduced by almost a factor two as compared to the epoxy-amine thermoset control when only 7% wt. of metal salts was added. ZnAc was found to be slightly more effective than CoAc. The morphological analysis of the char residues suggested that the main reason for the fire retardant action was the formation of a metal oxide inorganic layer that covered the surface of the underlying polymer. This char residue slowed down the release of any flammable fragments from the burning polymer and also reduced the heat transfer to the degrading polymer. An interesting additional feature of the metal salts composites discovered here was that in addition to a considerable reduction of PHRR, there was no generation of extra smoke. In fact, generated smoke was even slightly suppressed as compared to the epoxy-amine thermoset control.

Acknowledgments

The authors thank the Office of Naval Research, award number N00014-07-1-1057, for the financial support of this project.

References

1. Petrie, E. M. *Handbook of Adhesives and Sealants*; McGraw-Hill: New York, 2000.
2. Licari, J. J. *Coating Materials for Electronic Applications. Polymers, Processes, Reliability, Testing*; William Andrew Publishing: New York, 2003.
3. Yung, K. C.; Wu, J.; Yue, T. M.; Xie, C. S. *J. Compos. Mater.* **2006**, *40*, 567.
4. Hamerton, I. *Recent developments in epoxy resins*; Rapra review report 91; Rapra Technology Ltd: Shewbury, 1996.
5. La Rosa, A.; Recca, A.; Carter, J.; McGrail, P. *Polymer* **1999**, *40*, 4093.
6. Schartel, B.; Braun, U.; Balabanovich, A. I.; Artner, J.; Ciesielski, M.; Döring, M.; Perez, R. M.; Sandler, J. K. W.; Altstädt, V. *Eur. Polym. J.* **2008**, *44*, 704.
7. Wang, C.; Berman, J.; Walker, L.; Mendoza, A. *J. Appl. Polym. Sci.* **1991**, *43*, 1315.
8. Hoerold, S (Clariant). U.S. Patent 6,420,459, 2002.
9. Nara, S.; Matruyama, K. *J. Macromol. Sci.* **1971**, *5*, 1205.
10. Morgan, A. B. A review of transition metal-based flame retardants: transition-metal oxide/salts, and complexes. In *Fire and Polymers V. Materials and Concepts for Fire Retardancy*; Wilkie, C. A., Morgan, A. B., Nelson, G. L. ACS Symposium Series 1013; American Chemical Society: Washington, DC, 2009; ISBN 978-0-8412-6988-0
11. Kashiwagi, T.; Danyus, R.; Liu, M.; Zammarano, M.; Shields, J. R. *Polym. Degrad. Stab.* **2009**, *94*, 2028.
12. Linteris, G. T.; Rumminger, M. D.; Babushok, V. I. *Prog. Energy Combust. Sci.* **2008**, *34*, 288.
13. Aseeva, R. M.; Zaikov, G. E. *Adv. Polym. Sci.* **1985**, *70*, 171.
14. Nie, S.; Hu, Y.; Song, L.; He, S.; Yang, D. *Polym. Adv. Technol.* **2008**, *19*, 489.
15. Lewin, M.; Endo, M. *Polym. Adv. Technol.* **2003**, *14*, 3.
16. Zammarano, M.; Franceschi, M.; Bellayer, S.; Gilman, J. W.; Meriani, S. *Polymer* **2005**, *46*, 9314.
17. Manzi-Nshuti, C.; Songttipya, P.; Manias, E.; Jimenez-Gasco, M. M.; Hossenlopp, J. M.; Wilkie, C. A. *Polymer* **2009**, *50*, 3564.
18. Leroux, F.; Besse, J. –P. *Chem. Mater.* **2001**, *13*, 3507.

19. Manzi-Nshuti, C.; Zhu, L.; Nyambo, C.; Wang, L.; Wilkie, C. A.; Hossenlopp, J. M. Use of Layered Double Hydroxides as Polymer Fire-Retardant Additives: Advantages and Challenges. In *Fire and Polymers V. Materials and Concepts for Fire Retardancy*; Wilkie, C. A., Morgan, A. B., Nelson, G. L., Eds.; ACS Symposium Series 1013; American Chemical Society: Washington, DC, 2009; ISBN 978-0-8412-6988-0
20. Wang, G. –A.; Wang, C. C.; Chen, C. Y. *Polymer* **2005**, *46*, 5065.
21. Gilman, J. W.; Kashiwagi, T.; Nyden, M.; Brown, J. E. T.; Jackson, C. L.;Lomakin, S.; Giannelis, E. P.; Manias, E. In *Chemistry and Technology of Polymer Additives*; Al-Malaika, S., Golovoy, A., Wilkie, C. A., Eds.; Blackwell Scientific: Oxford, 1999; pp 249−265.
22. Schartel, B.; Hull, T. R. *Fire Mater.* **2007**, *31*, 327.
23. Weil, E. D. *Handbook of Organophosphorus Chemistry*; Engrl, R., Ed.; Marcel Dekker: New York, 1992; p 693.
24. Morgan, A. B. *Polym. Adv. Technol.* **2006**, *17*, 206.
25. Gilman, J. W.; Jackson, C. L.; Morgan, A. B.; Harris, R.; Manias, E.; Giannelis, E. P.; Wuthenow, M.; Hilton, D.; Phillips, S. H. *Chem. Mater.* **2000**, *12*, 1866.

Chapter 7

Fire Retardancy of Mineral Fillers in EVA Copolymers

Artur Witkowski,*,[1] Luke Hollingbery,[1,2] and T. Richard Hull[1]

**[1]Centre for Fire and Hazards Science, University of Central Lancashire,
Preston PR1 2HE, U.K.
[2]Minelco Ltd., Raynesway, Derby DE21 7BE, U.K.
*E-mail: awitkowski@uclan.ac.uk**

A simple numerical model quantifies the four contributions made by mineral fillers to fire retardancy. This model has been applied to samples of EVA filled with calcium carbonate (as a control), aluminium hydroxide, magnesium hydroxide, hydromagnesite, and naturally occurring mixtures of huntite and hydromagnesite in various ratios. The model shows good correlation between the magnitude of the endotherm and the ignition behavior, in both limiting oxygen index test and cone calorimeter. The heat release rate, measured by oxygen depletion, masks the contribution of the endotherm in the cone calorimeter. The intial peak derives from chain stripping EVA, releasing acetic acid in the molten polymer, which reacts with the hydroxides to form acetates, which are subsequently converted to acetone, and volatilized as fuel, but delayed, relative to the release of acetic acid by EVA.

Mineral Filler Fire Retardants

Mineral fillers are an important class of fire retardants with many inherently sustainable attributes, including cleaner manufacture, reduction in polymer (hence hydrocarbon) use, no reported environmental hazards, and no adverse effect on the biggest causes of death and of injury in fire, smoke and toxicity (*1*). However, mineral fillers are more difficult to incorporate into a polymer and to achieve the required level of fire retardancy than halogenated flame retardants, so better

In Fire and Polymers VI: New Advances in Flame Retardant Chemistry and Science; Morgan, A., et al.;
ACS Symposium Series; American Chemical Society: Washington, DC, 2012.

understanding of the details of their mode of action is required. Incorporation of any non-combustible filler will reduce the flammability of a polymer, by reducing the total amount of fuel, the rate of diffusion of oxygen into, and fuel from, the polymer bulk while increasing the heat capacity, thermal conductivity, reflectivity and emissivity. There may also be synergistic or antagonistic catalytic (*2*) or other surface effects associated with the filler, and effects on the polymer melt rheology (*3*).

To date, a fairly simplistic view of their mode of action has been generally assumed. Mineral filler fire retardants (FRs) decompose endothermically, with the release of inert gases or vapour, resulting in a fire retardancy effect. In order to be effective, this decomposition must occur in a narrow window above the polymer processing temperature, but at, or below, its decomposition temperature. In practice most of the suitable materials are group II or III carbonates or hydroxides. Four effects can be considered to contribute to its fire retardancy.

- Heat capacity of the filler prior to decomposition.
- Endothermic decomposition, absorbing heat and therefore keeping the surrounding polymer cooler.
- Production of inert diluent gases absorbing heat from the flame. Flaming reactions require a critical concentration of free radicals to be self-sustaining. If this concentration falls sufficiently, through temperature reduction or dilution, for example by the release of water or carbon dioxide, flame extinction will occur.
- Accumulation of an inert layer of inorganic residue on the surface of the decomposing polymer. This will shield it from incoming radiation, and act as a barrier, to oxygen reaching the fuel, flammable pyrolysis products reaching the gas phase, and radiant heat reaching the polymer.

For example, the most widely used FR, aluminium hydroxide ($Al(OH)_3$), (commonly referred to as alumina trihydrate (ATH) and incorrectly formulated as $Al_2O_3.3H_2O$, even though it is neither an alumina, nor a hydrate (*4*)), decomposes to form alumina (Al_2O_3) with the release of water. $Al(OH)_3$ breaks down endothermically forming water vapour, diluting the radicals in the flame, while the residual Al_2O_3 builds up to form a protective layer.

$$2\ Al(OH)_3\ (s) \xrightarrow{180\text{-}200°C} Al_2O_3(s) + 3\ H_2O(g) \quad \Delta H = +1.3\ kJ\ g^{-1}$$

It is worth noting that the heat capacity of organic polymers (*5*) vary from 1.6 to 3.0 J $K^{-1}g^{-1}$, over the temperature range ambient to decomposition, thus the decomposition enthalpy of an FR mineral filler is around the same as that required to heat 2 g of polymer between 250 and 500 °C – the decomposition enthalpy of 1 g $Al(OH)_3$ is equal to the heat (q) required to raise the temperature of a mass (m) of 1.2 g of polypropylene from ambient temperature to decomposition (424°C)($\Delta\theta$), assuming constant heat capacity (c) during heating, ($q = m\ c\ \Delta\theta$, so $q = 1.2 \times 2.8 \times 400 = 1.3$ kJ).

Production methods for both ATH and another mineral filler FR, magnesium hydroxide (MH) involve the use of minerals (bauxite or lime) followed by a chemical process, and in the case of ATH, the storage and disposal problems of a caustic red sludge by-product. As well as ATH and MH, naturally occurring mixtures of hydromagnesite ($Mg_5(CO_3)_4(OH)_2.4H_2O$) and huntite ($Mg_3Ca(CO_3)_4$) have similar potential as FRs, some of which are sold as UltraCarb®. Commercially exploited natural reserves of huntite and hydromagnesite mixtures, are already very pure and do not need chemical processing, or precipitation of the final product. This makes production of fine particle size mixtures of huntite and hydromagnesite much less energy intensive. The only by product is a small quantity of dolomite, $MgCa(CO_3)_2$, a mineral closely related to huntite, $Mg_3Ca(CO_3)_4$, that occurs naturally in the mixture and is removed during the grinding process.

Previous authors have discussed the decomposition of huntite and hydromagnesite (*6–8*). Natural hydromagnesite particles have a blocky morphology (*7*, *9*) and once processed, the majority of the particles are usually between 1 and 10 µm in diameter, depending on the processing. It thermally decomposes (*1*, *3*), between about 220 °C and 550 °C in two stages, initially releasing water then carbon dioxide, leaving a solid residue of magnesium oxide.

$$Mg_5(CO_3)_4(OH)_2{\cdot}4H_2O \rightarrow 5MgO + 4CO_2 + 5H_2O$$

Huntite particles have a platy morphology and the particles are usually about 1 µm or less in diameter, much smaller than hydromagnesite particles. It thermally decomposes between about 450 °C and 750 °C in two stages, releasing only carbon dioxide, leaving a solid residue of magnesium oxide and calcium oxide.

$$Mg_3Ca(CO_3)_4 \rightarrow 3MgO + CaO + 4CO_2$$

The thermal decomposition of mixtures of these minerals, through endothermic release of carbon dioxide and water, has led to several studies showing their potential applications, including FR additives for polymer compounds. The endothermic decomposition of hydromagnesite coincides with the temperature range at which polymeric materials, such as ethylene vinyl acetate and polyethylene, thermally decompose. This is a good indicator that hydromagnesite has potential to perform well as an FR. Huntite decomposes between about 450 °C and 750 °C, a temperature range where most of the polymer has completely volatilised. This has led to a suggestion that huntite has little more influence than an inert diluent filler in terms of fire retardancy. It has been argued by the current authors (*9*) that the evidence in the literature does not back up this assertion. Recent work (*10*) demonstrates that both huntite and hydromagnesite contribute significantly to the FR properties of polymer compounds.

Ethylene-vinyl acetate (EVA) is an elastomeric copolymeric material capable of maintaining its flexibility at filler loadings as high as 70% by weight. In combination with metal hydroxide or carbonate FRs, it makes an ideal alternative to polyvinyl chloride for fire retarded communication and power cable sheathing. The FR behaviour of combinations of EVA with ATH and MH have been widely reported (*11*, *12*). In studies reported elsewhere (*13*), for samples containing ATH, water is evolved around 250 °C, and for samples containing MH around 300 °C. At about 320 °C the acetate groups are released as acetic acid and the resulting polyene cross-links to form a protective layer. Of greater interest and significance are the more recent studies (*14*) of the trapping of acetic acid by $M(OH)_x$, as aluminium or magnesium acetate, followed by a catalytic conversion occurring on the oxide surface, forming acetone, carbon dioxide (CO_2) and water, delaying and diluting the fuel released from the decomposing polymer. The early peak of HRR for EVA formulations gives high peak HRRs, and FIGRA (fire growth rate) values, giving an initial boost to flame spread. These early peaks were eliminated by trapping of acetic acid by aluminium or magnesium hydroxide, which is only released after dehydration, with the formation of aluminium or magnesium oxide, following the ketonic decarboxylation of acetic acid to acetone, carbon dioxide and water.

Thermochemically, the heat of combustion of two moles of acetic acid (2 x -876.1= -1752 kJ) is sufficiently similar to the heat of combustion of 1 mole of acetone product (-1785.7 kJ) that the process is unlikely to have a noticeable impact on the total heat release.

The four contributions to fire retardancy have been crudely calculated for some mineral fillers (*8*). The heat absorbed by the filler from ambient to its decomposition temperature was calculated from the heat capacity over that range; the heat absorbed by the inorganic residue was determined from its representative heat capacity from the decomposition temperature to the final residue temperature (estimated as 600 °C), for the fraction remaining in the condensed phase; the heat absorbed by endothermic decomposition was obtained from DSC studies and published data; the heat absorbed by the water or carbon dioxide released to the gas phase is their representative heat capacity from the filler decomposition temperature to the maximum flame temperature (estimated as 900 °C) (*8*). While the temperature of premixed flames of typical hydrocarbon fuels in air, and the adiabatic flame temperature (corresponding to the maximum temperature attainable from thermodynamic considerations without loss of heat) can reach 2000 °C (*15*), and a candle flame has been reported to have a peak temperature of 1400 °C, polymer diffusion flames have only been reported to reach a peak temperature of around 900 °C (*16*, *17*).

These data, together with the average values of heat capacities of the filler, its residue, and its gaseous decomposition products have been used to estimate the heat absorption by the filler, the residue, the evolved water vapour and carbon dioxide and the decomposition endotherm, shown in Figure 1. The selection of mineral fillers is matched to the current work, including those fillers for which experimental data is reported. As the data have been calculated in energy units, the contribution to the individual fillers may be compared in absolute terms. Figure 1 shows the energy absorption per gram of each of the processes undergone by the filler.

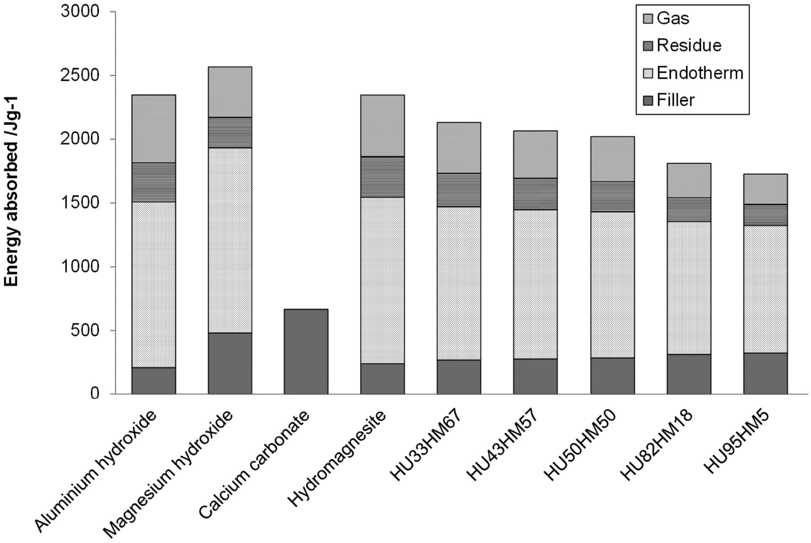

Figure 1. Absolute estimation of heat absorbed by potential FR mineral fillers (labels such as HU40HM60 show the % huntite (HU) and hydromagnesite (HM) in the mixture).

The higher decomposition temperature of MH and particularly the greater contribution of the filler, increase its energy absorbing capacity by about 250 J g^{-1}, compared to aluminium hydroxide. Comparing aluminium and magnesium hydroxide, it is evident that the difference between their relative effects arises from the higher decomposition temperature of $Mg(OH)_2$, giving a larger contribution to the heat capacity of the undecomposed filler, but a smaller contribution from the heat capacity of the residue, and from the heat capacity of the greater volume of water vapour released by the $Al(OH)_3$ – even though the energy for such a release is almost identical for both fillers. For the hydromagnesite, huntite and HU43HM57 mixture, which has been proposed as an alternative to $Al(OH)_3$, it can be seen that the higher decomposition temperature of huntite gives a greater filler contribution, although overall HU43HM57 absorbs less energy than either ATH or MH.

This approach is deliberately simplistic, and involves the following assumptions:

- The thermal conductivity of the polymer composite is unaffected by the presence of the filler. This is not realistic, particularly if incorporation of the filler results in significant changes to the melt flow behaviour.
- The final temperature reached by the solid residues and the CO_2 and water in the gas phase do not vary significantly from one filler to another. This is discussed further.

- The heat capacity of the filler, and residue is not affected by the presence of polymer.
- The decomposition endotherm of the filler is unaffected by incorporation into the polymer.
- The only effect of the solid residue is its ability to act as a heat sink (in practice it will also change the reflectivity and the absorption of radiant heat).
- The only effect of the gas phase diluent is an absorber of heat, neglecting any effects reducing the free radical concentration below a critical threshold, by collisional quenching.
- It takes no account of particle size or morphology of the filler, which have been shown to be important in experimental studies.

It might be that the greatest value of simple models, such as the one presented here, is to observe deviations from the predicted behaviour in order to identify other properties, obscured by the physical effects of the filler, which also contribute to (improvements in) the burning behaviour. For example, the superior performance of mixtures of huntite and hydromagnesite compared to aluminium hydroxide reported here, or the unexpected FR performance of the micro and nano-boehmites.

Experimental

Materials

Mixtures of huntite and hydromagnesite with different ratios of the two minerals were supplied by Minelco Ltd. The samples are labelled throughout this work according to the ratio of the two minerals. For example HU43HM50 signifies that the sample contained a mixture of the minerals in the ratio: 43% huntite and 50% hydromagnesite. The remaining percentage comprises of closely related minerals, such as dolomite. For simplicity, in the calculation described earlier and in comparisons with it, the remaining percentage is taken to be huntite (which is closely related to dolomite). The actual HU:HM ratios, and those used in the calculations are shown in Table 2. In addition, natural calcium carbonate was supplied by Minelco under the name MicroCarb ST10H; aluminium hydroxide supplied by Nabaltec under the name Apyral AP40; magnesium hydroxide supplied by Martinswerk under the name Magnifin H5A;

The following polymer formulation referred to as "EVA" (Table 1) was chosen as a typical, general purpose, halogen free compound found in the wire and cable industry. It has been used throughout this study to investigate the effects of huntite and hydromagnesite.

Limiting oxygen index (LOI) tests were carried out according to BS EN ISO 4589-2:1999, using a Stanton Redcroft instrument with a total gas flow of 18 L min^{-1}. Samples of 10 x 125 x 3 mm were cut from compression moulded plaques, and measurements were taken to the nearest 0.5% O_2. A Fire Testing Technologies (FTT) cone calorimeter was used in accordance with ISO 5660, in triplicate, with a heat flux of 50 kW m^{-2}, and samples of 100 x 100 x 6 mm. Py-GC-MS experiments were carried out on a CDS-5200 Pyrolyser (Chemical Data Systems Co.) coupled with a PerkinElmer TurboMass gas chromatography-mass spectrometry (GC-MS) system. Around 0.8 mg of polymer in a quartz tube was inserted into a platinum coil on the probe tip, connected to a temperature programmer. The pyrolyzer, under helium, was heated from 50 to 450°C at 10°C min^{-1}, and the decomposition products collected on Tenax TA trap at 50 °C. The trap was then heated at 280 °C for 2 min, the desorbed vapour transferred at 310 °C to the GC-MS.

Table 1. Typical wire and cable formulation

Tradename	*Supplier*	*Description*	*Quantity (phr)*
Escorene UL00328	Exxon	Ethylene vinyl acetate (28%)	55
Exact 8201	ExxonMobil	Polyolefin elastomer	30
Fusabond MB226D	DuPont	Maleic anhydride grafted polyethylene	10
Borealis BS2581	Borealis	High density polyethylene	5
Irganox 1010	Ciba (BASF)	phenolic antioxidant	1
Mineral filler	Various	metal hydroxide / carbonate	160
		Total	261

Results

The limiting oxygen index (LOI) values in Table 2, show a significant improvement for all the FR additivies considered, with the exception of HU93HM5, which shows a similar value to the calcium carbonate. Other studies (*18*) have reported that increasing the proportion of hydromagnesite from 0% up to 40% increases the oxygen index, but further increase in the proportion of hydromagnesite has no further benefit to the LOI. Figure 2 shows the correlation between the calculated effects of the filler and the measured LOI. The clearest correlation is with the endotherm, which increases the LOI as it increases. The only significant exception to this is the HU77HM18 material, which may form a more strongly adherent residue, as described by Rothon (*19*), who showed the influence of a resilient inorganic residue on the tip of the burning LOI specimen.

The heat release rate (HRR) of EVA compounds filled with ATH, MH, hydromagnesite and the various blends of huntite and hydromagnesite was measured using cone calorimetry at applied heat fluxes of 30, 50 and 70 kW m^{-2}, as shown in Figure 3. As the time to ignition increases as the heat flux is reduced, direct comparison is less apparent. Therefore, the HRR has been plotted against time *following* ignition, rather than time from the start of the test. Unfortunately data is only available for MH at 50 kW m^{-2}, and this is plotted from the start of the test.

Table 2. Effect of huntite/hydromagnesite ratio on limiting oxygen index

FR additive	*Ratios used for calculation*	*LOI*
Aluminium hydroxide		30.0
Magnesium hydroxide		31.5
Calcium carbonate		23.0
Hydromagnesite		29.5
HU24HM67	HU33HM67	29.5
HU41HM57	HU43HM57	29.0
HU43HM50	HU50HM50	28.0
HU77HM18	HU82HM18	29.5
HU93HM5	HU95HM5	24.5

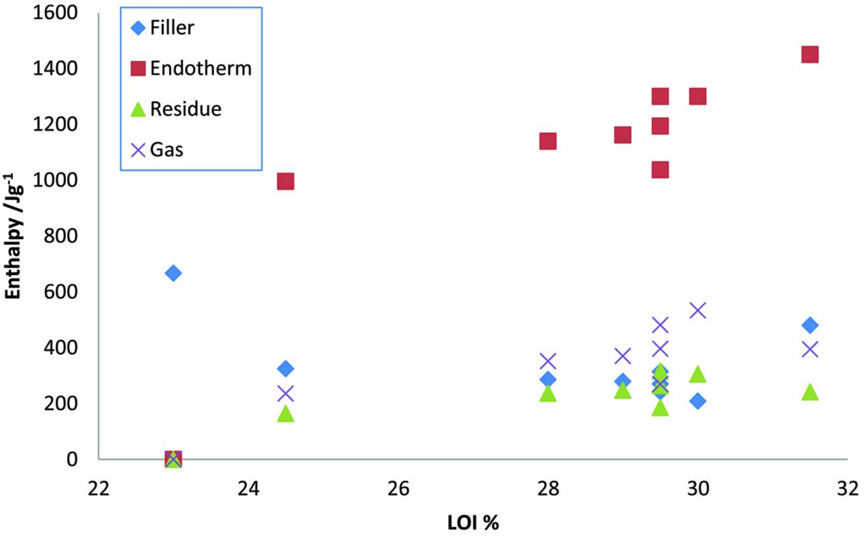

Figure 2. Comparison of calculated FR contributions and measured LOI values.

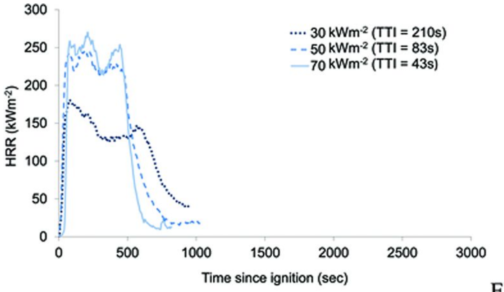

EVA_CaCO$_3$

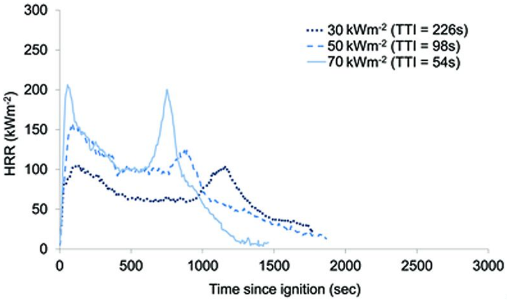

EVA_ATH

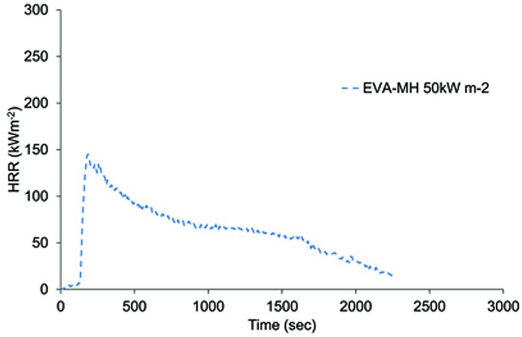

EVA_MH

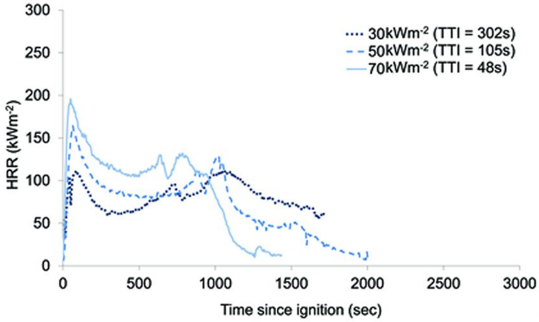

HM100

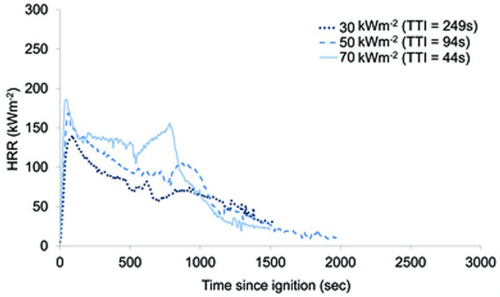

HU24HM67

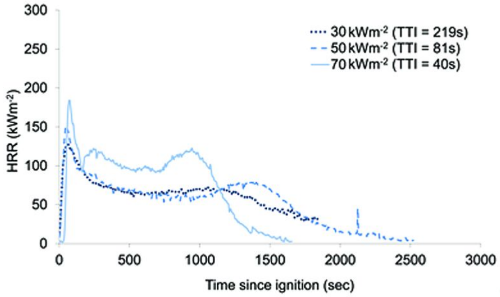

HU43HM50

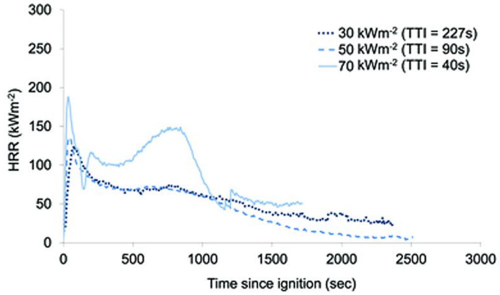

HU77HM18

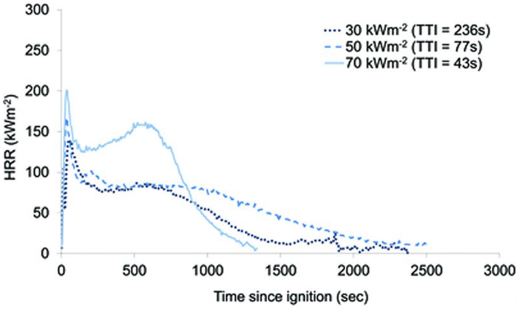

HU93HM5

Figure 3. HRR at varying heat fluxes of diferent samples of FR EVA.

Calcium carbonate, as may be expected, and as predicted by the calculation, makes only a small contribution to reducing the flammability, despite being present at a high loading (160 phr or 61%), particularly at the higher heat fluxes. Relative to calcium carbonate, ATH, MH, hydromagnesite and huntite-hydromagnesite mixtures reduced the rate of heat release over the entire burning period. The hydromagnesite filled compounds behave in a very similar manner to the ATH filled compound, showing an initial peak, followed by a second fairly sharp peak associated with movement and collapse of the residue. The compounds filled with a blend of huntite and hydromagnesite have a lower rate of heat release than the ATH or hydromagnesite filled compounds for most heat fluxes for most of the burning time, showing benefit from almost half of the hydromagnesite being replaced by huntite. As reported elsewhere (*10*), the use of a mixture of huntite and hydromagnesite leads to a stronger more stable char which does not collapse during the test period and gave a longer slower burn. This is particularly evident in the samples containing a higher proportion of huntite, and not addressed in the simple calculation model described earlier. The heat release characteristics of the magnesium hydroxide filled compound were different to the ATH or huntite-hydromagnesite filled compounds. The compound shows a much slower reduction in rate of heat release following the initial peak. It was quite clear that the formation of the residue from this compound was different to that of the ATH and hydromagnesite filled compounds.

Table 3. Summary of Cone Calorimeter data at 30, 50 and 70 kW m^{-2}

Sample	*Time to iginition /s*			*Peak HRR /kW m^{-2}*			*Average HRR /kW m^{-2}*		
Applied Heat Flux /kW m^{-2}	***30***	***50***	***70***	***30***	***50***	***70***	***30***	***50***	***70***
ATH	226	98	54	117	169	208	81	84	102
MH		125			163			88	
$CaCO_3$	210	83	43	186	257	251	107	129	187
Hydromagnesite	302	101	48	117	168	197	83	89	106
HU24HM67	249	93	44	139	162	190	73	74	90
HU41HM57		88			168			71	
HU43HM50	219	81	40	130	154	191	68	56	84
HU77HM18	227	90	40	135	138	189	64	41	85
HU95HM5	236	78	43	154	174	202	52	57	103

EVA-huntite-hydromagesite mixtures also show similar sharpness and intensity of the initial peak of heat release with increasing heat flux. The cone calorimeter has been shown (*20*) to heat the surface of a ceramic board to about 500 °C, 610 °C, and 700 °C when heat fluxes of 30 kW m^{-2}, 50 kW m^{-2} and 70 kW m^{-2} are used. Huntite and hydromagnesite go through a series of decompositions (*21*) commencing at about 220 °C and completing at about 750 °C. ATH decomposes over a temperature range of about 180 – 350 °C. Therefore a heat flux of 30 kWm^{-2} is sufficient to ensure total decomposition of ATH, at higher heat fluxes the decomposition of the ATH will remain the same as at 30 kW m^{-2}. As hydromagnesite and huntite have stages of decomposition that occur at higher temperatures these will be activated sooner at the higher heat fluxes. The additional heat flux activates the higher temperature decompositions in the hydromagnesite and huntite which means that it actually becomes more efficient at higher heat fluxes and keeps the rates of heat release closer that which was measured at 30 kW m^{-2}.

Table 3 provides a summary of numerical data which is used as the basis for comparing the behaviour of the formulations to the simple model. For HU41HM57 (and MH) data are only available at 50 kW m^{-2}.

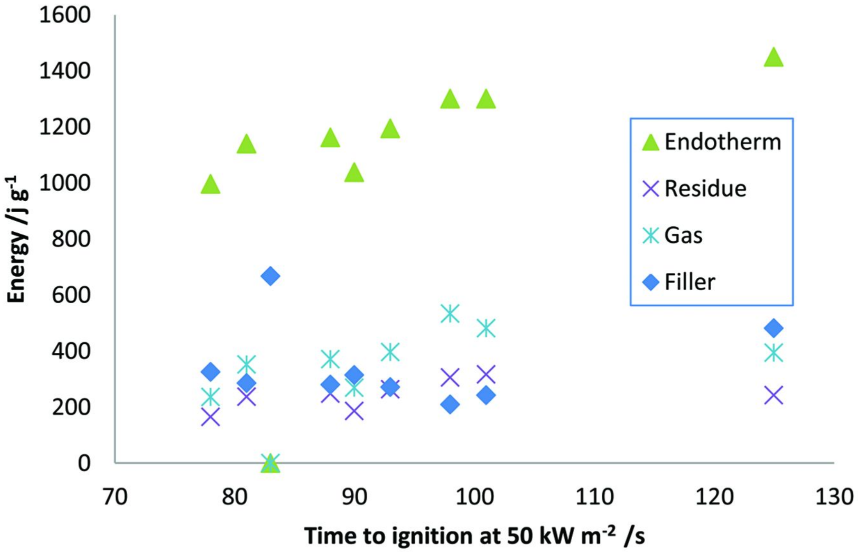

Figure 4. Relationship between individual energy contributions to FR effect, and time to ignition in the cone calorimeter at 50 kW m^{-2}.

Figure 4 shows a reasonable correlation between the time to ignition and the magnitude of the decomposition endotherm. This fits with the general principle that the LOI, as an ease of extinction test (with the same criteria as ignition, that the heat feedback from the flame must equal or exceed the heat required to gasify the fuel), is driven by the same material parameters as the time to ignition.

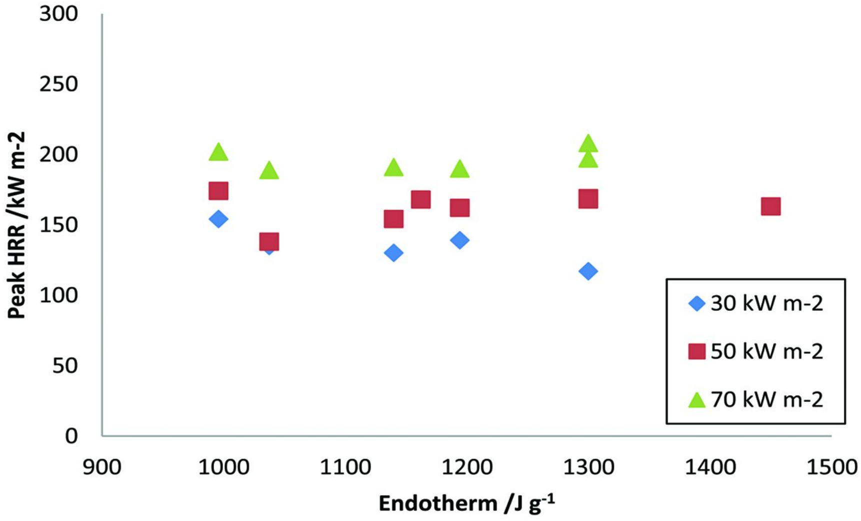

Figure 5. Relationship between Peak Heat Release Rate, measured in the cone calaorimeter, and the contribution from the endothermic decomposition of the filler.

In contrast to Figure 4, Figure 5 shows only a very modest contribution of the filler decomposition endotherm to the magnitude of the peak HRR. In part, this is due to the method of measurement of HRR by oxygen depletion calorimetry (13.1 kJ released for every gram of oxygen consumed). Endothermic decomposition, and the production of water and CO_2 will have no effect on the magnitude of the HRR when measured in the cone calorimeter, whereas in a real fire, or in experiments measuring the HRR using a thermometric device, this heat absorption would reduce the overall HRR. The slight trend showing reduction in peak HRR at 30 kW m^{-2} probably results from the cooling effect of the endotherm, resulting in a reduction of the rate of gasification of the pyrolysed EVA.

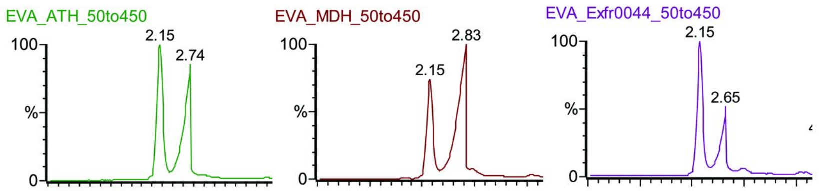

Figure 6. Pyrolysis GC-MS traces showing distribution between acetone and acetic acid from decomposition of EVA containing ATH, MH,and EXFR 0044, a commercial HU-HM blend containing roughly equal proportions of each mineral.

Figure 6 shows the acetone (2.15) and acetic acid (~2.7) peaks from the GC traces of the pyrolysis products of FR filled EVA, identified by MS. Under these pyrolysis conditions, the conversion of acetic acid to acetone is most efficient for HU-HM and least efficient for EVA-ATH. As described earlier, the acetone:acetic acid ratio is impotant, as acetic acid or acetone release is considered responsible for the first sharp peak in the HRR curve. As acetic acid is trapped on the hydroxides as an acetate, then subsequently released as acretone, this will delay the initial peak until the decomposition of the hydroxide. This explains the longer time to ignition of the EVA-MH sample, though is hidden behind the axis in the plots in Figure 3.

Conclusions

Different tests for quantifying flammability focus disproportionately on particular aspects of burning behaviour. Thus, the LOI, which shows the least correlation to other tests, seems to be more strongly influenced by the presence and resilience of the inorganic residue (*19*); only the side effects of the endotherm decomposition, not the endotherm itself, are quantified in cone calorimetry (the time to ignition may be delayed and peak heat release lowered and delayed by endothermic decomposition of the filler, but the measured value of the total heat release, or effective heat of combustion will be unaffected by the endothermic event). The model analysis (*8*) described here shows reasonable correlation with overall flammability parameters, and particularly the magnitude of the endotherm to the ignition behaviour. However, it is limited in its scope, and some effects of filler, such as the reduction of dripping (UL94) and action as a radiant heat shield the inorganic residue (cone calorimeter), are not included. This simple model also fails to address the enhanced FR effects achieved from incorporation of huntite into EVA, reinforcing the barrier layer with a platy resilient mineral. The UltraCarb mixture can outperform both hydromagnesite, and aluminium hydroxide as an FR. This indicates that the FR mechanism of huntite is not simply the endothermic release of inert diluent vapour typical of other mineral fillers, since it has been shown that mixtures of huntite and hydromagnesite perform similarly to aluminium hydroxide in measurements involving cone calorimetry. Huntite certainly has much greater effect than an inert diluent filler, such as calcium carbonate (Figure 3).

The endothermic release of water and carbon dioxide from hydromagnesite at temperatures between 220 °C and 500 °C helps to reduce the initial peak of heat release and increase the time to ignition. It shows that the partial decomposition of huntite at temperatures between 450 °C and 600 °C helps to reduce the rate of heat release during the later stages of combustion by providing a physical barrier, slowing the release of combustible gases to the flame. This has been ascribed to the platy morphology of huntite, reinforcing the barrier properties of the residual layer (*9*). The additional heat absorbed during the endothermic, partial decomposition, of huntite also reduces the heat transferred to the underlying polymer and further dilutes the gas phase with non-combustible carbon dioxide.

In summary the FR action of mixtures of huntite and hydromagnesite comes from a combination of the actions of the two minerals.

References

1. Hull, T. R.; Wills, C. L.; Artingstall, T.; Price, D.; Milnes, G. J. In *Fire Retardancy of Polymers: New Applications of Mineral Fillers*; Royal Society of Chemistry: Cambridge, U.K., 2005; Chapter 28, p 372−384.
2. Hull, T. R.; Quinn, R. E.; Areri, I. G.; Purser, D. A. *Polym. Degrad. Stab.* **2002**, *77*, 235–242.
3. Rothon, R. N. Effects of Particulate Fillers on Flame Retardant Properties of Composites. In *Particulate-Filled Polymer Composites*, 2nd ed.; Rothon, R. N., Ed.; Rapra Technology: Shawbury, U.K., 2003; Chapter 6.
4. Horn, W. E. Inorganic hydroxides and hydroxycarbonates: Their function and use as flame retardants. In *Fire Retardancy of Polymeric Materials*; Grand, A., Wilkie, C. A., Ed.; Marcel Dekker: New York, 2000; Chapter 9.
5. Stoliarov, S. I.; Safronava, N.; Lyon, R. E. *Fire Mater.* **2009**, *33*, 257–271.
6. Ozao, R.; Otsuka, R. *Thermochim. Acta* **1985**, *86*, 45–58.
7. Hollingbery, L. A.; Hull, T. R. *Thermochim. Acta* **2010**, *509*, 1–11.
8. Hull, T. R.; Witkowski, A.; Hollingbery, L. A. *Polym. Degrad. Stab.* **2011**, *96*, 1462–1469.
9. Hollingbery, L. A.; Hull, T. R. *Polym. Degrad. Stab.* **2010**, *95*, 2213–2225.
10. Hollingbery, L. A.; Hull, T. R. *Polym. Degrad. Stab.* **2012**, *97*, 504–512.
11. Hull, T. R.; Price, D.; Liu, Y.; Wills, C. L.; Brady, J. *Polym. Degrad. Stab.* **2003**, *82*, 365–371.
12. Rothon, R. N.; Hornsby, P. R. *Polym. Degrad. Stab.* **1996**, *54*, 383–385.
13. Zilberman, J.; Hull, T. R.; Price, D.; Milnes, G. J.; Keen, F. *Fire Mater.* **2000**, *24*, 159–164.
14. Witkowski, A.; Stec, A. A.; Hull, T. R. *Polym. Degrad. Stab.* **2012**, in press.
15. Bradley, J. N. *Flame Combustion and Phenomena*; Methuen's Monographs on Chemical Subjects; Methuen & Co. Ltd.: London, 1969; p 29.
16. Audoin, L.; Kolb, G.; Torero, J. L.; Most, J. M. *Fire Safety J.* **1995**, *24*, 107–130.
17. Yuan, L.-M.; Cox, G. *Fire Safety J.* **1997**, *27*, 123–139.
18. Kirschbaum, G. *Ind Miner.* **2001**, 61–67.
19. Ashley, R. J.; Rothon, R. N. *Plast. Rubber Process. Appl.* **1991**, *15*, 19–21.
20. Schartel, B.; Hull, T. R. *Fire Mater.* **2007**, *31*, 327–354.
21. Hollingbery, L. A.; Hull, T. R. *Thermochim. Acta* **2010**, *509*, 1–11.

Chapter 8

Some Developments in Halogen-Free Flame Retardancy of Polycarbonate and Its Blends

Jie Feng, Jianwei Hao,* and Jianxin Du

National Laboratory of Flame Retardant Materials, School of Materials Science and Engineering, Beijing Institute of Technology, 5 South Zhongguancun Street, Beijing 100081, PR China
***E-mail: hjw@bit.edu.cn**

In this chapter, some recent developments of halogen-free flame retardancy of polycarbonate (PC) and its blends are reviewed. Conventional halogen-free flame retardants used in PC and its blends include phosphorus-containing compounds, siloxanes and sulfur-containing compounds. In the conventional category, some compounds with new structures have been used; combined usage of conventional compounds has been also studied. Nanocomposites of PC and its blends with improved flame retardancy have been noticed, whereas combining nanocomposites technology and conventional flame retardants to take advantages of synergistic effects between them has appeared to be a solution for the usually worsened self-extinguishing properties of the nanocomposites. In general, in order to suit the distinct applications of the material, different systems should be carefully designed according to the features of the components used.

Introduction

Polycarbonate (PC) is an engineering thermoplastic with remarkable mechanical properties, high heat distortion temperature (HDT) and excellent transparency. Thus PC, especially the bisphenol A type, and its blends are widely used in the fields of electrical and electronic devices, aeronautics and astronautics, transport and building. By itself, PC has an inherent fire risk and

In Fire and Polymers VI: New Advances in Flame Retardant Chemistry and Science; Morgan, A., et al.;
ACS Symposium Series; American Chemical Society: Washington, DC, 2012.

hazard. Although it usually has a rating of V-2 in the UL-94 vertical burning test and its limiting oxygen index is ca. 25%, better flame retardant property is often required in a lot of cases.

Many attempts have been made to improve the flame retardancy of PC and its blends as well as simultaneously keep their other outstanding properties. Levchik *et al* reviewed the flame retardants used in PC and its blends (*1*, *2*) during the year 2005, and since then there are some new trends in this topic which will be discussed in this chapter.

Like other polymers, halogenated flame retardants, such as brominated aromatic compounds (*3*), were primarily used because of their high efficiency of flame retardancy improvement and little influence on the other properties of PC and its blends. However, when the negative effect of halogenated compounds on environmental and health safety was realized, this kind of flame retardant is gradually restricted since the recent decade. Therefore, halogen-free flame retardants suitable for PC and its blends have been developed and studied abundantly in both industry and academia.

Typical conventional halogen-free flame retardants used for PC and its blends mainly include phosphorus-containing compounds, siloxanes, and sulfur-containing compounds. Also since the discovery of nanocomposite technology to be a new route for flame retardancy of polymers (*4*), this technology has also been adapted for developing flame retardant PC and its blends.

In this chapter, the recent development of conventional halogen-free flame retardants used for PC and its blends will be briefly reviewed first; then, we will focus on studies of using nanocomposite technology for flame retardant PC and its blends; finally, synergistic effect of nanocomposite technology and conventional halogen-free flame retardants applied in PC and its blends will be discussed.

Conventional Halogen-Free Flame Retardants

Phosphorus-Containing Compounds

Red phosphorus is not often used in PC or its blends not only because its dark red color would compromise the transparency of PC but also its hydrophilicity and hygroscopicity would degenerate many other good properties of the matrix. However, Jian *et al* encapsulated red phosphorus with polysiloxane (MRP) and applied it to polycarbonate/acrylonitrile-butyldien-styrene (PC/ABS) blend (*5*). With 15 wt. % MRP, the blend reached UL-94 V-0 rating and the flame retardancy of the sample could still be preserved after a long time of hot water bath.

Organic phosphate is more effective and compatible with PC and its blend. In the early 1990s, there were already some attempts to use brominated phosphate in PC (*6*, *7*). Because of their high effectiveness and compatibility with PC and its blends, triphenyl phosphate (TPP), resorcinol bis(diphenyl phosphate) (RDP) and bisphenol A bis(diphenyl phosphate) (BDP) are the common aromatic phosphate used; TPP is highly volatilizable, thus it is less preferable than the latter two. Mechanistic studies showed all these three phosphates exhibited gas phase action for they could generate volatile phosphorus-containing species to trap combustible radicals; TPP reacted mainly in the gas phase, whereas RDP and BDP had an additional condensed phase action; the condensed phase action of BDP was more prominent than that of RDP (*8*). The different mechanisms of these three phosphates were due to their different decomposition temperatures (*9*). Though these phosphates are effective in improving flame retardancy, they have a negative effect of reducing the mechanical modulus and HDT of the matrix due to their intrinsic plasticizing effects. Also, RDP and BDP are usually in liquid form which is not convenient during transport and processing.

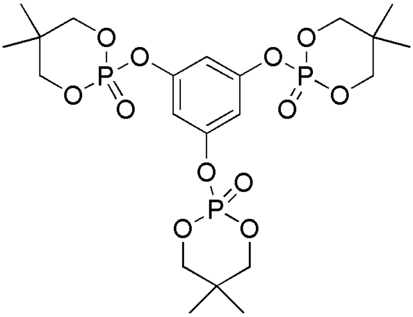

Scheme 1

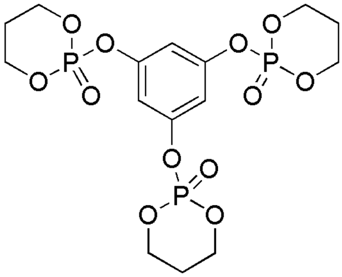

Scheme 2

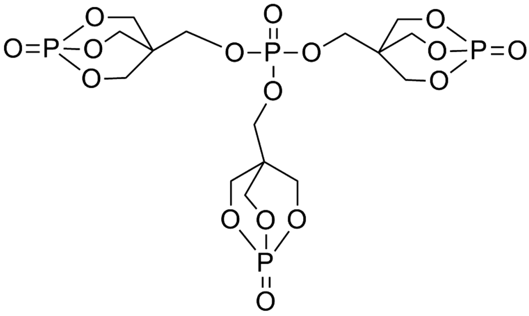

Scheme 3

Besides the commercially available RDP and BDP, some new structural phosphates with high phosphorus contents have been developed at the laboratory or pilot scale. For example, solid phosphates, phloroglucinol tris(cyclic 2,2-dimethyl-1,3-propanediol phosphate) (PCBMPP, Scheme 1) and phloroglucinol tris(cyclic 1,3-propanediol phosphate) (PCPP, Scheme 2) were synthesized with a phosphorus content of 16.29 wt. % and 19.11 wt. %, respectively. PCBMPP and PCPP left more char residue in thermogravimetric analysis (TGA) than RDP, and with 3-5 wt. % loadings of these phosphates, PC could reach UL-94 V-0 ratings (*10*). Zhao *et al* synthesized a cage-shaped solid phosphate, tris(1-oxo-2,6,7-trioxa-1-phosphobicyclo[2,2,2]octane methylene-4) (Trimer, Scheme 3), with a phosphorus content of 21.2 wt. %. PC loaded with 8 wt. % of Trimer had a UL-94 V-0 rating, unchanged mechanical and even an enhanced flexural modulus (*11*); this Trimer has been already produced at the pilot scale.

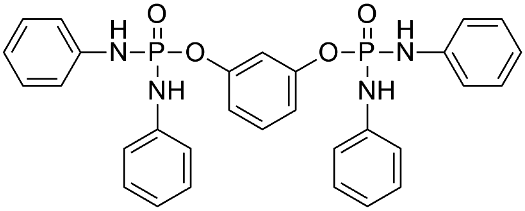

Scheme 4

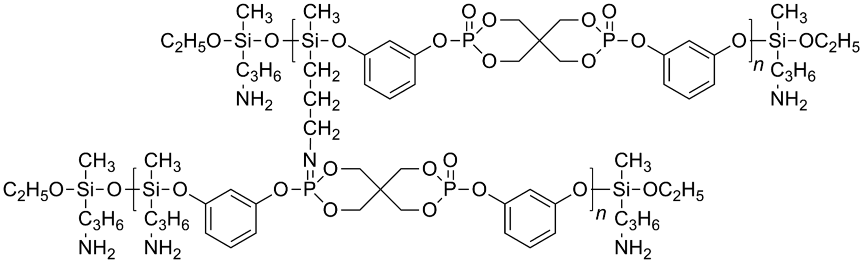

Scheme 5

With the expectation of synergistic effects, other flame retardant elements were also introduced in the phosphorus-containing flame retardants. With an analogous structure of RDP, resorcinol bis(*N*,*N′*-diarylphosphoramidate) (4N-RDP, Scheme 4) exhibited more char residue than RDP in TGA and only 3 wt. % loading was needed in PC to reach a V-0 rating whereas 5 wt. % loading was needed for RDP. The authors claimed that coupling reactions, such as intermolecular transesterification reactions between the –NH– and the pentavalent phosphorus in a neighboring molecule, would form thermally stable P–N rich residue, and this thermally stable residue was beneficial for enhancing the flame retardancy (*12*). Li *et al* synthesized a complicated phosphate structure containing phosphorus, silicon and nitrogen. With 15 wt. % loading of this phosphate, poly(3-aminopropyl methylsiloxane bis(3-hydroxyphenyl spirocyclic pentaerythritol bisphosphate)) (PSBPBP, Scheme 5), PC exhibited a UL-94 V-0 rating. Although the flame retardant efficiency of PSBPBP was not as good as RDP or BDP, it should be mentioned that the mechanical properties of the matrix remained almost unchanged with even 15 wt. % loading of PSBPBP, while RDP or BDP usually worsens the mechanical properties, especially the toughness (*13*).

To sum up, the development of phosphorus-containing flame retardants used for PC and its blends trends towards high phosphorus content phosphate in solid phase within the temperature range that the polymer will be used, and also introducing other flame retardant elements to react with phosphorus.

Siloxanes

Siloxane derivatives are effective flame retardants for PC and its blends. Due to their good compatibility with PC and its blends, siloxanes do not compromise much of the excellent mechanical or thermal properties of the matrix. Siloxanes with a branched structure, relatively low molecular weight and bearing both methyl and phenyl side group in the chain were quite effective to improve the flame retardancy of PC and PC/ABS blend; the impact strength of PC was reduced to a certain extent (*14*). These siloxanes would react with the polymer to crosslink and form thermally stable char residue to be a good insulating barrier on the surface of the samples (*14*, *15*).

In order to preserve or even enhance the impact strength, some new siloxanes were developed.

A core-shell structure latex containing a polysiloxane rubbery core (MSiS) was blended into recycled PC. With the help of some compatibilizers, MSiS was well dispersed in the matrix and thus the impact strength and flame retardancy of the sample were improved simultaneously (*16*).

Methylhydrosilicone oil was condensation reacted with phenol, and then the resulting siloxane product was blended into PC. With 5 wt. % loading of this siloxane, notched impact strength of the sample was increased by 48.9% and a UL-94 V-0 rating was reached (*17*).

A ladder structure polyphenylsilsesquioxane (PPSQ, Scheme 6) was synthesized and blended into PC. 4 wt. % loading of PPSQ was enough to obtain a UL-94 V0 rating at 3.2 mm thickness. Although no impact strength data was presented, the almost unchanged elongation at break was an indication of persevered toughness of the matrix. It is also noted that the HDT was also unchanged (*18*).

Generally, siloxanes are good choices to improve flame retardancy of PC and its blends as well as to preserve or even enhance the mechanical and thermal properties of the matrix.

Sulfur-Containing Compounds

Sulfonates were found to be extremely effective flame retardants for PC as early as 1970s (*19*). Typically, the sample exhibited sufficient flame retardancy with less than 1 wt. % loading of sulfonate. The flame retardant mechanism is not yet fully understood, but many cases suggested that the earlier initial thermal decomposition and crosslinking of the matrix catalyzed by the sulfonates is the main explanation (*20*, *21*). The effectiveness of the flame retardancy was related to the decomposition temperature of the sulfonate salts, and the best result was obtained when the decomposition temperature of the sulfonate matched the maximum decomposition temperature of the matrix (*20*). Also the decomposition of the matrix, promoted by the additive, leads to an accelerating evolution of CO_2 and a dilution effect in the flame (*21*).

Sulfonates are often used together with fluoride and siloxanes. When 0.1-0.3 wt. % loading of potassium diphenylsulfone sulfonate, poly(aminopropyl/phenylsilsesquioxane) and poly(vinylidenefluoride) were added to PC, the LOI of the samples increased to approximate 38 % and UL-94 V-0 ratings were achieved. A synergistic effect between sulfonate, fluoride and siloxane was detected (*22*).

Since the necessary loading of sulfonates is quite small, unchanged transparency and mechanical properties of PC is the major feature. Therefore, sulfonates are suitable for the applications focused on optical and mechanical properties of PC. However, the thermal stability of the sample is deteriorated, thus it is not appropriate for samples with high temperature applications.

Besides sulfonates, other sulfur-containing compounds were also used. Liu *et al* loaded 10 wt. % poly(ether sulfones) (Scheme 7) and 0.5 wt. % polysiloxane/acrylate copolymer into PC. A UL-94 V-0 rating was obtained with the sample thickness of 1.6 mm, while the toughness and rigidity of the matrix was retained (*23*).

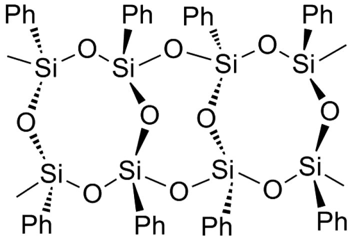

Scheme 6

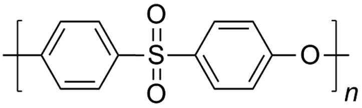

Scheme 7

Nanocomposite Technology

Nanocomposite technology is abundantly studied in various polymer systems because of the enhanced properties of the polymers with a small loading of nano-fillers (*24*). Among these properties, flame retardancy improvement is also noticed especially by the remarkably reduced heat release rate (HRR) in cone calorimetry (*25*, *26*). PC/PC-blends nanocomposites are discovered with improved flame retardancy as well.

Nano-sized silica was blended into PC-polydimethylsiloxane (PC-PDMS) copolymer. With only 0.5 wt. % loading of silica, the PDMS domains in PC dispersed more evenly leading to decreased haze; LOI of the sample was increased a little, and maximum weight loss rate was reduced (*27*).

The LOI value of PC/nano-hydroxyapatite (HAP) reached 34 % with 0.5 wt % HAP compared with 26 % for the pure polymer. It was speculated that the small amount of the nano-additive could help to increase the thermal stability of PC in the earlier degradation (*28*).

Trisilanolphenyl polyhedral oligomeric silsesquioxane (TPOSS) was dispersed in PC at the nano-scale. The char residue layer on the surface of the sample with TPOSS was found to be of higher thermal oxidative stability, and the peak HRR was reduced by 46 % with 2 wt. % of TPOSS in the matrix (*29*).

Multiwall carbon nanotubes (MWNT) could largely reduce the peak HRR under lower irradiations in cone calorimetry. However, the LOI of PC was not affected and UL-94 result was worsened by the loading of MWNT (*30*).

PC/nano-magnesium oxide (MgO) nanocomposites were also developed. There was a significant increase of LOI with small loadings of MgO. The mechanism of the improvement of flame retardancy was explained by the catalyzed initial decomposition of the matrix by MgO and formation of thermal stable char layer on the surface (*31*).

Generally, PC/PC-blends nanocomposites with enhanced flame retardancy may also exhibit enhanced thermal and mechanical properties (for example: increased mechanical strength, elevated HDT). Thus, they are suitable for applications where higher strength or service temperature is required. However, despite the reduced HRR, samples tend to be easier to ignite with a decreased time to ignition in the cone calorimeter test; self-extinguishing property of the samples is compromised showing a worsened UL-94 test result. With respect to these shortcomings, studies of nanocomposites combined with conventional halogen-free flame retardants have emerged recently.

Synergy between Nanocomposites Technology and Conventional Halogen-Free Flame Retardants

Nanocomposite technology combined with conventional halogen-free flame retardants not only might introduce separate effects of the two components into the matrix at the same time, but also a synergy between them could occur. This method could be a solution to overcome the possible drawbacks when each is used alone. Phosphorus-containing compounds have been chosen to combine with nanocomposites technology to be used in PC and its blends.

Trisilanolphenyl-POSS (TPOSS) and BDP were blended into PC. Results showed a synergistic effect on flame retardancy at an optimized ratio between TPOSS and BDP. In this case, 2 wt. % TPOSS combined with 3 wt. % BDP exhibited the best performance in reducing the peak HRR of the matrix in the cone calorimeter (*32*). Taking advantages of the variability of the organic side group of POSS, Zhang *et al* synthesized a POSS bearing 9,10-dihydro-9-oxa-10-phosphaphenanthrene-10-oxide (DOPO) side groups and used it in both PC (*33*) and PC/ABS blend (*34*). This is a case which actually tied the nano-filler and a conventional flame retardant together, thus nano-dispersion of the nano-filler and the conventional flame retardant could be achieved simultaneously. Only 4 wt. % and 10 wt. % loading of this DOPO-POSS was needed to allow PC and PC/ABS blend, respectively, to achieve a UL-94 V-0 rating.

Clays are another type of nano-fillers used. A novel DOPO-containing siloxane (DOPO-VTES) was synthesized and used in PC. 5 wt. % loading of DOPO-VTES increased the LOI of PC but failed to improve the UL-94 rating. When an additional 2 wt. % of montmorillonite (MMT) was added, a UL-94 V-0 rating was achieved (*35*). Solid BDP was also combined with organo-MMT. A synergistic effect between these two components could be noticed in UL-94 test and cone calorimeter results. The mechanism was explained by enhanced condensed phase effect of BDP in the present of organo-MMT (*36*, *37*). Further investigations showed BDP and organo-MMT filled samples had higher mechanical strength and modulus; the types of organic modifier of the organo-MMT had an impact on the final properties of the flame retarded PC nanocomposites (*38*).

Clays combined with phosphorus-containing flame retardants have been also used for PC blends. Boehmite and three aryl phosphates (TPP, RDP and BDP) were combined in PC/ABS blend. BDP with 5 wt. % boehmite showed a positive effect of reducing peak HRR and increasing LOI of the matrix (*39*). Feyz *et al* used TPP combined with MMT in PC/ABS blend. Synergistic effects revealed by LOI, UL-94 and cone calorimetry appeared with enhanced mechanical properties (*40*). RDP was absorbed on the surface of MMT (RDP-MMT) and used in a PC/poly(styrene-co-acrylonitrile) (SAN) blend. Morphological analysis showed RDP-MMT enhanced the compatibility between PC and SAN. Reduced HRR was detected with an improved char residue layer after cone calorimetry (*41*).

From above examples, the various phosphorus-containing flame retardants have already been proven to work with nanocomposites technology showing synergistic effects, especially exhibiting improved self-extinguishing property; however research on the change of time to ignition of nanocomposites is not yet fully understood. Whether other conventional flame retardants could be combined with nanocomposite technology is a topic that should be studied further. Combining nanocomposite technology with conventional flame retardants should be a promising route to develop PC and its blends with improved flame retardancy and other properties.

Conclusion

PC and its blends are very important engineering plastics, and recent developments of halogen-free flame retardancy of PC and its blends are summarized here.

Conventional halogen-free flame retardants used in PC and its blends include phosphorus-containing compounds, siloxanes and sulfur-containing compounds. With regards to the drawbacks of these flame retardants, some new structures have emerged: phosphates should be solids with a high phosphorus content. In addition to sulfonates, sulfones were also found effective for PC. Also, combinations of different kinds of conventional flame retardants have been studied.

Nanocomposite technology has been applied in flame retardancy of PC and its blends as well. Various kinds of nano-fillers showed possibilities to enhance the flame retardancy, mechanical and thermal properties of PC and its blends. However, ease of ignition and difficulty of self-extinguish remain problems, as with other polymer nanocomposite systems. Thus, methods of combining conventional halogen-free flame retardants, especially phosphorus-containing ones, with nanocomposite technology have arisen; synergy between the conventional flame retardants and nano-fillers are assumed to be a solution of the problem of difficulty of self-extinguishment. Regarding the topic of ease of ignition and combining nanocomposites technology with other sorts of the conventional flame retardants, more research is expected in the future.

References

1. Levchik, S. V.; Weil, E. D. *Polym. Int.* **2005**, *54* (7), 981–998.
2. Levchik, S. V.; Weil, E. D. *J. Fire Sci.* **2006**, *24* (2), 137–151.
3. Fox, D. W. U.S. Patent 3,855,277, 1974.
4. Gilman, J. W.; Kashiwagi, T.; Lichtenhan, J. D. *SAMPE J.* **1997**, *33* (4), 40–46.
5. Jian, R. K.; Chen, L.; Hu, Z.; Wang, Y. Z. *J. Appl. Polym. Sci.* **2012**, *123* (5), 2867–2874.
6. Green, J. *J. Fire Sci.* **1991**, *9* (4), 285–295.
7. Green, J. *J. Fire Sci.* **1994**, *12* (4), 388–408.
8. Pawlowski, K. H.; Schartel, B. *Polym. Int.* **2007**, *56* (11), 1404–1414.
9. Perret, B.; Pawlowski, K. H.; Schartel, B. *J. Therm. Anal. Calorim.* **2009**, *97* (3), 949–958.
10. Vothi, H.; Nguyen, C.; Lee, K.; Kim, J. *Polym. Degrad. Stab.* **2010**, *95* (6), 1092–1098.
11. Zhao, Y.; Ou, Y. X.; Li, X. M. *China Synth. Resin Plast.* **2008**, *25* (6), 25–28.
12. Nguyen, C.; Kim, J. *Polym. Degrad. Stab.* **2008**, *93* (6), 1037–1043.
13. Li, L. K.; Wei, P.; Li, J.; Jow, J.; Su, K. *J. Fire Sci.* **2010**, *28* (6), 523–538.
14. Masatoshi, I.; Serizawa, S. *Polym. Adv. Technol.* **1998**, *9* (10-11), 593–600.
15. Zhou, W.; Yang, H. *Thermochim. Acta* **2007**, *452* (1), 43–48.
16. Sun, S. Y.; He, Y. D.; Wang, X. D.; Wu, D. Z. *J. Appl. Polym. Sci.* **2010**, *116* (4), 2451–2464.

17. Ding, L. P.; Song, R. J.; Li, B. *Polym. Mater. Sci. Eng.* **2011**, *27* (10), 138–142.
18. Jiang, Y. Y.; Li, X. M.; Yang, R. J. *J. Appl. Polym. Sci.* **2012**, *124* (5), 4381–4388.
19. Nouvertne, W. U.S. Patent 3,775,367, 1973.
20. Nodera, A.; Kanai, T. *J. Appl. Polym. Sci.* **2004**, *94* (5), 2131–2139.
21. Huang, X. B.; Ouyang, X. Y.; Ning, F. L.; Wang, J. Q. *Polym. Degrad. Stab.* **2006**, *91* (3), 606–613.
22. Liu, S. M.; Ye, H.; Zhou, Y. S.; He, J. H.; Jiang, Z. J.; Zhao, J. Q.; Huang, X. B. *Polym. Degrad. Stab.* **2006**, *91* (8), 1808–1814.
23. Liu, S. M.; Yang, Y.; Jiang, Z. J.; Zhou, Y. H.; Zuo, J.; Zhao, J. Q. *J. Appl. Polym. Sci.* **2012**, *124* (6), 4502–4511.
24. Paul, D. R.; Robeson, L. M. *Polymer* **2008**, *49* (15), 3187–3204.
25. Morgan, A. B. *Polym. Adv. Technol.* **2006**, *17* (4), 206–217.
26. Kiliaris, P.; Papaspyrides, C. D. *Prog. Polym Sci.* **2010**, *35* (7), 902–958.
27. Nodera, A.; Kanai, T. *J. Appl. Polym. Sci.* **2006**, *101* (6), 3862–3868.
28. Dong, Q. X.; Chen, Q. J.; Yang, W.; Zheng, Y. L.; Liu, X.; Li, Y. L.; Yang, M. B. *J. Appl. Polym. Sci.* **2008**, *109* (1), 659–663.
29. Song, L.; He, Q. L.; Hu, Y.; Chen, H.; Liu, L. *Polym. Degrad. Stab.* **2008**, *93* (3), 627–639.
30. Schartel, B.; Braun, U.; Knoll, U.; Bartholmai, M.; Goering, H.; Neubert, D.; Potschke, P. *Polym. Eng. Sci.* **2008**, *48* (1), 149–158.
31. Dong, Q. X.; Gao, C.; Ding, Y. F.; Wang, F.; Wen, B.; Zhang, S. M.; Wang, T. X.; Yang, M. S. *J. Appl. Polym. Sci.* **2012**, *123* (2), 1085–1093.
32. He, Q. L.; Song, L.; Hu, Y.; Zhou, S. *J. Mater. Sci.* **2009**, *44* (5), 1308–1316.
33. Zhang, W.; Li, X.; Guo, X.; Yang, R. *Polym. Degrad. Stab.* **2010**, *95* (12), 2541–2546.
34. Zhang, W. C.; Li, X. M.; Yang, R. J. *Polym. Adv. Technol.* **2012**, *23* (3), 588–595.
35. Hu, Z.; Chen, L.; Zhao, B.; Luo, Y. A.; Wang, D. Y.; Wang, Y. Z. *Polym. Degrad. Stab.* **2011**, *96* (3), 320–327.
36. Feng, J.; Hao, J. W.; Du, J. X.; Yang, R. J. *Polym. Degrad. Stab.* **2010**, *95* (10), 2041–2048.
37. Feng, J.; Hao, J. W.; Du, J. X.; Yang, R. J. *Polym. Degrad. Stab.* **2012**, *97* (4), 605–614.
38. Feng, J.; Hao, J. W.; Du, J. X.; Yang, R. J. *Polym. Degrad. Stab.* **2012**, *97* (1), 108–117.
39. Pawlowski, K. H.; Schartel, B. *Polym. Degrad. Stab.* **2008**, *93* (3), 657–667.
40. Feyz, E.; Jahani, Y.; Esfandeh, M. *J. Appl. Polym. Sci.* **2011**, *120* (6), 3435–3442.
41. Pack, S.; Kashiwagi, T.; Cao, C. H.; Korach, C. S.; Lewin, M.; Rafailovich, M. H. *Macromolecules* **2010**, *43* (12), 5338–5351.

Chapter 9

Antiflammable Properties of Capable Phosphorus−Nitrogen-Containing Triazine Derivatives on Cotton

SeChin Chang,* Brian Condon, Thach-Mien Nguyen, Elena Graves, and Jade Smith

Southern Regional Research Center (SRRC), United States Department of Agriculture (USDA) – Agricultural Research Service (ARS),
1100 Robert E. Lee Blvd., New Orleans, Louisiana 70124
***E-mail: sechin.chang@ars.usda.gov**

Herein we present the synthesis and application of triazine derivatives as flame retardants on cotton. Novel phosphorus−nitrogen-containing compounds (*TPN1*, *TPN2*, *TPN3* and *TPN4*) were prepared by organic reactions of cyanuric chloride and phosphonates. They were characterized by analytical tools such as proton (^{1}H) and carbon (^{13}C) nuclear magnetic resonance (NMR) spectroscopy, and elemental analysis (EA). Cotton twill fabrics were soaked in 10-20% aqueous sodium hydroxide and then treated with *TPN1*-*TPN4* in various organic solvent mixtures. The compounds were grafted onto the fabric by traditional pad, dry, cure methods to produce semi-durable flame resistance. Thermogravimetric analysis (TGA) provided degradation and char content information on all materials by measuring the change in mass as a function of rising temperature. Treated fabrics were evaluated for flame resistance by such methods as vertical flammability test (ASTM D6413-08), 45° angle flammability test (ASTM D1230-01) and limiting oxygen index (LOI, ASTM D2863-09).

Not subject to U.S. Copyright. Published 2012 by American Chemical Society
In Fire and Polymers VI: New Advances in Flame Retardant Chemistry and Science; Morgan, A., et al.;
ACS Symposium Series; American Chemical Society: Washington, DC, 2012.

Introduction

In response to increasing government regulation for fire safety and environmental issues, new flame retardants such as non-halogenated, non-toxic, and environmentally friendly materials are needed (*1*). Phosphorus-containing compounds are widely used in the textile industry to make cotton textiles flame resistant (*2*, *3*). Phosphorus-containing flame retardant compounds have been chemically reacted with cotton, producing products with an ether cross linker between the phosphorus compound and the cellulosic material. In the condensed phase, the phosphorus-containing functional groups are converted by thermal decomposition to phosphoric acid, forming a protective char. Char development and intumescence provide low flammability to cotton textiles (*4*, *5*).

Nitrogen-containing flame retardants, in combination with phosphorus compounds, have multifunctional advantages: 1) low toxicity during combustion, 2) high efficiency as measured by cone calorimetry, and 3) low smoke development in fire accidents (*6*). Some nitrogen-containing compounds, such as urea, dicyandiamide, and melamine, will accelerate phosphorylation of cellulose through formation of a phosphorus-nitrogen intermediate, and thus synergize the flame retardant action of phosphorus (*7*, *8*).

Triazine and its derivatives are known as flame retardant materials and good charring agents because of their abundant nitrogen and structure of tertiary nitrogen (*9*). Furthermore, triazines are of beneficial merit since they are commercially available, comparatively cheap, and environmentally clean materials.

This research is focused on an organophosphorus flame retardant. Mono- and di-substituted diethyl phosphonate (*TPN1* and *TPN2*) and dimethyl hydroxymethylphosphonate (*TPN3* and *TPN4*) derivatives of cyanuric chloride were chosen as potential flame retardants for cotton. The choice of cyanuric chloride is based on its affordability and the advantage of its chemical structure, with abundant nitrogen. Utilizing the existing dye and flame retardant chemistry between cyanuric chloride and cotton (*10–13*), cyanuric chloride was derivatized with phosphonate. This article presents the preparation of *TPN1-TPN4*, and the comparison of the synthesis and characterization, flame retardant performance, including vertical and 45° angle flammability and LOI testing, as well as thermal properties by thermogravimetric analysis (TGA) of the flame retardant treatments on cotton twill fabric.

Experimental

Materials and Measurements

Some of the synthesis and characterization of the flame retardants covered in this paper were as reported (*14*, *15*). Triethylphosphite, dimethylphosphate, paraformaldehyde, potassium carbonate, and cyanuric chloride were purchased from Sigma-Aldrich. Regent grade solvents and all other commercially available reagents were used as received. All reactions were carried out under nitrogen atmospheric conditions and monitored using silica gel 60 F_{254} thin layer chromatography (TLC) purchased from EMD. Twill fabric, 258g/m^2 (Testfabrics, Inc., Style 423) was bleached and mercerized. ^{1}H and ^{13}C NMR spectra were recorded on a Varian Unity plus 400 spectrometer (400 MHz) at ambient probe temperature. Tetramethylsilane and $CDCl_3$ were used as internal reference. GC/MS was carried out on an Agilent 6890GC coupled to a time-of-flight mass spectrometer (Leco Corporation, St. Joseph, MI) with a DB-5 (Supelco, Bellefonte, PA) capillary column of 30 m x 0.25 mm ID x 0.25 µm as stationary phase. Elemental analyses were carried out on a 2400 series II CHNS/O Analyser, PerkinElmer and ICP Leeman Labs Prodigy/Prism at 253 and 561 nm.

Synthesis of Diethyl 4,6-dichloro-1,3,5-triazin-2-ylphosphonate, *TPN1*

A mixture of cyanuric chloride (20.0 g, 110 mmol) and anhydrous toluene (250 mL) were stirred at room temperature until dissolved, and then this solution was stirred 1 hour at 0°C. To this solution, triethylphosphite (21.6 g, 130 mmol) in anhydrous toluene (100 mL) was added dropwise at 0°C. When the addition was complete, the reaction mixture was cooled to 0°C for 7-8 hours, then allowed to warm to room temperature and stirred overnight. The solvent was removed via rotary evaporation and a light yellow oil was obtained (32.0g, 86.0% yield). ^{1}H NMR (400MHz, $CDCl_3$) δ-ppm: 1.46 (t, 6H, $POCH_2\mathit{CH_3}$), 4.45 (q, 4H, $PO\mathit{CH_2}CH_3$). ^{13}C NMR (100MHz, $CDCl_3$) δ-ppm: 16.4, 65.5, 172.3-176.7. *m/z* observed 286.0 (calcd. 286.05). Anal. Calcd for $C_7H_{10}Cl_2N_3O_3P$: C=29.39%; H=3.52%; N=14.69%. Found C=30.02%; H=5.50%; N= 11.18%.

Synthesis of Tetraethyl 6-chloro-1,3,5-triazin-2,4-diyldiphosphonate, *TPN2*

Cyanuric chloride (19.9 g, 0.11 moles) in anhydrous toluene (400ml) was stirred for 1 hour with gentle heating to a temperature of approximately 60°C. A solution of triethylphosphite (37.7 g, 0.23 moles) in anhydrous toluene (200 ml) was added dropwise over 1 hour under nitrogen atmosphere with increased heating to 90°C. The mixture was refluxed for 18 hours and the solvent was evaporated after filtration. A light yellow oil was obtained (40.7 g, 98.0 % yield). ^{1}H NMR (400 MHz, $CDCl_3$): δ 1.33 (t, 12H, $POCH_2\mathit{CH_3}$), 4.32 (q, 8H, $PO\mathit{CH_2}CH_3$). ^{13}C NMR (100 MHz, $CDCl_3$): δ 16.1, 65.0, 170.6-175.2. *M+Na* observed 410.05 (calcd 387.69). Anal calcd for $C_{11}H_{20}ClN_3 O_6P_2$: C=34.04%; H=5.20; N=10.84; Found C=30.02%; H=5.50; N=11.18 %.

Synthesis of Dimethyl (4,6-dichloro-1,3,5-triazin-2-yloxy)methyl Phosphonate, *TPN3*

A mixture of cyanuric chloride (5.0 g, 27 mmol) and acetone (170 mL) was stirred at room temperature until dissolved. The solution was then cooled to 0°C. To this solution, dimethyl hydroxymethyl phosphonate (3.80 g, 27 mmol) in H_2O (100 mL) was added dropwise. The pH of the reaction mixture was adjusted to 5.5-6 with solid anhydrous K_2CO_3 as needed throughout the experiment. The reaction progress was followed by TLC using 5% MeOH/EtOAc as eluent. When the addition was complete, the ice bath was removed, and the reaction was allowed to warm to room temperature. After fifteen minutes at room temperature, TLC confirmed the disappearance of cyanuric chloride and the appearance of the desired product. The solid was then filtered off, and the acetone was removed via rotary evaporator. Brine (100 mL) was added, and the solution was extracted with $CHCl_3$ (3 x 200 mL). The organic layer was combined, dried over Na_2SO_4, filtered and evaporated to obtain a colorless oily compound. This was further dried under high vacuum to give an off-white solid at 75-80 % yield. ^{1}H NMR (400MHz, $CDCl_3$) δ-ppm: 3.86 (d, 6H, PO*CH$_3$*), 4.80 (d, 2H, -O*CH$_2$*P). ^{13}C NMR (100MHz, $CDCl_3$) δ-ppm: 53.6, 60.5, 171.0, 173.0. ^{31}P NMR (162MHz, $CDCl_3$) δ-ppm: 18.8 (m). *m/z* observed 288.0 (calcd. 288.03). Anal. Calcd for $C_9H_{16}ClN_3O_8P_2$: C= 25.02%; H= 2.80%; N= 14.60%; P= 10.75%. Found C= 25.27%; H= 2.91%; N= 14.72%; P= 10.71%.

Synthesis of Tetramethyl (6-chloro-1,3,5-triazine-2,4-diyl)bis(oxy)bis(methylene) Diphosphonate, *TPN4*

A mixture of cyanuric chloride (2.0 g, 10.85 mmol) and acetone (70 ml) was stirred until dissolved. To this solution, dimethyl hydroxymethyl phosphonate (3.36 g, 24 mmol) was added dropwise. The solution was then cooled to 0°C. A mixture of aqueous 50% w/w NaOH in 30 ml of distilled water was added dropwise to the above solution. The reaction was allowed to warm to room temperature after 2 hours and was monitored by the Fujiwara test (*19*) and TLC with MeOH/EtOAc as an eluent. After the solvent was removed via rotary evaporation, the aqueous solution was then extracted with $CHCl_3$. The organic layer was combined, dried over Na_2SO_4, filtered, and evaporated to obtain a colorless oily compound. This was further dried under high vacuum to give a white solid at 76–82% yield. ^{1}H NMR (400 MHz, $CDCl_3$) δ (ppm): 3.85 (d, 12H, PO*CH$_3$*), 4.80 (d, 4H, -O*CH$_2$*P). ^{13}C NMR (100 MHz, $CDCl_3$) δ (ppm): 53.5, 60.0, 172.0, 173.2. 31P NMR (162 MHz, $CDCl_3$) δ (ppm): 19.9 (septet). m/z observed 392.0 (calcd. 391.64). Anal. calcd. for $C_9H_{16}ClN_3O_8P_2$: C = 27.60%; H = 4.12%; N = 10.73%; P = 15.82%. Found C = 26.70%; H = 4.21%; N= 10.23%; P = 16.10%.

Fabric Treatment

The fabric used was cotton twill (238 g/m^2) that was desized, scoured, bleached and mercerized. Fabric samples (17 x 9 in.) were soaked in a 20 % sodium hydroxide solution for 2 hours and processed on a two roll padder at 40 psi pressure. The cotton fabric was then treated with 50% aqueous isopropanol formulations containing various percentages of *TPN1-TPN4*. Fabric samples were immersed in the treatment solution overnight for thorough wetting, then padded (10 psi), dried (100°C, for 5 min), and cured in air (140°C, for 5 min). After curing, the fabric was allowed to cool to room temperature. Weight of the fabric before and after treatment was recorded. The wet pick-up weight after padding and the dry pick-up weight after drying in the dessicator were obtained. Flammability testing was carried out immediately after obtaining the add-on value.

Limiting Oxygen Index (LOI) and Flammability Test (Vertical and 45° Angle)

The limiting oxygen index (LOI) values were measured on a limiting oxygen index chamber (Dynisco polymer test) with strips of fabrics (6.35×12.7 cm) according to ASTM D-2863-09 (*16*). Vertical flame tests were conducted on a vertical flammability model VC-2 instrument (Govmark Inc.) with strips of fabrics (30×7.6 cm) according to ASTM D-6413-08 (*17*). 45° angle flame tests were performed on strips of fabric (15 x 6 cm) according to ASTM D-1230-01 (*18*).

Thermogravimetric Analysis (TGA)

Onsets of degradation (*20–22*) and char content at 600°C were obtained from thermogravimetric analysis (TGA) thermograms. Fabric degradations were observed for untreated and treated fabrics in nitrogen atmosphere by TGA (from 20 to 600°C, heating rate 10°C/min).

Results and Discussion

Synthesis and Characterization of Flame Retardants, *TPN1-TPN4*

Diethyl 4,6-dichloro-1,3,5-triazin-2-ylphosphonate, *TPN1*, and tetraethyl 6-chloro-1,3,5-triazin-2,4-diyldiphosphonate, *TPN2*, were prepared in one step as shown in Scheme 1. *TPN1* was synthesized by cyanuric chloride and triethylphosphite in anhydrous toluene at 0°C. Following work up, *TPN1,* was obtained in 86.0% yield as a light yellow oil. It afforded baseline ^{1}H and ^{13}C NMR spectra and needed no further purification. Tetraethyl 6-chloro-1,3,5-triazine-2,4-diyldiphosphonate, *TPN2*, was also prepared in one step through the Michaelis-Arbrusov reaction followed by oxidation of cyanuric chloride and triethylphosphite in toluene at reflux condition as light yellow oil (98.0 % yield) (*14*). ^{1}H and ^{13}C data for *TPN1* and *TPN2* are consistent with structure as explained in Table I. In Figure 1(a) ^{1}H NMR spectrum of *TPN1*, the chemical shift at 4.48-4.40 ppm belongs to the -OCH_2CH$_3$ protons and the chemical shift at 1.48-1.35 ppm are assigned to the -OCH$_2$$CH_3$ protons. Figure 1(b) shows the ^{13}C NMR spectrum of *TPN1*. The peak at about 16.4 and 65.5 ppm are assigned to -OCH$_2$$CH_3$ and -OCH_2CH$_3$. Also, the peaks at about 171.0-177.0 ppm belong to aromatic back bond carbons. Synthesis and characterization of *TPN2* was reported earlier, and most of the chemical shifts of NMR data had very similar values to *TPN1* (*14*).

Dimethyl(4,6-dichloro-1,3,5-triazin-2-yloxy)methyl-phosphonate, *TPN3*, and tetramethyl (6-chloro-1,3,5-triazine-2,4-diyl)bis(oxy)bis(methylene) diphosphonate, *TPN4* (*15*), were successfully synthesized in one simple step in high yield of 75-82% (Scheme 1). The product could be used without further purification. *TPN3* readily dissolved in MeOH, THF, acetone, and chloroform. It dissolved slowly in ethyl acetate and methylene chloride. Like *TPN4* (*15*), the temperature, pH of reaction medium, and molar ratio between cyanuric chloride and dimethyl hydroxylmethyl phosphonate were important factors in preparation of *TPN3*. *TPN3* formation favored low temperature and slightly acidic medium, while *TPN4* could be obtained at room temperature and in slightly basic medium. The chemical structure of *TPN3* was studied by NMR, GC-MS, and elemental analysis. Chemical shift of NMR results for *TPN3* and *TPN4* are listed in Table I for comparison. Both compounds have 2 signals in ^{1}H NMR data and 4 signals in ^{13}C NMR data. Figure 1(c) shown ^{1}H NMR of *TPN3*. The six protons at 3.87 ppm and two protons at 4.84 ppm, are assigned to methoxy and methylene protons, respectively. Figure 1(d) showed 4 signals of carbon. The peak at about 53.6 and 61.3 ppm are assigned to -OCH_3 and -OCH_2POCH$_3$, respectively. Also, the peaks at about 171.0 and 173.0 ppm belong to the aromatic back bond carbons.

From Table I, it is obvious that the chemical shifts in proton and carbon data of two compounds are close to each other. It is noticeable that the carbon which attaches to oxygen of phosphorus group (C-O) appears as a doublet. When comparing peak amplitude for this carbon and the carbon attaches to chlorine (C-Cl), it is obvious that both types of carbon exhibit the same amplitude in *TPN4*, but the C-O amplitude is intensively reduced in *TPN3*. This may due to the substituent's type and the number of the substituent on the cyanuric ring. The GC-MS spectrum of *TPN3* provided a molecular ion peak of product 288 and its isotope. The experimental values of elemental analysis are close to the calculated ones. These instrumental analyses results confirm that the chemical structure of *TPN3* is the same as that proposed in Scheme 1.

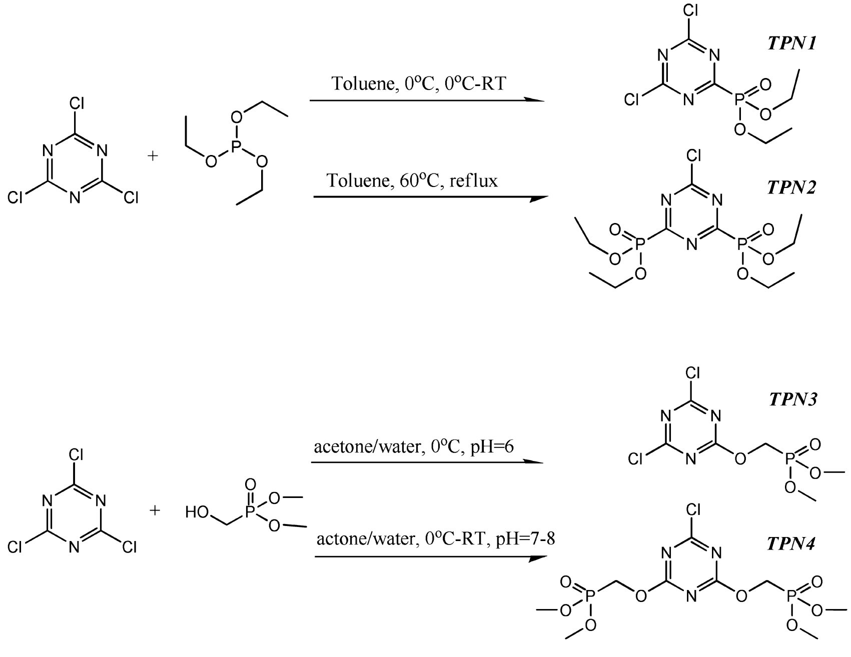

Scheme 1. Synthesis of TPN1, TPN2, TPN3 and TPN4

Fabric Treatment and Phosphorus and Nitrogen Contents

Cotton twill fabric was treated with solutions of *TPN1-TPN4* (w/v in 50% aqueous isopropanol) at room temperature. The fabric was weighed before and after treatment and the data were fitted to equation 1 and 2 to obtain wet pick-up and add-on percents.

$$\text{wet pick-up (\%)} = \frac{\text{(weight after padding - weight before treatment)}}{\text{weight before treatment}} \times 100 \qquad (1)$$

$$\text{add-on (\%)} = \frac{\text{(weight after drying - weight before treatment)}}{\text{weight before treatment}} \times 100 \qquad (2)$$

Table I. Chemical structure and NMR shift data for *TPN1, TPN2, TPN3* and *TPN4*

<table>
<tr><td></td><td colspan="4"><i>TPN1</i> and <i>TPN2</i></td><td colspan="4"><i>TPN3</i> and <i>TPN4</i></td></tr>
<tr><td>Structure</td><td colspan="4">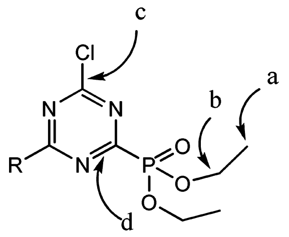 R = -Cl (<i>TPN1</i>)
-P(O)(OCH$_2$CH$_3$)$_2$ (<i>TPN2</i>)</td><td colspan="4">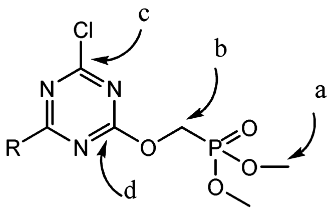 R = -Cl (<i>TPN3</i>)
-OCH$_2$P(O)(OCH$_3$)$_2$ (<i>TPN4</i>)</td></tr>
<tr><td>Position</td><td colspan="2"><i>TPN1</i></td><td colspan="2"><i>TPN2</i></td><td colspan="2"><i>TPN3</i></td><td colspan="2"><i>TPN4</i></td></tr>
<tr><td>ppm</td><td>^{1}H</td><td>^{13}C</td><td>^{1}H</td><td>^{13}C</td><td>^{1}H</td><td>^{13}C</td><td>^{1}H</td><td>^{13}C</td></tr>
<tr><td>a</td><td>1.46</td><td>16.4</td><td>1.33</td><td>16.1</td><td>3.86</td><td>53.6</td><td>3.85</td><td>53.5</td></tr>
<tr><td>b</td><td>4.45</td><td>65.3</td><td>4.32</td><td>65.0</td><td>4.83</td><td>60.5</td><td>4.80</td><td>60.0</td></tr>
<tr><td>c</td><td>-</td><td rowspan="2">171.0-177.0</td><td>-</td><td rowspan="2">170.6-175.2</td><td>-</td><td rowspan="2">171.0-173.0</td><td>-</td><td rowspan="2">172.0-173.2</td></tr>
<tr><td>d</td><td>-</td><td>-</td><td>-</td><td>-</td></tr>
</table>

Overall, *TPN3* samples show more wet pick-up than *TPN4* samples. Surprisingly, 10 wt% add-on of *TPN3* achieved the same wet pick-up as 19 wt% add-on of *TPN4*. After curing, all *TPN4* samples appeared off-white but samples treated with *TPN3* turned grey. In addition, *TPN3* samples were stiffer and more brittle than *TPN4* samples.

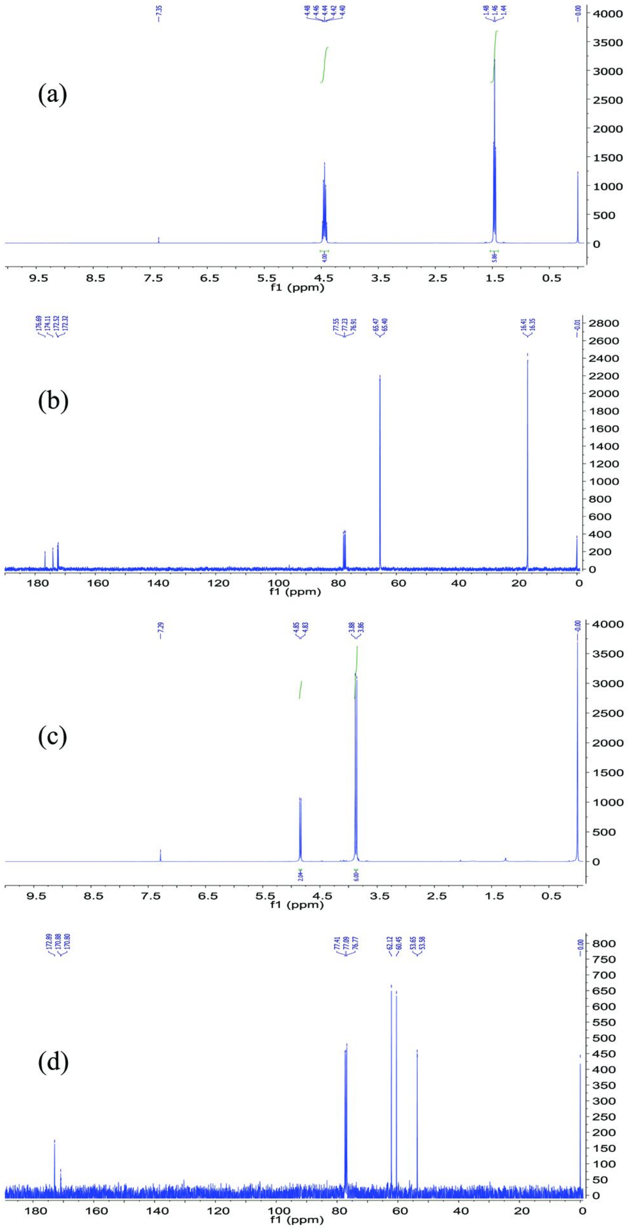

Figure 1. ^{1}H and ^{13}C NMR spectra of TPN1(a:^{1}H and b:^{13}C) and TPN3(c:^{1}H and d:^{13}C).

All add-on percents and their phosphorus and nitrogen percent results were summarized in Figure 2. Content of phosphorous and nitrogen for *TPN1* and *TPN2* were determined analytically for each add-on sample with three observations for nitrogen and six observations for phosphorous. It is apparent that the content of phosphorous and nitrogen increases with the increase of add-on value, and nitrogen content is always higher than phosphorous content in each sample. Nitrogen has been recognized to play a role in fire retardancy and adding nitrogen often reduces the need for phosphorous (*23*). The graphical P-N synergistic effect for a variety of phosphorus-nitrogen systems on cotton twill showed that P+N should be 3.5-6% for flame retardancy (*24*, *25*).

Flame retardants	*TPN1*	*TPN2*	*TPN3*	*TPN4*
Add-ons (wt %)	4, 12, 17, 26, 33	4, 10, 15, 24, 31	5, 10, 16, 21	5, 9, 14, 19

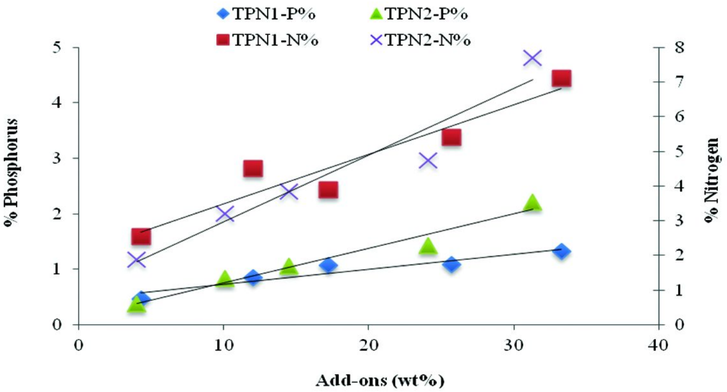

Figure 2. Add-ons (wt %) and contents of phosphorus and nitrogen in treated fabric of TPN1 and TPN2.

Thermal Properties of Flame Retardant Treated Fabric

The thermal degradation data were obtained in a nitrogen atmosphere. Degradation of untreated control twill and various add-ons (wt %) of treated twill samples with *TPN1-TPN4* are presented graphically in Figure 3. Untreated twill fabric showed an onset temperature at 327°C and char residue of 3% of the original weight at 600°C. Treated twill fabric for *TPN1* and *TPN2* with 4-33 add-on (wt %) were degraded between 260 and 295°C, and provided char yield between 15 and 27%. In general, onsets of degradation of the *TPN1* series are very similar to results with the *TPN2* series. However, onsets of degradation of the *TPN3* series are lower than that of the *TPN4* series. Furthermore, the

TPN3 series degrades at a lower temperature than *TPN4* but provides higher char content at 600°C. 5 and 10 wt% add-on *TPN3* samples show onset of degradation at 244 and 242°C; whereas, the onset of degradation of 5 and 9 wt% add-on *TPN4* samples are 287 and 283°C. Within *TPN3* and *TPN4* indivially, these percent yield almost the same char content. Although *TPN3* with 16 and 21 wt% add-ons and *TPN4* with 14 and 19 wt% add-ons provide the same char content, 16 and 21 % samples display the same onset of degradation, while the onset temperature of 14 wt% add-on is higher than that of 19 wt% add-on. The onset temperature of the compound decreases with increasing concentration of the phosphorus moiety, while the onset temperature of the treated fabric decreases with decreasing concentration of phosphorous moiety.

Limiting Oxygen Index (LOI) and Flame Tests (Vertical and 45° Angle) of Fabrics

LOI values indicate the minimum amount of oxygen needed to sustain a candle-like flame when a sample is burned in an atmosphere of oxygen and nitrogen. Textiles are considered to be flammable when LOI values are below 21% oxygen in nitrogen and are considered to be flame retardant when LOI values fall in the range of 26–28%. At these LOI values, flame retarded test fabric samples are expected to pass open flame tests in either the 45° angle or vertical direction (*26*, *27*). Passing an open flame test means that the ignited test sample self extinguished following a very short after-flame time, did not glow after the flame extinguished by itself, and showed a char length that did not equal the length of the test sample.

LOI values and vertical flame tests of untreated fabrics and those treated with *TPN1* and *TPN2* are shown in Table II. LOI values of untreated fabrics were 18% oxygen in nitrogen. LOI data for treated fabrics ranged between 28 and 48%. *TPN1* series provided LOI values of 28, 37, 45, 38 and 48% when add-on values were 4, 12, 17, 26 and 33 wt %. With the *TPN2*, LOI values were 28, 36, 42, 45 and 48% when add-on values were 4, 10, 15, 24 and 31 wt %. All samples treated with *TPN1* and *TPN2* have high LOI values. The lowest, 4 wt% add-on, and the highest, 33 wt% add-on, have LOI values of 28 and 48%, respectively. LOI value increases seem to reach a limiting value with respect to add-on which higher phosphorus content for improved flame resistance. Convinced that our new triazine based monomers will afford flame resistance to fabrics of different constructions, we tested the treated fabrics by the vertical flame test, ASTM D-6413-08 and observed satisfying results. Following 12-sec exposure to flame, treated fabric with more than 12 and 10 wt% add-on for *TPN1* and *TPN2* samples, respectively showed no observable after-flame and after-glow times, and char lengths were less than 6-8.5cm. Based on vertical flammability and LOI results, it can be concluded that *TPN1* and *TPN2* act as good flame retardants when applied to cotton twill fabrics at a level of 10 wt% add on or higher. The results are particularly useful for textile articles of commerce protected under 16CFR Parts 1610.17

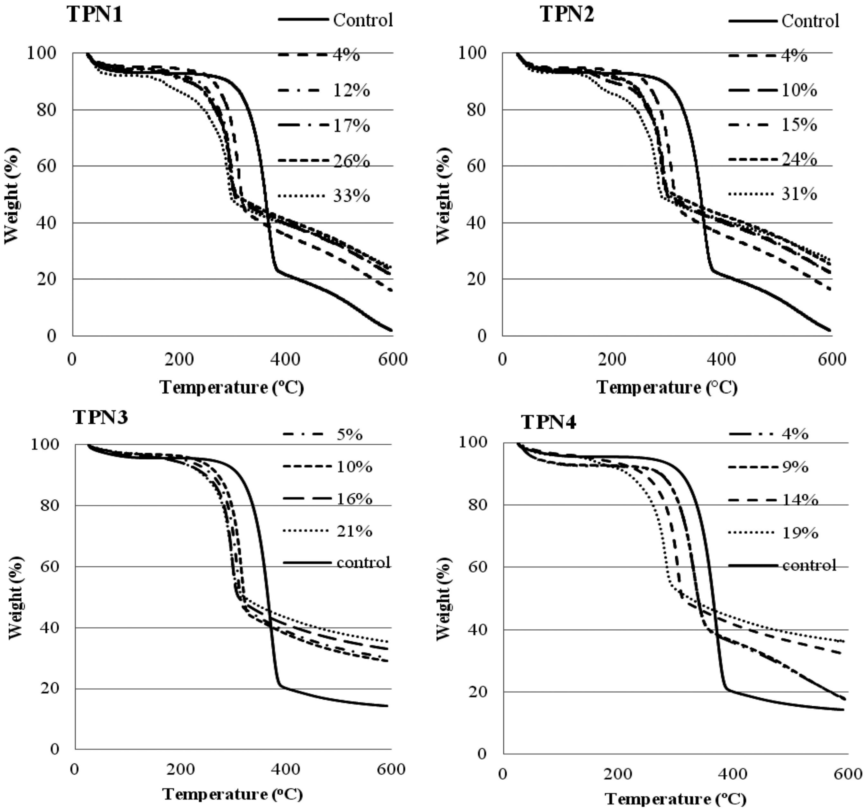

Figure 3. Degradation thermograms of TPN1, TPN2 (14), TPN3, and TPN4 (15) treated fabrics at various add-ons (wt %) by TGA in nitrogen atmosphere.

To evaluate the flame retardancy of *TPN3* and *TPN4*, treated samples with different add-on values were selected for modified standard 45° angle flammability and standard limiting oxygen index testing. Standard 45° angle flammability test (*18*) establishes flammability requirements that all clothing textiles, as defined in the *Standard for the Flammability of Clothing Textiles*, must meet before sale or introduction into commerce. The Standard provides a method for testing and establishes three *classes* of flammability performance of textiles and textile products used for clothing, thereby restricting the use of any dangerously flammable clothing textiles. In this test procedure, a 16 mm (5/8 in) flame impinges on a specimen mounted at a 45° angle for 10 second. The specimen is allowed to burn its full length or until the stop thread is broken, a distance of 127 mm (5 in). Samples of *class I* or *II* meet the requirements of the Standard. If the sample is assigned as *class III*, rapid and intense burning, it fails to meet the requirements of the Standard. The results of LOI and 45° angle flammability test results for samples treated with *TPN3* and *TPN4* are presented in Table III (*28*).

Table II. Vertical flammability (ASTM D-6413-08) (*17*) and limiting oxygen index (LOI) (ASTM D-2863-09) (*16*) test for different add-ons (wt %) of treated twill fabrics for *TPN1* and *TPN2*. [σ]= standard deviation

TPN1 series	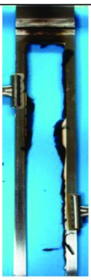	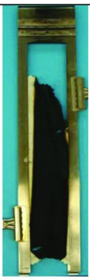	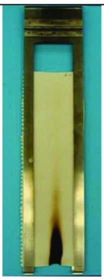	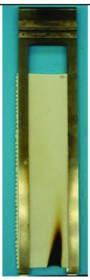	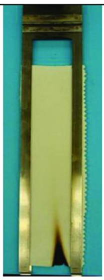	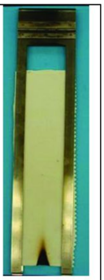
Add-on (wt %)	control	4	12	17	26	33
After-flame (sec)	10	18	2	0	0	0
After-glow (sec)	30	3	0	0	0	0
Char length (cm)	NA	>30	6.0	5.0	3.5	2.5
Ave. LOI (%)[σ]	18[0.12]	28[0.26]	37[0.13]	45[0.26]	38[0]	48[0.20]
TPN2 series	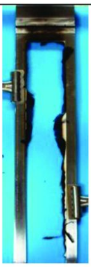	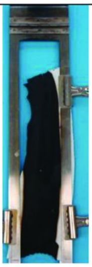	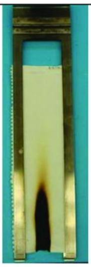	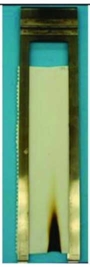	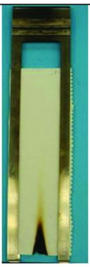	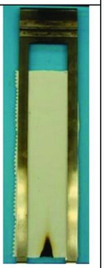
Add-on (wt %)	control	4	10	15	24	31
After-flame (sec)	10	24	0	0	0	0
After-glow (sec)	30	2	0	0	0	0
Char length (cm)	NA	>30	8.5	5.0	3.5	2.5
Ave. LOI (%)[σ]	18[0.12]	28[0]	36[0]	42[0.20]	45[0.20]	48[0.26]

From Table III, it is seen that *TPN4* with 14 and 19 wt% add-ons *TPN4* and all *TPN3* samples did not exhibit ignition after removal of the flame. Although obtaining the same add-on, 5 wt% add-on *TPN4* had 80 seconds of flame spread and 35 seconds of glowing, while 5 wt% add-on *TPN3* did not display ignition or glowing. The *TPN4* sample with 9 wt% add-on had 46 seconds of flame spread and went out but 10 wt% add-on *TPN3* did not exhibit ignition. Based on the Standard, at a concentration of 5 wt% add-on or higher of *TPN3* or *TPN4*, treated fabric can be designated *class 1* textile.

Table III. 45° angle flammability (ASTM D-1230-01) (*18*) and limiting oxygen index (LOI) (ASTM D-2863-09) (*16*) test for different add-ons (wt %) of treated twill fabrics for *TPN3* and *TPN4* (*28*). [σ]= standard deviation

TPN3 series	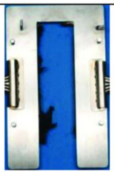	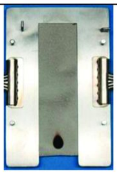	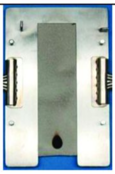	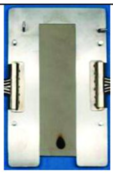	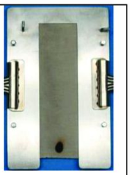
Add-on (wt %)	control	5	10	16	21
Flammability (sec) Class	 Class III[b]	DNI[a] Class I[c]	DNI Class I	DNI Class I	DNI Class I
Ave. LOI (%)[σ]	18[0.12]	30.0[0]	32.0[0]	34.2[0.41]	40.2[1.1]
TPN4 series	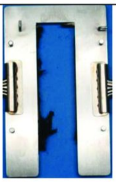	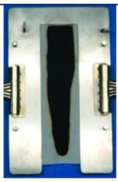	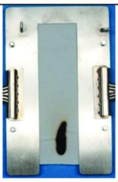	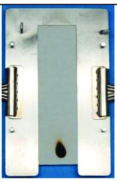	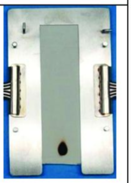
Add-on (wt %)	control	5	9	14	19
Flammability (sec) Class	 Class III	80[d] Class I	46[d] Class I	DNI Class I	DNI Class I
Ave. LOI (%)[σ]	18[0.12]	19.6[0.55]	22.7[0.52]	31.0[1.0]	36.0[5.03]

All samples treated with *TPN3* had high LOI values. The lowest, 5 wt% add-on, and the highest, 21 wt% add-on, had LOI values of 30 and 40%, respectively. *TPN4* samples had high LOI value of 31 and 36% only at high add-on levels of 14 and 19 wt%, respectively. It has been established (*29*) that materials with LOI values in the range of 20.95 to 28% are known as slow burning. Above this range, materials are considered to be self-extinguishing. As a result of the LOI experiment, *TPN3* can be classified as a flame retardant even at low add-on values.

Conclusions

A new derivative of triazine based phosphorus–nitrogen containing monomers, *TPN1*, *TPN2*, *TPN3* and *TPN4*, were successfully synthesized and characterized. All monomers were prepared in high yield 75-98%. Their flame resistant properties on cotton twill fabric were compared. TGA results showed that all treated fabrics were degraded at much lower temperatures and produced higher char yields at 600°C in nitrogen compared to that of untreated fabrics. In flammability test, such as LOI, 45° angle, and vertical test, most of treated fabrics with triazine based monomers were acceptable for their flame resistance performance.

Fabric treated with *TPN1* and *TPN2* showd very similar results for onset of degradation, LOI values and char contents. Moreover, fabric treated with *TPN3* exhibited lower onset of degradation than fabric treated with *TPN4*, and low add-on *TPN3* samples obtained higher char content than *TPN4* samples. In conclusion, these four monomers of triazine based phosphorus−nitrogen-containing derivatives are promising flame retardants for applications to cotton fabric. In the future, pyrolysis mechanism will be investigated to understand their flame retardant pathway.

Acknowledgments

The authors wish to acknowledge the USDA-ARS CRIS for financial support. We also appreciate the skillful experimental assistance of Dr. Minori Uchimiya, Linda Wartelle, and Christa Madison.

References

1. Lewin, M. *Polym. Degrad. Stab.* **2005**, *88*, 13.
2. Weil, E. D.; Levchik, S. V. *Flame Retardants for Plastics and Textiles*; Carl Hanser Verlag: Munich, 2009; pp 197−225.
3. Horrocks, A. R. *Polym. Degrad. Stab.* **2011**, *96*, 377.
4. Horrocks, A. R.; Kandola, B. K.; Davies, P. J.; Zhang, S.; Padbury, S. A. *Polym. Degrad. Stab.* **2005**, *88*, 3.
5. Hörold, S. *Polym. Degrad. Stab.* **1999**, *64*, 427.
6. Horacek, H.; Grabner, R. *Polym. Degrd. Stab.* **1996**, *54*, 205.
7. Levchik, S. V. Introduction to Flame Retardancy and Polymer Flammability. In *Flame Retardant Polymer Nanocomposites*; Morgan, A. B., Wilkie, C. A., Eds.; John Wiley & Sons, Inc.: Hoboken, New Jersey, 2007.
8. Weil, E. D. Synergists, Adjuvants and Antagonists in Flame Retardant Systems. In *Fire Retardancy of Polymeric Materials*; Grand, A. F., Wilkie,C. A., Eds.; Marcel Dekker: New York, 1999.
9. Hu, X. P.; Li, W. Y.; Wang, Y. Z. *J. Appl. Polym. Sci.* **2004**, *94*, 1556.
10. Chance, L. H.; Moreau, J. P. Paper presented at the 9th Cotton Utilization Res. Conf., New Orleans, LA, April, 1969.
11. Chance, L. H.; Moreau, J. P. *Am. Dyest. Rep.* **1970**, 37.
12. Fierz-David, H. E.; Matter, M. *J. Soc. Dyers Colour.* **1937**, *424*, 12.
13. Sharawat, B. S.; Handa, I.; Bhatnaga, H. L. *Proc. Indian Acad. Sci., Chem. Sci.* **1980**, *89* (3), 289.
14. Chang, S.; Condon, B.; Graves, E.; Uchimiya, M.; Fortier, C; Easson, M; Wakelyn, P. *Fibers Polym.* **2011**, *12* (3), 334.
15. Nguyen, T-M.; Chang, S.; Condon, B.; Uchimiya, M.; Graves, E.; Smith, J.; Easson, M.; Wakelyn, P. *Polym. Adv. Technol.* **2012**, *23*, 1036.
16. Standard test method for measuring the minimum oxygen concentration; American Society for Standards and Testing, ASTM D-2863-09, 2009.
17. Standard test method for flame resistance of textiles (vertical flame test); American Society for Standards and Testing, ASTM D-6413-08, 2008.

18. Standard test method for flammability of apparel textiles (45 degree angle flame test); American Society for Standards and Testing, ASTM D-1230-01, 2001.
19. Fang, Q.; Ding, X.; Wu, X.; Jiang, L. *Polymer* **2001**, *42*, 7595.
20. Kroschwitz, J. I. *Polymer: Polymer Characterization and Analysis*; John Wiley & Son, Inc.: New York, 1990; pp 837–870.
21. Sachinvala, N. D.; Ju, R. F.; Litt, M. H.; Niemczura, W. P. *J. Polym. Sci, Part A: Polym. Chem.* **1995**, *33*, 15.
22. Sachinvala, N. D.; Winsor, D. L.; Hamed, O.; Niemczura, W. P.; Maskos, K.; Vigo, T. L.; Bertoniere, N. R. *Polym. Adv. Technol.* **2002**, *13*, 413.
23. Lyons, J. W. *The Chemistry and Uses of Fire Retardants*; John Wiley & Son, Inc.: Hoboken, NJ, 1970; Chapters 5 and 7.
24. Tesoro, G. C. *Textilveredlung* **1967**, *2*, 435.
25. Tesoro, G. C.; Sello, S. B.; Willard, J. J. *Text. Res. J.* **1969**, *39*, 180.
26. Horrocks, A. R.; Anand, S. C. Heat and flame protection. In *Handbook of Technical Textiles*; Woodhead Publishing Ltd and CRC Press LLC: Boca Raton, FL, 2000; Chapter 10.
27. Lyons, J. W. *The Chemistry and Uses of Fire Retardants*; John Wiley & Son, Inc.: Hoboken, NJ, 1970; Chapter 5.
28. Nguyen, T.-M.; Chang, S.; Condon, B.; Slopek, R. *Fibers Polym.* **2012**, accepted.
29. Nguyen, C. T.; Kim, J. W. *Polym. Degrad. Stab.* **2008**, *93*, 1037.

Chapter 10

Halogen-Free Flame Retardant Flexible Polyurethane Foams via a Combined Effect of Flame Retardants

Feng Yang* **and Gordon L. Nelson**

Department of Chemistry, Florida Institute of Technology,
150 West University Blvd., Melbourne, Florida 32901
***E-mail: fyang@fit.edu**

Flame retardant flexible polyurethane foams were developed through four different approaches including the utilization of inorganic flame retardant, phosphorus-containing flame retardants, a combination of phosphorus compounds and inorganic additives, and the combination of phosphorus compounds and reactive silicone. Cone results of the obtained flexible foams strongly support "synergism" among the combined systems. With 15 pbw of phosphorus FR, Antiblaze® 230, an alkyl arylphosphate/phosphonate, in PUR, the peak heat release rate was reduced by 23% However, the combined use of Antiblaze® 230 with zinc stannate (ZS) reduced the PHRR of the resulting PUR foams by over 40%. Moreover, the combined use of ZS or zinc hydorxystannate (ZHS) with Antiblaze® 230 significantly reduces smoke generation. Flame retardant flexible foams are also successfully obtained with functionalized silicone component, and with the combination of silicone and phosphorus-containing FR, which follow a different flame retardant mechanism.

In Fire and Polymers VI: New Advances in Flame Retardant Chemistry and Science; Morgan, A., et al.;
ACS Symposium Series; American Chemical Society: Washington, DC, 2012.

Introduction

Polyurethane foams, both rigid and flexible, are one of the most widely used polymeric foams. Polyurethane foams and molded materials have a wide range of industrial applications including packaging, seat cushions in transportation, insulation, as well as furniture (*1–5*). Polyurethanes are very flammable and produce extensive smoke on burning (*6–8*). For practical use of these foams, fire-retardant properties are required to fulfill different requirements depending on national or international standards and end-use applications. Flame-retardancy of PU foam is achieved through use of reactive or additive flame-retardants (*9–12*): the first are chemically linked to the polymer backbone while the latter are added to foam formulations as separate compounds.

The majority of the approaches to achieve flame retardant polyurethane foams in the past utilized halogen containing flame retardants, especially brominated compounds, in the formulation, which could cause potential problems to human health and environment. There is thus a need for environmentally friendly and affordable polyurethane foams that offer desired fire, smoke and toxicity behavior, processability and physical performance.

It was originally found by us that the combined use of a phosphonate based flame retardant with ZS or ZHS can significantly reduce the smoke generation of flexible polyurethane foams (*13*). We postulate that the mechanism of this phenomenon is the chelating effect of phosphonate compounds with ZS or ZHS, which will prevent them from forming insoluble precipitates (scale) and suppress their catalytic activities. The characteristics of phosphonates may benefit by deactivating the reactivity of free radicals during the burning process, thus following a totally different flame retardant pathway than phosphate. In the present research, optimizing the amount of ZS and/or ZHS with phosphonate flame retardant is reported, and the comparison between phosphonate and phosphate of this combination on the flammability of PUR foams is evaluated.

Finally, an alternative approach to combine reactive silicone with the phosphorus compound to achieve flame retardant PUR foams with reduced smoke generation is also reported. We reported previously that the use of amine functionalized silicone alone in PUR foams can significantly enhance the flame retardancy of polyurethane foams in the cone. However, such enhancement only introduced a physical barrier effect to PUR foams instead of making the foams inherently flame retardant. Therefore, the combined use of reactive silicone along with other flame retardants in PUR is attempted, and its impacts on heat release as well as smoke generation are discussed.

Experimental

Preparation of Flexible Polyurethane Foams

All polyurethane formulations were prepared by using a one-shot method. The Bayfit® 566 component B (polyol), which contains a mixture of polyether polyols together with blowing agent and water (less than 5%), was stirred with a high speed mixer. The hydroxyl number of the polyol mixture was 210. To this, the component A of Bayfit® 566, which is polymeric diphenylmethylene diisocyanate (MDI) with NCO content of 32.5%, was introduced in 5 seconds under stirring. The stoichiometry of polyol to isocyanate is 100% of theoretical. The above mixture was then poured into a preheated (120°F) mold that was pre-treated with Chemtrend® MR515 mold release agent. Flexible PUR foam was obtained after 4-5 min of mold time, and then was removed and crushed to eliminate trapped carbon dioxide. As for the formulation of additive containing flexible foams, the additive was introduced into component B (polyol) in the above procedure. For reactive additives, their hydoxyl numbers were used as part of the alcohol number calculation to meet 100% stoichiometry of polyol to isocyanate. Table 1 lists flame retardant additives studied in this work. Moreover, Silpak® SP 200-4 two-components PUR is also investigated in the current research. The Silpak® 200 is a self-skinning, non-CFC (chlorofluorocarbon), flexible foam, and the component B (polyol) contains a mixture of polyether polyols together with blowing agent and water (less than 5%). It was prepared by identical procedure as the Bayfit® foams.

Table 1. Flame Retardant Additives list

Bayfit® 566 component A: polymeric MDI
Bayfit® 566 component B: polyether polyol
Dow Corning Powdered Silicone Additives 9641: siloxan with reactive amine groups
Zn Stearate
Mg Stearate
$Al(OH)_3$
Fyrol® RDP: Resorcinol bis(diphenyl phosphate)
Fyrol® FR2: tri-(1,3-dichloro-2-propyl)phosphate
Antiblaze® 100: chloroalkyldiphosphate ester
Antiblaze® 230: alkyl aryl phosphate/Phosphonates

The following additives were used in the present research: Antiblaze® 230: alkyl aryl phosphate/phosphonates, from Albemarle; zinc stannate(ZS), and zinc hydroxyl stannate(ZHS) were purchased from 3N International, Inc. Dow Corning silicone I-9641 was used as is, which is an amine terminated silicone. Fyrolflex® RDP, an oligomeric phosphate ester flame retardant, is from ICL-IP, as listed in Table 1.

Flammability Evaluation

The prepared flexible polyurethane foams were evaluated by cone calorimetry (ASTM 1354). The size of the cone specimen is 4”x4”x1”. Tests were conducted under 25 and 35 kW/m^2 external heat flux in a horizontal position. Oxygen Index testing (OI) was performed on all samples according to ASTM D2863.

Discussion

Flexible PUR Foams from Inorganic Flame Retardant Additives Approach

Polymers can be given flame retardant characteristics by introducing elements of organic, inorganic and halogen origin. Such elements include magnesium, aluminium, phosphorus, molybdenum, antimony, tin, chlorine and bromine. The most common inorganic flame retardants are the hydroxides or aluminium and magnesium. Aluminium trihydroxide (ATH) is by far the most widely used flame retardant on a tonnage basis. Magnesium hydroxide (MDH) is used in polymers which have higher processing temperatures, because it is stable up to temperatures of around 300 °C versus ATH which decomposes around 200 °C. Zinc compounds were initially developed as smoke suppressants for PVC (Zinc hydroxystannate). Later it was found that they also act as flame retardants in certain plastics mainly by promoting char formation. To investigate the impact of inorganic flame retardants on the flammability of flexible polyurethane foams, ATH, magnesium stearate, zinc stearate, as well as amine terminated silicone were incorporated into flexible PUR foams, and the Cone results are shown as Table 2.

The cone calorimeter data for non-halogen containing inorganic additive modified polyurethane foams at 25 kW/m^2 external heat flux as shown in Table 2 suggested that the largest reduction in peak heat release rate was achieved for a sample containing 5 pbw amine functionalized silicone power (I-9641), which reduced the peak heat release rate of polyurethane from 412 to 249 (-40%). Average heat release rate and total heat released were also lowest with this formulation. The 13% residue further indicated that the addition of I-9641 can significantly promote the char formation of PUR foams.

Table 2. A Comparison of the Fire Performance of Non-Halogen Additive Modified Polyurethane Foams at 25 kW/m^2 External Heat Flux

Formulation	*TTI (s)*	*PHRR (kW/m^2)*	*Ave. HRR (kW/m^2)*	*THR (kW/m^2)*	*Ave. SEA*	*Ave CO*	*Residue (%)*
Control	15.6	412	225	57.4	413	0.018	6.6
I-9641-5*	13.7	249	126	54.2	404	0.01	13.0
Zn Stearate-17	372	340	174	64.4	597	0.01	9.9
Mg Stearate-17	39.1	444	194	70.8	431	0.02	11.7
$Al(OH)_3$-37	16.0	401	218	60.1	446	0.02	15.2

* Last number is the pbw (parts by weight) of FR based on 100 parts of B-side in the formulation.

On the other hand, metal containing addives, i.e. zinc stearate, magnesium stearate and aluminum trihydrate in Table 2, had less impact on the flammability of PUR foams.Minor to no change in PHRR can be observed when 37 pbw of ATH was incorporated into the foams, which suggested that there is a strong linkage between the flammability of polyurethanes and the chemical composition of additives used. As reported on the thermal degradation of polymeric nanocomposites (*14*, *15*), metal containing and non-metal containing nanoparticles affect the decomposition pathways of polymeric materials differently. It is believed that an inorganic additive can catalyze the degradation of polymer through heterogeneous catalysis effects, which facilitate the decomposition of carbonyl–containing polymers. Fillers that belong to this class usually are metal oxides and metal hydroxides. The investigation in this part of research clearly demonstrated that utilizing inorganic based flame retardants alone can not obtain flame retardant PUR foams with desirable cone performance unless at high loading of metal hyroxides.

PUR Foams from Phosphorus Flame Retardants

To minimize the usage of halogen containing flame retardants is a current concern of the plastics industry. One approach that has been widely practiced by materials scientists is substituting halogen containing compounds by phosphorus compounds, because phosphorus based flame retardants are generally accepted as environmentally friendly additives. Phosphorus flame retardant modified flexible polyurethane foams were successfully prepared and the Cone results shown in Table 3.

Table 3. Phosphorus and Halogen-Phosphorus Based Additives Modified Polyurethane Foams at 25 kW/m^2 External Heat Flux

Formulation	*TTI (s)*	*PHRR (kW/m^2)*	*Ave. HRR (kW/m^2)*	*THR (kW/m^2)*	*Ave. SEA*	*Ave CO*	*Residue (%)*
Control	15.6	412	225	57.4	413	0.018	6.6
Fyrolflex RDP-17*	22.6	429	210	56.7	793	0.08	8.2
Fyrol FR2-37	18.4	326	163	48.2	745	0.08	13.2
Antiblaze 100-37	28.4	315	144	19.9	881	0.11	10.2
Antiblaze 230-15	26.1	274	154	49.2	727	0.10	9.9

* Last number is the pbw of FR based on 100 parts of B-side in the formulation.

With 17 pbw phosphorus flame retardant, Fyrolflex RDP, in PUR foam, no change in flame retardancy was achieved, as indicated by the same level of PHRR, THR and average heat release rates (*16*). Unlike Fyrolflex RDP, Fyrol FR2-37 and Antiblaze 100, belong to chlorinated organophosphate based flame retardants. Antiblaze 230 is a phosphate/phosphonate based flame retardant. At 15 pbw loading of Antiblaze 230 (unlike 37 pbw for Fyrol FR2 or Antiblaze 100), a 33% reduction in peak heat release rate and delayed ignition time were achieved. Phosphonates or phosphonic acids are organic compounds containing C-PO(OH)$_2$ or C-PO(OR)$_2$ groups (where R=alkyl, aryl). Phosphonates are effective chelating agents that bind tightly to di- and trivalent metal ions, preventing them from forming insoluble precipitates (scale) and suppressing their catalytic properties. The characteristics of phosphonates may benefit by deactivating the reactivity of free radicals during the burning process, thus following a totally different flame retardant pathway than phosphate. The phosphonate family of flame retardants will be explored. To take advantage of the "chelating agent" characteristics of phosphonates, combined usage of phosphonates and ZS, which is known as a "smoke supression" agent, will also be investigated to lower the emission of carbon monoxide and soot.

PUR Foams from The Combination of Flame Retardants and Inorganic Flame Retardant Additives

A number of other inorganic substances show flame retarding effects and are used in commercial applications. Most of them are used as synergists *i.e.* they enhance the performance of other flame retardants or they are used for specific effects like the suppression of smoke formation. The combined use of phosphorus flame retardant with organometallic compounds in flexible polyurethane foams was attempted with monoactylferrocene (FcCOCH$_3$), and the resulting materials were tested at 35 kW/m^2 (Table 4).

Table 4. Cone Results of Ferrocene Containing Oligomer and Phosphorus Additive Modified Polyurethane Foams at 35 kW/m^2 External Heat Flux

Formulation	*TTI*	*PHRR*	*Ave. HRR*	*THR*	*Ave. SEA*	*Ave. CO*	*Residue*
Control	7.3	563	163	58	442	0.024	3.8
FcCOCH$_3$-5*	8.2	447	140	47	327	0.021	0
FcCOCH$_3$-5/ Fyrol RDP-15	5.2	490	117	40	720	0.06	6.0

* Last number is the pbw of FR based on 100 parts of B-side in the formulation.

The introduction of organoferrocene to PUR reduced the PHRR of PUR by 21%. As discussed previously (Table 3), 17 pbw of phosphorus compound increased the PHRR of polyurethane foams and increased the evolution of CO gas 4 times. The combined useage of organo-ferrocene and Fyrol RDP significantly enhanced the char formation of polyurethane, while the reductions in THR and average HRR were maintained.

Table 5. Cone Calorimetry of PUR Foams @25kW/m^2

MATERIAL	*PUR*	*PUR/230(25)/ZS(5)/ Zn Stearate (5)*	*PUR/230(25)/ ZS (10)*	*PUR/230(25)/ ZHS (10)*
PHRR (kW/m2)	890	485(-46%)	424(-52%)	471 (-47%)
TTI (s)	26	9	31	36
TTP (s)	90	137	88	148
THR (MJ/m2/g)	2.50	1.98	1.86	1.95
AvgMLR (g/m2s)	22.3	13.6	13.3	15

To take advantage of the "chelating agent" characteristics of phosphonates, combined usage of phosphonates and zinc stannate, which is known as a "smoke suppression" agent, is investigated to lower the emission of carbon monoxide and soot. Investigation on the flammability of optimized PUR foams with Antiblaze 230 and smoke suppression agent, zinc stannate or zinc hydroxystannate was carried out with cone at 25 kW/m^2 heat flux as shown in Table 5. As low as 52% reduction in PHRR is achieved when 25 pbw of Antiblaze 230 is used together with zinc stannate as indicated in Table 5. The time to ignition for FR added PUR foams is also prolonged, while substantial reduction in total heat released is achieved. On the other hand, 5 pbw of smoke suppression agent, zinc stannate, with 5 pbw of inorganic flame retardant additive, zinc stearate, showed less flame retardant effect than ZS alone in the PUR foams, i.e. the foam ignited much earlier than pristine PUR foams.

The performance of ZHS is because of its dual phase mechanism. In addition to exhibiting vapor phase action, similar to antimony trioxide, ZHS also exhibits condensed phase action where it acts as an excellent char promoter. The condensed phase action of zinc hydroxystannate enhances the formation of a thermally stable carbonaceous layer at the expense of aromatic, volatile and flammable products. ZHS is effective in both halogen-free and halogen containing systems. The foam with ZHS alone does not exhibit noticeable changes in the varying aspects of cone test results, although a slightly increased time to peak is observed. However, when combining ZHS with FR, Antiblaze® 230, the resulting foam shows significant reduction in PHRR, as low as 47%, while all the other flame characteristics are also improved. It also shoulbe be noted that the combined use of zinc stannate and zinc stearate is not as good as zinc stannate or zinc hydroxylstannate alone, suggesting that tin compounds played a critical role in the reduction of heat release rate and smoke generation of PURs.

Besides the improvement in heat release rates and mass loss rates, the interactive flame retardant effect between FR and ZS or ZHS also has significantly impact on the smoke production of PUR foams, as shown in Figure 1. The addition of FRs to PUR foams significantly increased the smoke production rates of PUR foams. However, PUR with the combination of ZS with FR exhibits a similar level of smoke production as pristine PUR foam.

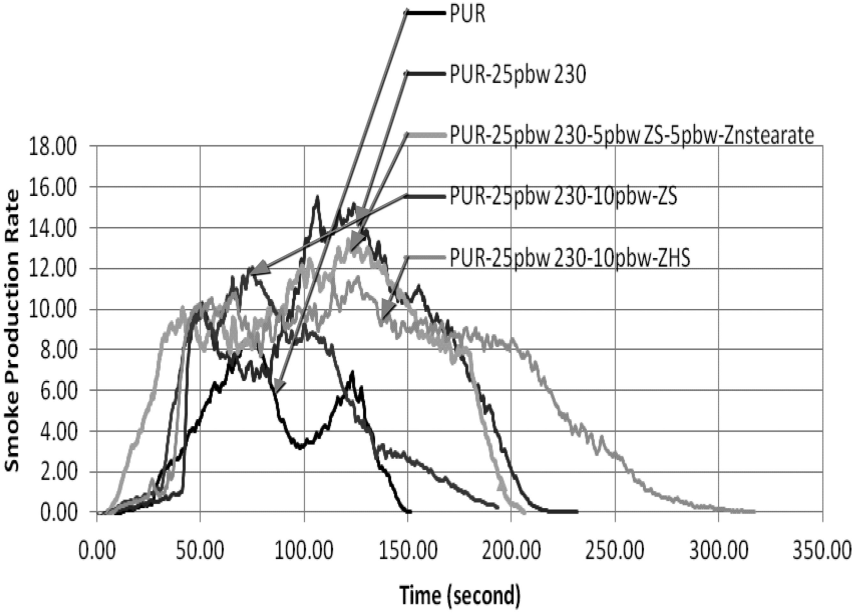

Figure 1. Smoke generation of flame retardant PUR foams.

Table 6. Comparison of Cone Calorimetry of PUR Foams from RDP vs. 230 @25kW/m²

MATERIAL	*PUR*	*PUR/ Antiblaze 230(25)*	*PUR/ RDP (25)*	*PUR/ ZS(5)/ Zn Stearate(5)/RDP(25)*
PHRR (kW/m²)	890	548 (-38%)	910	720 (-19%)
TTI (s)	26	41	65	33
TTP (s)	90	130	132	132
AvgHRR (kW/m²)	308	200	318	358
Total HR (MJ/m²/g)	2.50	1.86	--	1.93

In order to compare the efficacy of different types of phosphorus compounds as flame retardants, the flammability of PUR foams formulated with RDP and ZS/Zn stearate is evaluated as shown in Table 6.

Fyrolflex® RDP, an oligomeric phosphate ester flame retardant, is designed for use in engineered resin applications. Because of its low volatility and high heat stability, this non-halogen flame retardant can tolerate high temperature processing required of many engineered resins. However, when used alone in PUR foams, RDP is not effective, and visible leaking of RDP from the resulting foams can be observed 1 month after sample preparation. According to Table 6, poorer performance in flammability tests was observed when RDP was used alone or used together with ZS/Zn stearate. The poor performance of RDP alone indicated that no solid phase inhibition mechanism occurred in the foams. The low volatility and high heat stability characteristics of RDP also led to the absence of gas phase inhibition. Therefore, the comparison between PUR foams formulations based on Antiblaze 230 versus RDP indicated that phosphonate based FRs are much more effective than phosphate based FRs for PUR foams.

PUR Foams from the Combination of Flame Retardants and Reactive Silicone

It was previously reported by the authors that the application of silicone in polyurethanes, both flexible foams and flexible coatings, could significantly reduce the flammability of polyurethane materials (*17*). It was found that silicone modified polyurethanes microphase segregate forming a silicone rich surface on cast films. Oxygen Index values were silicone-like even at 30-50% silicone. Silicone surface undergoes a solid phase FR mechanism to produce a silicon dioxide layer on the surface. However, silicone alone in PUR foams only inputs a physical barrier effect to the foams. In order to take advantage of silicone as a flame retardant enhancer, it is used together with FRs to achieve PUR foams with inherent flame retardancy as well, and the results are shown in Table 7. The PUR foam for this part of research is based up Silpak 400 instead of Bayfit 566, and the thickness of cone sample is 1 inch instead of 2 inches.

Amine functionalized silicone in the backbone of PUR foams alone offered excellent flame retardancy to the foams, and as low as 48% reduction in PHRR was achieved with only 5pbw of silicone in the B-side formulation. The combined use of silicone with FR can further reduce the PHRR to 53%, which suggests that the introduction of FR into silicone modified PUR foams can further enhance the flammability of the resulting foams. Oxygen Indices indicated that silicone alone will not input inherent flame retardancy to PUR foams, while the combination of silicone with Antiblaze® 230 exhibited inherent flame retardancy as indicated by an OI of 27.3. This result suggested that the silicone modified PUR coupled with traditional flame retardant not only improves the fire performance evaluated by the cone, but also one has a better chance to pass other regulatory tests.

Moreover, the average smoke extinction area result suggested that the smoke generation from the foams was significantly reduced when modified by silicone, 344.7 to 286.4 m/kg. Antiblaze® 230 as a phosphonate based FR followed both a solid phase and gas phase inhibition mechanism, which led to incomplete burning of combustible fuel and heavy smoke generation, 652.7 m/kg at 25pbw. However, the combined use of silicone and 230 reduced the smoke generation of PUR foams to an acceptable level, close to that of pristine PUR.

Table 7. Cone Calorimetryand OI of PUR Foams with silicone

MATERIAL	*PUR*	*PUR/ Antiblaze 230(25)*	*PUR/ silicone 9641(5)*	*PUR/ Antiblaze 230(15)/ silicone 9641 (5)*
PHRR (kW/m^2)	890	548	459	425
TTI (s)	26	41	10	24
TTP (s)	90	130	182	103
THR (MJ/m^2/g)	2.50	1.86	2.40	2.04
AvgSEA(m/kg)	344.7	652.7	286.4	463.8
OI	21.2	27.3	21.2	27.3

Conclusion

It was found that utilizing inorganic based flame retardants alone can not obtain flame retardant PUR foams with desirable cone performance, and the type of phosphorus FRs (phosphonate vs. phosphate) can significantly impact on the flammability of flexible PUR foams. Halogen-free flame retardant flexible PUR foams were successfully developed (46-52% reduction in PHRR). "Synergistic" flame retardant effects were observed between phosphorous containing flame retardants and ZS/ZHS. While the addition of Antiblaze 230 increases smoke production, the combined use of ZS or ZHS with Antiblaze 230 significantly reduces smoke generation.

Silicone modified PUR foams showed as much as 48% reduction in PHRR, while using phosphorus-containing FR together with silicone can further enhance the reduction of PHRR, as well as exhibit inherent flame retardancy. The combined use of silicone and FR also helps in reducing smoke generation.

References

1. de Mello, D.; Pezzin, S. H.; Amico, S. C. *Polym. Testing* **2009**, *28* (7), 702–708.
2. Wakabayashi, A. U.S. Patent Appl. Publ. 12 pp., Patent No. U.S. 20,110,003,042.
3. Kozlowski, R.; Malgorzata, M.; Bozena, M. Comfortable, flexible upholstery fire barriers on base of bast, wool and thermostable fibres. *Polym. Degrad. Stab.* **2011**, *96* (3), 396–398.
4. Neff, R. A.; Smiecinski, T. M. Patent No. U.S. 20100160473.
5. Hillier, K.; King, D. A.; Henneuse, C. Study of odours coming out of polyurethane flexible foam mattresses. *Cell. Polym.* **2009**, *28* (2), 113–144.
6. Singh, H.; Jain, A. K. Ignition, combustion, toxicity, and fire retardancy of polyurethane foams: a comprehensive review. *J. Appl. Polym. Sci.* **2009**, *111* (2), 1115–1143.

7. Hirschler, M. M. *Polym. Adv. Technol.* **2008**, *19* (6), 521–529.
8. Bashirzadeh, R.; Gharehbaghi, A. *J. Cell. Plastics* **2010**, *46* (2), 129–158.
9. Levchik, S. V.; Weil, E. D. *Polym. Int.* **2004**, *53*, 1585–1610.
10. Weil, E. D.; Levchik, S. V. *J. Fire Sci.* **2004**, *22*, 183–209.
11. Levchik, S. V.; Weil, E. D. *J. Fire Sci.* **2006**, *24*, 345–364.
12. Wang, J. Q.; Chow, W. K. *J. Appl. Polym. Sci.* **2005**, *97*, 366–376.9.
13. Yang, F.; Nelson, G. L. Proceedings of the 22th Annual BCC Conference on Flame Retardancy, May 23-25, 2011.
14. Yang, F.; Bogdanova, I.; Nelson, G. L. *Polym. Adv. Technol.* **2008**, *19*, 602–608.
15. Kashiwagi, T. In *Flame Retardant Polymer Nanocomposites*; Morgan, A. B., Wilkie, C. A., Eds.; Wiley-Interscience: New York, 2007; pp 285−324.
16. Jayakody, C.; Myers, D.; Sorathia, U.; Nelson, G. L. *J. Fire Sci.* **2000**, *18*, 430–455.
17. Jayakody, C.; Nelson, G. L.; Sorathia, U.; Lewandowski, S. *J. Fire Sci.* **1998**, *16*, 351–382.

Chapter 11

Novel Biomass-Based Non-Halogenated FR Styrenic Blends

Tze-Wei Liu,[1] Cameron R. Youngstrom,[2] Sushant Agarwal,[1] Adam Al-Mulla,[1] Satish K. Gaggar,[2] and Rakesh K. Gupta*,[1]

**[1]Department of Chemical Engineering, West Virginia University,
Morgantown, West Virginia 26506
[2]SABIC Innovative Plastics, Route 892, Washington, West Virginia 26181
*E-mail: rakesh.gupta@mail.wvu.edu**

Flame retardant (FR) additives are commonly used in polymeric materials, with non-halogenated variants being preferred for environmental, health and safety reasons. Developing non-halogenated FRs for styrenic polymers such as acrylonitrile-butadiene-styrene (ABS) is a challenge since these polymers burn very easily and produce minimal char. This work describes a novel technical approach to increase char formation in ABS by utilizing sustainable natural fibers and ammonium polyphosphate (APP) to provide V-0 burn ratings in UL–94 testing. The effects of various phosphates and natural ingredients on flame retardancy and some thermal and mechanical properties are presented. These types of ABS blends were found to suffer from lower impact strength, darker base color and lower thermal stability versus traditional formulations. Technical strategies for improving these properties are described leading to blend formulations that show good balance of mechanical, flow and flame retardant properties in a cost effective manner.

In Fire and Polymers VI: New Advances in Flame Retardant Chemistry and Science; Morgan, A., et al.;
ACS Symposium Series; American Chemical Society: Washington, DC, 2012.

Introduction

In general, ABS polymers possess good strength, rigidity, toughness, and processability. They also have good chemical resistance, especially to inorganic salt solutions, alkalis, relatively weak acids, and some mineral, vegetable, and animal oils. Thus, there are a wide variety of applications for ABS, including appliances and consumer electronics, automobiles, football helmets and pipes (*1*). However, ABS is flammable, and this can limit its use if flame retardants are not added. A common approach employed is to use halogenated flame retardants with antimony oxide as a synergist to impart FR properties to ABS. The use of halogenated flame retardants, however, results in the potential production of toxic gases during combustion. As a consequence of this hazard, the European Community (EC) has restricted the use of brominated diphenyl oxide flame retardants because of the possibility of producing furans and dioxins upon combustion (*2*), while eight states in the U.S. (CA, HI, IL, MD, ME, MI, OR, and NY) have also passed legislation to ban octabromodiphenyl oxide (OBDPO) and pentabromodiphenyl oxide (PBDPO) from further use (*3*). Consequently, research efforts have increasingly focused on developing halogen-free flame retardants for ABS, and many approaches have been examined in order to achieve the desired UL-94 rating. The most common approach is to introduce a charring agent, a good example being the blending of polycarbonate (PC) with ABS and phosphates; this allows one to achieve a V-0 rating (1.6 and 3.2 mm) on the UL-94 test, but a relatively high loading level of PC is required (*4*). In addition to PC, it has been reported that phenol and epoxy can also serve as char formers. These are effective to flame retard ABS when tetra-2,6-dimethyl resorcinol diphosphate (DMP-RDP) is used as the flame retardant; a V-1 rating on the UL-94 test and a limiting oxygen index (LOI) value of up to 53 can be obtained (*5*).

Another approach has been to use natural bio-based materials as charring agents. Li and He (*6*) used wood fibers together with ammonium polyphosphate (APP) in linear low density polyethylene (LLDPE) and observed the formation of char on burning which led to increase in thermal decomposition temperatures in thermogravimetric tests. De Chirico et al. (*7*) used lignin in polypropylene (PP) together with aluminum trihydroxide and observed reduced heat release rates in cone calorimeter tests. On the other hand, Le Bras et al. (*8*) used flax fibers in PP together with APP as acid catalyst, pentaerithrytol as carbon source and melamine as spumefic to make composites. Increased char formation was observed which resulted in samples with V-0 ratings on the UL-94 test. However, no data on mechanical testing was provided. Bakar et al. (*9*) studied PP filled with wood fibers and APP. They found that V-0 UL-94 rating could be achieved with 30% wood fiber and 30% of APP with increased formation of char residue, although they also observed deterioration in mechanical properties which improved marginally with the addition of maleated anhydride PP. More recently, Song et al. (*10*) studied ABS filled with lignin for thermal stability and used SEBS-g-MA as the coupling agent. Addition of lignin led to formation of more char at high temperatures and reduction in heat release rates. In this work, it is shown that phosphorus-containing compounds together with wood fibers, cellulose fibers or starch powder as charring material can be used effectively to impart flame

In Fire and Polymers VI: New Advances in Flame Retardant Chemistry and Science; Morgan, A., et al.;
ACS Symposium Series; American Chemical Society: Washington, DC, 2012.

retardant properties to ABS in a cost-effective manner. Various formulations are described which lead to ABS blends that have a good balance of mechanical, flammability and flow properties. Furthermore, various processing methods are described to improve the base color and thermal stability of the FR-ABS blends.

Experimental Details

Materials Used

ABS was either utilized in pellet form [CYCOLAC* (Trademark of SABIC Innovative Plastics IP BV) grade MG94 melt flow index = 13 g/min (220 °C/5.0 kg)] or through the blending of a high rubber content ABS powder (CYCOLAC* resin IMP362) and SAN (CYCOLAC* experimental grade 29355), and was supplied by GE Plastics (now SABIC Innovative Plastics). Ammonium phosphate dibasic (ADP) and triphenyl phosphate (TPP), a white flakey solid, were purchased from the Sigma-Aldrich company. Ammonium polyphosphates, Exolit AP423 and AP750, were obtained from Clariant. Bisphenol A bis-diphenyl phosphate (BPADP), resorcinol bis-diphenyl phosphate (RDP), diphenyl decyl phosphate (DPDP), zinc stearate, nitrile rubber (NBR) and ethylene bis-stearamide (EBS wax) were obtained through SABIC Innovative Plastics. The cellulose that was used (TC90) was the product of the CreaFill company, maple wood flour (Maple 8010, size of 80-mesh, about 177 μm) was provided by American Wood Fiber and corn starch was purchased from Bob's Red Mill.

Sample Preparation

Compounding of the cellulose and wood flour samples was carried out using either a Leistritz Micro-27 co-rotating twin screw extruder (L/D = 40, D = 27mm) or a Thermo Haake internal mixer. For the twin screw extruder, materials were fed to the hopper using K-Tron loss-in-weight feeders at a total feeding rate of 3 kg/hr, and the screw speed was 80 rpm. The extruder has ten heating zones, and the temperature was set at 60 °C at the hopper, while at the die it was 170 or 180 °C depending on the formulation used. For the internal mixer, all the constituents were fed to the hopper, and the total sample weight was about 50 grams. The rotor speed and the temperature were set to 70 rpm and at 190 °C, respectively. Since wood and cellulose are hygroscopic (moisture content over 5%), they were dried at 100 °C for 7 hours before use. Similarly, ABS and the compounded pellets were each dried at 90 °C for 6 hours before extrusion or molding operations. Cellulose and wood flour samples were molded using a Battenfeld injection molding machine or in a compression molding hot press. The process temperature profile for injection molding was in the range of 182 to 200 °C (hopper) to the range of 175 to 225 °C (nozzle) depending on the materials. All starch and the improved color cellulose samples were compounded on a lab Banbury (Ferrel 82BR), milled on a Farrel 50-HB steam heated 2-roll lab mill, cut into slabs and ground in a Cumberland ½ grinder. The ground pellets were injection molded (5 oz, 150 ton Van Dorn) into

UL94 flame bars of 0.125-inch thickness, 3.3 mm multiaxial impact (MAI) disks and 3.3 mm ISO izod bars. Banbury flux and drop temperatures were about 135 °C and 177 °C, respectively.

Flammability, Color, and Mechanical Characterization

For flammability characterization, a UL-94 type vertical burn test (5th edition, 1996) was carried out on test specimens of dimensions (127 × 12.7 × 3 mm^3). At least 5 specimens were tested for each sample. A methane flame was used. The flame was applied to the vertical sample twice for 10 s each and the afterflame time was noted after each application of the flame. Afterglow time was recorded after the second application of flame. Any burning material dripping or cotton pad ignition was also noted. Based on these observations, the flame retardancy was classified as V-0, V-1 or not classified (NC) as prescribed by the UL-94 test method, with V-0 being the most desirable. It should be noted that our labs are not UL certified. Burn time data for some of the samples are given in the data tables to enable the assessment of effect of various additives.

Color measurements were performed as necessary on molded articles using a Macbeth color eye 7000 (CRIOLL 10 degrees D65) spectrophotometer.

Multiaxial impact test (Dynatup) and Izod impact (TMI 43-02) (ISO180) were conducted for impact tests. Melt flow index (MRI) (200 °C/10kg) was determined using a Dynisco D4004 rheometer according to ISO649. Flexural properties were measured on an Instron 5567 universal testing machine according to the ASTM D790 procedure at a crosshead rate of 1.3462 mm/min at room temperature. A test specimen having dimensions of 127 × 12.7 × 3 mm^3 was subjected to a three point bending test, and a stress-strain curve was generated.

Thermal Characterization

Thermogravimetric analysis was carried out at a heating rate of 10 °C/min under nitrogen on a TA Instruments TGA model Q500.

A TA Instruments Q100 differential scanning calorimeter (DSC) was used to determine the glass transition temperature for ABS. DSC scans were obtained at a heating rate of 10 °C/min under a helium flow of 25 ml/min.

Morphology Characterization

For examining the ability of char formation of a flame retardant, a bar (127 × 12.7 × 3 mm^3) was burned using a LOI tester for 3 minutes. After burning, the unburned end of the bar was fixed, and then, using pliers, the burned end was broken to obtain the fracture surface. The above fractured pieces were then sputter coated with gold and examined using a Hitachi S-4700 Field Emission Scanning Electron Microscope (FESEM).

Table I. Flammability of ABS with wood fibers

Component composition (%mass)						*Flammability*
Samples	*ABS*	*Wood*	*ADP*	*AP423*	*AP750*	*UL-94 type*
1	100	–	–	–	–	NC
2	70	30	–	–	–	NC
3	70	–	30	–	–	NC
4	70	–	–	30		NC
5	70	–	–	–	30	NC
6	50	20	30	–	–	V-0
7	45	30	25	–	–	V-0
8	40	40	20	–	–	V-0
9	50	20	–	30	–	V-0
10	50	30	–	20	–	V-0
11	45	40	–	15	–	V-0
12	45	20	–	–	35	V-0
13	40	30	–	–	30	V-0
14	32.5	40	–	–	27.5	V-0

Results and Discussion

Cellulose and Wood Flour

Flammability Properties

Wood-Based Flame Retardant Systems

To improve the flame retardance of ABS by char formation mechanism, both char promotors like phosphates, and char forming materials such as bio materials are needed. One component in itself is not enough. This is shown by the data in Table I, where it can be seen that the addition of 30 wt% of wood, ADP, AP423 or AP750 alone to ABS does not improve the fire resistance of ABS. If, however, one adds wood and phosphates together in a proper amount to ABS, a V-0 rating on a UL-94 type test can be obtained. Also, it is seen that increasing wood content decreases the ratio of phosphates to wood when UL-94 ratings of V-0 have been achieved. This indicates that the role of phosphoric acids, indeed, is to serve as catalysts since wood is the source of char. The efficiency of phosphates in dehydrating wood can be ranked in decreasing order: AP423>ADP>AP750.

However, the sum of the loading level of wood plus phosphates increases with increasing wood content. This indicates that the increased formation of char leads to decreased protection for ABS, and this is probably due to mixing problems.

Cellulose-Based Flame Retardant Systems

The need to have both char promotors and char forming materials is also corroborated for cellulose containing blends. It can be seen from Table II that like the cases of wood and phosphates, the addition of 30 wt% of cellulose or TPP alone to ABS does not improve the fire resistance of ABS. If, again, one adds cellulose and phosphates together in a proper amount to ABS, a V-1 or V-0 rating on a UL-94 type test can be obtained. Note that the combination of cellulose and TPP does not give a UL-94 rating when compared to the combination of cellulose and AP423. However, TPP can be employed as a synergist when added to a combination of AP423 and cellulose in flame retarding ABS.

Table II. Flammability of ABS with cellulose fibers

Component composition (%mass)						*Flammability*
Samples	*ABS*	*Cellulose*	*ADP*	*AP 423*	*TPP*	*UL-94 type*
1	70	30	–	–	–	NC
2	62.5	20	17.5	–	–	V-0
3	55	30	15	–	–	V-0
4	62.5	20	–	17.5	–	V-1
5	57.5	30	–	12.5	–	V-0
6	70	–	–	–	30	NC
7	60	20	–	20	–	V-1
8	60	20	–	–	20	NC
9	60	20	–	10	10	V-1
10	65	10	–	10	15	V-0

Effect of Feed Location

One of the major findings of this work was that when ABS, cellulose and APP were fed together in an extruder at the feed-hopper, the resulting blend was not classified in the UL-94 test, as shown in Table III. However, when APP was fed downstream, the resulting blend showed a V-0 rating (*11*) and it also improved the appearance of the blend. It is believed that when all components are fed together some precharring and cross-linking of cellulose occurs due to the relatively prolonged exposure to high processing temperatures causing a deterioration in properties. However, if APP is fed down stream, exposure to elevated temperature is for shorter periods of time resulting in much less precharring.

Table III. Effect of APP feed location in extruder on FR performance

Component (%)	*APP fed down stream*					*Fed in feed hopper*
ABS	50	55	50	55	57.7	57.5
Cellulose	30	25	20	15	30	30
APP	20	20	30	30	12.5	12.5
FR rating	V-0	V-1	V-0	V-1	V-0	NC

Mechanical Properties

Selected samples from Table I were subjected to mechanical testing to see the effects of wood, and phosphates on the flexural properties of ABS-FR blends. For this purpose samples were prepared in a twin screw extruder. Mechanical properties were characterized in terms of flexural strength and flexural modulus, and results are displayed in Figures 1-2. These figures show that the addition of additives to ABS at a loading level from 30 wt% to 60 wt% has an insignificant effect on the flexural strength, while a significant improvement on modulus is observed.

Thermogravimetric Analysis

TGA was used to examine the thermal degradation behavior of these composites. Figure 3 gives the thermogravimetric and differential thermogravimetric curves for various ABS/flame retardant systems. It is seen that the degradation of ABS/wood proceeds through two steps below 500 °C (curve a). The first step is attributed to the degradation of wood, and the second step is the degradation of ABS. Clearly, with the addition of phosphates, the first peak of R_{max} (maximum weight change rate) occurs earlier, below 300 °C (Figure 3b), and an increased weight loss is observed in the first step of decomposition below 360 °C (Figure 3a). These results indicate that char formation has taken place, and these actions have caused the disappearance of the first peak of ABS/wood composite attributed to wood producing flammable volatiles around 360 °C. Apparently, these are converted into char with the addition of phosphates by means of dehydration reactions (*12*).

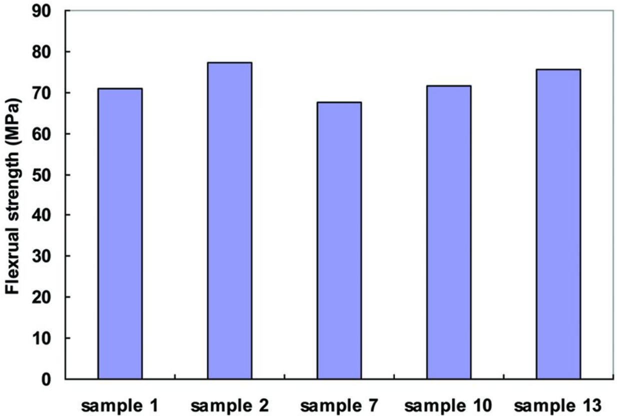

Figure 1. Flexural strength of samples listed in Table I.

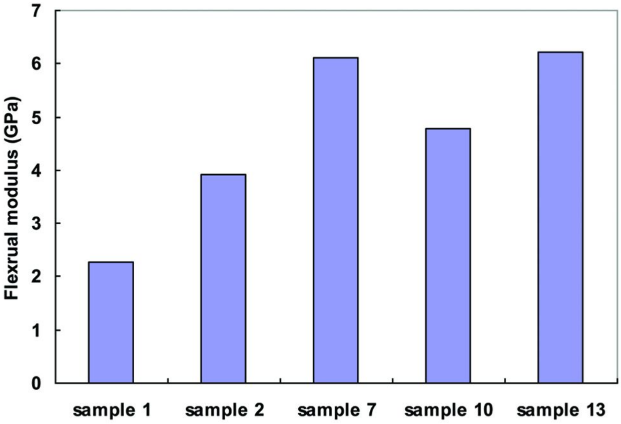

Figure 2. Flexural modulus of samples listed in Table I.

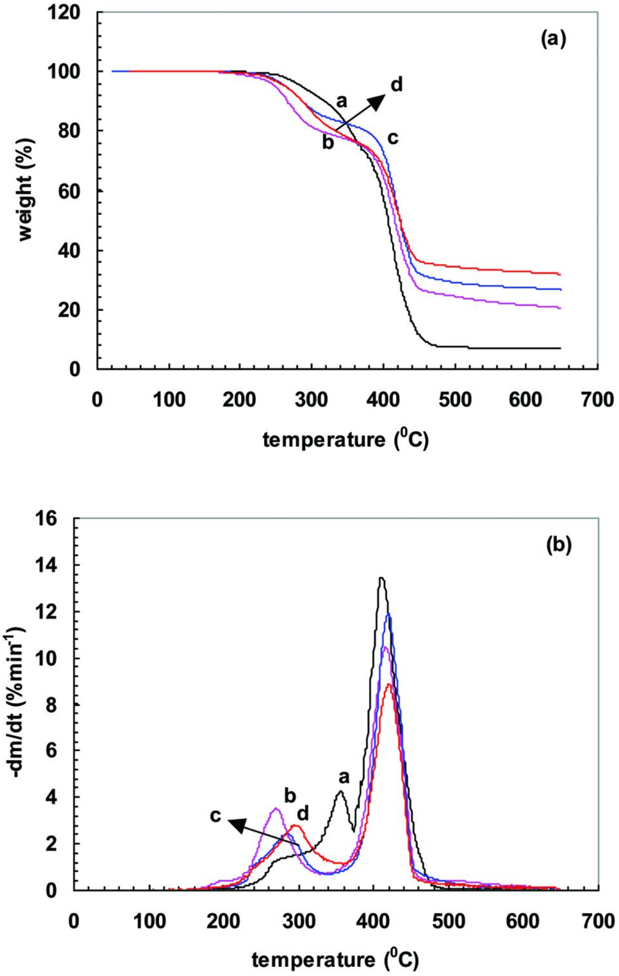

Figure 3. TG and DTG curves of a variety of samples in Table I under nitrogen. Curve a (sample 2); curve b (sample 7); curve c (sample 10); curve d (sample 13).

Glass Transition Temperature

The glass transition temperature (T_g) is an important parameter that affects processing and many end use applications, thus it is important to evaluate T_g of the FR-ABS system containing wood or cellulose, TPP/RDP/BPADP and phosphates. The measured T_g values of the different ABS blends are listed in Tables IV and V. As can be seen from Table IV, the glass transition point of ABS does not change significantly with the addition of wood or cellulose in the range of 10 wt% to 30 wt% natural fiber. Indeed, even with the addition of phosphates to the mixture of

ABS and wood or cellulose, there is only a minor change in the T_g (0.52-3.9 °C). However, in the presence of TPP, RDP or BPADP, as shown in Table V as well, the T_g of the ABS blends containing cellulose and AP423 decreases by 30 to 40 °C. This is due to the plasticization effect of low melting liquid additives (TPP T_m ~ 50.54 °C, RDP pour point -12 °C, BPADP pour point 8 °C).

Table IV. Glass transition data of ABS blends

Component composition (%mass)							*Tg (°C)*
Samples	*ABS*	*Wood/ cellulose*	*ADP*	*AP 423*	*AP 750*	*TPP*	
1	100	–	–	–	–	–	103.8
2	90	10	–	–	–	–	102.0
3	80	20	–	–	–	–	104.3
4	70	30	–	–	–	–	102.3
5	70	30	25	–	–	–	102.3
6	70	30	–	20	–	–	103.1
7	70	30	–	–	30	–	99.9
8	63	20	–	17	–	–	104.9
9	71.5	12.5	–	11	–	5	73.7
10	53	20	–	17	–	10	62.7
11	–	–	–	–	–	100	50.7

Morphology

Morphology of the burned samples was studied using SEM to examine their pore structure. From the SEM image of a burned sample in Figure 4a, it can be seen that big pores formed at the burned surface indicating that the char density is low for ABS with only added wood. However, further adding ADP significantly increases the char density as shown in Fig. 4b by the presence of much smaller pores, and this verifies that ADP is the effective catalyst for triggering char formation of wood.

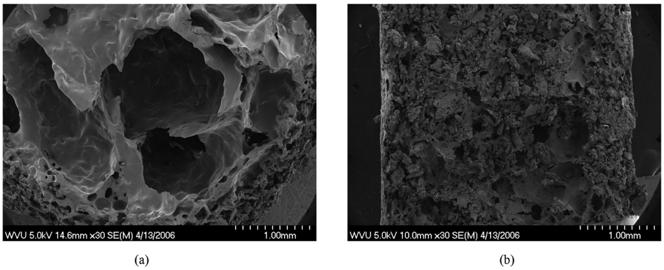
WVU 5.0kV 14.6mm x30 SE(M) 4/13/2006
1.00mm
(a)
WVU 5.0kV 10.0mm x30 SE(M) 4/13/2006
1.00mm
(b)

Figure 4. Burned surfaces of WPCs with wood at 30wt% by SEM. (a) ABS/wood; NC and LOI=21; (b) ABS/wood/ADP; V-0 and LOI=27.

Table V. Plasticization flow improvements

Components	*1*	*2*	*3*	*4*	*5*	*6*	*7*
Cellulose, phr	24	24	24	24	24	24	24
HR-ABS, phr	30	30	30	30	30	30	30
SAN, phr	26	26	46	26	26	26	26
AP423, phr	20	20	20	20	20	20	20
EBS wax, phr	2	2	2	2	2	2	2
Zn stearate, phr	1	1	1	1	1	1	1
RDP, phr		3	5	10			
BPADP, phr					3	5	10
Notched Izod, kJ/m^2	2.61	2.33	1.89	1.3	2.41	2.17	1.51
MAI Dynatup, J	8.7	6.7	6.0	4.0	7.2	7.3	5.2
MFI,(200 °C/10kg), g/10min	1.59	4.7	9.2	27.5	4.6	8.3	25.4
T_g, mid point, °C	105.2	91.2		68.4	103.4		77.6
Flammability, UL-94	V-1	V-1	V-0	V-0	V-0	V-0	V-0
Burn times for UL-94 tests- 1st Ign time (s) / 2nd Ign time (s)							
Bar 1	1 / 1	1 / 1	1 / 6	1 / 1	1 / 1	1 / 1	1 / 1
Bar 2	1 / 1	1 / 23	1 / 1	1 / 1	1 / 1	1 / 1	1 / 1
Bar 3	1 / >30	1 / 1	1 / 1	1 / 1	1 / 1	1 / 1	1 / 1
Bar 4	1 / 1	1 / 1	1 / 1	1 / 3	1 / 1	1 / 1	1 / 1
Bar 5	1 / 1	1 / 1	1 / 1	1 / 1	1 / 1	1 / 4	1 / 1

Table VI. Starch vs Cellulose

Component		*Cellulose*	*Starch*	*non-FR*
Corn starch, phr		-	24	24
Cellulose, phr		24	-	-
HR-ABS, phr		30	30	30
SAN, phr		26	26	46
AP423, phr		20	20	-
EBS wax, phr		2	2	2
Zn stearate, phr		1	1	1
DPDP, phr		0.5	0.5	0.5
BPADP, phr		3	3	3
Notched Izod, kJ/m^2		2.41	1.76	1.39
MAI, Dynatup, J		8.4	7.74	3.46
MFI,(200 °C/10kg), g/10min		9.94	34.45	61.01
Flammability, UL-94		V-0	V-0	NC
Color	L*	73.52	77.96	85.96
	a*	3.49	1.91	1.78
	b*	16.09	10.9	8.04
Burn times for UL-94 tests- 1st Ign time (s) / 2nd Ign time (s)				
Bar 1		1/1	1/1	-
Bar 2		1/1	1/1	-
Bar 3		1/1	1/1	-

Starch

Flammability

Experiments utilizing corn starch as a natural fiber char agent versus cellulose in ABS are summarized in Table VI. At 24 phr loading, along with 20 phr AP423, both natural products were found to exhibit V-0 UL-94 flame ratings while a non-AP423 containing version had no flame retardancy. ABS blends with starch were found to exhibit the added advantage of improved base color in molded disks (lighter and 48% less yellow) and were also shown to have significantly higher (3.5x) flow characteristics than cellulose. Conversely, starch blends suffered lower ductility than the cellulose analogs with 27% lower notched Izod and 8% lower Dynatup impact.

Property Improvements for FR Natural Fiber Blends

Base Color Improvements

The base color of polymer blends with cellulose, wood or starch is typically found to be darker than that of virgin polymer due to the low thermal stability of natural fibers. This phenomenon is worsened upon the addition of the FR phosphorous compounds, such as AP423 or AP750, due to the onset of pre-charring that occurs upon thermal processing of the blends. As can be seen in Table VII, a 20 unit improvement in L* (see samples 4 and 8) can be obtained in molded articles through the use of a combination of the lubricants EBS wax and zinc stearate. These color improvements were achieved without detrimentally affecting the UL-94 type flammability ratings of the blends.

Table VII. Color improvements

Components		*1*	*2*	*3*	*4*	*5*	*6*	*7*	*8*
HR-ABS, phr		25	25	25	25	25	25	25	25
SAN, phr		33	33	33	33	33	33	33	33
Cellulose		25	25	25	25	25	25	25	25
AP423, phr		17	17	17	17	17	17	17	17
EBS wax, phr		-	1	3	2	-	1	3	2
Zn stearate, phr		-	-	-	1	-	-	-	1
Process		mixer	mixer	mixer	mixer	mold	mold	mold	mold
Flammability		-	-	-	-	V-1	V-1	V-1	V-1
Color	L*	46.8	55.5	69.9	82.9	46.3	49.2	47.3	67
	a*	4.3	5.1	3.2	0.4	2.4	2.2	3.7	4
	b*	12.2	16.4	15	14.1	5.2	5.8	7.6	14.5
Burn times for UL-94 tests- 1st Ign time (s) / 2nd Ign time (s)									
Bar 1		-	-	-	-	2/1	1/22	3/1	6/10
Bar 2		-	-	-	-	1/8	1/8	2/9	3/10
Bar 3		-	-	-	-	1/30	1/1	4/7	1/11
Bar 4		-	-	-	-	1/9	3/16	1/15	2/12
Bar 5		-	-	-	-	4/15	1/12	2/15	6/25

Table VIII. Improved ductility with added NBR

<table>
<tr><td colspan="10"><i>Corn starch = 24 phr, APP = 20 phr, EBS wax = 2 phr, Zn stearate = 1 phr, BPADP = 3 phr</i></td></tr>
<tr><td><i>Component</i></td><td><i>1</i></td><td><i>2</i></td><td><i>3</i></td><td><i>4</i></td><td><i>5</i></td><td><i>6</i></td><td><i>7</i></td><td><i>8</i></td><td><i>9</i></td></tr>
<tr><td>HR-ABS, phr</td><td>30</td><td>30</td><td>30</td><td>30</td><td>30</td><td>30</td><td>22</td><td>14</td><td>6</td></tr>
<tr><td>SAN, phr</td><td>26</td><td>26</td><td>26</td><td>26</td><td>26</td><td>26</td><td>29</td><td>32</td><td>35</td></tr>
<tr><td>NBR</td><td></td><td>1</td><td>3</td><td>5</td><td>9</td><td>11</td><td>5</td><td>10</td><td>15</td></tr>
<tr><td>Flammability</td><td>V-0</td><td>V-1</td><td>V-1</td><td>V-1</td><td>V-1</td><td>NC</td><td>V-0</td><td>V-0</td><td>V-0</td></tr>
<tr><td>HDT (1.8MPa), °C</td><td>69.8</td><td>66.5</td><td>63.6</td><td>61.8</td><td>58.8</td><td>55.3</td><td>64.2</td><td>61.2</td><td>59.6</td></tr>
<tr><td>Izod, notched, kJ/m^2</td><td>1</td><td>1.2</td><td>3.6</td><td>4.6</td><td>5.7</td><td>7.4</td><td>2.9</td><td>2.5</td><td>2.6</td></tr>
<tr><td>Izod, un-notched, kJ/m^2</td><td>4.6</td><td>4.4</td><td>8.9</td><td>11.0</td><td>13.3</td><td>19.1</td><td>8.4</td><td>11.6</td><td>14.0</td></tr>
<tr><td>MAI,Dynatup, J</td><td>5.3</td><td>7.9</td><td>9.0</td><td>8.6</td><td>9.5</td><td>9.3</td><td>9.1</td><td>9.3</td><td>8.8</td></tr>
<tr><td>MFI, g/10min</td><td>31.2</td><td>27.8</td><td>23.7</td><td>19.0</td><td>18.4</td><td>13.3</td><td>33.6</td><td>30.0</td><td>45.4</td></tr>
<tr><td colspan="10">Burn times for UL-94 tests- 1st Ign time (s) / 2nd Ign time (s)</td></tr>
<tr><td>Bar 1</td><td>1 / 1</td><td>11/1</td><td>2/1</td><td>3/15</td><td>2/11</td><td>1/30</td><td>1/1</td><td>1/1</td><td>1/1</td></tr>
<tr><td>Bar 2</td><td>9 / 1</td><td>1 / 1</td><td>2/11</td><td>2/1</td><td>1/1</td><td>2/30</td><td>1/1</td><td>1/8</td><td>1/3</td></tr>
<tr><td>Bar 3</td><td>1 / 1</td><td>10/2</td><td>2/1</td><td>1/1</td><td>4/2</td><td>-</td><td>2/1</td><td>2/1</td><td>1/1</td></tr>
<tr><td>Bar 4</td><td>1 / 1</td><td>1/13</td><td>1/2</td><td>1/2</td><td>2/9</td><td>-</td><td>2/1</td><td>1/1</td><td>1/1</td></tr>
<tr><td>Bar 5</td><td>1 / 1</td><td>1/1</td><td>2/2</td><td>2/15</td><td>1/2</td><td>-</td><td>1/1</td><td>1/1</td><td>1/1</td></tr>
</table>

Improved Ductility

As would be expected in most highly filled polymer systems, the ductility of the ABS-natural fiber FR blends is significantly lower than that of virgin ABS polymer. Table VIII shows the unexpected benefits that can be gained through the use of NBR rubber in the formulation. A three fold improvement in un-notched izod and about 1.8 times improvement in Dynatup impact were achieved when total rubber content increased from about 21% (sample 1) to about 30% (sample 5). It should be noted that this improvement in ductility has minimal to no effect on FR performance. At a constant rubber contant of about 20%, V-0 ratings are again obtained (samples 7-9) but also result in reduced MFR values and lowered thermal mechanical properties as demonstrated by the ~10 °C drop in HDT.

Conclusions

An eco-friendly FR-ABS can be obtained using wood, cellulose or starch, phosphates and TPP/RDP/BPADP as FR additives. Phosphorous compounds work as catalysts for charring while natural fibers act as charring materials. The loading levels of these additives can be optimized to achieve desirable flammability properties. As expected, these additives increase the modulus. The base color of the blends can be affected through the utilization of a combination of EBS wax and zinc stearate. Additionally it has been shown that significant ductility improvements can be achieved through the incorporation of NBR rubber in the formulation. By carefully balancing the formulation of the blends it should be possible to achieve a non-halogenated product that has flammability and impact properties similar or better than traditional FR high impact polystyrene with the added benefit of significantly higher melt flow. This work has resulted in the issuance of three U.S. patents (*11*, *13*, *14*).

References

1. Placek C. *ABS Resin Manufacture*; Noyes Data Corp.: Park Ridge, NJ, 1970.
2. Lu, S. Y.; Hamerton, I. *Progr. Polym. Sci.* **2002**, *27*, 1661–1712.
3. Dawson, R. B.; Landry, S. D.; Steukers, V. In the 16th Annual BCC Conference on Flame Retardancy, Stamford, CT, U.S.A., May 22−25, 2005.
4. Levchik, S. V.; Bright, D. A.; Alessio, G. R.; Dashevsky, S. *J. Vinyl Addit. Technol.* **2001**, *7*, 98–103.
5. Sumi K.; Tsuchiya, Y. *Building Research Note No. 111*, Division of Building Research, National Research Council of Canada, April, 1976.
6. Li, B.; He, J. *Polym. Degrad. Stab.* **2004**, *83*, 241–246.
7. De Chirico, A.; Armanini, M.; Chini, P.; Cioccolo, G.; Provasoli, F.; Audisio, G. *Polym. Degrad. Stab.* **2003**, *79*, 139–145.
8. Le Bras, M.; Duquesne, S.; Fois, M.; Grisel, M.; Poutch, F. *Polym. Degrad. Stab.* **2005**, *88*, 80–84.
9. Bakar, M. B. A.; Ishak, Z. A. M.; Taib, R. M.; Rozman, H. D.; Jani, S. M. *J. Appl. Polym. Sci.* **2010**, *116*, 2714–2722.
10. Song, P.; Cao, Z.; Fu, S.; Fang, Z.; Wu, Q.; Ye, J. *Thermochim. Acta* **2011**, *518*, 59–65.
11. Gaggar, S. K.; Gupta, R. K.; Liu, T.-W.; Agarwal, S.; Al-Mulla, A. U.S. Patent 7,939,585, 2011.
12. Gao, M.; Sun, C. Y.; Zhu, K. J. *Therm. Anal. Calorim.* **2004**, *75*, 221–232.
13. Gaggar, S. K.; Yongstrom, C. R. U.S. Patent 7,915,328, 2011.
14. Gaggar, S. K.; Yongstrom, C. R.; Moore, J. F. U.S. Patent 7,915,329, 2011.

In Fire and Polymers VI: New Advances in Flame Retardant Chemistry and Science; Morgan, A., et al.;
ACS Symposium Series; American Chemical Society: Washington, DC, 2012.

Chapter 12

Thermal Degradation and Fire Behaviors of Glass Fiber Reinforced PA6 Flame Retarded by Combination of Aluminum Hypophosphite with Melamine Derivatives

Bin Zhao, Li Chen, and Yu-Zhong Wang*

**Center for Degradable and Flame-Retardant Polymeric Materials,
College of Chemistry, National Engineering Laboratory of
Eco-Friendly Polymeric Materials (Sichuan), Sichuan University,
Wangjiang Road 29, Chengdu 610064, China
*E-mail: yzwang@scu.edu.cn**

Low-cost aluminum hypophosphite (AP) was used as the flame retardant for glass fiber reinforced polyamide 6 (GFPA6) together with melamine pyrophosphate (MPyP) or melamine cyanurate (MCA) to prepare halogen-free flame-retardant GFPA6 composites. The thermal degradation behavior and fire behavior of the resulting GFPA6 composites were investigated via thermogravimetric analysis (TGA) together with evolved gas analysis (TG-FTIR) and via limiting oxygen index (LOI) test, vertical burning test (UL-94) and cone calorimetry, respectively. Both AP/MPyP and AP/MCA flame retardant systems could endow GFPA6 composites V-0 rating in UL 94 test and increase the LOI values to 29.0% at 20wt% of total loading. Cone calorimeter results showed that AP combined with melamine derivatives could efficiently reduce the smoke production of the flame-retardant composites, particularly the production of CO. Thermal analysis indicated that some reactions occurred among AP, melamine derivatives and PA6 matrix during heating. The phosphorus- and nitrogen-containing volatile products were detected

In Fire and Polymers VI: New Advances in Flame Retardant Chemistry and Science; Morgan, A., et al.;
ACS Symposium Series; American Chemical Society: Washington, DC, 2012.

in the TG-FTIR. The burning residues showed compact, continuous and bladder-like char layers from the observation of morphologies by scanning electronic microscopy (SEM). All the results indicated that both condensed phase and vapor phase flame retardant mechanisms occur in these composites.

Keywords: Flame retardance; composites; polyamide 6; thermal degradation

1. Introduction

Glass fiber reinforced polyamide 6 (GFPA6) is an important engineering plastic composite due to its excellent properties, including high strength, wear and abrasion resistance and chemical resistance (*1*). However, the applications of GFPA6 are limited because of its flammability when subjected to fire. The flame retardation of GFPA6 is much more difficult than that of PA6 because of the "candlewick effect" caused by glass fibers (*2*, *3*). Many effective solutions to flame retard GFPA6 have been found for additive-type substance containing halogen, phosphorus and/or nitrogen (*3–7*). However, the utilization of some halogen-containing additives has been forbidden due to environmental and health considerations. Thus, development of halogen-free flame-retardant GFPA6 systems is urgently needed to solve the potential fire hazard. In recent years, phosphorus- and nitrogen-based flame-retardant systems including organic and inorganic compounds were frequently used in GFPA6 and other polymers (*8*, *9*); red phosphorus is an efficient halogen-free flame retardant but limits the color of products (*10*, *11*). Recently, metal phosphinates, especially aluminum or zinc salts of diethylphosphinic acid, have been found to be effective flame retardants for polyesters, polyamides, and their glass fiber reinforced composites (*12*, *13*). In addition, when the metal phosphinates were combined with some nitrogen-containing substance, the flame-retardant effect could be enhanced. Braun *et al.* have done some important work in the flame-retardant mechanism of the metal phosphinates (*14–16*). The study on the flame retardant mechanism of aluminum diethylphosphinate in combination with melamine polyphosphate and zinc borate in glass-fiber-reinforced PA6,6 revealed that using a combination of aluminum phosphinate and melamine polyphosphate resulted in some charring and dominant barrier effects (*15*). Gallo *et al.* (*16*) reported that the metal oxides could change the PBT decomposition behavior and promote the formation of additional stable carbonaceous char in the condensed phase. Although these metal phosphinate salts have been proven to be very efficient for some polymers, the flame retardants are of high cost due to the complicated synthetic route of the organic phosphinate. In our previous study, a low-cost inorganic hypophosphite, aluminum hypophosphite (AP), was found to be an efficient flame retardant for glass-fiber-reinforced engineering plastics based on PA6 (*17*) and poly(butylene terephthalate) (*18*). Both the GFPA6 and GFPBT achieved a V-0 (1.6 mm) rating in UL 94 test and have high LOI values. At the same time, PHRRs of flame-retardant GFPA6 and GFPBT have been decreased markedly. However, more smoke is produced when AP was used alone. In this chapter, we use AP as the flame retardant together with melamine pyrophosphate (MPyP) or melamine cyanurate (MCA) to prepare a series of halogen-free flame-retardant glass-fiber-reinforced PA6 composites, and tried further to enhance the flame-retardant efficiency and reduce the smoke and CO production of GFPA6. The thermal degradation and fire behavior as well as flame-retardant mechanism of the systems were investigated via thermogravimetric analysis, degradation products analysis (TG-FTIR), flammability tests (UL 94, LOI) and monitoring the fire behavior under forced flaming conditions (cone calorimeter).

2. Experimental

2.1. Materials

Neat PA6 pellets (Mn≈30000; product code: YH-800) were purchased from Hunan Yueyang Baling Petrochemical Co., Ltd., China. Glass fiber (ECS301-CL) was supplied by Chongqing Polycomp International Co., Ltd., China. Melamine pyrophosphate (MP_yP) was obtained from Shandong Shian Chemical Co., Ltd., China. Melamine cyanurate (MCA) was a commercial product from Bluestar Chengrand Chemical Co., Ltd, China. Aluminum hypophosphite (AP) was prepared in our laboratory (*17*).

2.2. Sample Preparation

PA6 and the flame retardants were dried in an oven at 100 °C for 5 h prior to blending. Then neat PA6 pellets and 30 wt% glass fiber were mixed with the flame retardants by tumbling the ingredients in a tumbler. Then the mixtures were fed into a twin-screw extruder (SLJ230, L/D = 30) operating at about 230-240 °C, and the exudates were clipped into pellets. The pellets were finally compression-molded and cut into standard test bars.

2.3. Measurements

Thermogravimetric analysis (TGA) was carried out on an TG 209F1 (NETZSCH, Germany) thermal analyzer under a 60 mL/min flowing nitrogen atmosphere at a scan rate of 20 °C/min, and the weight of the testing samples was kept within 3.0 to 5.0 mg. Thermogravimetric analysis/infrared spectrometry (TG-IR) of GFPA6 composites was performed using the TG 209F1 IR thermogravimetric analyzer interfaced to the Nicolet 6700 FTIR spectrophotometer. Each sample of about 10.0-15.0 mg in weight was placed in an alumina oxide crucible and heated from 40 to 700 °C. The heating rate was set as 10 °C/min in a nitrogen atmosphere with a flow rate of 50 mL/min. The LOI was evaluated according to GB/T2406.2-2009 and the dimensions of all samples were 130 mm×6.5 mm×3.0 mm. The vertical burning test was performed according to UL-94 and the dimension of all samples was 130 mm×13 mm×3.0 mm. Scanning electronic microscopy (SEM, JEOL JSM-5900LV) was used to investigate char residues of the flame-retardant GFPA6 after the LOI test. SEM graphs of the char residues were recorded after coating with gold. The fire behavior in flaming conditions was characterized using a cone calorimeter (Fire Testing Technology, East Grinstead, UK) according to ISO 5660-1 at an external heat flux of 50 kW/m^2. The dimension of all specimens was 100 mm×100 mm×3.0 mm.

3. Results and Discussion

3.1. Thermal Degradation Behavior

The Thermogravimetric results of GFPA6 and the flame-retardant composites based on AP and/or different nitrogen-containing chemicals are listed in Table I, and the corresponding curves are shown in Figure 1 and Figure 2, respectively.

Table I. Thermogravimetry results of GFPA6 composites under N_2 atmosphere[a]

Samples	*$T_{5\%}$ /°C*	*T_{max1} /°C*	*R_{d1} /%/min*	*T_{max2} /°C*	*R_{d2} /%/min*	*Residues at 700 °C /%*
GFPA6	403	/	/	446	22.6	31.6
GFPA6-AP_{20}	342	384	12.4	/	/	52.5
GFPA6-MCA_{20}	330	349	10.6	461	15.0	31.7
GFPA6-MP_yP_{20}	338	374	22.8	419	7.6	40.2
GFPA6-$AP_{13.3}$-$MCA_{6.7}$	327	391	15.6	451	3.6	42.8
GFPA6-$AP_{13.3}$-$MP_yP_{6.7}$	320	387	14.6	441	4.1	45.8

[a] R_{d1} : The decomposition rate at T_{max1}; R_{d2} : the decomposition rate at T_{max2}.

In detail, neat GFPA6 showed a single decomposition step with a maximum mass loss rate at 446 °C, resulting from the release of water, carbon dioxide, carbon monoxide, ammonia and hydrocarbon fragments (*19*), and the residue is only 31.5 %, which mostly results from the glass fibers added. When different flame retardants are added to the GFPA6 composites, the degradation behavior of the flame-retardant composites change greatly. Both the onset decomposition temperatures ($T_{5\%}$) (approximately 50-70 °C below that of the virgin GFPA6) and the maximum- decomposition-rate temperature (T_{max}) of the samples decrease when AP is added, meaning that AP can decrease the thermal stability of GFPA6 as AP is a weak Lewis acid-base, which can interact with the matrix (*17*). When MCA is added, two degradation steps can be observed (Figure 1. b).

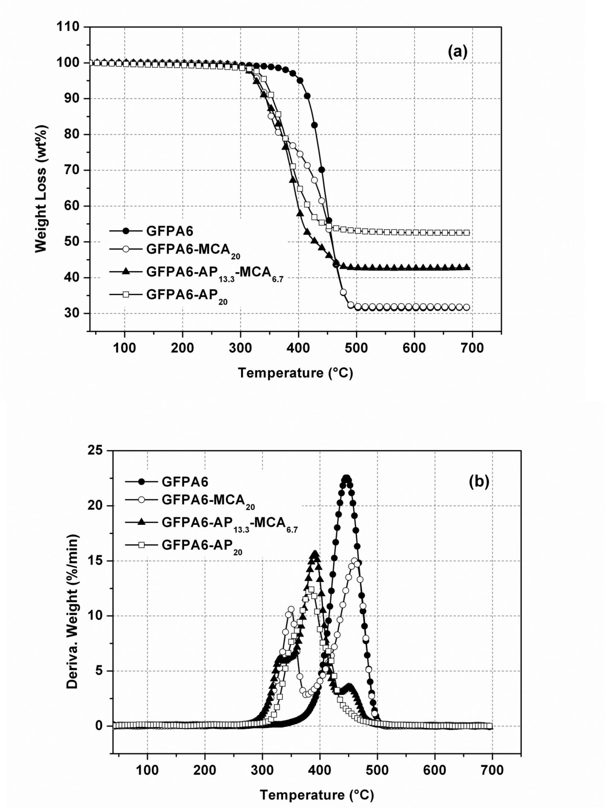

Figure 1. TG (a) and DTG (b) curves of the GFPA6-AP-MCA composites at the heating rate of 20 °C/min in N_2.

The decomposition rate (10.6 %/min) at T_{max1} (349 °C) is lower than that (15.0 %/min) at T_{max2} (461 °C). The first degradation stage is attributed to the decomposition of MCA, which increased the T_{max2} of the material (461 °C) compared to the T_{max} of neat GFPA6 (446 °C). Unfortunately, more stable products are not formed in the high temperature zone, and the residue is the same as the virgin GFPA6. When MPyP is added, the decomposition rate at T_{max1} is 22.8 %/min, which is higher than that of other samples; Compared to virgin GFPA6, T_{max2} also decreases, indicating that MPyP promotes the decomposition of the matrix. As shown in Table I, when AP is combined with MPyP or MCA to flame retard GFPA6, the initial decomposition temperature of the composites are lower than those of the composites containing only one of the flame retardants. When AP is combined with MCA, there appear three weight loss peaks in DTG curve (Figure 1, b): The first small peak is attributed to the decomposition of MCA; T_{max1} (the second peak) is postponed to 391 °C; However, the decomposition rate (15.6 %/min) at T_{max1} is higher than that of the system in which AP or MCA is used alone. The results indicate that the presence of MCA and AP can promote the decomposition of the matrix. As shown in Figure 2, when AP and MPyP are added to GFPA6, $T_{5\%}$ of the sample is 320 °C (the lowest in the samples studied), indicating that reaction occurs upon heating and the composites decompose earlier. The decomposition promotes the earlier formation of char, which could restrain the degradation of composites.

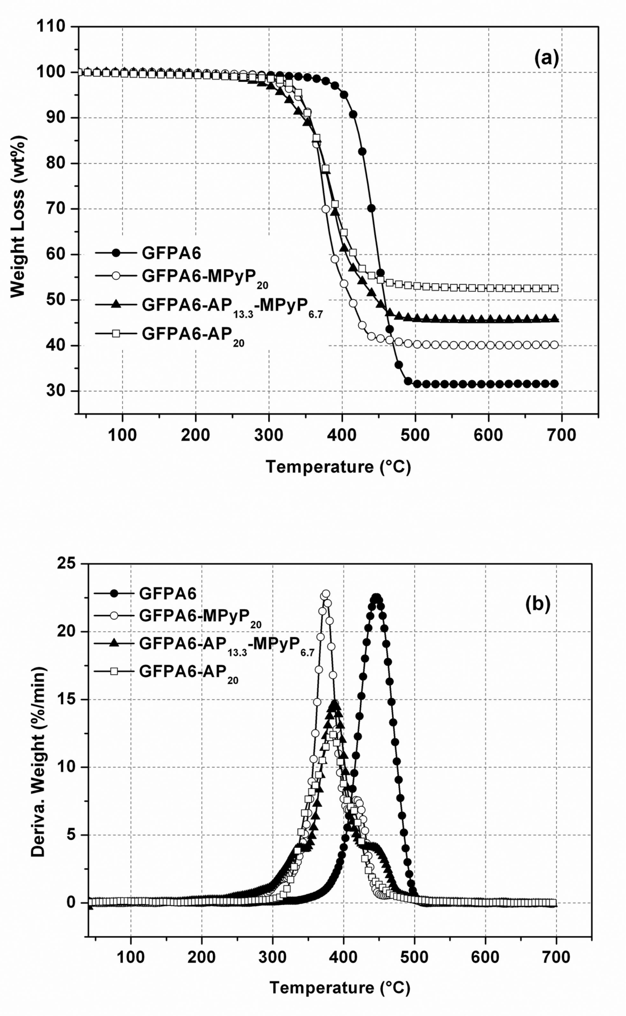

Figure 2. TG (a) and DTG (b) curves of the GFPA6-AP-MPyP composites at the heating rate of 20 °C/min in N_2.

3.2. Flame Retardance of the Composites

The flame-retardant results of GFPA6 composites with different formulations at 30wt% of total flame retardant loading are summarized in Table II, including Underwriters Laboratories (UL) 94 and limiting oxygen index (LOI) tests. The LOI value of GFPA6 sample is only 22.5 % and it is not classified in the UL-94 test. Specifically, during UL-94 test, GFPA6 sample burns over 70 s at the first ignition and the dripping ignites the cotton below. MCA or MPyP does not improve the UL-94 rating of GFPA6 when they are used alone as a flame retardant, though they can increase the LOI values of GFPA6 to 24.5 and 26.3 %, respectively. In our previous work, AP was shown to be an effective flame retardant for GFPA6 (*17*). As shown in Table II, when 20 wt% AP is added, the composite can obtain the UL-94 V-0 rating and the LOI value increases to 27 %. Moreover, when MCA or MPyP is added to GFPA6-AP composites to replace part of the AP in an appropriate proportion, the composites show improved flame retardancy: the LOI values of both GFPA6-AP-MCA and GFPA-AP-MPyP are further increased to 28.5% and 29.0%, respectively, meanwhile the two composites achieve the V-0 rating in UL-94 tests.

Table II. Results of UL-94 and LOI tests for the composites

Samples	*t_1 (s)*	*t_2 (s)*	*UL-94 rating (3.0 mm)*	*LOI (%)*
GFPA6	70 (BC[a])	--	NR[b]	22.5
GFPA6-AP_{20}	0	2	V-0	27.0
GFPA6-MCA_{20}	41 (BC)	--	NR	24.5
GFPA6-$MPyP_{20}$	32 (BC)	--	NR	26.3
GFPA6-$AP_{13.3}$-$MCA_{6.7}$	0	3	V-0	28.5
GFPA6-$AP_{13.3}$-$MPyP_{6.7}$	0	1	V-0	29.0

[a] BC means burning to the clamp. [b] NR denotes No Rating.

3.3. Cone Calorimetric Analysis

The cone calorimeter has been widely used for assessing the fire performance of polymer materials. Results from cone calorimetry provide a comprehensive understanding for the burning performance of the tested sample in a rather well-defined fire test scenario (*20*). Table III lists the main results of the GFPA6 composites after cone tests at an external heat flux of 50 kW/m^2, including time to ignition (TTI), peak heat release rate (PHRR), total heat release (THR), fire growth rate (FIGRA, which is defined as the calculated value by dividing the peak HRR by the time to HRR (*21*)), average effective heat of combustion (Av-EHC) and average HRR (Av-HRR).

Table III. Cone calorimetric data obtained at a heat flux of 50 kW/m^2

Samples	*GFPA6*	*GFPA6-AP$_{20}$*	*GFPA6-AP$_{13.3}$-MCA$_{6.7}$*	*GFPA6-AP$_{13.3}$-MPyP$_{6.7}$*
TTI (s)	37	29	28	20
pHRR (kW/m^2)	520	206	194	263
FIGRA[a]	4.9	3.2	2.9	4.8
THR (MJ/m^2)	73	56	49	36
Av-EHC (MJ/kg)	28	26	22	22
Av-HRR (kW/m^2)	249	107	116	139
Residue (wt%)	32.3	51.3	44.2	48.1

[a] FIGRA: the calculated value obtained from dividing the peak HRR by the time to HRR.

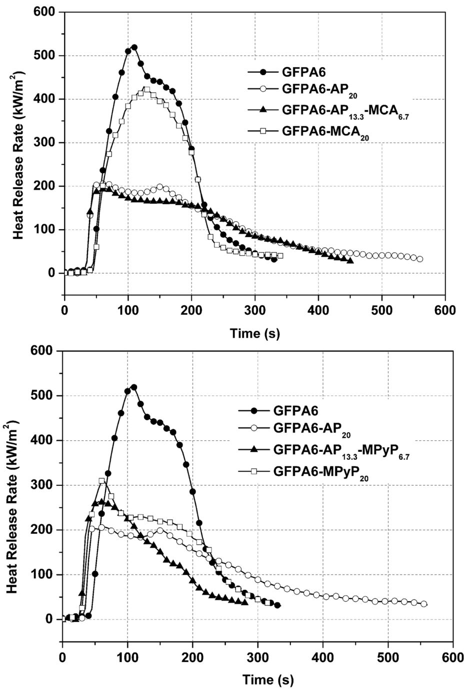

Figure 3. Heat release rate (HRR) curves of the composites at an external heat flux of 50 kW/m^2.

HRR curves of the examined specimens are given in Figure 3. It can be seen that GFPA6 without the interference of flame retardant burns quickly after ignition and an intensive peak turns up with a PHRR value of 520 kW/m^2, followed by a sudden decrease with a small flat, which is a typical HRR plot for glass fiber reinforced materials (*22*). The addition of MCA or MPyP to GFPA6 reveals radically different HRR plots. HRR of GFPA6-MCA$_{20}$ quickly decreases after the peak value is achieved; however, the curve of GFPA6-MPyP$_{20}$ is flat when it arrives at the maximum. The difference between them is due to the different mechanisms during their combustion: MCA is a classic flame retardant which mostly acts in the gaseous phase; while MPyP can promote the formation of a carbonaceous char layer during combustion by the release of pyro-/ultra- or poly-phosphoric acid (*23*), similar to the mechanism of ammonium polyphosphate (APP) (*24*). Lower PHRR and more typical HRR curve of a char-forming material are revealed when MCA or MPyP is combined with AP to flame retard GFPA6. When the flame retardants are added, especially AP is combined with MCA or MPyP, the values of TTI are decreased, suggesting that they could promote the decomposition of the matrix PA6, which is in agreement with the TG test. The reduction of TTI may be due to the initial decomposition of flame retardants which promotes the decomposition of the composites (*25*). The relationship between TTI and HRR could be explained on the basis of an early ignition allowing less accumulation of combustible vapors to give rise to the reduction of HRR after ignition (*26*). Furthermore, it can be seen that AP-MCA is the most effective flame retardant system, which can decrease the PHRR of GFPA6 composite by about 60% compared to virgin GFPA6, to 194 kW/m^2.

Based on the cone test, FIGRA, calculated by dividing the peak HRR by the time to HRR (PHRR/t_{PHRR}), is usually used to assess the fire hazard of materials (*27*). The flame retardant samples show lower FIGRA value than neat GFPA6, while the specimen GFPA6-AP$_{13.3}$-MCA$_{6.7}$ has the lowest FIGRA value, 2.9, which means it has highest fire safety. A low FIGRA value indicates the delayed time to flashover, which allows more time to evacuate and survive in a fire hazard (*28*).

THR is the integral of HRR during the cone test and according to the external radiant flux levels (*29*). At the same radiant flux, the THR is related to several factors, including the effective heat of combustion (EHC) of the volatiles, the total mass loss, and the combustion efficiency in the fire zone (*30*). As shown in Table III, THR of the flame retardant GFPA6 composites decrease from 73 MJ/m^2 of virgin GFPA6 to 36-56 MJ/m^2, respectively. Moreover, the two combined flame-retardant systems (GFPA6-AP/MCA and GFPA6-AP/MPyP) show lower THR values than AP used alone (GFPA6-AP).

EHC is the heat release of the volatile portion of the material during combustion, which is determined by dividing the heat release rate by the mass loss rate (HRR/MLR). From Table III, it can be seen that the Av-EHC of the flame-retardant sample with AP/MCA or AP/MPyP decreases compared to that of virgin GFPA6 and GFPA6-AP$_{20}$; the Av-HRR of combined flame-retardant composites increases compared to that of the flame retarded GFPA6 by AP$_{20}$ alone, indicating that the MLR of the flame-retardant materials containing melamine derivatives are higher than that of GFPA6-AP$_{20}$. The higher gas

In Fire and Polymers VI: New Advances in Flame Retardant Chemistry and Science; Morgan, A., et al.;
ACS Symposium Series; American Chemical Society: Washington, DC, 2012.

production and lower EHC value indicate that noncombustible gases exist in the gas phase. Combustion residues of the flame-retardant samples decrease from 51.3 wt% of GFPA6-AP$_{20}$ to 44.2 and 48.1 wt% by incorporation of MCA and MPyP, respectively, which also confirms that in the presence of melamine salts, the flame-retardant samples produce more gaseous materials than GFPA6-AP$_{20}$. However, combustion residues of all flame-retardant samples are higher than that of the virgin GFPA6, which means that a condensed phase mechanism for flame retardation occurs in such melamine-containing systems.

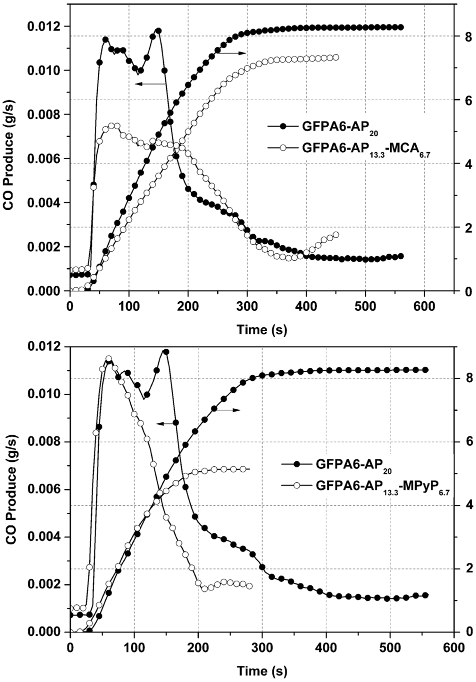

Figure 4. CO Produce (COP) and total smoke produce (TSP) curves of the composites at an external heat flux of 50 kW/m².

In order to investigate the smoke of the flame-retardant composites during combustion, CO production (COP) and total smoke production (TSP) curves were recorded (shown in Figure 4). By comparing the flame-retardant systems containing both AP and melamine derivatives with the system flame-retarded by AP alone, it can be seen that the former has lower TSP value than the latter. In addition, the GFPA6 composite flame-retarded with AP/MCA could reduce the CO production during the combustion. Those results show that the melamine derivatives combined with AP could efficiently reduce the smoke of the flame-retardant GFPA6 composites compared to AP alone as a flame retardant at the same loading of flame retardants.

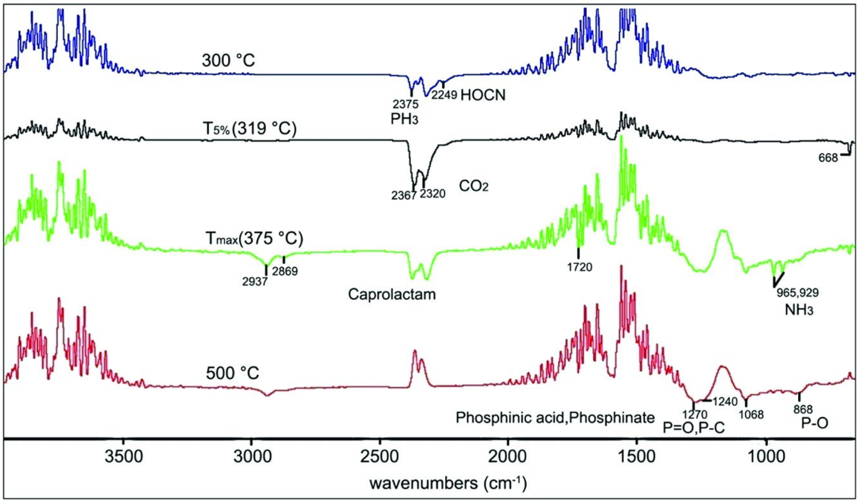

Figure 5. FTIR spectra of volatilized products during the thermal decomposition of GFPA6-AP$_{13.3}$-MCA$_{6.7}$ composite.

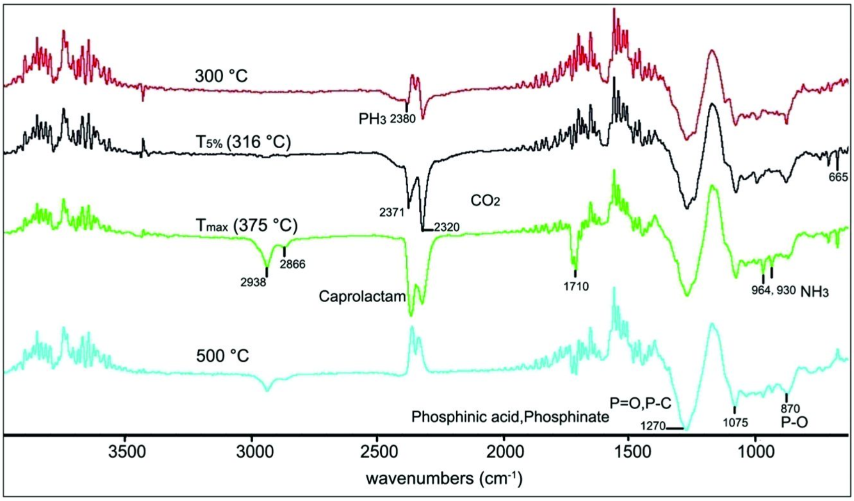

Figure 6. FTIR spectra of volatilized products during the thermal decomposition of GFPA6-AP$_{13.3}$-MPyP composite.

3.4. Degradation Products and Residue Analysis

Identification of degradation products are studied by the TG-IR technique. Figure 5 and Figure 6 give the FTIR spectra of volatilized products during the thermal decomposition of the flame-retardant composites with different melamine salts. The main evolved substances from thermal degradation of GFPA6 include caprolactam, ammonia, water and carbon dioxide (*31*). From Figure 5, it can be observed that PH_3 (2375 cm^{-1}) and isocyanic acid (2249 cm^{-1}) have been released in the temperature range between 300-319 °C; these are the volatile products generated in the initial decomposition of AP and MCA. When the temperature increased to 375 °C (the temperature of the maximum-mass-loss rate), the caprolactam (2937, 2869, 1720 cm^{-1}) and NH_3 (965, 929 cm^{-1}) were released (*29*). Meanwhile, some phosphorus-containing substances like phosphinic acid, phosphinate at 1270 and 1240 cm^{-1} (P=O, P-C) as well as 868 cm^{-1} (P-O) were generated from the reaction of AP and/or the corresponding phosphorization of MCA with the resin during the heating process. The signal of PO_2^- was detected at 1067 cm^{-1} (*32*). Subsequently, the degradation products of PA6 (caprolactam, NH_3) are observed in very small amounts, indicating that thermally stable chars were formed during heating. Figure 6 shows the spectra of the AP/MPyP system, different from the AP-MCA system, phosphorus-containing substances are released at relatively low temperature (300 °C), indicating that the volatile products were generated in the initial decomposition of MPyP. In addition, the release of the phosphorus-containing gas was not reduced at high temperature (500 °C), which could produce more smoke than the samples containing MCA during cone calorimeter test. The signal for isocyanic acid was not detected during the test, which is in accordance with the literature (*14*, *33*).

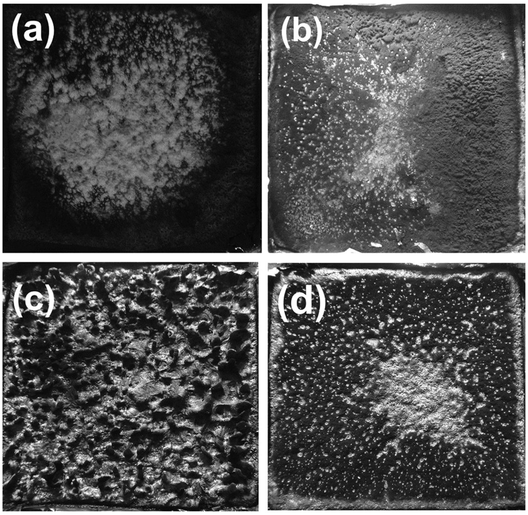

Figure 7. Digital photographs of the char residues after cone calorimeter test: (a) GFPA6, (b) GFPA6-AP_{20}, (c) GFPA6-$AP_{13.3}$-$MCA_{6.7}$, (d) GFPA6-$AP_{13.3}$-$MPyP_{6.7}$.

Figure 7 shows the vertical view of the samples after cone test. The char layer can be observed on the surface of flame retardant GFPA6 composites especially for the sample of GFPA6-AP_{20}. As shown in Figure 7c, the material containing MCA formed "small lumps" char layer after cone test, which is due to the noncombustible gases released during the combustion. On the contrary, only glass fibers remained on the surface of the virgin GFPA6 as shown in Figure 7a.

The outer chars of the four composites after LOI test were analyzed by SEM (Figure 8). After burning, the neat GFPA6 left glass fibers; while the PA6 matrix was burnt out (Figure 8a). When flame retardants were added, chars with different topography formed after LOI test. The AP-containing samples formed thick and discontinuous char layer; when melamine derivatives are added together with AP, the char residues changed to more compact, continuous and bladder-like morphology caused by the volatilization of the decomposition products generated mostly from the melamine derivative. This morphology could prevent heat/oxygen transfer and protect the inner polymer.

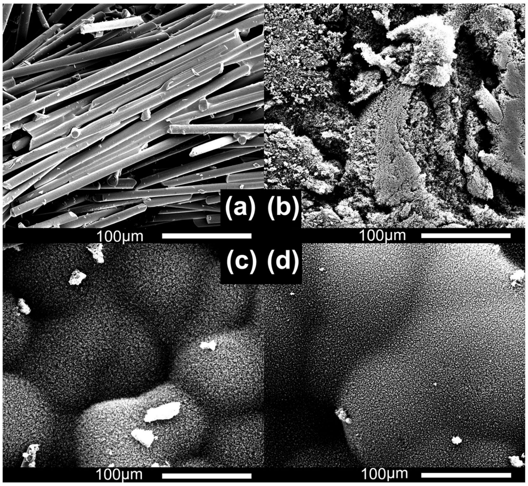

Figure 8. SEM images of residues from the investigated composites after LOI tests: (a) GFPA6, (b) GFPA6-AP_{20}, (c) GFPA6-$AP_{13.3}$-$MCA_{6.7}$, (d) GFPA6-$AP_{13.3}$-$MPyP_{6.7}$.

4. Conclusions

In this work, flame-retardant GFPA6 composites were fabricated by adding aluminum hypophosphite (AP) together with melamine pyrophosphate (MPyP) or melamine cyanurate (MCA). The resulting combined flame-retardant systems could endow the GFPA6 composites V-0 rating in UL 94 testing and higher limiting oxygen index than AP alone, and could efficiently reduce the smoke production of the flame-retardant composites, particularly the production of

CO; meanwhile, the fire safety degree (FIGRA) of the composites was also increased. Thermal analysis showed that some reactions occurred among AP, melamine derivatives and PA6 matrix during heating, which accelerated the decomposition of composites. The early decomposition promoted the formation of char, which could restrain the degradation of the composites. Degradation products and residue analysis showed that the flame retardation of MPyP or MCA on GFPA6 was based on a gas fuel-dilution effect and the formation of the phosphorus-containing residues acting as the protecting barrier.

Acknowledgments

This work was supported by the National Science Foundation of China (Grant Nos. 50933005, 51121001) and the Program for Changjiang Scholars and Innovative Research Team in University (IRT1026)

References

1. Akkapeddi, M. K. Glass fibre reinforced polyamide-6 nanocomposites. *Polym. Compos.* **2000**, *21*, 576–85.
2. Isitman, N. A.; Gunduz, H. O.; Kaynak, C. Nanoclay synergy in flame retarded/glass fibre reinforced polyamide 6. *Polym. Degrad. Stab.* **2009**, *94*, 2241–50.
3. Gunduz, H. O.; Isitman, N. A.; Aykol, M.; Kaynak, C. Interfacial interactions and flammability of flame retarded and short fibre reinforced polyamides. *Polym. Plast. Technol. Eng.* **2009**, *48*, 1046–54.
4. Weil, E. D.; Levchik, S. V. Current practice and recent commercial developments in flame retardancy of polyamides. *J. Fire Sci.* **2004**, *22*, 251–64.
5. Levchik, S. V.; Weil, E. D. Combustion and fire retardancy of aliphaticnylons. *Polym. Int.* **2000**, *49*, 1033–73.
6. Xiong, W. C.; Chen, L.; Zhao, B.; Wang, D. Y.; Wang, Y. Z Polyamide 6 with a flame retardant encapsulated by polyamide 66: flame retardation, thermal-decomposition and the potential mechanism. *Chin. J. Polym. Sci.* **2012**, *30*, 297–307.
7. Xiong, W. C.; Chen, L.; Wang, D. Y.; Song, F.; Wang, Y. Z. Synergistic effects of novolac-based char former with a phosphorus/nitrogen- containing flame retardant in polyamide 6. *Chin. J. Polym. Sci.* **2012**, *30*, 72–81.
8. Chen, L.; Wang, Y. Z. A review on flame retardant technology in China. Part I: development of flame retardants. *Polym. Adv. Technol.* **2010**, *21*, 1–26.
9. Lu, S. Y.; Hamerton, I. Recent developments in the chemistry of halogen-free flame retardant polymers. *Prog. Polym. Sci.* **2002**, *27*, 1661–712.
10. Levchik, G. F.; Vorobyova, S. A.; Gorbarenko, V. V.; Levchik, S. V.; Weil, E. D. Some mechanistic aspects of the fire retardant action of red phosphorus in aliphatic nylons. *J. Fire Sci.* **2000**, *18*, 172–82.

11. Jou, W. S.; Chen, K. N.; Chao, D. Y.; Lin, C. Y.; Yeh, J. T. Flame retardant and dielectric properties of glass fibre reinforced nylon-66 filled with red phosphorus. *Polym. Degrad. Stab.* **2001**, *74*, 239–45.
12. Kleiner, H. J.; Budzinsky, W.; Kirsch, G. U.S. Patent 5,780,534, 1998.
13. Jenewein, E. Kleiner, H. J.; Wanzke, W.; Budzinsky, W. U.S. Patent 6,365,071, 2002
14. Braun, U.; Schartel, B.; Fichera, M. A.; Jager, C. Flame retardance mechanisms of aluminium phosphinate in combination with melamine polyphosphate and zinc borate in glass-fibre reinforced polyamide 6, 6. *Polym. Degrad. Stab.* **2007**, *92*, 1528–45.
15. Braun, U.; Bahr, H.; Sturm, H.; Schartel, B. Flame retardance mechanisms of metal phosphinates and metal phosphinates in combination with melamine cyanurate in glass-fibre reinforced poly(1,4-butylene terephthalate): the influence of metal cation. *Polym. Adv. Technol.* **2008**, *19*, 680–92.
16. Gallo, E.; Braun, U.; Schartel, B.; Russo, P.; Acierno, D. Halogen-free flame retarded poly(butylene terephthalate) (PBT) using metal oxides/PBT nanocomposites in combination with aluminium phosphinate. *Polym. Degrad. Stab.* **2009**, *94*, 1245–53.
17. Zhao, B.; Hu, Z.; Chen, L.; Liu, Y.; Liu, Y.; Wang, Y. Z. A phosphorus-containing inorganic compound as an effective flame retardant for glass-fiber-reinforced polyamide 6. *J. Appl. Polym. Sci.* **2011**, *119*, 2379–85.
18. Chen, L.; Luo, Y.; Hu, Z.; Lin, G. P.; Zhao, B.; Wang, Y. Z. An efficient halogen-free flame retardant for glass-fibre-reinforced poly(butylene terephthalate). *Polym. Degrad. Stab.* **2012**, *97*, 158–65.
19. Hornsby, F. R.; Wang, J.; Rothon, R.; Jackson, G.; Wilkinson, G.; Cossick, K. Thermal decomposition behaviour of polyamide fire-retardant compositions containing magnesium hydroxide filler. *Polym. Degrad. Stab.* **1996**, *51*, 235–49.
20. Schartel, B.; Bartholmai, M.; Knoll, U. Some comments on the use of cone calorimeter data. *Polym. Degrad. Stab.* **2005**, *88*, 540–47.
21. Schartel, B. Considerations regarding specific impacts of the principal fire retardancy mechanisms in nanocomposites. In *Flame retardant polymer nanocomposites*; Morgan, A. B., Wilkie, C. A., Eds.; John Wiley &Sons: Hoboken, 2007; p 122.
22. Casu, A.; Camino, G.; DeGiorgi, M.; Flath, D.; Laudi, A.; Morone, V. Effect of Glass Fibres and Fire Retardant on the Combustion Behavior of Composites, Glass Fibres-Poly(butylene terephthalate). *Fire Mater.* **1998**, *22*, 7–14.
23. Levchik, S. V.; Costa, L.; Camino, G. Effect of the fire-retardant ammonium polyphosphate on the thermal decomposition of aliphatic polyamides. Part III—Polyamides 6.6 and 6.10. *Polym. Degrad. Stab.* **1994**, *43*, 43–54.
24. Laoutid, F.; Bonnaud, L.; Alexandre, M.; Lopez-Cuesta, J. M.; Dubois, P. New prospects in flame retardant polymer materials: From fundamentals to nanocomposites. *Mater. Sci. Eng., R* **2009**, *63*, 100–125.
25. Gallina, G.; Bravin, E.; Badalucco, C.; Audisio, G.; Armanini, M.; Chirico, A. D.; Provasoli, F. Application of cone calorimeter for the

assessment of class of flame retardants for polypropylene. *Fire Mater.* **1998**, *22*, 15–18.

26. Babrauskas, V. Y.; Parker, W. J. Ignitability Measure ments with the Cone Calorimeter. *Fire Mater.* **1987**, *11*, 31–43.
27. Fangrat, J.; Hasemi, Y.; Yoshida, M.; Kikuchi, S. Relationship between heat of combustion, lignin content and burning weight loss. *Fire Mater.* **1998**, *22*, 1–6.
28. He, S. Q.; Hu, Y.; Song, L.; Tang, Y. Fire safety assessment of halogen-free flame retardant polypropylene based on cone calorimeter. *J. Fire Sci.* **2007**, *25*, 109–118.
29. Schartel, B.; Kunze, R.; Neubert, D. Red phosphorus-controlled decomposition for fire retardant PA 66. *J. Appl. Polym. Sci.* **2002**, *83*, 2060–2071.
30. Schartel, B.; Hull, T. R. Development of fire-retarded materials-interpretation of cone calorimeter data. *Fire Mater.* **2007**, *31*, 327–54.
31. Levchik, S. V.; Weil, E. D.; Lewin, M. Thermal decomposition of aliphatic nylons. *Polym. Int.* **1999**, *48*, 532–57.
32. Thomas, L. C. *Interpretation of the IR spectra of organophosphorus compounds*; Heyden: London, U.K., 1974.
33. Braun, U.; Schartel, B. Effect of red phosphorus and melamine polyphosphateon the fire behavior of HIPS. *J. Fire Sci.* **2005**, *23*, 5–30.

Chapter 13

Study of Intumescent Flame Retardant Copolyester Hot Melt Adhesive

Mingming Zhang, Jianxin Du,* and Jianwei Hao

National Laboratory of Flame Retardant Materials, School of Materials Science and Engineering, Beijing Institute of Technology, 5 South Zhongguancun Street, Beijing 100081, PR China
***E-mail: tonydjx@bit.edu.cn**

Halogen-free flame retardant copolyester (PES) hot melt adhesive was prepared using an intumescent flame retardant (IFR) consisting of ammonium polyphosphate (APP), pentaerythritol (PER) and melamine (MEL) with Zeolite 4A as a synergistic agent. The effect of IFR on flame retardancy of PES and synergistic effect between IFR and Zeolite 4A were studied. It was found that a small quantity of Zeolite 4A could enhance the flame retardant effect of IFR on PES. When 30 wt% IFR was used, PES/IFR achieved an LOI value of 30.7%, UL-94 V-0 rating, and significantly reduced maximum heat release rate. The LOI value increased to 35.1% when 3wt% Zeolite 4A was added. TGA, SEM and XPS showed that Zeolite 4A could catalyze esterification reactions of IFR and facilitate the formation of much denser char. Zeolite 4A decomposed and participated in carbonization reactions at high temperature, which stabilize the carbon residue and increased its amount.

Introduction

Copolyester (PES) hot melt adhesive, which is random copolymer of one or more polybasic acids and polyatomic alcohols, has wide application in shielding materials. For instance, conductive fabric plays an important role in the electronics industry, where the surface is coated with a thin layer of hot melt adhesive film, requiring a high level of flame retardancy. Currently flame-retardants used in hot melt adhesives applied to conductive fabric are generally halogenated. The

In Fire and Polymers VI: New Advances in Flame Retardant Chemistry and Science; Morgan, A., et al.;
ACS Symposium Series; American Chemical Society: Washington, DC, 2012.

halogens may be harmful to the environment and the ydo not meet the requirements of environmental protection (*1*, *2*). The European Union Restriction of Hazardous Substances (RoHS) on Electric and Electronic Production came into effect on July, 1st, 2006 (*3*) and there is an urgent need for halogen-free flame retardant hot melt adhesives in the electronics industry. However, research on this topic has not been reported.

In this report, halogen-free flame retardant PES hot melt adhesive was prepared using a conventional intumescent flame retardant (IFR) with Zeolite 4A as synergistic agent. The effect of IFR on flame retardancy of PES and synergistic effect between IFR and Zeolite 4A are studied.

Experimental

Materials

PES hot melt adhesive (a random copolymer of terephthalic acid, isophthalic acid and ethylene glycol, melt index = 28g/10min, melting point=120±5 °C), was offered by Shanghai HeHe hot melt adhesives Co., Ltd. Ammonium polyphosphate (APP) was produced by Hangzhou JLS Flame Retardants Chemical Co., Ltd., Pentaerythritol (PER) by Beijing Tong county YuCai Fine Chemical Factory, Melamine (MEL) by Tianjin Guangfu Fine Chemical Research Institute and Zeolite 4A by Dalian Yixiu Molecular Sieve Catalyst Co., Ltd.

Sample Preparation

The materials (include PES, APP, PER, MEL and Zeolite 4A) were mixed in a high-speed mixer, then extrusion pelletized on a twin-screw extruder and finally sheets of various dimensions were obtained by injection molding.

Performance Test

Limiting Oxygen Index (LOI) data of all samples were obtained at room temperature on an oxygen index instrument (FTA ‖) produced by UK PL company according to GB/T 2406.2-2009 standard; the dimensions of all samples are 120×6×3 mm. Vertical burning rates were measured on a CZF-3 instrument produced by Jiangning Analysis Instrument Factory, with sample dimensions of 127×12.7×3.2 mm, according to the UL-94 standard. Cone calorimeter tests were measured on a FTT 0007 cone calorimeter produced by UK FTT Company with sample dimensions of 100×100×3mm, according to ASTM E 1354 standard. Thermogravimetry experiments were carried out under N_2 atmosphere using a Netzsch 209 F1 Iris® thermoanalyzer at a heating rate of 10 °C/min. The morphological observation of the char residues obtained from cone calorimeter tests were examined by Scanning Electron Microscope (SEM, Supra 55 type) produced by Zeiss. X-ray photoelectron spectroscopy (XPS) data were obtained on a PHI 5300 spectrometer produced by PERKIN-ELMER Physics Electronics Company.

Results and Discussion

Flame Retardancy

Limiting oxygen index (LOI) and vertical burning rate (UL-94) are simple and important methods to evaluate the flame retardancy of polymeric materials. Table 1 shows the effect of IFR and Zeolite 4A on the LOI values and UL94 ranking for flame retardant PES system; in all formulations containing IFR, the ratio of APP, PER and MEL was 3:1:1.

Table 1. Effect of IFR and 4A Zeolite on flame retardant PES

Samples (PES/IFR/4A Zeolite)	*LOI (%)*	*UL-94 (3.2mm)*	*t_1+t_2 (5 specimens, s)*
100/0/0	21.3	no rating	—
70/30/0	30.7	V-0	18
70/30/1	31.3	V-0	15
70/30/2	34.5	V-0	10
70/30/3	35.1	V-0	9
70/30/4	34.6	V-0	9

Exp.: IFR-(APP:PER:MEL=3:1:1).

From LOI data shown in Table 1, PES is an easily flammable polymeric material with a LOI value of 21.3% and it undergoes melt dripping. When the amount of IFR in PES was 30wt%, the LOI increased to 30.7%.

It is known that Zeolite 4A is a synergist of intumescent flame retardants and can effectively enhance the mechanical strength of the char layer by the formation of Si-O-P-C and Al-O-P-C bonds (*4*). Therefore Zeolite 4A was added to flame retardant PES systems in this research (samples 3 to 6).

When the amount of IFR was unchanged and 3% Zeolite 4A was added to the system, the LOI value was increased to 35.1%.

Furthermore, from UL94 data shown in Table 1, PES has no rating in UL94 vertical burning test, but all of the flame retardant PES systems could obtain a UL94 V-0 rating, further demonstrating that IFR is very effective in PES.

Cone Calorimeter

Cone Calorimetry provides a number of parameters to describe a fire, including time to ignition, heat release rate, smoke production and so on. These parameters have wide application in fire safety engineering and design, research and evaluation on flame retardant performance of material. Table 2 gives CONE data of flame retardant PES systems. Figure 1(a) shows heat release rate curves of PES, before and after adding flame retardants. The shape of the heat release rate curve of PES without flame retardants is high and narrow, with a high peak heat release rate (PHRR). When flame retardants are added, the shape becomes quiote different, simply rising to a low value and then continuing at that value for some time, with a much lower PHRR.

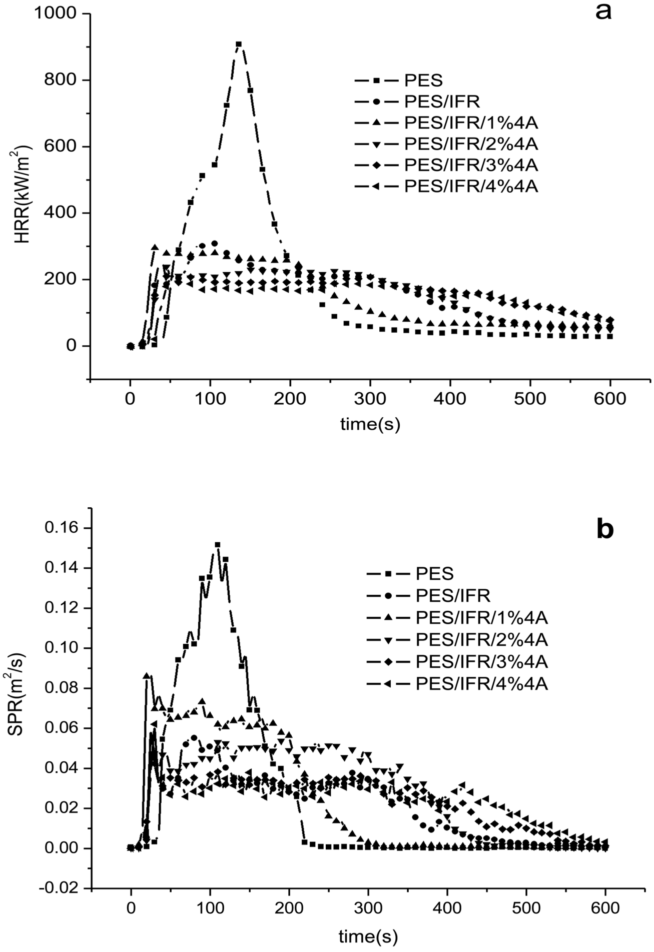

Figure 1. HRR(a) and SPR(b) curves of PES before and after adding IFR and 4A Zeolite.

Table 2. CONE data of flame retardant PES

Samples (PES/IFR/ 4A Zeolite)	*Cone data(50kW/m²)*					
	TTI (s)	*T_{PHRR} (s)*	*PHRR (kW/m²)*	*THR (MJ/m²)*	*PSPR (m²/s)*	*TSP (m²/kg)*
100/0/0	34	135	908	105	0.152	15.2
70/30/0	20	85	312	106	0.056	12.7
70/30/1	16	35	303	91	0.088	14.4
70/30/2	19	45	241	97	0.056	14.7
70/30/3	23	50	225	109	0.045	14.0
70/30/4	30	55	222	102	0.062	14.2

Exp.:TTI-Time to ignition; TPHRR-Time to PHRR; PHRR-Peak heat release rate; THR-Total heat release; PSPR-Peak smoke production rate; TSP- Total smoke production.

The peak heat release rate is further reduced by adding Zeolite 4A, and with an increased amount of Zeolite 4A, the peak heat release rate continued to reduce, finally tending to be constant at 3 and 4%.

Figure 1(b) shows smoke production rate curves of PES before and after adding flame retardants. The smoke production seems to track quite well with the heat release rate. The peak smoke production rate (PSPR) of the material was markedly reduced when flame retardants were added but no change in smoke as the amount of Zeolite is increased. CONE test results clearly show that the presence of IFR will enhance the flame retardancy of PES.

Table 3. TG and DTG data of PES, PES/IFR, PES/IFR/3% 4A

Samples	*T1% (°C)*	*T5% (°C)*	*Tp (°C)*	*Rp (%/°C)*	*W_{700} (%)*
PES	324	369	404	1.57	7.6
PES/IFR	195	266	235(s1)	0.08(S1)	21.1
			391(s2)	1.37(S2)	
PES/IFR/3%4A	217	306	242(s1)	0.05(S1)	32.0
			391(s2)	1.16(S2)	

Exp.:T1%,T5%-Temperature at mass loss of 1% and 5%; Tp-Temperature at maximal mass loss rate; Rp-Maximal mass loss rate; W700- Residue at 700°C;S1-Stage1; S2-Stage2.

In Fire and Polymers VI: New Advances in Flame Retardant Chemistry and Science; Morgan, A., et al.;
ACS Symposium Series; American Chemical Society: Washington, DC, 2012.

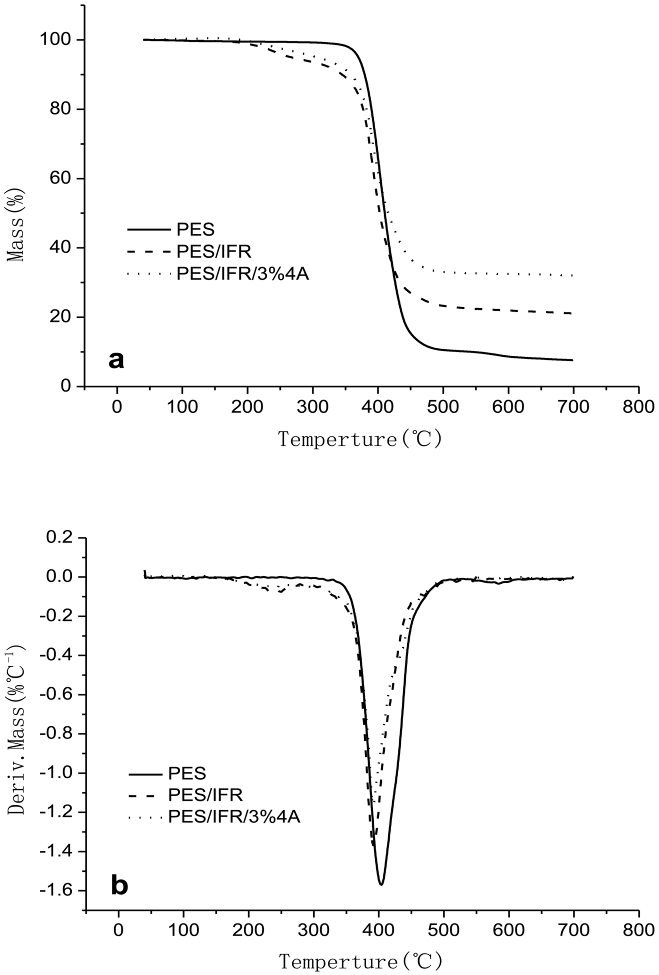

Figure 2. TG(a) and DTG(b) curves of PES, PES/IFR and PES/IFR/3% 4A.

Thermal Degradation and Charring Behavior

By combining the results from LOU, UL94 and the cone calorimeter, it can be seen that the PES/IFR/3% Zeolite 4A system (sample 5) showed the best results. Therefore this system was chosen for further study for thermal degradation and charring behavior.

Thermogravimetry (TG) results are shown in Table 3 and Figure 2. PES exhibits only one weight loss region, while flame retardant PES systems showed two weight loss regions, the first is due to the thermal decomposition of flame retardants, and the second is mainly the degradation of PES. The following can be noted from this data: (1) the initial decomposition temperature of the two flame retardant PES systems is less than that of PES; (2) the weight loss temperature T1% and T5% of PES/IFR/3% Zeolite 4A are higher than PES/IFR, and this may be due to Zeolite 4A facilitating the esterification of IFR, which brings about char formation and reduces volatiles; (3) Tp, the maximum mass loss rate of flame retardant PES systems is reduced as is the maximum weight loss rate Rp, which help to form char; (4) when 30wt% IFR is added to PES, the residual mass at 700 °C increased from 7.6% to 21.1%, and when 3% Zeolite 4A is also added, the residue increased to 32.0%, which demonstrates that Zeolite 4A plays a role to facilitate the formation of char. TG test results demonstrate that the enhanced fire retardancy due to IFR is due to char formation.

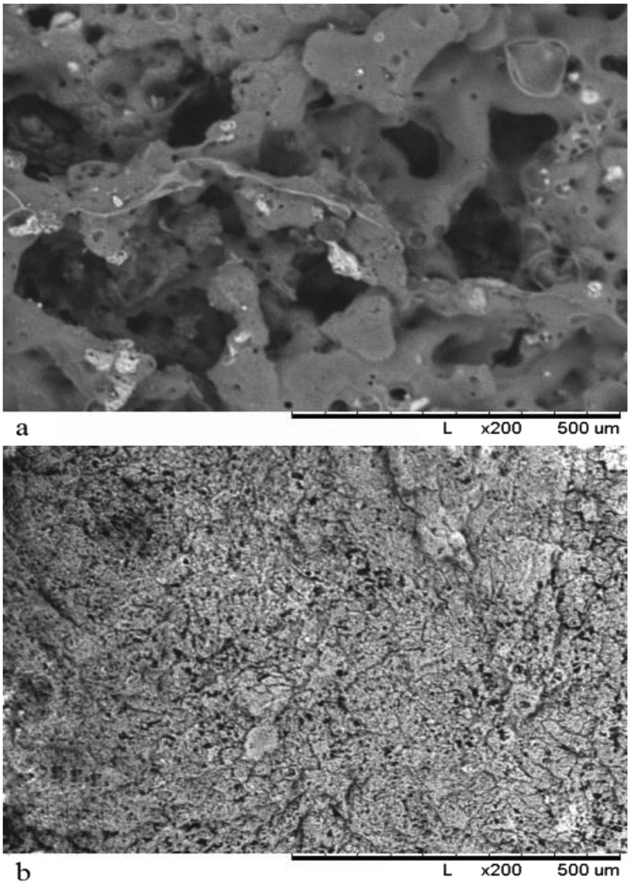

Figure 3. Morphologies of char of PES/IFR (a) and PES/IFR/3%4A (b).

The Morphology of the Carbonaceous Residue

The carbonaceous residue of the two systems PES/IFR and PES/IFR/3% Zeolite 4A after cone calorimetry were observed by scanning electron microscopy (SEM) and the results are shown in Figure 3. From SEM images at 200 times magnification, we can see that the internal structure of PES/IFR/3% Zeolite 4A system is denser and more uniforme than that without Zeolite 4A (PES/IFR system). This can provide better insulation for both thermal and oxygen transfer.

XPS Analysis of Carbonaceous Residue

The residues of the two systems PES/IFR and PES/IFR/3% Zeolite 4A after cone calorimetry were analyzed by X-ray Photoelectron Spectroscopy (XPS) and the results are shown in Table 4.

Table 4. XPS data of PES/IFR and PES/IFR/3%4A

Elements	*PES/IFR -chars*	*PES/IFR/3%4A*	*PES/IFR/3%4A -chars*
C(%)	38.33	61.47	55.04
N(%)	1.01	4.09	2.13
O(%)	54.04	30.4	36.25
P(%)	6.62	0.92	1.89
Si(%)	—	2.58	4.54
Al(%)	—	0.53	0.15
C/O	0.71	—	1.52
Si/Al	—	4.87	30.27

The content of carbon shows the degree of charring while the amount of oxygen shows the degree of oxidation. The more carbon and the less oxygen, the greater is the charring ability and antioxidation. Here the value of C/O is taken as a comparison standard (*5*).

The value of C/O for the flame retardant PES system rose from 0.71 to 1.52 when Zeolite 4A was added, indicating a greater ability for charring and antioxidation after Zeolite 4A is added.

The value of Si/Al in the residue of PES/IFR/3% Zeolite 4A system is higher than that before burning. At high temperature (the temperature can reach higher than 700 °C in the cone calorimeter) aluminosilicate decomposes, and SiO_2 and Al_2O_3 compete on the surface layer, finally leading to the enrichment of SiO_2. Meanwhile Zeolite 4A participates in charring reactions and the charring reaction could be promoted because of increased acid catalytic activity on the surface (*6*).

In Fire and Polymers VI: New Advances in Flame Retardant Chemistry and Science; Morgan, A., et al.;
ACS Symposium Series; American Chemical Society: Washington, DC, 2012.

Conclusion

When IFR is added to the PES system, the material has very good flame-retardancy but, adding a small quantity of Zeolite 4A, the flame retardancy can be improved. When the ratio of PES, IFR and Zeolite 4A is 70:30:3, LOI value can reach 35.1%. Likewise the PHRR and PSPR of material are greatly reduced.

The addition of Zeolite 4A increases the amount of char and catalyzes esterification reactions to facilitate much denser char.

References

1. Li, W.; Bouzidi, L.; Narine, S. S. Current research and development status and prospect of hot-melt adhesives: A review. *Ind. Eng. Chem Res.* **2008**, *47*, 7524–7532.
2. Jeong, H. M.; Kim, D. H.; Jung, J. S.; Kim, T. K.; Kim, B. K.; Kim, Y. S.; Cho, Y. L.; Hwang, J. M. The effect of organoclay on the properties of a reactive hot melt polyurethane adhesive. *Compos. Interfaces* **2007**, *14*, 467–476.
3. Tang, X.; Xu, H. M. The EU Environmental Directives and Environmentally Friendly China Mechanical and Electrical Products. *Market Modernization* **2009**, *572*, 3–4 (in Chinese).
4. Bourbigot, S.; Le Bras, M.; Delobel, R.; Bréant, P.; Tremillon, J-M 4A zeolite synergistic agent in new flame retardant intumescent formulations of polyethylenic polymers-study of the effect of the constituent monomers. *Polym. Degrad. Stab.* **1996**, *54*, 275–287.
5. Zhang, J.; Ji, K. J.; Xia, Y. Z. Combustion and Flame Retardancy of Polymer. *Chem. Ind. Press* **2005** (in Chinese).
6. Wei, P.; Wang, J. Q. The TGA/XPS study on the synergy of 4A zeolites in the intumescent flame retardant APP/PER. *Polym. Mater. Sci. Eng.* **2003**, *19*, 179–181.

Chapter 14

Analysis of Combustibility of Brominated Epoxies

Stanislav I. Stoliarov,*,[1] Qaadir Williams,[2] Richard N. Walters,[2] Sean Crowley,[2] and Richard E. Lyon[2]

[1]Department of Fire Protection Engineering, University of Maryland, College Park, Maryland 20742
[2]FAA W. J. Hughes Technical Center, Airport and Aircraft Safety Research and Development Division, Atlantic City International Airport, New Jersey 08405
***E-mail: stolia@umd.edu**

A widespread use of brominated flame-retardants and recent concerns about their environmental impact prompted a study to understand the mechanism by which bromine inhibits the combustion of polymeric materials as a first step toward identifying alternative compounds. The heats of combustion of bromine-containing epoxies were calculated from known atomic compositions and compared to experimental values. The experimental heats were obtained using a cone calorimeter, microscale combustion calorimeter, and by burning volatile pyrolysis products in a methane diffusion flame and measuring oxygen consumption (pyrolysis-flaming-combustion calorimeter). In all experiments, the heat released by a unit amount of material decreased with increasing fraction of bromine. Further analysis revealed that, in the case of cone calorimeter experiments, the decrease is caused by incomplete combustion of volatile degradation products and, to a lesser degree, by the formation of char.

Keywords: Gas-phase flame retardants; cone calorimetry; heat of combustion

1. Introduction

During the past 50 years, a substantial amount of research has been done to understand the mechanism of inhibition of the gas-phase combustion of hydrocarbons by brominated compounds. It has been established that brominated fire-suppressing agents (such as CF3Br) act as scavengers of reactive radicals (chemical mode of action), heat capacity energy sinks and diluents (physical modes of action) (*1*). Dependencies of premixed burning velocity on the concentration of the agents have been analyzed and the inhibitors have been ranked in terms of their efficiency (*2*). The mechanism of action of brominated flame-retardants used in plastics is not understood nearly as well. While it is known that these additives affect both condensed-phase degradation of a polymer and gas-phase combustion of the degradation products (*3*), the quantitative contributions of these effects have not been established. In the light of recent environmental concerns (*4*), quantification of these effects becomes an important first step toward elucidation of the mechanism of action of these additives and identification of environmentally benign alternatives.

In the present study, the heats of combustion of blends of bisphenol-A epoxy, brominated bisphenol-A epoxy, and brominated bisphenol A were calculated from known atomic compositions and compared with the heats released by these materials in flaming and non-flaming combustion. The main combustion scenario realized in a cone calorimeter (*5*) showed the largest bromine-induced reductions in the measured heats. These reductions were analyzed further to determine contributions associated with dilution, charring, and change in the efficiency of the gas-phase combustion.

2. Experimental

The materials used in this study were prepared by blending diglycidylether of bisphenol A (DBA) with tetrabromodiglycidylether of bisphenol A (BDBA) or with tetrabromobisphenol A (BBA). A range of blends containing up to 80 wt.% of BDBA and up to 40 wt.% of BBA was made. The blends were cured using 1-2 wt.% of 2-ethyl-4-methylimidazole in a convection oven. The oven temperature was increased from 20°C to 120°C in 50°C steps; after each increase, it was maintained constant for 4 hours.

The materials were evaluated using cone calorimetry (CC), pyrolysis-combustion flow calorimetry (PCFC), and pyrolysis-flaming-combustion calorimetry (PFCC). The CC and PCFC methods are described in references (*5*) and (*6*), respectively. PFCC is a new method. A schematic diagram of the PFCC setup is shown in Figure 1. In this method, a small sample of material, about 30 mg, is pyrolyzed at a constant heating rate. 2 K s^{-1} was used in this study. Gaseous products of pyrolysis are swept by a flow of methane, 0.8 cm^3 s^{-1}, feeding a laminar diffusion flame, which is open to the atmosphere. The heat released as a result of combustion is measured by means of oxygen consumption (*7*). The sample size and heating rate were selected to insure that, during the sample degradation, most of the released heat is associated with the combustion of its products.

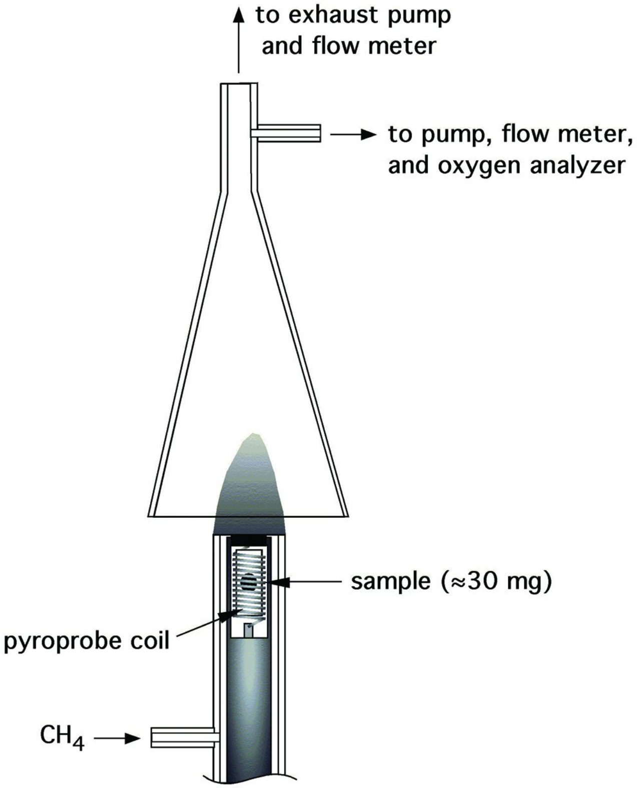
to exhaust pump and flow meter
to pump, flow meter, and oxygen analyzer
sample (≈30 mg)
pyroprobe coil
CH_4

Figure 1. Pyrolysis-Flaming-Combustion Calorimetry Apparatus.

3. Results

All experimental methods used in this study rely on the oxygen consumption technique for the measurement of heat released by materials. This technique is based on the fact that for a large number of organic compounds, the heat released per 1 g of oxygen consumed in combustion is constant and equal to 13.1 kJ (*7*). To make sure that this approach is still valid when applied to brominated materials, the heat release constant was used to calculate the heats of combustion of 20 small (6-20 atoms) brominated organic compounds with known enthalpies of formation (*8*). The amount of oxygen consumed by a unit amount of compound was determined from the stoichiometry of a complete combustion reaction:

$$C_xH_yO_zBr_k[\text{gas}] + (x+(y-k)/4-z/2)\,O_2 = x\,CO_2 + (y-k)/2\,H_2O[\text{gas}] + k\,HBr$$

The calculated heats of combustion were found to be, on average, within 3% of those determined from the enthalpies of formation at standard conditions (pressure=1.013×10^5 Pa and temperature =298 K). The maximum deviation was

8%. This comparison indicates that the accuracy of the oxygen consumption technique is not compromised by the presence of bromine and that, provided that sample atomic composition is known, the heat of its complete combustion can be easily computed from the reaction stoichiometry.

Table 1. Summary of the Cone Calorimetry Data Obtained at the External Heat Flux of 50 kW m^{-2}

Material[a]	*Avg.HRR kW m^{-2}*	*THR kJ g^{-1}*	*Avg.MLR g s^{-1} m^{-2}*	*Char wt.%*
DBA	552	22.6	22.0	5.5
20 wt.% BDBA (9.3 wt.% Br)	541	16.0	37.1	7.4
40 wt.% BDBA (19.5 wt.% Br)	346	10.8	34.7	16.4
60 wt.% BDBA (29.2 wt.% Br)	228	9.3	28.4	13.4
80 wt.% BDBA (38.5 wt.% Br)	180	6.4	--	15.1
10 wt.% BBA (5.9 wt.% Br)	519	19.3	28.7	8.2
20 wt.% BBA (11.2 wt.% Br)	346	13.0	26.9	13.1
30 wt.% BBA (18.2 wt.% Br)	279	9.9	28.7	17.2
40 wt.% BBA (22.9 wt.% Br)	272	9.2	31.4	12.9

The results of CC, PCFC, and PFCC tests are summarized in Table 1 and 2. The CC tests were performed on 10×10×0.45(±0.10) cm samples subjected to 50 kW m^{-2} of radiant heat flux. All testing procedures followed the standard (*5*). The average heat release rate (Avg.HRR) and average mass loss rate (Avg.MLR) were obtained from the data collected during the time between the initial increase of the heat release rate above 150 kW m^{-2} and its final decrease below 150 kW m^{-2}. This threshold was used to exclude noise-dominated parts of the heat release and mass loss rate curves from impacting the averages. PCFC experiments were also performed following recommended practices (*6*). 5-7 mg samples were pyrolyzed in nitrogen using 1 K s^{-1} heating rate; the gaseous pyrolysis products were oxidized by mixing them with oxygen and sending the mixture through a tubular reactor maintained at 900°C. The total heat released (THR) measured in the CC, PCFC, and PFCC experiments was normalized by the initial sample mass. All tests indicate that THR decreases systematically with increasing amount of brominated compounds. This trend is also followed by Avg.HRR. Addition of these compounds also promotes the formation of char. However, the char yield increase does not show the same level of correlation with additive amount as THR. All data suggest that, on the wt.% basis, BBA is a more efficient flame-retardant than BDBA.

Table 2. Summary of the Pyrolysis-Combustion Flow Calorimetry and Pyrolysis-Flaming-Combustion Calorimetry Data

Material	*PCFC THR kJ g⁻¹*	*PCFC Char wt.%*	*PFCC THR kJ g⁻¹*	*PFCC Char wt.%*
DBA	25.7	5.3	19.2	9.6
20 wt.% BDBA (9.3 wt.% Br)	21.0	8.4	18.3	14.4
40 wt.% BDBA (19.5 wt.% Br)	18.2	11.3	16.7	18.7
60 wt.% BDBA (29.2 wt.% Br)	15.8	13.6	13.1	16.6
80 wt.% BDBA (38.5 wt.% Br)	12.9	14.9	9.6	20.0
10 wt.% BBA (5.9 wt.% Br)	23.0	7.7	19.4	13.5
20 wt.% BBA (11.2 wt.% Br)	21.3	8.7	17.6	13.5
30 wt.% BBA (18.2 wt.% Br)	19.3	8.5	15.7	17.2
40 wt.% BBA (22.9 wt.% Br)	17.7	10.7	14.5	14.8

4. Analysis

To perform in-depth analysis of the THR and Avg.HRR trends, it is necessary to determine the heats of complete combustion (HCC) of the materials under study. As stated in the previous section, these heats can be computed from the stoichiometry of the corresponding reactions and the heat release constant (13.1 kJ / 1 g of O_2). Assuming that the atomic composition of the materials is not a significant source of uncertainties, these calculations should be at least as accurate as the measurements performed in this work because both approaches are based on the same empirical relation between the oxygen consumption and released heat. The results of the calculations are shown in Table 3. Note that two heat values are reported: one is normalized by the initial mass of a given sample, the other by the number of moles of monomers comprising the sample. The same approach was used to calculate the HCC of char (also given in Table 3). The char was assumed to consist of pure carbon.

Knowledge of the heats of complete combustion makes it possible to determine the efficiencies of the gas-phase combustion processes that took place in the CC, PCFC, and PFCC tests.

$$\text{Comb.Eff.} = \frac{\text{THR}}{\text{HCC(material)} - \text{HCC(char)} * \text{ch.yld.}}$$

where ch.yld. is the mass fraction of char formed in a given experiment. Dependencies of the combustion efficiencies on the mass fraction of bromine (in the initial material) are shown in Figure 2.

Table 3. Calculated Heats of Complete Combustion

Material	*HCC* *$kJ\ g^{-1}$*	*HCC* *$kJ\ mol^{-1}$*
DBA	30.8	10.7×10^3
20 wt.% BDBA (9.3 wt.% Br)	27.8	10.5
40 wt.% BDBA (19.5 wt.% Br)	24.4	10.4
60 wt.% BDBA (29.2 wt.% Br)	21.2	10.3
80 wt.% BDBA (38.5 wt.% Br)	18.1	10.1
10 wt.% BBA (5.9 wt.% Br)	29.0	10.5
20 wt.% BBA (11.2 wt.% Br)	27.3	10.2
30 wt.% BBA (18.2 wt.% Br)	25.1	9.8
40 wt.% BBA (22.9 wt.% Br)	23.6	9.5
Char (carbon)	34.9	--

The CC dependencies are consistent with the notion that bromine acts as a suppressant of the gas-phase combustion. However, PCFC and PFCC data indicate that addition of brominated compounds produces a slight increase in the combustion efficiency. In the case of PCFC, the increase can be explained by significantly lower temperature of the combustion process. Typical diffusion flame temperature peaks at around 1600°C (*9*), which is significantly higher than 900°C used in the PCFC reactor. According to the observations summarized in reference (*3*), the role of bromine may shift from that of an inhibitor of the gas-phase combustion to that of a promoter with decreasing temperature. Similar upward trend observed in PFCC is harder to explain. The laminar diffusion flame used in this apparatus is expected to create gas-phase combustion conditions similar to those observed in the CC tests. One possible explanation is that the use of methane to maintain the flame in this apparatus (gaseous pyrolysis products are mixed with CH_4 prior to reaching the flame) lowers the bromine concentration in the gaseous fuel stream and distorts the flame chemistry and structure. A new version of this apparatus, which does not use methane, is currently being designed to address this potential deficiency.

Since cone calorimetry is the most realistic flammability test used in this work, further analysis is focused on the CC data (see Table 1). By performing heat of complete combustion and combustion efficiency calculations, we have implicitly identified all mechanisms by which addition of brominated compounds reduces THR. The heats of complete combustion of BDBA and BBA are lower than that of DBA. Thus, when one of the brominated compounds is added to DBA, the heat of complete combustion of a unit amount of material decreases (see Table 3). In this manuscript, this effect is referred to as dilution (a more combustible material is diluted by a less combustible material). The brominated compounds promote the formation of char – an after-burn residue that retains carbon in the condensed phase. This constitutes the second mechanism by which THR is reduced. Finally, brominated compounds also promote incomplete gas-phase combustion (i.e., decrease the combustion efficiency), which constitutes the third mechanism.

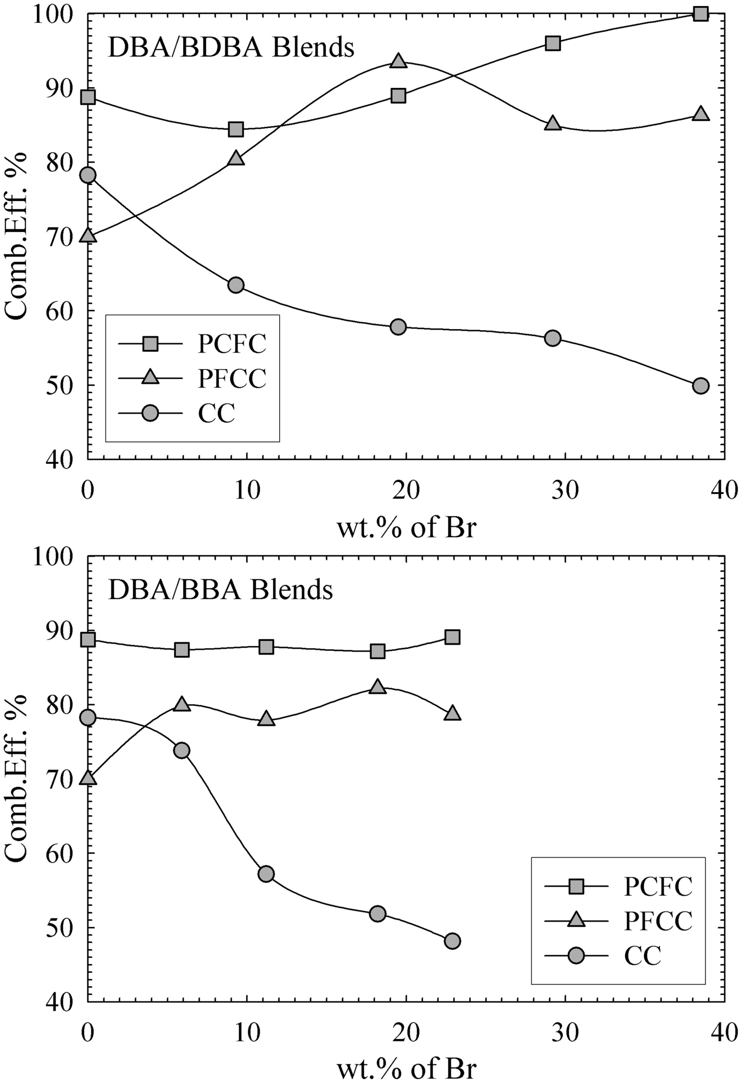

Figure 2. Gas-Phase Combustion Efficiencies.

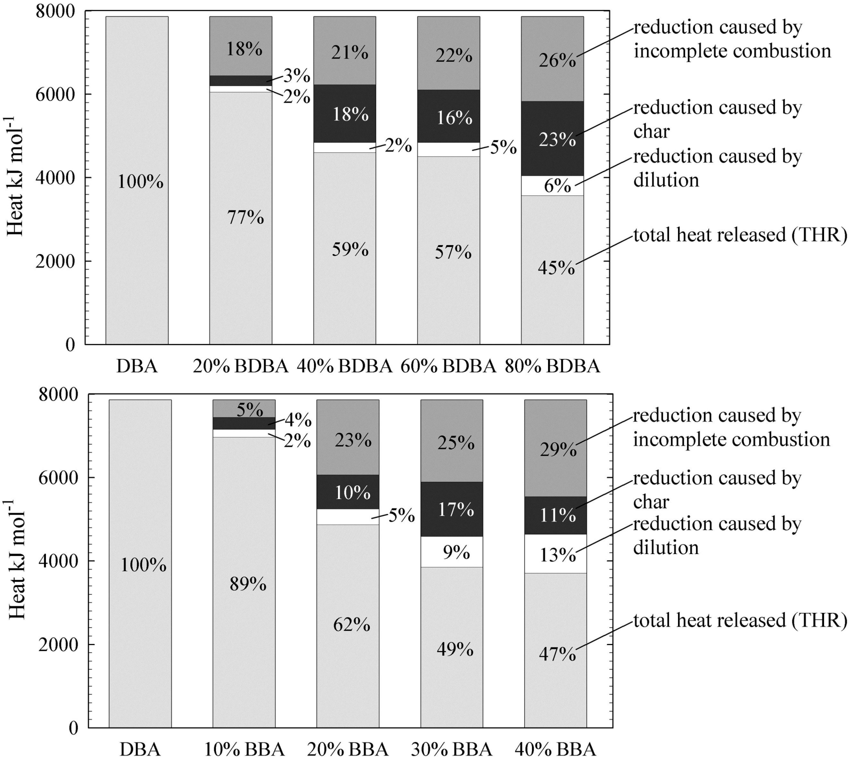

Figure 3. Reductions in the Cone Calorimetry THR Associated with the Addition of Brominated Compounds.

An evaluation of the contributions of these mechanisms to reductions in the CC THR (these contributions were calculated from the HCC values, char yields, and combustion efficiencies) indicates that the dilution is the most significant contributor. This result is not unexpected because the THR is a mass-based value. To a large degree, the reductions reflect increases in the average molecular weight of the structural units of material (due to introduction of heavy atoms of bromine), which is the reason why mass-based THR may not be an objective measure of the flammability for the polymeric systems under study. To correct this deficiency, the total heats released in the CC tests were renormalized by the number of moles of DBA, BDBA, and BBA used to make the samples. Subsequently, the THR reductions caused by dilution, char, and incomplete combustion were recalculated on the molar basis. The results of these calculations are shown in Figure 3. Note that the char yield and combustion efficiency obtained for pure DBA serve as a baseline; i.e., it is the reductions in the THR produced by increases in the fractional amount of char above that of DBA and by decreases in the combustion efficiency below that of DBA that are shown in the figure. According to these results, suppression of the gas-phase combustion is the main mechanism by which the brominated compounds reduce the molar THR. The ability of BDBA and BBA to promote the formation of char also has a significant effect on the THR values.

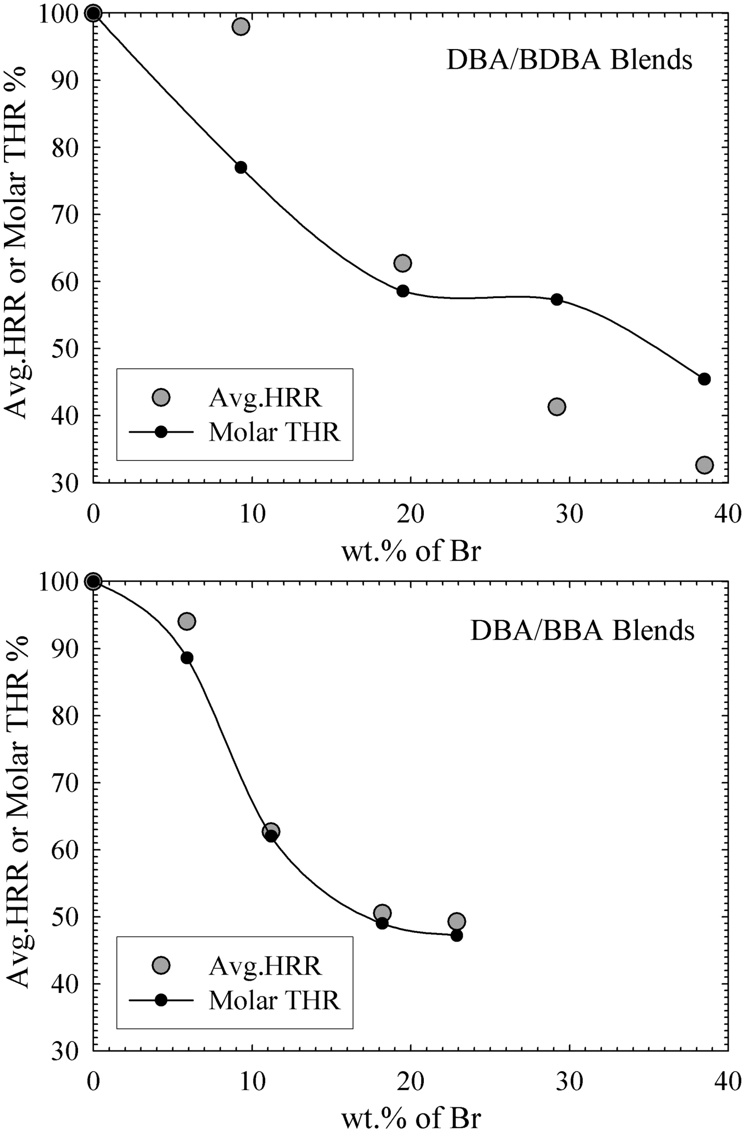

Figure 4. Comparison of the Relative Avg.HRR and Relative Molar THR.

Under the assumptions that the average molar rate of decomposition of all materials in the CC tests is the same (regardless of the composition) and that the decomposition is the rate-limiting step of the gasification process, the Avg.HRR is expected to be proportional to the molar THR. Dependencies of the Avg.HRR and molar THR, which were normalized by the corresponding values obtained for DBA, on the mass fraction of bromine are shown in Figure 4. An excellent agreement between the Avg.HRR and molar THR observed for DBA/BBA blends indicates that for these systems, the assumptions are valid. It also means that all mechanisms by which addition of BBA affects heat release have been accounted for. DBA/BDBA show notable discrepancies between the Avg.HRR and molar THR trends. These discrepancies can be explained as follows. According to the mass loss data shown in Table 1, addition of the first 20 wt.% of BDBA to DBA sharply increases the average rate of mass loss. This increase suggests that this change in the composition reduces the thermal stability, which results in the Avg.HRR being notably higher than the molar THR. At the same time, high concentrations (60-80 wt.%) of BDBA cause a significant reduction in the average molar rate of decomposition. This is, perhaps, due to a more thermally insulating char layer, which results in the Avg.HRR being lower than molar THR.

5. Conclusions

The analysis presented in this manuscript indicates that bromine-based flame-retardants used in polymers are effective because of their ability to significantly reduce the efficiency of the gas-phase combustion and, to a lesser degree, because they also promote the formation of char. This analysis is based on cone calorimetry measurements performed at a high external radiative heat flux (50 kW m^{-2}) simulating material response to a relatively large fire. In these measurements, the energy feedback from the surface flame does not contribute significantly to the total energy flow into the material. In contrast, in many standard scenarios testing material ignitability by a small heat source, such as UL-94 (*10*), the heat flow from the surface flame drives the flame spread and, therefore, defines fire growth. Understanding how bromine affects flame energy feedback is these scenarios is critical for developing a comprehensive knowledge of its modes of action in polymers and will be a subject of future investigation.

References

1. Sheinson, R. S.; Penner-Hahn, J. E.; Indritz, D. *Fire Saf. J.* **1989**, *15*, 437.
2. Babushok, V.; Tsang, W. *Combust. Flame* **2000**, *123*, 488.
3. Cullis C. F.; Hirschler M. M. *The Combustion of Organic Polymers*; Clarendon Press: Oxford, 1981.
4. D'Silva, K.; Fernandes, A.; Rose, M. *Crit. Rev. Environ. Sci. Technol.* **2004**, *34*, 141.
5. ASTM E 1354 – 09. *Standard Test Method for Heat and Visible Smoke Release Rates for Materials and Products Using an Oxygen Consumption Calorimeter*; ASTM International: West Conshohocken, PA, 2009.

6. ASTM D 7309 – 07. *Test Method for Determining Flammability Characteristics of Plastics and Other Solid Materials Using Microscale Combustion Calorimetry*; ASTM International: West Conshohocken, PA,(2007.
7. Huggett, C. *J. Fire Mater.* **1980**, *12*, 61.
8. *NIST Chemistry WebBook, NIST Standard Reference Database Number 69*; Linstrom, P. J., Mallard, W. G., Eds.; National Institute of Standards and Technology: Gaithersburg, MD, 2003, http://webbook.nist.gov.
9. Smyth, K.; Miller, J. H.; Dorfman, R. C.; Mallard, W. G.; Santoro, R. J. *Combust. Flame* **1985**, *62*, 157.
10. UL 94. *Flammability of Plastic Materials*; Underwriters Laboratories, Inc.: Northbrook, IL, 1991.

Chapter 15

Fire Performance of Curable Silicone-Based Coatings

**B. Gardelle,[1,2,3,4] S. Duquesne,[1,2,3,4] P. Vandereecken,[5]
and S. Bourbigot*,[1,2,3,4]**

**[1]Univ. Lille Nord de France, F-5900 Lille, France
[2]ENSCL, ISP-UMET, F-59652 Villeneuve d'Ascq, France
[3]USTL, ISP-UMET, F-59655 Villeneuve d'Ascq, France
[4]CNRS, UMR 8207, F-59652 Villeneuve d'Ascq, France
[5]Dow Corning S.A., 7180 Seneffe, Belgium
*E-mail: serge.bourbigot@ensc-lille.fr. Tel: +33 (0)320434888**

Polysiloxane elastomers are widely used because of their high thermal stability and low thermal conductivity. In this study, the fire performance of silicone based coatings containing ground calcium carbonate (GCC) are evaluated using a fire testing methodology similar to the "Torch Test" fire testing method. Two kinds of room temperature vulcanized silicone resins containing 50% GCC are used. The two resins, S1 and S2, are based on polydimethylsiloxane (PDMS) and are composed of D [$SiO_2(CH_3)_2$] and T [$CH_3Si(O_{1/2})_3$] structures. The two resins mainly differ in their chain length. It is shown that the performance of the silicone based coating used as thermal barrier are better when the coating is mainly composed of D structures and has high crosslinking density. This is explained by its lower thermal diffusivity at high temperature and by its higher thermal stability.

In Fire and Polymers VI: New Advances in Flame Retardant Chemistry and Science; Morgan, A., et al.;
ACS Symposium Series; American Chemical Society: Washington, DC, 2012.

Introduction

Polydimethylsiloxane (PDMS) is widely used in construction and electrical utilities because of its excellent thermal stability and fire properties including low heat of combustion and low rate of heat released compared to organic polymers (*1*, *2*). This polymer is available in different forms from liquid to cross-linked rubber. The rubbers can be found in two main classes (*3*): one cross-linked by poly-addition, and another by poly-condensation.

For poly-addition, cross-linking of silicone rubber is achieved using vinyl endblocked polymers and reacting them with the SiH groups carried by functional oligomers. This reaction is catalyzed by Pt or Rh metal complex (*3*) as illustrated in Figure 1.

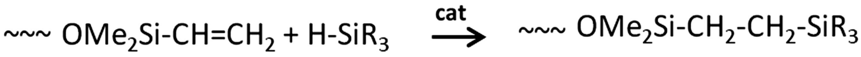

$$\sim\sim\sim OMe_2Si\text{-}CH{=}CH_2 + H\text{-}SiR_3 \xrightarrow{cat} \sim\sim\sim OMe_2Si\text{-}CH_2\text{-}CH_2\text{-}SiR_3$$

Figure 1. Poly-addition reaction.

Silicones prepared via the poly-condensation method are used to make sealants that find applications in original equipment manufacturing for glazing sealing windows and doors for either residential or public buildings. They are also used as building components providing a barrier against severe environments such as humidity or dust (*4*). These products are ready to use and require no mixing: cross-linking starts when the product is exposed to moisture. Most silicone sealants are formulated from a reactive polymer prepared from an hydroxy-polydimethylsiloxane and a large excess of methyltrimethoxysilane. The poly-condensation reaction is illustrated in Figure 2.

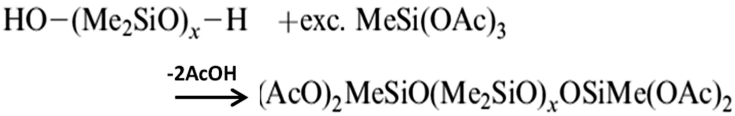

$$HO-(Me_2SiO)_x-H \quad +\text{exc. } MeSi(OAc)_3 \xrightarrow{-2AcOH} (AcO)_2MeSiO(Me_2SiO)_xOSiMe(OAc)_2$$

Figure 2. Poly-condensation reaction.

On the other hand, calcium carbonates have attracted more and more interest due to the availability of these raw materials and its low cost. This filler is mainly used in PDMS to improve its mechanical (*3*) and flame retardant properties (*5*, *6*). Calcium carbonate also enhances the thermal stability of PDMS. Upon heating, silicones containing calcium carbonate form ceramic-like calcium silicate residues (*6*). When incorporated in thermoplastics, the formation of this type of residue acts as a protective barrier which provides significant flame retardancy.

In this work, passive fire protection of steel using silicone-based coating is investigated. The protection of metallic materials against fire has become an important issue in the construction industry. Steel begins to lose its structural properties above 500 °C and it must be therefore protected against fire (*7*).

Prevention of the structural collapse of the building is paramount to ensure the safe evacuation of people from the building, and is a prime requirement of building regulations in many countries.

In this field, the use of silicone-based protective coating is very seldom reported in the literature. Beigbeder et al. evaluated the fire protective performance of PDMS/Carbon nanotube based coating on an aluminium plate. They highlighted that in convective/radiative heating test, this coating exhibited improved properties compared to virgin aluminum.

In this paper, fire performance of two silicone sealants containing calcium carbonate is investigated using a homemade fire test based on the Torch test. Since the formation of protective coating at the surface of steel will be involved, thermal parameters including heat conductivity and thermal diffusivity should be low in order to limit heat transfer. These parameters will be measured as a function of temperature using the Hotdisk method and will be discussed (*8*). The structure formed by the silicone based-coatings upon heating will be then investigated by ^{29}Si solid state NMR and potential correlations between the structure and the thermal properties will be examined.

2. Experimental

2.1. Materials

The two curable PDMS were formed from three main components: an hydroxyl PDMS, methyltrimethoxysilane as cross-linking agent and an organometallic catalyst such as tin and titanium catalyst. All the materials were supplied by Dow Corning, Seneffe (Belgium).

The first resin, hereafter called silicone 1 (S1), was composed of an hydroxylated PDMS with a viscosity of 80 cS (viscosity is measured using cone/plate rheometer CP-52), a large excess of methyltrimethoxysilane (MTM) and a tin catalyst.

The second, hereafter called silicone 2 (S2), was composed of a hydroxylated PDMS with a viscosity of 2000 cS (viscosity is measured using cone/plate rheometer CP-52), a large excess of MTM and a titanium catalyst. S1 and S2 mainly differ in their chain length, with S2 having a longer chain length than S1.

50% of stearic acid coated ground calcium carbonate (GCC) with an average particle size of 4.5μm supplied by Dow Corning is incorporated into the matrix to enhance the fire performance of the coating. Both formulations were applied on a 10 cm x 10 cm x 3 mm steel plate to obtain 400 ± 40 μm coating. Steel plates were cleaned before application with ethanol and a primer (Primer 1200 from Dow Corning) was applied to enhance the coating adhesion.

2.2. Solid State NMR

^{29}Si NMR spectroscopy is a powerful tool for examining silicon surrounding. This technique can distinguish between several kinds of structures including D and T structures which characterize silicone network (Figure 3).

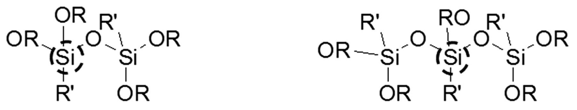

T^1 structure T^2 structure

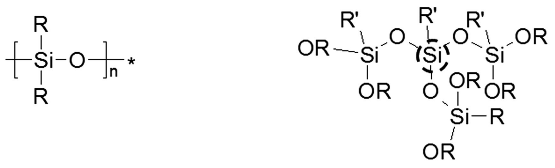

D structure T^3 structure

Figure 3. Schematics presentation of D, T^i silicone structures.

^{29}Si NMR spectra were recorded on a Bruker Advance II 400 operating at 9.4T and equipped with 7 mm probe. NMR spectra were acquired with MAS (magic angle spinning) at 5 kHz. The reference used for ^{29}Si NMR is tetramethylsilane (TMS). A delay of 180s between the pulses and a $\pi/2$ pulse length were used. For S1 and S1/GCC materials respectively 64 scans and 784 scans were accumulated. For S2 and S2/GCC materials respectively 1250 scans and 7620 scans were accumulated. In order to quantify the amount of D and T structure within each resin, simulation of ^{29}Si NMR spectra were obtained using DMfit99 software (*9*).

2.3. Fire Performance

Fire performance of the coatings were evaluated using a homemade fire testing method (Figure 4) based on Torch Test method (American Bureau of Mines Fire Endurance Test (4), 1966). The coating is exposed to an open flame (temperature of the flame around 1100°C).

The temperature at the back side of the plate is measured as a function of time using a pyrometer (temperature measured in the center of the plate). The backside of the plate is coated with black paint (Jeltz) having a constant emissivity (0.92) and thermally resistant up to 800°C in order to get reliable temperature measurements with the pyrometer. This test allows evaluating the fire performance of a coating in radiative/convective heating scenario.

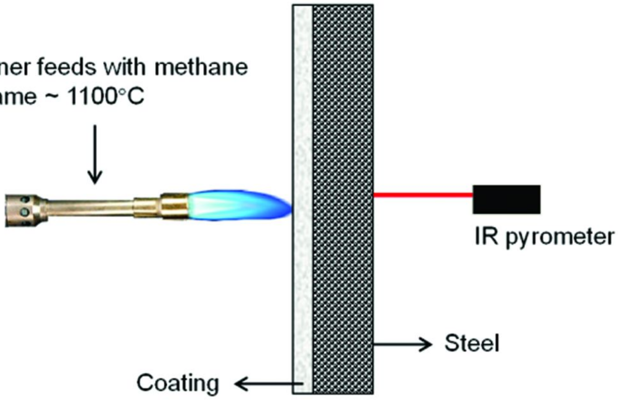

Figure 4. Schematic representation of the Torch Test.

2.4. Thermal Properties

Thermogravimetric analyses (TGA) were carried out using a TGA Q5000 from TA Instruments at 10 °C/min in a nitrogen flow (25 mL/min). For each sample, 15 mg of sample were positioned in alumina pans. Gases released during the degradation of the material were analyzed using a thermo gravimetric analysis (TGA Q5000, TA Instrument) connected to a Fourier transformed infrared (FTIR) spectrometer (ThermoScientific) Nicolet iS10. The IR spectra were recorded between 400 cm^{-1} and 4000 cm^{-1} (spectra recorded every 11 s). For each experiment, samples of 15mg material (powder) were positioned in alumina pans. All the analyses have been carried out in nitrogen flow (75 mL/min).

Thermal conductivity and diffusivity of both formulations: S1 + 50%GCC and S2 + 50%GCC were measured from 25°C to 500°C using a hot disk thermal constant analyzer (Hot Disk TPS 2500 S) from Thermoconcept (Bordeaux, France), which is a transient plane source technique (*8*). The sensor, which is warmth emitter and thermocouple, is directly molded in the sample to ensure a good contact between the sample and the sensor during the experiment. The temperature is stabilized each 100°C with less than 0.1°C deviation. The conductivity measurements were made by applying a power of 0.03–0.15 W for between 5 and 60 s, depending on the thermal conductivity of the sample. The furnace is directly connected to nitrogen flow and all experiments are carried out in inert atmosphere to prevent the oxidation of the sensor. For each sample, two experiments are carried out to evaluate the uncertainty of measurement. This experimental set up allows measuring the thermal conductivity and diffusivity of the material versus the temperature.

3. Results and Discussion

3.1. Resin Characterization

Figure 5 illustrates chemical reactions which occur during the cross-linking of the hydroxylated PDMS (*3*). Exposed to moisture, hydroxyl group reacts with the methoxy group of MTM which lead mainly to T^1 and T^2 structures. Without any fillers, the crosslinking is complete and no silanol group remain.

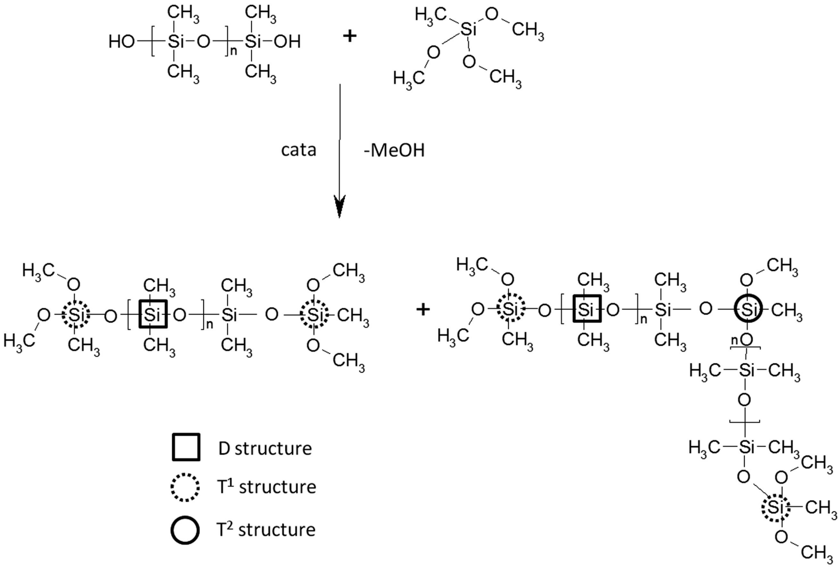

Figure 5. Chemical pathway of resin cross-linking.

Figure 6 shows ^{29}Si NMR spectra of resins S1 and S2. Band assignments have been made according to the literature (*10*). Three bands appear in both spectra at -22 ppm, -58 ppm and -67 ppm corresponding to respectively D, T^1 and T^2 structures. It demonstrates that the two resins have similar chemical structure composed of D, T^1 and T^2 units.

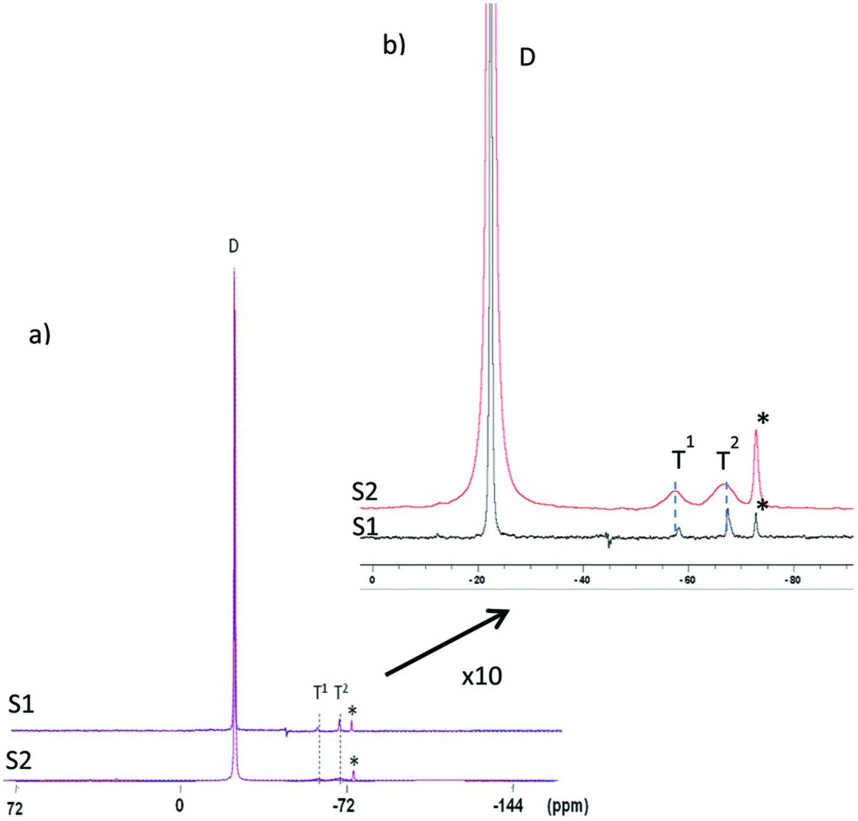

Figure 6. a) blue line- ^{29}*Si solid state MAS NMR spectra / red line - calculated spectra with DMFIT software b) zoom of T bands.*

It is noteworthy that in handling S2 is more rigid than S1 rubber which could be due to a different crosslinking degree of the two resins. Indeed, it is well known that the crosslinking degree of polymers is directly linked with its mechanical properties (*11*) (in particular highly cross-linked elastomers exhibit high modulus).

Deconvolution of the spectra allows quantifying the ratio between D and T in each siloxane resin and so, it allows evaluating the crosslinking density of each resin. Results are summarized in Table I. S1 contains more T structure than S2. For S1, polymeric chains are shorter than those of S2 and so, there are more reactive hydroxyl group in S1. Consequently, the amount of MTM in S1 is higher than in S2 to make the resin cross-linked. The crosslink density of S1 is thus higher than S2.

Table I. Deconvolution results of S1 and S2 resin

Material	*D*	*T*
S1	93%	7%
S2	95%	5%

The next step of the study is to evaluate the influence of T structures and of the silicone network on fire performances of S1 and S2 based coating containing GCC.

3.2. Fire Performance

The temperature profiles obtained in the Torch Test of the silicone-based coatings on steel plate are compared with that of the uncoated steel plate (Figure 7). It is observed in all cases that the temperature increases until around 400 s and then a steady state is reached. The temperature at the steady state for the uncoated steel plate is around 380°C whereas those obtained for S1/GCC and S2/GCC coated steel plate are respectively around 320°C and 295°C evidencing the heat barrier properties of the coatings.

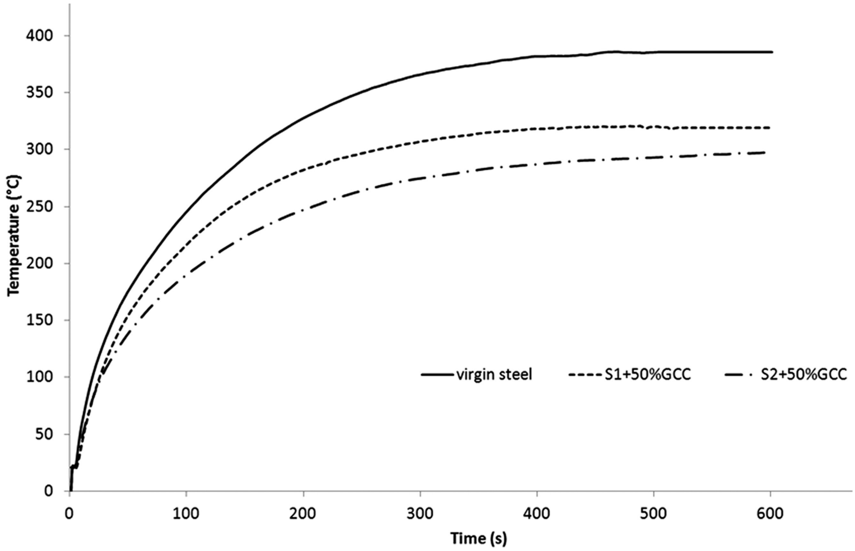

Figure 7. Time/temperature curves for the virgin steel plate and for the silicone coatings plate.

Figure 8 illustrates S1/GCC and S2/GCC based coating after torch test experiment. It shows that no swelling of the coating occurs during experiment and that some cracks are visible for S2 based coating.

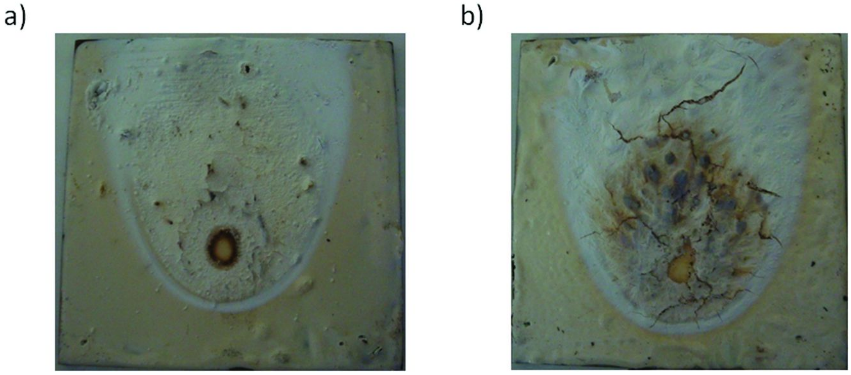

Figure 8. a) S1+50%GCC b) S2 + 50%GCC steel plate after torch test.

To explain the fire performance of the coatings, several parameters have to be taken into account. Staggs demonstrates that the fire performance of intumescent coatings are governed by their thickness (their expansion during the fire test) and their thermal properties such as heat conductivity (*12*). In this last case, fire protection is due to the formation of thick insulative foam with low thermal conductivity at high temperature. In the present work, silicone based coating do not swell during fire experiment and we can reasonably assume that the main parameters governing fire performance are their thermal properties at high temperature, such as thermal conductivity and diffusivity.

3.3. Thermal Properties

In this section, thermal diffusivity and thermal conductivity are thus investigated from ambient temperature to 500°C using the hot disk technology. Heat conductivity is one of the parameters governing the performance of the coating in terms of insulation. Very few articles in the literature deal with the measurement of thermal conductivity at high temperature of material. Staggs determined the thermal conductivities of intumescent char at high temperature by numerical simulation (*13*). He evaluated thermal conductivity from ambient temperature to 1200K and its dependence on the porosity of the material. He calculated that thermal conductivity of intumescent char material varies from 0.1 W/m.K. to 0.4 W/m.K. from ambient temperature to 600°C suggesting the heat insulative properties of these materials.

Thermal conductivity of S1/GCC and S2/GCC are measured from ambient temperature to 500°C (Figure 9).

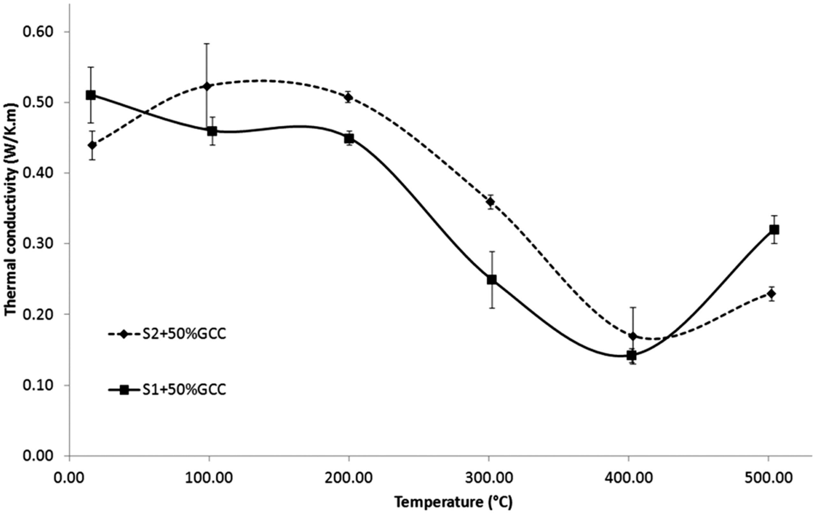

Figure 9. Thermal conductivity versus temperature curve for S1/GCC and S2/GCC adding with GCC.

For the two materials, heat conductivity decreases from 25°C to 400°C due to the formation of some alveolus inside the material (Figure 10). Indeed, the heating rate in the furnace is very low compared to that in the fire test and therefore, it allows the material to encapsulate gases evolved during the matrix degradation. During the torch test, the coating is directly exposed to an open flame and the temperature of the coating reaches 800°C in few seconds. Because of this high heating rate, the coating does not swell and cracks appear on the coating after testing (Figure 8).

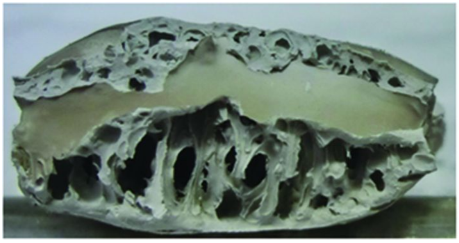

Figure 10. Picture of S2/GCC residue at 500°C.

For S1 and S2 based material, thermal conductivities are similar and reach respectively 0.32 ± 0.02 W/K.m and 0.23 ± 0.01 W/K.m at 500°C.

The other important parameter when dealing with heat transfer is the thermal diffusivity α (eq. 1) which depends on the thermal conductivity k, the density ρ, and the specific heat capacity C_p.

Equation 1 : Thermal diffusivity Eq.1

$$\alpha = \frac{k}{\rho . c_p} \qquad \text{Eq. 1}$$

Figure 11 shows the thermal diffusivity versus temperature for S1/GCC and S2/GCC material. When S2/GCC material is heated, thermal diffusivity varies from 0.05 ± 0.03 mm²/s to 0.15 ± 0.01 mm²/s. According to the errors on the measurement, we may say there are no significant changes of the thermal diffusivity as a function of temperature. However, the thermal diffusivity of S1/GCC material increased significantly when heated to 500°C. At ambient temperature, thermal diffusivity is 0.04 ± 0.02 mm²/s (as that of S2 based material) and reachs 0.45 ± 0.04 mm²/s at 500°C which is 4 times higher than that of S2/GCC.

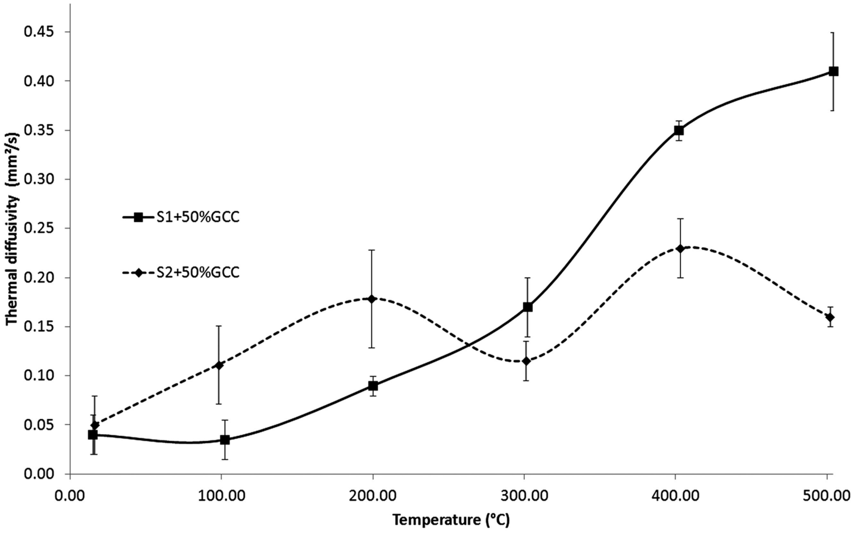

Figure 11. Thermal diffusivity versus temperature curve for S1 and S2 adding with GCC.

Thermal diffusivity describes the ability of a material to conduct heat (k) compared to storing the heat ($\rho.c_p$). In a material with high thermal diffusivity, heat moves through rapidly. Heat diffuses therefore more rapidly in S1/GCC matrix than in S2/GCC. Since k of the two materials are similar, the change of thermal diffusivity is explained by the changes of $\rho.c_p$, *i.e.* by the heating storage (lower heating storage of S1 compared to that of S2).

This strong difference of heat diffusivity of the two materials should be due to different thermal stability. Depending on its degradation pathway, the resin exhibits morphological modification and hence modification of its thermal properties.

Thermal stability of the two materials is thus investigated (Figure 12).

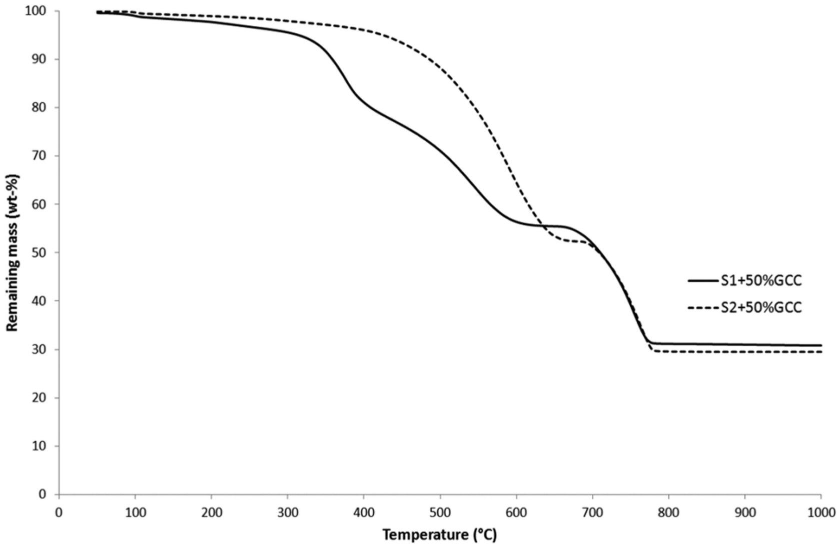

Figure 12. TG curve of S1/GCC and S2/GCC in nitrogen flow at 10°C/min.

It is observed that S2/GCC is more stable than S1/GCC. Thermal degradation of S1/GCC occurs in three main steps (the last step corresponding to the degradation of calcium carbonate). The temperatures for each step where degradation rate is maximum, are respectively 376°C, 540°C and 760°C. The weight loss of each degradation step for S1/GCC is respectively 20%, 24% and 25%. Concerning S2 based material, thermal degradation occurs in two main steps (the last corresponding to the degradation of calcium carbonate). The temperatures for each step where degradation rate is maximum, are respectively 590°C and 760°C and the weight loss of each degradation step are 47% and 23%. The two resins contain 50% calcium carbonate. The thermal degradation of calcium carbonate is well known and lead to the formation of CaO, releasing carbon dioxide (*5*). Theoretically, the amount of CO_2 released by the calcium carbonate is 22%. This demonstrates that the last step of degradation of each material is mainly due to calcium carbonate and the gas released should be carbon dioxide. This will be confirmed by TGA-FTIR experiment.

To explain the lower thermal stability of S1/GCC compared to S2/GCC, the chemical structure of the two materials is examined by solid state ^{29}Si NMR (Figure 13). As for the pure resin, three main bands appears in ^{29}Si NMR spectra at -22 ppm, -58 ppm and -67 ppm corresponding to respectively D, T^1 and T^2 structures.

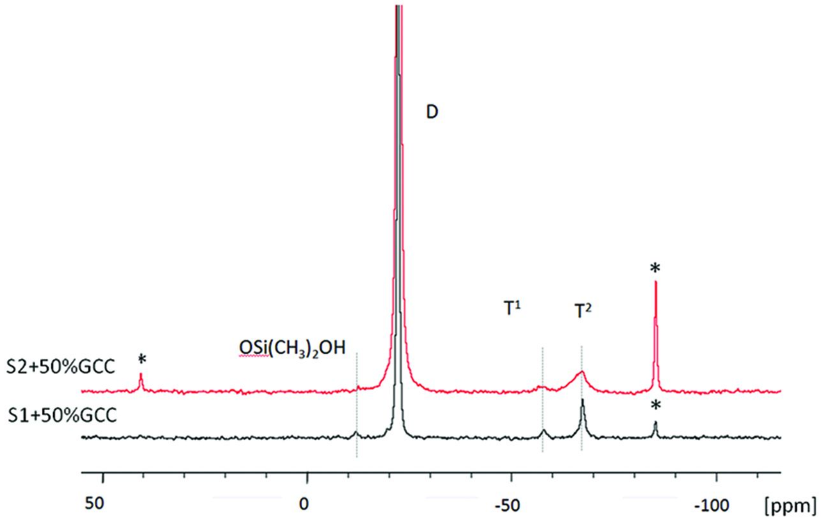

Figure 13. ^{29}Si NMR spectra of S1/GCC and S2/GCC materials.

Deconvolution of the bands allows determining the ratio D/T in each resin and so, to evaluate the crosslinking degree of the material. The results are reported in Table II. This evidences that S1 based resin is more cross-linked (it contains more T structure) when calcium carbonate is incorporated. On the contrary, there is no modification of the crosslinking density of S2 when calcium carbonate is incorporated.

In Fire and Polymers VI: New Advances in Flame Retardant Chemistry and Science; Morgan, A., et al.;
ACS Symposium Series; American Chemical Society: Washington, DC, 2012.

Moreover, for S1/GCC, an additional band appears at -12 ppm corresponding to silanol site. The presence of this residual silanol could explain the lower thermal stability of S1/GCC compare to S2/GCC.

Table II. Deconvolution results of S1 ; S2 ; S1/GCC and S2/GCC

Resin	*$OSi(CH_3)_2OH$*	*D*	*T*
S1	-	93%	7%
S1/GCC	1%	87%	12%
S2	-	95%	5%
S2/GCC	<1%	95%	5%

Indeed, the silanol function is known to induce depolymerization by an "un-zipping reaction" and to lead to the formation of cyclic silicone compounds (*5*) that evolved in the gas phase. This reaction is due to intramolecular interaction and is illustrated in Figure 14.

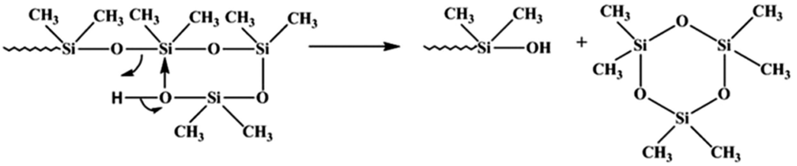

Figure 14. Schematic illustration of "un-zipping" reaction.

In order to verify the un-zipping reaction due to silanol group, TGA coupled with FTIR was used. Figure 15 and Figure 16 respectively show the infrared spectra of gases released during the degradation of S1/GCC and S2/GCC material. For both material, the same gases are released and are composed of cyclic silicone oligomers and carbon dioxide at high temperature. Peak at 2950 cm^{-1} corresponding to the bending vibration of CH_3 bond; peaks between 1000-1100 cm^{-1} corresponding to the bending vibrations of Si-O-Si bond and a peak at 1260 cm^{-1} assigned to the bending vibration of Si-CH_3 bond are observed. From 200°C to 650°C, cyclic oligomers are thus released from the two materials. However, Figure 15a illustrates the intensity of the peak at 1080 cm^{-1} (corresponding to the bending vibration of Si-O-Si) versus time during TG analysis. It shows that cyclic oligomers are released in two steps when S1/GCC is heated whereas only one is observed for S2/GCC (Figure 16a).

During the last step of degradation (for T>700°C), carbon dioxide from calcium carbonate is released.

The analysis of the gas phase during the degradation of each material confirms that the lower thermal stability of S1/GCC is due to the remaining silanol group in the coating. Indeed, upon heating, the remaining silanol promotes the depolymerization of the polymer evolving cyclic oligomers at lower temperature and in two steps. The resulting residue exhibits therefore different thermal properties at high temperature.

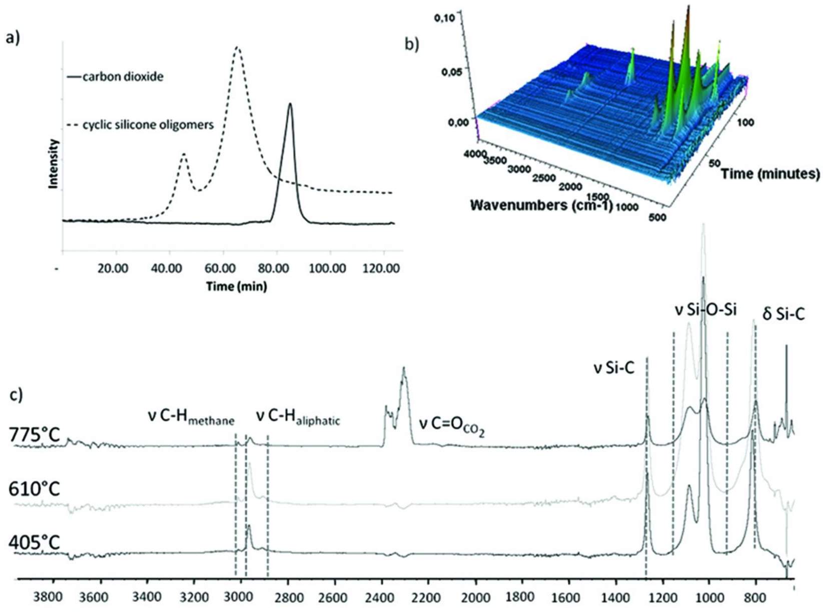

Figure 15. a) Intensity of the band at 1080 cm^{-1} versus time b) IR spectra of the gas released during TG experiment c)IR spectra of the gas evolved during the thermal degradation of the S1/GCC at 405°C, 610°C and 775°C.

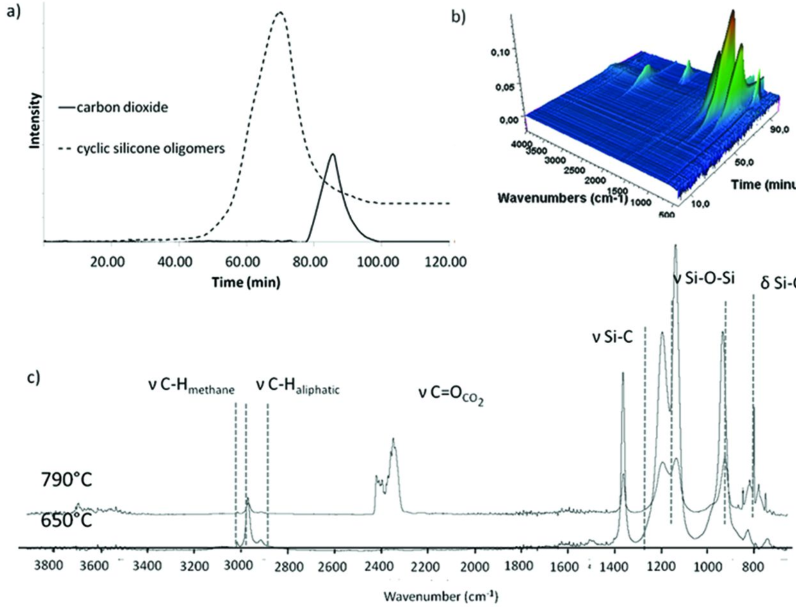

Figure 16. a) Intensity of the band at 1080 cm^{-1} versus time b) IR spectra of the gas released during TG experiment c)IR spectra of the gas evolved during the thermal degradation of the S2/GCC at 650°C, 790°C.

3.4. Discussion and Conclusion

In this study, fire performance of two silicone resins containing GCC have been evaluated in convective/radiative heating source. The two silicone resins exhibit heat barrier properties. When GCC is incorporated in the silicone resins, remaining silanol group are present in S1/GCC based material. This leads to a lower thermal stability due to depolymerization reaction occurring at lower temperature (250°C). Because of this lower thermal stability (and also because of different degradation pathway), S1/GCC has a higher thermal diffusivity than S2/GCC as a function of temperature explaining its lower fire performance compared to S2/GCC.

This work has evidenced that in the field of resistance to fire, methyl-silicone based coatings have to be composed of mainly D structure and no silanol group to ensure a high thermal stability combined with appropriate thermal parameters (low heat conductivity and thermal diffusivity).

References

1. Genovese, A.; Shanks, R. A. Fire performance of poly(dimethyl siloxane) composites evaluated by cone calorimetry. *Composites, Part A* **2008**, *39* (2), 398–405.
2. Buch, R. R. Rates of heat release and related fire parameters for silicones. *Fire Saf. J.* **1991**, *17* (1), 1–12.
3. de Buyl, F. Silicone sealants and structural adhesives. *Int. J. Adhes. Adhes.* **2001**, *21* (5), 411–422.
4. Wolf, A. Material Properties of Construction Sealants. *Kautsch. Gummi, Kunstst.* **1988**, *41* (2), 173–178.
5. Hamdani, S.; Longuet, C.; Perrin, D.; Lopez-cuesta, J.-M.; Ganachaud, F. Flame retardancy of silicone-based materials. *Polym. Degrad. Stab.* **2009**, *94* (4), 465–495.
6. Hermansson, A.; Hjertberg, T.; Sultan, B.-Å. The flame retardant mechanism of polyolefins modified with chalk and silicone elastomer. *Fire Mater.* **2003**, *27* (2), 51–70.
7. Gardner, L.; Baddoo, N. R. Fire testing and design of stainless steel structures. *J. Construct. Steel Res.* **2006**, *62* (6), 532–543.
8. Gustafsson, S. E. Transient plane source techniques for thermal conductivity and thermal diffusivity measurements of solid materials. *Rev. Sci. Instrum.* **1991**, *62* (3), 797–804.
9. Massiot, D.; Fayon, F.; Capron, M.; King, I.; Le Calvé, S.; Alonso, B.; Durand, J.-O.; Bujoli, B.; Gan, Z.; Hoatson, G. Modelling one- and two-dimensional solid-state NMR spectra. *Magn. Reson. Chem.* **2002**, *40* (1), 70–76.
10. Babonneau, F.; Baccile, N.; Laurent, G.; Maquet, J.; Azaïs, T.; Gervais, C.; Bonhomme, C. Solid-state nuclear magnetic resonance: A valuable tool to explore organic-inorganic interfaces in silica-based hybrid materials. *C. R. Chim.* **2010**, *13* (1-2), 58–68.
11. Kim, D. J.; Park, Y. J.; Kim, H. J.; Park, H. J.; Lee, B. W. Mechanical properties of alkoxy type silicone sealants. *J. Ind. Eng. Chem.* **2002**, *8* (3), 241–246.
12. Staggs, J. E. J. Thermal conductivity estimates of intumescent chars by direct numerical simulation. *Fire Saf. J.* **2010**, *45* (4), 228–237.
13. Staggs, J. E. J. Thermal conductivity estimates of intumescent chars by direct numerical simulation. *Fire Saf. J.* **2010**, *45* (4), 228–237.

Chapter 16

Thermal and Burning Properties of Poly(lactic acid) Composites Using Cellulose-Based Intumescing Flame Retardants

**Douglas M. Fox,*,1,2,§ Srilatha Temburni,[1] Melissa Novy,[1]
Laura Flynn,[1] Mauro Zammarano,[1,2,§] Yeon S. Kim,[2,§]
Jeffrey W. Gilman,[3] and Rick D. Davis[2]**

**[1]Chemistry Department, American University, Washington, DC 20016
[2]Fire Research Division, Engineering Laboratory, National Institute of Standards and Technology, Gaithersburg, Maryland 20899-8665
[3]Polymers Division, Material Measurement Laboratory, National Institute of Standards and Technology, Gaithersburg, Maryland 20899-1070
§Guest Researcher at NIST
*E-mail: dfox@american.edu**

Poly(lactic acid) was flame – retarded using cellulose-based intumescing flame retardants. Cellulose was found to be an excellent carbon source, and when added in combination with ammonium polyphosphate (APP), PLA composites exhibited good thermal stabilities and UL-94 ratings of V-0. Nanofibrillated cellulose was phosphorylated to eliminate the need for APP. The fibers were further modified by quaternization and with glycidyl phenyl POSS to increase the char yield during pyrolysis. Fibers were analyzed by elemental analysis, potentiometric titration, and thermogravimetric analysis. The composites prepared without APP exhibited good thermal stability, but they failed the UL-94 vertical burn test.

In Fire and Polymers VI: New Advances in Flame Retardant Chemistry and Science; Morgan, A., et al.;
ACS Symposium Series; American Chemical Society: Washington, DC, 2012.

Introduction

There has been a surge in research and product development of environmentally sustainable materials over the past twenty years. Company managers have learned how to manufacture products that are derived from renewable materials, are less toxic, and produce little waste while maintaining and, in some cases, increasing company profits (*1*, *2*). The production of polymer resins and use of polymers is the third largest industry globally, with 265 million tonnes produced annually (*3*). One of the more promising bio-derived and biodegradable polymers is poly(lactic acid), or polylactide (PLA) (*2*, *4*, *5*). A key disadvantage to the use of polymers is their inherent flammability. Depending on their use, most polymers, including PLA, require the addition of flame retardants to pass regulatory and safety requirements. Due to increasing regulatory pressures, public perceptions of the hazards and toxicities of the most commonly used flame retardants, and a perceived need for enhanced fire retardancy of materials, there is a need to develop more sustainable flame retardants with lower risks to the public and environmental health. Intumescing flame retardants (IFRs) have emerged as possible alternatives to address these issues.

One of the most effective methods for reducing flammability is the generation of carbonaceous char. One of the flame retardant classes that generates a foaming char barrier to heat and fuel transport is an intumescent (*6*, *7*). Intumescing flame retardants (IFRs) typically consist of three components: an acid source, a carbon source, and a blowing agent. Like many other flame retardants, a relatively high loading (15 % to 25 % by mass) for the polymer matrix is needed to successfully pass fire tests. As a result, the composites suffer significant reductions in both mechanical strength and melt viscosity (*8*, *9*). Furthermore, the components are often water soluble, leading to loss of the additives, hydrolysis reactions, and a loss in fire protection under warm, humid conditions (*10*, *11*). Finally, the lower thermal stability of the components than that of many high performance polymers, such as polyamides or poly(ethylene terephthalate), preclude their use as flame retardants in these systems.

These issues have been addressed by incorporating nanofibrillated cellulose fibers (NFC) in intumescing flame retardant formulations (*12*). This takes advantage of the reinforcing nature of fibers, while retaining the use of an underutilized, sustainable resource. In this study, cellulose fibers were modified to include an acid source and blowing agent on the fiber, producing an all – fiber IFR for polymers. Phosphorylation of cellulose using phosphoric acid was used to add an acid source to the fibers. This method produces only monosubstituted glucose units (*13*) and has been shown to be less efficient than other phosphorylation techniques, such as the use of phosphorus oxychloride (*14*, *15*), phosphorus trichloride (*14*), phosphorus pentachloride (*14*, *16*), organophosphoryl chlorides (*17*) or phosphoroamidates (*18*). However, these other phosphorylating agents are significantly more toxic, are more hazardous to handle, or involve more reaction steps. A primary goal of this study was to establish a greener process for flame retarding polymers, so it was determined that the less efficient pad-bake phosphorylating method presented here was the most appropriate procedure for initial studies.

The modified cellulose was characterized using potentiometric titration, elemental analysis, and thermogravimetric analysis (TGA). Composites were prepared by a melt blending technique. Thermal stability was determined using thermal gravimetric analysis (TGA) and flammability was characterized by UL-94 tests. Reinforcing effects were examined using dynamic mechanical analysis (DMA). The effects on flammability properties and the remaining challenges to producing an all-fiber IFR are discussed.

Experimental

Materials

Nanofibrillated cellulose (NFC), prepared from Lyocell fibers with a precursor length of 6 mm and low degree of nanofibrillation (≈ 500 nm diameter), was obtained from Engineered Fibers. Rice hull flour (RHF) was obtained from Composition Materials Co. Toluene (anhydrous, 99.8 %), N,N-dimethylformamide (DMF, anhydrous, 99.8 %), glacial acetic acid (HAc, 99.8 %), orthophosphoric acid (99 %), urea (99 %), and (3-chloro-2-hydroxypropyl) trimethylammonium chloride (97 %) were purchased from Sigma-Aldrich. Sodium hydroxide (ACS reagent, ≥ 98.6 %) was purchased from Fluka, ammonium polyphosphate (APP, EXOLIT AP422 $(NH_4PO_3)_{1000+}$) was purchased from Clariant, pentaerythritol (PER, > 98%) was purchased from Avacado, ammonium hydroxide (ACS reagent, 14.8 M) was purchased from Fisher Scientific, ethanol (dehydrated, 200 Proof) was purchased from Pharmco, and glycidyl isobutyl POSS and glycidyl phenyl POSS were purchased from Hybrid Plastics, Inc. Poly(lactic acid) (PLA) was purchased from NatureWorks (PLA2002D grade) and dried 60 min at 90 °C prior to use.

POSS – modified nanofibrillated cellulose (PNFC) was prepared as previously described (*19*). Cellulose phosphate fibers were prepared by soaking in a 1 M H_3PO_4 / 3 M urea solution for 90 min, filtering until the fibers retained enough solution to equal 4 times the mass of fibers, and placing in a 150 °C oven for 15 min or 40 min. The excess phosphoric acid was neutralized with either 1 M aqueous NaOH (NFC-PO4) or 1 M aqueous NH_4OH (NFC-PO4NH4). RHF phosphate (RHF-PO4) and PNFC phosphate (PNFC-PO4) were prepared in the same manner, baking for 40 min and neutralizing with an aqueous NH_4OH solution. Nitrogen was added to the fibers by mixing a 1:3 ratio of (3-chloro-2-hydroxypropyl) trimethylammonium chloride to fibers in 15% by mass aqueous NaOH solution for 60 min. The quaternized cellulose (QNFC) and quaternized cellulose phosphate (NFC-PO4Q) were neutralized by dialysis in 3.5 kDa cellulose SnakeSkin tubing. Dialysis water was replaced daily for 3 days, or until pH = 7 was obtained. POSS – modified QNFC (QPNFC) was prepared by adding ethanol to the pre-dialyzed solution, filtering until the solution uptake was 2 times the mass of fibers, then reacting in toluene in the same manner as PNFC. All reactions were performed consecutively prior to manual shredding the fibers and drying them overnight at 90°C.

Instrumentation

Duplicate elemental analyses of the fibers were performed by Galbraith Laboratories. Carbon, hydrogen, and nitrogen contents were analysized by combustion. Silicon and phosphorus contents were measured using an ICP – OES technique. Carbon, hydrogen, and nitrogen analyses were performed in duplicate on 2 mg ± 0.3 mg samples and phosphorus and silicon analyses were performed on 75 mg ± 2 mg samples. The repeated measurements were within 5% of each other, and the mean values are reported here. Acid-base titrations and chloride ion concentrations were measured using an Orion 5-Star meter, equipped with an AquaPro pH combination electrode and an IonPlus chloride ion selective electrode. PLA composites were prepared by melt blending at 180 °C and 21 rad/s for 5 min in an Xplore 15 mL twin-screw co-rotating mini-compounder (DSM Instruments). Thermal stabilities were measured using a Netzsch TG449 F1 Jupiter Thermo-nanobalance or a TA Instruments Q-500 thermogravimetric analyzer. Samples (5.0 mg ± 0.3 mg) were placed in open ceramic pans and heated at a scan rate of 10°C/min while purged with nitrogen at a rate of 100 mL/min. The mean of typically two replicate measurements was reported. The temperature of both the onset (5 % mass fraction loss) and peak mass loss rate have an uncertainty of $\sigma = \pm 2$ °C. All samples were held at 90 °C for 30 min prior to each scan to remove any residual water and to remove any residual oxygen from the furnace. Horizontal and vertical burn tests were conducted in a fume hood using UL-94 standard procedures. Composite samples were hot pressed (25 MPa) into 125 mm x 13 mm x 3 mm molds at a temperature of 180 °C using a Carver hydraulic heated press. The reported burn rate had an uncertainty of $\sigma = \pm 0.2$ mm/min. Storage modulus, storage loss, and tan δ were determined using a TA Instruments Q-800 Dynamic Mechanical Analyzer. Samples were hot pressed into 36 mm x 13 mm x 3 mm plate molds at 180 °C and 25 MPa. They were quench cooled with forced air, annealed at 90 °C for 45 min to induce crystallization, and clamped into the 35 mm single/dual cantilever attachment. The samples were heated from 35 °C to 130 °C at a rate of 3 °C/min using the single cantilever mode (17.5 mm) with a displacement amplitude of 15 μm and frequency of 1 Hz. Storage modulus and T_g had uncertainties of $\sigma = \pm 100$ MPa and $\sigma = \pm 1$ °C, respectively.

Results and Discussion

Fiber Characterization

Fibers were analyzed for C, H, N, P, and Si content by elemental analysis. (cf Table 1) All fibers had higher than expected hydrogen content, which is likely due to surface absorbed water. The phosphorylation process was found to be inefficient, resulting in the incorporation of only about 20% of the expected phosphorus. The nitrogen content was below the instrument detection limit for almost all fibers. It has been noted that elemental analysis underestimates the degree of quaternization in cellulose (*20*). Since carbon, hydrogen, and nitrogen contents were determined by combustion, the lower than expected carbon content in POSS – containing fibers is likely due to the large amount of char that results during combustion (*19*).

The degree of substitution for the modified fibers were determined from the elemental analysis and by potentiometric techniques, and is shown in Table 2. Phosphate content by potentiometric titration were slightly lower than those from elemental analysis, but values were comparable. On average, the phosphorylation adds a phosphate group about every 5 glucose units. Implied nitrogen content by potentiometric Cl^- concentrations were lower than those suggested by elemental analysis, indicating that potentiometric Cl^- content is an ineffective method for determining the extent of the quaternization reaction. The higher phosphorus and silicon content for PNFC-PO4 may suggest that some of the phosphate ions cross-link with the trisilanols that form during the PNFC reaction, similar to what was found for APP-PNFC mixtures (*12*).

Table 1. Elemental Analysis of Modified Fibers

Fiber	*%C expt (theor)*	*%H expt (theor)*	*%N expt (theor)*	*%P expt (theor)*	*%Si expt (theor)*
NFC	41.6 (44.4)	6.4 (6.2)	---	---	---
RHF	38.8 (38.7)	5.5 (5.4)	0.9 (0.7)	0.3 (0)	7.6 (6.8)
PNFC	41.9 (50.3)	6.1 (5.0)	0 (0)	---	3.2 (13.0)
NFC-PO4	39.5 (29.8)	6.2 (4.5)	0.9 (0)	2.1 (12.8)	---
NFC-PO4NH4	41.7 (27.8)	6.3 (5.4)	0 (5.4)	0.6 (12.0)	---
QNFC	46.2 (46.0)	6.4 (6.8)	0 (1.8)	---	---
QPNFC	32.4 (50.5)	4.1 (5.3)	0 (0.8)	---	5.4 (12.1)
NFC-PO4Q	39.7 (31.6)	6.4 (6.0)	0.9 (6.1)	1.7 (10.2)	---
RHF-PO4	37.0 (30.4)	5.4 (4.6)	0.7 (3.4)	3.2 (6.3)	7.8 (6.8)
PNFC-PO4	37.2 (43.0)	5.3 (4.9)	1.1 (2.1)	3.6 (4.6)	6.7 (11.1)

The thermal stabilities of cellulose phosphate prepared under different reaction conditions are shown in Figure 1. Phosphorylating cellulose resulted in a 50 °C decrease in both onset and peak degradation temperatures, and the char yield significantly increased to over 20% of the original mass. Increasing the pad bake time decreased the thermal stability and increased char yield only slightly, despite nearly doubling the phosphate concentration. Neutralizing the product with ammonium hydroxide solution increased the char yield without significantly altering the thermal stability.

Table 2. Degree of Substitution of Modified Fibers

Fiber	*DS_P by pot*	*DS_P by EA*	*DS_N by pot*	*DS_N by EA*	*DS_{Si} by EA*
PNFC	---	---	---	---	0.062
NFC-PO4 (15min)	0.10	---	---	---	---
NFC-PO4 (40min)	0.20	0.16	---	---	---
NFC-PO4NH4	0.03	0.05	---	---	---
QNFC	---	---	0.010	0	---
QPNFC	---	---	0	0	0.11
NFC-PO4Q	0.19	0.16	0.013	0.037	---
RHF-PO4	0.20		---	---	
PNFC-PO4	0.31	0.78	---	---	0.15

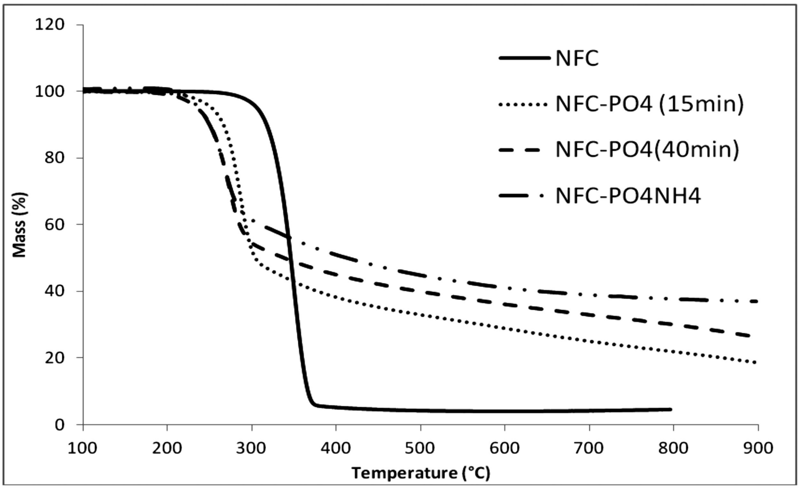

Figure 1. TGA of cellulose phosphate prepared under different reaction conditions under a flow of N_2 at 10°C/min.

The addition of phosphate by phosphoric acid hydrolysis added an acid source to the cellulose fibers. The thermal stability of the cellulose phosphate depended significantly on the other modifications performed, as shown in Figure 2. Quaternizing the fibers with glycidyltrimethylammonium ions slightly increased the thermal stability of the fibers, but reduced the char yield at all temperatures. Adding POSS to the fibers produced very high amounts of char (over 60% by mass), which were thermally stable to over 850 °C. Rice hull flour phosphate had a nearly identical thermal profile to nanofibrillated cellulose phosphate. This was a bit surprising because RHF contains lignin and hemicelluloses (*21*), which both have significantly lower thermal stabilities and produce higher char yields than cellulose (*22*). It is likely that the lignin, which is water soluble, was removed from the final product during filtration, leaving predominately phosphorylated cellulose. Further characterization of these materials is under investigation.

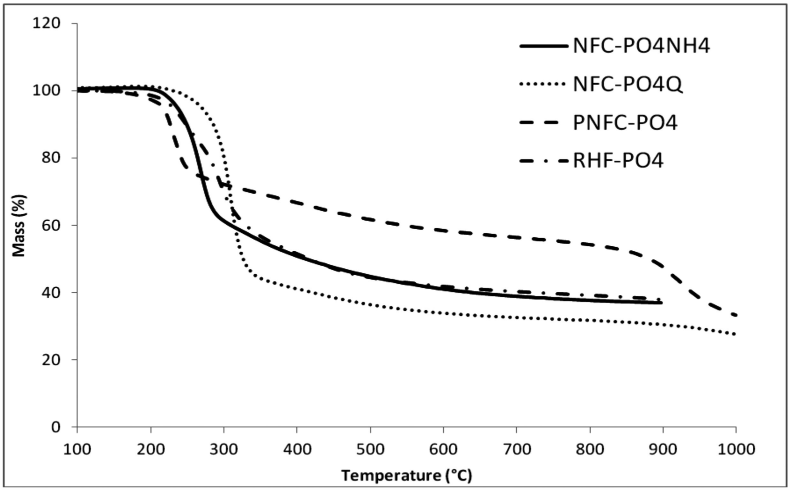

Figure 2. Thermal stability of cellulose phosphate fibers with different modifications while purged with a flow of N_2 at a heating rate of 10°C/min.

PLA Composite Properties

Intumescing flame – retarded PLA composites were prepared by melt blending. Thermal stabilities of APP based IFR formulations using NFC, PNFC, RHF, and PER as the carbon source are shown in Figure 3. Thermal stabilities of cellulose phosphate based IFRs are shown in Figure 4. Addition of 15% by mass of the conventional IFR, APP-PER, to PLA increased the thermal stability by 2 °C and the char yield to 6 % of the original mass. Replacing the PER with a cellulose based carbon source further increased the thermal stability by 3 °C to 8 °C and resulted in char yields of 8% to 9% by mass. The onset of degradation temperature was increased by a few degrees, but the peak decomposition temperature remained unchanged in PLA composites containing 15% by mass cellulose fibers. The char yield only slightly increased. Phosphorylation of the fibers resulted in 5% to 10% loss in mass between 200 °C and 250 °C for the composites, but increased final char yield to about 6% of the original mass. Since less than the total mass of fibers degraded at the earlier stage, fiber char was likely formed and may show some intumescing behavior when burned.

In Fire and Polymers VI: New Advances in Flame Retardant Chemistry and Science; Morgan, A., et al.;
ACS Symposium Series; American Chemical Society: Washington, DC, 2012.

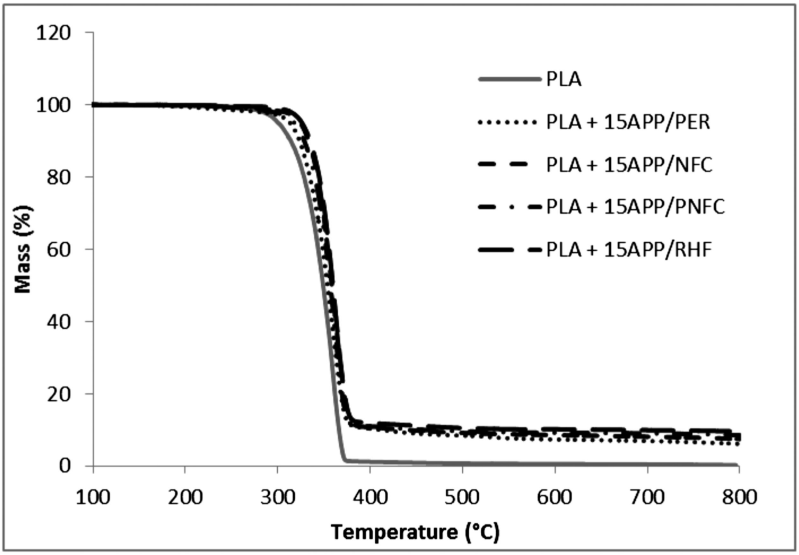

Figure 3. Thermal stability of PLA composites using APP-based IFRs with different cellulose carbon sources while purged with a flow of N_2 at a heating rate of 10°C/min.

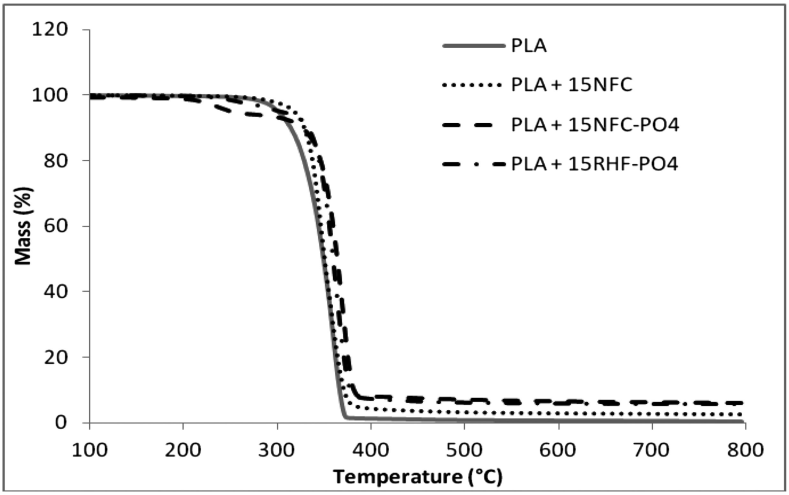

Figure 4. Thermal stability of PLA composites using cellulose phosphate fibers as an IFR while purged with a flow of N_2 at a heating rate of 10°C/min.

Horizontal and vertical burn tests were conducted for the PLA composites. In the horizontal burn test, neat PLA burned at a rate of 9.4 mm/min and had a burn length between 0 mm and 20 mm. Since this polymer showed some resistance to burning, it was expected that the flame – retarded samples would not burn in the horizontal direction. So all other samples were burned only in the vertical direction, and the results are reported in Table 3. As expected, neat PLA completely burned in the test, producing burning drips. The use of APP-based intumescents eliminated burning, resulting in a V-0 rating, regardless of the carbon source used. It was observed, however, that APP/PER produced the most dripping, while APP/NFC and APP/PNFC produced only a few non-burning drips. APP/RHF exhibited a dripping behavior somewhat between that of the PER and cellulose fiber samples. The reduction in melt flow during burning was attributed to the higher aspect ratio of the carbon source. Replacing the APP with phosphorylated cellulose resulted in composites that produced burning drips and failed the UL-94 test. However, the charring behavior observed was similar to the action of an intumescent, and the flame in the NFC-PO_4 composite did extinguish after about a minute, prior to reaching the holding clamp. This suggests that further modification of the fibers may result in an efficient IFR based solely on cellulose fibers.

Table 3. UL-94 Tests of PLA Composites*

Composite	*HB rate (mm/min)*	*t_1 (s)*	*t_2 (s)*	*UL-94*
PLA	9.4	complete		NR
PLA + 15APP/PER		DNB	DNB	V-0
PLA + 15APP/NFC		DNB	DNB	V-0
PLA + 15APP/PNFC		DNB	DNB	V-0
PLA + 15APP/RHF		DNB	DNB	V-0
PLA + 15NFC		complete		NR
PLA + 15NFC-PO4		DNB	73	NR
PLA + 15RHF-PO4		DNB	complete	NR

* - DNB = did not burn, NR = not rated.

Dynamic mechanical analysis was used to assess the changes in semi-crystalline composite stiffness and polymer mobility. As noted in Table 4, the addition of APP/PER reduced composite stiffness and increased the glass transition relative to pure PLA. This is consistent with the reduction in melt viscosity during extrusion that was visually observed. Other studies have noted losses in mechanical strength when incorporating PER in flame retarded polymers (*8*). Replacing the PER with fiber based carbon sources increased both storage modulus and glass transition for the polymer. This was as expected, since the addition of fibers has a reinforcing effect on polymer composites. The addition of rice hull flour had the smallest increase in storage modulus and greatest increase in glass transition temperature. This is likely due to the lower aspect ratio of the filler. The storage modulus and glass transition temperatures of the composites containing phosphorylated cellulose fibers were similar to those of APP/fiber containing composites and slightly lower than the PLA + 15NFC composite. This is consistent with partial degradation of the polymer, which occurs during extrusion in the presence of acidic components. A more complete analysis of the role of IFR formulations in polymer degradation and in composite viscoelastic behavior is currently under investigation (*9*).

Table 4. Dynamic Mechanical Analysis of Composites

Composite	*Storage Modulus (MPa)*	*tan δ peak (T_g, °C)*
PLA	2050	61.8
PLA + 15APP/PER	1900	69.2
PLA + 15APP/NFC	2350	67.6
PLA + 15APP/PNFC	2450	69.9
PLA + 15APP/RHF	2300	71.7
PLA + 15NFC	2550	71.5
PLA + 15NFC-PO4	2400	70.6

Conclusions

Cellulose fibers were modified variously with phosphoric acid, glycidyltrimethylammonium chloride, and glycidylphenyl POSS to increase char yield, gas generation, and thermal oxidative stability upon pyrolysis. The fibers were used as intumescing flame retardants for poly(lactic acid). Elemental analysis indicated that the phosphorylation modifications resulted in a fairly low degree of substitution. Nitrogen elemental analysis by combustion and potentiometric analysis of Cl^- were both found to be ineffective for determining the extent of the quaternization reactions. Despite the low DS, the additions, especially of phosphate and POSS, resulted in significant increases in char yield with only small decreases in thermal stabilities. Using nanofibrillated cellulose fibers, POSS modified cellulose, or rice hull flour as the carbon source in APP based IFRs for PLA increased the thermal stability by up to 10 °C, increased char yield to nearly 10% of the original mass, and resulted in UL-94 ratings of V-0. Composites using phosphorylated celluloses instead of APP formulations exhibited similar thermal properties, but failed UL-94 tests. Despite poor UL-94 results, the composites were observed to exhibit intumescing behavior and did extinguish the flame prior to complete combustion. Dynamic mechanical analysis illustrated that the use of fibers in intumescing formulations prevented losses in stiffness normally observed for APP/PER containing composites. The glass transition temperatures were found to be 6 °C to 10 °C higher than the neat PLA, which is comparable to the composite containing APP/PER.

Acknowledgments

The policy of the National Institute of Standards and Technology (NIST) is to use metric units of measurement in all its publications, and to provide statements of uncertainty for all original measurements. In this document however, data from organizations outside NIST are shown, which may include measurements in non-metric units or measurements without uncertainty statements. The identification of any commercial product or trade name does not imply endorsement or recommendation by NIST. Opinions, interpretations, conclusions, and recommendations are those of the authors and are not necessarily endorsed by NIST.

This material is based upon work supported by the NIST – BFRL Extramural Fire Research Grants Program under Award No. 60NANB11D174. Research was carried out at the National Institute of Standards and Technology (NIST), an agency of the U. S. government and by statute is not subject to copyright in the United States.

Certain commercial equipment, instruments, materials or companies are identified in this paper in order to adequately specify the experimental procedure. Such identification is not intended to imply recommendation or endorsement by the National Institute of Standards and Technology, nor is it intended to imply that the materials or equipment identified are necessarily the best available for this purpose.

References

1. Ruiz-Mercado, G. J.; Smith, R. L.; Gonzalez, M. A. Sustainability Indicators for Chemical Processes: I. Taxonomy. *Ind. Eng. Chem. Res.* **2012**, *51*, 2309–2328.
2. Álvarez-Chávez, C. R.; Edwards, S.; Moure-Eraso, R.; Geiser, K. Sustainability of bio-based plastics: general comparative analysis and recommendations for improvement. *J. Cleaner Prod.* **2012**, *23*, 47–56.
3. *Plastics - The Facts 2011*. In Manufacturers, P.-A. o. P., Ed..; Brussels, Belgium, 2011.
4. Gupta, B.; Revagade, N.; Hilborn, J. Poly(lactic acid) fiber: An overview. *Prog. Polym. Sci.* **2007**, *32*, 455–482.
5. Bhardwaj, R.; Mohanty, A. K. Advances in the Properties of Polylactides Based Materials: A Review. *J. Biobased Mater. Energy* **2007**, *1*, 191–209.
6. Horacek, H.; Pieh, S. The importance of intumescent systems for fire protection of plastic materials. *Polym. Int.* **2000**, *49*, 1106–1114.

7. Bourbigot, S.; Le Bras, M.; Duquesne, S.; Rochery, M. Recent advances for intumescent polymers. *Macromol. Mater. Eng.* **2004**, *289*, 499–511.
8. Li, B.; He, J. Investigation of mechanical property, flame retardancy and thermal degradation of LLDPE–wood-fibre composites. *Polym. Degrad. Stab.* **2004**, *83*, 241–246.
9. Fox, D. M.; Novy, M.; Flynn, L.; Zammarano, M.; Jr., R. H. H.; McCarthy, E.; Gilman, J. W. Flame Retarded Poly(lactic acid) Using POSS-Modified Cellulose. 2. Effects of Intumescing Flame Retardant Formulations on Crystalline and Viscoelastic Properties. *Polymer*, in preparation.
10. Wang, Z.; Han, E.; Ke, W. Influence of expandable graphite on fire resistance and water resistance of flame-retardant coatings. *Corros. Sci.* **2007**, *49*, 2237–2253.
11. Braun, U.; Wachtendorf, V.; Geburtig, A.; Bahr, H.; Schartel, B. Weathering resistance of halogen-free flame retardance in thermoplastics. *Polym. Degrad. Stab.* **2010**, *95*, 2421–2429.
12. Fox, D. M.; Lee, J.; Citro, C.; Novy, M. Flame Retarded Poly(lactic acid) Using POSS-Modified Cellulose. 1. Thermal and Combustion Properties of Intumescing Composites. *Polym. Degrad. Stab.*, submitted.
13. Kaputskii, F. N.; Yurkshtovich, N. K.; Yurkshtovich, T. L.; Golub, N. V.; Kosterova, R. I. Preparation and physicochemical and mechanical properties of low-substituted cellulose phosphate fibers. *Russ. J. Appl. Chem.* **2007**, *80*, 1135–1139.
14. Reid, J. D.; Mazzeno, L. W. Preparation and Properties of Cellulose Phosphates. *Ind. Eng. Chem.* **1949**, *41*, 2828–2831.
15. Reid, J. D.; Mazzeno, L. W.; Buras, E. M. Composition of Two Types of Cellulose Phosphates. *Ind. Eng. Chem.* **1949**, *41*, 2831–2834.
16. Granja, P. L.; Pouysegu, L.; Petraud, M.; De Jeso, B.; Baquey, C.; Barbosa, M. A. Cellulose phosphates as biomaterials. I. Synthesis and characterization of highly phosphorylated cellulose gels. *J. Appl. Polym. Sci.* **2001**, *82*, 3341–3353.
17. Horrocks, A. R.; Kandola, B. K.; Davies, P. J.; Zhang, S.; Padbury, S. A. Developments in flame retardant textiles - a review. *Polym. Degrad. Stab.* **2005**, *88*, 3–12.
18. Gaan, S.; Rupper, P.; Salimova, V.; Heuberger, M.; Rabe, S.; Vogel, F. Thermal decomposition and burning behavior of cellulose treated with ethyl ester phosphoramidates: Effect of alkyl substituent on nitrogen atom. *Polym. Degrad. Stab.* **2009**, *94*, 1125–1134.
19. Fox, D. M.; Lee, J.; Zammarano, M.; Katsoulis, D.; Eldred, D. V.; Haverhals, L.; Trulove, P. C.; Long, H. C. D.; Gilman, J. W. Char-forming behavior of nanofibrillated cellulose treated with glycidyl phenyl POSS. *Carbohydr. Polym.* **2012**, *88*, 847–858.
20. Schwarzinger, C.; Pfeifer, A.; Schmidt, H. Determination of the nitrogen content of cationic cellulose fibers by analytical pyrolysis. *Monatsh.. Chem.* **2002**, *133*, 1–7.
21. Yang, H. P.; Yan, R.; Chen, H. P.; Lee, D. H.; Zheng, C. G. Characteristics of hemicellulose, cellulose and lignin pyrolysis. *Fuel* **2007**, *86*, 1781–1788.
22. Rangel-Vazquez, N. A.; Leal-Garcia, T. Spectroscopy Analysis of Chemical Modification of Cellulose Fibers. *J. Mex. Chem. Soc.* **2010**, *54*, 192–197.

In Fire and Polymers VI: New Advances in Flame Retardant Chemistry and Science; Morgan, A., et al.;
ACS Symposium Series; American Chemical Society: Washington, DC, 2012.

Chapter 17

Comparison of the Impact of Phosphorus and Phosphorus/Nitrogen on the Flammability of Styrenic Oligomers

Bob A. Howell*[*] and Adina Dumitrascu

Department of Chemistry, Center for Applications in Polymer Science, Central Michigan University, Mt. Pleasant, Michigan 48859-0001
[*]E-mail: bob.a.howell@cmich.edu

Phosphorus compounds have long been utilized as flame-retarding additives for polymeric materials. The development of new, highly effective, nontoxic phosphorus flame retardants is an area of great current interest because of the increasing regulatory restrictions on the use of organohalogen compounds for flammability control. It has been broadly suggested that the flame retardant activity of phosphorus compounds may be enhanced by the presence of nitrogen. To provide a direct assessment of the merits of this suggestion, the flammability behavior of oligomers derived from styrene monomers containing phosphorus moieties has been compared to that of similar structures containing both phosphorus and nitrogen.

Introduction

Organophosphorus compounds have been widely used as flame retardants for polymeric materials (*1–4*). Many of these have been utilized as polymer additives while others have been incorporated into the polymer either as components of the mainchain or as pendant groups (*5–29*). The development of new, more effective organophosphorus agents has been stimulated by the increasing regulatory restrictions on the use of organohalogen flame retardants (*30*). Organohalogen compounds, particularly the brominated aryl ethers, are persistent in the environment, tend to bioaccumulate and may pose potential to human health risks (*31–34*). A significant advance has been the utilization of derivatives of 9,10-dihydro-9-oxa-10-phosphaphenanthrene-10-oxide (DOPO) to replace tetrabromobisphenol A as flame-retarding entities in epoxy resins and poly(carbonate) (*35–41*). These materials are effective at low levels of incorporation and do not significantly degrade the physical properties of the polymer into which they are placed. It has often been suggested that the effectiveness of organophosphorus flame retardants may be enhanced by the presence of nitrogen (*42–49*). To assess the impact of nitrogen on the effectiveness of phosphorus flame retardants two sets of styrene oligomers, one containing only phosphorus and the other containing both phosphorus and nitrogen, have been synthesized, characterized by thermal and spectroscopic methods, and subjected to pyrolysis combustion flow calorimetry.

Experimental

General

In general, reactions were carried out in a dry three-necked, round-bottomed flask fitted with a Liebeg condenser bearing a gas-inlet tube, a magnetic stirring bar, and a pressure-equalizing dropping funnel. All glassware was flame-dried and allowed to cool under a stream of dry nitrogen prior to use. Chromatography was accomplished using ultrapure synthetic silica gel SilaFlash P60 (230-400 mesh silica) in a column of appropriate size, and combinations of hexane and ethyl acetate as eluents. Silica-coated (fluorescence UV_{254}) Whatman plates (Whatman Ltd.) were used for thin layer chromatography (TLC).

Materials

Diethylphosphite (98%), diphenylphosphite (~85%), 4-*tert*-butylcatechol (TBC) and sodium hydride (NaH) as a 60% suspension in mineral oil were purchased from the Aldrich Chemical Company and dimethylphosphite (98%) from Alfa-Aesar, and used as received. 4-(Chloromethyl)styrene (min. 90%), 4-aminostyrene and 9,10-dihydro-9-oxa-10-phosphaphenanthrene-10-oxide (DOPO) were supplied by TCI America and used as received. Styrene (≥ 99%, Sigma Aldrich) was passed through a column of basic alumina prior to use, in order to remove polymerization inhibitors. 2,2′-Azobis(isobutyronitrile) (AIBN) (Sigma Aldrich), which was used as a radical initiator, was recrystallized from methanol. All solvents and other common reagents were obtained from usual laboratory suppliers and were purified prior to use by standard methods.

Analytical Techniques

Nuclear magnetic resonance (NMR) spectra were obtained using 10% to 25% solutions in deuterochloroform and a Varian Mercury 300 MHz spectrometer. Proton and carbon chemical shifts (δ) were reported in parts-per-million (ppm) with respect to tetramethylsilane (TMS) as internal reference (δ = 0.00 ppm). ^{31}P-NMR spectra were referenced relative to the signal for triphenylphosphate at δ : –18.0.

Infrared (IR) spectra were obtained using thin films between sodium chloride plates or solid solutions (1%) in anhydrous potassium bromide (as discs) and a Nicolet MAGNA-IR 560 spectrometer. Absorptions were recorded in wavenumbers (cm^{-1}), and absorption intensities were classified in the usual fashion as very weak (vw), weak (w), medium (m), strong (s), and very strong (vs) relative to the strongest band in the spectrum.

Mass spectra were obtained using a Hewlett-Packard 5890A gas chromatograph/mass spectrometer (GC-MS) with an ionizing potential of 70 electron volts and temperature programmed elution into the spectrometer inlet (90-200°C).

Melting points were determined by differential scanning calorimetry (DSC) using a PYRIS Diamond DSC (Perkin Elmer). All samples were analyzed in a constant nitrogen purge of 50 ml/min at a heating rate of 5°C/min.

Thermogravimetric analysis (TGA) was performed using a TA Instruments 2950 Hi-Res TGA instrument interfaced with the Thermal Analyst 2100 control unit. Most generally, a heating rate of 10°C/min was used. Samples (5-10 mg) were contained in a standard platinum pan. The sample compartment was purged with dry nitrogen at 50 ml/min during analysis. TA Universal Analysis software was used for data analysis.

Glass transition temperatures (T_g) were determined using a DSC Q 2000 (TA Instruments). The samples were contained in standard aluminum DSC pans. Samples were heated from –20 to 200 °C in a nitrogen atmosphere at a rate of 10 °C/min. The T_gs were obtained from the second heating cycle, using TA Universal Analysis software.

Gel permeation chromatography (GPC) was used to determine molecular weights and molecular weight distributions of polymer samples using a Waters 1525 GPC system equipped with a differential refractive index detector and Wyatt Technologies Dawn Helios II multi-angle light scattering detector. Tetrahydrofuran was used as eluent at a flow rate of 1.0 mL/min. Sample concentration of 20 mg/mL and injection volumes of 20 µL were used.

Pyrolysis combustion flow calorimetry (PCFC) was performed using a Govmark microscale combustion calorimeter. Small polymer samples (1-10 mg) were dried for at least 8 hours at 75°C in a convection oven and held in a dessicant chamber until testing. The samples were heatead at a constant rate (1°C/sec) from 150 to 700 °C. The volatile pyrolysis products generated during the temperature ramp were swept from the pyrolyzer into the combustion chamber (900 °C) by nitrogen gas flowing at 80 cm^3/min to which was added 20 cm^3/min of pure oxygen. Deconvolution of the oxygen consumption signal was performed during the test, and the heat release rate was calculated in watts per gram of sample.

Monomer Synthesis

The styrene monomers required for this study are shown below. A detailed description for the synthesis of two of these is presented below. All others were prepared in an analogous manner (*5*, *42*).

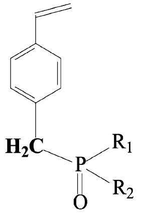

$R_1 = R_2 = OCH_3$ Dimethyl-(4-vinylbenzyl)phosphonate **(M_1)**

$R_1 = R_2 = OC_2H_5$ Diethyl-(4-vinylbenzyl)phosphonate **(M_2)**

$R_1 = R_2 = OC_6H_5$ Diphenyl-(4-vinylbenzyl)phosphonate **(M_3)**

R_1, R_2 = DOPO 4-[(6-Oxido-6H-dibenz[c, e][1, 2]oxaphosphorin-6-yl)]methyl styrene **(M_4)**

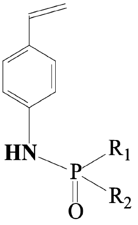

$R_1 = R_2 = OCH_3$ Phosphoramidic acid, *N*-(4-vinyl-phenyl)-dimethylester **(M_5)**

$R_1 = R_2 = OC_2H_5$ Phosphoramidic acid, *N*-(4-vinyl-phenyl)-diethylester **(M_6)**

$R_1 = R_2 = OC_6H_5$ Phosphoramidic acid, *N*-(4-vinyl-phenyl)-diethylester **(M_7)**

R_1, R_2 = DOPO 4-[(6-Oxido-6H-dibenz[c, e][1, 2]oxaphosphorin-6-yl)]amino styrene **(M_8)**

Dimethyl (4-Vinylbenzyl)phosphonate

Sodium hydride (0.55 g, 0.024 mmol) as a 60% suspension in mineral oil was added to 20 mL of dry THF and the suspension was stirred at room temperature, under nitrogen for 0.5 hours. A solution of dimethyl phosphite (2.6 g, 0.024 mol) and 10 mL of THF was added slowly and the mixture was allowed to cool at 0-5°C and stirred for 0.5 hours. 4-(Chloromethyl)styrene (3 g, 0.02 mol) and TBC (100 mg, 0.6 mmol) in 25 mL of THF were added dropwise. The reaction mixture was stirred at ambient temperature for 2 hours and then at the solvent reflux for 12 hours. The salt which formed during the reaction was removed by filtration. The solvent was removed from the filtrate by rotary evaporation at reduced pressure. The residual material was dissolved in 100 mL of methylene chloride. The solution was washed, successively, with two 100-mL portions of distilled water and 100 mL of saturated aqueous sodium chloride solution. The solution was dried over anhydrous magnesium sulfate and the solvent was removed by rotary evaporation at reduced pressure. The residue was purified by flash chromatography (eluant: ethyl acetate/hexane 50/50, v/v). The pure product was obtained as a pale yellow oil (4.02 g, yield 90.13 %): **IR** (thin film, cm^{-1}) 3003 (w, Ar-H), 2909 (m, CH_2), 1630 (m, vinyl), 1515 ($C{=}C_{aromatic}$), 1410 (m, P-C), 1250, vs (P=O), 1030 (vs, P-O-C); **^{1}H-NMR** (300 MHz, $CDCl_3$, δ) 2.75 (d, 2H, J_{PH}=21.7 Hz, $C\underline{H}_2$-P); 3.1 (d, 6H, J_{PH}=10.89 Hz, $C\underline{H}_3$–O); 5.09 (d, 1H, J_{HH}=10.8 Hz, $CH{=}C\underline{H}_2$); 5.42(d, 1H, J_{HH}=17.6 Hz, $CH{=}C\underline{H}_2$); 6.61-6.71 (dd, 1H, *cis* J_{HH}=10.8 Hz, *trans* J=17.6 Hz, $C\underline{H}{=}CH_2$); 6.95-7.33 (m, $4\underline{H}_{aromatic}$); **^{13}C-NMR**

(75.46 MHz, $CDCl_3$, δ) 33.5 (d, J_{PC}=127.8 Hz, $C\underline{H}_2$-P), 53.3 (d, J_{PC}=6.8 Hz, $C\underline{H}_3$-O); 113.6 (1C, CH=$\underline{C}H_2$), 130.04, 131.10 (d, J=9.8 Hz, $\underline{C}H$=CH_2), 126.15, 126.25 (d, J_{PC}=3.45 Hz, 1$\underline{C}_{aromatic}$), 130.5, 136.3 (2C aromatic); **^{31}P-NMR** (121.48 MHz, $CDCl_3$, δ) + 34.5; **GC-MS**: calcd. for $C_{11}H_{15}O_3P$: 226, found: 226.

Phosphoramidic Acid, *N*-(4-Vinylphenyl)dimethylester

A stirred mixture of dimethyl phosphite (3.3g, 0.03 mol) and 30 mL of carbon tetrachloride was allowed to cool to 0°C, in a nitrogen atmosphere. 4-Aminostyrene (3.0 g, 0.025 mol) and TBC (100 mg, 0.6 mmol) dissolved in 25 mL of THF were then added and the mixture was stirred for one hour. Triethylamine (TEA) (3 g, 0.03 mol) in 10 mL of carbon tetrachloride was added dropwise and the resulting solution was stirred overnight. After approximately 20 hours, TLC (eluant: ethyl acetate) indicated that 4-aminostyrene had been completely consumed. The triethylammonium chloride formed in the reaction was removed by filtration and washed with 30 mL of carbon tetrachloride. The organic solution was washed successively with two 100-mL portions of distilled water and 100 mL of saturated aqueous sodium chloride solution. The organic layer was dried over anhydrous magnesium sulfate and the solvent was removed by rotary evaporation at reduced pressure. The residue was purified by column chromatography using a mixture of ethyl acetate:hexane (50:50, v/v) as eluant to provide 5.1 g of phosphoramidic acid, *N*-(4-vinyl-phenyl)dimethylester (89.5% yield) as a colorless liquid: **IR** (thin film, cm^{-1}) 3200 (N-H), 1610 (s, vinyl group); 1025, 1400 (s, m P–O–alkyl); 1520 ($\upsilon_{C=C \text{ in the phenyl ring}}$); 1167 (P=O stretching); 1230, 840 (m, vs, $\upsilon_{C\text{-}N}$ and $\upsilon_{P\text{-}N}$); **^{1}H-NMR** (300 MHz, $CDCl_3$, δ) 3.7 (d, J_{PH}=11.4 Hz, OCH_3); 5.12 (d, 1H, J_{HH}=10.8 Hz, CH=$C\underline{H}_2$); 5.61 (d, 1H, J_{HH}=17.6 Hz, CH=$C\underline{H}_2$); 6.59-6.68 (dd, 1H, *cis* J_{HH}=10.8 Hz, *trans* J=17.6 Hz, $C\underline{H}$=CH_2); 6.75 (d, J_{PH}= 9, N$\underline{H}$); 6.96-6.99 (dd, 2$\underline{H}_{aromatic}$); 7.28-7.31 (dd, 2$\underline{H}_{aromatic}$); **^{13}C-NMR** (75.46 MHz, $CDCl_3$) 53.10-53.15 (d, J_{PC}=5.2 Hz, $\underline{C}H_3$ from phosphoramidate P(O)$\underline{C}H_3$); 112.0 (CH=$\underline{C}H_2$); 117.25-117.34 (d, J_{PC}=6.79 Hz, $C_{aromatic}$–P); 127.2, 131.4, 136.1, 139.2 (s, 4$C_{aromatic}$); **^{31}P-NMR** (121.48 MHz, $CDCl_3$, δ) +6.6; **GC-MS**: calcd. for $C_{10}H_{14}NO_3P$: 227, found: 227.

Polymer Synthesis

In a typical preparation a solution in *N,N*-dimethylacetamide (DMAC) of monomer (40% wt) and initiator (0.5% mol AIBN/mol monomer) was placed in a Pyrex polymerization tube, sealed under nitrogen, and heated in an oil bath for a period of 3 hours at 70°C. Subsequently, the tube was transferred to an oven and kept at 110°C for 16 hours, to provide a viscous solution of polymer. The polymer was separated by precipitation in water. The crude polymer was dried and re-dissolved in DMAC and then precipitated by the addition of hexane. The polymer was washed repeatedly with hexane then dried at 15 torr and 50°C for 24 h. The purity of the polymers was assesed by ^{1}H-NMR spectroscopy which showed no traces of monomer. **^{31}P-NMR** (121.48 MHz, δ) of the polymers: HMP_1 ($CDCl_3$):+30.2; HPM_2 ($CDCl_3$): +5.9; HPM_3 ($CDCl_3$): +21.1; HPM_4

($CDCl_3$): +34.4; HPM_5 ($DMSO-d_6$): +7.9; HPM_6 ($DMSO-d_6$) +3.9; HPM_7 ($DMSO-d_6$): -5.2; HPM_8 ($DMSO-d_6$): +9.4. The structures of the polymers generated are shown below.

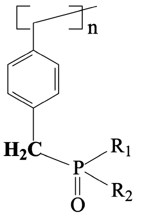

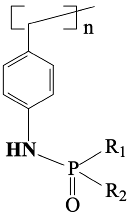

$R_1 = R_2 = OCH_3$	**PM_1**	$R_1 = R_2 = OCH_3$	**PM_5**
$R_1 = R_2 = OC_2H_5$	**PM_2**	$R_1 = R_2 = OC_2H_5$	**PM_6**
$R_1 = R_2 = OC_6H_5$	**PM_3**	$R_1 = R_2 = OC_6H_5$	**PM_7**
R_1, R_2 = DOPO	**PM_4**	R_1, R_2 = DOPO	**PM_8**

Results and Discussion

Phosphorus compounds are commonly used as flame retardants for polymeric materials. It has widely been suggested that the effectiveness of these flame retardants is enhanced in the presence of a nitrogen-containing compound. To directly assess the impact of the presence of nitrogen on the effectiveness of phosphorus compounds as flame retardants in styrene polymers, two series, one containing only a phosphorus moiety and the second containing both phosphorus and nitrogen, have been prepared, characterized, and evaluated for potential flame retarding effect.

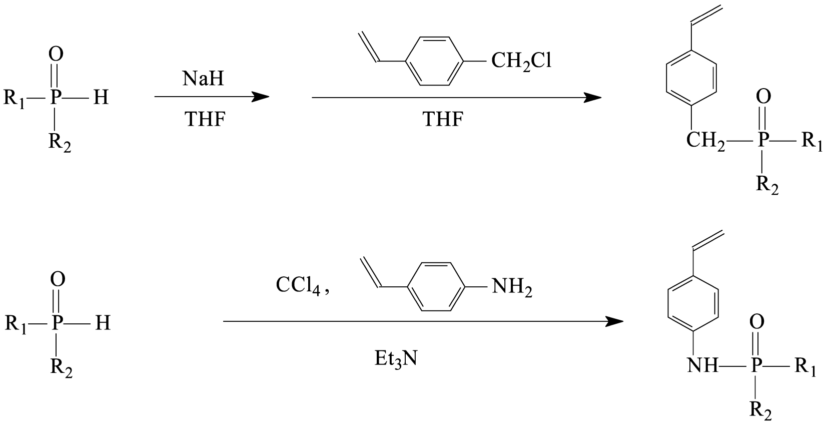

Scheme 1. Synthesis of styrene monomers containing flame-retarding moieties

Monomers were prepared from 4-chloromethylstyrene or 4-aminostyrene as illustrated in Scheme 1.

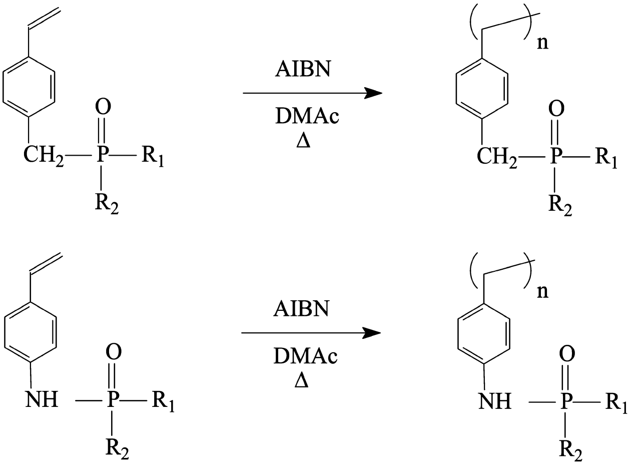

Scheme 2. Polymerization of styrene monomers containing flame-retarding moieties

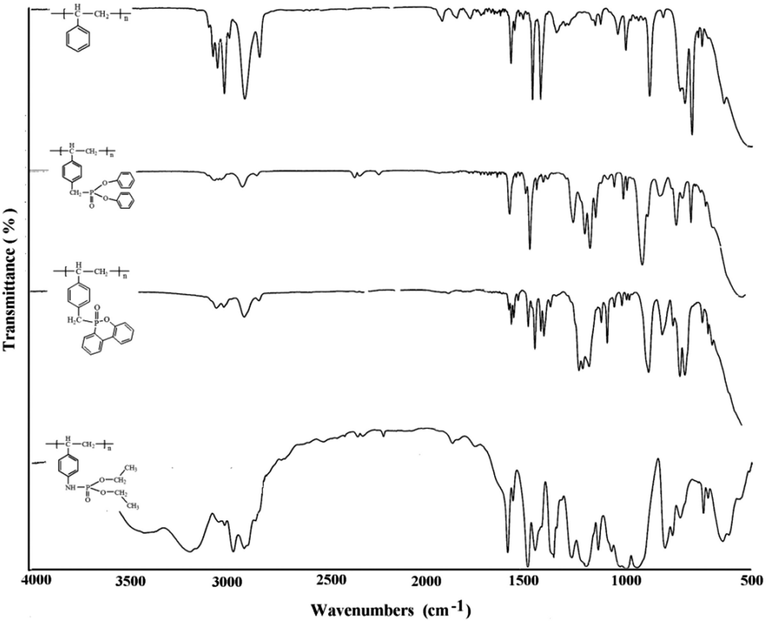

Figure 1. Infrared spectra of styrenic polymers containing phosphonate or phosphoramide flame-retarding moieties.

These monomers were purified by chromatography and characterized spectroscopically (*5*, *42*). The monomers were converted to the corresponding polymers using standard radical techniques as illustrated in the Scheme 2. The polymers were purified by repeated precipitation, dried at reduced pressure and characterized using chromatographic and spectroscopic techniques. A sample of poly(styrene) was prepared under the same conditions to be used as refernce. Molecular weights [SEC; THF; refractive index] were 70,000-82,000 with dispersities of 1.4-1.6.

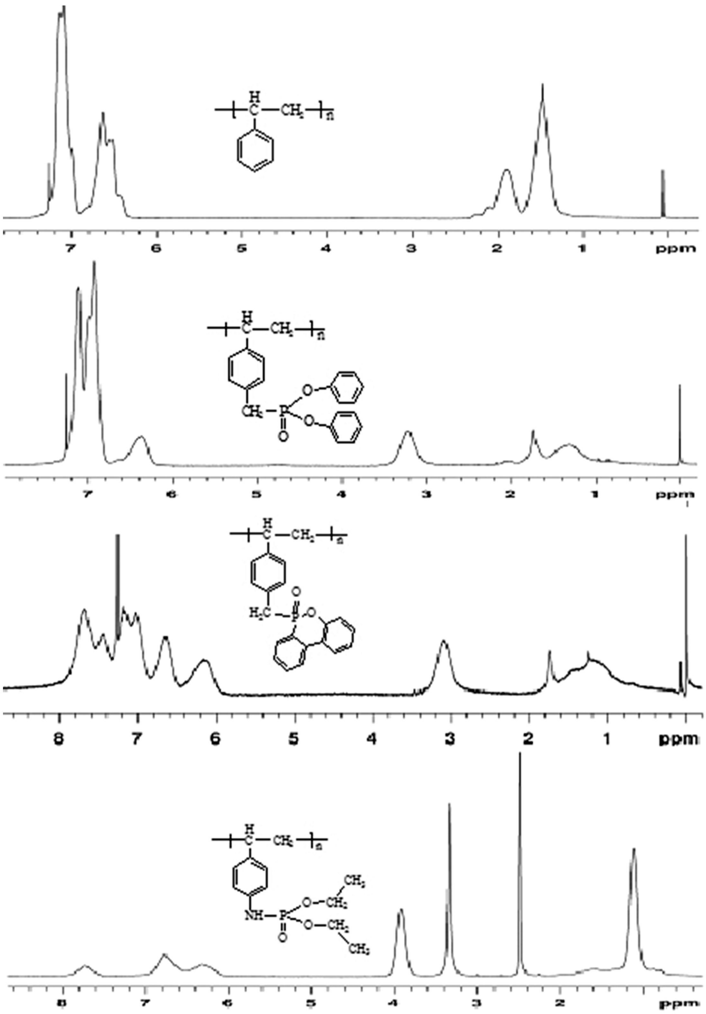

Figure 2. Proton NMR spectra of styrenic polymers containing phosphonate or phosphoramide flame-retarding moieties.

The infrared spectra of phosphorus-containing polymers contains specific absorptions not present in the poly(styrene) spectrum at 1200-1275 cm^{-1} (very strong, -P=O), 1116 and 967 cm^{-1} (-P-O-Ph) and 1030 cm^{-1} (-P-O-C), reflecting the presence of the phosphonate groups pendant to the polymer chain and peaks at 1000-1250, 870 due to $\upsilon_{C\text{-}N}$, $\upsilon_{P\text{-}N}$ absorptions. In the phosphoramidate series, the presence of a broad absorbtion at about 3200 cm^{-1} due to the N-H stretch may be noted. These features are illustrated in Figure 1.

Table I. Glass transition temperatures for styrenic polymers containing phosphonate or phosphoramide flame-retarding moieties

Polymer	*T_g [°C]*	*Polymer*	*T_g [°C]*
HPM_1	122.4	***HPM_5***	131.5
HPM_2	130.2	***HPM_6***	132.4
HPM_3	-	***HPM_7***	136.1
HPM_4	153.4	***HPM_8***	126.2
PS	102	***PS***	102

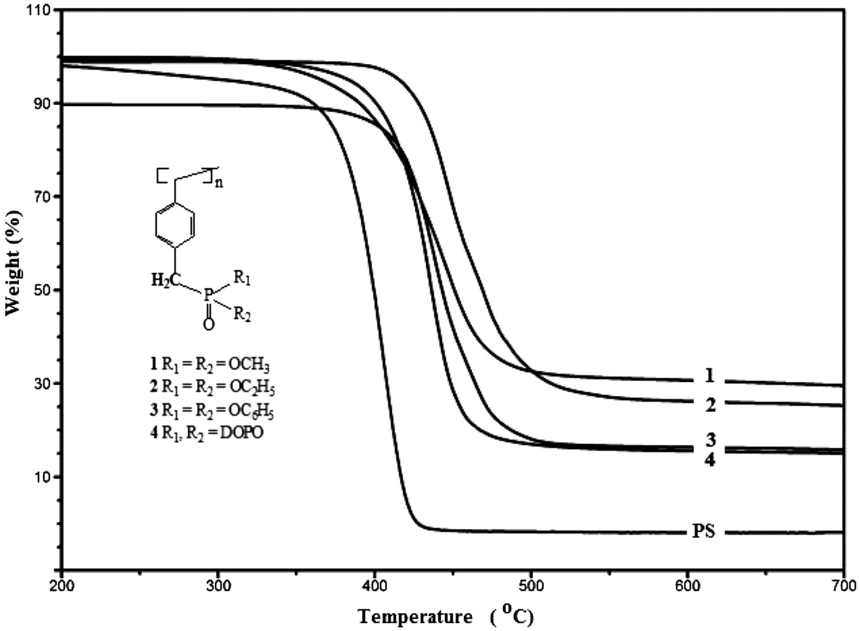

Figure 3. Thermal degradation of styrene polymers bearing phosphorus-containing pendant groups.

The ^{1}H-NMR spectra of these polymers are illustrated in Figure 2 and contain the following characteristic peaks: $\delta \approx 1.4$ (Ph- CH- C$\underline{H}_2$); $\delta \approx 1.8$, (Ph- C$\underline{H}$- CH$_2$), aromatic protons from former vinyl segments, at $\delta \approx 6.5$ and $\delta \approx 7.05$; methyl protons (P-CH$_2$-C$\underline{H}_3$) from diethylphosphonate groups at $\delta \approx 1.2$-1.25; methylene protons (P-C$\underline{H}_2$-CH$_3$) from phosphonate groups at 4-4.25 ppm; benzylic Ph-C$\underline{H}_2$-P signals at $\delta \approx 3$ - 3.4, aromatic protons from diphenylphosponate residues at 7.2-7.3 ppm and signals at $\delta \approx 4$ due to N$\underline{H}$ protons from phosphoramidate pendants.

The glass transitions temperatures (T_g) for these polymers are generally higher than that for poly(styrene) as shown in Table I. This may be reflective of strong intermolecular interactions between the polar groups pendant to the polymer mainchain.

Thermal decomposition of the polymers bearing only phosphorus-containing pendants is depicted in Figure 3. As can be seen, the onset temperature for degradation is higher for the polymers with phosphorus–containing pendant groups than for unsubstituted poly(styrene).

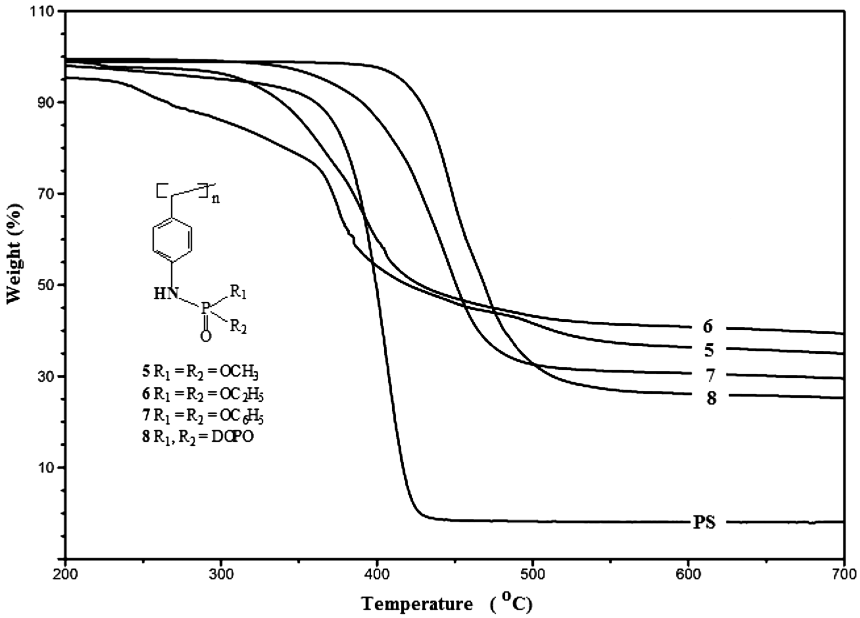

Figure 4. Thermal degradation of styrene polymers bearing pendant groups containing both phosphorus and nitrogen.

Further, the residue from degradation of the phosphorus–containing polymer is significantly greater (16-27 % of the initial sample mass) than for the degradation of unsubstituted poly(styrene) (0%). The degradation of the polymers bearing pendants groups containing both phosphorus and nitrogen is depicted in Figure 4. Again, the onset temperature for degradation of the polymers with phosphorus/ nitrogen containing pendant groups is generally higher than that for unsubstituted poly(styrene). Degradation of these polymers also leads to significant levels of residual material (25-40% of the initial sample mass). Not only is the level of residue much higher than that for unsubstituted poly(styrene) but is significantly greater than that for degradation of polymers with pendant groups containing only phosphorus. Based on these simple observations, it would seem that the beneficial impact of phosphorus on the thermal stability of poly(styrene) is strongly enhanced by the presence of nitrogen. Data for the degradation of both sets of polymers are displayed in Table II.

Table II. Thermal degradation data for the polymers from phosphorus- and phosphorus- and nitrogen- containing monomers

Sample	*T_{onset} [°C]*	*Mass loss [%]*	*Residue at 600 °C [%]*	*Sample*	*T_{onset} [°C]*	*Mass loss [%]*	*Residue at 600 °C [%]*
PM_1	414	64.2	32.5	***PM_5***	239; 366	63.6	36.4
PM_2	425	69.9	26.5	***PM_6***	340	59.2	40.8
PM_3	412	84.4	15.6	***PM_7***	391	68.7	31.3
PM_4	416	83.6	16.3	***PM_8***	426	72.8	26.2
PS	384	100	0	***PS***	384	100	0

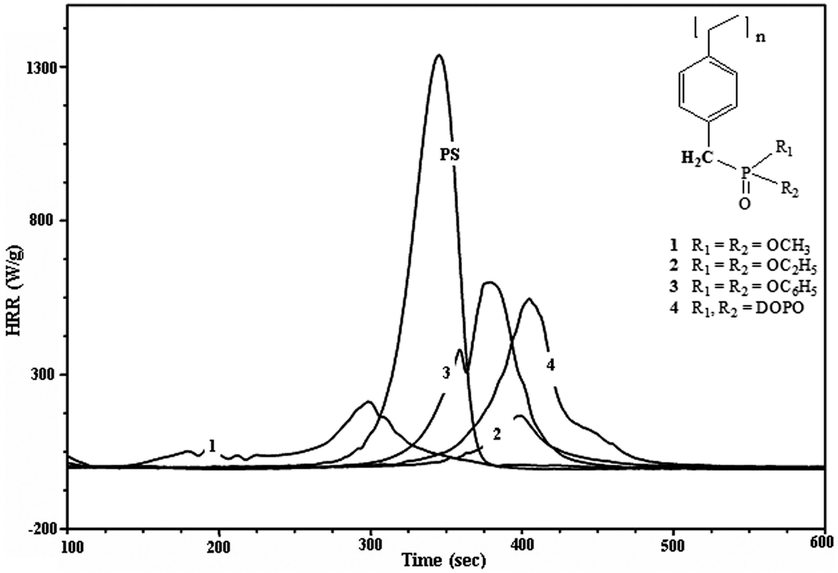

Figure 5. Heat release rate for the combustion of styrene polymers bearing phosphorus-containing pendant groups.

A reflection of the impact of the presence of the pendant groups on the combustion of the polymers is provided by the data from pyrolysis combustion flow calorimetry. Plots of heat release rates versus time for the polymers are displayed in Figures 5 and 6.

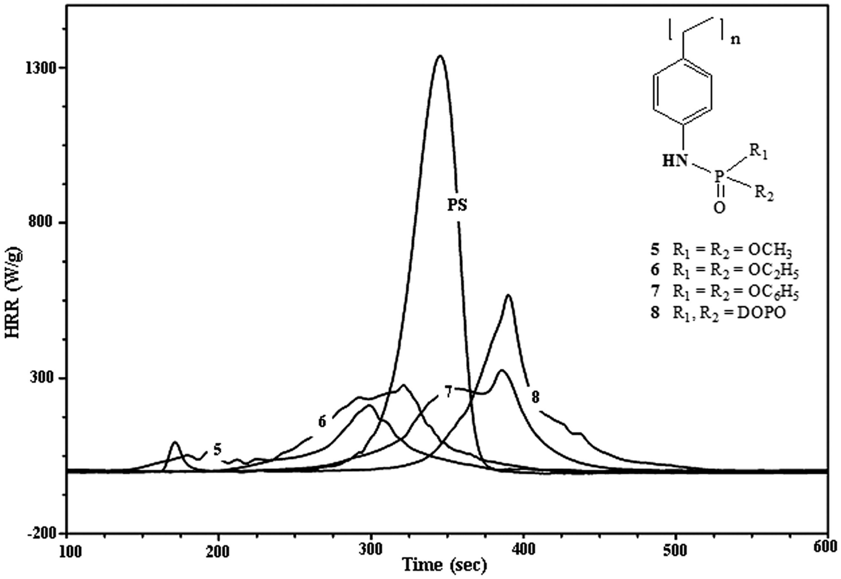

Figure 6. Heat release rate for the combustion of styrene polymers bearing phosphorus/nitrogen-containing pendant groups.

Table III. Heat release (HR) values for the combustion of the homopolymers from phosphorus- and phosphorus- and nitrogen- containing monomers

Homopolymer	*HR [kJ/g]*	*Homopolymer*	*HR [kJ/g]*
P1	25.8	**PM_5**	14.02
PM_2	27.9	**PM_6**	22.6
PM_3	28.3	**PM_7**	22.9
PM_4	26.6	**PM_8**	25.23
PS	42.4	***PS***	42.4

First, it is apparent that the presence of phosphorus in the polymer dramatically alters heat release rate for combustion of the polymer. As may be seen from the plots in Figure 6, this impact is enhanced by the presence of nitrogen in the phosphorus/nitrogen-containing pendant groups.

Heat release values for the polymers are collected in Table III. The heat release values for the combustion of polymers containing both phosphorus and nitrogen are only marginally smaller than those for the polymers containing only phosphorus.

Conclusions

Two sets of styrene monomers, one containing a phosphorus moiety as a substituent and the other containing a substituent with both phosphorus and nitrogen components, have been prepared, characterized, and used to generate a set of polymers containing, in the first instance, only phosphorus and, in the second, both phosphorus and nitrogen. Both the thermal degradation and the combustion characteristics of the polymers have been examined. Thermogravimetry suggests that the presence of nitrogen enhances the impact of phosphorus on the stability of the polymers (higher onset temperature for degradation and significantly higher levels of residue after decomposition). Polymers containing both phosphorus and nitrogen display slightly depressed combustion heat release rates compared to those containing only phosphorus.

References

1. Weil, E. D. Phosphorus-based Flame Retardants. In *Handbook of Organophosphorus Chemistry*; Engel, R. E., Ed.; Marcel Dekker: New York, NY, 1992.
2. Weil, E. D.; Levchik, S. V.; Ravey, M.; Zhu, W. M. A Survey of Recent Progress in Phophorus-based Flame Retardants and Some Mode of Action Studies. *Phosphorus Sulfur Silicon Relat. Elem.* **1999**, *146*, 17–20.
3. Lu, S. Y.; Hamerton, I. Recent Developments in the Chemistry of Halogen-free Flame Retardant Polymers. *Prog. Polym. Sci.* **2002**, *27*, 1661–1712.
4. Davis, J. The Technology of Halogen-free Flame Retardant Additives For Polymeric Systems. *Eng. Plast.* **1996**, *9*, 403–419.
5. Dumitrascu, A.; Howell, B. A. Flame-retarding Vinyl Polymers Using Phosphorus-Functionalized Styrene Monomers. *Polym. Degrad. Stab.* **2011**, *96* (3), 342–349.
6. Joseph, P.; Tretsiakova-Menally, S. Reactive Modifications of Some Chain- and Step-growth Polymers with Phosphorus-Containing Compounds- A Review. *Polym. Adv. Technol.* **2011**, *22*, 395–406.
7. Furukawa, J.; Kobayashi, E.; Wakui, T. Phosphorus-containing Polystyrene Derivatives As Flame Resistance. *Polym. J.* **1980**, *12* (5), 277–285.
8. Yu, Z.; Zhu, W.-E. Synthesis and Polymerization of Vinylbenzylphosphonate Diethyl Ester. *J. Polym. Sci., Part A: Polym. Chem.* **1990**, *28*, 227–230.
9. Boutevin, B.; Hamoui, B.; Bessière, J.-M. M. Synthesis of a Phosphonated Styrene Monomer. Instability of the Diacidic Moiety and Polymerization. *Macromol. Chem. Phys.* **1995**, *196*, 1865–1873.

10. Ebdon, J. R. Flame Retardancy in Styrenic and Acrylic Polymers with Covalently Bound Phosphorus-containing Groups. *Recent. Adv. Flame Retard. Polym. Mater.* **1997**, *8*, 161–170.
11. Ebdon, J. R.; Price, D.; Hunt, B. J.; Joseph, P.; Gao, F.; Milnes, G. J.; Cunlife, L. K. Flame Retardance in Some Polystyrenes and Poly(methyl methacrylate)s with Covalently Bound Phosphorus-containing Groups: Initial Screening Experiments and Some Laser Pyrolysis Mechanistic Studies. *Polym. Degrad. Stab.* **2000**, *69*, 267–277.
12. Dworak, C.; Koch, T.; Varga, F.; Liska, R. Photopolymerization of Biocompatible Phosphorus-containing Vinyl Esters and Vinyl Carbamates. *J. Polym. Sci., Part A: Polym. Chem.* **2010**, *48*, 2916–2924.
13. Catel, Y.; LePluart, L.; Madec, P.-J.; Pham, T.-N. Synthesis and Photopolymerization of Phosphonic Acid Monomers for Applications in Compomer Materials. *J. Appl. Polym. Sci.* **2010**, *117*, 2676–2687.
14. Chang, S.-J.; Sheen, Y.-C.; Chang, R.-S.; Chang, F.-C. The Thermal Degradation of Phosphorus-containing Polyesters. *Polym. Degrad. Stab.* **1996**, *54*, 365–367.
15. Wang, C. S.; Liu, C. H.; Chen, C. Y. Synthesis and Properties of Phosphorus-containing Polyesters Derived From 2-(6-Oxido-6H-dibenzáe,eñá1,2ñoxaphosphorin-6-yl)-1,4-hydroxyethoxy phenylene. *J. Polym. Sci., Part A: Polym. Chem.* **1998**, *36*, 3051–3061.
16. Wang, C. S.; Shieh, J. Y.; Sun, Y. M. Synthesis and Properties of Phosphorus-containing PET and PEN. *J. Appl. Polym. Sci.* **1988**, *70*, 1959–1964.
17. Wang, C. S.; Liu, C. H. Synthesis and Properties of Phosphorus-containing PEN and PBN Copolyesters. *Polymer* **1999**, *40*, 747–757.
18. Wang, C. S.; Shieh, J. Y. Synthesis and Flame Retardancy of Phosphorus-containing Polycarbonate. *J. Polym. Res.* **1999**, *6*, 149–154.
19. Wang, Y.-Z.; Chen, X.-T.; Tang, X.-D. Synthesis, Characterization and Thermal Properties of Phosphorus-containing, Wholly Aromatic Thermotropic Copolyesters. *J. Appl. Polym. Sci.* **2002**, *86*, 1278–1284.
20. Park, J. M.; Park, Y. H. Synthesis and Properties of Novel Flame Retardant Poly(butylene terephtalate). *Macromol. Res.* **2005**, *13*, 128–134.
21. Hamciuc, C.; Vlad-Bubulac, T.; Sava, I.; Petreus, D. New Phosphorus-containing Copolyesters. *J. Macromol. Sci., Part A: Pure Appl. Chem.* **2006**, *43*, 1355–1364.
22. Du, X.-H.; Zhao, C.-S.; Wang, Y.-Z.; Zhou, Q.; Deng, Y.; Qu, M.-H.; Yang, B. Thermal Oxidative Degradation Behaviours of Flame-retardant Thermotropic Liquid Crystal Copolyester/PET blends. *Mater. Chem. Phys.* **2006**, *98*, 172–177.
23. Balabanovich, A. I.; Pospiech, D.; Korwitz, A.; Hausler, L.; Harnisch, C. Pyrolysis Study of a Phosphorus-containing Aliphatic-aromatic Polyester and its Nanocomoposites with Layered Silicate. *Polym. Degrad. Stab.* **2009**, *94*, 355–364.
24. Li, Q.-L.; Wang, X.-L.; Wang, D.-Y.; Xiong, W.-C.; Zhong, G.-H.; Wang, Y.-Z. A Novel Organophosphorus Flame Retardant: Synthesis and Durable Finishing of Poly(ethylene terephtalate)/ Cotton Blends. *J. Appl. Polym. Sci.* **2010**, *117*, 3066–3074.

25. Hu, Z.; Chen, L.; Zhao, B.; Luo, Y.; Wang, D.-Y.; Wang, Y.-Z. A Novel Efficient Halogen-free Flame Retardant System for Polycarbonate. *Polym. Degrad. Stab.* **2011**, *96* (3), 320–327.
26. Annakutty, K. S.; Kishore, K. Synthesis and Properties of Flame-retardant Polyphosphate Esters-A Review. *J. Sci. Ind. Res.* **1989**, *48*, 479–493.
27. Ranganathan, T.; Zilbermann, J.; Farris, R. J.; Coughlin, E. B.; Emrick, T. Synthesis and Characterization of Halogen-free Antiflammable Polyphosphonates Containing 4,4′-bisHydroxydeoxybenzoin. *Macromolecules* **2006**, *39*, 5974–5975.
28. Ranganathan, T.; Ku, B. C.; Zilbermann, J.; Beaulieu, M.; Farris, R. J.; Coughlin, E. B.; Emrick, T. Poly(arylate-phosphonate) Copolymers with Deoxybenzoin in the Backbone: Synthesis, Characterization and Properties. *J. Polym. Sci., Part A: Polym. Chem.* **2007**, *45*, 4573–4580.
29. Chong, Y.-L.; Wang, Y.-Z.; Ban, D.-M.; Yang, B.; Zhao, G.-M. A Novel Phosphorus-containing Polymer as a Highly Effective Flame Retardant. *Macromol. Mater. Eng.* **2004**, *289*, 703–707.
30. Hess, G. Industry Drops Flame Retardant. *Chem. Eng. News* **2010**, *88* (1), 10.
31. Ravichandran, S.; Nagarajan, S.; Ku, B. C.; Coughlin, B.; Emrick, T.; Kumar, J.; Nagarajan, R. Halogen-free Ultra-high Flame Retardant Polymers Through Enzyme Catalysis. *Green Chem.* **2012**, *14*, 819–824.
32. Alace, M.; Wenning, R. J. The Significance of Brominated Flame Retardants in the Environment: Current Understanding, Issues and Challenges. *Chemosphere* **2002**, *46*, 579–582.
33. Darnerud, P. D. Brominated Flame Retardants as Possible Endocrine Disrupters. *Int. J. Androl.* **2008**, *31*, 152.
34. Herbstman, J. B.; Sjodin, A.; Kurzon, M.; Lederman, S. A.; Jones, R. S.; Rauth, V.; Needham, L. L.; Tang, D.; Niedzwiecki, M.; Wang, R. Y.; Perera, F. Prenatal Exposure To PBDEs and Neurodevelopment. *Environ. Health Perspect.* **2010**, *118*, 712–719.
35. Artner, J.; Ciesielski, M.; Walter, O.; Doring, M.; Perez, R. M.; Sandler, J. K. W.; Altstadt, V.; Schartel, B. A Novel DOPO-based Diamine as Hardener and Flame Retardant for Epoxy Resin Systems. *Macromol. Mater. Eng.* **2008**, *293*, 503–514.
36. Ciesielski, M.; Schafer, A.; Doring, M. Novel Efficient DOPO-based Flame-retardants for PWB Relevant Epoxy Resins with High Glass Transition Temperatures. *Polym. Adv. Technol.* **2008**, *19*, 507–515.
37. Schartel, B.; Balabanovich, A. I.; Braun, U.; Knoll, U.; Artner, J.; Ciesielski, M.; Doring, M.; Perez, R.; Sandler, J. K. W.; Altstadt, V.; Hoffman, T.; Pospiech, D. Pyrolysis of Epoxy Resins and Fire Behavior of Epoxy Resin Composites Flame-retarded with 9,10-dihydro-9-oxa-10-phosphaphenanthrene-10-oxide Additives. *J. Appl. Polym. Sci.* **2007**, *104*, 2260–2269.
38. Perez, R. M.; Sandler, J. K. W.; Altstadt, V.; Hoffman, T.; Pospiech, D.; Artner, J.; Ciesielski, M.; Doring, M.; Balabanovich, A. I.; Knoll, U.; Braun, U.; Schartel, B. Novel Phophorus-containing Hardeners with

Tailored Chemical Structures for Epoxy Resins: Synthesis and Cured Resin Properties. *J. Appl. Polym. Sci.* **2007**, *105*, 2744–2759.

39. Perez, R. M.; Sandler, J. K. W.; Altstadt, V.; Hoffman, T.; Pospiech, D.; Artner, J.; Ciesielski, M.; Doring, M.; Balabanovich, A. I.; Schartel, B. Effective Halogen-free Flame Retardancy for a Monocomponent Polyfunctional Epoxy Using an Oligomeric Organophosphorus Compound. *J. Mater. Sci.* **2006**, *41*, 8347–8351.
40. Perez, R. M.; Sandler, J. K. W.; Altstadt, V.; Hoffman, T.; Pospiech, D.; Artner, J.; Ciesielski, M.; Doring, M.; Braun, U.; Knoll, U.; Schartel, B. Effective Halogen-free Flame Retardants for Carbon-reinforced Epoxy Composites. *J. Mater. Sci.* **2006**, *41*, 4981–4984.
41. Perez, R. M.; Sandler, J. K. W.; Altstadt, V.; Hoffman, T.; Pospiech, D.; Ciesielski, M.; Doring, M. Effect of DOPO-based Compounds on Fire Retardancy, Thermal Stability, and Mechanical Properties of DGEBA Cured with 4,4′-DDS. *J. Mater. Sci.* **2006**, *41*, 341–353.
42. Dumitrascu, A.; Howell, B. A. *Impact of the Incorporation of the Nitrogen into Phosphorus Flame Retardant Styrene Monomers*, Proceedings of the 22nd Annual Conference on Recent Advances in Flame Retardancy of Polymeric Materials; BCC Research: Wellesley, MA, 2011; Chapter 10.
43. Tai, Q.; Song, L.; Hu, Y.; Yuen, R. K. K.; Feng, H.; Tao, Y. Novel Styrene Polymers Functionalized with Phosphous-nitrogen Containing Molecules : Synthesis and Properties. *Mater. Chem. Phys.* **2012**, *134*, 163–169.
44. Chen, Y.; Wang, Q. Reaction of Melanine Phosphate with Pentaerythritol and its Products for Flame Retardation of Polypropylene. *Polym. Adv. Technol.* **2007**, *18*, 587–600.
45. Singh, H.; Jain, A. K.; Sharma, T. P. Effect of Phosphorus-nitrogen Additives on Fire Retardancy of Rigid Polyurethane Foams. *J. Appl. Polym. Sci.* **2008**, *109*, 2718–2728.
46. Nguyen, C.; Kim, J. Synthesis of a Novel Nitrogen-phosphorus Flame Retardant Based on Phosphoramidate and its Application to PC, PBT, EVA, and ABS. *Macromol. Res.* **2008**, *16*, 620–625.
47. Gao, F.; Tong, L.; Fang, Z. Effect of a Novel Phosphorus-nitrogen Containing Intumescent Flame Retardant on the Fire Retardancy and the Thermal Behaviour of Poly(butylene terephthalate). *Polym. Degrad. Stab.* **2006**, *91*, 1295–1299.
48. Gaan, S.; Salimova, V.; Heuberger, M.; Rupper, P.; Schoenholzer, P. *Phosphoramidate Flame Retardants: Mechanism and Application*, Proceedings of the 20th Annual Conference on Recent Advances in Flame Retardancy of Polymeric Materials; BCC Research: Wellesley, MA, 2009.
49. Gaan, S.; Mauclaire, L.; Rupper, P.; Salimova, V.; Tran, T.-T.; Heuberger, M. Thermal Degradation of Cellulose Acetate in Presence of Bis-phosphoramidates. *J. Anal. Appl. Pyrol.* **2011**, *90*, 33–41.

Chapter 18

Recent Developments in Flame Retardancy of Flexible Polyurethane Foams

N. Matthias Neisius,[1] Shuyu Liang,[1] Henri Mispreuve,[2] and Sabyasachi Gaan*,[1]

[1]Empa Swiss Federal Laboratories for Materials Science and Technology, Lechenfeldstrasse 5, CH-9000 St. Gallen, Switzerland
[2]Foampartner, Fritz Nauer AG, Oberwolfhauserstrasse 9, CH-8633 Wolfhausen, Switzerland
***E-mail: Sabyasachi.Gaan@empa.ch**

This short review is focused on scientific developments and studies in flame retardancy of flexible polyurethane (PU) foams that has been published during the last three years. Since an increasing number of brominated flame retardants are banned and chloro-phosphate esters like TCEP, TDCPP, TDCP are either banned or under investigation by environmental agencies, the industrial and academic flame retardant research in PU foams has gained impetus. It is a mutual understanding that more environmentally benign and less hazardous materials should be used in the future. In the first part of this article we have reviewed the recent efforts of various research groups towards the development of such kind of flame retardants for PU foams. The second part of this article details some investigations on possible synergistic or antagonistic interactions between phosphoramidate compounds and melamine in flame retardancy of flexible polyurethane foam (FPUF).

Introduction

Polyurethane (PU) is one of the most versatile polymers finding application in diverse areas such as manufacturing of flexible- and rigid- thermoplastic foams, coatings, adhesives, sealants, elastomers, binders, reaction injection molding products, dispersions etc (*1*). The world consumption of PU has been steadily

In Fire and Polymers VI: New Advances in Flame Retardant Chemistry and Science; Morgan, A., et al.; ACS Symposium Series; American Chemical Society: Washington, DC, 2012.

increasing in the past decades and the potential for new applications never ceases (*2*). Flexible polyurethane foams (FPUFs) are primarily used in manufacturing of cushioning materials for application in furniture, bedding, automobiles carpets, textiles and packaging (*3*). FPUFs due to their low density, open cell structure and chemical nature (relatively higher percentage of carbon and hydrogen) are quite easy to ignite and usually burn rapidly. Thermal decomposition and combustion of FPUFs is a highly exothermic process and leads to formation of toxic gases like isocyanates, hydrogen cyanides, carbon dioxide and carbon monoxide. Thus FPUFs need to be made flame retardant so as to meet various fire safety requirements for application in rail, aircraft interior, mattress etc (*4*).

A wide range of flame retardants such as inorganic phosphorus-, organic phosphorus-, halogen- and phosphorus-halogen organic compounds are used in rendering FPUF flame retardant. The choice of flame retardant system usually depends on the field of application, price, and environmental and fire safety regulations (*4*, *5*). One of the most commonly used flame retardant (FR) in FPUF industry in Europe is TCPP (tris-(chloropropyl) phosphate). TCPP is especially suitable as it is relatively cheap, liquid and it does not interfere in the foam build up process. However TCPP containing PU foams suffers from several problems such as fogging, releasing more carbon monoxide during burning as compared to virgin foam (*6*) and more recently it is being reviewed by European Union Risk assessment body (*7*). Therefore researchers all over the world have focused on flame retardant FPUF research that uses much more environmentally acceptable materials *i.e* melamine or expandable graphite. The use of melamine and graphite as a flame retardant for PU is well known in the literature for a long time and has been reviewed by Chattopadhya *et al.* in detail in 2009 (*4*).

This paper reviews the scientific research in the field of flame retardancy of FPUFs undertaken by various research groups during the last three years and is an addition to the already published review article of Chattopadhya *et al.* on PU (*4*). This paper will also highlight some of our efforts in the flame retardancy of FPUFs.

Non-Phosphorus Additives

One of the most commonly used compounds for rendering polymeric materials flame retardant are metal compounds like ATH (aluminum trihydroxide). ATH finds usage in a broad range of polymers, for example in epoxy resins or in polypropylene, because it is cheap, environmentally benign, readily available and it exhibits good smoke suppressant properties (*8*, *9*). In 2009 König *et al.* reported the application of ATH as FR in flexible polyurethane foams (*10*). A comparison between normal, unfunctionalized ATH and silane modified ATH was presented in their paper. It was shown that relatively large amounts (up to 60 (phpp) parts per hundred parts polyol) of ATH had to be applied to pass the FMVSS 302 test standards for M3 vehicles, which requires a burning rate of less than 100 mm/min. It was observed that the viscosity of the polyol dispersion increased significantly with addition of large amounts of ATH and thus the foam preparation became much more difficult. To overcome this problem König *et al.* modified the ATH with 3-aminopropylsiloxane to improve the compatibility with the foaming procedure. By using a process similar to the sol-gel process, the siloxane group was covalently bound onto the ATH surface so that the amino group was still left unreacted. The free amino group was meant to react with the isocyanate groups from TDI to incorporate the siloxane-linked ATH in the polyurethane matrix. Through this modification, the viscosity of the resulting polyol dispersion could be significantly reduced, the preparation of the PU foam remarkably facilitated and flammability test results were not affected by this modification.

In the same year, König *et al.,* also reported a detailed and comprehensive study regarding the thermal decomposition of slabstock flexible polyurethane foams in the presence of melamine (*11*). As melamine is environmentally more acceptable, readily available and cheap chemical, it is extensively used in flame retardant applications as well as polyurethane foams (*12–14*). Until 2009 the main application of melamine as FR in flexible polyurethane foams was limited to higher density foams (>50kg/m^3) (*11–13*). König *et al.* were the first to apply melamine in lower density foams (≈25 kg/m^3) and investigate the flammability properties and thermal degradation behavior in detail (*11*). Prior to this research, it was commonly understood that the flame retardant efficiency of melamine was its capability to act as a heat sink, that is cooling the flame due to sublimation and degradation with release of ammonia (*15*). König *et al.* could show that the flame temperature of the burning polyurethane foam was not affected by the presence of melamine during the first stage of decomposition. They further showed that the flame temperature increased during the subsequent stage of decomposition. The temperature increased more or less linearly with the increasing amount of melamine in the FPUFs formulation. The authors attributed this effect to the exothermic oxidation of the temporary char being formed from the condensation products of melamine and the resulting higher surface area of the residual material. This assumption of a more efficient oxidation could further be supported by the fact that the amount of released CO_2 constantly increased by adding more melamine. It was also shown that melamine acted as a very efficient smoke suppressant because the smoke density could already be significantly reduced by addition of only 20 phpp. The authors could not find strong evidence of reactivity of melamine with the TDI during the polymerization process but speculated that the sublimed melamine and its condensation products could react with the TDI which is formed during the decomposition of PU in the first stage. The flammability of the FPUFs were evaluated by the FMVSS 302 test which was passed with 60 phpp of melamine. With 60 phpp of melamine all samples extinguished by themselves. The authors finally concluded that the FR mechanism of melamine is more attributed to the dilution of the flame by sublimed melamine or its degradation products rather than to a certain heat sink effect (*11*).

Similar studies were performed and published by Bashirzadeh and Gharehbaghi in 2010 (*16*). They investigated and compared the influence of melamine and expandable graphite (EG) on the reactivity, mechanical and fire properties of flexible PU foams (density between 40 and 57 kg/m^3). Due to its mode of action EG can be seen as a kind of intumescent flame retardant. The volume of EG can be expanded up to 500 times by applying an external heat source. Subsequently a voluminous carbonaceous char layer can be formed to inhibit the heat and mass transfer of the burning material. Furthermore intercalated oxidants, like sulfuric acid, react upon heating with the EG to form non-combustible gases like CO_2, H_2O and SO_2 which act as blowing agent and diluents in the flame zone.

It could be clearly inferred from their studies that the application of solid flame retardants, like melamine and EG, affected the mechanical properties of PU foams remarkably. Melamine and EG treated foams became more inhomogeneous and softer, with EG having a significantly higher adverse effect than melamine. Particularly EG increased the compression set and the tear strength of the foams as its flake shape acted as a kind of solid reinforcement in the foam structure. The results of the flammability tests according to UIC code 564-2 and ISO 9772 revealed that EG had a strong effect on the reduction of burning length and burning time when 16 phpp or more were applied. EG with a bigger particle size i.e. 0.25 mm exhibited better flame retardant efficiency compared to smaller ones (0.18 mm) whereas various particle size of melamine did not have such a considerable influence. Cone calorimeter measurements showed a very interesting behavior of the EG treated PU foams. The total heat released (THR), the heat release rate (HRR) and the smoke emission were reduced significantly. Especially EG had a much higher impact on these parameters than melamine. A further big difference between EG and melamine containing foams was the measured CO/CO_2 ratio. In case of EG it was significantly increased due to incomplete combustion whereas it was reduced in case of melamine due to more efficient oxidation as described by König *et al.*

Similar observations were reported in 2012 by Wolska *et al.* (*17*).In their report they described the application of EG, cellulose and both together as FR in PU foams (density $\approx$ 25 kg/m^3). Each additive was used in a relatively low concentration of 5 wt% and the resulting foams were investigated for their flame retardant properties (linear flammability test ISO 3795), thermal degradation behavior (thermogravimetirc analysis, TGA, pyrolysis combustion flow calorimetry, PCFC) and mechanical properties. Low levels of FR additive did not affect the mechanical properties of foams. The thermal stability of the FPUFs was also not affected by the addition of EG and cellulose because the TGA curves revealed no significant difference between them and the untreated PU foam. Subsequent PCFC analyses exhibited a big difference between the various foams. The cellulose treated PU foam had 30% higher maximum heat release rate compared to the untreated foam. This could be explained by the formation of levoglucosan, a very combustible material, during the degradation of the cellulose treated PU foam. The EG treated foam had a slightly lower maximum heat release rate which could be explained by the formation of a carbonaceous char layer due to the expansion of the EG which may inhibit mass transfer. The linear flammability test showed that both additives, EG and cellulose, when added separately, downgrade the flame retardant properties. This could be seen by an increased burning rate compared to the untreated foams. In contrast, the burning rate decreased when both additives are applied together in on PU foam as a synergistic pair. That means the burning rate of a PU foam treated with 2.5 wt% EG and 2.5 wt% cellulose had a slower burning rate than the untreated foam. This is a clear indication for a very good synergism between these two additives. More detailed investigations on this topic are currently in progress.

Synergistic Interaction between Non-Phosphorus and Phosphorus-Based FRs

In 2011 Ahmadi, Bashirzadeh and Gharehbaghi applied the same flame retardant systems (EG, melamine) to PU foams for application in airplane seats (*18*). They observed similar detrimental effects as discussed above for EG and melamine containing FPUFS. A FAA 25.853 flammability test, required for aircraft seat cushions, was performed to evaluate the flame retardant properties of the solid FR systems. The PU foams treated with 20 phpp of melamine could pass the required test although some dripping was also observed. In contrast to that, the EG treated foams (20 phpp) failed the test and burned completely without showing any significant flame retardant effect. Therefore the EG had to be combined with a liquid halogen-free phosphorus based flame retardant (obtained from Clariant) for possible synergistic effect. Indeed a combination of 4 phpp of liquid phosphorus FR and 20 phpp of EG exhibited very good flame retardant properties and the FAA 25.853 could be passed easily without any dripping. The observed smoke density was also slightly lower compared to melamine treated foams and much lower compared to untreated foams. Thus the smoke density and toxicity test prescribed by the Airbus Directive ABD0031 could easily be passed. From this research it becomes very obvious that EG does not work for each kind of PU foams and that sometimes a second additive, a synergist was needed to achieve the demanded flame retardant properties.

One year later Wolska *et al.* published an analogous study on flame retardant PU foams using EG and Fyrol PNX, an oligomeric liquid alkylphosphate flame retardant (*19*). The FR foams were evaluated as noted above. The mechanical properties were not affected very much by the addition of both FRs. The addition of Fyrol PNX reduced the thermal stability of the PU foam slightly whereas the addition of EG had no significant effect on their mechanical properties. As mentioned above, the addition of 5 wt% EG caused a very slight increase in the burning rate of the PU foam during the linear flammability test. Compared to that, the addition of 5 wt% Fyrol PNX had a much better impact on the flame retardant properties because it led to a decrease in the burning rate of more than 30%. As a possible synergistic combination, Fyrol PNX and EG were mixed together (2.5 wt% each) in PU foam and the FR properties were evaluated. As in the examples mentioned above, a significant synergistic effect could again be observed. The burning rate of this mixed foam had the same burning rate as the foam with 5 wt% Fyrol PNX. Thus half of the amount of the phosphorus based FR could be readily replaced by EG without any loss in FR efficiency. Furthermore the thermal stability of this foam was better than that with 5 wt% Fyrol PNX.

In 2012 Benin, Durganala and Morgan reported their work on the development of new boron- and phosphorus-containing aromatic compounds as FR for polyurethane foams (*20*). They successfully elaborated new synthetic pathways to boronated and phosphonated terephtalic acid derivatives by means of transition metal catalysis. As multigram quantities of flame retardants were needed for the preparation of even small blocks of flexible polyurethane foams and the synthesized flame retardants were not easily available in such quantities, they chose to use thermoplastic polyurethane (TPU) as model system for preliminary investigations. Thus the authors pre-screened their novel flame retardants by means of PCFC analysis for their flame retardant capability. After identification of the most promising candidates (giving best char yields, lowest HRRs and THCs) they were blended with TPU and subsequently analyzed by PCFC. The best candidate amongst all the synthesized compounds, a boronated terephthalic acid derivative, could significantly reduce the maximum heat release rate (HRR) and the total heat of combustion (≈ 19-20%). Furthermore the char formation could be increased from about 1% for non-treated TPU to 15% for treated TPU. The authors attributed these phenomena to the reaction of boronic acid moiety with the TPU during thermal decomposition. Further studies on this topic are ongoing.

Phosphorus-Based Flame Retardants

The synthesis and application of a novel gas phase flame retardant, namely Methyl-DOPO **1** (figure 1), in flexible polyurethane foams was reported by König *et al.* (*21*).

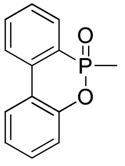

1

Figure 1. Methyl-DOPO.

In this report the authors described an efficient two step synthesis and detailed analyses of the flame retardant properties of **1** FPUF. Additionally, to prove the proposed gas-phase mechanism of this compound, they performed TGA-MS measurements to detect low molecular weight reactive phosphorus species, like *PO or *PO_2, which were presumably responsible for the gas-phase flame retardant action (*22–26*). The authors were able to detect minor amounts of such fragments during the decomposition of the FR foam at a temperature around 200°C. This could be seen as a first indirect hint for the efficient gas-phase action of **1**. Further investigations, like cone calorimeter measurements, were performed to find more evidence of the gas-phase action of **1**. It was proposed that the amount of smoke release, CO and the CO/CO_2 ratio were also good indicators for the efficiency of a gas-phase flame retardant (*27*, *28*). Higher amounts of smoke and CO and thus a higher CO/CO_2 ratio could be the outcome of incomplete combustion. This incomplete combustion was presumably a result of the scavenging of reactive *OH radicals by *PO or *PO_2, that were released by **1** during decomposition. The higher the smoke density, CO amount and the CO/CO_2 ratio, the more efficient is the gas-phase action of the FR (*27*, *28*). The authors could show that the smoke density and CO/CO_2 ratio increased significantly with addition of Methyl-DOPO to the FPUF. Furthermore the FPUF did not even ignite in the cone calorimeter when 10% of **1** were added to the foam. Additionally small scale burner tests FMVSS 302 revealed that the FR foam with 10% Methyl-DOPO led to an excellent SE classification.

In a follow up article, the same group investigated the reason for the gas-phase efficiency of Methyl-DOPO in more detail (*29*). It was proposed earlier by Döring *et al.* that the release of *PO and *PO_2 and thus the gas-phase FR action was caused by the ring strain within the DOPO moiety (*30*). To test this, Koenig and Kroke prepared a "ring-opened" analogue (Methylphenoxyphenyl-phosphinate **2**, figure 2) of **1** and compared their FR efficiency in FPUF by means of TGA-MS, cone calorimeter and small scale burner test.

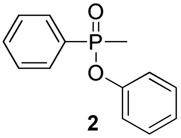

2

Figure 2. Methylphenoxyphenyl-phosphinate (MPPP).

There was more or less no significant difference between **1** and **2** in the majority of the test results. The abundance of *PO and *PO_2 detected by TGA-MS was very comparable for both compounds. The only obvious difference was the difference in the temperature of the volatilization and *PO/*PO_2 detection. In case of MPPP it was remarkably shifted to lower temperatures and showed a maximum at 160°C whereas Methyl-DOPO had its maximum at 200°C. The smoke density and CO/CO_2 ratio measured by the cone calorimeter exhibited comparable values for both compounds as well. Finally the small scale burner test FMVSS 302 revealed that foams treated with 10% MPPP also had a very good SE classification like the ones treated with 10% Methyl-DOPO. The most significant difference could be found within the FMVSS 302 results of foams treated with 7.5 % of MPPP and Methyl-DOPO. Methyl-DOPO caused a classification between B and SE whereas MPPP led only to a B rating. From these results the authors concluded that the ring tension in Methyl-DOPO did not have a significant influence on the release of *PO/*PO_2 species and hence on the flame retardant efficiency.The temperature of the volatilization and decomposition of the flame retardants have a major influence on their flame retardant efficiency in FPUF.

In 2012 Gaan *et al.* reported an investigation of the structural influence of organophosphorus compounds on the flame retardancy and thermal degradation of FPUF (*31*).

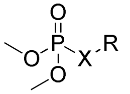

X = O, N or Ø
R = propyl, allyl or benzyl

Figure 3. General structure of phosphorus FRs evaluated by Gaan et al. (30).

In this study the authors compared three classes of organophosphorus moieties (phosphates, phosphoramidates and phosphonates, figure 3) regarding their flame retardant efficiency in FPUF. Within these three classes the substituent at the heteroatom was systematically varied from a propyl to an allyl and finally a benzyl moiety. The flame retardant properties and thermal decomposition analyses were performed by means of TGA, PCFC and flammability tests (LOI, UL-94 HB and swiss BKZ vertical test). The TGA measurements revealed that phosphates and phosphonates catalyzed the first stage of decomposition more efficiently than phosphoramidates. This could be attributed to their more acidic character which helps in degradation of the urethane bond at lower temperatures. The PCFC analyses showed no remarkable differences between the investigated compounds. The BKZ vertical burning test as well showed no difference because all samples passed upon the addition of 1% of organophosphorus FR. In contrast to these results, LOI measurements showed that phosphonates and phosphoramidates, which had similar values for all three different compounds, performed significantly better than phosphates. Within the three different groups of FRs the allyl-substituted compound exhibited in all cases the best FR behavior. The UL-94 HB test result corresponds very well with these results. Phosphonates and phosphoramidates outperformed phosphates and the allyl-substituted compounds had the best classification. With the addition of 10% allyl phosphonate and allyl phosphoramidate, the best classification of HF-1 rating, could be achieved. Commercially available flame retardant TCPP achieved only the lower HF-2 rating at similar concentration. In order to get a better understanding of these results and to find an explanation for the superior performance of allyl phosphonate and allyl phosphoramidate, the authors analyzed the mass spectrometric fragmentation pattern of all compounds carefully. This analysis revealed that the scission of the P-O bond was much more difficult and less favored than the P-N or P-C bond scission. The more facile P-heteroatom bond scission supported an easier degradation of the FR compound via different *P fragments. They concluded that an efficient *PO formation was easier for phosphonates and phophoramidates and hence a better gas-phase action was thus expected.

Phosphoramidates and Melamine: Synergism/Antagonism?

It has been reported in our recent research that phosphoramidates are efficient flame retardant compounds for FPUF (*32*) and melamine has been reported as synergist together with TCPP and TDCP in polyurethane foams (*25*). Thus, it seemed reasonable to investigate the interaction between phosphoramidates and melamine in FPUF flame retardancy.

Two different bidentate phosphoramidate compounds were synthesized, used as FR in FPUF and finally analyzed for their flame retardant properties with melamine. Figure 4 shows the structure of flame retardant compounds synthesized in this research.

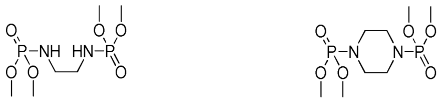

3

Phosphoramidicacid-1,3-ethanediylbis-tetramethylester (PAED)

4

Phosphonic acid-1,4-piperazinediylbis-tetramethylester (PAPD)

Figure 4. Flame Retardants compounds.

TCPP was used as a standard commercially available flame retardant (FR) for comparison with the synthesized phosphoramidates. PAED **3** and PAPD **4** were synthesized according to the method outlined in Scheme 1.

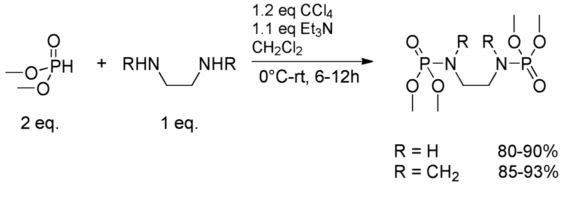

Scheme 1. Synthesis of PAED and PAPD

PAED and PAPD were white, crystalline solids with melting points of 98 °C and 119 °C respectively and could easily be dispersed in the poylol. It was also realized that the foaming process was affected if some impurities (traces of triethylamine hydrochloride) remained in the FR after the synthesis and thus every attempt was made to make the compounds as pure as possible. The compounds were synthesized in good yields and were more than 99% pure. The FPUF were manufactured according to the recipe given in Table 1.

Table 1. Formulation for PFUF manufacturing

FPUF	
Ingredients	*pphp*
All PO polyol	97
Compatibilizers	3.4
Tin(II)octanoate	0.25
Catalyst (dimethyl ethanolamine)	0.5
Silicone Stabilizer	0.5
H_2O (total)	1.85
Toluene diisocyante TDI	29.8
FR*	X
Mel**	Y

* TCPP, PAPD, PAED, concentration of FR : 0, 1, 2, 5, 10%; ** Melamine: 0, 5, 10%.

Table 2. BKZ flammability test

Classification *(Degree of flammability)*	***Requirements***
Class 3	time 5 - 20 s
Class 4	time, duration of burning > 20 s
Class 5*	flame does not reach the top level of the sample holder (150 mm). duration ≤ 20 s

* Any foam which achieves classification 5 passes the BKZ test and is described as ‘pass’ in the subsequent discussions.

The foams having a density of ≈43±1 kg/m³ were then tested for their flammability according to Swiss flammability standard (BKZ), a vertical burning test for foamed materials with a specific sample size (length: 160 mm, width: 60 mm, thickness: 6 mm ± 10% tolerance). For each specimen the flame test (BKZ) was performed in triplicate. If the results were not consistent, each specimen was tested 6 times. For the BKZ test an air dried specimen was placed in a vertical position and subjected to flame at the lower front edge by a standardized flame. The flame height of 20 mm was maintained and should burn constantly with sharp outlines. The burner position was adjusted 45° so that the flame hit the specimen vertically in the middle of the lower front edge. The flame was brought in contact with the foam for 15 sec and should be placed such that the foam bottom was approximately 4 ± 1 mm inside the flame from the tip. The analysis of the burning test was then made according to the details given in Table 2.

FPUF with various concentrations of synthesized FRs and TCPP were prepared (Table 1) and subjected to the BKZ vertical burning test as described above. It could be seen from Table 3 that the virgin foam burned completely and did not pass the BKZ test. The addition of TCPP as FR reduced the flammability of the foam significantly and the vertical burning test could be passed even with only 1% of TCPP. The time required to stop burning and as well as the height of burned material decreased an with increase in concentration of TCPP remarkably.

Table 3. Flammability results TCPP treated FPUF

FR	***FPUF***				
	Vertical Burning test (15cm×5cm×0.6cm)				***LOI*** *(O_2%)*
	PASS/NO	*Time (s)*	*1st Burned Height (cm)*	*2nd Burned Height (cm)*	
Blank	NO	20.6±2	15	15	20.5±0.2
1%TCPP	PASS	14.2±2	6.2±1	11.6±2	21.7±0.2
2%TCPP	PASS	12.2±2	6.0±1	11.5±2	21.9±0.2
5%TCPP	PASS	11.0±2	5.4±1	10.2±2	22.5±0.2
10%TCPP	PASS	9.7±2	5.2±1	9.6±2	23.0±0.2

Table 3 also shows the results of the limiting oxygen index (LOI) test of TCPP treated foams. The blank foam had a LOI value of around 20.5% while addition of TCPP increased the LOI values of the foam.

It has been reported in literature that nitrogen containing additives, like melamine, urea and guanidine derivatives, sometimes exhibit synergistic interaction with phosphorus flame retardants (*31*). The synergistic effect between melamine and TCPP on flame retardancy in FPUF has been also been reported (*24*).

Based on such reported literature, we wanted to investigate if such synergism (phosphoramidate/TCPP-melamine) could occur in the flame retardancy of FPUF. Therefore various FPUFs with different amounts and ratios of TCPP and melamine were prepared and evaluated.

Table 4 shows the effect of melamine as a co-additive in flame retardant formulation of TCPP.

It can be seen from Table 4 that the addition of melamine had no obvious effect on the LOI values of the FPUF. In contrast, the results of the BKZ test changed dramatically. The addition of melamine led to complete failure of all investigated foams so that all burned completely. These results could be attributed to certain antagonistic interaction of TCPP and melamine during the burning of foams.

Table 4. Effect of Melamine on flame retardancy of TCPP containing foams

FR	***BKZ test (15cm×5cm×0.6cm)***				***LOI*** *(O_2%)*
	PASS/NO	*Time (s)*	*1st Burned Height (cm)*	*2nd Burned Height (cm)*	
5%TCPP +10%melamine	NO	26.9±2	15	15	22.6±0.2
10%TCPP +5%melamine	NO	24.2±2	15	15	23.0±0.2
10%TCPP +10%melamine	NO	28.1±2	15	15	23.0±0.2

We further analyzed the synthesized phosphoramidates (PAED and PAPD) for their FR efficiency in FPUF. Table 5 and 6 show the flammability results of PAED and PAPD containing foams.

Table 5. Effect of PAED and melamine as flame retardants for FPUFs

FR	***BKZ test (15cm×5cm×0.6cm)***				***LOI (O_2%)***
	PASS/NO	*Time (s)*	*1st Burned Height (cm)*	*2nd Burned Height (cm)*	
Blank	NO	20.6±2	15	15	20.5±0.2
1%PAED	NO	21.7±2	15	15	21.6±0.2
2%PAED	NO	21.9±2	15	15	21.7±0.2
5%PAED	NO	22.8±2	15	15	22.0±0.2
10%PAED	NO	24.1±2	15	15	22.6±0.2
5%PAED +10%melamine	NO	24.9±2	15	15	22.0±0.2
10%PAED +5%melamine	NO	24.3±2	15	15	22.5±0.2
10%PAED +10%melamine	NO	28.3±2	15	15	22.5±0.2

As can be seen from Table 5, the addition of PAED to the FPUF increased the LOI values and the LOI values are slightly lower compared to TCPP treated foams. All PAED treated foams failed the BKZ test even at 10% concentration. Compared to the blank foam, there was some improvement in flame retardancy of FR PAED containing foams, as the time that was needed for complete burning of the foams increased. An addition of melamine (co-additive to PAED) led to a decreased burning rate but did not really improve the flame performance of the foams either.

Table 6 shows the BKZ and LOI results of PAPD treated foams. Unlike PAED treated foams, these passed the BKZ test even at a concentration of 1% FR. The LOI values were also higher than those for PAED treated foams and were comparable to the LOI values achieved with TCPP containing foams. As was observed in case of TCPP and PAED, the addition of melamine had a detrimental effect on the fire performance of the PAPD foams.

Table 6. Effect of PAPD and melamine as flame retardants for FPUFs

FR	***BKZ test (15cm×5cm×0.6cm)***				***LOI** (O₂%)*
	PASS/NO	*Time (s)*	*1st Burned Height (cm)*	*2nd Burned Height (cm)*	
Blank	NO	20.6±2	15	15	20.5±0.2
1%PAPD	PASS	14.1±2	6.4±1	12.5±2	21.5±0.2
2%PAPD	PASS	12.8±2	6.1±1	11.8±2	21.8±0.2
5%PAPD	PASS	11.6±2	5.6±1	11.1±2	22.4±0.2
10%PAPD	PASS	10.1±2	5.3±1	9.8±2	23.0±0.2
5%PAPD +10%melamine	NO	25.0±2	15	15	22.2±0.2
10%PAPD +5%melamine	NO	23.2±2	15	15	22.9±0.2
10%PAPD +10%melamine	NO	31.2±2	15	15	22.8±0.2

All foams containing melamine as additive failed the BKZ test and burned completely. The burning rate was again slower as compared to the melamine free foams. The LOI values were again not effected by the addition of melamine.

The flammability tests revealed that the bidentate Phosphoramidate PAPD **4** exhibited better flame retardant properties than the similar PAED **3** and comparable results to the commercially available TCPP. In order to find an explanation for these results and the fact that the co-addition of melamine led to a dramatic deterioration of the flame retardant properties, some more detailed analyses were performed with the FR foams.

The organophosphorus treated foams were subjected to thermal decomposition studies like TGA and PCFC analyses. Figure 5 shows the heat release rate profile for the virgin foam and the foams treated with 5% of FR measured by pyrolysis combustion flow calorimeter (PCFC). It can be seen from the figure 5 that the foams primarily decompose in two stages. The maximum heat release rate for stage 1 (200-300 °C) was small as compared to stage 2 (350-450 °C). All three flame retardants catalyzed the first stage of decomposition which could be seen since it occurred at lower temperatures as compared to the untreated foam.

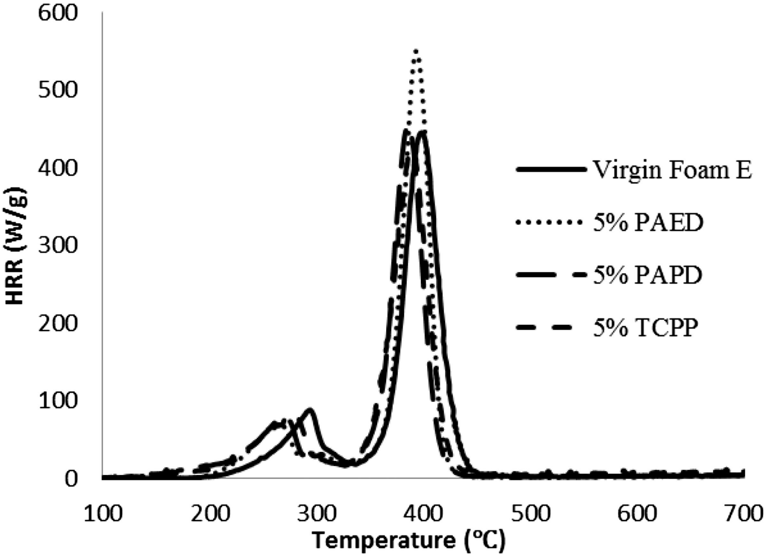

Figure 5. Heat release rates of Foams with and without any FR (heating rate 1K/sec).

The second decomposition stage was also shifted to slightly slower temperatures - 4-9°C. Looking at the maximum heat release rate, MHRR, of the second stage one could clearly see that PAED treated foam had a much higher heat release rate as compared to the other three foams, which could indicate the reason for failing the BKZ test. The heat release rates of the virgin, TCPP and PAPD treated foams were all in a similar range. The detailed pyrolysis data are tabulated in Table 7. It can be seen from this table that the addition of TCPP and PAPD had only a negligible effect on the THC values of the foam whereas the addition of PAED led to a reduction of THC of about 7%. The absence of any char residues indicated strongly possible gas phase action.

Figure 6 shows the thermogravimetric analysis (TGA) data performed in air for the virgin foam and FR treated foams. The TGA showed that the thermal decomposition of the virgin foam occurred in roughly three stages where stage 1 started at around 220 °C, stage 2 at around 320 °C and stage 3 at around 380 °C. After the third decomposition stage (>550°C) there was no detectable char residue left.

Table 7. PCFC data for foams

Foam E	*T_M 1 (°C)*	*MHRR 1 (W/g)*	*T_M 2 (°C)*	*MHRR 2 (W/g)*	*THC 1 (J/g)*	*THC 2 (J/g)*	*THC (J/g)*	*Char (%)*
0% FR	296	72	399	470	4747	18841	23587	0
5%TCPP	278	80	390	434	5634	18081	23715	0
5%PAED	266	70	394	551	4492	17595	22086	0
5%PAPD	272	74	395	461	4913	18799	23712	0

T_M 1: Temperature for maximum heat release rate (stage 1), MHRR 1: Maximum heat release rate (stage 1), THC 1: Total heat of combustion (stage 1), T_M 2: Temperature for maximum heat release rate (stage 2), MHRR 2: Maximum heat release rate (stage 2), THC 2: Total heat of combustion (stage 2), THC: Total Heat of combustion (stage 1 + stage 2).

In accordance with the PCFC measurements the TGA measurements of the FR treated foams showed that the first decomposition stage was shifted to lower temperatures due to the acid catalyzed decomposition of the urethane bond (Figure 6).

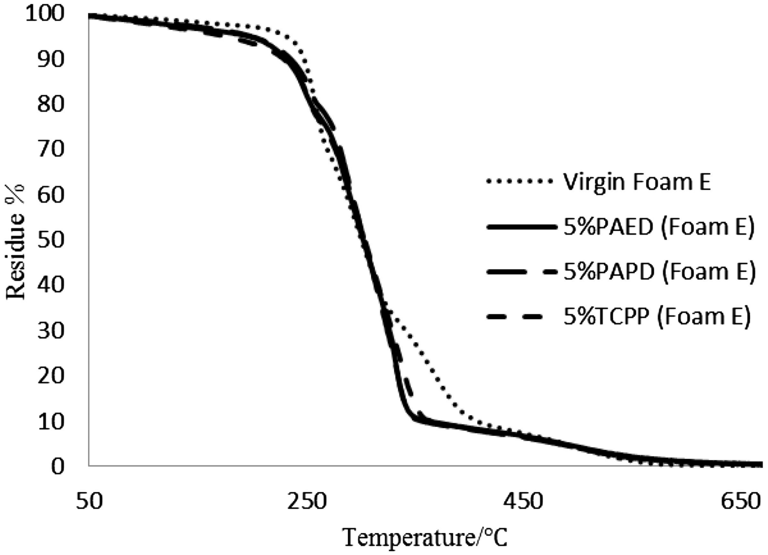

Figure 6. Thermal decomposition of Foam E with 5% of FR's under air (10 k/min heating rate).

Furthermore one could see that the decomposition of FR treated foams proceeded only via two stages. The curves of the three FR treated foams appeared to be very similar and the first stage started at around 130°C and the second stage at around 350°C. There was also no detectable char residue for FR treated foams which confirmed the PCFC results and emphasizes the gas-phase action of the FRs.

In order to determine why melamine caused such an antagonistic effect, PCFC and TGA analyses were performed with the appropriate foams. The results of these analyses are compared with the PAPD + melamine treated foams.

Figure 7 shows the PCFC measurement curves of melamine, PAPD and PAPD + melamine treated foams. One can clearly see that the melamine treated foam had a much lower maximum heat release rate as compared to the PAPD treated one. Foams with additives, PAPD and melamine, showed a maximum heat release rate that was very similar to the one with only melamine. It seems likely that the combination of both FRs resulted in a slight shift of the temperature of the maximum heat release rate to higher temperatures. The most obvious difference between the PCFC curves could be found in the range of 100 to 330°C. The foams with both additives showed a more complex multistep degradation which did not occur when both additives were added separately. This could give a first hint why foams with melamine as co- additive failed the BKZ test.

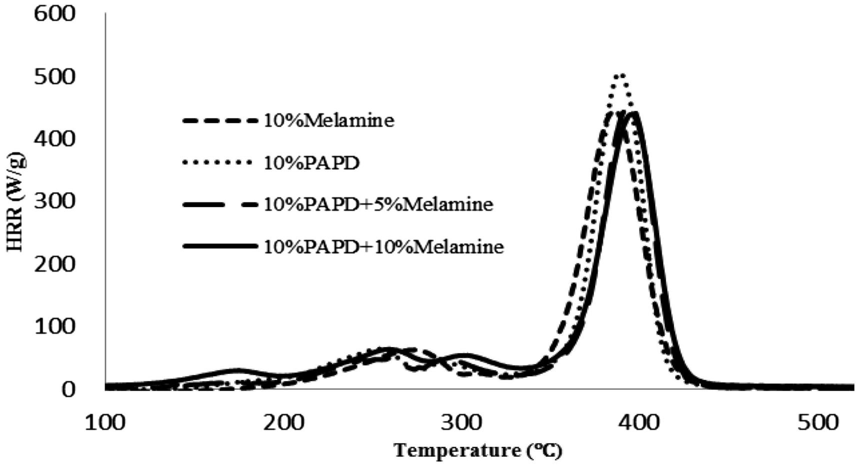

Figure 7. PCFC analysis of PAPD and PAPD + melamine treated foams (heating rate 1K/sec).

This complex multistep decomposition could not be detected with the TGA measurements of the investigated foams, figure 8. In accordance with the PCFC measurements, the PAPD + melamine treated foams decomposed at lower temperature and no char residue could be detected at a temperature higher than 600°C.

The TGA curves of the foams with both additives showed a very smooth shape in the temperature range between 150 and 350°C and did not provide any explanation for the antagonistic effect of melamine.

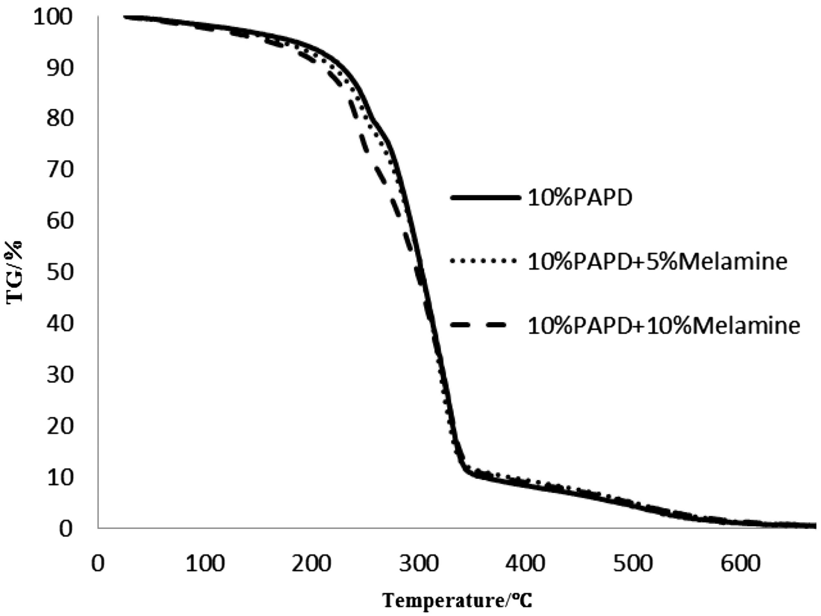

Figure 8. TGA analysis of PAPD and PAPD + melamine treated foams under air (10 k/min heating rate).

A possible explanation for the antagonistic effect of melamine with TCPP and phosphoramidates can be drawn from Scheme 2. The phosphorus based FRs support the first stage of decomposition of the FPUF by acid catalyzed polyurethane bond scission. This faster depolymerization leads to a faster melting away of the FPUF from the flame and resulting in a better flame retardant effect. The addition of melamine may interfere with this mode of action by neutralization of acidic species and thus retarding a faster melting away from the flame.

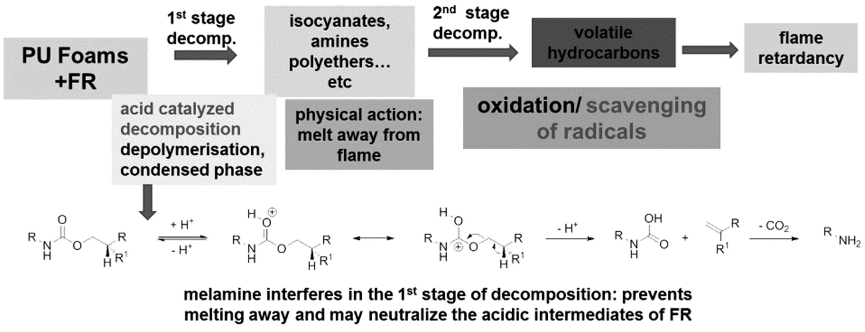
PU Foams
+FR
1st stage
decomp.
isocyanates,
amines
polyethers…
etc
2nd stage
decomp.
volatile
hydrocarbons
flame
retardancy
acid catalyzed
decomposition
depolymerisation,
condensed phase
physical action:
melt away from
flame
oxidation/ scavenging
of radicals
+ H+
- H+
- H+
- CO2
R
NH2
melamine interferes in the 1st stage of decomposition: prevents
melting away and may neutralize the acidic intermediates of FR

Scheme 2. Flame retardant action in FPUF

Subsequently this inhibition of fast melting away from the flame results in a much worse flame retardant performance of the FPUF.

Conclusion

In the first part of this paper we have reviewed the recent scientific developments in flame retardancy in FPUF over the last three years. Different systems, like inorganic and/or organic fillers as well as phosphorus-based FRs, have been used in scientific studies on flame retardant FPUF. Inorganic and organic fillers, such as ATH or melamine, need to be used at relatively high loading up to 60 phpp to impart good flame retardant properties. These high loadings of solid particles result in problems in the foam manufacturing process which results in a decrease of mechanical properties. Better results could be achieved by a combination of different materials, like EG together with melamine, cellulose or liquid phosphorus based flame retardants. By means of these synergistic combinations, the flame retardant as well as the mechanical properties of the resulting FPUF could be significantly improved. The synthesis and application of novel organoboron and organophosphorus FRs in FPUF was also reported in this period. These compounds showed very promising results regarding their flame retardant action and compatibility with the foam manufacturing process.

In the second part of this article we present our efforts on the synthesis and application of halogen free flame retardants PAED and PAPD. PAPD has similar fire performance characteristics as compared to TCPP when incorporated in FPUF. The prepared FPUF passed the BKZ fire test when only 1% TCPP or PAPD were used as FRs. In contrast to that PAED had no beneficial influence on the flame retardancy of the FPUF with regard to the BKZ test. All PAED treated foams even with 10% failed the BKZ test. PCFC measurements showed that FR foams with PAED as FR have a much higher maximum heat release rate as compared to TCPP-, PAPD treated and the virgin foam. TGA measurements of all foams exhibited that the investigated organophosphorus compounds catalyzed the first stage of decomposition (urethane bond scission) which was shifted to lower temperatures. Investigation on the use of melamine as co-additive revealed that melamine had a detrimental effect on fire performance of foams. All foams treated with melamine as co-additive failed the BKZ test and burned completely although the burning rate was significantly reduced. PCFC measurements of PAPD and melamine treated foams showed a complex multistep decomposition behavior in a temperature range of 150-350°C. Further studies on the interaction of phosphoramidates and melamine in FPUF need to be undertaken in future to ascertain the real cause of this antagonistic effect.

Acknowledgments

The authors would like to thank FoamPartner, Switzerland, for steady material supply knowledge transfer and financial support. This research was also funded by CTI, Commission for Technology and Innovation Switzerland. Furthermore may thanks go to Elisabeth Michel for great support in analytical measurements.

References

1. Adam, N.; Avar, G.; Blankenheim, H.; Friederichs, W.; Giersig, M.; Weigand, E.; Halfmann, M.; Wittbecker, F.-W.; Larimer, D.-R.; Maier, U.; Meyer-Ahrens, S.; Noble, K.-L.; Wussow, H.-G. *Polyurethanes. Ullmann's Encyclopedia of Industrial Chemistry*; Wiley-VCH Verlag GmbH & Co. KGaA: New York, 2005; p 546.
2. Volker, B. http://www.sinopu.com/lunwen/119-125.doc.
3. *American Chemistry Council*; http://www.polyurethane.org/s_api/sec.asp?CID=908&DID=3621.
4. Chattopadhyay, D. K.; Webster, D. C. *Progr. Polym. Sci.* **2009**, *34*, 1068–1133.
5. Levchik, S. V.; Weil, E. D. *Polym. Int.* **2004**, *53*, 1585–1610.
6. Chung, Y.; Kim, Y.; Kim, S. *J. Ind. Eng. Chem.* **2009**, *15*, 888–893.
7. *Risk Assessment Report on Tris(2-Chlor-propyl) Phosphate (TCPP), Scientific Committee on Health and Environmental Risks, Environmental Part*, EINECS No. 237-158-7; 2007.
8. Formicola, C.; De Fenzo, A.; Zarrelli, M.; Frache, A.; Giordano, M.; Camino, G. *Polym. Lett.* **2009**, *3*, 376.
9. Plentz, R. S.; Miotto, M.; Schneider, E. E.; Forte, M. C.; Mauler, R. S.; Nachtigall, S. M. B. *J. Appl. Polym. Sci.* **2006**, *101*, 1799.
10. König, A.; Malek, A.; Fehrenbacher, U.; Brunklaus, G.; Wilhelm, M.; Hirt, T. *J. Cell. Plast.* **2010**, *46*, 18.
11. König, A.; Kroke, E.; Wilhelm, M.; Hirt, T. *J. Fire. Sci.* **2009**, *27*, 187.
12. Kageoka, M.; Tairaka, Y.; Kodama, K. *J. Cell. Plast.* **1997**, *33*, 219.
13. Falke, P.; Hendreich, R.; Jackson, G.; Schroeder, H. J.; Schuster, M. BASF-AG Germany, Ger. Offen., DE 2000-10047024, 2002.
14. Lutter, H.-D.; Zschische, R.; Gabbert, H.-J.; Haase, V.; Fimmel, K. BASF AG Germany, Eur. Pat. Appl., EP 91-117703, 1992.
15. Price, D.; Liu, Y.; Milnes, G. J. *Fire Mater.* **2002**, *26*, 201.
16. Bashirzadeh, R.; Gharehbaghi, A. *J. Cell. Plast.* **2010**, *46*, 129.
17. Wolska, A.; Gozdzikiewicz, M.; Ryszkowska, J. *J. Mater. Sci.* **2012**, *47*, 5693.
18. Gharehbaghi, A.; Bashirzadeh; Ahmadi, Z. *J. Cell. Plast.* **2011**, *47*, 549.
19. Wolska, A.; Gozdzikiewicz, M.; Ryszkowska, J. *J. Mater. Sci.* **2012**, *47*, 5627.
20. Benin, V.; Durganala, S.; Morgan, B. M. *J. Mater. Chem.* **2012**, *22*, 1180.
21. König, A.; Kroke, E. *Polym. Adv. Technol.* **2010**, *22*, 5.
22. Schäfer, A.; Seibold, S.; Lohstroh, W.; Walter, O.; Döring, M. *J. Appl. Polym. Sci.* **2007**, *105*, 685.
23. Artner, J.; Ciesielski, M.; Ahlmann, M.; Walter, O.; Döring, M.; Perez, R. M.; Altstädt, V.; Sandler, J. K. W.; Schartel, B. *Phosphorus Sulfur* **2007**, *182*, 2131.
24. Granzow, A. *J. Am. Chem. Soc.* **1978**, *11*, 177.
25. Lefebvre, J.; Le Bras, M.; Bastin, B.; Paleja, R.; Delobel, R. *J. Fire Sci.* **2003**, *21*, 343.

26. Lewin, M.; Weil, E. *Fire Retardant Materials*; Horrocks, A. R., Price, D., Eds.; Woodhead Publishing Limited: Cambridge, U.K., 2001; pp 32–34.
27. Bastin, B.; Paleja, R.; Lefebvre, J. *J. Cell. Plast.* **2003**, *39*, 323.
28. Koenig, A. *Flame retardancy for flexible polyurethane foams*. Ph.D. Thesis, TU Bergakademie Freiberg, 2009.
29. König, A; Kroke, E. *Fire Mater.* **2012**, *36*, 1.
30. Artner, J.; Ciesielski, M.; Ahlmann, M.; Walter, O.; Döring, M. *Arkivoc* **2007**, *3*, 132.
31. Liang, S.; Neisius, N. M.; Mispreuve, H.; Naescher, R.; Gaan, S. *Polym. Degrad. Stab.* **2012** DOI:10.1016/j.polymdegradstab.2012.07.019.
32. Gaan, S.; Sun, G.; Hutches, K.; Engelhard, M. H. *Polym. Degrad. Stab.* **2008**, *93*, 99.

Chapter 19

Synthesis of Phosphate-Urethane Block Copolymers: Effect of Bound Phosphorus in the Soft Moiety of Block Copolymers on Thermal and Flame Retardant Characteristics of Polyphosphate Polyurethane Block Copolymers

Ramazan Benrashid[1] **and Gordon L. Nelson***

Department of Chemistry, Florida Institute of Technology,
150 West University Boulevard, Melbourne, Florida 32901
[1]Current Address: 3644 Summit Trail Court, Carlsbad, California 92010
***E-mail: nelson@fit.edu**

Oligomers with a phosphorus moiety were prepared. Phosphate urethane block copolymers were made with these phosphorylated oligomers, diisocyanate and a diol as chain extender. Gel permeation chromatography (GPC) was performed on both the oligomeric materials and on block copolymers. Differential scanning calorimetry (DSC) shows a glass transition above room temperature and two melting temperatures for hard and soft blocks of these block copolymers. Thermo-gravimetric analysis results show these phosphorylated block copolymers have a tendency to form char when they were heated in nitrogen and air. Weight residue at 700 °C in air was higher for phosphate polyurethanes than ether urethane block copolymers without phosphate. Electron scanning microscopy (ESM) and electron dispersive x-ray spectroscopy (EDX) do not support the segregation of phosphorus onto the surface as is found with silicone block copolymers in polyurethanes. Oxygen indices of these materials were measured. The results

In Fire and Polymers VI: New Advances in Flame Retardant Chemistry and Science; Morgan, A., et al.;
ACS Symposium Series; American Chemical Society: Washington, DC, 2012.

show that even with a low level of phosphorus in the building blocks of the copolymers, some of these block copolymers were resistant to ignition and some had higher OI values compared to control and reference materials. Halogen in the building blocks of the copolymer showed "synergistic effects." However, some of these block copolymers containing phosphorus and halogen did not show significant improvement in flame retardancy given the low phosphorus content (under 2%). Based on flammability testing (OI results) these block copolymers were categorized as a) ignition resistant, b)higher Oxygen Index materials, and c) comparable to non-phosphorylated controls. These materials showed less flame retardancy compared to siliconated polyurethane block copolymers previously reported.

Introduction

Phosphorus containing compounds as additives or as part of the backbone in polymeric materials are considered as flame retardant materials. These flame retardants include inorganic ammonium phosphate, organophosphates, chlorophosphates. bromophosphates. phosphine oxides and red phosphorus. Phosphorus containing flame retardants can have an effect on flammability through a condensed phase mechanism or a vapor phase effect or a combination of the two. The mechanism of flame retardancy of phosphorus compounds depends upon the type of chemical and also polymer type, e.g., in some cases phosphate compounds decompose in the condensed phase to form phosphoric acid or a polyphosphoric acid which can form a viscous liquid or a ceramic on the surface, or may react with the polymer and form an insulating char which interferes with fire progress. In these cases the substrate will be protected from heat and oxygen, therefore, preventing any further decomposition of material to produce fuel to feed the fire. Formation of a dense carbon char or inorganic phosphate on the polymer surface leads to protection of the substrate from heat and oxygen, which causes decomposition of polymers to smaller fragments and volatiles and combustion of these fragments. For example triarylphosphate is a flame retardant filler for modified polyphenylene oxide. This additive functions with both vapor phase and condensed phase characteristics. In the case of fire it vaporizes and forms radicals which hinder and inhibit the fire by interfering with the combustion process and forms char on the surface of the polymer to protect it from heat and further decomposition.

Review of the literature reveals that phosphorus compounds as an additive or as part of a backbone are well known and have been studied for decades (*1–45*). Phosphorus materials can significantly contribute to thermal stability and flame retardancy of polymers. Such polymers have a variety of applications in household and office equipment. Flame retardant chemicals recently have become controversial. Much of the recent controversy about flame retardants has its origins in the ability of monomeric flame retardants to migrate from the product containing flame retardant additives out into the environment. Polymeric additives would either not do that or clearly to a much less extent. Continuing our interests in polyurethane flame retardancy (*46–49*), the purpose of the current work was to synthesize phosphate urethane block copolymers of a variety of structures and study their chemical thermal stability and flame retardancy characteristics. Given the small quantities, cast films and powders were characterized by oxygen index (*50*, *51*).

Experimental Materials

Dicyclohexylmethane-4,4′-diisocyanate (Desmodur W) $H_{12}MDI$, diphenylmcthane 4,4′-diisocyanate MDI, toluene diisocyanate TDI, and isophrone diisocyanate IPDI were supplied by Bayer Corp, 1 ,6-hexanediol (HDO) was supplied by the Aldrich Chemical Co. Phosphorylated diol FRD was supplied by FMC. Phosphorylated polyol (Vireo M.WT 545) was supplied by Albright & Wilson. Dimethylacetamide (DMAC) was stirred over MgO for one week, then distilled under vacuum and kept over molecular sieves 4, and under a nitrogen atmosphere. Methylene chloride was refluxed over CaH_2 and distilled immediately before use. Tetrahydrofuran (THF) and 1,4-dioxane were distilled from benzophenone kctyl immediately before use.

Synthesis of Oligomeric Hexafluoroisopropyl 4,4′-bisphenol-A-benzyl phosphate (General Procedure)

Phenyl phosphonic dichloride (15 g, 0.071 mol) was dissolved in 50 mL dried dichloromethane and slowly added dropwise (1 hr) to 28.7 g (0.085 mol) hexafluoroisopropyl 4,4′-bisphenol-A and 15.05g (0.149 mol) triethyleneamine in 200 mL dichloromethane under nitrogen atmosphere at room temperature. This solution was refluxed for 5 hrs. The solution was kept under nitrogen overnight at room temperature. The triethylammonium chloride was removed by filtration. The dichloromethane solution was washed with HCI(l.O N) and then with water at neutral pH. The solution was dried over anhydrous magnesium sulfate. The solution was filtered and the dichloromethane was evaporated at reduced pressure. The product was dried at room temperature under vacuum for 24 hrs. Weight of product after drying was 19.0g. Molecular weight was determined by GPC. Mn was 1393 and polydispersity was 1.73. Scheme 1A shows the general method of oligomer synthesis.

Synthesis of Phosphate Urethane Block Copolymer (General Procedure)

$H_{12}MDI$ (16.5 g 0.063 mol) was dissolved in 20 mL dichloromethane and added to 8g (0.003) of M3-5 oligomer (Mwt.2403) and 7.50 g (0.06 mol) 1.6-hexanediol was dissolved in 120 mL of dried THF. Eight drops of dibutyltin dilaurate were added. The reaction mixture was stirred by a mechanical stirrer at 56-70 °C (oil bath) under nitrogen atmosphere for 14 hrs. The completeness of reaction was monitored by FT-IR for disappearance of the isocyanate peak at 2765 cm-1. The viscous solution was cast as a film on glass plates by using an applicator. The molecular weight of the block copolymer using Gel Permeation Chromatography (GPC) was 27,265. Scheme 1B shows the general reaction for block copolymer synthesis. Table I presents examples of the oligomers. Table II presents the synthetic conditions which were used for select block copolymers.

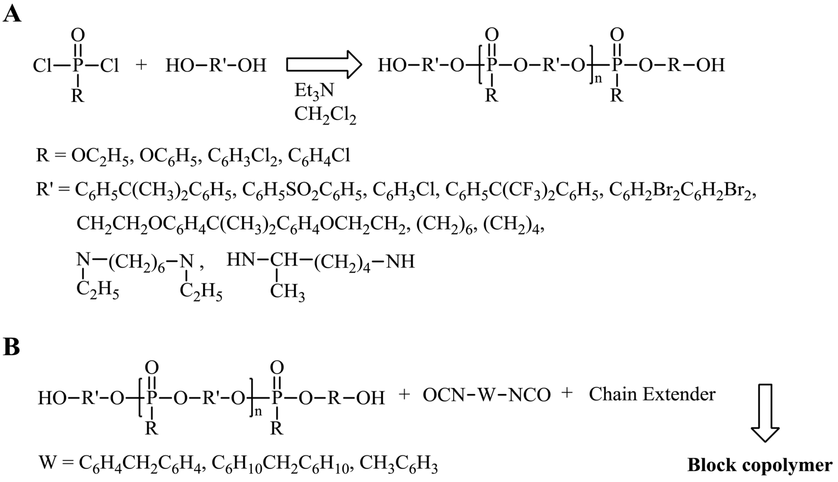
A
Cl–P(O)(R)–Cl + HO–R'–OH
Et3N
CH2Cl2
HO–R'–O–[P(O)(R)–O–R'–O]n–P(O)(R)–O–R–OH
R = OC2H5, OC6H5, C6H3Cl2, C6H4Cl
R' = C6H5C(CH3)2C6H5, C6H5SO2C6H5, C6H3Cl, C6H5C(CF3)2C6H5, C6H2Br2C6H2Br2,
CH2CH2OC6H4C(CH3)2C6H4OCH2CH2, (CH2)6, (CH2)4,
N(C2H5)–(CH2)6–N(C2H5), HN–CH(CH3)–(CH2)4–NH
B
HO–R'–O–[P(O)(R)–O–R'–O]n–P(O)(R)–O–R–OH + OCN–W–NCO + Chain Extender
W = C6H4CH2C6H4, C6H10CH2C6H10, CH3C6H3
Block copolymer

Scheme 1. 1A and 1B

Characterization

FT-IR Analysis

FT-IR spectra were obtained on a Nicolet Magna IR 550 spectrophotometer. A Spectro Tee Attenuated Total Internal Reflectance (ATR) with a ZnSe crystal at the incident angle of 45 was mounted on the attachment as an internal reflection was used. The resolution and number of scans was 4 cm-1 and 512 respectively. A Spectra-Tech Diffuse Reflectance attachment also was used for surface studies. The reference spectra were obtained from a silver mirror.

^{1}HNMR and ^{13}CNMR

^{1}HNMR and ^{13}CNMR spectra were performed on a Brucker AMX-360 instrument, deutrated chloroform was used as the solvent.

Table I. List of Oligomers Synthesized for this Study

No	Oligomer ID	Composition
1	M2-19	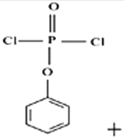 + $HOCH_2CH_2CH_2OH$
2	M3-1	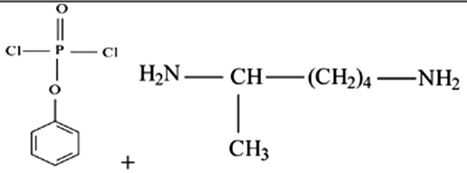
3	M3-2	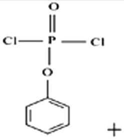 + $HO_2HC— (CH_2)_4 — CH_2OH$
4	M3-3	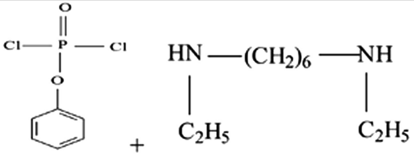
5	M3-4	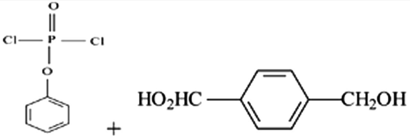
6	M3-5	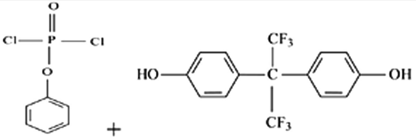
7	M3-6	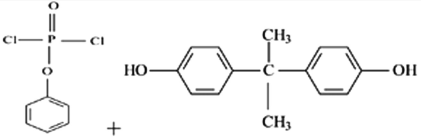

Continued on next page.

Table I. (Continued). List of Oligomers Synthesized for this Study

8	M3-7	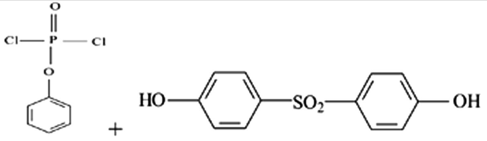
9	M3-8	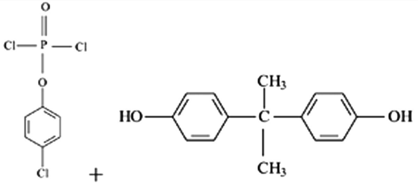
10	M3-9	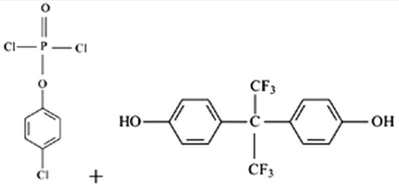
11	M3-10	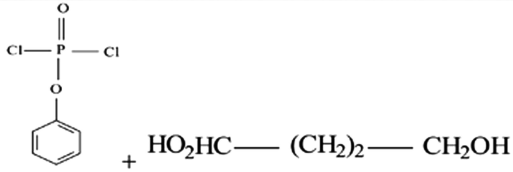
12	M3-11	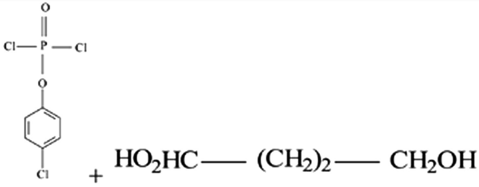
13	M3-12	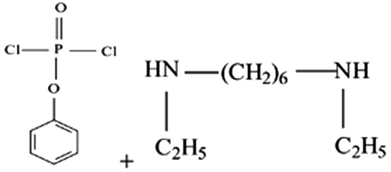
14	M3-13	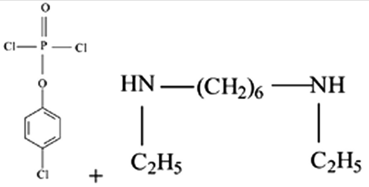

Continued on next page.

Table I. (Continued). List of Oligomers Synthesized for this Study

No	Oligomer ID	Composition
1	M4-1	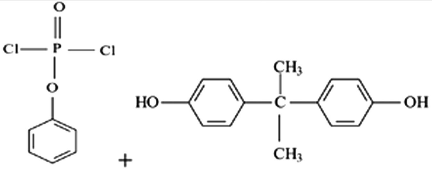
2	M4-2	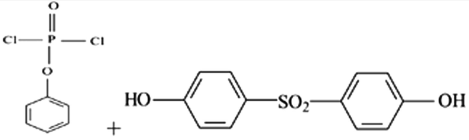
3	M4-3	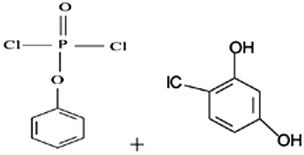
4	M4-4	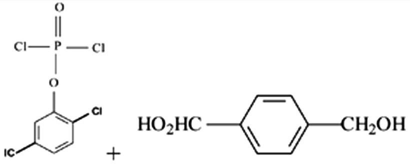
5	M4-5	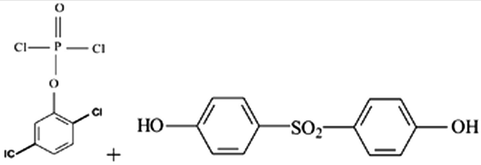
6	M4-6	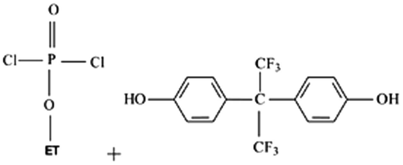
7	M4-7	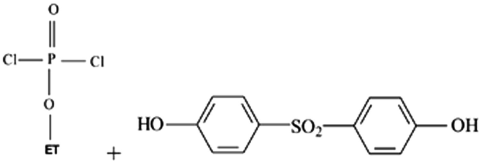

Continued on next page.

Table I. (Continued). List of Oligomers Synthesized for this Study

8	M4-8	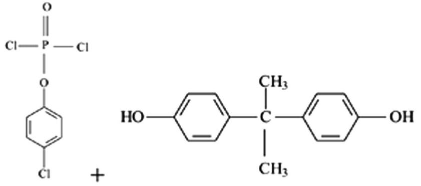
9	M4-9	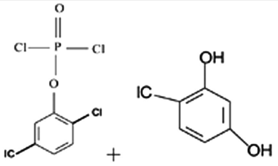
10	M4-10	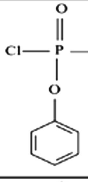 + FRD Phosphorylated diol
11	M4-11	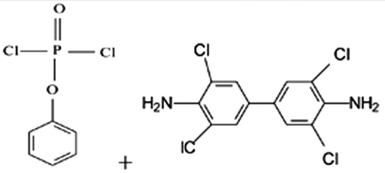
12	M4-12	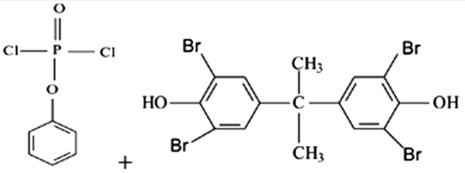
13	M4-13	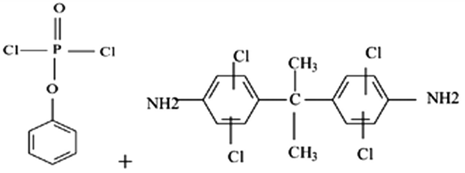
14	M4-23	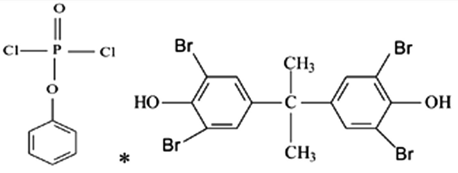

Table II. Examples of Block Copolymers Synthesized for this Study

Block Copolymer#	*Percent Soft Segment*	*Oligomer (g)*	*Diisocyanate (g)*	*Chain Extender (g)*	*Solvent THF/CH_2Cl_2*	*Reaction Time RT/80-85 °C*
M3-14	50	M3-1, 5.4	Des-W, 3.4	Hexanediol, 1.6.1	20/20	24/24
M3-15	25	M3-5, 8.0	Des-W, 16.5	Hexanediol, 16.5	120/20	24/24
M3-16	10	M3-5, 4.0	Des-W, 24.8	Hexanediol, 11.2	120/20	24/16
M3-17	35	M3-5, 9.0	Des-W, 11.5	Hexanediol, 5.2	120/20	24/20
M3-18	5	M3-5, 2.0	Des-W, 26.8	Hexanediol, 11.2	120/20	20/24
M3-20	10	M3-5, 2.0	IPDI, 11.8	Hexanediol, 6.2	100/20	25/35
M3-21	20	M3-5, 3.30	IPDI, 8.6	Hexanediol, 4.6	100/20	42/24
M3-22	5	M3-6, 6.0	Des-W, 26.2	Hexanediol, 11.8	100/20	38/20
M3-23	10	M3-6, 5.0	Des-W, 31.0	Hexanediol, 14.0	140/20	24/24
M3-24	15	M3-6, 6.0	Des-W, 22.4	Hexanediol, 10.6	140/20	24/24
M3-25	20	M3-6, 8.0	Des-W, 22.0	Hexanediol, 10.0	140/20	44/36
M3-26	25	M3-6, 5.0	Des-W, 10.3	Hexanediol, 4.7	120/20	44/24
M3-27	10	M3-9, 5.0	Des-W, 31.0	Hexanediol, 14	120/20	24/24
M3-28	20	M3-9, 8.0	Des-W,22.0	Hexanediol, 10	140/20	24/24
M3-29	30	M3-9, 11.0	Des-W, 17.9	Hexanediol, 8.1	120/20	24/44
M3-30	5	M3-7, 2.0	Des-W, 26.2	Hexanediol, 11.8	140/20	48/50

Continued on next page.

Table II. (Continued). Examples of Block Copolymers Synthesized for this Study

Block Copolymer#	*Percent Soft Segment*	*Oligomer (g)*	*Diisocyanate (g)*	*Chain Extender (g)*	*Solvent THF/CH_2Cl_2*	*Reaction Time RT/80-85 °C*
M3-31	20	M3-9, 8.0	Des-W, 22	Hexanediol, 10	120/20	24/44
M3-22	10	M3-7, 5.0	Des-W, 31.0	Hexanediol, 14.0	140/20	48/50
M3-33	10	M3-10, 5.0	Des-W, 31.0	Hexanediol, 14.0	140/20	54/50
M3-34	10	M3-11, 5.0	Des-W, 31.0	Hexanediol, 14	140/20	48/75
M3-35	25	M3-10, 8.0	Des-W, 16.5	Hexanediol, 7.5	140/20	58/24
M3-36	25	M3-11, 8.0	Des-W, 16.5	Hexanediol, 7.5	140/20	92/95
M3-37	10	M3-2, 5.0	Des-W, 31.0	Hexanediol, 15.0	140/40	24/58
M3-38	10	M2-19, 5.0	Des-W, 31.0	Hexanediol, 14.0	140/50	48/60
M3-39	25	M2-19, 8.0	Des-W, 16.5	Hexanediol, 7.5	140/20	24/100
M3-40	10	M2-19, 5.0	Des-W, 23.0	Hexanediol, 22	140/20	14/120
M3-41	10	M3-4, 5.0	Des-W, 31.0	2,3-Dibromo-1,4-butanediol	140/40	48/26
M3-43	10	M3-8, 5.0	Des-W, 31.0	Hexanediol, 14.0	140/40	50/78

Gel Perameation Chromatograhy (GPC)

GPC was performed on a Water Associate GPC system with an Acott 728 auto-sampler using a Pheodyne injector, a Waters model 510 I-IPLC solvent delivery pump, three ultrastragel column of minimal pore size 500, 103, and 104A, and a Waters model 410 differential refractometer detector operating at 33 °C. Tetrahydrofuran (THF), freshly distilled from calcium hydride, served as the mobile phase. Sample concentrations were approximately 0.5% (w/w) in THF, with an injection volume of 50 microL. Data acquisition and analysis were achieved using Polymer Laboratories PL Caliber software. Tables III and IV exhibit the Mn, Mw, and polydispersity for some of the oligomers and some block copolymers synthesized.

Thermal Analysis

A TA Instruments 2910 Differential Scanning Calorimeter with modulated capability was used to determine the glass temperatures (Tg) and melting points of the block copolymers. Scans were run at a rate of 5 °C per minute, with a modulation of ±0.5 per 80 cycles per second in helium. Samples were analyzed in a crimped aluminum pan with a lid. An empty pan with a lid served as a reference. The purge rate was 34 mL/min helium and the heating rate was 5 °C/min from -50 to 180 °C. Selected glass transition temperatures (Tg) and melting temperatures (mT) are exhibited in Table V.

Thermoxidative stabilities were determined on a TA Instruments 250 High Resolution Thermogravimetric Analyzer (TGA). The sample was heated in air or nitrogen from ambient temperature to 950 °C. The gas f1ow rate was 40 cm^3 per minute and resolution was set at 4.0. Ten percent, 50% weight loss and weight residue at 700 °C are exhibited in Table VI.

Scanning Electron Microscopy (SEM) and Energy Dispersive Spectroscopy (EDS)

SEM and EDS and HDS analyses were performed on a model S-2700 Hitachi Scanning Electron Microscope with attached Kevex light element detector. Electron beam energies were 20Kev. Data were collected from a scanned region of approximately 100 X 100 square micrometers. The x-ray detector was operated in the thin window mode at less than 20 percent dead-time. A Denton Desk II Sputter Coater with a Pd/Au target was employed for coating SEM samples to reduce surface charging affects. EDX spectra were taken for both sides of a cast film. EDX spectra were taken of the phosphorylated block copolymer before and after combustion and char formation. EDX shows a higher peak ratio for phosphorus for the char compared to the material before combustion since most of organic layer burned out. EDX spectra of front and back of a phosphorylated block copolymer film does not support a high concentration of phosphorus on the film surface, indicating a lack of high segregation of the phosphate moiety on the surface.

Table III. Molecular Weight of Example Oligomers by GPC

Sample #	*Mn*	*Mw*	*Polydispersity*
M3-2	482	515	1.07
M3-4	460	479	1.04
M3-5	1393	2403	1.73
M3-6	1091	1692	1.55
M3-7	1433	2211	1.54
M3-8	1273	2347	1.84
M3-9	1549	3146	2.03
M3-10	404	407	1.00
M3-11	426	430	1.01
M4-7	1583	2251	1.42
M4-12	1023	1590	1.55
M4-23	1380	2163	1.57

Table IV. GPC of Example Block Copolymers by GPC

Sample #	*Mn*	*Mw*	*Polydispersity*
M3-15	5923	27265	4.6
M3-16	10910	31949	2.9
M3-19	5195	16237	3.1
M3-22	9019	20734	2.3
M3-24	3984	11214	2.8
M3-26	21365	25638	1.2
M3-27	5947	16414	2.8
M3-32	7566	21680	2.9
M3-33	5652	14695	2.6
M3-34	7843	24712	3.2

Table V. DSC Characteristics of Block Copolymers

Sample #	*Tg °C*	*mT1 °C*	*mT2 °C*
M3-15	58.7	113.6	165
M3-15	46.5	96.0	170
M3-18	49.1	106.3	-
M3-19	56.9	112.0	-
M3-22	38.1	95.3	202.0
M3-23	34.9	96.4	160.2
M3-26	61.5	112.0	-
M3-31	59.0	112.0	-
M3-32	26.0	93.6	154.7
M3-33	30.3	96.6	218.3
M3-34	38.3	97.6	249.7
M3-47	-	99.4	-
M4-62 (Control)	48.5	103.2	-

Table VI. Thermal Analysis of Block Copolymers in Nitrogen and (Air)

Polymer #	***Temperature C related to 10% weight loss***	***Temperature C related to 50% weight loss***	***% Weight at 700 °C***
M3-15	310.0(316.4)	348.6(359.7)	1.8(1.8)
M3-18	290.9(310.1)	351.0(358.2)	0.5(0.5)
M3-19	311.9(319.7)	352.8(360.6)	0.4(1.5)
M3-22	274.8(290.1)	301.7(317.1)	0.8(3.2)
M3-23	279.1(291.5)	306.2(311.7)	1.8(5.1)
M3-25	291.4(292.9)	308.2(316.3)	3.4(9.5)
M3-26	282.5(287.6)	306.2(340.9)	3.8(11.6)
M3-31	302.9(318.8)	355.8(377.4)	0.0(2.5)
M3-32	268.0(268.4)	309.7(341.6)	2.4(4.0)
M3-33	268.3(270.4)	303.9(313.2)	0.4(3.7)
M3-34	257.0(264.1)	269.8(314.7)	0.7(3.0)
M4-47	277.9(242.8)	362.0(387.0)	1.4(3.1)
M4-48	271.5(299.5)	374.9(369.2)	1.9(5.3)

Continued on next page.

Table VI. (Continued). Thermal Analysis of Block Copolymers in Nitrogen and (Air)

Polymer #	*Temperature C related to 10% weight loss*	*Temperature C related to 50% weight loss*	*% Weight at 700 °C*
M4-49	271.5(264.5)	389.1(403.5)	1.9(4.6)
M4-62(Control 1)	279.2(284.9)	298.2(329.6)	0.5(0.3)
M4-65(Control 2)	278.0(286.0)	288.9(342.3)	0.4(0.3)

Oxygen Index

Oxygen indices (ASTM 2843) were performed on a original GE oxygen index tester on powders and cast films (*50*, *51*).

Oxygen index measures the ease of the extinction of the materials and the minimum percent of oxygen in a oxygen/nitrogen atmosphere that will just sustain combustion of a top ignited test specimen. A higher OI value is an indication of higher fire resistance for the material tested. OI = (Volume of O_2)/(Volume N_2+Volume O_2)x100. Table VII presents the OI values for different phosphorylated, siliconated and regular block copolymers.

Table VII. Oxygen Index (OI) Values of Block Copolymers and Reference Materials

Block Copoly-mer ID	*Oligomer + Diisocyanate + Chain Extender*				*% Soft Seg-ment*	*OI*
		% P	*% Cl*	*% Br*		
M3-14	M3-12 + Des-W + Hexanediol	5			50	20.1
M3-15	M3-5 + Des-W + Hexanediol	1.6			25	20.0
M3-18	M3-5 + Des-W + Hexanediol	0.33			5	17.7
M3-19	M3-5 + Des-W + Hexanediol	0.98			15	18.6
M3-20	M3-5 + Des-W + Hexanediol	0.65			10	18.6
M3-21	M3-5 + IPDI + Hexanediol	0.65			10	19.8
M3-22	M3-6 + Des-W + Hexanediol	0.43			5	18
M3-23	M3-6 + Des-W + Hexanediol	0.85			10	18.8
M3-24	M3-6 + Des-W + Hexanediol	1.28			15	18.8
M3-25	M3-6 + Des-W + Hexanediol	1.69			20	18.8

Continued on next page.

Table VII. (Continued). Oxygen Index (OI) Values of Block Copolymers and Reference Materials

Block Copolymer ID	*Oligomer + Diisocyanate + Chain Extender*				*% Soft Segment*	*OI*
		% P	*% Cl*	*% Br*		
M3-26	M3-6 + Des-W + Hexanediol	2.1			25	19.5
M3-27	M3-9 + Des-W + Hexanediol	0.61	0.70		10	18.8
M3-28	M3-9 + Des-W + Hexanediol	1.22	1.40		20	19.8
M3-29	M3-9 + Des-W + Hexanediol	1.83	2.10		30	19.8
M3-30	M3-7 + Des-W + Hexanediol	0.37			5	18.8
M3-31	M3-9 + Des-W + Hexanediol	1.22	1.40		20	19.5
M3-32	M3-7 + Des-W + Hexanediol	0.74			10	18.8
M3-33	M3-10 + Des-W + Hexanediol	1.4			10	18.1
M3-34	M3-11 + Des-W + Hexanediol	1.08	1.23		10	19.5
M3-35	M3-10 + Des-W + Hexanediol	3.4			25	19.5
M3-36	M3-11 + Des-W + Hexanediol	2.95	3.38		25	
M3-37	M3-2 + Des-W + Hexanediol	1.2			10	18.8
M3-41	M3-4 + Des-W + 2,3-Dibromo-1,4-butanediol	1.12		64	10	No ignition
M3-42	M3-4 + Des-W + Hexanediol	1.12			10	19.6
M3-43	M3-8 + Des-W + 1,6-Hexanediol	0.77	0.89		10	19.6
M3-44	M3-8 + Des-W + 1,6-Hexanediol	3.08	3.56		40	24.6
M4-14	M4-2 + Des-W + Hexanediol	2.22			30	19.8
M4-15	M4-2 + Des-W + FRD Diol				20	23
M4-18	M4-2 + TDI + Hexanediol	0.74			10	19.5
M4-19	M3-7 + MDI + Hexanediol	0.74			10	19.8
M4-20	M3-8 + TDI + Hexanediol	0.77	0.89		10	18
M4-21	M3-8 + TDI + 2,3-Dibromo-1,4-butanediol	0.77	38.8		10	
M4-22	M3-11 + TDI + Hexanediol	1.18	1.35		10	21.5
M4-24	M3-7 + Des-W + N,N’-Dimethylhexanediamine	0.74			10	19.1
M4-25	M4-7 + Des-W + Hexanediol	0.83			10	18.4
M4-26	M4-7 + Des-W + Hexanediol	1.66			20	No ignition

Continued on next page.

Table VII. (Continued). Oxygen Index (OI) Values of Block Copolymers and Reference Materials

Block Copolymer ID	*Oligomer + Diisocyanate + Chain Extender*				*% Soft Segment*	*OI*
		% P	*% Cl*	*% Br*		
M4-27	M4-13 + TDI + Hexanediol	0.61	2.83		10	19.8
M4-28	M4-8 + Des-W + Hexanediol	0.77	0.89		10	18
M4-29	M4-8 + TDI + Hexanediol	0.77	0.89		10	18.8
M4-30	M4-13 + Des-W + Hexanediol	0.61	2.83		10	18.4
M4-31	M4-13 + TDI + Hexanediol	1.22	5.66		20	19.8
M4-32	M4-13 + TDI + Hexanediol	1.86	8.49		30	21.8
M4-33	M4-12 + TDI + Hexanediol	1.84		18.1	40	26.6
M4-37	M4-4 + Des-W + Hexanediol	0.90	2.1		10	18.8
M4-39	M4-4 + TDI + Hexanediol	0.90	2.1		10	26.6
M4-41	M4-6 + Des-W + Hexanediol	0.72			10	18.9
M4-42	M4-6 + Des-W + Hexanediol	1.44			20	19.8
M4-43	M4-23 + Des-W + Hexanediol	0.45		4.69	10	18.6
M4-44	M4-23 + Des-W + N,N'-Dimethylhexanediamine	0.45		4.69	10	17.8
M4-45	M4-23 + Des-W + Hexanediol	0.90		9.38	20	20.3
M4-47	M4-1 + Des-W + FRD Diol + Hexanediol (1:1)	4.17			10	21.8
M4-48	M4-1 + Des-W FRD Diol + Hexanediol (1:2)	3.40			10	20.3
M4-49	M4-1 + Des-W FRD Diol + Hexanediol (2:1)	5.18			10	22.2
M4-50	M4-1 + Des-W + 1,4-(2-butene)diol	0.85			10	25.5
M4-51	M4-3 + TDI + Hexanediol	1.09	1.26		10	19.1
M4-53	M4-3 + Des-W + 1,4-(2-butene)diol	1.09	1.26		10	26.0
M4-54	M4-3 + Des-W + N,N'-Dimethylhexanediamine	1.09	1.26		10	19.1
M4-55	M4-3 + Des-W + FRD Diol				10	21.8
M4-56	M4-11 + TDI + Hexanediol	0.67	3.09		10	19.8
M4-57	M4-9 + Des-W + N,N'-Dimethylhexanediamine	0.88	3.03		10	18.6

Continued on next page.

Table VII. (Continued). Oxygen Index (OI) Values of Block Copolymers and Reference Materials

Block Copoly-mer ID	*Oligomer + Diisocyanate + Chain Extender*				*% Soft Seg-ment*	*OI*
		% P	*% Cl*	*% Br*		
M4-58	OH terminated PDMS + Des W + N,N'-Dimethylhexanediamine	No P			10	20.1
M4-59	NH_2 terminated PDMS + Des-W + Hexanediol	No P			10	20.1
M4-60	OH terminated PDMS + N,N'-Dimethylhexanediamine	No P			30	25.8
M4-62	OH terminated Poly THF + Des-W + Hexanediol	No P			10	19
M4-63	OH terminated Poly THF + Des-W + Hexanediamine	No P			10	17.5
M4-65	OH terminated Poly THF + Des-W + Hexanediol	No P			20	17.8
M4-66	OH terminated Poly THF + Des-W + Hexanediamine	No P			30	19.5
M4-67	NH_2 terminated PDMS + Des-W + Hexanediamine	No P			20	17.3
M4-68	NH_2 terminated PDMS + Des-W + Hexanediamine	No P			30	17.7
M4-69	NH_2 terminated PDMS + Des-W + Hexanediamine	No P			40	19.1
M4-70	OH terminated PDMS + Des-W + Hexanediamine	No P			10	17.8
M4-71	OH terminated PDMS + Des-W + Hexanediamine	No P			20	21.7
M4-73	OH terminated PDMS + Des-W + Hexanediamine	No P			40	21.7
Reference (*1*)	Hexadecane	No P			-	14.5
Reference (*2*)	Dodecanol	No P			-	18
Reference (*3*)	Silicone oil	No P			-	23.7
M4-77	OH terminated PDMS + TDI + N,N'-Dimethylhexamethylene-diamine	No P			10	25.2

Continued on next page.

Table VII. (Continued). Oxygen Index (OI) Values of Block Copolymers and Reference Materials

Block Copolymer ID	*Oligomer + Diisocyanate + Chain Extender*				*% Soft Segment*	*OI*
		% P	*% Cl*	*% Br*		
M4-78	OH terminated PDMS + TDI + N,N'- Dimethylhexamethylenediamine	No P			20	27.4
M4-80	OH terminated PDMS + TDI + N,N'- Dimethylhexamethylenediamine	No P			40	30.2
M4-81	OH terminated PDMS + TDI + N,N'- Dimethylhexamethylenediamine	No P			50	30.2
M4-90	NH_2 terminated PDMS + Des-W + Hexamethylenediamine	No P			40	22.6

Results

It is well documented that introduction of a specific moiety such as phosphate, silicone, as a block into the structure of a polymer can impart specific properties to the whole system. In this study we are investigating the impact of the phosphate ester moiety on the flame retardant characteristics of phosphate urethane block copolymers.

Hydroxy terminated oligomers were prepared by condensation of phenyl phosphonic dichloride, diol, diphenol or diamine in excess in the presence of an acid acceptor (Scheme 1). The molecular weight of oligomers was determined by GPC. The molecular weight of these oligomers was in the range of 407 to 2403, Table III. Molecular weight of the block copolymers was determined by GPC and it was in the range up to 32,000, Table IV.

The hydroxyl terminated phosphate ester oligomers were reacted with diisocyante and a chain extender in the presence of dibutyltin dilaurate. Completion of reactions was monitored by disappearance of the isocyanate IR absorption peak at 2270 cm^{-1}. Some of these block copolymers formed good films. Molecular weight of block copolymers was determined by GPC.

FTIR of the dried film cast from the block copolymer was determined using an ATR attachment. The results show absorption peaks related to P=O, P-O-C, and O-P-O stretching or bending. The IR spectra of the phosphorous containing polyurethane show the following characteristic absorption bands: NH stretching at 2216 cm^{-1}; C=O stretching 1690 cm^{-1}; P:C:=O 1236 cm^{-1} and P-O-C (1183-957 cm^{-1}). The relatively low P=O frequency is due to a hydrogen bonded phosphonyl group. IR spectrum of the polyurethane copolymers which was prepared from reaction of Des-W, chain extender and oligomers shows a strong absorption band at 2940-2861 cm-^{1}. The block copolymers which contain 4,4′-hexafluoroisopropyl diphenol show an absorption band which relates to C-F stretching. The block copolymer which contains 4,4′-diphenyl sulfone shows a S+O absorption.

Attempts were made to measure Tg and other thermal transition of these block copolymers by differential scanning calorimetry (DSC). The results show that these materials have a glass transition above room temperature. Most of these block copolymers exhibit two melting temperatures for soft and hard segments, Table V.

Thermogravimetric analyses results show introduction of a phosphate ester moiety into the structure of block copolymers increased the thermal stability of many block copolymers in air compared to an ether-urethane block copolymer as a reference material (Table VI). The thermograms showed that the phosphate ester urethane block copolymers have a tendency to form char in air. The formation of char in this temperature range is clear for some of the phosphate ester urethane block copolymers (in Table VI M3-22 through M3-26 5, 10, 20, 25% phosphorylated soft block, respectively, with char in air increasing from 3.2 to 11.6%). Char forms when they were heated in air compared to when they were heated in nitrogen.

The char formation and char decomposition processes for the block copolymer with and without phosphate moiety are different for the char forming process of non-phosphorylated polyurethane. Char burns out at higher temperature (600 °C), whereas, for the phosphorylated copolymers the char formation of organic polyphosphate has good thermal resistance up to 700°C. The weight residue for phosphate block copolymers is much higher than polyether polyurethane (control material) block copolymers.

Oxygen index is a parameter to evaluate whether the material is to be considered as flame retardant. Oxygen index measurements were performed on the dried block copolymer films or powders with and without polyphosphate moiety, Table VII. These materials were dried in an oven for extended time to insure the evaporation of the casting solvents and volatiles in the polymers by checking the weight consistency during extended drying. Some of these block copolymers show higher oxygen index values compared to the ether urethane block copolymer reference material. Some of these phosphate urethane block copolymers did not tend to ignite when they were exposed to a torch flame for 50-60 seconds. During this period the block copolymers degrade and low molecular weight products tend to burn. Based on oxygen index results the flammability of some of these synthesized block copolymers can be categorized into three classes, Table VIII. Class A is those block copolymers which did not ignite to the ignition flame. Class B constitutes those block copolymers which were ignited but have higher oxygen indices compared to the control. Class C is those block copolymers which showed similar flame retardant characteristics compared to the control. Testing of two hydrocarbons, silicone oil, and materials without any phosphate or silicone moiety was performed as controls and reference materials (*50*, *51*) A synergistic effect was observed when halogenated components were used along with polyphosphate in the structure of the block copolymers.

Table VIII. General Categorizing Block Copolymers Synthesized Based on OI Results

Class A: Non ignition or igniting with delay time (more than 55 sec) block copolymers					
Block Copolymer	*% Soft Segment*	*%P*	*% Halogen*	*N2:O2 Ratio Time to Ignite (sec)*	*OI*
M3-36	25	2.95	C1 3.38	Up to 55 sec torching	
M4-26	20	1.66	-	Did not ignite	
M3-41	10	1.12	Br 64	Did not ignite	
Class B: High OI block copolymers					
M4-50	10	0.85		(Butenediol)	25.5
M4-53	10	1.09	Cl 1.26	(Butenediol)	26.0
M4-32	30	1.86	Cl 8.49	(TDI)	21.8
M4-33	40	1.84	Br 18.1	(TDI)	26.6
M4-39	10	0.90	Cl 2.1	(TDI)	26.6
M3-44	40	3.08	Cl 3.56		24.6
Class C: Low OI block copolymers					
M3-15	25	1.6			20.0
M3-26	25	2.1			19.5
M3-29	30	1.83	Cl 2.10		19.8
M3-35	25	3.4			19.5
M4-14	30	2.22			19.8
Control and reference materials					
Hexadecane					14.5
Dodecanol					18.0
Poly THF					17.3
M4-62 Poly THF Urethane					18.0
M4-63 Poly THF Urethane					17.3
Silicone Oil					23.7

Discussion

The theoretical value of phosphorus in these polyphosphate polyurethane block copolymers was relatively low, in the range of 0.3 to 3.0%. The structure of the block copolymers in this study was designed to have phosphorus as one component of the soft segment and the phosphorus content is dependent on the soft segment content of the block copolymer which is in the range of 10-50%

soft segment. The hard segments which contain polyurethane can form hydrogen bonds which influence the mechanical integrity of the block copolymers. Contrary to silicone urethane block copolymers in which there exists microphase segregation of the silicone to the surface due to low surface energy of the silicone block, there is no microphase segregation in polyphosphate block copolymers (*52*). Polyphosphate soft segments and polyurethane hard segments have similar surface energy which does not cause or promote microphase segregation of the polyphosphate and urethane as was seen in silicone urethane block copolymers. It is very clear that there is a significant "synergistic effect" on these block copolymers when the block copolymer has a combination of phosphorus and halogen in the structure (e.g. M3-36 and M3-44). In most cases either these materials did not ignite during OI measurement, there was a delay in ignition of these test materials or the oxygen index value was much higher than the control.

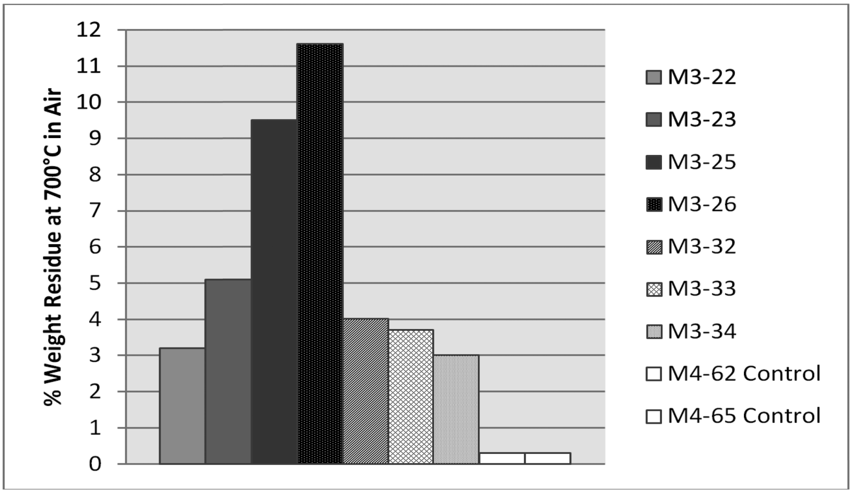

Figure 1. Bar graph of percent char residue in air at 700°C for phosphorylated and non-phosphorylated polyurethane block copolymer.

A TGA study in air shows the percent weight residue for phosphorylated block copolymer is higher than non-phosphorylated urethane block copolymers, Figure 1. It is postulated that the phosphorus in the structure of block copolymers even at a low level of 0.5 to 1.5% can enhance intumescent char formation which is one of the mechanisms to promote polymer flame retardancy. For example, the ignition was delayed for 55 seconds for a block copolymer containing 2.95% phosphorus and 3.38% chlorine (M3-36). Block copolymer M4-50 containing 0.85% phosphorus had an oxygen index value of 25.5. Block copolymer M4-53 with 1.09% phosphorus and 1.26% halogen had an OI value of 26. Energy dispersive spectroscopy of polyphosphate polyurethane blocks supports this assumption, since comparison of phosphorus peak ratios of polyphosphate polyurethane shows a higher phosphorus peak ratio for the char residue compared to the control. Gas phase and char retardation may take place for halogenated polyurethanes which can impart a significant effect on flame retardancy of the block copolymers.

Olefinic alcohol as a chain extender (M4-50 and M4-53) showed a significant effect on oxygen index of polyphosphate polyurethane block copolymers compared to similar phosphorylated block copolymers with saturated block copolymers. It is possible that the combination of phosphorus and olefinic diol may lead to higher char formation because of more cross linking because of the double bond.

The experimental design, given the clear need for polymeric flame retardant materials (i.e., flame retardants bound in), was to synthesized organophosphate oligomers with a variety of structures and have them bound into the polyurethane polymer chain. The use of 10% soft segments and moving to higher loading thus began with under 1% phosphorus loading for the polymer. The highest MW polymer made was 32,000 (M3-22). One then increased the soft segment content looking for structural features which might lead to enhanced OI.

Oligomers had 8-15% phosphorus loading. Five final formulations have OI values in the 24-27 range (not including those containing FRD diol): M3-44, M4-33, M4-39, M4-50 and M4-53. While most polymers in this study had saturated MDI (Des-W) as the isocyanate, two of the above had TDI as the isocyanate as did two of four of those with OI values in the low 20’s. Comparison of M4-37 and M4-39 shows the impact of TDI versus saturated MDI, an OI of 18.8 versus 26.6. That aromatic TDI is easier to flame retard is not surprising. That M4-50 and M4-53 have OI values of 25.5-26.0 is interesting given the butenediol and particularly the fact that M4-50 does not contain halogen in the oligomer. All the other four contain halogen in the oligomer. Thus from Table VIII, this work favors TDI, use of butenediol, and the use of a combination of phosphorus and halogen in the oligomer rather than phosphorus alone. A number of Des-W polymers shown in Table VIII had soft segments of 25-30% with a resulting percent P of about 2%. Yet their OI values were under 20.

Conclusions

Given the need for non-migrating phosphorus containing flame retardants, numerous block copolymers from hydroxyl or amine terminated polyphosphate or polyphosphate amide, diisocyanate and a chain extender were synthesized. Cast films were obtained for each. These novel materials show glass transition temperatures above room temperature and two melting temperatures for the soft and hard segments of the polyphosphate urethane block copolymers. Phosphorylated polyurethane block copolymers showed higher char formation at 700 °C. Char formation is one indication of improving flame retardancy of polymeric materials. Halogen in the structure of the block copolymer along with phosphorus showed “synergistic effects” and enhanced flame retardancy. Some of the polymers that did not ignite during OI measurement had both phosphorus and halogen in their structure. Oxygen index is only one parameter to assess polymer flame retardancy characteristics, but is measurable with small sample size. TDI polymers were easier to flame retard than saturated MDI polymers (Des-W). When olefin diols were used as a chain extender a significant improvement in OI was also observed.

References

1. Carnahan, J.; Hall, W.; Nelson, G. L.; Lee, G.; Abolins, V.; Shank, P. *Proceedings of the 4th International Conference on Flammability and Safety (January 15−19, 1979)* **1979**, *4*, 312–323.
2. Green, J. *J. Fire Sci.* **1992**, *10*, 470–487.
3. Troev, K.; Todorov, K.; Borisov, G. *J. Appl. Polym. Sci.* **1984**, *29*, 1701–1708.
4. Cullis, C. F.; Hirschler, M. M.; Tao, Q. M. *Eur. Polym. J.* **1991**, *27*, 281–289.
5. Allen, C. W. *J. Fire Sci.* **1993**, *11*, 320–328.
6. Mateva, R. P.; Dencheva, D. *J. Appl. Polym. Sci.* **1993**, *47*, 1185–1192.
7. Derouet, D.; Morvan, F.; Brosse, J. C. *J. Appl. Polym. Sci.* **1996**, *62*, 1855–1868.
8. Abed, J. C.; Mercier, R.; McGrath, J. E. *J. Polym Sci.,Part A: Polym. Chem.* **1997**, *35*, 977–987.
9. Fukatsu, K. *J. Fire Sci.* **1992**, *10*, 323–333.
10. Jensen, B. J.; Partos, R. D. *NASA Tech. Briefs* **1993**, 98–99.
11. Mikroyannidis, J. A. *J. Polym. Sci., Polym. Chem. Ed.* **1984**, *22*, 891–903.
12. Koutides, D.; Mikroyannidis, J. A. *NASA Tech. Briefs* **1985**Spring, *94*.
13. Banerjee, S.; Palit, S. K.; Maiti, S. *J. Polym. Sci., Part A: Polym. Chem.* **1994**, *32*, 219–227.
14. Antony, R. *J. Polym. Sci., Part A: Polym. Chem.* **1993**, *31*, 3187–3191.
15. Bilow, N.; Giants, T. W. *NASA Tech. Briefs* **1982**, *7*, 41.
16. Sarkis, H. K.; Yavrouian, A. H. *NASA Tech. Briefs* **1985**, *94*.
17. Gravalos, K. G. *J. Polym. Sci., Part A: Polym. Chem.* **1992**, *30*, 2521–2529.
18. Kishore, K.; Kannan, P. *J. Polym. Sci., Part A: Polym. Chem.* **1990**, *28*, 3481–3488.
19. Kim, K.-S. *J. Appl. Polym. Sci.* **1983**, *28*, 1119–1123.
20. Richards, M.; Dahiyat, B. I.; Arm, D. M.; Lin, S.; Leong, K. W. *J. Polym. Sci., Part A: Polym. Chem.* **1991**, *29*, 1157–1165.
21. Zentfman, H.; Wright, A. R. *Br. Plast.* **1952**, 374–871.
22. Natansohn, A. *J. Appl. Polym. Sci.* **1986**, *32*, 2961–2968.
23. Millich, F.; Carraher, C. E. *J. Polym. Sci., Part A-1: Polym. Chem.* **1970**, *8*, 163–169.
24. Chang, S.-J.; Sheen, Y.-C.; Chang, R.-S.; Chang, F.-C. *Polym. Degrad. Stabil.* **1996**, *54*, 365–371.
25. Liu, Y.-L.; Hsiue, G.-H.; Lan, C.-W.; Kuo, J.-K.; Jeng, R.-J.; Chiu, Y.-S. *J. Appl. Polym. Sci.* **1997**, *63*, 875–882.

26. Liu, Y.-L.; Hsiue, G.-H.; Lee, R.-H.; Chiu, Y.-S. *J. Appl. Polym. Sci.* **1997**, *63*, 895–901.
27. Liu, Y.-L.; Hsiue, G.-H.; Chiu, Y.-S. *J. Polym. Sci., Part A: Polym. Chem.* **1997**, *35*, 565–574.
28. Liaw, D.-J.; Lin, S.-P. *Eur. Polym. J.* **1996**, *32*, 1377–1380.
29. Kishore, K.; Kannan, P.; Iyanar, K. *J. Polym. Sci., Part A: Polym. Chem.* **1991**, *29*, 1039–1044.
30. Wang, T.-S.; Yeh, J.-F.; Shau, M.-D. *J. Appl. Polym. Sci.* **1996**, *59*, 215–225.
31. Delaviz, Y.; Gungor, A.; McGrath, J. E.; Gibson, H. W. *Polymer* **1993**, *34*, 210–213.
32. Hussein, M. A.; Asiri, A. M. *Des. Monomers Polym.* **2012**, *15*, 207–251.
33. Joseph, P.; Tretsiakova-Mcnally, S. *Polym. Adv. Technol.* **2011**, *22*, 395–406.
34. Vlase, T.; Vlase, G.; Doca, N.; Iliescu, S.; Ilia, G. *High Perform. Polym.* **2010**, *22*, 863–875.
35. Lebel, M.; Baumann, M.; Blubaugh, C. A new Family of flame retardant polymers and additives. *Conference Paper, ANTEC 2010, Proceedings of the 68th SPE Annual Technical Conference*, Orlando, FL, June 16−20, 2010.
36. Chen, L.; Wang, Y.-Z. *Materials* **2010**, *3*, 4746–4760.
37. Fang, K.; Li, J.; Ke, C.; Zhu, Q.; Zhu, J.; Yan, Q. *Polym.-Plast. Technol. Eng.* **2010**, *49*, 1489–1497.
38. Schartel, B. *Materials* **2010**, *3*, 4710–4745.
39. Özarslan, Ö.; Bayazıt, M. K.; Çatıker, E. *J. Appl. Polym. Sci.* **2009**, *114*, 1329–1338.
40. Schut, J. H. *Plast. Technol.* **2009**, *55*, 19–20.
41. FRX Polymera LLC. *Plast. Technol.* **2009**, *55*, 17.
42. Chen, H.; Luo, Y.; Chai, C.; Wang, J.; Li, J.; Xia, M. *J. Appl. Polym Sci.* **2008**, *110*, 3107–3115.
43. Lyon, R. E.; Speitel, L.; Walters, R. N.; Crowley, S. *Fire Mater.* **2003**, *27*, 195–208.
44. Kim, K.-S. *J. Appl. Polym. Sci.* **1983**, *28*, 2439–2443.
45. Poisson, P.; Sturtz, G. *Polym. Bull.* **1979**, *1*, 897–907.
46. Benrashid, R.; Nelson, G. L. *J. Polym. Sci., Part A: Polym. Chem.* **1994**, *32*, 1847–1865.
47. Jayakody, C.; Nelson, G. L.; Sorathia, U.; Lewandowski, S. *J. Fire Sci.* **1998**, *16*, 351–382.
48. Najafi-Mohajeri, N.; Nelson, G. L.; Benrashid, R. *J. Appl. Polym. Sci.* **2000**, *76*, 1847–1856.
49. Jayakody, C.; Myers, D.; Sorathia, U.; Nelson, G. L. *J. Fire Sci.* **2000**, *18*, 430–455.
50. Nelson, G. L.; Webb, J. L. *J. Fire Flammability* **1973**, *4*, 325.
51. Nelson, G. L.; Webb, J. L. *J. Fire Flammability* **1973**, *4*, 210.
52. Benrashid, R.; Nelson, G. L. In *Fire and Polymers II*; Nelson, G. L., Ed.; ACS symposium Series 599; American Chemical Society: Washington, DC, 1995; Chapter 14, pp 217−235.

Chapter 20

Synergistic Flame Retardant Mixtures in Epoxy Resins

Manfred Döring,*,[1] Michael Ciesielski,[1] and Christian Heinzmann[2]

[1]Fraunhofer Institut for Structural Durability and System Reliability LBF,
Schlossgartenstrasse 6, D-64289 Darmstadt, Germany
[2]University of Fribourg, Adolphe-Merkle-Institute, Avenue de ĺEurope 20,
CH-1700 Fribourg, Switzerland
***E-mail: manfred.doering@kit.edu**

Synergistic flame retardant mixtures were successfully tested as halogen-free flame retardants in two prepreg epoxies relevant in printed wired boards (PWB). The first epoxy system is composed of epoxy-novolac DOW DEN 438®, dicyandiamide (DICY) as hardener and fenurone as accelerator. The second one is based on the diglycidyl ether of bisphenol A (DGEBA) and uses the same hardener / accelerator combination. Reactive organophosphorus compounds were incorporated into these resins together with low-priced inorganic substances to give efficient flame-retardant systems. Samples without synergists or with tetrabromo bisphenol A (TBBA) were tested as well. Combinations of 9,10-dihydro-9-oxa-10-phosphaphenanthrene-10-oxide (DOPO) and 30% of crystalline boehmite (Nabaltec®) showed outstanding flame retardant efficiencies, so that low phosphorus contents (0.4% in DEN 438® / DICY / fenurone, 1.3% in DGEBA / DICY / fenurone) were sufficient to reach UL 94 V0 rating. Melamine polyphosphate (MPP) amplifies the activity of organophosphorus flame retardants, too. Additionally, novel salt-like additives were found to be efficient fire-retardants in the epoxy resins examined. Their flame-retardant efficiencies could be further enhanced by combination with boehmite or

In Fire and Polymers VI: New Advances in Flame Retardant Chemistry and Science; Morgan, A., et al.;
ACS Symposium Series; American Chemical Society: Washington, DC, 2012.

MPP. Using these synergistic mixtures allows the maintainence of the glass transition temperature (T_g) of the cured samples and to reduce the loading of phosphorus compounds. Such synergistic mixtures surpass the flame retardant efficiency of TBBA.

Introduction

Virtually all the modern day electronic devices contain at least one printed wired board (PWB) to support and connect their electronic components. The insulating backbone of most PWBs consists of epoxy composites manufactured by the so-called prepreg process. For meeting different application requirements, some grade designations for prepreg epoxy laminates have been specified by the National Electrical Manufacturers Association (NEMA). Of these, FR-4 is by far the most common material used in the PWB industry composed of the following three ingredients: epoxy resin, woven glass fibers and a flame retardant. For a long time bromine containing compounds have been employed to impart flame retardancy into FR-4 laminates. Among these tetrabromobisphenol A (TBBA) is the primary flame retardant used in conventional FR-4 composites.

Because of environmental and end-of-life issues, there is a general tendency to replace bromine-based flame retardants by halogen-free alternatives. Several companies are working on developing halogen-free versions of FR-4 laminates. Moreover, the development of novel flame-retardant epoxies is necessary because of the increasing application of lead-free soldering carried out at considerably higher temperatures than the traditional soldering process.

The application of flame-retarding phosphorus compounds instead of TBBA offers an ecologically friendly way to obtain improved FR-4 materials. Among the few phosphorus-based flame retardants successfully introduced into the PWB market, 9,10-dihydro-9-oxa-10-phosphaphenanthrene-10-oxide (usually denoted as DOPO) is by far the most relevant one. Two decades ago, DOPO was only a niche product in the PWB industry. However, during the last years its application has grown to an extent of several thousands of metric tons manufactured nowadays. Currently, the production of this powerful flame retardant is still increasing. Due to its P-H functionality DOPO is a reactive flame retardant like TBBA. Thus it can be incorporated into the epoxy network in an analogous manner using a fusion process (so-called preformulation) whereby the phosphorus containing unit is covalently bond to the epoxy network and becomes a part of the polymer matrix. Since DOPO is only mono-functional towards oxirane groups, it decreases the amount of crosslinks within the network of epoxy resins and causes a moderate drop of the T_g. The adduct of benzoquinone and DOPO (usually denoted as DOPO-HQ) is bifunctional and therefore it suffers only marginally from this disadvantage. DOPO-HQ has also been commercialized but its higher price prevented a broad application in the PWB industry. Due to a relatively high price of DOPO and the strong reduction of the T_g, there is a strong request to reduce the loading of DOPO necessary to reach the V0 classification in the UL 94 test demanded for FR-4 composites. These negative effects induced by halogen-free flame retardancy can be brought down if the organophosphorus compounds are applied together with low-priced components amplifying their efficiencies by synergistic interactions.

Our present study is a contribution to the growing field of research in this area. The main subject of this chapter will deal with the flame retardant properties of several synergistic mixtures investigated in two different prepreg epoxies relevant in PWB (see Figure 1). Flame retardant properties of phosphorus compounds without the addition of a synergist will be presented for comparison as well.

The first one of the chosen PWB based materials is composed of epoxy-novolac DOW DEN 438® (DOW Chemical Co.), dicyandiamide (DICY, Dynhard 100 SF, AlzChem AG) as hardener, and fenurone as accelerator. It is characterized as a polyepoxide-based resin system with high content of aromatic units, so that it forms a strong and dense network. Therefore, the cured resin has a high T_g (182°C). Samples of this epoxy material are not self-extinguishing if not flame retarded, but they show rather moderate burning behavior. The second epoxy system investigated in this study is based on the diglycidyl ether of bisphenol A (DGEBA, Baxxores TM ER 2200, BASF SE, 182 g / mol) and comprises the same hardener / accelerator combination. Unlike the epoxy-novolac, it has a lower epoxy functionality and a higher content of aliphatic substructures. Thus, it forms a weaker network, has a lower T_g (136°C) and burns more vigorously. Hence, higher loadings of phosphorus-based flame retardants are necessary to render this material flame retardant.

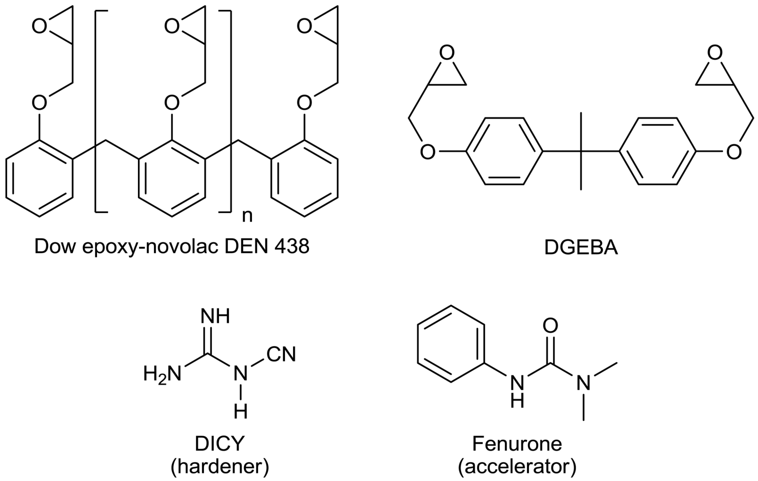

Figure 1. Epoxy resin formulations investigated in this study.

The present article will start with an evaluation of fire protecting behavior of several reactive flame retardants in the two selected epoxy matrixes while no synergist is present. Among these substances are commercially available ones, substances already reported in the literature, as well as some novel phosphorus-containing compounds. Afterwards, the synergistic amplification of the flame retardant efficiencies induced by metal hydroxides and melamine polyphosphate will be presented. The third part of this chapter will include the flame retarding properties of novel phosphorus-containing melaminium and guanidinium salts. These nonreactive salt-like additives are to be considered as synergistic systems too, because they both contain phosphorus and several nitrogen atoms. These nitrogen-containing additives were tested together with metal hydroxides and melamine polyphosphate as well. All of these synergistic systems were incorporated into the two chosen epoxy materials. The phosphorus content necessary to achieve the V0 rating in the UL 94 test will be presented together with the concentrations of the synergists applied and the corresponding T_g values.

All investigations of flame retarding properties have been restricted to non-reinforced epoxy samples. Glass fiber reinforced laminates containing the most promising formulations will be prepared and tested within continuative experimental series in the future.

Reactive Flame Retardants for PWB Epoxy Materials

As already mentioned above, the DOPO molecule can be introduced into the epoxy network because of its P-H functionality. Several other reactive phosphorus compounds were also incorporated into the chosen prepreg base materials using analogous fusion processes. The flame retardant properties of cured samples containing different amounts of these substances were determined. No synergists have been applied in these cases (synergistic mixtures containing these phosphorus compounds will be highlighted within the next section).

The investigations allow the evaluation of the dependence of flame retardant properties on the structures of phosphorus compounds. The influence of the type of base materials have been determined too. As seen in Figure 2, the chemical structures of the reactive organophosphorus compounds selected for this study are characterized by a broad variety of patterns. In these compounds the phosphorus atoms are in different chemical environments. According to the number of carbon-phosphorus bonds, the chosen substances are classified as phosphine oxides (Ph_2PO, DPPO), phosphinates (DOPO, DOPO-HQ), or phosphonates (DDPO). Sulfur derivatives of DOPO and DDPO have also been involved in this study. For comparison, TBBA as the most common commercial halogen-based flame retardant for epoxies was also applied in the test series.

Most of the chosen compounds, including DOPO, have one P-H functionality, but DOPO-HQ as well as $DDPO_2$-HQ are bifunctional phenolic hardeners just as TBBA.

DOPO, DOPO-HQ, Ph_2PO and TBBA are commercially available substances. The synthesis of DDPO has been performed according to a reported method (*1*). The remaining substances are novel compounds and were synthesized in our research group (*2–5*). The flammabilities of cured epoxy samples containing those organophosphorus compounds were characterised by the UL 94 vertical burning test (*6*).

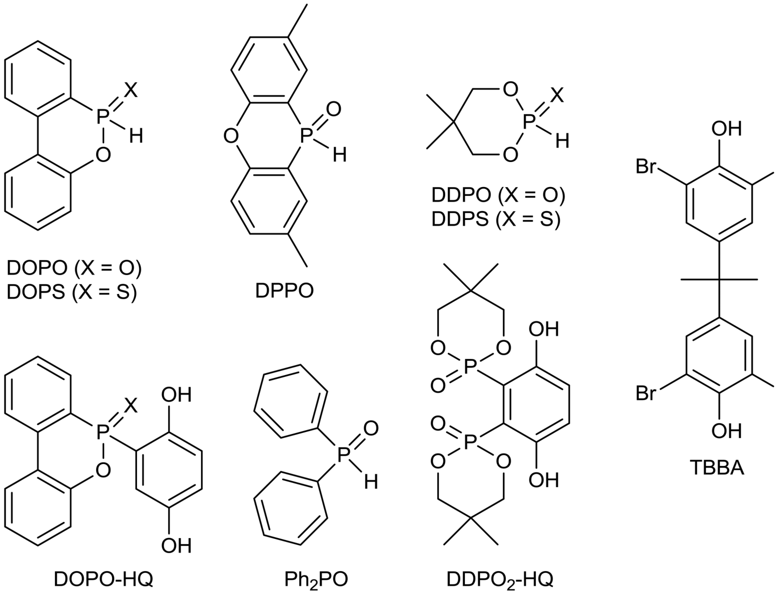

Figure 2. Selected reactive flame retardants for epoxies.

The phosphorus contents in the resin system DEN 438® / DICY / fenurone necessary to achieve the V0 rating are summarized in Table I for each compound together with the loadings and corresponding T_g values.

The flammability tests revealed that DOPO, its derivatives, DPPO and Ph_2PO are efficient flame retardants in the epoxy-novolac based resin. They mainly consist of aromatic substructures. The concentrations necessary to achieve the V0 rating were found to be similar or even lower than for TBBA. All of the mentioned compounds are expected to be predominantly gas phase active flame retardants. Characteristic for these compounds are the carbon-phosphorus bonds, which are known to be able to release P-O radicals during thermal decomposition (*3*). The P-O radical acts as a radical scavenger in the gas phase, which then extinguishes the flame. Among them DOPS (as the sulfur derivative of DOPO) has the highest flame retardant activity in this matrix, so that only 1% of phosphorus was required to reach the V0 classification in the UL 94 test. The superior flame retardant efficiency of DOPS may be explained by a synergistic interaction between phosphorus and sulfur.

DDPO and its derivatives showed rather poor flame retardant efficiencies in the DEN 438® / DICY / fenurone resin. In contrast to the aforementioned substances, these compounds are mainly acting in the condensed phase. High loadings of at least 15% had to be applied to achieve the V0 classification corresponding to a phosphorus content of 3%. In the case of $DDPO_2$-HQ the samples wee even not self-extinguishing and achieved no classification.

The flame retardant properties of four selected reactive phosphorus compounds were also investigated in the DGEBA / DICY / fenurone epoxy resin system having lower network density and higher content of aliphatic substructures compared to the epoxy-novolac-based resin. The results of UL 94 flammability tests show that it is a real challenge to render this PWB matrix material flame retardant using phosphorus-containing compounds alone (see Table II).

Table I. DOW DEN 438® resin hardened with DICY / fenurone (neat resin)[a]. Amounts of reactive flame retardants necessary for UL 94 V0 classification

Flame retardant	*UL 94 (4 mm)*	*P (Br) content (%)*	*FR-content (%)*	*T_g (DSC) (°C)*
-	n.c.	-	-	182
DOPO	V0	1.6	11.2	155
DOPS	V0	1.0	7.5	159
DOPO-HQ	V0	1.4	14.6	177
DPPO	V0	1.5	11.9	162
Ph_2PO	V0	1.5	9.8	158
DDPO	V0	3.0	14.5	148
DDPS	V0	3.0	16.2	135
$DDPO_2$-HQ	n.c.	3.0	19.7	182
TBBA	V0	8.0 (Br)	13.6	168

[a] Preformulation and curing procedures are described in (*3*).

With none of the P-H functionalized compounds was a V0 rating achieved below a phosphorus content of 3%. DOPO, Ph_2PO as well as DDPO failed in the flammability tests regardless of which flame retarding mechanism is predominant. All of them provoke remarkable drops of the T_g, because they strongly decrease the network density of the DGEBA-based resin. DOPO-HQ, as a bi-functional reactive flame retardant, performed considerably better in the UL 94 test. V1 rating could be achieved at a phosphorus content of 2% and a loading of 21%, respectively. The T_g of the cured samples was almost unaffected by the flame retardant in this case. Among all compounds tested in this epoxy matrix the bromine-containing substance TBBA showed by far the best flame-retarding performance. However, a bromine content in the considerable amount of 20% was required to reach the UL 94 V0 classification. Since TBBA has two reactive OH groups like DOPO-HQ, it does not weaken the network significantly. Thus, the T_g remains nearly unchanged despite the very high loading applied to the matrix.

Table II. DGEBA resin cured with DICY / fenurone (neat resin)[a]. Amounts of reactive flame retardants necessary for UL 94 V0 classification

Flame retardant	*UL 94 (4 mm)*	*P (Br) content (%)*	*FR-content*	*T_g (DSC) (°C)*
-	n. c.	-	-	136
DOPO	n. c.	3.0	20.9	93
DOPO-HQ	V1	2.0	20.8	128
Ph_2PO	n. c.	2.5	16.3	88
DDPO	n. c.	2.5	12.1	105
TBBA	V0	20 (Br)	33.5	126

[a] Preformulation and curing process: The DGEBA resin and the organophosphorus compounds were stirred at 60°C for 20 min using a lab dissolver (Dispermat® DS, VMA-Getzmann GmbH). Then, the hardener and accelerator were added. After stirring for 5 min the formulations were transferred to aluminium molds and cured at 100-130°C for 2 h and postcured at 180°C.

The results allow the following conclusions:

- Fire-retardant efficiencies of reactive organophosphorus compounds are strongly influenced by the structural pattern of the epoxy matrix used. The structures of the flame retardants and the respective epoxy resin should be adapted to each other (i.e. DOPO and other monofunctional gas phase active FR work well in the novolac-based epoxy resin, but they fail in the DGEBA-based resin completely).
- It is a lot easier to render novolac-based epoxy resins flame retardant than those based on DGEBA. The latter have more aliphatic components and form less dense networks making them more inflammable. Generally, high loadings are required to render DGEBA resins flame retardant. TBBA performed much better than all reactive organophosphorus compounds investigated in this matrix.
- Reactive flame retardants having only one functional group decrease the network density. Therefore they deteriorate the T_g as an important material property, most crucial in the case of DGEBA-based resins (which already has a low T_g as a neat material).

Moreover, the investigations revealed the shortcomings of reactive flame retardants, particularly of monofunctional ones. The goal of subsequent investigations was to find improved flame retardant systems working at lower concentrations without strong impact on material properties.

Flame Retardant Mixtures of Reactive Organophosphorus Compounds and Synergistic Additives

The performance and limits of reactive phosphorus-containing compounds as flame retardants for PWB materials have been exemplified in the previous section. Some of these compounds worked well in an epoxy-novolac-based resin (DEN 438), but they showed low activity in a DGEBA-based material. However, their efficiencies can be improved by application of appropriate synergists.

This section deals with the flame retardant properties of synergistic mixtures composed of reactive organophosphorus compounds and low-cost additives.

Table III. DOW DEN 438® resin hardened with DICY / fenurone (neat resin)[a]. Amounts of reactive flame retardants and synergists necessary for UL 94 V0 classification

Flame retardant (%)	*Synergist, specific surface (%)*	*UL 94 (4 mm)*	*P content (%)*	*T_g (DSC) (°C)*
-	Boehmite[b], 3 m^2/g (30)	V1	-	195
DOPO (2.8)	Boehmite[c], 3 m^2/g (30)	V0	0.4	168
DOPO (7.0)	Boehmite[c] 18 m^2/g (30)	V0	1.0	159
DOPO (11.2)	Boehmite[c] 100 m^2/g (30)	V0	1.6	153
DOPO (2.8)	ATH, 4 m^2/g (30)	V0	0.4	170
DOPO (7.0)	MDO, 4 m^2/g (30)	n. c.	1.0	153
-	MPP (11.3)	V1	1.5	195
DOPO (6.5)	MPP (6.5)	V0	0.9 + 0.8	157
DOPO (1.75)	MPP (15)	V0	0.25 + 2.0	188
DOPO-HQ (12.3)	Boehmite (30)	V0	1.2	178
DOPO-HQ (7.5)	MPP (7.5)	V0	0.7 + 1.0	185
DDPO (9.1)	MPP (15)	V0	1.9 + 2.0	168

[a] Preformulation and curing process: The DOW DEN 438® resin, the organophosphorus compound and the synergist were stirred at 80°C for 20 min using a lab dissolver (Dispermat® DS, VMA-Getzmann GmbH). Then, the hardener and accelerator were added. After stirring for 5 min the formulations were transferred to aluminium molds and cured at 100-130°C for 2 h and postcured at 200°C for 1 h. [b] crystalline boehmite, [c] amorphous boehmite.

Aluminium trihydroxide (ATH), boehmite (Al(O)OH, Apyral AOH 30, Nabaltec AG), magnesium dihydroxide (MDO) and melamine polyphosphate (MPP Melapur 200, BASF SE) were chosen as potential synergists and incorporated into epoxy materials together with the selected phosphorus compounds already tested (see previous section). As inert fillers, these synergists are completely insoluble in the epoxy resins. Therefore they did not show any deteriorating effects on the T_g of either epoxy material investigated (see Tables III and IV, corresponding values of neat resins are listed in Tables I and II). Surprisingly, the T_gs seem to be even somewhat enhanced by the chosen additives. These insoluble additives are broadly used in the thermoplastic sector but are known to have only moderate fire-protecting efficiencies in epoxy materials (see Tables III and IV). However, they are able to amplify the flame retardant action of reactive organophosphorus compounds as seen from the results listed in Tables III and IV (only MDO was found to be inefficient).

Table IV. DGEBA resin cured with DICY / fenurone (no glass-fiber)[a]. Amounts of reactive flame retardants and synergists necessary for UL 94 V0 classification

Flame retardant (%)	*Synergist, specific surface (%)*	*UL 94 (4 mm)*	*P content (%)*	*T_g (DSC) (°C)*
-	Boehmite, 3 m²/g(30)	V2	-	142
DOPO (10.5)	Boehmite, 3 m²/g(30)	V0	1.3	113
-	MPP (17)	V1	2.2	140
DOPO (9.5)	MPP (9.5)	V0	1.4 + 1.2	110
DOPO (10.5)	MPP (15)	V0	1.5 + 1.6	120
DOPO-HQ (10.4)	MPP (15)	V0	1.0 + 2.0	144
Ph_2PO (9.8)	MPP (15)	V0	1.5 + 2.0	114

[a] Preformulation and curing process: DGEBA resin, the organophosphorus compound and the synergist were stirred at 60°C for 20 min using a lab dissolver (Dispermat® DS, VMA-Getzmann GmbH). Then, the hardener and accelerator were added. After stirring for 5 min the formulations were transferred to aluminium molds and cured at 100-130°C for 2 h and postcured at 180°C for 1 h.

Synergistic combinations of crystalline boehmite and DOPO showed superior flame-retarding properties in the epoxy-novolac material. If 30% of boehmite was added to this resin, only a very small amount of DOPO (2.8%, 0.4% P) was necessary to reach the V0 classification and the T_g was maintained near the level of the neat resin. Furthermore, the synergistic mixture of DOPO and boehmite (30%) worked well in the DGEBA / DICY / fenurone resin. As expected, a considerably higher amount of DOPO (10.5%) was required to fire-protect this easily inflammable matrix. V0 rating could be achieved too, but the T_g was decreased more significantly in this case. If DOPO was replaced by DOPO-HQ, surprisingly no pronounced synergistic amplification of flame retardancy could be achieved. Using DOPO-HQ, the phosphorus content necessary to pass V0 was nearly as high as the corresponding one without boehmite in the novolac-based resin.

Generally, the application of very high loadings of boehmite is definitely profitable, because it has an even lower price than epoxy materials relevant for PWB. Surprisingly, only a special kind of crystalline boehmite (Al(O)OH, Nabaltec® APYRAL AOH 30®) having low specific surface (3 m^2/g) was found to be efficient as a synergist. In contrast, amorphous boehmite fractions showed much less synergistic activities even further diminishing with increasing specific surface (see Table III). Up to now there is no explanation available for this unexpected dependance.

ATH amplifies the flame retardant efficiency of DOPO quite similar to crystalline boehmite. However, it should be noted, that ATH has low thermal stability, so that its use is not compatible with lead-free soldering having increasing importance. Unlike crystalline boehmite and ATH, MDO showed no synergistic activity if combined with DOPO.

Combinations of reactive organophosphorus compounds and MPP have also been successfully tested as synergistic flame-retardant systems for both epoxy materials used in this study. If 15% of MPP was incorporated into the epoxy-novolac resin, a marginal amount of DOPO (1.75%) was already sufficient to achieve UL 94 V0 rating. DSC measurements revealed that this flame-retardant system does not decrease the T_g of the epoxy-novolac resin at all. The DGEBA-based resin could also be efficiently flame-protected using mixtures of DOPO and MPP, but higher loadings of DOPO were required to achieve V0 rating resulting in a moderate drop of T_g. This kind of synergy is not restricted to DOPO. Combinations of MPP with DOPO-HQ, Ph_2PO, and even with DDPO known as mainly condensed-phase active flame retardant showed high flame-retardant efficiencies.

These testing series revealed that these synergistic flame-retarding systems are characterized by following advantages:

- Superior flame-retardant properties
- Significantly lower amounts of phosphorus-based compounds are necessary if they are applied together with appropriate synergists
- None or low impact on T_g of the epoxy materials
- Reduced costs of flame retardancy because of the application of low-priced fillers.

Additive Flame Retardants for Epoxy Materials

Unlike the reactive flame retardants, the additive (non-reactive) flame retardants have no functionality to interact with the epoxy system. These compounds can be introduced into the epoxy polymer system by physical mixing of the resin with the flame retardant before adding an accelerator and hardener.

Without the reaction of the flame retardant with the epoxy resin, the disadvantage of weakening the polymer matrix is not important. Additionally, the time consuming preformulation is not needed.

One should note that without the interaction of the flame retardant with the epoxy resin, the flame retardant shows the same disadvantage as any other additive. It is necessary to disperse them well in the epoxy resin to prevent phase separation and bleeding out of the later product.

The additive flame retardants described here are organic salts containing nitrogen in the cation and phosphorus in the anion (*7–10*). Crystal structures confirm the salt-like structure, which is determined by a complex hydrogen-bonded system (*11*). The materials were synthesized by the reaction of melamine or guanidinium carbonate with hydroxyl functionalized organic phosphorus compounds (Figure 3).

Combining gas-phase and condensed-phase active flame retardants was the main goal of our research. Both nitrogen and phosphorus compounds show either behaviour, depending on their molecular environment (*12–14*). Tuning the structures allows to synthesize tailor-made flame retardants for the desired application. Our results are the first step in that process.

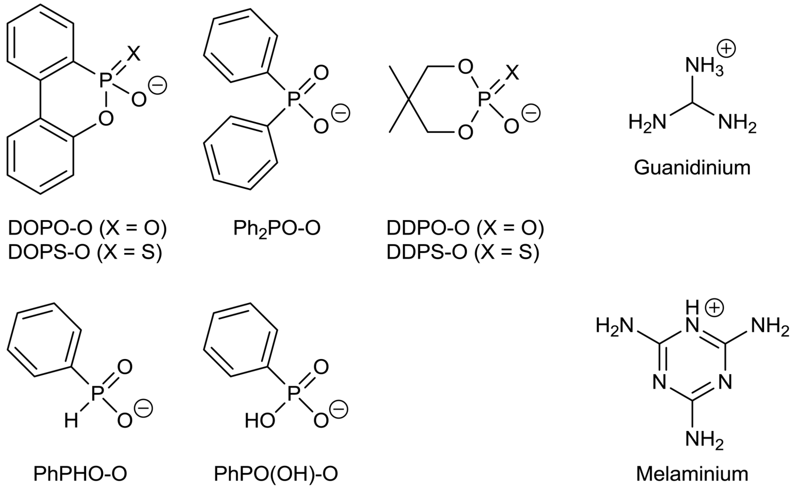

Figure 3. Chemical structures of organic cations and anions containing nitrogen and phosphorus, respectively.

The phosphorus contents in the resin system DEN 438® / DICY / fenurone necessary to pass the V0 rating are summarized in Table V for each compound together with the loadings and corresponding T_g values. Table VI shows additional loadings with common flame retardants like aluminium oxide hydroxide (Al(O)OH, crystalline boehmite, Nabaltec®) or melamine polyphosphate (MPP).

The results for the resin system DGEBA / DICY / fenurone for the organic phosphorus salts are shown in Table VII. Table VIII shows these compounds with the addition of commercial available additives.

As already mentioned before, the DGEBA based epoxy system requires a higher loading of the flame retardant than the novolac system (DEN 438®). It could be shown, that the new phosphororganic compounds have improved flame retardant behavior regarding the phosphorus loading in both systems. The flame retardant effect of phosphorus is enhanced by adding a nitrogen containing compound, which itself has only a weak flame retardancy.Combining a organophosphate and a nitrogen containing organic in one compound shows a synergistic effect, which allows one to reduce the loading of the usually more expensive organophosphate flame retardants. By adding additional inorganic fillers such as aluminium oxide hydroxide or melamine polyphosphate, the loading of the organophosphate could be even more decreased. This benefits not only to the thermal properties of the material such as the T_g, but also reduces the processing time of the epoxy materials.

Table V. DOW DEN 438® resin hardened with DICY / fenurone (neat resin)[a]. Amounts of additive flame retardants necessary for UL 94 V0 classification

Flame retardant	*UL 94 (4 mm)*	*P content (%)*	*FR-content (%)*	*T_g (DSC) (°C)*
-	n.c.	-	-	182
DOPO (preformulation)	V0	1.6	11.2	155
Melaminium salts				
DOPO-O	V0	1.0	11.6	174
DOPS-O	V0	1.0	12.1	161
PhPHO-O	V0	1.6	13.8	158
Ph_2PO-O	V0	1.0	11.1	162
DDPO-O	V0	1.25	11.8	169
Guanidinium salts				
DOPO-O	V0	1.25	11.8	178
DOPS-O	V0	1.0	9.9	170
PhPO(OH)-O	V0	1.25	8.8	181
Ph_2PO-O	V0	1.0	9.0	176

[a] The preparation and curing of the samples is described in (*15*).

Table VI. DOW DEN 438 resin hardened with DICY / fenurone (neat resin)[a]. Amounts of additive flame retardants necessary for UL 94 V0 classification

Flame retardant, synergist	*UL 94 (4 mm)*	*P content (%)*	*FR-content (%)*	*Tg (DSC) (°C)*
Melaminium salts				
DOPO-O + 30% boehmite[b]	V0	0.8	7.0	171
DOPO-O + MPP (1:1)	V0	0.9 + 0.7	5.2 + 5.2	179
DOPO-O + 15% MPP	V0	0.4 + 2.0	3.5	184
DOPS-O + 15% boehmite[b]	V0	0.8	9.1	156
PhPH(O)-O + 30% boehmite[b]	V0	0.8	6.9	168
PhPH(O)-O + 15% MPP	V0	0.5 + 2.0	4.3	175
Ph_2PO-O + 15% MPP	V0	0.5 + 2.0	5.6	170
Guanidinium salts				
DOPS-O + 30% boehmite[b]	V0	0.7	7.0	170

[a] The preparation and curing of the samples is described in (*15*). [b] crystalline boehmite, specific surface 3 m^2/g.

Table VII. DGEBA resin hardened with DICY / fenurone (neat resin)[a]. Amounts of additive flame retardants necessary for UL 94 V0 classification

Flame retardant	*UL 94 (4 mm)*	*P content (%)*	*FR-content (%)*	*Tg (DSC) (°C)*
-	n.c.	-	-	136
DOPO (preformulation)	V2	2.5	17.5	110
Melaminium salts				
DOPO-O	V0	2.5	31.4	137
PhPHO-O	V0	2.0	17.3	141
Ph_2PO-O	V0	1.8	19.4	125
DDPO-O	V0	2.0	18.9	139
Guanidinium salts				
DOPS-O	V0	2.5	24.8	125

[a] The preparation and curing of the samples is described in (*15*).

In Fire and Polymers VI: New Advances in Flame Retardant Chemistry and Science; Morgan, A., et al.;
ACS Symposium Series; American Chemical Society: Washington, DC, 2012.

Table VIII. DGEBA resin hardened with DICY / fenurone (neat resin)[a]. Amounts of additive flame retardants necessary for UL 94 V0 classification

Flame retardant, synergist	*UL 94 (4 mm)*	*P content (%)*	*FR-content (%)*	*Tg (DSC) (°C)*
Melaminium salts				
DOPO-O+ 30% boehmite[b]	V0	1.5	17.4	140
DOPO-O+ 15% boehmite[b]	V0	2.0	23.2	137
DOPO-O+ MPP (1:1)	V0	1.75 + 1.0	7.9 + 7.9	145
PhPH(O)-O +30% boehmite[b]	V0	1.0	8.7	132
PhPH(O)-O + 15% MPP	V0	0.3 + 2.0	2.6	131
Ph_2PO-O + 15% MPP	V0	1.0 + 2.0	11.3	128
Guanidinium salts				
DOPO-O + 30% boehmite[b]	V0	1.75	16.5	141

[a] The preparation and curing of the samples is described in (*15*). [b] crystalline boehmite, specific surface 3 m^2/g.

During the preparation of the loaded epoxy resins, some materials were incompatible with the neat epoxy system, which was illustrated by phase-separation. But due to its modularity, the salt-like substructures are higly variable and can be changed easily to accommodate different epoxy systems. By understanding the structure-property relations, it would contribute to a database of tailor-made flame retardants. Our research therefore shows where future studies should focus.

Summary and Conclusions

The goal of this study was to develop powerful fire-retardant systems suitable for epoxy resins relevant in composites, for example for lightweight structures. In order to reach that aim, several mixtures consisting of an organophosphorus component and a synergist were incorporated into epoxy resins. The flame retardant properties of cured samples containing these synergistic systems were determined. For comparison, sets of specimen with TBBA or without synergist were tested as well. An epoxy-novolac and a DGEBA based resin were used as matrix materials within this study (the latter has a higher content of aliphatic substructures, forms a weaker network and burns more vigorously). Therefore, it needs higher loadings of flame retardants.

Synergistic mixtures consisting of reactive organophosphorus compounds and metal hydroxides were successfully tested in both epoxy resins. Of these, combinations of DOPO with low surface crystalline boehmite were found to be the most effective, so that only small amounts of the phosphorus-containing component had to be applied to achieve the UL 94 V0 norm demanded for FR-4 materials. Moreover, MPP induces strong synergistic amplification of the flame-retardant efficiency of several organo-phosphorus compounds.

Novel melaminium or guanidinium salts of phosphorus-containing acids were incorporated as additive flame retardants into the resins. Some of them were found to be highly efficient flame retardants suitable for both epoxy resins investigated in this study. The flame retardant efficiencies of these organic salts can be further enhanced when combined with MPP or boehmite. Using these synergistic systems allows to reduce the loading of phosphororganic flame retardants substantially and to maintain the T_g near the level of neat epoxy materials (the synergists are inorganic fillers and do not influence the T_g). Furthermore, lower contents of the usually more expensive phosphororganic compound bring down the overall costs for manufacturing composites.

It could be demonstrated within this study that such mixtures can outperform the flame-retardant efficiency of TBBA as the most common bromine-based flame retardant used in PWB. The results presented here revealed that the application of synergistic mixtures offers an ecologically-friendly and cost-efficient way to obtain improved epoxy composite materials.

However, only nonreinforced epoxy materials have been investigated within the experimental series. The preparation and testing of reinforced composites containing novel flame-retarding systems will be the subject of future studies.

References

1. Wadsworth, W. S.; Emmons, W. D. *J. Am. Chem. Soc.* **1962**, *84*, 610–617.
2. Rakotomalala, M.; Wagner, S.; Zevaco, T.; Ciesielski, M.; Walter, O.; Döring, M. *Heterocycles* **2011**, 743–753.
3. Schäfer, A.; Seibold, S.; Lohstroh, W.; Walter, O.; Döring, M. *J. Appl. Polym. Sci.* **2007**, *105*, 685–696.
4. Wagner, S.; Rakotomalala, M.; Bykov, Y.; Walter, O.; Döring, M. *Heteroat. Chem.* **2012**, *23*, 216–222.
5. Müller, P.; Bykov, Y.; Walter, O.; Döring, M. *Heteroat. Chem.* **2012**, *23*, 383–394.
6. Underwriters Laboratories Inc. UL 94. *Test for Flammability of Plastic Materials for Parts in Devices and Applications*; 1996.
7. Simon, E. U.S. Patent 4,061,605A, 1977.
8. Nachbur, H.; Guth, C. Patent EP0057668A2, 1982.
9. Fuchs, S.; Weiss, T. Patent WO2010057851A1, 2010.
10. Fuchs, S.; Weiss, T.; Xalter, R. Patent WO2010063623A1, 2010.
11. Najafpour, M. M.; McKee, V *Acta Crystallograph., Sect. E* **2006**, *62* (4), 1365–1368.
12. Lewin, M.; Weil, E. D. *Fire Retard. Mater.* **2001**, 31–57.
13. Lewin, M. *Polym. Adv. Technol.* **2001**, *12*, 215–222.
14. Rakotomalala, M.; Wagner, S.; Döring, M. *Materials* **2010**, *3*, 4300–4327.
15. Heinzmann, C. Diploma Thesis, University of Heidelberg, Heidelberg, Germany, 2011.

In Fire and Polymers VI: New Advances in Flame Retardant Chemistry and Science; Morgan, A., et al.;
ACS Symposium Series; American Chemical Society: Washington, DC, 2012.

Chapter 21

Characterization of Melt Dripping Behavior of Flame Retarded Polypropylene Nanocomposites

B. K. Kandola,*,[1] D. Price,[1] G. J. Milnes,[1] A. Da Silva,[1] F. Gao,[2] and R. Nigmatullin[2]

[1]Institute for Materials Research and Innovation, University of Bolton, Bolton, BL3 5AB, U.K.
[2]School of Science and Technology, Nottingham Trent University, Nottingham, NG11 8NS, U.K.
***E-mail: B.Kandola@bolton.ac.uk**

This work presents the effect of a nanoclay and/or phosphorus/halogen based flame retardants on melt and burn dripping behavior of polypropylene. An experimental setup has been constructed to record the real-time melt-dripping behavior in a furnace. All experiments were repeated in a UL-94 set-up to replicate their melt dripping behavior in flaming conditions. A relationship between melt viscosity/rheology and melt dripping intensity of these polymers has been studied. The physical and chemical changes occurring during melt dripping have also been studied by conducting thermal analysis and rheology experiments on molten drops and comparing them with those of respective original polymer samples. The results have shown that during melt dripping a polymer degrades to a considerable extent and its viscosity is affected by the action of the flame retardant at that particular temperature range.

Introduction

The fire behavior of polymers is extensively studied and reported. Over the years, many tests to measure the flammability of polymers have been developed. Underwriters laboratories, UL-94 test (*1*) is a simple test method used to measure the flammability of polymers. The test although not very scientific in nature, is commonly used by industry for quality control. There are many other tests to

In Fire and Polymers VI: New Advances in Flame Retardant Chemistry and Science; Morgan, A., et al.; ACS Symposium Series; American Chemical Society: Washington, DC, 2012.

measure the flammability of polymers, e.g., limiting oxygen index (LOI), flame spread, cone calorimeter etc. However, none of the test methods quantitatively measures the melt dripping behavior of polymers.

For most melt-processed polymeric materials, resolving melt-dripping problems is more difficult than improving their flame retardancy and the two are often interlinked (*2*). This is partly because there always exists a conflict between reducing both melt dripping and polymer flame retardancy since imparting anti-dripping means the heat applied cannot be transferred and remains in the burning polymer. This makes the flame retardation of the polymer more difficult and presents a major problem when char-forming flame retardants are present. Presence of flame retardants increases the melt viscosity of polymers and affects their rheological behavior (*3*, *4*). A higher melt viscosity is beneficial for reducing melt dripping while burning, although it can be a disadvantage for processing techniques such as extrusion and injection molding. The melt viscosity of the polymer system not only determines the ease of drip formation but also influences the formation of the char and its physical properties during burning (*5*). High shear viscosity results in a slower burning velocity and reduced flame spread. Moreover higher shear viscosities at temperatures near the melting point reduce dripping (*6*). To prove this hypothesis, in this work the effect of different flame retardants on melt dripping in a furnace, melt/flame dripping in the UL94 test and melt viscosity of a commercially important thermoplastic material, polypropylene has been studied. The samples used have been studied in our previous papers where layered silicates were combined with selected flame retardants to enhance fire resistance of polypropylene polymer and fibers (*7–9*). To enhance the dispersion of nanoclays, maleic anhydride grafted polypropylene was used as a compatabilizer. It was observed that nanoclays, although increasing the thermal stability of polypropylene and helping in char formation, did not reduce the flammability of PP to a large extent. When nanoclay and 5% flame retardant were added together to PP containing compatibilizer, the resultant polymer had much reduced flammability (*7–9*). Flame retardants were selected based on their mode of action. These included those acting via chemical mechanisms: phosphorus containing - working in condensed phase, halogen containing - working in vapor phase; and layered silicates (clays) in nanocomposites acting via physical mechanisms. It was also observed that presence of clay reduces the melt dripping tendency of the polymer (*9*). This work aims to quantify this melt dipping behavior and to identify parameters affecting this behavior.

Experimental

Samples

Following materials were used in these samples: *polypropylene* (PP) Moplen HP 516R (Basell Polyolefins), *nanoclay* (E) Bentone E-107, which is montmorillonite modified with dimethyl, dehydrogenated tallow quaternary ammonium ion (Elementis, UK); and pentaerythritol phosphate, NH 1197 (Great Lakes), tris(tribromoneopentyl) phosphate, FR 372 (DSBG, Israel) as *flame retardants (FR).*

Table I. Mass percentages of various components in the formulations

Sample	*PP (%)*	*NOR (%)*	*PB (%)*	*E (%)*	*FR* (%)*
PP	99.0	1.0	-	-	-
PP-E	95.2	0.9	0.9	2.9	
PP-FR*	94.3	0.9	-	-	4.7
PP-E-FR*	90.9	0.9	0.9	2.7	4.5

Note: * FR = NH 1197 or FR 372.

The different formulations prepared for this work are given in Table I. For PP composites the level of clay has been kept at approximately 3% (w/w) and flame retardant about 5% (w/w). All samples contained 1% (w/w) UV stabilizer (Flamstab NOR 116 FF, Ciba SC). Samples containing nanoclays also contained 1% (w/w) maleic anhydride grafted PP (Polybond 3200, Crompton Corp), which was used to improve dispersion of the nanoclay in polypropylene (*7*). Polypropylene and additives were hand mixed in a plastic container prior to compounding. A twin screw extruder (Thermoelectron) with a temperature profile over six heating zones between 179 – 190 °C was used for compounding samples. Polymer was pelletized after cooling in the water bath. Plaques (ca. 3 mm thickness) were cast from the blends by compression molding with spacer plates between aluminium foil-coated steel plates at a set plate temperature of 190 °C for 2.5 minutes followed by rapid cooling.

Sample Characterization

The characterization of polymers and their nanocomposites by X-ray diffraction and transmission electron microscopy has been discussed in our previous publications (*7–9*). These demonstrated that although a high extent of clay exfoliation in the polymer could not be obtained, the organoclay was intercalated with the evidence of a considerable extent of increasing interlayer spacing of the clay platelets. Thermogravimetric analysis and differential thermal analysis (DTA) were performed on all of these sample and their molten drops using an SDT 2960 simultaneous DTA–TGA instrument under flowing air and nitrogen.

Melt Dripping Testing

The experimental set up constructed to measure the melt dripping behavior of polymers is shown in Figure 1. This consists of a home-built, movable electric furnace, details of which are discussed in a previous report (*10*). This 800 Watt furnace has a bore of 25 mm diameter and 120 mm length. The furnace is managed by a temperature controller with adjustable temperature limit up to 900 °C. The temperature controller measures the core surface temperature in the middle of the furnace by a thermocouple.

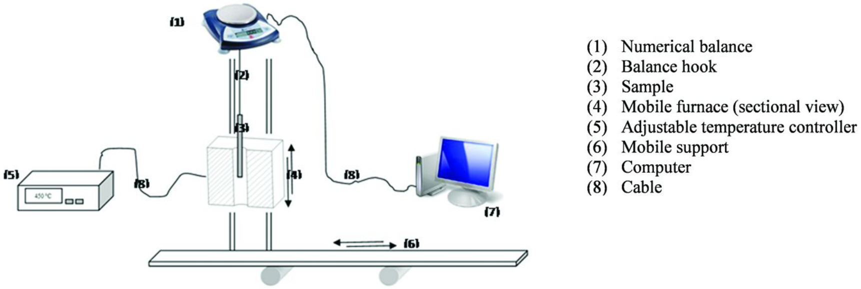

Figure 1. Schematic of the melt dripping experiment.

Dynamic recording of the mass of the polymer sample is made by a digital mass balance (Ohaus Scout Pro) connected to a computer. The mass of the sample is shown to the nearest 0.001 g. Mass lost data are recorded in real time via the data acquisition software provided by the manufacturer. The scale allows weighing of the polymer sample, attached to the bottom of the scale via a thin wire and built-in hook at the bottom of the scale. The sample is fixed and the furnace is raised on rails via a pulley arrangement (See Figure 1), until the bottom of sample is in the centre of the furnace. The temperature is pre-determined and pre fixed before the furnace is mounted. Under the bore of the furnace, a long strip of aluminium foil is placed on a conveyer belt to collect the drops. The conveyer belt moves at a pre-determined uniform speed. The size and the distance between the drops are measured by taking images of the aluminium foils and analyzing the images by an image analysis software, Image J® (image processing and analysis in Java). The experiment is handled in a fume hood. The time when the sample is in position inside the oven is set at zero. Using a video camera the images of falling drops are also taken, which give information about their size and shape.

Sample sizes were 100 x 6 x 3 mm. To determine the temperature setting for the furnace, the control polypropylene sample was tested at different furnace temperatures, the minimum being that at which melt dripping starts and the maximum where the sample begins to burn. Experiments were conducted at four temperatures (625, 660, 690 and 725 °C) (*10*). This paper only presents the results obtained at 660 °C.

Melt Dripping during UL-94 Vertical Burning Test

For this experiment, the same test rig as discussed above was used. However, the furnace was removed and the sample hanging on the hook was ignited with a Bunsen burner of 20 mm flame height according to standard UL-94 procedure. Two different sample sizes were used:

1. 100 x 6 x 3 mm (small size), similar to the one used for melt dripping experiments in a furnace.
2. 125 x 12.5 x 3 mm (standard size), similar to the one used for standard UL-94 tests.

Rheology

Rheological measurements of the polymers and their molten drops were carried out using a Bohlin C-VOR torque dynamic mechanical tester (Malvern Instruments, Malvern, UK) equipped with an oven extended temperature controller. Cone-plate geometry was used with the diameter of the plate 25 mm, cone angle 2.5° and gap size of 75 μm. The measurements were performed in air with heating rate 5 °C/min in a strain-controlled mode with shear strain of 0.1 and oscillation frequency of 1 Hz. A program was applied to heat the samples from 170 to 380 °C.

Results and Discussion

The effect of nanoclay and flame retardants alone and in combination with each other on the thermal stability, flammability and char formation tendency of PP has been discussed in detail in our previous publication (*9*). Here, thermal analysis was used to study the thermal properties, and limiting oxygen index (LOI) values and a slightly modified UL-94 test for the flammability of the samples. All flame retardants acting in the condensed phase (phosphorus- and nitrogen-containing, e.g. NH 1197 discussed here) lowered the rate of decomposition, whereas halogenated flame retardants (e.g., FR 372) had little effect. The addition of nanoclay with or without flame retardants increased the thermal stability of all samples and enhanced char formation. All samples with flame retardants and no clay burnt completely, which is not unexpected, given the low levels (5%) of flame retardants used there. Please note that these samples were intended to be extruded into fibers for potential use in textile structures. Thus the total additive level had to be less than 10% (w/w) to enable processability. Even so, the flame spread for the flame retarded samples was low. On addition of clay, a change in burning behavior was observed, flame spread was reduced and some samples self-extinguished. In the following sections the effect of these components on the melt dripping of PP is discussed.

Melt Dripping in Furnace

The numerical balance connected to the computer (Figure 1) allows obtaining the mass loss as a function of time. As an example mass loss curves for three replicate samples of polypropylene are shown in Figure 2 (a), which shows that the reproducibility of this test method is good in comparison with the UL-94 test data (Figure 2(b)). Results for all samples are given in Figure 3. On analyzing these mass loss curves it can be seen that within first 10 s, there is a sharp mass loss, which corresponds to the first drop of polypropylene. After this sharp mass loss, monotonic mass loss occurs, which corresponds to rapid melting into small drops. This was also observed visually and by taking video images. The images of falling drops collected on the aluminium foil are shown in Figure 4. By dividing the total mass loss in the second mass loss range by total number of drops (counted digitally from Figure 4), the mass of each drop could also be obtained. At the end of each experiment one drop fell, which was of larger mass and diameter compared to the others. The diameters of the drops, measured from images using image analysis software and thicknesses measured manually using digital calipers, are given in Table 2. From the difference in total mass loss (Figure 3) and total mass of drops (weighing the foil before and after the experiment), any volatilization occurring was also calculated.

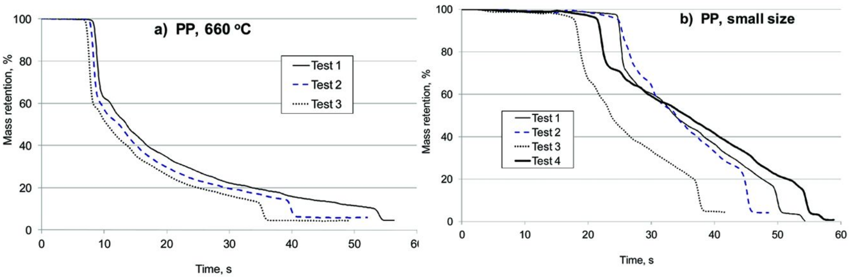

Figure 2. Replicate mass loss test results for PP in a) furnace and b) UL-94 equivalent test showing reproducibility of the test.

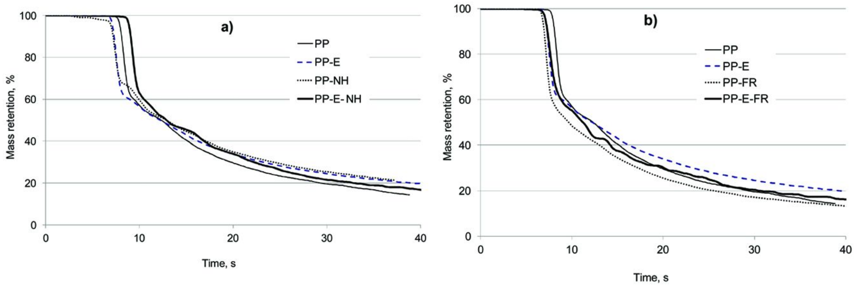

Figure 3. Mass loss test results for PP, PP containing clay and flame retardants, a) NH 1197 and b) FR 372 in furnace tests.

The melt dripping behavior of a polymer is related to its glass transition temperature (*11*) and pyrolysis mechanisms. Polymers pyrolyzing through random chain scission, such as PP (see Scheme 1), are reported to form wax like small-size drips (as also seen here in Figure 4(a)), whereas those pyrolyzing by unzipping reactions, such as PMMA result in large-size dripping in fires (*12*).

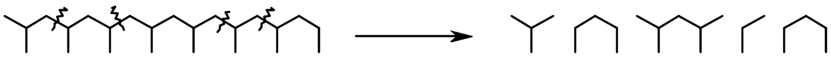

Scheme 1. Thermal decomposition mechanism of polypropylene

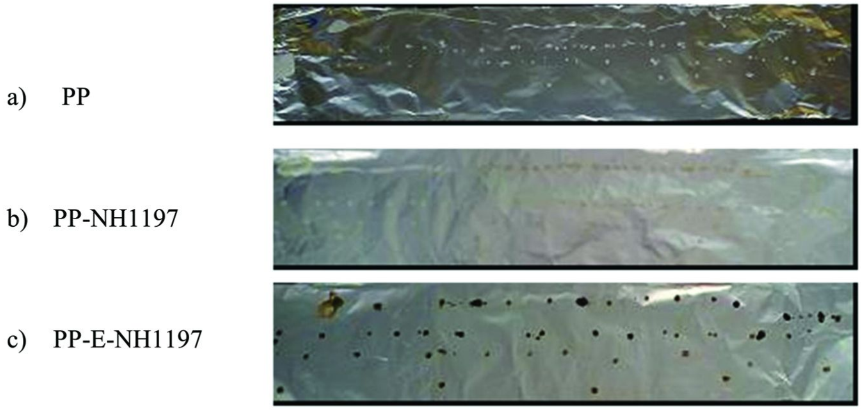

Figure 4. Digital images of a) PP, b) PP-NH 1197 and c) PP-E-NH 1197 drops, collected on aluminium foils.

As can be seen from Table 2, the presence of clay (sample PP-E) had little effect on number or size of drops compared to those of the PP sample. In general the numbers of drops increased and their size decreased; these changes however, are within experimental error range. Similarly both flame retardants had little effect on number and size of drops. However, when both clay and flame retardants are present, the number of drops is significantly reduced and their sizes are increased as also seen visually from Figure 4 (c). Flame retardants however, reduced volatilization indicating that they are active at this temperature and affect decomposition of PP. However, the presence of clay on its own (sample PP-E) or with flame retardants (PP-E-NH 1197 and PP-E-FR 372), had little effect on volatilization. From these results it can be concluded that the combination of nanoclay and flame retardants helps in reducing both the melt dripping and flammability of polypropylene, which is consistent with our earlier observations through other tests (*9*).

Melt Dripping during UL94 Vertical Burning Test

The mass loss curves for small samples shown in Figure 2 (b) indicate that the reproducibility of the test is not as good as for the tests performed in the furnace. Results for all samples are given in Figure 5. Here the first 10 s represent the time taken to ignite the polymer. Compiled results for both sample sizes are given in Table 3. Mass loss in this experiment is due to burning as well as flaming drips.

Table 2. Summary of melt dripping results for PP in furnace at 660 °C

Sample	***First drop***					***Main dripping range***					*Vol (%)*
	T.R.	*N.D.*	*Ms (mg)*	*Dm (mm)*	*Th (mm)*	*T.R. (s)*	*N.D.*	*Ms (mg)*	*Dm (mm)*	*Th (mm)*	
PP	7-9	1	231±21	19.8±8.0	2.5±0.2	10-42	77±3	5±0.25	6.2±1.8	0.4±0.1	35.2±3.6
PP-E	6-8	1	209±25	17.7±6.7	3.0±0.4	8-42	86±6	4±0.4	5.8±1.3	0.5±0.1	40.8±3.7
PP-NH1197	6-8	1	367±34	27.4±4.3	2.5±0.5	8-39	77±1	7±0.7	5.3±0.8	0.3±0.1	14.5±2.5
PP-E-NH1197	9-12	1	221±54	21.8±4.0	2.6±0.5	12-45	50±1	4±0.9	6.7±1.7	0.8±0.3	45.8±8.0
PP-FR372	6-8	1	307±35	22.2±0.7	2.2±0.5	8-41	85±5	5±0.7	6.8±1.5	0.3±0.1	26.5±2.1
PP-E-FR372	6-8	1	244±14	17.4±4.4	2.7±0.3	8-40	23±4	13±1.1	9.2±1.9	1.1±0.3	43.0±1.7

Note: Polym = polymer; T.R. = Time range; N.D. = No of drops; Ms = Mass; Dm = Diameter; Th = Thickness; Vol = Volatilization.

Table 3. Summary of melt/burn dripping results in UL-equivalent test

Sample	***Small size***						***Standard size***					
	T (s)	*N.D.*	*Ms (mg)*	*Dm (mm)*	*Th (mm)*	*B.M. (%)*	*T (s)*	*N.D.*	*Ms (mg)*	*Dm (mm)*	*Th (mm)*	*B.M. (%)*
PP	32±8	163±4	3±1	5.4±1.7	≤0.1	34.8±7.6	107±7	397±29	5±1	/	0.1±0.02	43.4±3.5
PP-E	57±6	93±4	6±1	5.4±3.4	1.1	25.5±5.2	81±46	331±34	6±1	6.7±3.2	0.7±0.3	42±1.0
PP-NH1197	52±3	159±4	2±0.2	5.7±2.1	≤0.1	37.9±6.9	8±2	575±16	0.7±0.1	6.4±1.2	0.3±0.02	0.3±0.05
PP-E-NH1197	40±2	48±6	20±2	5.7±2.6	0.9	12.4±5.4	93±11	196±22	12±2	6.8±3.1	1.2±0.5	31.3±7.0
PP-FR372	34±6	127±8	2±0.3	6.5±1.5	≤0.1	12.6±4.0	6±3	12±18	3.3±0.3	9.7±2.2	0.2±0.05	0.9±0.2
PP-E-FR372	30±3	16±3	21±1.2	8.4±3.3	0.8	38.4±15.4	87±7	295±70	11±6	8.6±5.1	2.9±0.2	28.6±1.7

Note: Polym = polymer; T = Time ; N.D. = No of drops; Ms = Mass; Dm = Diameter; Th = Thickness; B.M. = Burnt Mass.

The number of drops for PP was more for the large sample sizes than for the smaller sample sizes, their diameters however, were similar. There was no trend for samples containing flame retardants. This is due to the fact that some flame retarded samples of large size did not burn. The burnt mass for PP samples containing clay alone or with flame retardants is much higher than PP containing flame retardants only. This is due to the fact that the clay increased the melt strength of the polymer and holds the polymer together, resulting in increased burning as also seen in our previous work (*9*). PP samples containing clay produced fewer drops compared to pure PP. On comparing these results with melt dripping in furnace, although no numerical co-relationship could be observed, the trend observed for small sized samples is similar to those in furnace. Larger samples due to lack of reproducibility, showed no real trend.

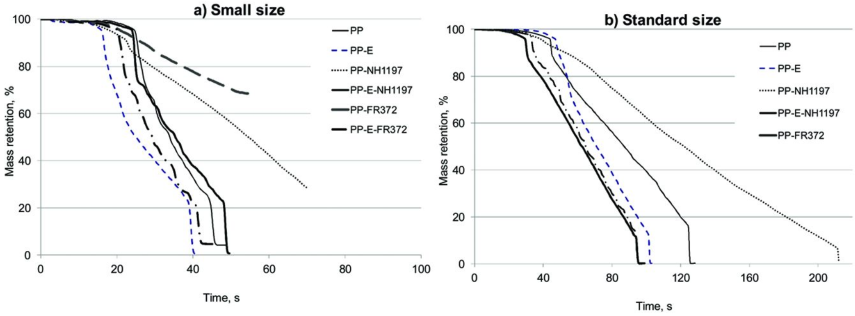

Figure 5. Mass loss as a function of time for a) small and b) standard size samples in UL-94 equivalent test.

Rheology

The complex viscosity values for all samples are plotted as a function of temperature in Figure 6. The viscosity of pure polymer decreases in the entire temperature range, which is predominantly due to the temperature influence on the viscosity. However, the decomposition into smaller molecules contributes to some extent to a viscosity decrease above the onset temperature of PP decomposition. The details of this will be discussed in a separate paper. It should be indicated that the viscosity data is only valid before the evolution of volatiles occurs. Gas bubbles and voids could be present during volatile formation and evolution. Therefore the viscosity data obtained at higher temperatures may not represent the inherent viscosity of the polymer and is better regarded as an apparent viscosity. The minimum viscosities and their temperatures are reported for all samples in Table 4. For clay and flame retarded samples, the viscosity increases above 250 °C due to char nucleation. The nucleation temperature of char formation is in the order: PP-NH 1197 < PP-E ≈ PP-E-NH 1197 ≈ PP-E-FR 372 < PP-FR 372. This shows that presence of clay plays an important role in nucleation and char formation.

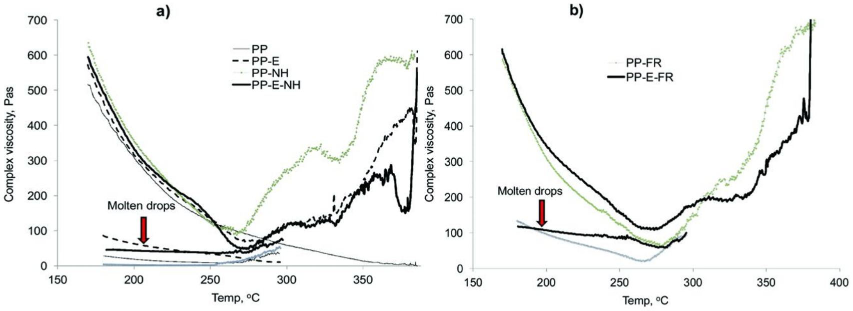

Figure 6. Complex viscosity of flame retarded PP samples and their molten drops as a function of temperature.

Table 4. Complex viscosity of polymers and their molten drops

Sample	*Temp., where viscosity is minimum (°C)*	*Viscosity of polymers at min temp (Pas)*	*Viscosity of polymers at 200 °C (Pas)*	*Viscosity of molten drops at 200 °C (Pas)*	*% Loss in viscosity of molten drips at 200 °C*
PP	370	4.6	305.4	18.7	93.9
PP-E	275	74.5	317.5	63.5	80.0
PP-NH	268	92.7	354.3	3.2	99.1
PP-E-NH	275	50.3	333.6	43.1	87.1
PP-FR	280	63.3	309.5	96.7	68.8
PP-E-FR	274	113.9	344.9	107.4	68.9

Characterization of Molten Drops

In a separate experiment, the molten drops of the control polypropylene sample were collected in a pan just below the furnace hole. The pan was lined with aluminium foil and insulated on three sides with ceramic wool. Two thermocouples were inserted in the pan to record the temperature as they were falling. The temperature varied between 245 and 345 °C. As can be seen from TGA curves of polymer samples in Figure 7 and their analyzed results in Table 5, at 345 °C, decomposition has started and hence, the molten drops are not the pure polymer but decomposed version of the polymer. This is more evident from the TGA curves of the molten drops in Figure 7, which are very different compared to the polymer samples.

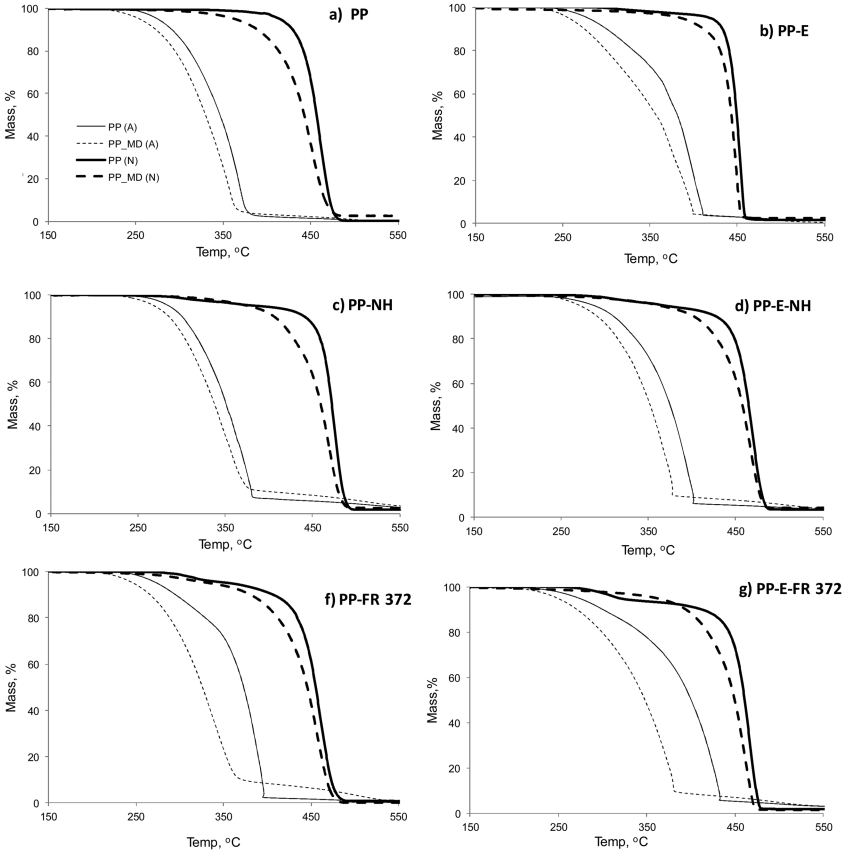

Figure 7. Themogravimetric curves of polymer samples (solid line) and their molten drops (dashed lines) in air (lighter lines) and nitrogen (bold lines).

The degree of degradation has been calculated by measuring the temperature (T_{50}) where 50% mass loss occurs in the polymer and at the same temperature the residual mass of the molten drop, and from the mass difference between the these two relative to the mass of the pure polymer.

Complex viscosities of molten drops were also measured similar to those of pure polymers, and were shown to be significantly lower than viscosities of the starting polymer and composite (Figure 6(b) and viscosity values at 200 °C in Table 4). In Figure 8, loss in viscosity is plotted against the degradation observed from TGA. Good corelaton in air is observed. In air the decomposition is oxidative, hence the viscosity of the polymer decreases. No such conclusion can be drawn from a similar plot for the results obtained in nitrogen Figure 8 (b), this is interesting information as in the furnace experiments the environment is air. In future work, melt dripping in the furnace will be studied under nitrogen atmosphere to understand these observations in depth.

Table 5. Thermal analysis results of PP, PP containing clay and FRs

Polymer		*DTA Peaks*		*TGA Analysis*		*Degradation** (%)*
		Melting endo (°C)	*Decomp. peak; Exo or Endo(-) (°C)*	*T_{Onset}**	*DTG maxima (°C)*	
PP	Polymer	172 (172)	232, 366 (-458)	274 (415)	367 (459)	36.8 (49.0)
	Molten drops	164 (164)	218, 356 (-447)	254 (356)	357 (450)	
PP-E	Polymer	172 (168)	289, 411 (-454)	280 (417)	369, 398 (453)	27.5 (23.5)
	Molten drops	167 (163)	261, 400 (-449)	258 (385)	373, 395 (448)	
PP-NH1197	Polymer	172 (171)	265, 348, 358, 375 (365, -475)	285 (385)	349, 360, 377 (475)	34.1 (22.8)
	Molten drops	166 (164)	230, 343, 355, 458 (365, -467)	268 (375)	343, 358 (469)	
PP-E-NH1197	Polymer	171 (171)	237, 402 (-470)	285 (359)	392, 398 (469)	19.5 (35.6)
	Molten drops	164 (164)	228, 377(-467)	270 (357)	364, 375 (467)	
PP-FR372	Polymer	170 (171)	253, 393 (460)	271 (344)	287, 392 (461)	9.8 (33.2)
	Molten drops	150 (152)	214, 349, 465 (459)	243 (327)	339, 507 (455)	
PP-E-FR372	Polymer	171 (172)	238, 433 (-466)	273 (362)	295, 429 (466)	8.7 (24.4)
	Molten drops	149 (136)	245, 380 (-461)	249 (317)	377 (461)	

* T_{Onset} = Onset of decomposition temp, where 5 % mass loss occurs ** Degradation = (50% Mass loss in polymer at T_{50} – mass loss of molten drops at T_{50})/ 50 X 100.

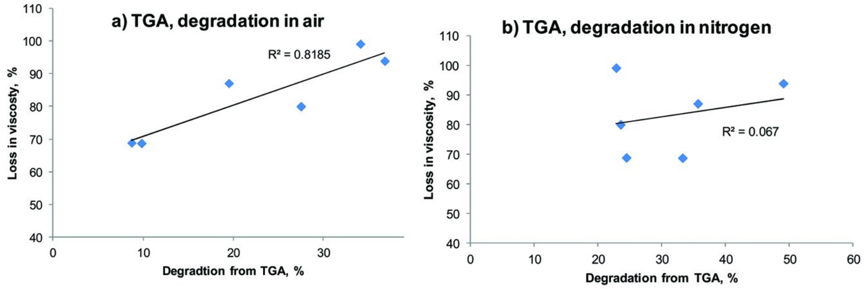

Figure 8. Relationship between % loss in viscosity (Table 4) and % degradation of molten drops observed from TGA (Table 5).

Conclusions

This work has shown that melt dripping of polypropylene (PP) can be quantified in a reproducible manner. The number of melting drops produced as well as their masses, diameters and thicknesses can be determined. These parameters have been found to be effected by the presence of clay, flame retardants or their combination. Flame retardants with minimal effect on PP rheology also have minimal effect on its melt dripping behavior. However, the presence of clay with a flame retardant reduced the number of molten drops observed but increased their sizes. This behavior could be related to an increase in the complex viscosity of these samples above 250 °C due to char nucleation, whereas for pure PP the viscosity decreases with increase in temperature. Characterization of the molten drops by thermogravimtery established that during melt dripping considerable degradation of the polymer occurs. Also, the viscosity of the molten drops was much less than that of the respective PP/clay/FR polymers. Thus, this work has proven experimentally that melt dripping of a polymer is due to the combined effect of physical melting and polymer decomposition. This behavior can be altered by suitable choice of flame retardants active at the temperature range where melt dripping of the polymer occurs

Acknowledgments

Authors wish to acknowledge late Prof Menachem Lewin (1918 – 2011) for the inspiration and initial discussions for designing the experimental strategy. Authors also thank Victor Fabre from École Polytechnique Universitaire de Montpellier, France for calibration of the melt dripping test rig as a part of his undergraduate internship programme at University of Bolton.

References

1. Test for Flammability of Plastic Materials for Parts in Devices and Appliances; UL-94, 1996.
2. Wang, Y-Z. *Advances in Fire Retardant Materials*, Horrocks, A. R.; Price, D., Eds.; Woodhead Publishing: Cambridge, U.K., 2008; Chapter 4.
3. Zhang, J.; Lewin, M.; Pearce, E.; Zammarano, M.; Gilman, J. W. *Polym. Adv. Technol.* **2008**, *19* (7), 928.
4. Lewin, M.; Zhang, J.; Pearce, E.; Zammarano, M. *Polym. Adv. Technol.* **2010**, *21* (11), 825.
5. Duquesne, S.; Delobel, R.; Le Bras, M.; Camino, G. *Polym. Degrad. Stab.* **2002**, *77*, 333.
6. Bartholmai, M.; Schartel, B. *Polym. Adv. Technol.* **2004**, *15*, 355.
7. Horrocks, A. R.; Kandola, B. K.; Smart, G.; Zhang, S.; Hull, T. R. *J. Appl. Polym. Sci.* **2007**, *106* (3), 1707.
8. Kandola, B. K.; Smart, G.; Horrocks, A. R.; Joseph, P.; Zhang, S.; Hull, T. R.; Ebdon, P.; Hunt, B. *J. Appl. Polym. Sci.* **2008**, *108* (2)–816.
9. Kandola, B. K.; Yenilmez, A.; Horrocks, A. R.; Smart, G. In *Fire and Polymers*; Morgan, A., Nelson, G. L., Wilkie, C. A., Eds.; ACS Symposium

Series 1103; American Chemical Society: Washington, DC, 2009; Chapter 5, p 47.

10. Kandola, B. K.; Price, D.; Milnes, J.; Da Silva, A. *Polym. Degrad. Stab.* **2012**, submitted for publication.
11. Zhang, J.; Shields, T. J.; Silcock, G. W. H. *Fire Mater.* **1997**, *21*, 1.
12. Ohlemiller, T. J.; Butler, K. Influence of polymer melt behavior on flammability; NIST Report NISTIR 6588, 2000.

Chapter 22

Textile Flame Retardancy Through Surface-Assembled Nanoarchitectures

Federico Carosio,* Jenny Alongi, Alberto Frache, Giulio Malucelli, and Giovanni Camino

**Dipartimento di Scienza Applicata e Tecnologia, Politecnico di Torino,
Alessandria Campus, Viale T.Michel 5, 15121 Alessandria, Italy
*E-mail: federico.carosio@polito.it**

Single step and multi-step adsorption processes have been investigated in order to enhance flame retardancy of poly(ethylene terephthalate) fabrics and their blends with cotton. The first strategy concerns single step nanoparticle adsorption in a finishing-like process upon plasma surface activation. This approach aims at evaluating the effectiveness of nanoparticle simple adsorption on fabric combustion properties and the enhancement promoted by the plasma surface activation performed at different processing conditions. Subsequently, the layer by layer assembly technique has been investigated as an evolution of the nanoparticle adsorption. This technique, which consists in a multi-step adsorption process, allows the build-up of coatings made of different kinds of nanoparticles and polymers, each one bearing a specific functionality. By using the multi-step approach, hybrid organic-inorganic or completely inorganic coatings have been deposited on selected fabrics and subjected to flammability and combustion tests.

Introduction

Nowadays fabric flammability still represents a severe threat to the safety of people and buildings. The use of natural and synthetic fibers involves different problems: the former can catch fire very easily and burn with vigorous flame, while the latter can melt during combustion, leading to the formation of incandescent drops that are able to spread the fire to other ignitable materials.

In Fire and Polymers VI: New Advances in Flame Retardant Chemistry and Science; Morgan, A., et al.;
ACS Symposium Series; American Chemical Society: Washington, DC, 2012.

Since 1950, chemists have been continuously developing flame retardant treatments able to reduce fabric flammability; in particular, the 1950-80 period is often referred as "the golden age" for what concerns flame retardancy chemistry (*1*). This period was really a golden age when the combination of increased fire safety concerns, which led to several legislations and regulations (*2–4*), and the virtual absence of constraints in the use of chemicals, promoted the development of most of the presently used flame retardants (*5–8*). Meanwhile, governments started worrying about environmental and health risks related to the use of certain types of flame retardants. As a result, most of the high performing flame retardants developed in the early 1950-80 were banned or limited as far as their application field is concerned (*1*). As a consequence, during the last decades, scientists had to refine the chemistry of the 50-80's in order to obtain more cost-effective flame retardants and remove the treatments that have shown an unacceptable level of environmental risk (*9*, *10*).

The above scenario opened the way for novel and non-conventional procedures such as surface or bulk modifications achieved by exploiting nanotechnology. However, when applied to the bulk, this technology had to face several problems such as compatibility between polymer and nanoparticles (*11*), effect on rheology during compounding (*12*, *13*), and a level of achieved flame retardancy often not completely satisfactory (*14*, *15*). On the contrary, a valuable and promising application of nanotechnology has been found in the surface modifications. Indeed, in the last ten years, nanotechnology has been applied for surface modifications in order to develop after-treatments capable of adding flame retardant properties to the selected textiles without significant modifications of the underlying fabric properties. Among the different approaches, techniques based on nanoparticle adsorption such as single- and multi-step (layer by layer) processes can be found. The single step nanoparticle adsorption represents the easiest way for pursuing a surface modification using nanoparticles and simply consists in the immersion of the fabric into a water suspension of nanoparticles in order to promote their adsorption on the fiber surface similarly to a finishing treatment (impregnation and exhaust). The adsorption process can be repeated several times (using different reagents at each adsorption step), leading to a multi-step process known as layer by layer (*16*).

This step-by-step film build-up based on electrostatic interactions was introduced in 1991 for polyanion/polycation films in order to obtain the so-called *polyelectrolyte multilayers* (*17*) and subsequently extended to inorganic nanoparticles (*18*). The procedure for obtaining such multilayer films requires the alternate immersion of the substrate into an oppositely charged polyelectrolyte solution (or nanoparticle dispersion); this process, which leads to a total surface charge reversal after each immersion step (*19*), creates a structure of positively and negatively charged layers piled up on the substrate surface.

Surface adsorption techniques mimic their flame retardant mechanism on that of bulk nanocomposites, for which a physical effect exerted by a ceramic barrier developed during combustion is observed (*20–23*). Upon adsorption from a suspension, the nanoparticles are already on the surface of the polymer and thus the aforementioned physical barrier can protect the substrate from the very beginning of the combustion.

In the present work, we discuss different approaches based on surface adsorption techniques, in order to build simple or complex nanoarchitectures able to enhance the flame retardancy of poly(ethylene terephthalate) (PET) fabrics and their blends with cotton. The first strategy concerns the single step adsorption of nanoparticles (namely hydrotalcite, silica and sodium montmorillonite) in a finishing-like process. Furthermore, the effects of cold plasma pre-treatment (etching), that should enhance the surface interaction and favor the nanoparticle adsorption, will be discussed (*24*, *25*). Subsequently, the layer by layer assembly technique will be presented as an evolution of the single-step adsorption for depositing simple or complex architectures characterized by completely inorganic or hybrid organic-inorganic compositions (*26–29*).

Results and Discussion

Single-Step Adsorption

This approach consists in the fabric immersion from 30 min to 1 h in a 0.3 to 1 wt.-% water suspension of nanoparticles. The surface morphology changes after the immersion and subsequent thermal treatment have been investigated by Scanning Electron Microscopy (SEM). Figure 1 shows the typical micrographs of PET treated by a single step adsorption of hydrotalcite (HT), silica (SiO_2) and sodium montmorillonite (CloNa), respectively.

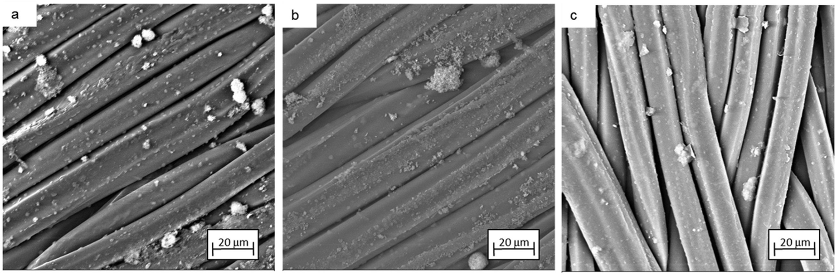

Figure 1. SEM micrographs of PET fabrics coated by single step adsorption of hydrotalcite (a), silica (b) and sodium montmorillonite (c).

As clearly observable, all the treated samples are characterized by a rougher surface with respect to untreated PET; this finding is ascribed to the presence of adsorbed nanoparticles that are homogeneously distributed on the fabric surface and form agglomerates with dimensions ranging from sub-micrometers to several micrometers.

The combustion resistance turns out to be enhanced only in the case of PET fabrics treated with HT and CloNa, as can be seen in Figure 2.

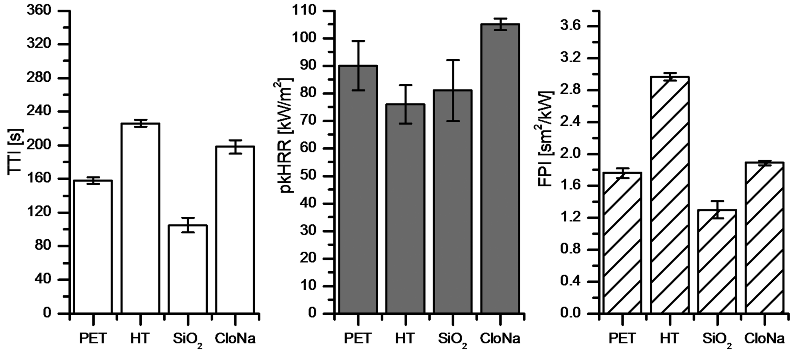

Figure 2. Cone calorimetry data (35 Kw/m²) for neat PET and PET coated by single-step adsorption of hydrotalcite (HT), silica (SiO_2) and sodium montmorillonite (CloNa). [data from refs. (24) and (25)]

Indeed, while SiO_2 treated samples show a 53 s reduction of Time to Ignition (TTI), this value increases by 68 and 48 s in the presence of HT and CloNa, respectively. Contrasting effects of nanoparticles on TTI of polymer nanocomposites have been previously found in the literature, the reasons for which are not yet understood (*30*). Furthermore, a 16% reduction of the peak of Heat Release Rate (pkHRR) is observed for HT whereas CloNa unexpectedly on the basis of literature data (*31*), shows a 17 % increase; SiO_2 samples yielded a reduction of 10% which falls in the accepted error of the cone calorimeter measurements. The Fire Performance Index (FPI =TTI/pkHRR), which averages TTI and PkHRR in the evaluation of Fire Risk, increasing when fire risk decreases (*32*), increases by 69 and 8 % in the case of HT and CloNa, respectively. Thus, with CloNa pkHRR increase is compensated by increase of TTI. On the contrary, in the case of SiO_2 the slight reduction in pkHRR does not overcome the TTI decrease, leading to a lower FPI as compared to pure PET.

A cold plasma surface treatment has been developed for PET textiles in order to increase the fiber hydrophilicity and produce a suitable substrate for further nanoparticle adsorption. Such different process parameters of the plasma treatment as power (50, 80 and 120 W) and etching time (15, 60 and 180 s) have been investigated and related to the final combustion properties achieved after the subsequent CloNa nanoparticle adsorption. Figure 3 depicts the obtained results.

As far as TTI is concerned, it is possible to observe an overall improvement for all the cold plasma-treated fabrics, in particular when the activation is performed for the longest time (180 s) and intermediate power (80 W) in the explored range, with doubling of TTI with respect to untreated PET. Comparing pkHRR values, plasma activated fabrics show average pkHRR values that are within the error range of the reference. As a consequence, all the plasma-etched fabrics have a Fire Perfomance Index greater than 1.76 of the untreated fabric.

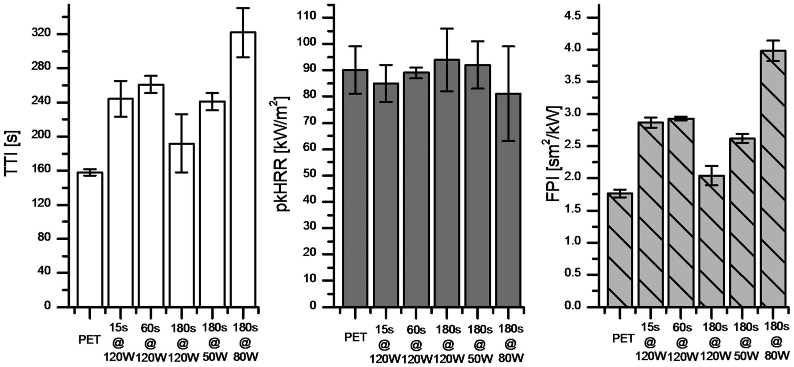

Figure 3. Cone calorimetry data for neat PET and PET coated by single-step adsorption of CloNa after cold plasma pre-activation performed at different powers and times. [data from ref. (25)]

Adsorbed CloNa nanoplatelets onto PET fabric surface can delay the sample ignition since they act as a barrier that protects the underlying polymer from heat and traps volatile products released from PET thermal degradation. Plasma etching can further promote this effect by: i) creating a more reactive and hydrophilic surface (*33*), which increases the amount of nanoparticles adsorbed during the immersion, and ii) developing stronger and more efficient interactions between the surface and the nanoparticles with respect to conventional adsorption phenomena. In addition, it is quite evident that power and etching time play different roles as depicted in Figure 3: indeed, high powers (120 W) combined with long treatment times can have a detrimental effect, while long treatment times can still lead to good properties when performed at lower powers.

Multistep Adsorption of Silica-Based Coatings

As an evolution of the single step process, a multi-step (i.e. layer by layer) adsorption has been applied in order to build up a completely inorganic silica coating on PET fabrics. To this aim, positively charged commercially available alumina coated silica nanoparticles (10 nm) have been coupled with negatively charged silica nanoparticles having different size (30 or 10 nm respectively) in order to build a coating made of bilayered (BL) architectures on the fiber surface (*26*). The best architectures, combustion behavior of which will be described in the following, turn out to be those made of the smallest nanoparticles (10 nm): their SEM micrographs show the formation of a thin and homogeneous coating, as shown in Figure 4.

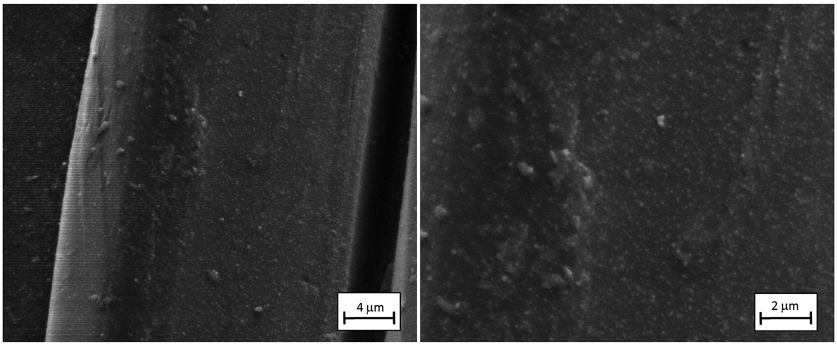

Figure 4. SEM micrographs of PET fabrics coated by 10 BL silica/silica 10/10 nm coating.

By vertical flame test, ASTM D6413, samples treated with 5 and 10 BL were found to reduce the burning time by 63 and 94%, respectively. The same samples were also able to suppress the incandescent melt-dripping phenomenon typical of PET fabrics, whereas dripping appears when the number of BL increases up to 20. This behavior suggests that a relationship exists between coating stability and fire performance achieved. Indeed, 5 and 10 BL treated samples appear to be very stable, unlike 20 BL coatings, which can likely flake off during the test, thus resulting in a less effective fire protection. A similar behavior has been found also during cone calorimetry tests (Figure 5).

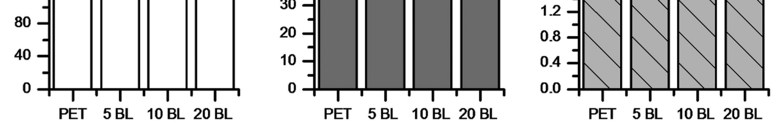

Figure 5. Cone calorimetry data (35kW/m²) for neat PET and PET treated by 5, 10 and 20 BL. [data from ref. (26)]

The histograms in Figure 5 indicate that, despite the great variability for TTI, the samples treated with 5 and 10 BL show a TTI increase of 99 and 32 s, respectively. A significant variation of pkHRR values can be appreciated only for 5 BL (-20%); as a consequence of both the great increase of TTI and the reduction of pkHRR, the FPI of 5 BL is strongly increased with respect to the uncoated fabric. Again, an increased number of BL does not necessary lead to better fire performances; this behavior could be ascribed to the coating instability during combustion (*26*).

Multistep Adsorption of α-Zirconium Phosphate-Based LbL Coatings

In the following, LbL will be extended to the use of negatively charged α-zirconium phosphate (ZrP) nanoplatelets with either octapropylammonium-functionalized POSS® (POSS/ZrP) or alumina-coated silica nanoparticles (SiO_2/ZrP), both bearing positive charges (*27*). Typical morphologies achieved after deposition of ZrP-based coatings are depicted in Figure 6.

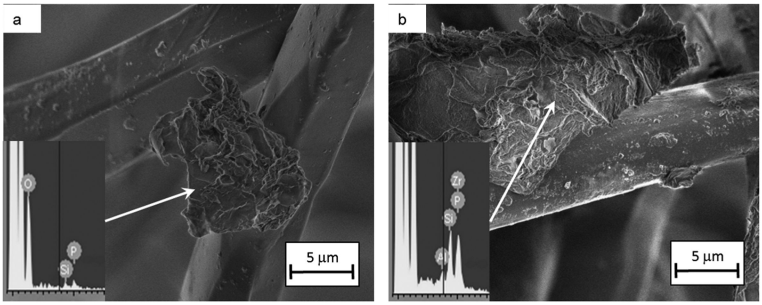

Figure 6. SEM micrographs of PET fabrics coated by 10BL POSS/ZrP (a) and 10BL SiO_2/ZrP (b). Inlets: EDS analyses.

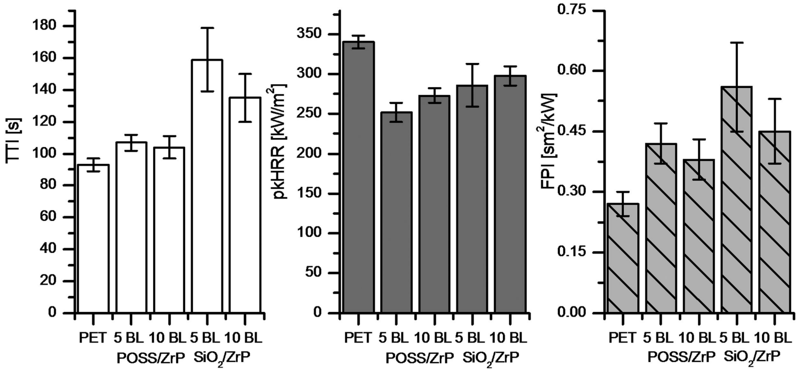

Figure 7. Combustion properties of neat PET and PET coated by 5 and 10 BL of POSS/ZrP and SiO_2/ZrP assemblies. Cone calorimeter at 35 kW/m^2. [data from ref. (27)]

A strong change in surface morphology is clearly observable after the LbL deposition: in particular, big aggregates are found on the fiber surfaces regardless of the coating composition. EDS analyses shown in Figure 6 suggest that such aggregates are complexes of ZrP and either POSS® or SiO_2 respectively, which are generated close to the fiber surface at each deposition step due to an un-optimized washing step. Although the typical LbL morphology is not achieved, the treated fabrics yielded good results when subjected to cone calorimetry tests as reported in Figure 7.

As far as POSS assemblies are concerned, a slight TTI increase is observed, while pkHRR is strongly reduced by 26 and 20 % for 5 and 10 BL, respectively. SiO_2-based assemblies show an inverse proportionality between BL number and both TTI increase and pkHRR decrease. From an overall point of view, the FPI values of the treated fabrics are higher than for uncoated PET and reach the highest value with 5 BL SiO_2/ZrP, due to the strong TTI increase. The smoke parameters are collected in Figure 8.

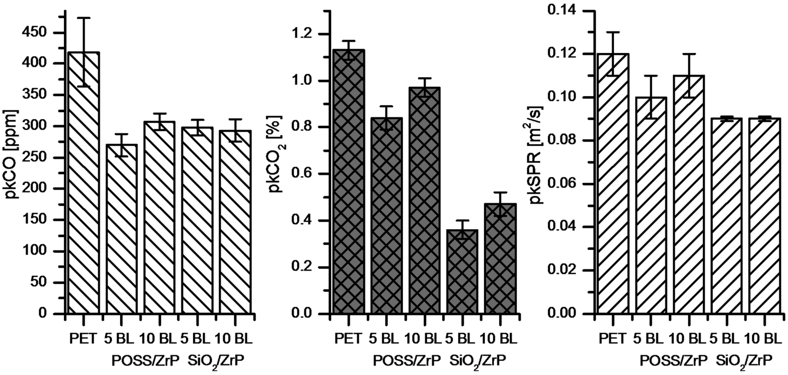

Figure 8. Smoke parameters of neat PET and PET coated by 5 and 10 BL of POSS/ZrP and SiO_2/ZrP. Cone calorimeter at 35 kW/m^2. Maxima for CO (pkCO), CO_2 ($pkCO_2$) and smoke evolution (pkSPR). [data from ref. (27)]

From a broad point of view, it seems that both the assemblies are capable of influencing the smoke parameters. However, as observed before, when referring to POSS assemblies, it is possible to detect an inverse proportionality between BL number and the smoke reduction efficiency, with 5 BL POSS showing greater effects on both pkCO (-35%) and $pkCO_2$ (-25%) reductions, while 10 BL affects pkCO and $pkCO_2$ for -26% and -14%, respectively. On the contrary, both SiO_2-based assemblies (5 and 10 BL) seem to affect smoke production at the same level (-20% pkSPR), with a 30% reduction of pkCO and an even larger effect on $pkCO_2$.

As clearly understandable from combustion and smoke data, even though each considered assembly did not promote the formation of a homogeneous coating, all the described LbL nanoarchitectures were able to enhance PET flame retardancy by increasing the time to ignition, decreasing the combustion kinetics and reducing the smoke production.

Multistep Adsorption of APP-Based Coatings

The layer by layer technique has been also applied to polyester-cotton blends (PET-CO, cotton-rich) in order to enhance their flame retardancy by exploiting the formation of a hybrid organic inorganic coating made of chitosan (Chi) and ammonium polyphosphate (APP) (*28*). PET-CO blends represent high performance and low price products; unfortunately, from the flame retardancy point of view, they also combine the flaws of both the fibers. The presented Chi/APP assembly should act as an intumescent-like system, in which chitosan represents both the carbon source and the foaming agent, while APP is able to generate phosphoric acid directly *in situ* at high temperatures (*34*). After the deposition of 5, 10 and 20 BL on PET-CO blends, a homogeneous surface coverage can be achieved, as depicted in Figure 9.

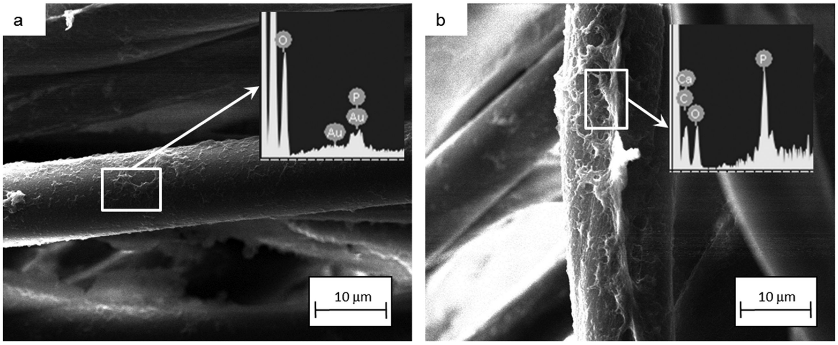

Figure 9. SEM micrographs of PET-CO fabrics coated by 20BL Chi/APP. Inlets: EDS analyses for PET (a) and cotton fibers (b).

Indeed, as clearly observable, the LbL coating homogeneously covers both cotton and PET fibers. Furthermore, it seems that, due to the more hydrophilic nature of cotton with respect to PET, the coating grows thicker on cotton fibers as qualitatively confirmed by EDS analyses (Figure 9).

When exposed to a small methane flame, irrespective of the considered BL number, such coatings do not significantly change the burning time of the pure blend but can suppress the afterglow phenomenon typical of the untreated PET-CO blend.

In addition, the deposited coatings are able to partially protect the blend during the combustion, yielding a consistent residue that increases by increasing the BL number (3, 5 and 8 % for 5, 10 and 20BL, respectively).

Referring to cone calorimetry tests, the deposited coating anticipates the time to ignition (12, 17 and 17 s for 5, 10 and 20BL vs. 22 s for the untreated blend). This behavior can likely be ascribed to the presence of hydroxyl groups in the chitosan molecules that are able to catalyze the thermal decomposition of cotton, as already described in the literature (*35*). In addition, a similar effect induced by the presence of APP is well documented in the literature (*1*). Although this could seem a detrimental effect, the anticipation induced by APP could be extremely

In Fire and Polymers VI: New Advances in Flame Retardant Chemistry and Science; Morgan, A., et al.;
ACS Symposium Series; American Chemical Society: Washington, DC, 2012.

advantageous since it promotes the formation of a thermally stable carbonaceous structure (*char*) at lower temperatures, avoiding the evolution of volatile species and limiting the further degradation and combustion of the polymer blend. As a consequence of the afore-mentioned mechanism, the Chi/APP pair turns out to significantly reduce the total heat release and the corresponding rate (evaluated as pkHRR) in a remarkable way (162, 138 and 128 kW/m^2 for 5, 10 and 20BL vs. 170 kW/m^2 for the untreated blend) as reported in Figure 10.

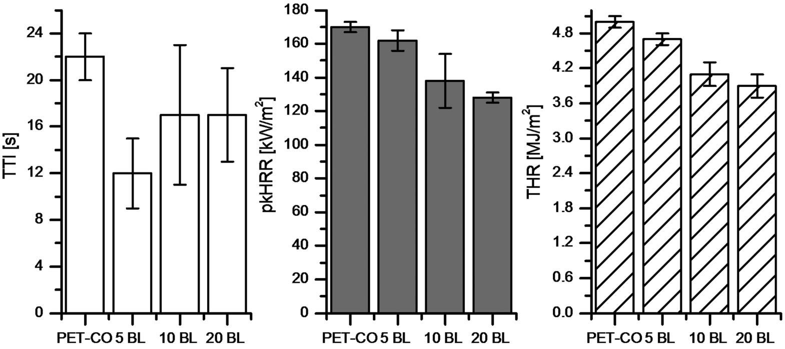

Figure 10. Cone calorimetry data (35 kW/m^2) for neat PET-CO and PET-CO coated by 5, 10 and 20 BL of Chi/APP. Time to Ignition (TTI), peak of Heat Release Rate (pkHRR), Total Heat Release (THR). [data from ref. (28)]

On the basis of these results, it is possible to conclude that the higher the BL number, the lower is the combustion rate. The most evident drawback of this system can be found in the significant release of smoke with respect to the pure blend, as depicted in Figure 11.

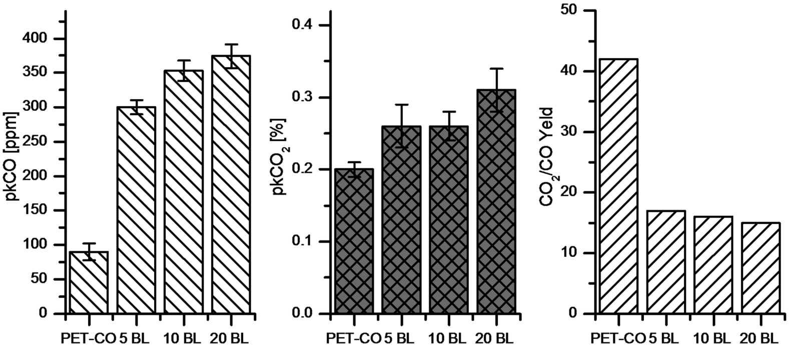

Figure 11. Smoke parameters of neat PET-CO and PET-CO coated by 5, 10 and 20 BL of Chi/APP. [data from ref. (28)]

Indeed, the formation of carbon monoxide and dioxide is favored for all the treated samples and the CO_2/CO ratio is considerably lower than that of the pure blend. This behavior confirms the occurrence of inefficient combustion, as observed in Figure 10, due to the restricted diffusion of oxygen into the pyrolysis zone (*36*). Again, as discussed for flammability, this effect is able to favor the char formation and yield coherent residue after combustion. SEM analyses performed on the 20BL residue show that the treated fabric is capable of partially maintain its original texture as depicted in Figure 12.

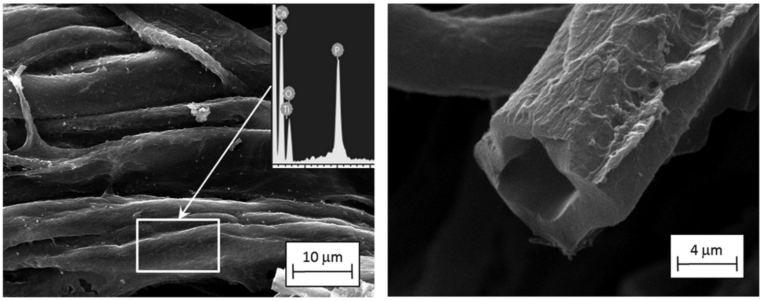

Figure 12. SEM micrographs performed on the cone combustion residue of PET-CO fabrics coated by 20BL Chi/APP. Inlets: EDS analysis.

EDS analysis evidences the presence of phosphorus and carbon, thus indicating that both the coating and the fiber char are partially present after the combustion process.

Hybrid Organic-Inorganic APP Based LbL Complex Architectures

Complex architectures made of chitosan, ammonium polyphosphate and silica have been built up on PET-CO fabrics in order to exploit the good HRR reduction achieved with chitosan and the consistent TTI increase derived from the presence of the above-mentioned silica/silica coating (*26*, *28*). Two different complex architectures containing all these constituents have been assembled, i.e. a quad-layer (QL) unit made of chitosan/ammonium polyphosphate/silica/silica and a bi-layer+bi-layer (BL+BL) unit, which consists of chitosan/ammonium polyphosphate bilayers (5 or 10) covered by silica/silica bilayers (5 or 10) (*29*). The morphology of the fibers after the LbL treatments has been assessed by SEM observations: some typical micrographs of the 10 QL and 10 BL+BL architectures are shown in Figure 13.

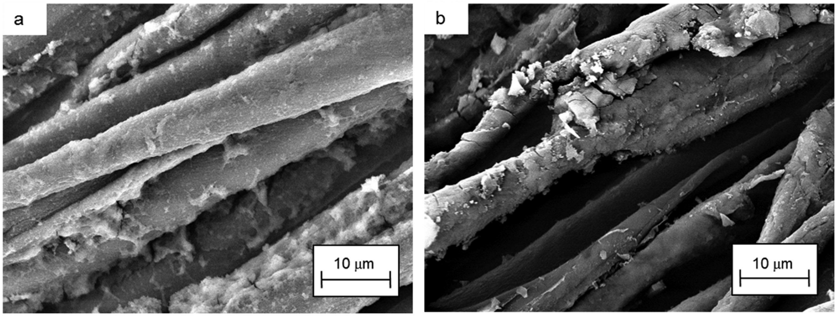

Figure 13. SEM micrographs performed on PET-CO fabrics coated by 10 QL (a) and 10 BL + BL (b).

As far as QL are considered, a continuous and homogeneous coating can be observed on both the fibers; a similar good surface coverage can be detected also for the BL + BL architecture, even though some cracks appear. This finding is likely due to the overloaded coating and therefore the crack formation presumably depends on the BL + BL deposited architecture.

Indeed, by comparing the structures of the two assemblies, it is quite evident that QL are potentially more flexible than BL+BL counterparts and thus the former are capable to maintain a good adhesion with both cotton and PET fibers and to prevent the crack formation.

When these architectures are subjected to flammability tests, as already observed for Chi/APP-based coatings, they lead to the suppression of the afterglow phenomenon and to an increased residue.

In addition, the morphology of the deposited coatings appears to play a key role as far as the combustion behavior is considered; indeed, as reported in Figure 14, the BL + BL architecture shows a detrimental effect for what concerns TTI and pkHRR.

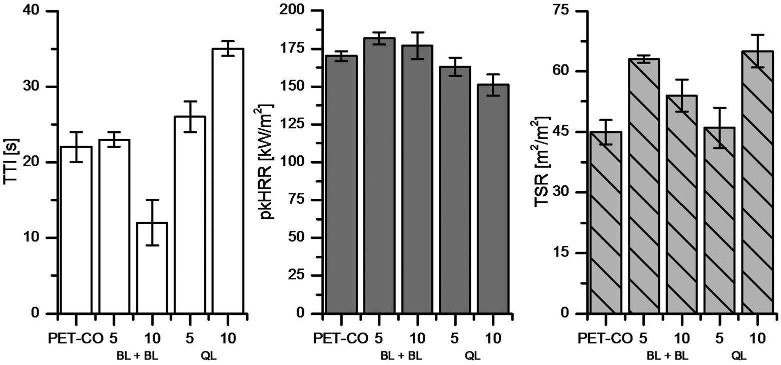

Figure 14. Cone calorimetry data for neat PET-CO and PET-CO fabrics coated by BL+ BL or QL architectures. [data from ref. (29)]

This finding can be ascribed to the numerous cracks exhibited by the samples that can act as preferential channels for the leakage of the gaseous species produced during heat exposure. On the contrary, TTI increases for both the quadlayer assemblies; indeed, as observed from SEM micrographs, the coating is compact and capable of protecting the substrate during the early stage of heat exposure and during the combustion process. However, only 10 QL, probably because of the high APP content as well as the very low number of cracks, proved to be quite efficient for both TTI and HRR. Conversely, the TSR increase assessed for all the treated fabrics is a clear confirmation of a detrimental effect exerted by the complex LbL architectures on the smoke production (Figure 10).

Conclusions

In the present work, we have successfully exploited single- or multi-step surface adsorption techniques, i.e. the adsorption of nanoparticles (namely hydrotalcite, silica, sodium montmorillonite, POSS® and zirconium phosphate) in a finishing-like process or the layer by layer assembly, in order to deposit nanostructures on the surface of poly(ethylene terephthalate) fabrics and of their blends with cotton. Furthermore, the effects of a cold plasma pre-treatment performed on the fabrics prior to the surface adsorption, have been deeply investigated. All the surface treatments turned out to significantly influence the flammability and combustion behavior of the fabrics, according to the adopted adsorption technique, the type, the number and the structure of the deposited nanoparticles and/or nanolayers.

Besides the surface-layered nanoparticles, exploitation of the intumescent shield generated by char and foaming precursors of multiple surface nanolayers has been shown to be suitable for fabric protection with potential performance enhancement by combination with inorganic particle layers.

The proposed surface adsorption methods have been shown to be quite interesting in promoting the development of novel cost-effective flame retardants with minimized environmental impact.

References

1. Horrocks, A. R. *Polym. Degrad. Stab.* **2011**, *96*, 377–392.
2. U.S. Government of Commerce, DOC FF 3-71, (as amended). *Standards for the flammability of children's sleepwear*; Washington, D.C.; 1971. Now 16 CFR Part 1615.
3. The nightdress (safety) regulation, S.I. 839:1967 and the nightwear (safety) regulations S.I. 2043:1985; London, U.K.: HMSO.
4. Bull, J. P.; Jackson, D. M.; Walton, C. *Br. Med. J.* **1964**, *2*, 1421–1427.
5. Horrocks, A. R. *Rev. Prog. Color.* **1986**, *16*, 62–101.
6. Weil, E. D.; Levchik, S. V. *J. Fire Sci.* **2008**, *26*, 243–281.
7. Weil, E. U.S. Patent 3,746,572, 1970.
8. Weil, E. U.S. Patent 3,695,925, 1972.

9. Horrocks, A. R. In *Textile finishing*; Heywood, D., Ed.; Society of Dyers and Colourists: Bradford, U.K., 2003; pp 214−50.
10. National Academy of Sciences. *Toxicological risks of selected flame-retardant chemicals*; Sub-committee on flame-retardant chemicals of the United States National Research Council, Washington, DC; National Academy Press: Washington, DC, 2000.
11. Awad, W. H.; Gilman, J. W.; Nyden, M.; Harris, R. H., Jr; Sutto, T. E.; Callahan, J. *Thermochim. Acta* **2004**, *409*, 3–11.
12. Yasue, K.; Katahira, S.; Yoshikawa, M.; Fujimoto, K. In *Polymer-Clay Nanocomposites*; Pinnavaia, T. J., Beall, G. W., Eds.; Wiley series in Polymer Science; Wiley: Chichester, 2000; pp 111−126.
13. Matayabas, J. C.; Turner, S. R.; Sublett, B. J.; Connell, G. W.; Barbee, R. B. Int. Appl.WO 98/29499, 1998.
14. Gilman, J. W.; Kashiwagi, T. In *Polymer-Clay Nanocomposites;* Pinnavaia, T. J., Beall, G. W., Eds.; Wiley series in Polymer Science; Wiley: Chichester, 2000; pp 193−206.
15. Gilman, J. W. *Appl. Clay Sci.* **1997**, *15*, 31–49.
16. *Multilayer thin films, sequential assembly of nanocomposite materials*; Decher, G., Schlenoff, J. B. Eds.; Wiley VCH: Weinheim, 2002.
17. Decher, G.; Hong, J. D. *Makromol. Chem., Macromol. Symp.* **1991**, *46*, 321–327.
18. Tang, Z.; Kotov, N. A.; Magonov, S.; Ozturk, B. *Nat. Mater.* **2003**, *2*, 413–418.
19. Bernt, P.; Kurihara, K.; Kunitake, T. *Langmuir* **1992**, *8*, 2486–2490.
20. Tang, Y.; Lewin, M.; Pearce, E. *Macromol. Rapid. Comm.* **2006**, *27*, 1545–1549.
21. Hao, J.; Lewin, M.; Wilkie, C. A.; Wang, J. *Polym. Degrad. Stab.* **2006**, *91*, 2482–2485.
22. Tang, Y.; Lewin, M. *Polym. Degrad. Stab.* **2007**, *92*, 53–60.
23. Lewin, M.; Tang, Y. *Macromolecules* **2008**, *41*, 13–17.
24. Tata, J.; Alongi, J.; Frache, A. *Fire Mater.* DOI:10.1002/fam.1105.
25. Carosio, F.; Alongi, J.; Frache, A. *Eur. Polym. J.* **2011**, *47*, 893–902.
26. Carosio, F.; Laufer, G.; Alongi, J.; Camino, G.; Grunlan, J. C. *Polym. Degrad. Stab.* **2011**, *96*, 745–50.
27. Carosio, F.; Alongi, J.; Malucelli, G. *J. Mater. Chem.* **2011**, *21*, 10370–10376.
28. Carosio, F.; Alongi, J.; Malucelli, G. *Carbohyd. Polym.* **2012**, *88*, 1460–1469.
29. Alongi, J.; Carosio, F.; Malucelli, G. *Cellulose* **2012**, *19*, 1041–1050.
30. Fina, A.; Camino, G. *Polym. Adv. Technol.* **2011**, *22*, 1147–1155.
31. Gilman, J. W. *Appl. Clay Sci.* **1999**, *15*, 31–49.
32. Schartel, B.; Bartholmai, M.; Knoll, U. *Polym. Adv. Technol.* **2006**, *17*, 772–777.
33. Cioffia, M. O. H.; Voorwalda, H. J. C.; Mota, R. P. *Mater. Charact.* **2003**, *50*, 209–215.
34. Zhang, J.; Horrocks, A. R.; Hall, M. E. *Fire Mater.* **1994**, *18*, 307–312.

35. Xie, W.; Gao, Z.; Pan, W. P.; Hunter, D.; Singh, A.; Vaia, R. *Chem. Mater.* **2001**, *13*, 2979–2990.
36. Kandare, E.; Kandola, B. K.; Price, D.; Nazarè, S.; Horrocks, A. R. *Polym. Degrad. Stab.* **2008**, *93*, 1996–2006.

Chapter 23

High-Temperature Flammability and Mechanical Properties of Thermoplastic Polyurethane Nanocomposites

Preejith Ambuken,[1] Holly Stretz,*,[1] Joseph H. Koo,[2] Jason Lee,[3] and Rosa Trejo[4]

[1]Department of Chemical Engineering, Tennessee Technological University, Cookeville, Tennessee 38505-0001
[2]Department of Mechanical Engineering, The University of Texas at Austin, Austin, Texas 78712-0292
[3]Massachusetts Institute of Technology, Department of Chemical Engineering, Cambridge, Massachusetts 02139-4307
[4]High Temperature Materials Laboratory, Oak Ridge National Laboratory, Oak Ridge, Tennessee 37831-6069
***E-mail: hstretz@tntech.edu**

Incorporation of nanoparticles into a polymer can result in enhancement of electrical, thermal and mechanical properties, particularly at high temperatures where the polymer alone might exhibit softening or degradation. The nanocomposite softening temperature may or may not coincide with the temperature at which the nanoparticle enhances char formation. This work describes the modulus enhancement of thermoplastic polyurethane (TPU) nanocomposites at high temperature (up to 300 °C) using dynamic mechanical analysis (DMA). Different compositions of TPU nanocomposites were prepared on a commercial scale twin-screw extruder using a montmorillonite organo-clay, carbon nanofibers and multiwall carbon nanotubes (MWNT). The onset of softening was found to increase with nanoparticle loading (tested at 1 Hz). Overall MWNT were found to produce the optimal reinforcement response in the

In Fire and Polymers VI: New Advances in Flame Retardant Chemistry and Science; Morgan, A., et al.;
ACS Symposium Series; American Chemical Society: Washington, DC, 2012.

char for TPU-based nanocomposites heated to 300°C. A gap in reinforcement was noted at certain temperatures as the samples developed char. A correlation can be drawn between crossover of dissipative versus elastic behavior (dominance of loss modulus versus storage modulus) and dripping in UL 94 tests.

Introduction

Polymer nanocomposites have generated a great deal of interest in the fire materials community because of their enhanced mechanical (*1*, *2*) and thermal properties (*3*, *4*).

Incorporation of nanoparticles into polymers has led to improvement in the flammability of polymers. This flame retardant property of polymers nanocomposites has been attributed for specific materials to the enhancement of char formation at the surface. If a significant amount of carbonaceous char is produced which consists of carbon formed from resin, one effect by mass balance considerations is that the amount of evolved gas (fuel) is reduced, *e.g.* the barrier effect and the same layer also limits heat transfer which prevents further oxidation of polymer. The reduction in fuel supply reduces peak heat release rate, an important contributor to fire risk (*5*). The heat shielding capacity which reduces peak heat release rate of the char (barrier property) is another desirable property. However, if the char is mechanically weak at any point in the development of char, its failure could result in breach of the heat shield and loss of any benefit in the mass or energy balance that the nanomaterial was designed for.

Thermoplastic polyurethane (TPU) nanocomposites are flame retardant materials that can provide high performance solutions for vehicle applications, such as cable jackets for electrically-charged car batteries among other important flame retardant applications. Reduction in heat release rate of TPU nanocomposites were observed when polyhedral oilgomeric silesquioxane (POSS) (*6*), organoclay (*7*), multi wall carbon nanotubes (MWNT) (*7*) and carbon nanofibers (CNF) (*7*, *8*) were used as nanoparticle composite modifiers. Lee *et al.* have shown the enhancement in flammability properties (UL-94 and cone calorimeter tests) of TPU compounded with various nanoparticles (*4*). Research of TPU-based nanocomposites is also of interest for ablative applications (*4*).

Flame retardant properties of TPU nanocomposites depend on the heat shielding properties of the char layer. If the char layer does not have structural integrity under mechanical action, then cracking or loss of the char layer will impact the fire retardant properties of the TPU nanocomposites and the efficiency of the protective layer. Therefore, it is very important to know the mechanical performance of the char layer which forms when exposed to higher temperature, particularly in relation to different nanoparticles incorporated into TPU. While strength and impact properties are important mechanical properties, strength of fragile char is very difficult to assess in a representative or intrinsic manner (*9*).

Reshetnikov *et al.* performed some early work studying the strength of intumescent chars using the rheological approach (*10*). Thermally stable structures were observed in the intumescent char residue. Avila *et al.* studied the degradation in mechanical properties using low velocity impact tests after exposing the sample under intense heat condition of oxyacetylene torch for carbon fiber –nano modified epoxy reinforced with nanographite and nanoclay. It was observed that there is a correlation between impact response and char layer thickness (*9*). Duquesne *et al.* have used dynamic testing to investigate the rheological and mechanical behavior of thermoset PU coating with traditional fire retardant additives. This technique helped to obtain real time information on the foaming process as well as the strength of intumescent char (*11*).

In the present study, dynamic mechanical properties of TPU nanocomposites at high temperatures have been investigated. Investigation of storage modulus, loss modulus and tan delta gives important information on high temperature stability of TPU nanocomposites during the charring process. As these nanocomposites behave differently when exposed to high temperature, it is of interest to investigate and compare the mechanical properties of the charred layer. Use of DMA enabled researchers to obtain real time information during the charring process, of particular interest when the char produced is potentially too weak to transfer from the oven to mechanical test equipment for analysis. However, the modulus reported in this paper is relative as modulus calculated by DMA depends on the area of the sample.

Experimental

Materials

The TPU used was DESMOPAN® 6065A. This polymer is an aromatic polyether-based TPU manufactured by Bayer Material Science. The polyether, Desmopan 6065A, is C3 ether-based whereas the hard segment is methylene diphenyl diisocyanate (MDI) (Lee *et al.* (*4*)). Three different types of nanoparticles were used in this study: Montmorillonite (MMT) nanoclay-Cloisite® 30B (Cl30B) was manufactured by Southern Clay Products. The modifier used to surface treat Cl30B is a methyl, tallow, bis-2-hydroxyethyl, quaternary ammonium (MT2EtOH) at 90 meq/100g exchange ratio. The d-spacing (001) for Cl30B is reported as 1.85 nm. Multiwalled carbon nanotubes (MWNT) were obtained from Arkema. MWNT under the name of Graphistrength® C100 were produced by chemical vapor deposition at elevated temperature of ethylene on a metal/ceramic catalyst. Typical dimensions for MWNT are 10 to 15 nm in diameter for 5 to 15 concentric tubes while the length ranges from 1 to 10μm. Carbon nanofibers (CNF) PR-19-XT-LHT were manufactured by Applied Sciences Inc./Pyrograf® Products and it was produced through pyrolysis of hydrocarbons. These loosened CNF have an average diameter of 150 nm and a length varying from 100μm to 1cm with a bulk density of 0.016-0.048 g/cc.

Processing of Materials

Twin screw extrusion was used for compounding the TPU with different loading of Cl30B, MWNT and CNF. For TPU/Cl30B and TPU/MWNT, four different loadings (2.5 wt%, 5 wt%, 7.5 wt% and 10%) of nanoparticles by weight are reported, while for TPU/CNF nanocomposites the nanoparticles loading were 5 wt%, 10 wt%, 15 wt% and 20 wt %. A summary of material designation used in this paper is presented in Table 1.

Flammability Analysis

Two flammability experiments were performed to observe the char structure and formation. The first test was a vertical UL 94 test. A hanging 12.7 cm (5”) long specimen was burned for 10 seconds by a 2.54 cm (1”) flame. The size and frequency that a sample will break during testing helped to distinguish the char structure. In addition, a 50 kW/m^2 horizontal cone calorimetry experiment was conducted (ASTM E1354). Cone calorimetry experiments were performed only on TPU nanocomposite samples at 5 wt% loading.

Dynamic Mechanical Analysis

DMA testing was performed with vacuum exhaust on a TA Instruments Dynamic Mechanical Analyzer Q800 with a compression clamp was used for DMA testing. The importance of the compression platform was that the samples might drip during testing, and only this mode protected the Q800 drive unit from sample incursion. Temperature sweep tests were carried out up to 300 °C with a heating rate of 5 °C/min. Samples were placed between the plates with a preload force of 1N. This ensured proper contact between the sample and plates. A test frequency of 1 Hz was chosen and initial strain of 0.5% was used for all the tests to prevent crushing of the sample during the test. All samples were heated in nitrogen to prevent the sample catching fire during the test and protect the fragile char long enough to obtain direct comparisons between the various nanocomposites. All samples were tested using nitrogen as the “air bearing” gas and with vacuum exhaust.

For DMA testing, injection molded TPU nanocomposites tensile test bars (ASTM D638 dimensions) were further processed in DSM microcompounder to obtain a melt which was then transferred into a custom made cylindrical mold. The melt in the cylindrical mold was compression molded using a plunger in a Carver press at 170°C for 5 min in order to obtain cylindrical flat samples necessary for the dynamic mechanical analyzer setup. The hot cylinder was kept in ambient condition to attain room temperature after removing it from Carver press. Dimensions of the sample after compression molding were around 26.5 mm in diameter and 2.2 mm in thickness.

Table 1. Material description and designation

Polymer	*Nanoparticle*	*Nanoparticle loading in wt%*	*Material designation used in this paper*
TPU	MWNT	2.5 wt%	TPU/MWNT/2.5
		5 wt%	TPU/MWNT/5
		7.5 wt%	TPU/MWNT/7.5
		10 wt%	TPU/MWNT/10
TPU	Cl30B	2.5 wt%	TPU/Cl/2.5
		5 wt%	TPU/Cl/5
		7.5 wt%	TPU/Cl/7.5
		10 wt%	TPU/Cl/10
TPU	CNF	5 wt%	TPU/CNF/5
		10 wt%	TPU/CNF/10
		15 wt%	TPU/CNF/15
		20 wt%	TPU/CNF/20
TPU	-	-	-

Results and Discussion

Flammability Studies

The purpose of this study was to examine the correlations between dynamic mechanical properties for TPU nanocomposite char formation and the corresponding flammability. Flammability will be discussed first in terms of UL 94 and cone calorimetry. Dynamic mechanical analysis results are then presented and comparison is made between the intrinsic measured mechanical properties of the char during formation and the flammability test results.

UL 94

In the UL 94 flammability tests, the neat TPU was found to have a very low viscosity exemplified by dripping. The continuous drip behavior affected the bulk material; the bulk did not burn. With addition of 2.5wt% nanoclay however, the material did not drip. The char structure at 2.5wt% loading appeared somewhat weak. Seven samples of each formulation were tested as required by UL 94. There were 4-8 small portions which fell these bulk seven samples. As nanoclay loading increased the char exhibited improved strength. Specimens with 7.5wt% nanoclay and higher had no falling bits of char. Scanning electron microscopy (SEM) images of the surface of the 10wt% nanoclay composite at different stages of a UL 94 experiment are shown in Figure 1. In Figure 1a the surface imaged had not burned; but had been thermally heated by proximity to a flame. The heat from the flame caused the material to begin to crack. In Figure 1b the surface imaged had burned for 30 seconds and was externally extinguished. Large degassing bubbles were observed. In Figure 1c shows the surface imaged continued to burn until no combustible material remained. The char began here to appear more plate-like in the cracks.

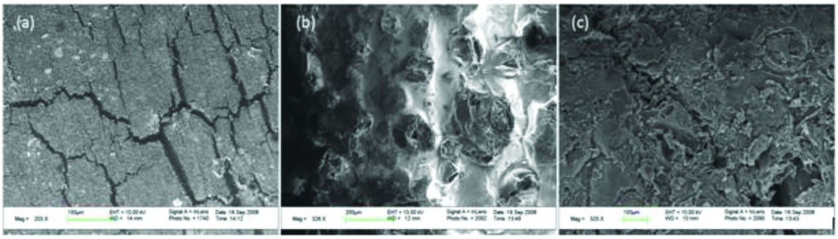

Figure 1. SEM images of TPU/Cl/10 at three burn stages: (a) heated surface, (b) 30 second burn surface, and (c) complete burn surface. Reprinted with permission from ref. (4). Copyright 2011 American Institute of Aeronautics and Astronautics.

The equivalent tests performed on the MWNT-based nanocomposite at 2.5wt% loading resulted in a very weak char structure just as the organoclay-based nanocomposite did. Small bits broke apart throughout the burning process. At 5wt% loading of the MWNT up to 4 specimens fell apart during the test. Even at 10wt%, one segment would break off during the test. The char structure formed had numerous large cracks resulting in a weak char structure. SEM images, (see Figure 2) show evidence of this cracking. In addition, higher resolution SEM images were taken. In Figure 3, SEM images of the virgin material show evidence of the morphology of the embedded MWNTs in the TPU. The burnt samples showed that the remaining char material morphology was dominated by the MWNTs.

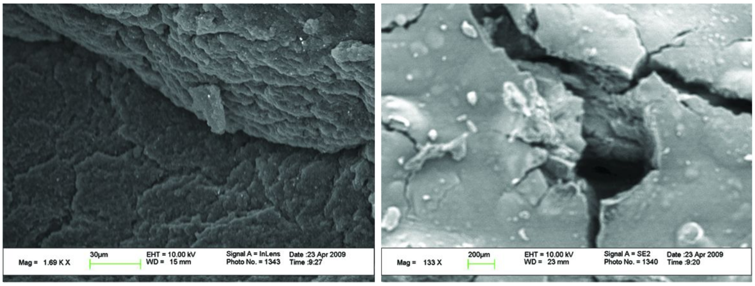

Figure 2. SEM images of burnt TPU/MWNT/10 after UL 94 test. Reprinted with permission from ref. (4). Copyright 2011 American Institute of Aeronautics and Astronautics.

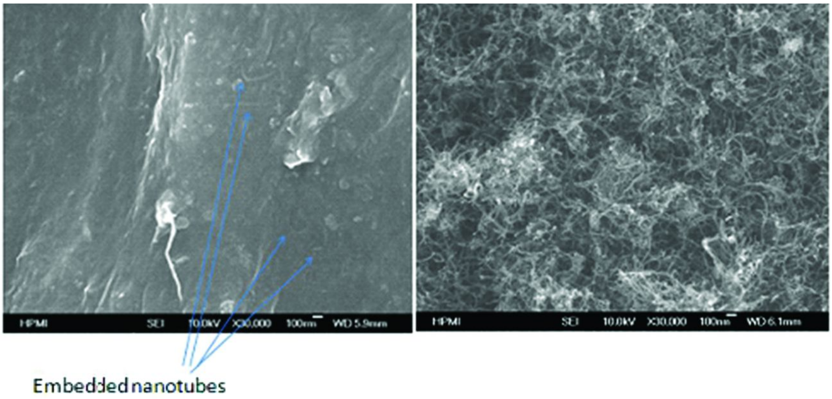

Figure 3. High resolution SEM images of virgin (Top) and burnt TPU/MWNT/10 (Bottom) after UL 94 test. Reprinted with permission from ref. (4). Copyright 2011 American Institute of Aeronautics and Astronautics.

The CNF bubbled on the surface while burning and degassing. TPU/CNF/5., which was not observed in either the nanoclay or MWNT PNCs. This bubbling occurs when the char is forming slowly; the material formed has both properties of the solid char and a viscous liquid. Small solid pieces not fully melted, flow through the elongating portion and speed up the drip process. TPU/CNF/10 elongated less rapidly but did not form a char able to maintain the melt flow. The pieces of TPU/CNF/15 and TPU/CNF/20 specimens that dropped can be distinguished, however, each deformed due to its liquid like properties. In Figure 4, SEM images show that after firing the CNF samples have many porous regions. Similar to the MWNT nanocomposite images, CNF morphology is shown to dominate the final char structure.

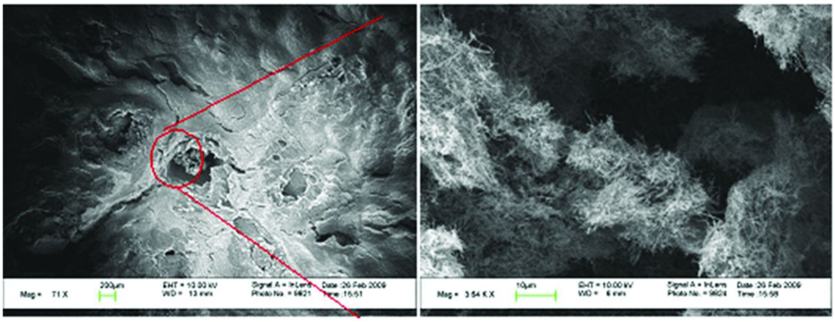

Figure 4. SEM image of TPU/CNF/20 after UL 94 test. Reprinted with permission from ref. (4). Copyright 2011 American Institute of Aeronautics and Astronautics.

These burn tests show how significantly each nanomaterial modified the melt and burning conditions of the nanocomposite. The mechanical stability of the char after the flame test was increased as the nanomaterial loading increased. (Mechanical stability is here approximated by the time a charred segment began to fall and the size of the charred segments that fell.) The failure mechanism of each TPU nanocomposite was different. Cracks appear in both the nanoclay and MWNT specimens. Nanoclay loadings above 7.5wt% show no cracking and as a result no charred segments dropped. The surface of the CNF specimens did not create char-like structure until a much higher loading was added. At low loadings, the CNF specimen burned like a very viscous melt. At higher loadings the CNF specimens behaved similar to that of the MWNT. These flammability tests show that adding nanoparticles to TPU drastically changes the viscosity, mechanical properties, and flammability properties. At higher loading, the composite integrity persists for a longer period of time. The nanoclay additives showed superior enhancement per weight percent filler added, with some benefit evident at 7.5% loading, and the CNF additives showed weak enhancements even at the high 20wt% loading.

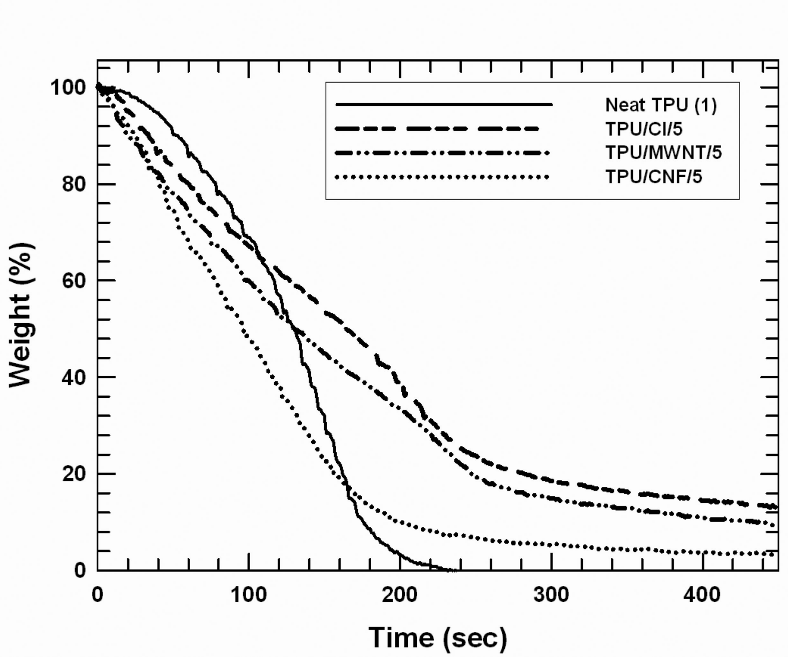

Figure 5. Mass loss of neat and 5% PNC cone calorimeter test at 50 kW/m^2. Reprinted with permission from ref. (4). Copyright 2011 American Institute of Aeronautics and Astronautics.

Cone Calorimetry

Cone calorimeter tests were performed for three nanocomposite samples at 5wt% loading. The average weight loss and heat release (HRR) rate curves are shown in Figures 5 and 6, respectively. Two neat TPU tests were conducted. The aluminum foil back melted during these experiments and material dripped. The HRR and mass loss data of the nanocomposite samples were more robust as the foil did not melt in these cases. The total heat released by each sample should be the same since each material was exposed to the same heat flux conditions. Thus the HRR curves from neat TPU that melts can be integrated and compared to HRR curves for the nanocomposites to determine if the TPU curves were appropriate. The energy released by each material was 101, 74, 102, 104, and 100 MJ/m^2 for the 1st neat TPU, 2nd neat TPU, 5wt% nanoclay, 5wt% CNF, and 5wt% MWNT nanocomposites, respectively. Thus the first neat TPU test absorbed and released energy consistent with the data observed for the nanocomposite cases. Of the nanocomposites, the nanoclay-based material had the lowest weight loss at any given time. The 50wt% mass loss occurred for the neat, 5wt% CNF, 5wt% MWNT, and 5wt% nanoclay specimens at 142, 116, 150, and 175 sec, respectively. Note that the onset of mass loss for all the nanocomposites (shown in Figure 5) was immediate, where the neat TPU appeared to maintain some mass slightly later into the burn before onset occurred significantly. This phenomena will be discussed later.

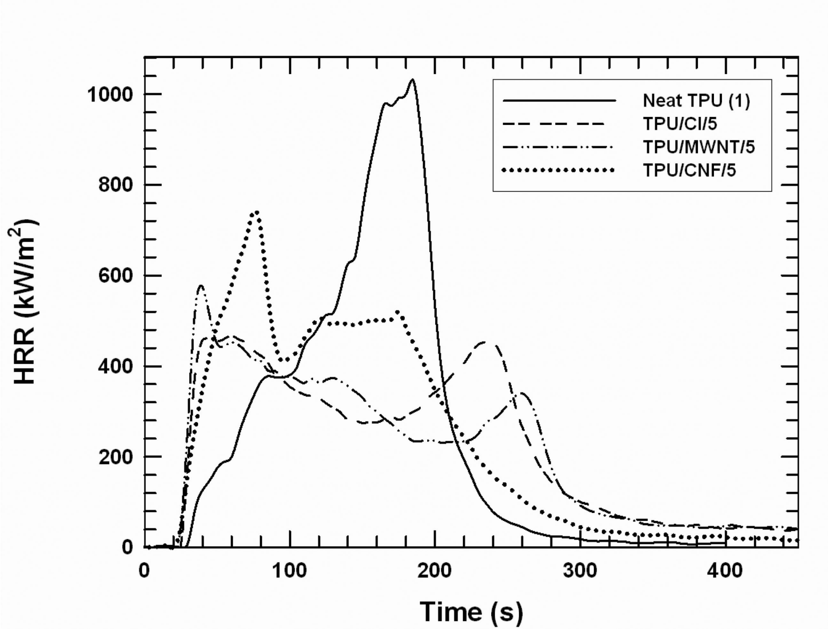

Figure 6. HRR of neat and 5% PNC for cone calorimeter test at 50 kW/m^2. Reprinted with permission from ref. (4). Copyright 2011 American Institute of Aeronautics and Astronautics.

Table 2. Summary of cone calorimetry data at irradiance heat flux of 50 kW/m²

Material	*t_{ig} (s)*	*PHRR (kW/m²)*	*Avg. HRR, 60s (kW/m²)*	*Avg. HRR, 180s (kW/m²)*	*Avg. Eff. H_c (MJ/kg)*	*Avg. SEA (m²/kg)*
Neat TPU(1)	28	1031	228	515	27	311
TPU/Cl/5	27	518	442	376	28	256
TPU/MWNT/5	21	571	436	492	28	297
TPU/CNF/5	21	808	508	361	27	298

t_{ig} = Time to sustained ignition; PHHR = Peak heat release rate; Avg. HRR = Average heat release rate after ignition; Avg. Eff, H_c = Effective heat of combustion; Avg. SEA = Average specific extinction area.

The flammability properties are summarized in Table 2. The material's time to sustained ignition was not affected by the addition of nanoclay. However, the carbon-based nanocomposite time to ignition decreased by 25%, due to the higher thermal conductivity. The suppression of PHRR in the nanocomposites was significant, 50%, 45%, and 22% from the nanoclay, MWNT and CNF nanocomposites, respectively. The effective heat of combustion was the same, a result to be expected since the masses of each material were approximately the same. The average specific extinction area (SEA) was also decreased slightly for the nanoclay-based nanocomposite (18%). The carbon-based nanocomposite SEAs were influenced by the high soot content of these materials. The nanoclay in TPU/Cl/5 potentially served as a good barrier against gas transport.

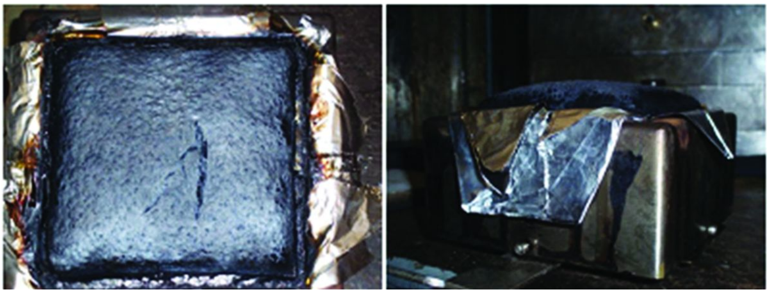

Figure 7. Post Desmopan-5% Cloisite® 30B cone calorimeter sample. Reprinted with permission from ref. (4). Copyright 2011 American Institute of Aeronautics and Astronautics.

The materials after firing are shown in Figures 7 to 9. The nanoclay-based material was shown to expand. This is evidence of the clay's gas barrier properties. Note that the CNF nanocomposite stayed flat. Additionally the center of the CNF sample showed cracking which was not observed for the nanoclay nanocomposite. Lastly, the MWNT nanocomposite showed a red pigment, attributed to the iron content from MWNT manufacturing. This material did not expand to the extent of the nanoclay composite.

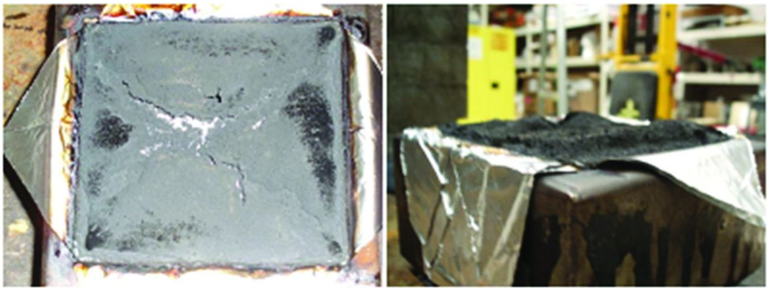

Figure 8. Post Desmopan-5% CNF cone calorimeter sample. Reprinted with permission from ref. (4). Copyright 2011 American Institute of Aeronautics and Astronautics.

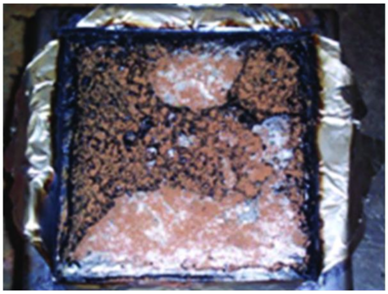

Figure 9. Post Desmopan-5% MWNT cone calorimeter sample. Reprinted with permission from ref. (4). Copyright 2011 American Institute of Aeronautics and Astronautics.

Dynamic Mechanical Analysis of TPU Nanocomposites

For the dynamic mechanical analysis, the nanoclay nanocomposites and MWNT nanocomposites at three different loadings were examined: 5, 7.5 and 10 wt%. For CNF nanocomposites the nanoparticle loadings were 15 and 20 wt%, the higher loading expected to give a more stable char based on previous flammability tests.

For TPU reinforced with nanoclay, the compressive storage moduli as a function of temperature are compared in Figure 10. The 5% nanoclay sample collapsed at 210 °C with an initial strain of 0.5%. The 7.5% and 10% nanoclay-based samples showed an increase in storage modulus developing after the softening event, and also an increase in the value of that char modulus with increased nanoparticle loading. At 210 °C where all three nanoclay nanocomposites were structurally stable, an increased storage modulus with increase in nanoparticles loading is observed. It was visually observed that both the 7.5 and 10% formulations were able to retain structural integrity after completion of the test. Note that these are the same formulations which did not drip or fall apart during UL 94 testing. At 300 °C, the 10% formulation showed higher storage modulus than the 7.5% did.

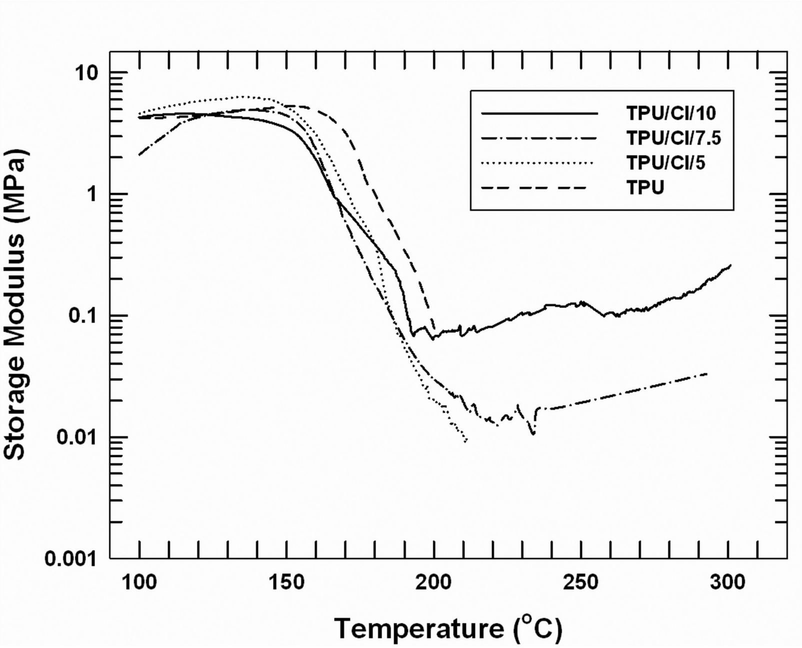

Figure 10. Variation of storage modulus versus temperature for TPU/Cl nanocomposites.

As shown in Figure 11, the MWNT-based TPU nanocomposites (after the initial softening) formed stable chars upto 250 °C with recordable storage moduli. The storage modulus of 7.5 and 10% formulations were comparatively higher than the 5% formulation at 200 °C where all nanocomposites where stable. This is attributed to the higher reinforcement provided by the high aspect ratio and entangled multiwalled carbon nanotubes. The 5% MWNT nanocomposite did not retain elasticity beyond 240 °C (*i.e.* would not respond properly to a cycle of loading and recovery necessary for a dynamic loading test) and it physically was observed to have collapsed upon opening the oven (cooled to 200 °C). As shown in Figure 11, both TPU/MWNT/7.5 and TPU/MWNT/10 exhibited the softening event seen for both TPU and the 5% nanocomposite, but the storage modulus recovered as char formed when the sample was exposed to higher temperatures. This gap where the sample modulus has experienced a decline at higher temperatures, and then at even higher temperatures recovers, will be heretofor termed a "reinforcement gap." A similar gap was noted for the nanoclay-based materials presented in Figure 10. At 300 °C for these high loadings (10 wt%), MWNT-based nanocomposites exhibited greater recovery of storage modulus than the nanoclay-based materials. (Note that modulus data here are taken to be relative, and can be compared within this study, but are not considered absolute values.)

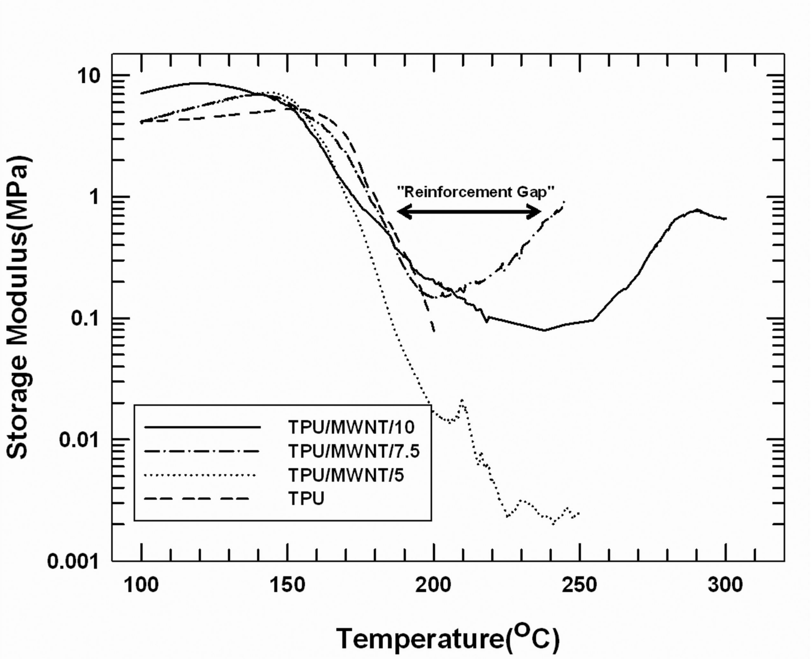

Figure 11. Variation of storage modulus versus temperature for TPU/MWNT nanocomposites.

For the CNF-based nanocomposites recordable data was measured only upto 220 °C as the samples lost their elasticity beyond 220 °C as shown in Figure 12. When the furnace was opened after the cool down step at 200 °C, a viscous melt was observed. This behavior is consistent with UL 94 testing where it was observed that TPU/CNF with such high loading had liquid melt like behavior and the samples also dripped. To avoid dripping and damage to the DMA instrument the test was stopped at 210 °C for neat TPU. Thus no evidence of char formation with a stable modulus could be recorded for CNF-based materials.

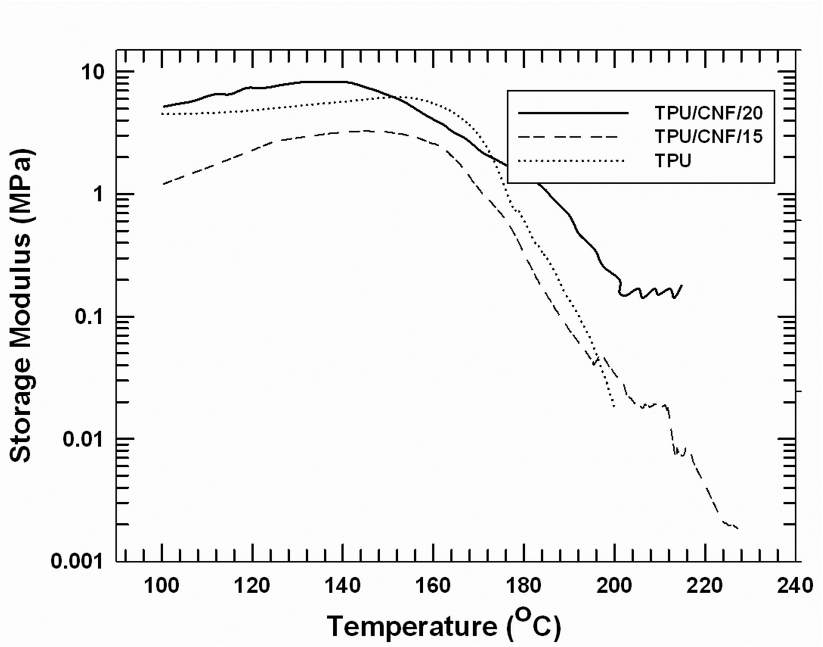

Figure 12. Variation of storage modulus versus temperature for TPU/CNF nanocomposites.

One important observation consistent for all TPU nanocomposites was that in the presence of nanoparticles, the onset of drop of storage modulus (softening) occurred in all cases at a lower temperature than compared with neat TPU (see Figure 13). With increased loading of nanoparticles the onset of drop in storage modulus also occurred at successively lower temperatures for a given nanocomposite. The onset of drop in storage modulus was found at 152 °C for neat TPU. It is not known if the early onset of softening and the subsequent development of char are related. Liff *et al.* has observed hard segments of the TPU melting and producing an endotherm using Differential Scanning Calorimetry (DSC) at 150 °C (*12*). Thermogravimetric Analysis (TGA) data by Lee *et al.* on the same set of injection molded samples showed chemical degradation of TPU well above 250 °C (*4*). Thus, it is not anticipated that this softening event for the TPU is due to chemical degradation, though it cannot be ruled out yet that the nature of the mechanism for reducing the temperature of the onset of softening might be due to some form of chemical degradation during processing. In Figure 13, note that the CNF-based nanocomposites were affected much less than the other two nanocomposites.

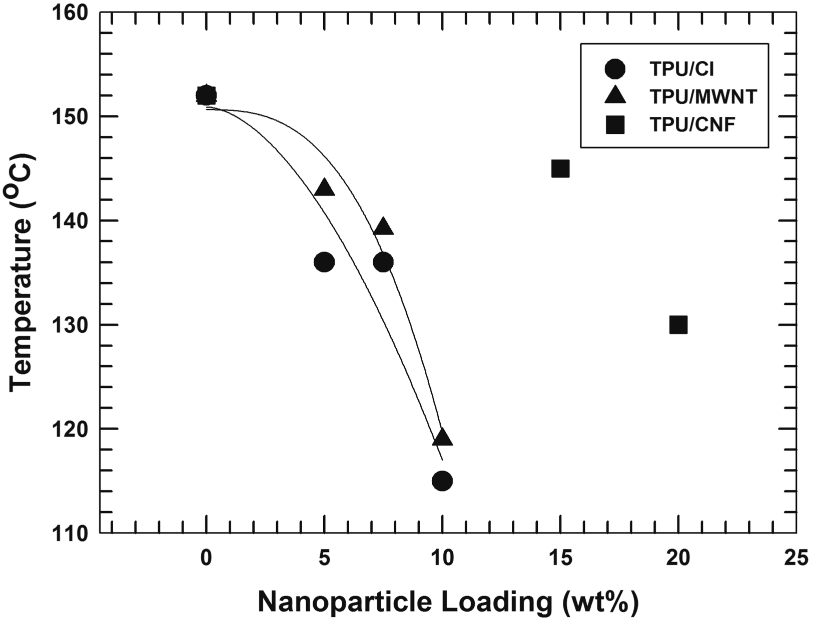

Figure 13. Effect of nanoparticle loading on onset of storage modulus depression. The lines superimposed on TPU/Cl30B and TPU/MWNT are guides for the eye.

Another way to quantify the softening event (other than onset) is to take advantage of the complex behavior of this material under dynamic loading that is to compare the storage and loss moduli. When the loss behavior becomes more dominant, the material behavior is no longer elastic but more dissipative. As an example, in Figure 14, for TPU/CNF/15 storage modulus intersects with loss modulus at 200 °C, and this is the so called "crossover temperature." When the furnace was opened after testing this material (at 220 °C) the sample was a viscous melt. The crossover behavior are compared to UL 94 dripping behavior qualitatively in Table 3. The existence of the crossover phenomena seems to correlate well with, and even predict the dripping behavior seen in the more empirical UL 94 test.

From the DMA results presented, it can be said that each material loses its storage modulus even before it forms a char. As shown in Figure 11, there is a "reinforcement gap" which exists between the onset of degradation of storage modulus and formation of reinforced char. To have good performance, the TPU nanocomposites should sustain the applied strain at lower temperatures (115 °C-160 °C) and should be able to cover the reinforced gap. As a part of future work blending TPU with another polymer or an additive is a possible route to help alleviate the reinforcement gap.

In Fire and Polymers VI: New Advances in Flame Retardant Chemistry and Science; Morgan, A., et al.;
ACS Symposium Series; American Chemical Society: Washington, DC, 2012.

From the high temperature performance of TPU reinforced with Cl30B and with MWNT at different concentrations (5 wt%, 7.5 wt% and 10 wt%), it was found that a loading of 7.5 wt% exhibited the best overall performance. These formulations exhibited good modulus at high temperatures. The temperature for onset of depression in storage modulus is uniformly higher for all loadings tested above the 7.5 wt% formulations, so 7.5 wt% was viewed as an optimum.

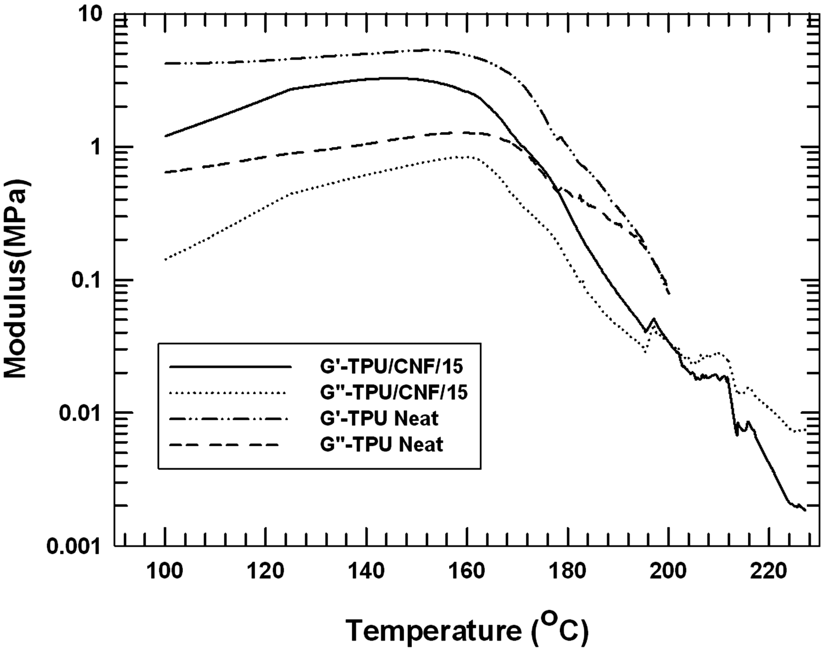

Figure 14. Storage modulus and loss modulus of TPU and TPU/CNF/15 nanocomposites.

A final word should be mentioned about DMA results and the correlations with cone calorimetry. The DMA results did not appear to predict any cone calorimeter data with one small exception. Mass loss data in cone calorimetry showed that neat TPU appeared to maintain some mass slightly later into the burn before onset of mass loss occurred significantly (see Figure 5). In the DMA testing, the temperature at which modulus loss was first noted (onset) was highest for the neat TPU compared to all nanocomposites (see Figure 13). These appear to be related, but we caution that the heat rate is not the same for both tests.

Table 3. Comparison of DMA Crossover Behavior to UL 94 Dripping Behavior

Sample Name	*Crossover of Loss Modulus versus Storage Modulus*	*UL 94 Dripping (# of drops)*
TPU/Cl/5	Yes	1
TPU/Cl/7.5	No	0
TPU/Cl/10	No	0
TPU/MWNT/5	Yes	2-4
TPU/MWNT/7.5	Maybe	0-1
TPU/MWNT/10	No	0-1
TPU/CNF/15	Yes	8

Summary and Conclusions

This paper has studied the high temperature flammability and mechanical properties of thermoplastic polyurethane (TPU) nanocomposites. From the UL 94 studies it was found that high loading of nanoparticles is needed for all the formulations to have a stable char structure. From the cone calorimeter studies on TPU nanocomposites, the lowest PHRR was observed for TPU/Cl30B formulation while the highest PHRR was shown by TPU/CNF nanocomposites. The char obtained after firing TPU/Cl30B nanocomposites was swollen and it retained its structural integrity while TPU/MWNT and TPU/CNF had cracks.

DMA testing was performed on the same materials to study complex modulus as a function of temperature up to 300 °C where the char was anticipated to have formed. TPU/MWNT displayed better char modulus in comparison to TPU/Cl30B. For TPU/CNF tests could not be completed above 220 °C as the sample turned into a viscous melt. All samples began to lose modulus (soften) in the range of 120-160 °C. For TPU/MWNT and TPU/Cl30B nanocomposite recovery in modulus (reinforced char formation) was observed at about 230 °C with loadings above 7.5 wt%. The temperature range at which modulus had decreased but char formation was not yet significant enough to exemplify modulus recovery was termed the “reinforcement gap.” A correlation can be drawn between crossover of dissipative versus elastic behavior (dominance of loss modulus versus storage modulus) and dripping in UL 94 tests.

Acknowledgments

This research through the Oak Ridge National Laboratory’s High Temperature Materials Laboratory User Program (where DMA testing was performed) was sponsored by the U. S. Department of Energy, Office of Energy Efficiency and Renewable Energy, Vehicle Technologies Program. The authors also would like to thank the following individuals for supporting our research: Dr. Wissler of 21st Century Polymers who performed the twin screw extrusion and injection molding. Student funding courtesy by Center for Energy Systems Research, Center for Manufacturing Research and Department of Chemical Engineering, Tennessee Technological University, Cookeville, TN,38505-0001.

References

1. Fornes, T.; Paul, D. *Polymer* **2003**, *44*, 4993–5013.
2. Lee, H.; Fasulo, P. D.; Rodgers, W. R.; Paul, D. *Polymer* **2005**, *46*, 11673–11689.
3. Ho, W. K.; Koo, J. H.; Ezekoye, O. A. *J. Nanomater.* **2010**, *2010*, 8–8.
4. Lee, J. C.; Koo, J. H.; Ezekoye, O. A. In *47th AIAA/ASME/SAE/ASEE Joint Propulsion Conference & Exhibit*; San Diego, California, 2011.
5. Kashiwagi, T.; Danyus, R.; Liu, M.; Zammarano, M.; Shields, J. R. *Polym. Degrad. Stab.* **2009**, *94*, 2028–2035.
6. Bourbigot, S.; Turf, T.; Bellayer, S.; Duquesne, S. *Polym. Degrad. Stab.* **2009**, *94*, 1230–1237.
7. Koo, J. H.; Nguyen, K. C.; Lee, J. C.; Ho, W. K.; Bruns, M. C.; Ezekoye, O. A. *J. Fire Sci.* **2010**, *28*, 49–85.
8. Morgan, A. B.; Liu, W. *Fire Mater.* **2011**, *35*, 43–60.
9. Ávila, A. F.; Koo, J. H.; Bracarense, A. Q. In *SAMPE fall technical conference and exhibition*; Memphis, Tennessee, 2008.
10. Reshetnikov, I. S.; Garashchenko, A. N.; Strakhov, V. L. *Polym. Adv. Technol.* **2000**, *11*, 392–397.
11. Duquesne, S.; Delobel, R.; Le Bras, M.; Camino, G. *Polym. Degrad. Stab.* **2002**, *77*, 333–344.
12. Liff, S. M.; Kumar, N.; McKinley, G. H. *Nat. Mater.* **2006**, *6*, 76–83.

Chapter 24

Pyrolysis-Combustion Flow Calorimetry: A Powerful Tool To Evaluate the Flame Retardancy of Polymers

R. Sonnier, H. Vahabi, L. Ferry, and J.-M. Lopez-Cuesta*

**Centre des Materiaux d'Alès (CMGD), Ecole des Mines d'Alès,
6, avenue de Clavières, 30100 Ales, France
*E-mail: jose-marie.lopez-cuesta@mines-ales.fr**

Pyrolysis-combustion flow calorimeter is becoming a common and useful tool to study the flammability of materials at a very small scale (several milligrams of sample). Most generally, it is used according to the method A described in the ASTM D7309 standard (anaerobic pyrolysis and complete combustion) since it is possible to monitor the conditions of pyrolysis and combustion to a large extent. Moreover, combining PCFC with thermogravimetric analysis allows a better understanding of the thermal degradation of materials. Even if there is no general correlation between PCFC and cone calorimeter (or other flammability tests) results, it has also been shown that the comparison of the results from both tests could help to identify the modes-of-action of flame retardants. This chapter reviews the multiple uses of PCFC and points out some issues or developments about this tool.

Introduction

Evaluating the flame retardancy of polymeric materials requires specific tools. Many tests are dedicated to one application and only allow classifying materials qualitatively according to their macroscopic behavior (self-extinguishibility, dripping…) in determined conditions (horizontal or tilted orientation, radiative heating source or flame…). On the contrary, some methods provide quantitative data about the mass loss, the heat or the smoke released during the burning.

In Fire and Polymers VI: New Advances in Flame Retardant Chemistry and Science; Morgan, A., et al.;
ACS Symposium Series; American Chemical Society: Washington, DC, 2012.

Cone calorimeter is probably the most used and complete apparatus which allows measuring accurately many flammability characteristics. Nevertheless, these characteristics are measured in certain conditions which could be significantly different from those used in other tests. In most cases, the correlations between these tests are only statistical. This problem arises for any new method of characterizing the fire behavior.

In 2004, Lyon and Walters (*1*) presented a new method to evaluate the combustibility of a small polymeric sample. This method is now frequently used in many fire laboratories, in particular when only a small amount of material is available (for example polymers synthesized at the laboratory scale). This method aims to evaluate the flammability of formulations before testing them using other tests (like cone calorimeter) which require larger amounts of material. This test is now described by a standard (ASTM D7309). It is designated according two names: Pyrolysis-combustion flow calorimeter (PCFC) or microscale combustion calorimeter (MCC). In our opinion, the former has the advantage of pointing out one of its main interesting characteristics: the de-coupling between pyrolysis and combustion.

Indeed, in PCFC, the degradation of the condensed phase occurs in the pyrolysis chamber under anaerobic conditions (under nitrogen flow - method A) or under aerobic conditions (80/20 nitrogen/oxygen flow – method B). The sample is heated up to 750 °C max, at a heating rate of 0.5-4 K/s (typically 1K/s). In both methods, gases released from pyrolysis are sent into a combustor chamber. Conditions in the combustor could be monitored but they are generally chosen to ensure complete combustion: combustion temperature is fixed at 900 °C and oxygen is in excess (80/20 nitrogen/oxygen flow). Gases are burnt and oxygen is consumed. An oxygen analyzer allows the consumption of oxygen and the heat release rate to be calculated according to the well-known Huggett's relation (*2*): 1 kg of consumed oxygen corresponds to 13.1 MJ of released energy whatever the organic material (Figure 1).

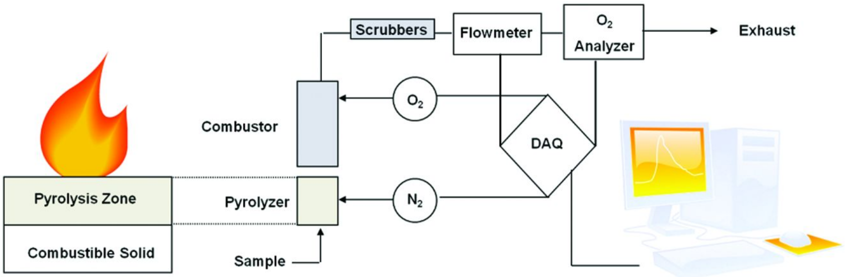

Figure 1. Scheme of PCFC apparatus. (Reproduced with permission from ref. (1). Copyright 2004 Elsevier.)

Therefore, a heat release rate curve is recorded versus the pyrolysis temperature. Characteristic data are peak of heat release rate (PHRR, W/g), heat release capacity (HRC, J/g.K, which will be discussed in greater detail later), total heat release (THR, kJ/g) and temperature at pHRR (T_{max}, °C). This temperature is not a temperature at ignition as claimed in some references (*3–6*) since PCFC is a non-flaming test.

It is now possible to review the use of PCFC from this literature, and to present all aspects of the method. This test is most generally carried out in standard conditions (method A and complete combustion), but other kinds of information could also be obtained. In the following, some important aspects of the PCFC test will be discussed prior to presenting all the data which could be calculated from PCFC measurements. A comprehensive comparison between PCFC and thermogravimetric analysis (TGA) will be presented and the interest of combining both techniques to thoroughly study material flammability will be highlighted. Then, the differences between PCFC and other calorimetric methods, in particular cone calorimetry, will be elucidated to point out the possibility to use PCFC as a screening tool. Correlations with other flammability tests, such as LOI or UL94, will be also discussed. Finally some issues and future developments concerning PCFC will be presented.

Some Important Aspects of PCFC

Heterogeneous Materials

Obviously, PCFC is not suitable for all types of material due to the small weight of samples (1-4mg). A material which is not homogeneous at this scale cannot be tested correctly in PCFC, e.g. multilayer materials. Textile fibers, and in particular surface-treated fibers were also questionable from this point of view. Yang and He (*7*) have studied the repeatability of PCFC measurements on various fibers (cotton, PP, polyester, kevlar, nylon, acrylic, silk) and on surface-treated cotton. In all cases, fibers were ground to powders before testing to improve the repeatability. The variance coefficient was generally found close to or lower than 3.0 % for pHRR, HRC, temperature at pHRR, THR (and char measured using a balance). Higher variance coefficients were found when the value of the considered property was low. For example, on surface-treated cotton, THR value was 1.8 kJ/g, and therefore the coefficient of variance was 17.8 %. The repeatability was not affected when pyrolysis was performed in aerobic atmosphere (20 wt% of oxygen).

Heat Release Capacity

The heat release capacity (HRC) is defined as the peak of heat release rate divided by the heating rate. It is believed that HRC is an intrinsic flammability parameter independent of the heating rate. It is a reasonable hypothesis if the pyrolysis mechanisms do not change when the heating rate is modified. If the heating rate is fixed at 1 K/s, pHRR = HRC and therefore it is not necessary to present values for both parameters, as seen in many studies (for example (*8*)).

Heat release capacity is considered a suitable parameter to assess the material fire hazard. But, when decomposition occurs in more than one step, considering only HRC (or pHRR) is not satisfying. For example, Jinping and Guoqiang (*9*) studied silk fabric modified via a graft copolymerization of organophosphorus flame retardant. The grafting of DMMEP (dimethyl 2-(methacryloyloxyethyl) phosphate) led to a decrease in pHRR but a small shoulder appeared at low temperature. In this study, other flammability tests showed that grafting was greatly favorable to improve flame retardancy. But the relative importance of a small peak (or shoulder) at low temperature in the fire hazard probably varied in each case.

In order to find a better parameter for taking into account multiple-steps degradation, sumHRC (sum of HRC of all peaks after deconvolution) and avgHRC (average HRC) have been proposed (*10*). These parameters are defined as follows:

$$sumHRC = \Sigma \frac{\Phi_n . \mathrm{Q}_n}{\beta . \mathrm{m}_n}$$

where Φ_n is the weight fraction of the component n, Q_n is the peak of heat release rate corresponding to the component n, β is the heating rate and m_n is the weight of the component n

$$avgHRC = \frac{THR}{\Delta T_p}$$

where ΔT_p is the pyrolysis temperature interval

The HRR curve should be deconvoluted in simple peaks before calculating Q_n. Few studies used sumHRC or avgHRC. It is not established that fire hazard should be better defined, taken into account HRC, sumHRC or avgHRC.

Anaerobic versus Aerobic Pyrolysis

Almost all studies use PCFC according to method A, meaning that the pyrolysis of condensed phase is carried out under nitrogen flow. But the aerobic pyrolysis (method B) could be carried out to evaluate the resistance of a material, or a char, to thermo-oxidation (*1*, *7*). Repeatability of this method is also good as evidenced by Yang and He (*7*).

In a next section, it will be shown that PCFC is not suitable to prove the formation of a thermal barrier effect because of the too small sample size. The barrier effect actually exhibits multiple aspects. Apart from the thermal barrier effect (a layer insulates the underlying material from a heat source), the formation of a barrier to oxygen diffusion is also able to delay the time to ignition when the material is heated in aerobic conditions (as in cone calorimeter).

Polyethylene (PE) composites filled with a mineral filler which is able to play an oxygen barrier effect have been studied (Figure 2). Under anaerobic conditions, no difference in heat release rate is observed between pure and filled polyethylenes. Temperature at pHRR is 495-500 °C in both cases. On the contrary, under aerobic conditions, the onset temperature is significantly shifted to higher temperatures for filled PE. The temperature at pHRR is 443 °C against only 395 °C for pure PE. This strong enhancement in thermal stability is assigned to the oxygen barrier effect of the filler.

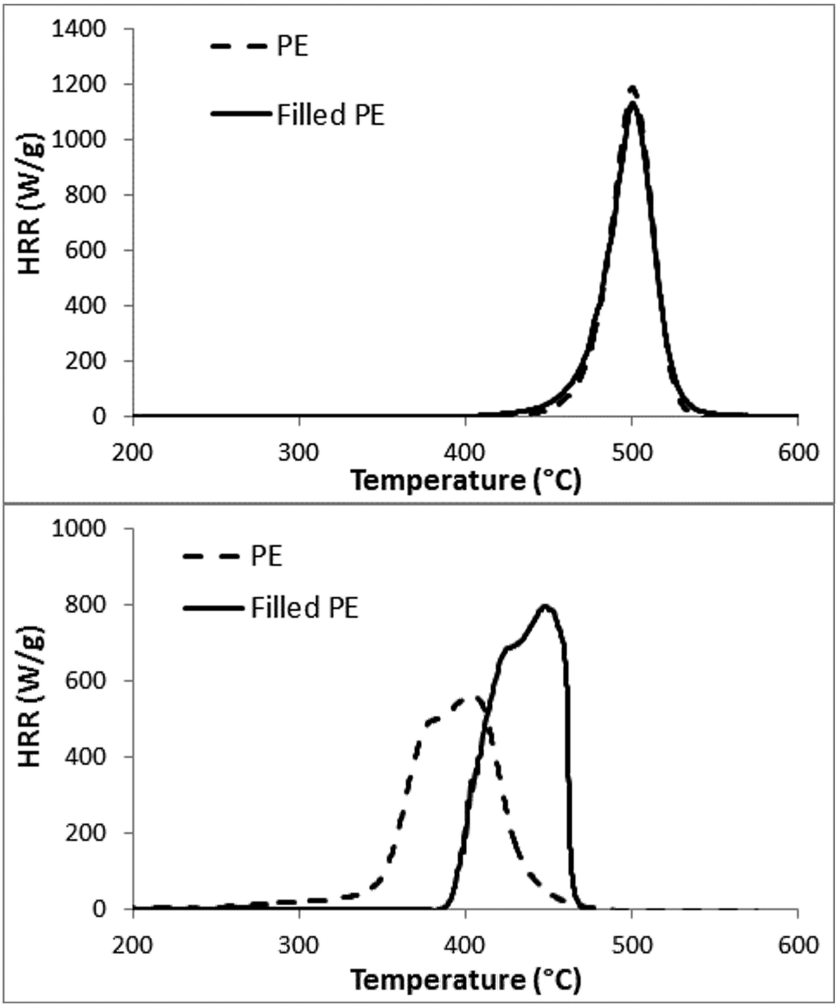

Figure 2. HRR curves for PE and filled PE under anaerobic pyrolysis (up) and aerobic pyrolysis (bottom).

Activation Energy of Pyrolysis

The thermal stability of a polymer could be quantitatively estimated by calculating its pyrolysis activation energy, which could be carried out very easily using thermogravimetric analysis at different heating rates. For example, the well-known Kissinger method allows calculating the activation energy from the temperatures at peak of mass loss rate. Of course this approach is only possible if the pyrolysis mechanism does not depend on the heating rate which is usually a reasonable hypothesis (even if there are some exceptions as for aluminium phosphinate (*11*)). Since pyrolysis in PCFC is carried out at a constant heating rate (exactly like in TGA), it is possible to calculate activation energy from PCFC tests as well. A peak of heat release rate in PCFC corresponds to a peak of mass loss rate in TGA, and therefore temperature at pHRR could be used to calculate activation energy using the Kissinger method. Such an approach was used by our research group to calculate activation energy of PA11 filled with nanoboehmites (*12*).

Calculating activation energy using PCFC rather than TGA has two advantages. First, the heating rate in PCFC is generally 1-4 K/s, close to the heating rate of the surface sample in cone calorimeter (*13*) while heating rate in TGA is generally much lower (10 °C/min typically). Therefore, if the mechanism of pyrolysis depends slightly on heating rate, the activation energy calculated from TGA would be less suitable than that calculated from PCFC. Secondly, due to higher heating rates, the test duration is 15 minutes or less in PCFC against more than one hour in TGA; practically, PCFC allows saving time.

Lyon has also defined the activation energy Ea from HRC as follows (*1*, *14*):

$$HRC = \frac{EHC \times (1-\mu) \times E_a}{e \times R \times T_p^2} \text{ and } \Delta T_p = \frac{e \times R \times T_p^2}{E_a}$$

where EHC is the effective heat of combustion of fuel gases, μ is the char yield, e and R are the natural number and gas constant, T_p is the temperature at peak of decomposition rate and ΔT_p is the pyrolysis temperature interval.

Combustion in PCFC

In most cases, combustion was carried out at 900 °C and in an excess of oxygen leading to complete combustion and maximal heat release. Nevertheless, Schartel et al. (*10*) have shown that it is possible to decrease the combustion temperature and the oxygen rate. Below the critical temperature and oxygen rate, the combustion is incomplete. The critical oxygen rate depends on the material and the sample weight. But the critical temperature depends only on the material, and more precisely on the gases released during the pyrolysis. Since pyrolysis is not affected when combustion conditions are modified because of the de-coupling between the processes, it is possible to calculate the combustion efficiency χ at a given temperature T according to the following equation:

$$X = \frac{THR(T)}{THR\ (900\ °C)}$$

THR at 900 °C is believed to correspond to the maximal heat release (complete combustion). This approach allows studying in detail the combustion of polymers using PCFC and the flame inhibition from some flame retardants. Sonnier et al. (*15*) have determined the combustion efficiency versus combustion temperature curves of various pure and filled polymers. The role of different chemical groups in the para-position on the aromatic ring of polystyrene was pointed out (three examples are shown in Figure 3). PS exhibits a complete combustion above 700 °C. Below this critical temperature, the combustion efficiency decreases quickly. Methyl and methoxy groups do not change the combustion efficiency profile. On the contrary, Br and Cl atoms lead to an increase of the critical combustion temperature, meaning that a higher temperature is needed to ensure complete combustion of brominated and chlorinated polystyrene. This is in perfect agreement with the well-known flame inhibition effect of halogens. Phosphonated PS exhibits a slower decrease of combustion efficiency when the temperature decreases. This polystyrene exhibits good flammability properties due to high charring but this result shows that phosphorus group is not efficient in the gas phase as aflame inhibitor. Similar results were obtained with ABS flame retarded with various additives: ammonium polyphosphate, tetrabromobisphenol A, and TBBA combined with antimony trioxide.

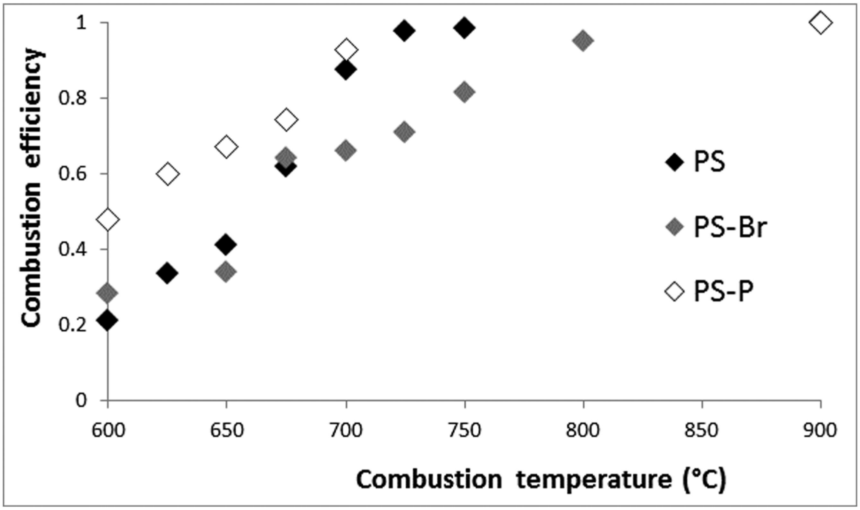

Figure 3. Combustion efficiency of various modified polystyrenes. (from ref. (15))

Moreover, the combustion efficiency profiles of pure polymers have been modelled using a phenomenological equation (by analogy with Avrami equation for isothermal crystallization). This equation is the following:

$$1 - X(T) = \exp(-A \times T^n)$$

where χ(T) is the combustion efficiency at the temperature T. A and n could be calculated by modifying the equation as follows:

$$Ln\left(-Ln\big(1 - X(T)\big)\right) = n \times LnT + LnA$$

Figure 4 shows the very good agreement between modelling curves and experimental data for three pure polymers: PA6, PS and PE. From results on 10 pure polymers, the authors have shown that the parameters n and A (and then the combustion efficiency profile) are related to the chemical structure of the polymer. In particular, the presence of aromatic rings leads to a steep decrease in combustion efficiency when decreasing temperature below 700 °C. On the contrary, this decrease is relatively gentle for PE, PMMA, EVA28 or polyamides.

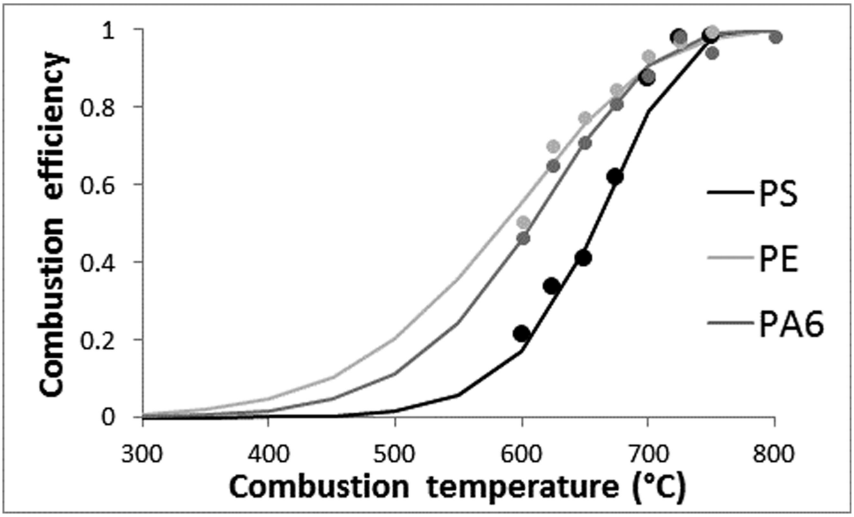

Figure 4. Combustion efficiency profiles for three polymers – Modeling curves (solid lines) and experimental data (circles). (from ref. (15))

FTIR coupled with TGA and cone calorimeter are well-established methods. But in both cases, combustion is not monitored. For TGA, combustion is negligible, even if analysis is carried out under air because pyrolysis of polymers occurs at relatively low temperature. For cone calorimeter, combustion efficiency could be calculated *a posteriori* but it is not a controlled parameter.

On the contrary, in PCFC, pyrolysis and combustion are two separate phenomena. Combustion could be perfectly controlled without modifying pyrolysis. We have carried out analyses on polystyrene and brominated polystyrene using FTIR-PCFC coupling. The combustion efficiency of both polymers was measured versus the combustion temperature (Figure 3). FTIR spectra of gases released after pyrolysis and combustion at combustion temperatures of 600, 650 and 700 °C were recorded at the pHRR temperature (Figure 5). At 600 and 650 °C, combustion efficiencies are similar for both polymers. Combustion is incomplete and CO peaks are clearly detected between 2000 and 2250 cm^{-1}. But at 700 °C, combustion is almost complete for PS (0.9) and CO is detected with difficulty. On the contrary, combustion efficiency is close to 0.65 for brominated PS and CO peaks are visible. Moreover, methane is observed for brominated PS between 2900 and 3150 cm^{-1} up to a combustion temperature of 750 °C (Figure 5 - details). For PS, methane is hardly detected only up to 650 °C. The presence of methane indicates that some organic gases are not fully oxidized in the chosen combustion conditions. Such preliminary results show that FTIR-PCFC coupling should bring new data on the combustion of polymers.

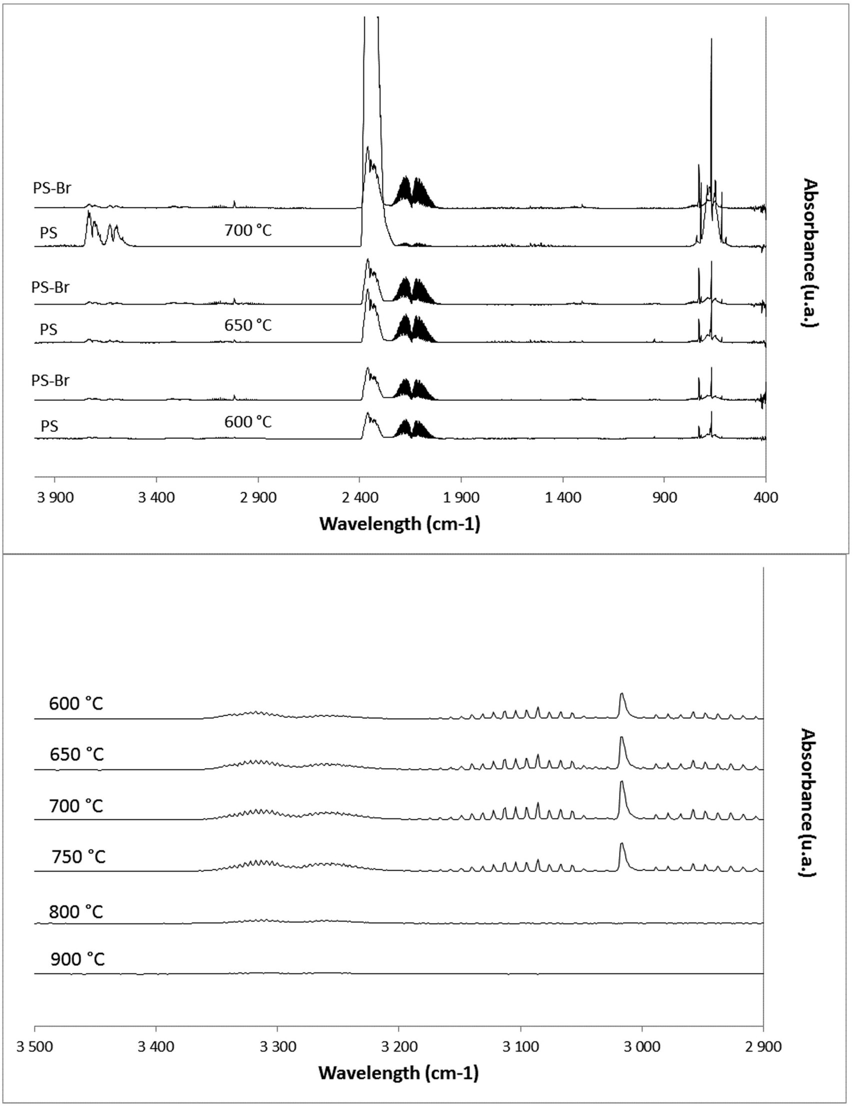

Figure 5. FTIR spectra of gases released after pyrolysis and combustion of PS and brominated PS at various combustion temperatures (up); Details of FTIR spectra for brominated PS at various combustion temperatures (bottom).

Predicting Flammability Using a Van Krevelen Approach

As said previously, PCFC allows measuring some important flammability characteristics of small amount of samples. Therefore it is a useful tool for chemists who synthesize new polymeric structures. In many articles where the synthesis of new polymers or the grafting of chemical groups onto macromolecules are reported, PCFC is the first and often the only method to characterize flammability: for example, phosphorus-modified polystyrenes (*3*, *4*, *16*), fluorinated polyurethanes (*5*), copolymers containing cyclic PBT oligomers (*17*), phosphorus containing PBT (*18*), siloxane grafted copolyimides (*8*), fluorinated poly(arylene ether phosphine oxide)s (*19*), bisphenol-1,2,3-triazole polymers (*20*), poly(arylate-phosphonate)s (*21*), polyphosphorinanes (*22*), polyphosphazenes (*23*), polysilphenylene-siloxanes (*23*), polycyanurates (*24*), cyanate ester-epoxy blends (*25*).

However, predicting the flammability of a polymer from its chemical structure could be an even better strategy avoiding a long and cost-expensive synthesis process. In a series of articles (*26–28*), Lyon and his team have proposed to calculate some important flammability data (HRC, heat of combustion, char content) using a Van Krevelen approach. A polymer structure is divided into simple chemical groups. Each flammability property P (HRC or sumHRC, EHC, THR or char yield) of this polymer is then calculated as follows:

$$P = \Sigma\,(w_i \times P_i)$$

where P_i is the contribution to this property of the chemical group I and w_i is the weight fraction of the group i

Using a statistical method, the contributions to HRC, EHC and char yield of almost forty chemical groups were calculated and a relative good agreement was found between the experimental and calculated flammability properties of more than 84 polymers (*26*). Nevertheless, there are some polymers for which the calculated flammability properties are significantly far from the experimental data. The reason is probably that this approach is quite simple. For example, the interactions between chemical groups are not taken into account.

Sonnier et al. (*29*) have attempted to calculate properties of two new chemical groups (dioxaphosphorinane and phosphonate) using the same approach and the first database proposed by Lyon et al. (*26*). They succeeded in calculating contributions to HRC and to THR of both groups when incorporated in two series of molecules (small molecules, oligomers and polymers –series A and B in Figure 6). But in a third series (series C), when these groups are present together with ester or acid groups, the contributions previously calculated were incorrect; experimental values of HRC (or THR) of the polymers from this series were systematically lower than the predicted values. The authors assumed that these results were due to the interactions between phosphorus groups and acid or ester groups and they proposed to calculate the interaction indices to evaluate the strength of these interactions for each polymeric structure. This approach is believed to identify the most promising structures to be used for flame retardancy.

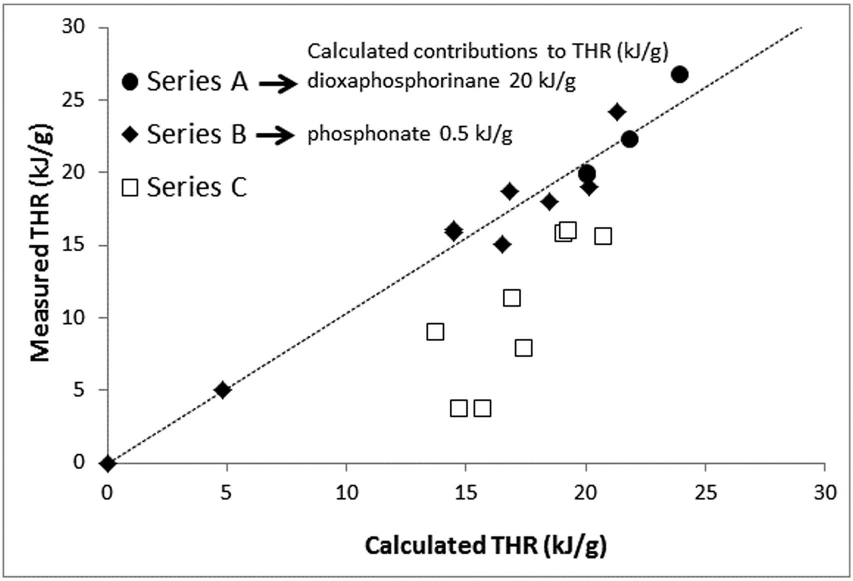

Figure 6. Measured versus calculated THR for phosphorus containing molecules (series A,B and C are described in the text). (Reproduced with permission from ref. (29). Copyright 2012 Elsevier.)

If interactions are expected between some chemical groups, it is not possible to calculate a unique contribution of these groups for a wide range of polymeric structures. The contribution of a given group should be modified according to the chemical environment of this group and the presence of other interacting groups. Vahabi et al. (*30*) have calculated the contributions to sumHRC, EHC and char yield of the phosphonate group incorporated into two comonomers polymerized with methyl methacrylate (MMA). One comonomer is a monophosphonated monomer and the other one is an aminobisphosphonated monomer. Since the ratio between MMA and the phosphorus comonomer varied, the calculated contributions allowed fitting quite well the predicted and the measured EHC and char yield. The agreement between measured and calculated sumHRC was less satisfying. This theoretical approach showed that both phosphonated comonomers contribute similarly to char yield but that the aminobisphosphonated monomer decreases the sumHRC more significantly.

Combining PCFC and TGA

Pyrolysis is generally carried out in similar conditions in PCFC and TGA: under aerobic or anaerobic conditions in both cases and at a constant heating rate. Only the heating rate is usually different. Sample weight is also slightly lower in PCFC. Due to these similar conditions, PCFC and TGA could be easily combined to bring new information about the flammability of materials. Heat release rate is the product of two quantities: the mass loss rate (MLR) and the (instantaneous) effective heat of combustion (EHC_i). Identically, total heat release is the product of total mass loss (ML) and mean effective heat of combustion (EHC_m).

$$HRR = MLR \times EHC_i$$

$$THR = ML \times EHC_m$$

By measuring HRR and MLR, it becomes possible to calculate EHC. For example, Schartel et al. (*10*) have well shown this coupling with PVC. PVC decomposition occurs in two main steps. The first one corresponds to a high mass loss but low heat release. The second one corresponds to high heat release and low mass loss. Indeed, the first peak is mainly attributed to the release of HCl corresponding to a high mass fraction of the polymer. Nevertheless, HCl is a non-combustible gas and therefore the EHC of the gases released during this step is low. During the second step, on the contrary, the rest of the molecules corresponding to relatively low mass fraction is decomposed and oxidized (in PCFC) to release heat. Therefore, the EHC of these gases is higher.

If pyrolysis is carried out at the same heating rate in PCFC and TGA, it should be possible to calculate not only the mean effective heat of combustion but also the instantaneous effective heat of combustion using HRR and MLR at each temperature. In other cases, instantaneous EHC could be calculated at pHRR. Indeed, pHRR corresponds to peak of MLR.

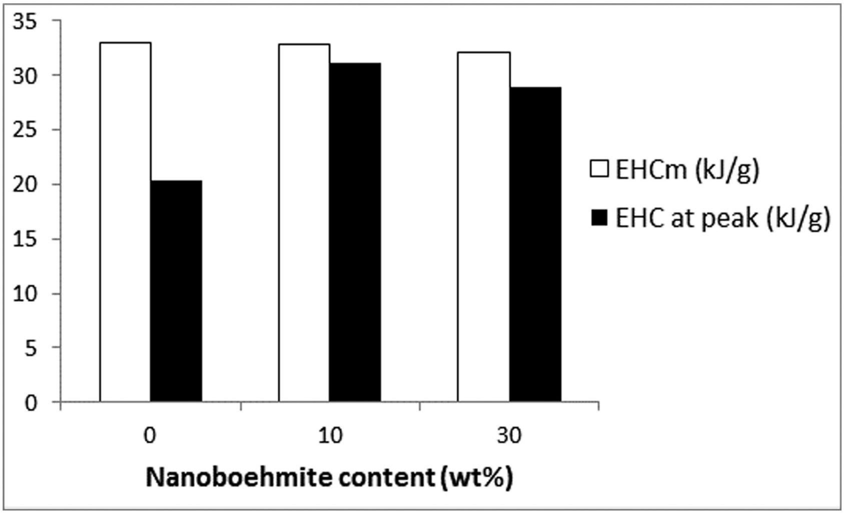

Figure 7. EHC_m and $EHC_{at\ peak}$ for PA11 pure and filled with nanoboehmites. (from ref. (12))

Using Mass Loss Capacity (MLC) as the peak of MLR divided by the heating rate (by analogy with HRC which is defined by the pHRR divided by the heating rate), it is possible to calculate the EHC at peak ($EHC_{at\ peak}$) as the ratio between

HRC and MLC. This approach was carried out on PA11 pure and filled with 10 and 30 wt% of nanoboehmites (*12*). While EHC_m is similar at 32-33 kJ/g for these three formulations (a slight decrease is observed due to the release of water from the decomposition of nanoboehmites), $EHC_{\text{at peak}}$ is significantly different (Figure 7). The value for pure PA11 is low (20 kJ/g) in comparison with EHC_m, while $EHC_{\text{at peak}}$ is close to EHC_m for filled PA11. These results are explained as follows: PA11 decomposition occurs in two steps. The first one corresponds to the main pHRR while a small shoulder at higher temperature corresponds to the degradation of a char formed previously. This char has a very high EHC because it is a carbon-rich product. Therefore, the EHC corresponding to the gases released during the first step is reduced. The incorporation of nanoboehmites significantly modifies the decomposition pathway of PA11 which exhibits only one step. In this case, EHC is the same over the whole pyrolysis temperature interval.RC HRC and MLC.

Some flame retardant additives could act both in condensed and gaseous phases. particularly for phosphorus containing compounds. Vahabi et al. (*30*) studied two chemically modified PMMA. Combining TGA, PCFC and phosphorus content measured by EDX (Energy Dispersive X-ray spectroscopy), they proposed two indicators to evaluate the relative influence of phosphorus in both condensed and gaseous phases. The first is the Charring Efficiency of Phosphorus (CEP) calculated as follows:

$$CEP = \frac{X_{char}(copo) - X_{char}(PMMA)}{100 \times f_{Pcond} \times X_{Pini}}$$

where X_{char} is the char yield (in %), f_{Pcond} is the fraction of phosphorus remained in condensed phase and X_{Pini} is the initial phosphorus content.

The second indicator was called “Efficiency of Phosphorus in the Vapor phase” (EPV) and was calculated using PCFC data:

$$EPV = \frac{EHC_{PMMA} - EHC_{copo}}{100 \times f_{Pvap} \times X_{Pini}}$$

where EHC is the effective heat of combustion (calculated as the ratio between the Total heat release and the mass loss), f_{Pvap} is the fraction of phosphorus in vapor phase.

Using this approach, the authors assumed that the phosphorus contained in the monophosphonated copolymer was more efficient in condensed phase (higher CEP) than the aminobisphosphonated copolymer. The efficiency of phosphorus in vapor phase was similar for both copolymers.

As shown above, the coupling between both methods is really interesting and allows calculating other flammability data in addition to pHRR (or HRC) and THR. Moreover, EHC could provide indirect indications about the gases released for a specific step of decomposition. Unfortunately, there are only few studies which discussed precisely the comparison between PCFC and TGA data (*12*, *30–34*). In most cases, TGA and PCFC are used separately.

In Fire and Polymers VI: New Advances in Flame Retardant Chemistry and Science; Morgan, A., et al.;
ACS Symposium Series; American Chemical Society: Washington, DC, 2012.

Thermal stability is mainly studied using TGA and some work has been done to try to correlate the time to ignition in cone calorimeter and the onset temperature of degradation in TGA (for example, (*35*)). These attempts are based on the fact that ignition occurs for a critical mass loss rate, and TGA measures basically the mass loss rate according to a constant heating rate. In our opinion, such correlations are more likely to be highlighted using PCFC rather than TGA. First of all, the critical mass loss rate as criterion for ignition could be turned on a critical energy density (*36*), meaning a critical HRR. Moreover, the heating rate in cone calorimeter is close to the typical heating rate in PCFC while the heating rate in TGA is much lower. Finally, mass loss rate could be due to non-combustible gases in some cases. This is particularly the case when hydrated fillers are incorporated into a polymer to delay its ignition by endothermic decomposition. In this case, time to ignition in cone calorimeter and onset temperature for mass loss rate in TGA should not be correlated, because the mass loss rate at low temperature is due to non-combustible gases which could not induce earlier ignition in cone calorimeter. Using a HRR criterion in PCFC allows avoiding this problem, because the release of non-combustible gases does not contribute to heat release rate. Therefore, the onset temperature (defined for a critical HRR) corresponds exactly to the release of combustible gases.

Correlations between PCFC and Other Calorimetry Methods

Some authors have attempted to use PCFC as a new screening tool before testing materials in cone calorimeter tests. Indeed, in PCFC only a small amount of materials is needed compared to cone calorimetry, where approximately a 50 g of material is needed to prepare the square sheets. Furthermore, the preparation of this type of specimen, for cone calorimeter test, needs extrusion and injection molding processes which require a great amount of material. This is a severe limitation in some cases when materials are difficult to synthesize or very expensive.

Some authors have found a quite good agreement between PCFC and cone calorimeter results. Here, we present briefly some of this work.

Lu and Wilkie have studied 13 brominated flame retardant polystyrene composites using both methods (*37*). Flame retardant systems contained decabromodiphenyl oxide, antimony trioxide, multi-wall carbon nanotubes (MWCNT) and organically modified montmorillonite clay (Cloisite 15A). Using the Minitab 15 statistical software, they calculated the correlation coefficients between cone calorimeter and PCFC data. They found relatively high correlation coefficients (absolute value > 0.8) between HRC in PCFC and pHRR and THR in cone calorimeter and between THR in PCFC and AEHC (average effective heat of combustion) in cone calorimeter. Moreover, the reduction in pHRR in PCFC was in good agreement with the reduction in pHRR in cone calorimeter even if at low flame retardant loadings (< 10 wt%), the reduction in PCFC was more significant than in cone calorimeter. The authors concluded that PCFC can provide evidence of the efficiency of flame retardants on smaller samples and in much less time than in cone calorimeter. These results are quite surprising, since organo-modified layered silicates and multiwall carbon nanotubes (MWCNT) act by barrier effect and brominated flame retardants decrease the combustion efficiency in cone calorimeter. However, both effects are not efficient in PCFC (as shown in the following). It should be noted that the value of the correlation coefficient to consider a good agreement between PCFC and cone calorimeter: 0.8 is a relatively low value.

Cogen et al. (*38*) have also used a statistical approach to evaluate the agreement between cone calorimeter and PCFC results. Halogen-free polyolefin compounds were studied as formulations for wire and cable industry. Many correlation coefficients were found higher than 0.7 between various data in both tests. The highest coefficients (> 0.9) were found between TTI and Fire Growth Rate (FIGRA) in cone calorimeter and temperature at pHRR in PCFC and between THR in PCFC and in cone.

Lyon et al. (*26*, *39*) have shown a good agreement between pHRR in cone calorimeter and HRC in PCFC for respectively 50 and 160 polymers. Some of them were charring polymers or contain halogens. Nevertheless, the authors admitted that PCFC properties could not correlate flame retardancy of polymers (as measured in other tests) over a broad range of flame retardant chemical compositions. These authors proposed a simple model to describe flaming combustion as occurred in cone calorimeter (*39*). This model includes the HRC measured in PCFC:

$$HRR = \frac{HRC\ \times q^{''}_{ext}}{n_g}$$

where HRR is the heat release rate of the solid in flaming combustion (steady burning), q”ext is the external heat flux and ηg is defined as follows:

$$n_g = \frac{\frac{h_g}{\Delta T_p}}{X\ \times\ \theta}$$

where hg is the heat of gasification per unit initial mass of solid, ΔTp is the pyrolysis temperature interval, χ is the combustion efficiency and θ is the relative efficiency of heat and mass transfer at the surface. The product χ.θ is the burning efficiency.

This model points out that the fire performance in cone calorimeter of a range of materials could be screened using PCFC only if hg, ΔTp, χ and θ values do not change. It means that the ratio between HRR and HRC at a given external heat flux is constant but this is a severe (and generally not expected) condition.

Thermal Barrier Effect

Since there is no general correlation between PCFC and cone calorimetry, PCFC should not be used as a screening tool (*10*, *32*, *40–46*). Several authors have correctly identified one of the major sources of non-correlation between both tests: thermal barrier effect could be effective in cone calorimeter when an organic or hybrid char layer is formed at the surface of the sample. This layer would be able to limit the heat transfer from the flame to the underlying material and the gases release rate from the condensed phase to the vapor phase. In the above equation, it means that θ decreases. But this effect vanishs and could be neglected in PCFC since a very small sample weight is used.

Chen et al. (*42*) have studied EVA copolymers containing aluminium trihydroxide (ATH) and Fe-OMT (Fe-montmorillonite). The best formulations in terms of flammability results are not the same in PCFC and in cone calorimeter. In fact, the best formulation in PCFC exhibits a low-strength char residue. This residue collapses during cone calorimetry, leading to poorer barrier effect and flame retardancy.

Hence, intumescent phenomena which involve very efficient barrier effect in cone calorimeter test could not be observed using PCFC. Gerard et al. (*43*) correctly addressed this problem studying the efficiency of intumescent flame retardant systems based on ammonium polyphosphate (APP) and nanoparticles (carbon nanotubes or organomodified polyhedral oligomeric silsesquioxane (POSS)) in epoxy resin using both tests.

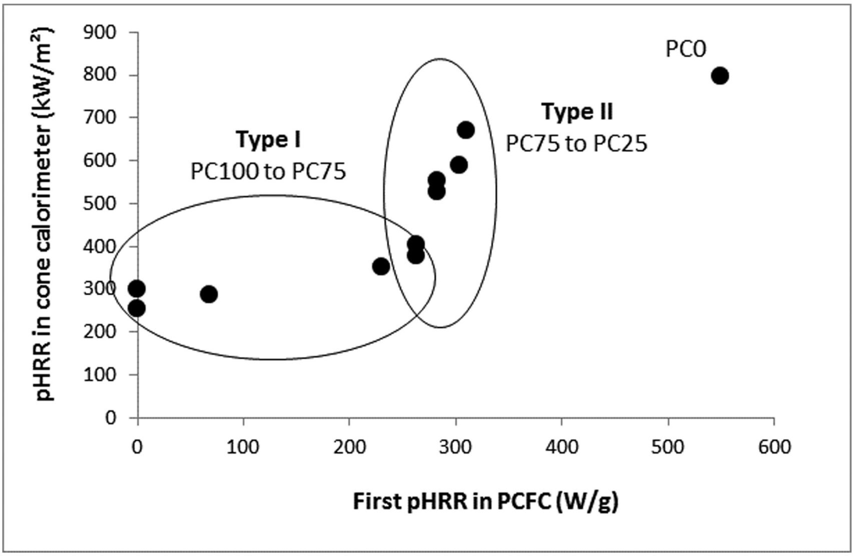

Figure 8. Comparison between pHRR in cone calorimeter and first pHRR in PCFC (corresponding to PBT decomposition) for PC/PBT blends (PCX means a blend containing X wt% of PC). (Reproduced with permission from ref. (44). Copyright 2012 John Wiley and Sons.)

Sonnier et al. (*44*) have attempted to correlate data from cone calorimetry and PCFC for various PC/PBT binary blends. The sumHRC was approximately the same for all blends because PC and PBT exhibited a similar HRC. Nevertheless, the decomposition temperature was much lower for PBT than for PC. Therefore, the authors assumed that HRR in the cone calorimeter should be mainly governed by pHRR of PBT in the PCFC (see Figure 8). Moreover, the relation between pHRR in the cone calorimeter and that of PBT in PCFC appeared complicated by an intumescent phenomenon. Two kinds of behavior could be observed according to the PBT content and the occurrence of intumescence: firstly, at low PBT content (type I), pHRR in the cone calorimeter slowly increases with increasing PBT content (and then first pHRR at PCFC). In the cone calorimeter, the corresponding formulations exhibit highly expanded char. But, when PBT content increases above 25 wt%, PBT becomes the continuous phase and no expansion occurs. Therefore, a fast increase in pHRR in cone calorimetry was observed (type II).

It was then proposed (*46*) to exploit the discrepancy between the results in PCFC and cone calorimeter tests to highlight a thermal barrier effect. Two parameters R1 and R2 were calculated:

$$R1 = \frac{pHRR(flame\ retarded\ polymer)}{pHRR(pure\ polymer)}\ in\ PCFC$$

$$R2 = \frac{pHRR(flame\ retarded\ polymer)}{pHRR(pure\ polymer)}\ in\ cone\ calorimeter$$

It was noticed that R1 is always higher (or at least equal to) than R2 (Figure 9); a flame retardant leads to a stronger decrease in pHRR in cone calorimetry than in PCFC. Considering that some modes-of-action are efficient in both cone calorimeter and PCFC while other modes-of-action (thermal barrier effect) are only efficient in cone calorimeter, it was concluded that when R1 = R2, a flame retardant does not act by barrier effect. On the contrary, when R2 < R1, thermal barrier effect is one of the significant modes-of-action of the flame retardant. An example is given in Figure 10. Various contents of MDH were incorporated into EVA (28 wt% of vinyl acetate). It could be seen that R2 becomes lower than R1 when the MDH content increases above 50 wt%. This corresponds to a significant char layer formed at the surface during the degradation. This method should allow quantifying barrier effect, which is often invoked only from visual observation.

This approach was applied in several cases to estimate the barrier effect as one of the modes-of-action of various flame retardant systems: nano-alumina and ATH in unsaturated polyester resins (*47*), ammonium polyphosphate/melamine polyphosphate/metal oxide (alumina and boehmite) in PMMA (*48*), ammonium polyphosphate and nanosilica in PMMA (*49*).

Nevertheless, this empirical approach is only valid if the barrier effect is the only source of non-correlation between both tests. The studied formulations should exhibit similar thermal stability, combustion efficiency and thermal properties, because these characteristics could also induce non-correlations, as will be shown in the following examples.

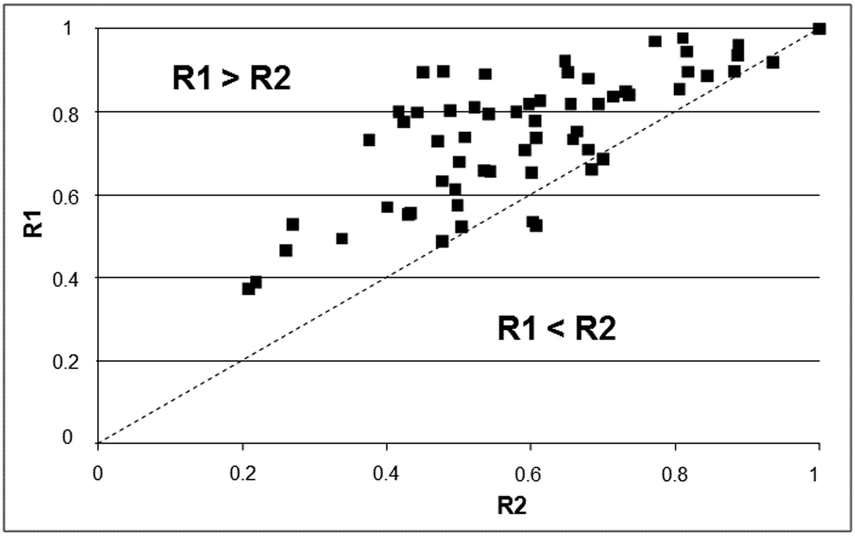

Figure 9. R1 versus R2 graph for more than 60 formulations. (Reproduced with permission from ref. (45). Copyright 2011 John Wiley and Sons.)

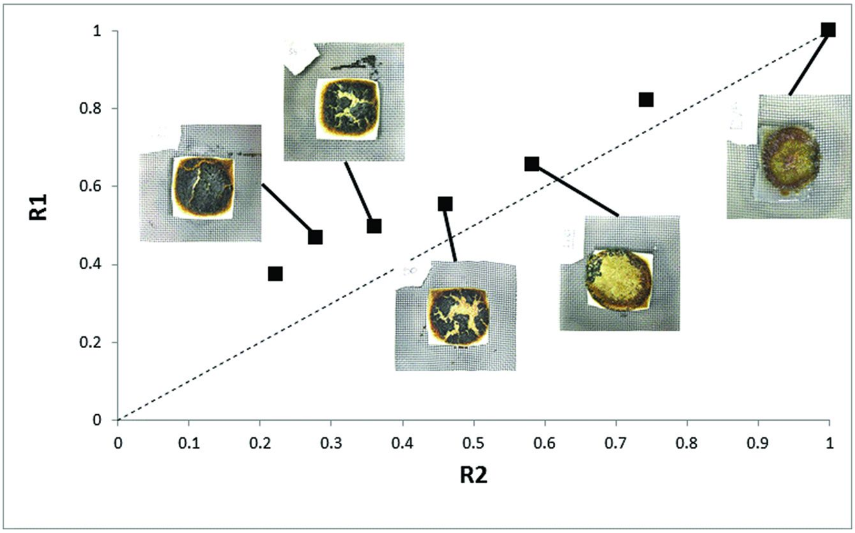

Figure 10. R1 versus R2 graph for EVA28-MDH formulations (figures give the weight content of MDH). (Reproduced with permission from ref. (45). Copyright 2011 John Wiley and Sons.)

Combustion Efficiency

Except thermal barrier effect, other sources of non-correlation have been identified by Lyon et al. (*39*). The second one is the combustion efficiency (*10*, *15*, *39*). Combustion efficiency is equal to 1 in PCFC standard test because the combustion is forced to be complete. On the contrary, in cone calorimetry, the combustion is not complete even if the combustion efficiency is often close to 0.9-1 because of well-ventilated conditions. Combustion efficiency in the cone calorimeter could be calculated by dividing the effective heat of combustion of fuel gases by the effective heat of complete combustion measured at PCFC (*14*). For example, Braun et al. (*11*) have shown that zinc or aluminium phosphinates decrease the combustion efficiency of PBT/glass fibers in the cone calorimeter, but not in PCFC (in standard conditions). This point explains also that the efficiency of halogenated flame retardants is underestimated in PCFC standard test, since these additives act mainly by flame inhibition.

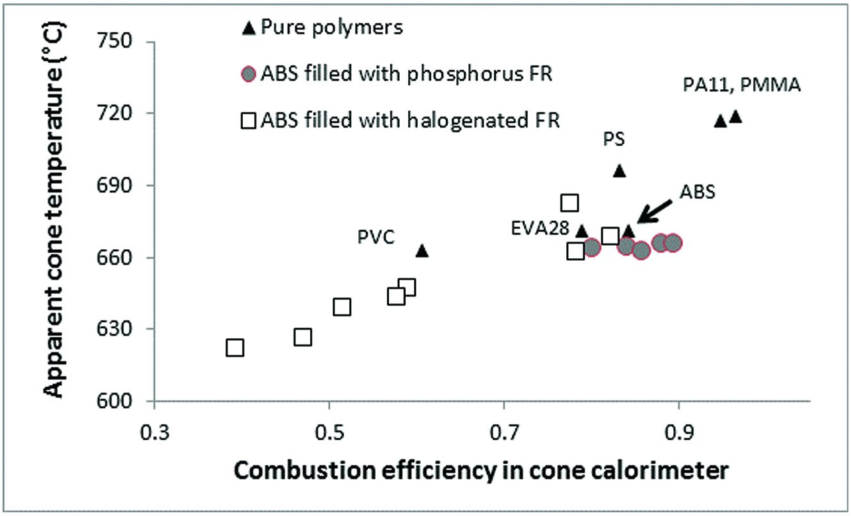

Figure 11. Apparent cone calorimeter temperature versus combustion efficiency in cone calorimeter (irradiance 50 kW/m²) for various pure polymers and flame retarded ABS. (from ref. (15))

As discussed earlier, Sonnier et al. have monitored the combustion temperature in PCFC to decrease the combustion efficiency (*15*). They compared the combustion efficiency in PCFC for different combustion temperatures with that measured in cone calorimetry for an irradiance of 50 kW/m². According to the analyses of some pure polymers and ABS flame retarded with various contents of TBBA, TBBA/Sb_2O_3 or APP, they found that the PCFC combustion temperature needed to obtain the same combustion efficiency at PCFC and cone calorimeter ranged from 650 to 700 °C for most formulations. This temperature, called “apparent cone calorimeter temperature”, decreased to 620 °C for ABS contained high amounts of halogenated flame retardants, and increased to 720 °C for some very flammable pristine polymers (PMMA, PA11) (Figure 11).

Such analysis should be confirmed by testing a larger variety of materials, but it suggests that it would be possible to predict the combustion efficiency in the cone calorimeter from tests carried out using PCFC at a combustion temperature in the 650-700 °C range. Moreover, it was showed that the comparison between pHRR in cone calorimetry and in the PCFC based on the calculations of R1 and R2 parameters (as seen earlier) could be applied to halogenated materials if PCFC tests are carried out at this apparent cone calorimeter temperature.

Thermal Stability

The third source of non-correlation is the thermal stability of materials. Two materials could exhibit similar peaks of heat release rate in PCFC but at various pyrolysis temperatures so that their behavior in the cone calorimeter test would not be the same. The most thermally stable material needs more heat to be decomposed and volatilized, therefore the mass loss rate is lower. Therefore, one should not correlate better flame retardancy with the lowering of HRC, THR or an increasing char yield in PCFC, if the decomposition starts at lower temperature as claimed in some articles (*50*, *51*). Patel et al. (*52*) have well shown the influence of pyrolysis temperature on the burning rate in cone calorimeter test using Thermakin, based on a one-dimensional pyrolysis model. With the selected properties used in this study, a change in pyrolysis temperature from 900 to 500 K leads to an increase in peak of heat release rate from 500 to 900 kW/m^2 and a decrease in time to ignition from approximately 130 to 10 s. Using the same approach, Stoliarov et al. (*53*) have shown that the Arrhenius pre-exponential factor and the activation energy (which are directly related to the pyrolysis temperature) are among the main important parameters to control the burning rate in cone calorimetry.

Results obtained from PCFC and cone calorimetry are not always in agreement, even for usual materials, and may be much more complex for multicomponent materials. Such materials could exhibit several decomposition steps, if their components have various thermal stability temperatures. In this case, considering heat release capacity derived from the main peak of heat release rate is not appropriate. Some other parameters (avgHRC and sumHRC) have been proposed as relevant parameters, as shown in the previous section (*10*). Nevertheless, data are too scarce to evaluate if these parameters are well-correlated to peak of heat release rate in the cone calorimeter. Further efforts should be made to address this problem.

Contrary to most of polymers, silicone (PDMS) exhibits a very different pyrolysis temperature according to its crosslinking density and the presence of fillers. Eight silicone-based formulations containing 20 wt% of silica and 20 wt% of various fillers were studied: mica, wollastonite, alumina, ATH, boehmite, calcite, precipitated calcium carbonate and calcium hydroxide. The peak of heat release rate in PCFC is close for seven formulations (between 120 and 160 W/g).

On the cone calorimeter, the peak of heat release rate seems to decrease when the pyrolysis temperature (measured in PCFC as the temperature of the pHRR) increases (Figure 12). Obviously, other characteristics influence the peak of heat release rate and therefore this tendency is not straightforward. Especially, the fact that mica-filled silicone exhibits a lower pHRR than other formulations in PCFC indicates a significant barrier effect while using the cone calorimeter.

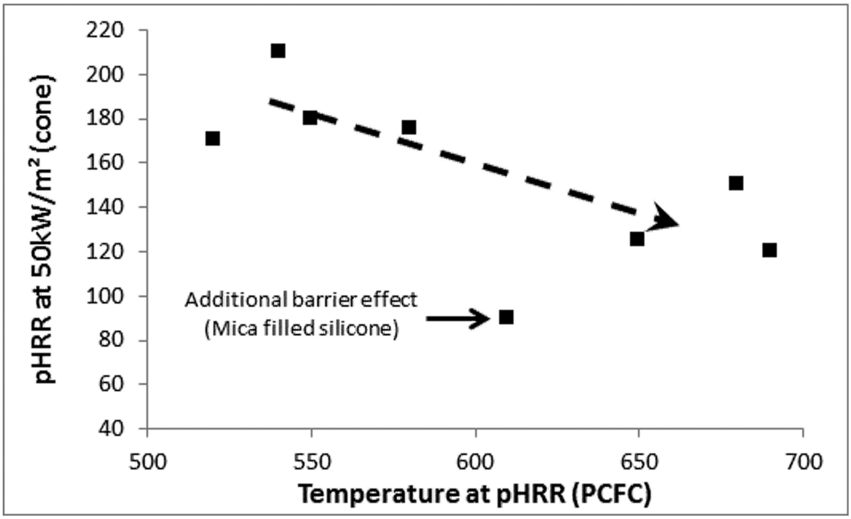

Figure 12. Peak of heat release rate in cone calorimeter of mineral fillers containing silicones versus temperature at peak of heat release rate in PCFC.

Thermo-Physical Properties

A fourth reason which could lead to different or contradictory results in both tests is related to thermo-physical properties of the materials: particularly thermal conductivity, reflectivity and heat absorption. Several works (*52*, *53*) have studied the influence of various properties on the heat release rate using the already mentioned Thermakin software. Higher thermal conductivity leads to a longer time to ignition and a faster increase in heat release rate after ignition. Higher reflectivity leads to a longer time to ignition and a lower peak of heat release rate. Lower heat absorption leads to a delayed time to ignition but a shorter time to peak of heat release rate. On the contrary, in PCFC, these properties could not have any influence on the flammability because of the small size of specimen.

We have incorporated nanoboehmites into a polyamide 11. 30 wt% of nanoboehmites increase the thermal stability, and the pHRR temperature at PCFC is shifted 25 °C towards higher temperatures (*12*). Nevertheless, the

In Fire and Polymers VI: New Advances in Flame Retardant Chemistry and Science; Morgan, A., et al.; ACS Symposium Series; American Chemical Society: Washington, DC, 2012.

time to ignition is significantly reduced in the cone calorimeter from 75 to 53s (at an irradiance of 50 kW/m²). This apparent discrepancy was attributed to higher heat absorption when incorporating nanoboehmites. Experimental data from epiradiator test (French standard based on the radiative heating of a 7x7 cm² sample sheet (NF P 92-505)) show that the surface temperature increases faster in the presence of nanoboehmites, despite a theoretically higher thermal conductivity of the filled polymers (Figure 13).

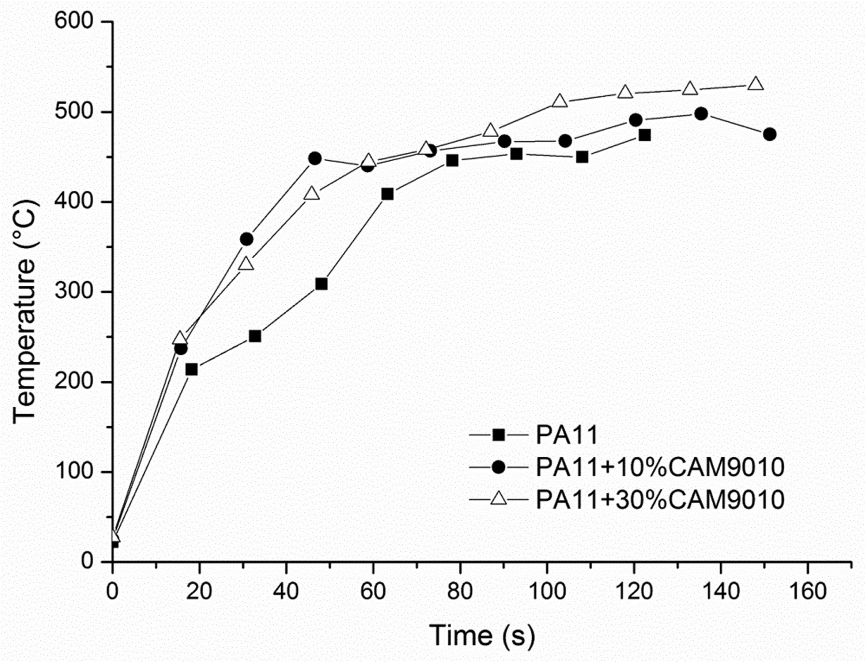

Figure 13. Surface temperature of PA11 and PA11 filled with nanoboehmites during the epiradiator test. (from ref. (12))

Other Physical Effects

Finally, some other physical phenomena are negligible in PCFC, like bubbling or dripping. Even if dripping is not observed in the cone calorimeter test, bubbling could have a strong effect on peak of heat release rate. Oztekin et al. (*54*) have shown that a very small amount of water in PEEK (0.73 wt%) could lead to bubbling after melting of PEEK. This phenomenon leads to a lower time to ignition but also a lower peak of heat release rate. Obviously, this influence could not be detected in PCFC.

Discrepancy in Total Heat Release

Up to now, the discussion has been focused on the comparison of the peak of heat release rate in both tests. Another important parameter is the total heat release. In the cone calorimeter, all the fuel is decomposed and volatilized if the temperature is high enough, which is generally the case for most of polymers which exhibit relatively low temperature of decomposition. Their peak of heat release rate in PCFC occurs most of the time at temperature lower than 500 °C while the temperature in the condensed phase in the cone calorimeter could easily reach 600 °C (*13*). In this case, a good agreement in THR is expected between PCFC and cone calorimetry. Cogen et al. (*38*) have found a correlation coefficient of 0.98 between both THR (in cone calorimeter and in PCFC) in their study on halogen-free polyolefin compounds.

Nevertheless, a discrepancy in THR may occur in four cases. The first is related to the thermal stability of the polymer. The temperature reached in the cone calorimeter could be too low to decompose all the fuel since PCFC standard heating ramp ends at 750 °C. Therefore, the Total Heat Release in the cone calorimeter is lower than for PCFC. The same remark could apply when a barrier layer is able to limit the heating of the underlying polymer. For example, polyurethane and polyphosphazenes containing expandable graphite exhibit a higher char yield in cone calorimetry than in anaerobic pyrolysis in PCFC due to the protective intumescent char layer (*23*).

When a char is formed, its thermal stability could be variable according to the presence of oxygen. In the cone calorimeter, thermo-oxidation could occur: char is degraded leading to heat release rate, even without flame (after flame is out). Conversely, for PCFC standard conditions, the pyrolysis atmosphere is nitrogen so the char could not undergo thermo-oxidation. Char is therefore higher in PCFC and THR should be lower. Such discrepancy in char yield was observed by Walters and Lyon between PCFC and OSU (Ohio State University) fire calorimeter in the case of cyanate ester-epoxy blends (*25*).

The combustion efficiency is the third reason for the discrepancy in THR between the two tests. If the combustion efficiency is lower than 1in the cone calorimeter, the THR should be lower than in PCFC, which is probably the reason why Lu and Wilkie did not observe a good correlation between THR in cone calorimeter and in PCFC (*37*). The materials studied in their work contained various contents of a well-known flame inhibitor (decabromodiphenyl oxide with antimony trioxide). Schartel et al. (*10*) did not observed any good correlation between the total heat release in PCFC and the EHC in the cone calorimeter for PC/ABS flame retarded with organo-phosphorous compounds. They also explained this discrepancy by the flame inhibition of these flame retardants. In fact, the combustion efficiency in the cone calorimeter (defined as the effective heat of combustion at cone calorimeter divided by the heat of complete combustion of volatiles in PCFC) ranged from 0.79 to 1 according to the formulation.

Finally, a fourth case leads to a difference not in THR but in EHC. Some fillers release water or carbon dioxide during their decomposition. For some of them, this decomposition occurs at a high temperature. Therefore, the decomposition takes place in PCFC but not in the cone calorimeter. EHC is higher for the latter test than for the former. As mentioned earlier, Cogen et al. (*38*) have studied halogen-free flame retardant polyolefin compounds containing $CaCO_3$. $CaCO_3$ releases CO_2 at high temperature (above 700 °C). The residue yield at cone calorimeter is close to the theoretical one considering no decomposition of $CaCO_3$. On the contrary, the residue yield from PCFC corresponds to the calculated char considering the decomposition of $CaCO_3$. Therefore, the EHC for both tests should be significantly different while THRs are very close.

A strong discrepancy in heat of combustion measured in PCFC and in oxygen bomb calorimeter was found by Schartel et al. (*10*) for ABS/PC blends containing various flame retardants (see Figure 13). Heat of combustion is always lower in PCFC because the char is not oxidized (method A). On the contrary, complete oxidation of the char takes place in bomb calorimeter. Therefore, the discrepancy of both tests allows measuring the potential heat release remaining in the char. This could be expressed as follows (*24*):

$$h^0_{c,x} = \frac{h^0_{c,p} - \mu \times h^0_{c,\mu}}{1 - \mu}$$

where $h^0_{c,v}$, $h^0_{c,p}$ and $h^0_{c,\mu}$ are respectively the heat of combustion of the volatile fuel gases at PCFC, the net heat of combustion of the polymer in oxygen bomb calorimeter and the heat of combustion of the char and μ the char yield at PCFC.

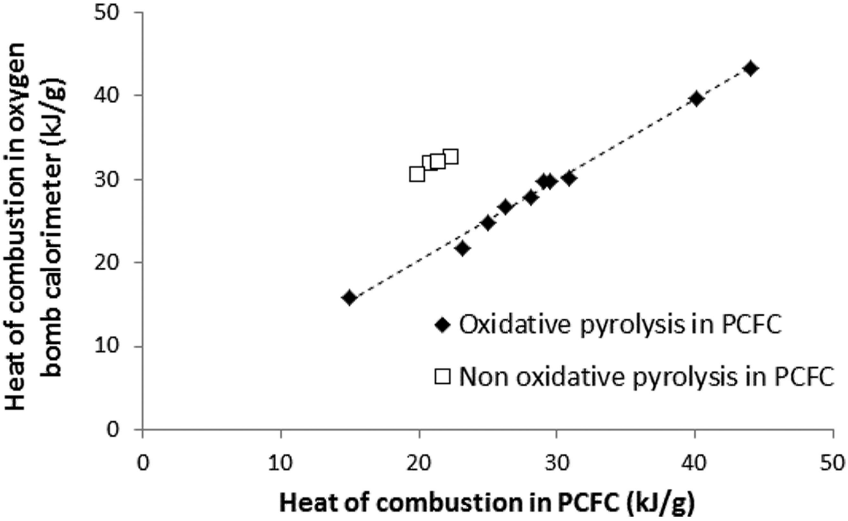

Figure 14. Comparison between the heat of combustion in PCFC and in oxygen bomb calorimeter for 10 polymers under oxidative pyrolysis in PCFC (from (1)) and for 5 flame-retarded PC/ABS blends under non oxidative pyrolysis in PCFC. (from ref. (10))

But, when pyrolysis of sample is carried out under air in PCFC (method B), the heat of combustion becomes very close to the value measured in oxygen bomb calorimeter. Lyon and Walters have measured the net heat of combustion of ten polymers using both methods (*1*). A very good agreement was observed between them, even for charring polymers (Figure 14).

Correlations between PCFC and Other Flammability Tests

Performances prediction would be also useful for other usual flammability tests as Limiting Oxygen Index or UL94. The same reasons which could limit the correlations between PCFC and cone calorimeter are also valid for these predictions. But the correlations between PCFC and these tests seem to be limited since physical effects such as dripping have considerable importance. Nevertheless, Lyon has developed statistical approach to establish correlations between these tests (*26*).

UL94

Lyon et al. (*26*, *27*, *39*) have measured flammability data in PCFC and vertical UL94 ratings of 110 polymers, plastics and composites. Poor correlation could be drawn between HRC and UL94 rating: one material exhibits the highest rating in UL94 (V0) with a HRC as high as 800 J/g.K. On the contrary, some polymers with low or moderate HRC (200 J/g.K) could be non-rated (HB) in UL94. Despite that, the authors noticed that the changeover from HB to V0 ratings corresponds to critical HRC values ranging between 200 and 400 J/g.K.

The authors have also calculated a probability of burning without auto-extinguishing in UL94 versus the thermal combustion properties measured in PCFC (HRC, heat of combustion, pyrolysis temperature and residue which includes char but also inorganic filler and fibrous reinforcement) (*26*, *39*). Relatively good correlations are found between this probability of burning and HRC or heat of combustion. Correlations are poorer with residues and pyrolysis temperature.

Schartel et al. (*10*) have studied seventeen PC/ABS blends flame retarded with various additives, including organophosphorus compounds. Since these blends exhibit multiple-step decomposition, they considered sumHRC or avHRC rather than HRC. The changeover from HB to V0 rating occurs for sumHRC between 400 and 500 J/g.K and for avHRC between 175 and 250 J/g.K. Since the majority of the studied formulations exhibits results corresponding to these ranges, this illustrates quite well that PCFC is unable to predict UL94 ratings with high confidence.

Limiting Oxygen Index

Cogen et al. (*38*) have compared the performances of seven halogen-free flame retardant polyolefin compounds according to various tests. Despite correlations between PCFC and flame spread tests or cone calorimeter were noticed, no correlation was observed between PCFC and LOI.

Schartel et al. (*10*) have compared LOI and PCFC data for PC/ABS blends flame retarded with various additives (in particular phosphorus additives). LOI and THR are relatively well-correlated. Comparison with HRC or sumHRC could not be stated since HRC varied only slightly. But the authors showed a very poor correlation for a wide range of polymers. For a HRC close to 400 J/g.K, LOI could vary from 15 to 45 %. The same conclusion could be drawn from Lyon's data (*39*) about many polymers including halogen-containing polymers.

Some equations were proposed to calculate theoretically LOI using various parameters, including PCFC data (*10*, *39*, *55*). These equations highlight in which cases correlation between PCFC and LOI should fail or succeed. Lyon et al. (*39*) proposed the following equation to estimate LOI:

$$LOI = \frac{\dfrac{h_g \times HRR^*}{b \times \Delta T_p}}{HRC \times X \times \theta} + \frac{\sigma \times T_{max}^4}{b}$$

with h_g is the heat of gasification per unit initial mass of solid, HRR^* is the critical heat release rate for burning of a condensed phase with a diffusion flame in air (≈ 60 kW/m^2), b is a proportionality constant between the heat flux from flame to the surface and the volume fraction of oxygen, ΔTp is the pyrolysis temperature interval, $\chi.\theta$ is the burning efficiency, σ is the Boltzmann radiation constant and T_{max} is the pyrolysis temperature. The authors showed also the influence of thermal stability (T_{max}) and burning efficiency ($\chi.\theta$) on the LOI calculation. HRC, ΔT_p and T_{max} could be measured by PCFC but χ and θ could not be estimated using PCFC standard conditions. It leads to discrepancy between PCFC and LOI, exactly as previously discussed about the comparison between PCFC and the cone calorimeter. Schartel et al. (*10*) used the same equation but substituting $HRC.\Delta T_p$ by THR because they noticed that THR and LOI were well-correlated in the case of the studied PC/ABS blends.

Yang et al. (*56*) used a slightly modified equation:

$$LOI = OI + \frac{\sigma \times T_{max}^4}{b} + \frac{\dfrac{n_g \times HRR^*}{b \times X^2}}{HRC \times (1 - \mu)^2}$$

with OI is the minimum oxygen volume fraction for combustion of gaseous fuels at the lower flammability limit (≈ 13.5 %), η_g is the heat absorption capacity (= $L_g/\Delta T_p$ with L_g the heat of gasification) and μ is the char or inert fraction in PCFC. A good correlation was found between measured and calculated LOI for various fibres. Some of them were surface-treated with MDPA (N-methylol dimethylphosphonopropionamide). But in this equation χ was kept equal to 1 since all formulations were halogen-free. It would be interesting to check if this equation could be suitable for materials exhibiting various combustion efficiencies.

Flame Spread Tests for Wires

In their study, Cogen et al. have used two flame spread tests to evaluate the flame performance of some halogen-free polyolefin compounds in addition to the cone calorimeter, PCFC and LOI (*38*). In MS-8288 test, the wire is suspended horizontally while in SAE J1128, the wire is suspended at a 45° angle. Self-extinguishibility is required in both tests but the authors have also measured the experimental flame spread velocity. The seven studied formulations were ranked according to their performances for both tests and the authors looked for possible correlations with other tests. If both flame spread tests were well-correlated, low correlation coefficients were generally found with cone calorimeter, LOI and PCFC. Especially, highest correlation coefficients between PCFC and flame spread tests were lower than 0.8. It should be noticed that the authors used an equation to predict the flame spread velocity. This velocity depends on various parameters, including heat capacity, density, thickness and angle of inclination of sample but not on heat release rate or total heat release. Pyrolysis temperature was also taken into account since the pHRR temperature in PCFC is the only parameter measured which correlated moderately with both flame spread tests (correlation coefficient is -0.75).

Conclusions and Propositions of Future Work

PCFC is now an essential tool in the field of research about the flame retardancy of polymers. It is an attractive technique to understand the fire behavior of a material since the test conditions could vary to a large extent: anaerobic versus aerobic pyrolysis, heating rate from 0.5 to 4 K/s, monitored oxygen rate and temperature in the combustion chamber. In addition, it appears to be very complementary to TGA. Moreover, it has been shown that the lack of correlation between PCFC and other methods (particularly the cone calorimeter) could be exploited to identify the mode-of-action of flame retardants.

However, up to now, PCFC has been used in standard conditions in most cases. Almost no studies were carried out using aerobic pyrolysis or incomplete combustion. Moreover, few studies have combined PCFC and TGA to obtain more flammability characteristics, such as effective heat of combustion (EHC).

Moreover, some issues are still remaining about the meaning of PCFC flammability data and the correlations between PCFC and other tests. These issues are briefly summarized now:

1 − Correlations between HRC in PCFC and pHRR in cone calorimeter are not systematic but could be obtained for a limited range of materials. But when formulations exhibit multiple decomposition steps, HRC is not suitable. It could be substituted by avgHRC or sumHRC but the practical interest of these parameters for correlations is not well established. Such formulations show several peaks at different pyrolysis temperatures, with various pHRR, THR, EHC and combustion efficiency profiles. How do the PCFC data of these formulations correlate with cone calorimeter results?

2 − Up to now, heating rate in PCFC is constant and ranged between 0.5 and almost 4 K/s. In cone calorimeter and other tests, heating rate is neither controlled, nor homogeneous and could change during the test. To the best of our knowledge, no study has been reported where the heating rate was modified during the PCFC analysis. Similarly, isothermal analysis has not been carried out. Hence, modifying the heating rate in PCFC to be closer to the actual conditions existing in other tests could be an interesting approach.

3 − We have shown that PCFC is not available for heterogeneous materials (for example multilayer composites). But PCFC analysis could be separately carried out on each layer. How do these analyses help rebuilding the fire behavior of the whole material?

4 − Incomplete combustion could be done in PCFC and some correlations with cone calorimeter test were found. Moreover FTIR-PCFC coupling has been recently carried out to identify the gases after pyrolysis and combustion. Comparing FTIR-PCFC and FTIR-TGA couplings should allow a better understanding of the combustion process. FTIR-TGA allows identifying the gases released during the pyrolysis since FTIR-PCFC should define that these gases become under determined combustion conditions.

5 − Similarly, comparing FTIR-PCFC and FTIR-cone calorimeter couplings should help specifying the combustion process in the cone calorimeter.

6 − Flame inhibition could be studied by measuring the burning velocity of fuels premixed with air in presence of an inhibitor (*56*). In PCFC, combustion is allowed when O_2 is introduced into the combustor and flame poisoning could happen if a flame inhibitor is incorporated into the material. But, another way to study the flame inhibition in PCFC could be possible if oxygen with a given concentration of a flame inhibitor was introduced into the combustor. The advantage of this method would be that the flame inhibitor could not modify the pyrolysis but only the combustion process.

References

1. Lyon, R. E.; Walters, R. N. *J. Anal. Appl. Pyrolysis* **2004**, *71*, 27–46.
2. Huggett, C. *Fire Mater.* **1980**, *4*, 61–65.
3. Tai, Q.; Chen, L.; Song, L.; Nie, S.; Hu, Y.; Yuen, R. K. K. *Polym. Degrad. Stab.* **2010**, *95*, 830–836.
4. Tai, Q.; Song, L.; Hu, Y.; Yuen, R. K. K.; Feng, H.; Tao, Y. *Mater. Chem. Phy.* **2012**, *134*, 163–169.
5. Xu, W.; Lu, B.; Hu, Y.; Song, L.; Nie, S. *Polym. Adv. Technol.* **2012**, *23*, 877–883.
6. Kunkel, B. M.; Peoples, B. C.; Yung, C. M.; Scott, S. L. *Macromol. Mater. Eng.* **2011**, *296*, 1075–1080.
7. Yang, C. Q.; He, Q. *Fire Mater.* **2012**, *36*, 127–137.
8. Ghosh, A.; Banerjee, S.; Wang, D-Y.; Komber, H.; Voit, B. *J. Appl. Polym. Sci.* **2012**, *123*, 2959–2967.
9. Jinping, G.; Guoqiang, C. *Fire Mater.* **2010**, *34*, 261–270.

10. Schartel, B.; Pawlowski, K. H.; Lyon, R. E. *Thermochim. Acta* **2007**, *462*, 1–14.
11. Braun, U.; Bahr, H.; Sturm, H.; Schartel, B. *Polymers for Advanced Technologies* **2008**, *19*, 680–692.
12. Ferry, L.; Sonnier, R.; Lopez-Cuesta, J.-M. *Polym. Degrad. Stab.*, submitted for publication.
13. Schartel, B.; Weib, A. *Fire Mater.* **2010**, *34*, 217–235.
14. Hergenrother, P. M.; Thompson, C. M.; Smith, J. G., Jr; Connell, J. W.; Hinkley, J. A.; Lyon, R. E.; Moulton, R. *Polymer* **2005**, *46*, 5012–5024.
15. Sonnier, R.; Otazaghine, B.; Ferry, L.; Lopez-Cuesta, J.-M. *23rd Annual Recent Advances in Flame Retardancy of Polymeric Materials* **2012** Stamford.
16. Dumitrascu, A.; Howell, B. A. *Polym. Degrad. Stab.* **2011**, *96*, 342–349.
17. A.R. Tripathy, A. R.; R.J. Farris, R. J.; W.J. Knight, W. J. *Polym. Eng. Sci.* **2007**, *47*, 1536–1543.
18. Sablong, R.; Duchateau, R.; Koning, C. E.; Pospiech, D.; Korwitz, A.; Komber, H.; Starke, S.; Haubler, L.; Jehnichen, D.; Auf der Landwehr, M. *Polym. Degrad. Stab.* **2011**, *96*, 334–341.
19. Ghosh, A.; Bera, D.; Wang, D-Y.; Komber, H.; Mohanty, A. K.; Banerjee, S.; Voit, B. *Macromol. Mater. Eng.* **2012**, *297*, 145–154.
20. Ryu, B-Y.; Emrick, T. *Angew. Chem., Int. Ed.* **2010**, *49*, 9644–9647.
21. Ranganathan, T.; Ku, B.-C.; Zilberman, J.; Beaulieu, M.; Farris, R. J.; Coughlin, E. B.; Emrick, T. *J. Polym. Sci., Part A: Polym. Chem.* **2007**, *45*, 4573–4580.
22. Negrell-Guirao, C.; Boutevin, B.; David, G.; Fruchier, A.; Sonnier, R.; Lopez-Cuesta, J.-M. *Polym. Chem.* **2011**, *2*, 236–243.
23. Lyon, R. E.; Speitel, L.; Walters, R. N.; Crowley, S. *Fire Mater.* **2003**, *27*, 195–208.
24. Lyon, R. E.; Walters, R. N.; Gandhi, S. *Fire Mater.* **2006**, *30*, 89–106.
25. Walters, R. N.; Lyon, R. E. *Fire Mater.* **2003**, *27*, 183–194.
26. Lyon, R. E.; Takemori, M. T.; Safronava, N.; Stoliarov, S. I.; Walters, R. N. *Polymer* **2009**, *50*, 2608–2617.
27. Walters, R. N.; Lyon, R. E. *J. Appl. Polym. Sci.* **2003**, *87*, 548–563.
28. Walters, R. N. *Fire Mater.* **2002**, *26*, 131–145.
29. Sonnier, R.; Negrell-Guirao, C.; Vahabi, H.; Otazaghine, B.; David, G.; Lopez-Cuesta, J.-M. *Polymer* **2012**, *53*, 1258–1266.
30. Vahabi, H.; Ferry, L.; Longuet, C.; Sonnier, R.; Negrell-Guirao, C.; David, G.; Lopez-Cuesta, J.-M. *Eur. Polym. J.* **2012**, *48*, 604–612.
31. Vahabi, H.; Longuet, C.; Ferry, L.; David, G.; Robin, J-J.; Lopez-Cuesta, J.-M. *Polym. Int.* **2012**, *61*, 129–134.
32. Lu, H.; Wilkie, C. A. *Polym. Adv. Technol.* **2011**, *22*, 14–21.
33. Tai, Q.; Chen, L.; Song, L.; Hu, Y.; Yuen, R. K. K. *Polym. Compos.* **2011**, *32*, 168–176.
34. Kramer, R. H.; Zammarano, M.; Linteris, G. T.; Gedde, U. W.; Gilman, J. W. *Polym. Degrad. Stab.* **2010**, *95*, 1115–1122.
35. Costache, M. C.; Wilkie, C. A. *Polym. Adv. Technol.* **2010**, *21*, 506–511.
36. Lyon, R. E.; Quintiere, J. G. *Combust. Flame* **2007**, *151*, 551–559.

37. Lu, H.; Wilkie, C. A. *Polym. Degrad. Stab.* **2010**, *95*, 564–571.
38. Cogen, J. M.; Lin, T. S.; Lyon, R. E. *Fire Mater.* **2009**, *33*, 33–50.
39. Lyon, R. E.; Walters, R. N.; Stoliarov, S. I. *Polym. Eng. Sci.* **2007**, *47*, 1501–1510.
40. Nakamura, R.; Netravali, A. N.; Morgan, A. B.; Nyden, M. R.; Gilman, J. W. *Fire Mater.* DOI:10.1002/fam.2113.
41. Hapuarachchi, T. D.; Bilotti, E.; Reynolds, C. T.; Peijs, T. *Fire Mater.* **2011**, *35*, 157–169.
42. Chen, X.; Jiao, C.; Zhang, J. *Polym. Eng. Sci.* **2012**, *52*, 414–419.
43. Gerard, C.; Fontaine, G.; Bourbigot, S. *Polym. Adv. Technol.* **2011**, *22*, 1085–1090.
44. Sonnier, R.; Viretto, A.; Taguet, A.; Lopez-Cuesta, J.-M. *J. Appl. Polym. Sci.* **2012**, *125*, 3148–3158.
45. Sonnier, R.; Ferry, L.; Longuet, C.; Laoutid, F.; Friederich, B.; Laachachi, A.; Lopez-Cuesta, J.-M. *Polym. Adv. Technol.* **2011**, *22*, 1091–1099.
46. Morgan, A. B.; Galaska, M. *Polym. Adv. Technol.* **2008**, *19*, 530–546.
47. Tibiletti, L.; Longuet, C.; Ferry, L.; Coutelen, P.; Mas, A.; Robin, J-J.; Lopez-Cuesta, J.-M. *Polym. Degrad. Stab.* **2011**, *96*, 67–75.
48. Friederich, B.; Laachachi, A.; Sonnier, R.; Ferriol, M.; Cochez, M.; Toniazzo, V.; Ruch, D. *Polym. Adv. Technol.* DOI:10.1002/pat.2056.
49. Quach, Y.; Cinausero, N.; Sonnier, R.; Longuet, C.; Lopez-Cuesta, J.-M. *Fire Mater.* DOI:10.1002/fam.1119.
50. Chen, L.; Song, L.; Lv, P.; Jie, G.; Tai, Q.; Xing, W.; Hu, Y. *Progr. Org. Coat.* **2011**, *70*, 59–66.
51. Cheng, X.; Yang, C. Q. *Fire Mater.* **2009**, *33*, 365–375.
52. Patel, P.; Hull, T. R.; Stec, A. A.; Lyon, R. E. *Polym. Adv. Technol.* **2011**, *22*, 1100–1107.
53. Stoliarov, S. I.; Safronava, N.; Lyon, R. E. *Fire Mater.* **2009**, *33*, 257–271.
54. Oztekin, E.; Crowley, S. B.; Lyon, R. E.; Stoliarov, S. I.; Patel, P.; Hull, T. R. *Combust. Flame* **2012**, *159*, 1720–1731.
55. Yang, C. Q.; He, Q.; Lyon, R. E.; Hu, Y. *Polym. Degrad. Stab.* **2010**, *95*, 108–115.
56. Noto, T.; Babushok, V.; Hamins, A.; Tsang, W. *Combust. Flame* **1998**, *112*, 147–160.

Chapter 25

Thermal Stability and Fire Retardancy of Polypropylene/Sepiolite Composite

W. C. Cao,[a] L. J. Wang,*,[a] X. L. Xie,[b] and C. A. Wilkie[c]

[a]College of Materials Science and Engineering, Guilin University of Technology, Guilin 541004, People's Republic of China
[b]College of Chemical and Biological Engineering, Guilin University of Technology, Guilin 541004, People's Republic of China
[c]Department of Chemistry and Fire Retardant Research Facility, Marquette University, P.O. Box 1881, Milwaukee, Wisconsin 53201
***E-mail: wlj@glite.edu.cn**

Polypropylene/sepiolite and PP/organo-sepiolite composites were prepared via melt extrusion, sepiolite was pre-modified with cetyltrimethyl ammonium bromide (CTAB). X-ray diffraction, transmission electron microscopy were used to characterize the morpohlogy of composites. Thermal stability and flame retardancy of the composites were evaluated by thermogravimetric analysis(TGA), cone calorimetric analysis, limiting oxygen index(LOI) and the UL94 protocol. The peak heat release rate of PP/sepiolite and PP/organo-sepiolite composites, with 10% sepiolite loading, decreased by 54% and 66%, respectively. The other fire retardancy also improved by addition of sepiolite, fire performance index (FPI) of PP/sepiolite composite and PP/sepiolite composite increased by 41.7% from 0.014sm^2/kW of PP to 0.024 sm^2/kW, and that of PP/organo-sepiolite composite increased by 150% reached 0.035 sm^2/kW. The smoke production rate (SPR) of PP/organo-sepiolite composite decreased by 40% , from 0.117m^2/s of PP to 0.07m^2/s of composite, while mass loss rate (MLR) decreased by 41%, from 0.45g/s of PP to 0.20g/s of composite. The limiting oxygen index of composite increased

In Fire and Polymers VI: New Advances in Flame Retardant Chemistry and Science; Morgan, A., et al.;
ACS Symposium Series; American Chemical Society: Washington, DC, 2012.

by 3, from 17.1(in PP) to 20.1. All of the composites could obtain an HB in the UL-94 horizontal burning test (UL-94HB) grade but were not classified in the vertical burning test (UL-94VB).

Keywords: Sepiolite; polypropylene; composite; fire retardancy

Introduction

Flammability is a major concern for polymeric materials. Because the important industrial applications of polymeric materials are restricted due to inherent high flammability, reducing the flammability of polymeric materials is a major and challenging task. Polypropylene (PP) is an important commodity plastic used extensively in many fields, such as housing, transportation, and electrical engineering materials, but its usage is often limited because of its poor flame retardancy (the limiting oxygen index (LOI) is often lower than 18%). Therefore, studies on flame-retardant PP have attracted considerable interest during the last decades (*1–3*).

Many flame retardant have been developed for PP in the last three decades. Early fire retardants were halogen-based, such as polybrominated biphenyls (PBB) and polybrominated diphenyl ethers (PBDE), which are very efficient and easy to use. However, interference with flame reactions inhibiting hydrocarbon oxidation and the conversion of CO to CO_2 results in very smoky, highly toxic fire effluents. In addition, halogen flame retardants have been shown to leach out of polymers into the natural environment, where their presence is now ubiquitous, and some are proven endocrine disruptors (*4*). European Union (EU) directive on the “Reduction of certain hazardous substances in electrical and electronic equipment” (RoHS, 2002/95/EC) prohibited the use of PBB and PBDE. These problems have driven the search for alternative “halogen free” fire retardants, which include metal hydroxide, carbonate fillers, phosphorus compounds and clays (*5–7*).

In general, halogen-free fire retardants are much more polymer-specific and less efficient than halogen based flame retardants, requiring higher loadings (up to 70% by weight) in order to meet required flammability standards. Flame retardants with very small particle size have been of great interest. Nanometer size fire retardants have been thought to have essential advantages over flame retardants with larger particle size in terms of efficiency. In these systems, concurrent improvements across multiple properties are typically achieved, such as improved barrier, flammability, and biodegradability behavior, compared to the unfilled polymer (*8*).

Polymer/clay nanocomposites have attracted wide interest in recent years for exhibiting improved mechanical, thermal, barrier, optical properties and fire retardancy. A great fraction of published data on polymer/clay nanocomposites focused on lamellar layered silicates, especially on the intercalation and exfoliation of montmorillonite and layered double hydroxides (*9*, *10*), whereas polymer/ sepiolite (nano)composites have not been studied to great extent.

Sepiolite, which belongs to the structural family of phyllosilicates, is a hydrated magnesium silicate clay with $Si_{12}Mg_8O_{30}(OH,-F)_4(OH_2)_4{\cdot}8H_2O$ as the theoretical half-unit-cell formula. This clay mineral has a nanometer-size tunnel structure and exhibits microfibrous morphology. The particular structure provides a high specific surface area (> 300 m^2g^{-1}) and porous volume (~0.4 cm^3 g^{-1}). Due to its specific structure, sepiolite can be easily modified. The modification can enhance the interaction between the polymer matrix and therefore sepiolite can improve the properties of polymers (*11*, *12*).

The objective of this paper is to prepare polypropylene/sepiolite composites via melt extrusion with CTAB modified sepiolite as an additive, and study the fire retardancy of sepiolite/PP (nano)composites using thermogravimetric analysis, limiting oxygen index, UL-94 and cone calorimetrcy.

Materials and Experimental

Materials

Polypropylene (PP, homopolymer, HD 120 MO) was supplied by China National Petroleum Co., Ltd., Maleic anhydride grafted polypropylene (MAH-g-PP, Exxelor PO1020) was supplied by Huadu Technology Co., Ltd. Nanjing. Sepiolite was provided by Xixia Wanli sepiolite Factory (China). Cetyltrimethyl ammonium bromide (CTAB) was purchased from Sinopharm Chemical Reagent (China).

Modification of Sepiolite

To improve the dispersion of sepiolites in PP, it is nessary to enhance the compatibility of sepiolites with PP. According to the structural characteristics of polypropylene, CTAB is an appropriate material used to modify sepiolite to enhance the compatibility of the interface between inorganic additive and organic matrix.

The typical method is as follows: 25g sepiolite and 240mL deionized water were mixed in a 500mL three-neck flask. 150mL of 1.2mol/L HCl was added dropwise into the flask with vigorous stirring for 6h at 75 °C and then centrifuged. The material was washed several times with deionized water. The resulting slurry was dried at 105 °C overnight and sieved to obtain a 200-mesh acidic-sepiolite. 12g acidic-sepiolite was mixed with 180mL deionized water in one-neck flask, 5.7mL of 10 wt% CTAB solution was added to the suspension. The mixture was vigorous stirred for 12h at 75 °C, then centrifuged and washed several times with deionized water, then dried overnight in a vacuum oven.

Preparation of PP/Sepiolite Composite

The (nano)composites were prepared by extrusion molding in a tightly intermeshing co-rotating twin screw extruder (TS-20,Nanjing rubber & plastic machinery co., Ltd) with screw diameter of 27mm and L/D ratio of 36. A masterbatch was fabricated by melting maleic anhydride grafted polypropylene (MAH-g-PP) and sepiolite. Then the masterbatch was melt mixed with pure PP. The temperature in the extruder barrel was 200 °C at the feed region and 225 °C at the die section; the screw speed was 12 rev/min; the feed rate was 5 kg/h. The formulations are shown in Table 1.

Table 1. Formulation of composites

Samples	*Pure PP (g)*	*MAH-g-PP (g)*	*Sepiolite (g)*	*Organo-sepiolite (g)*
PP	97	3	0	0
PP/3% sepiolite	94	3	3	0
PP/5% sepiolite	92	3	5	0
PP/10% sepiolite	87	3	10	0
PP/3% organo-sepiolite	94	3	0	3
PP/5% organo-sepiolite	92	3	0	5
PP/10% organo-sepiolite	87	3	0	10

Characterization

XRD experiments were performed on a PANalytical X'pert PRO powder diffractometer with Cu K_α generator (l5.5405Å) at 40 kV and 40 mA. Scans were taken at $2\theta=5°$to 80°at 2°/min. Polymer composite samples were pressed into $20\times15\times1mm^3$ thickness plaques by compression molding. Every sample was tested five times at different positions. FT-IR spectroscopic analyses were carried out on a NICOLET 470 Fourier transform infrared spectrometer using the KBr method. Spectra were recorded between 400 and 4000 cm^{-1} at a resolution of 4 cm^{-1}. The TEM imaging was carried out using a transmission electron microscope JEM-2100 with an accelerating voltage of 75 kV. The samples were ultramicrotomed with a glass knife on an AO-E microtome at room temperature to give sections of ~90 nm in thickness. The sections were transferred from the knife-edge to Cu grids.

Bending test was carried out on an AG-201 machine at room temperature according to Chinese National Standard GB/T 1040-1992. The specimens were $100\times4\times1.5mm^3$ in size and the crosshead speed was set at 50 mm/min. A minimum of five specimens were tested for each data point and the averages were reported. Thermogravimetric analysis data were obtained on a NETZSCH STA-449 thermal analysis instrument at 12-16mg scale under N_2 atmosphere; all TGA samples were run in duplicate and the average values were reported. The thermal degradation measurements were carried out at a heating rate of 10 °C /min at a temperature ranging from room temperature to 600 °C. The UL94 protocol was performed on a DMS Horizontal-Vertial flame chamber testing instrument. Sample size is length of 130±5mm, width of 13±0.5mm, thickness of 1.0±0.1mm, angular radius <1.3mm, smooth edges. Cone calorimetry was performed according to ASTM E 1354 at an incident flux of 35 kW/m^2 using a cone shaped heater, exhaust flow was set at 24 L/s; all samples were burned in triplicate. Cone samples (about 30 g) were prepared by compression molding into $100\times100\times$ $3mm^3$ square plaques.

Results and Discussion

Modification of Sepiolite

The X-ray diffraction patterns of sepiolite and the modified samples are shown in Fig.1. The peak at $2\theta = 7.3°$ corresponds to the (110) diffraction of sepiolite. The pristine sepiolite sample contained impurity of calcite ($2\theta = 29.44°$, 47.53°, 48.54°). X-ray diffraction analysis, together with the chemical analysis of pristine sepiolite sample (31.2% SiO_2, 12.6% MgO, 9.15% CaO, 33.68% $CaCO_3$ and loss of ignition 13.37%) indicate that sepiolite and calcite are the major components.

The basal spaces of pristine sepiolite and organo-sepiolite are observed at 1.19 and 1.23nm, respectively. The change in the basal spacing is only 0.04nm. This minimal expansion suggests that CTBA cations attach to the edges of sepiolite. The layers of sepiolite are linked by covalent bonds, but the layers of LDH and MMT are linked by Van der Waals force. The main influence of long-chain organic cations is surface modification or replacing the edge Si–OH groups of sepiolite (*13*).

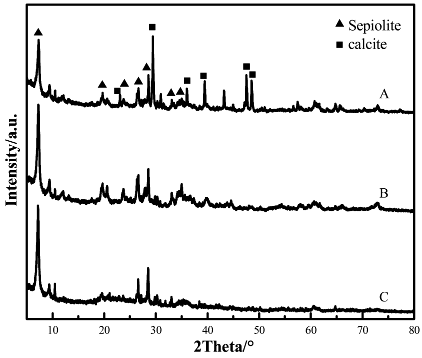

Figure 1. X-ray diffraction patterns of pristine sepiolite (A), acidic sepiolite (B) and organo-sepiolite (C).

This conclusion could be further proved using FT-IR of organo-modified sepiolite (Fig. 2). The FT-IR spectrum shows the characteristic absorption peaks at 2932 and 2857cm^{-1}, assigned to the –CH– and –CH_2– stretching vibrations in CTAB molecules. It assumed that the Si–OH groups of sepiolite surface have reacted with CTAB. The reduced absorption –OH band intensity indicates that the sepiolite surface structure is altered and the Si-OH group on the sepiolite surface decreases.

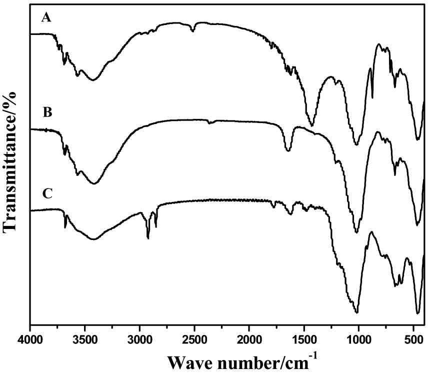

Figure 2. FT-IR spectrum of primitive sepiolite (A), acidic sepiolite (B), organo-sepiolite (C).

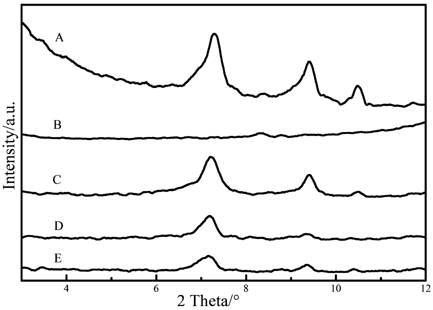

Figure 3. XRD patterns of PP and its composites (A: organo-sepiolite;B: PP;C: PP/10% organo-sepiolite;D: PP/5% organo-sepiolite;E: PP/3% organo-sepiolite).

Morphology of (Nano)composite

The XRD patterns of organic sepiolite and PP/sepiolite composites are shown in Fig.3. For the PP/organo-sepiolite composite, there was almost no change in the basal spacing of sepiolite compared with that of organo-sepiolite, but the relatively intensity of the diffraction peak of sepiolite increased as the loading of the organo–sepiolite increased, which is an indication of agglomeration of some sepiolite fibers. The modified sepiolite disperses in PP better than does the unmodified sepiolite (not shown here). Due to the typical feature of the zeolitic pores and impurities inside the sepiolite fibers, XRD analysis can be used only to discuss possible changes in the polymer structure and not the extent of dispersion of the filler, which was different from what is generally observed with layered phyllosilicates. XRD alone cannot completely describe the morphology of these additives in polymer matrices.

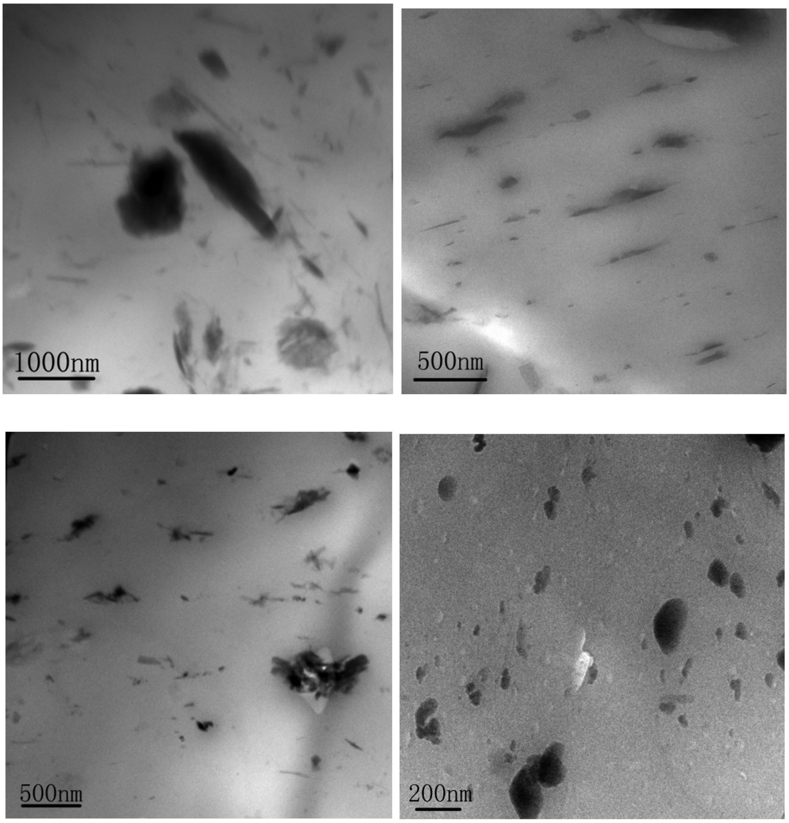

Figure 4. The TEM images of PP/sepiolite (up) and PP/organo-sepiolite (down)at low (left) and high (right) magnification.

The morphology of the composites was further accessed by TEM. A lower magnification image are used to determine the global dispersion of the layered clays in the polymer, while the higher magnification images evaluate the registry of the layers in more detail on the nanometer scale. The TEM images can provide some direct evidence for the formation of (nano)composites. Fig. 4 shows the TEM images of PP (nano)composites with 5% sepiolite and organo-sepiolite loading. Compared with pristine sepiolite, the diameter of organo-sepiolite shows an obvious change, and the surface of organo-sepiolite is no longer smooth. The TEM results indicate that the reaction of organo-sepiolite fibers with MA group of maleic anhydride grafted PP. The reaction improves the compatibility of sepiolite and PP matrix, and therefore the clay disperses more homogeneously in the PP matrix. The organo-sepiolite tactoids, typical sizes 10 - 60nm with very few larger ones (in the range of 100-250nm), are much smaller than the tactoids of the sepiolite in the PP matrix (typically 80 - 160nm). Several long clay layers of mainly tactoids appear in PP/sepiolite but do not appear in PP/organo-sepiolite composites, which suggests that the structure of the clay layers in the modified sepiolites is changed.

Mechanical Properties

The mechanical properties of PP and its composites with different loading of sepiolite are listed in table 2. Compared with PP, the addition of sepiolite and organo-sepiolite increase the bending strength and the elastic modulus of composites. As organo-sepiolite increased from 3, 5 to 10%, the bending strength increased from 69.9MPa, 71.22MPa to 74.94MPa, and the elastic modulus increased from 2562MPa, 3990MPa to 3120MPa. These values are much higher than these of PP/APP-MMT composites (less than 1000MPa for elastic modulus) (*14*) The improvement of bending strength and the elastic modulus may be due to the physical crosslinking of sepiolite, especially organic sepiolite with PP.

Table 2. Mechanical properties of PP and its composites

Samples	*Bending strength (MPa)*	*Elastic modulus (Mpa)*
PP	65.54±2.0	2370±120
PP/3% sepolite	70.07±3.0	2750±135
PP/5% sepolite	69.94±3.05	2675±140
PP/10% sepolite	72.17±3.2	2970±148
PP/3% organo-sepolite	69.90±2.4	2565±128
PP/5% organo-sepolite	71.22±2.8	2990±146
PP/10% organo-sepolite	74.94±3.5	3120±150

Dynamic Mechanical Analysis

Dynamic mechanical analysis is very sensitive to molecular motion, and has been widely used in plastic composite systems to investigate polymer chain dynamics. The loss modulus of PP and its composites are given in Fig. 5.

Compared with pristine PP, the curves of composites become flatter and the peak is less pronounced. At 10% loading, the loss modulus peak shows more relaxation and the peak value increased. This implies that the addition of sepiolite spreads the glass transition temperature (T_g) of composite into a relatively wide range.

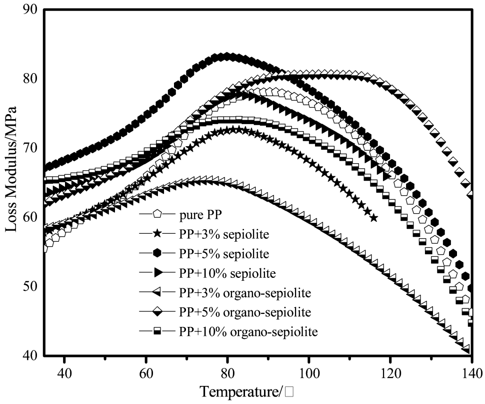

Figure 5. Loss modulus of the PP and its composites.

Thermal Stability and Flame Retardancy of Composites Thermal Stability Analysis

TGA curves of pristine PP and PP/sepiolite composites under nitrogen are shown in Fig. 6, and the detailed data are summarized in table 3. It is apparent that thermal decomposition temperature for PP/sepiolite composites shifts to higher temperature compared to pristine PP, which indicates an improvement in thermal stability. The temperatures corresponding to 10 and 50 wt% weight loss ($T_{0.1}$ and $T_{0.5}$) are used to evaluate the decomposition of PP. The major weight loss range of PP composites is 400-470℃, while that of PP is 350-470℃.

When 50% weight loss was selected as the point of comparison, the thermal decomposition temperatures for the pure sepiolite, 3% , 5% and 10% PP/organo-sepiolite samples increases by 8 to 15 °C. The onset temperature of degradation ($T_{0.1}$) increases by 16-20 °C. The fraction of non-volatile residue can be attributed to the sepiolite with perhaps a small amount of organic residue. A black sticky substance can be seen in the residue, which may indicate the presence of some carbonaceous material. The sepiolite function as a mass transport barrier to the volatile materials generated during decomposition and this role increases with dispersion of sepiolite.

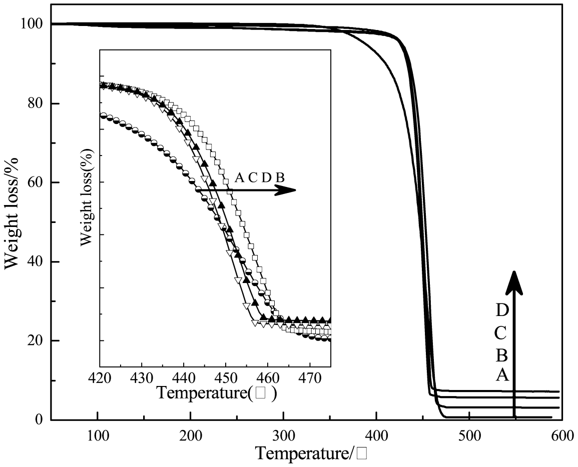

Figure 6. TGA curves of PP and its organic composites (A: PP;B: PP/3% organo-sepiolite;C: PP/5% organo-sepiolite;D: PP/10% organo-sepiolite).

Table 3. TGA summary results for PP and its organic composites

Formulation	$T_{0.1}$(℃)	$T_{0.5}$(℃)	*Char(%)*
PP	410	447	0.6
PP/3% organo-sepolite	436	462	3.2
PP/5% organo -sepolite	433	455	5.7
PP/10% organo -sepolite	434	458	7.3

LOI and UL94 Testing

Table 4 presents the LOI values of PP and PP/sepiolite composites. For both PP/sepiolite and PP/organo-sepiolite systems, the LOI values increase as the amount of additive increases but the difference between sepiolite and organo-sepiolite is not significant. The UL94 results on PP and its composites are listed in table 5. All the samples could obtain a UL94HB rating whereas all are unclassified according to the vertical burning protocol.

Table 4. LOI value of PP and its composites

Sample	*LOI value*	*Δ (%)*
PP	17.1	0
PP/3% sepolite	18.2	1.1
PP/5% sepolite	18.6	1.5
PP/10% sepolite	19.5	2.4
PP/3% organo-sepolite	18.5	1.4
PP/5% organo-sepolite	19.2	2.1
PP/10% organo-sepolite	20.1	3.0

Table 5. The results of UL94HB test of PP and its composites

sample	*UL94HB*			
	T_1(s)	*T_2(s)*	*Burning rate(mm/min)*	*Achieve or not*
PP/3% sepolite	30	192	31.2	Yes
PP/5% sepolite	33	208	28.8	Yes
PP/10% sepolite	35	217	27.5	Yes
PP/3% organo-sepolite	36	204	29.4	Yes
PP/5% organo-sepolite	42	212	28.2	Yes
PP/10% organo-sepolite	49	217	27.6	Yes

T_1 (s): the time of burning to 25 mm, T_2 (s): the time of burning to 100 mm.

Cone Calorimetric Characterization

Cone calorimeter is one of the most effective measures for researching fire retardancy at the bench-scale, which follows a well-defined fire scenario for a comprehensive fire performance (*15*, *16*). The results can be used to assess the fire properties of specific materials (*17*, *18*), setting it apart from many of the established fire tests intended to monitor the fire reaction of the samples. The data offered by cone calorimeter include the heat release rate (HRR), peak heat release rate (PHRR), average mass loss rate (AMLR), total heat release (THR), smoke production rate (SPR), and fire performance index (FPI). Much attention has been given to PHRR, which is due to concomitant changes in the mass loss rate (*19*). The reduction in the mass loss rate is attributed to the formation of a barrier which prevents mass transfer and thermally insulates the underlying polymer from the heat source (*20*). PHRR is considered one of the most important parameters in assessing the potential fire behavior (*21–24*).

The heat release rate plots of PP an PP/sepiolite composites, obtained at a heat flux of 35kW m^{-2}, are shown in Fig. 7 and table 6. It is routinely observed for composites that the time to ignition was a little shorter than that for the virgin polymer and this is also found with sepiolite and organo-sepiolite and the time of combustion is extended which is also normal for polymer-clay nanocomposites.

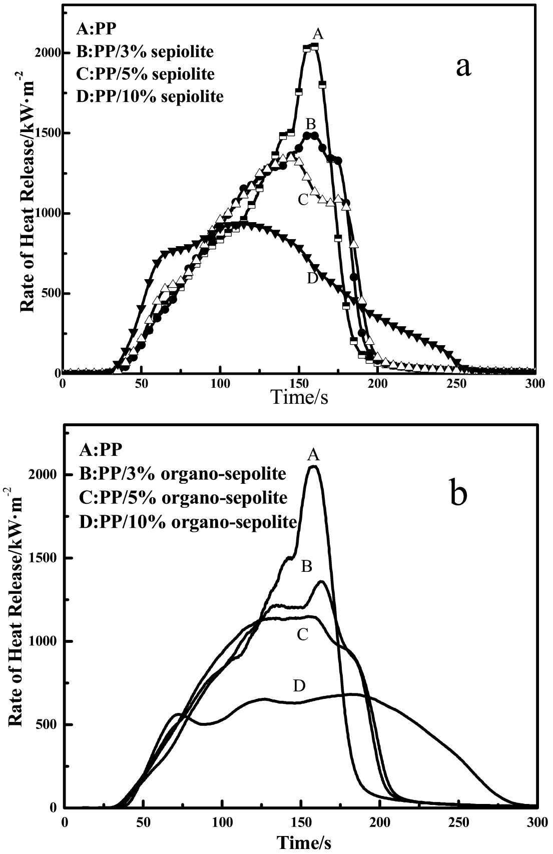

Figure 7. HRR curves of PP, PP/sepolite (a) and PP/organo-sepiolite (b) composites.

A very sharp HRR curve appears for PP with a peak heat release rate (PHRR) of 2086 kW/m^2; for pristine sepiolite, reductions in the PHRR up to 54% are observed (Fig.7a). For PP/organo-sepiolite composites the reductions are a little larger (Fig.7b). These reductions are significantly larger than what is seen with organically-modified MMT (*25*). The total heat released (THR) of PP/sepiolite and PP/organo-sepiolite decreased from 90MJ/m^3 for PP to one-half, or less than this value with samples containing 10% or either sepiolite or organically-modified sepiolite. This is very surprising as with MMT the entire sample burns and the THR is quite constant (*26*). The change in the mass loss rate suggests that not all of the sample burns, which is in accord with the TGA results.

Table 6. Cone calorimetric data of PP and its composites

Formulation	*PHRR (KW/m^2)*	*Reduction (%)*	*THR (mJ/ m^2)*	*MLR (g/s)*	t_{ig} *(s)*	t_{PHRR} *(s)*	*SPR (m^2/s)*
PP	2086	NA	90	0.45	30	142	0.117
PP/3% sepolite	1534	26	90	0.40	26	159	0.099
PP/5% sepolite	1401	32	78	0.37	19	103	0.087
PP/10% sepolite	957	54	44	0.28	23	145	0.075
PP/3% organo-sepolite	1368	34	47	0.39	24	154	0.090
PP/5% organo-sepolite	1193	42	43	0.27	25	149	0.081
PP/10% organo-sepolite	692	66	36	0.20	24	150	0.070

The error is between 30 to 95 KW/m^2 for PHRR, 1 to 5 mJ/m^2 for THR, 0.01 to 0.05g/s for MLR, 4 to 7s for t_{ig}, 8 to 15s for t_{PHRR} and 0.005 to 0.01m^2/s for SPR.

Fire performance index (FPI), the ratio of TTI/PHRR, is independent of the tested sample thickness and often used to predict how the flame may spread after ignition (*20*). Therefore, the greater the FPI value, the better the fire resistance. The FPI of PP/organo-sepiolite composite was 0.035sm^2/kW, which is twice that of pristine PP (0.014sm^2/ kW) and also higher than that of PP/sepiolite composite (0.024sm^2/kW).

The mass loss rate (MLR) curves of PP/sepiolite and PP/organo-sepioite composites are shown in Fig. 8. Quite similar trends for both HRR and MLR curves are seen. The MLR of pristine PP is 0.45g/s, and decreases from 0.4g/s to 0.37g/s and 0.28g/s as the loading of sepiolite increases from 3% to 5 and 10%. For the PP/organo-sepiolite composite , the change is even greater, which is accord with the change in the PHRR. The smoke production rate (SPR) is recognized as another important focus in the halogen-free flame retardant system. The SPR curves of PP/sepiolite and PP/organo-sepioite composite are shown in Fig. 9. The SPR again decreases as the amount of either sepiolite or organo-sepiolite increase; once again, the organo-sepiolite shows the best performance. Taking all of these cone calorimetric results together, sepiolite, and especially organo-sepiolite, offers very good fire performance in PP.

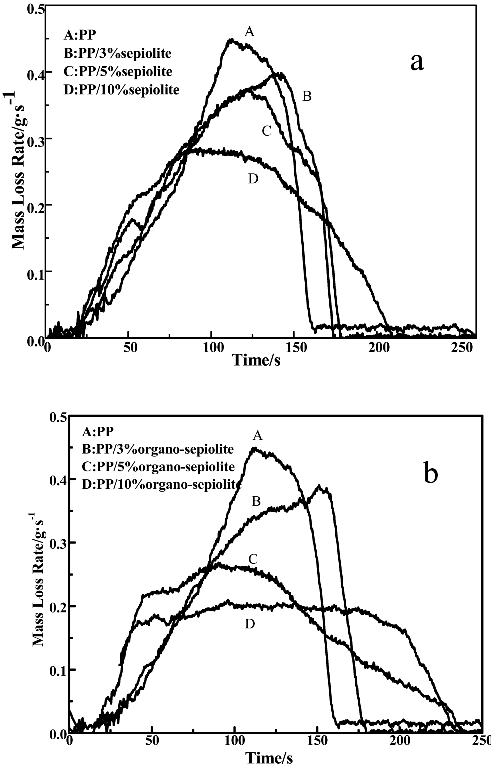

Figure 8. Mass loss rate curves of PP/sepiolite (a) and PP/organo-sepiolite (b) composites.

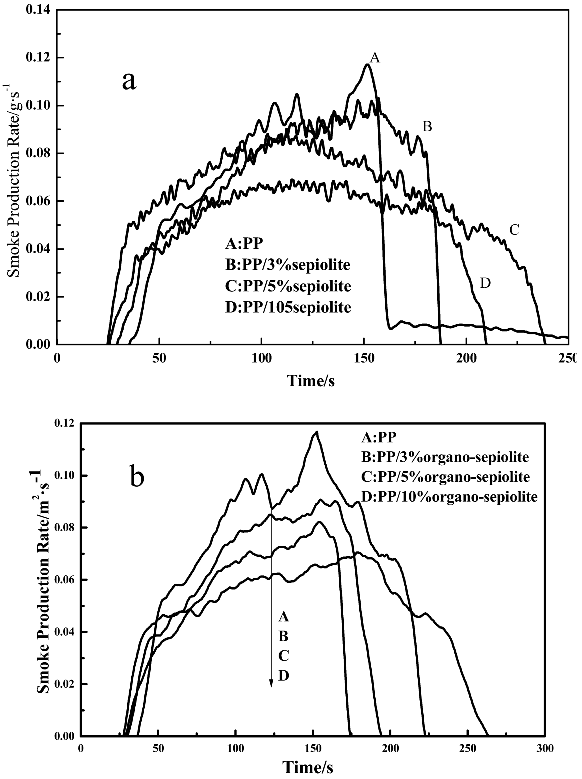

Figure 9. Smoke production rate curves of PP/sepiolite (a) and PP/organo-sepiolite (b) composites.

Conclusion

Sepiolite appears to offer very good fire properties in PP. There is an excellent reduction in the PHRR and a significant portion of the polymer does not burn. Other fire retardant parameters, such as, fire performance index, smoke production rate and mass loss rate, also show improvement. The bending strength and elasticity modulus increased but no real improvement in LOI or UL-94 are observed. The addition of sepiolite to a polymer will not solve the fire problem but it is quite possible that it may be combined with other (conventional) fire retardants and offer possibilities.

Acknowledgments

Partial support for this work by the Natural Science Foundation (No. 40972033) of China and Guangxi Science Foundation (No. 2010GXNFC013003) are gratefully acknowledged.

References

1. Zhang, K.; Wang, L. J.; Wu, X. M.; Zhang, G. W.; Xie, X. L. *Plast. Rubber Compos.* **2008**, *37* (5/6), 213–127.
2. Wang, L. J.; He, X. J; Lu, H. D; Feng, J. X.; Xie, X. L.; Su, S. P.; Wilkie, C. A. *Polym. Adv. Technol.* **2011**, *22* (7), 1131–1138.
3. Huang, N. H.; Chen, Z. J.; Wang, J. Q; Wei, P. *Exp. Polym. Lett.* **2010**, *4* (12), 743–752.
4. Shaw, S. D.; Blum, A.; Weber, R.; Kannan, K.; Rich, D.; Lucas, D.; Koshland, C. P.; Dobraca, D.; Hanson, S.; Birnbaum, L. *Rev. Environ. Health* **2010**, *25* (4), 261–305.
5. Wang, D. Y.; Zhu, J.; Yao, Q.; Wilkie, C. A. *Chem. Mater.* **2002**, *14*, 3837–3843.
6. Manzi-Nshuti, C.; Songtipya, P.; Manias, E.; Jimenez-Gasco, M. M.; Hossenlopp, J. M.; Wilkie, C. A. *Polymer* **2009**, *50* (15), 3564–3574.
7. Price, D.; Pyrah, K.; Hull, T. R.; Milnes, G. J.; Ebdon, J. R.; Hunt, B. J.; Joseph, P. *Polym. Degrad. Stab.* **2002**, *77* (2), 227–233.
8. Levchik, S. V. In *Flame retardant polymer nanocomposites;* Morgan, A. B., Wilkie, C. A., Eds.; John Wiley and Sons, Inc.: Hoboken, NJ, 2007; pp 1−23.
9. Zhu, J.; Wilkie, C. A. *Polym. Int.* **2000**, *49* (10), 1158–1163.
10. Wang, L. J.; Su, S. P.; Chen, D.; Wilkie, C. A. *Polym. Degrad. Stab.* **2009**, *94* (5), 1110–1118.
11. Ruiz-Hitzky, E. *J. Mater. Chem.* **2001**, *11* (1), 86–91.
12. Shafig, M.; Yasin, T.; Saeed, S. *J. Appl. Polym. Sci.* **2012**, *123* (3), 1718–1723.
13. Sabah, E.; Turan, M.; Çelik, M. S. *Water Res.* **2002**, *36* (16), 3957–3964.
14. Yi, D.; Yang, R. J. *J. Appl. Polym. Sci.* **2010**, *118* (2), 834–840.
15. Hull, T. R.; Witkowski, A.; Hollingbery, L. *Polym. Degrad. Stab.* **2011**, *96* (8), 1462–1469.
16. Tsai, K. C. *J. Hazard Mater.* **2009**, *172* (2-3), 763–772.
17. Schartel, B.; Bartholmai, M.; Knoll, U. *Polym. Degrad. Stab.* **2005**, *88* (3), 540–547.
18. He, X. J.; Wang, L. J.; Xie, X. L. *Plast. Rubber Compos.* **2010**, *39* (2), 54–60.
19. Chow, W. K.; Han, S. S. *Polym. Test.* **2005**, *24* (7), 125–131.
20. Schartel, B.; Hull, T. *Fire Mater.* **2007**, *31* (5), 327–354.
21. Costache, M. C.; Heidecker, M. J.; Manias, E. *Polymer* **2007**, *48* (22), 6532–6545.
22. Nyambo, C.; Kandare, E.; Wang, D. Y.; Wilkie, C. A. *Polym. Degrad. Stab.* **2008**, *93* (9), 1656–1663.
23. Jash, P.; Wilkie, C. A. *Polym. Degrad. Stab.* **2005**, *88* (3), 401–406.
24. Zhang, J. P.; Michael, A. *Combust. Flame* **2009**, *156* (11), 2056–2062.
25. Hu, Y.; Tang, Y.; Song, L. *Polym. Adv. Technol.* **2006**, *17* (4), 234–245.
26. Wang, L. J.; Xie, X. L.; Su, S. P.; Feng, J. X.; Wilkie, C. A. *Polym. Degrad. Stab.* **2010**, *95* (4), 572–578.

Chapter 26

Significance of Aspect Ratio on Efficiency of Layered Double Hydroxide Flame Retardants

Bashar Diar-Bakerly,[1] Günter Beyer,[2] Rainer Schobert,[3] and Josef Breu*,[1]

**[1]Department of Inorganic Chemistry I, University of Bayreuth,
Universitaetsstr. 30, 95447 Bayreuth, Germany
[2]Kabelwerk Eupen AG, 4700 Eupen, Belgium
[3]Department of Organic Chemistry I, University of Bayreuth,
Universitaetsstr. 30, 95447 Bayreuth, Germany
*E-mail: josef.breu@uni-bayreuth.de**

The effect of specific surface area and aspect ratio of different layered double hydroxides (LDHs) on flame retardant properties of PS/LDH nano-composites was systematically investigated. Carbonate LDH, with a Mg:Al molar ratio of 2:1, was synthesized by the urea hydrolysis method and external basal surfaces were selectively modified using a siderophilic ligand (3,4-dihydroxybenzo-phenone). The efficiency of this surface modification was investigated by studying the sedimentation kinetics in an organic solvent. PS/LDH nanocomposites were prepared by solution blending in a three roll mill. Cone calorimeter measurements showed little influence of specific surface areas but a pronounced influence of aspect ratio on flame retardancy. Optimizing aspect ratio yielded a significant reduction of the peak of heat release rate (PHRR) of 34 % at 5 wt% loading of LDH. A maximum reduction of PHRR of 51% could be achieved at a loading of 15wt%. Interestingly, at this loading an unusual increase of t_{ign} could be observed.

In Fire and Polymers VI: New Advances in Flame Retardant Chemistry and Science; Morgan, A., et al.;
ACS Symposium Series; American Chemical Society: Washington, DC, 2012.

Introduction

Most of the currently used, commercially available flame retardants are halogenated molecular compounds because of their high efficiency allowing for low loadings. However, in the last decade increasing environmental concerns (*1*, *2*) have generated growing interest for non-halogenated and environmentally benign flame retardants. Inorganic flame retardants, such as aluminum trihydroxide (ATH) and magnesium dihydroxide (MDH), in contrast to the organic additives are considered to be immobile and non-toxic. However, high loadings (40-70 wt%) of these fillers are required to achieve sufficient flame retardancy that, on the other hand, alter the mechanical properties of the polymer crucially and represent a major drawback of these fillers. As alternatives, layered double hydroxides (LDHs), which are structurally and chemically related fillers to ATH and MDH, were intensively studied as flame retardants or synergistic flame retardants (*3–12*). These LDHs are anionic clays having the same layer structure as brucite. Partial isomorphic substitution of the divalent cation by trivalent cations in the octahedral layer renders the layers to carry a permanent positive charge. The cationic layer charge is balanced by interlayer anions resulting in the general formula of $[M(II)_{1-x}\ M(III)_x\ (OH)_2]^{x+}[A^{n-}{}_{x/n}]^{x-}.\ mH_2O$, where M(II) and M(III) are divalent and trivalent metal cations, respectively, A^{n-} is the charge balancing interlayer anion, while x ranges between 0.20 and 0.33 and m refers to the number of interlayer water molecules (*13*).

Whereas the influence of cationic clays, like hectorite and montmorillonite (MMT), on the flame retardant properties of polymer nanocomposites is fairly well understood and the crucial role of the aspect ratio of fillers has been elucidated (*14*, *15*), the mechanism by which LDHs influence flame retardant properties is not yet clear. The individual contributions of the endothermic nature of the thermal degradation of the filler, the specific interface area between the polymer and filler, and the gas barrier or mechanical reinforcement of the char related to the filler´s aspect ratio is not obvious.

Additionally, LDHs are highly hydrated and cannot be dispersed effectively in hydrophobic polymer matrices without surface modification. Usually this problem has been solved by intercalation of different organic anions (sulfonates, carboxylates, and phosphonates) containing a hydrophobic aromatic/aliphatic chain (*16–20*). However, the ion exchange capacity of LDH is considerably higher as compared to montmorillonite and consequently, a lot of readily flammable organic matter is introduced by the ion exchange.

Here, we present a novel approach for organic modification of Mg/Al-CO_3 LDH, which selectively restricts organophilization to external surfaces, using siderophilic ligands, e.g. catechol derivatives like 1,2-dihydroxyphenyl. This functional group is well known to form stable complexes with aluminum cations in solution (*21*, *22*) and even Al immobilized at solid surfaces like external octahedral layers of Mg/Al-LDH or kaolinite (*23*). Modification of LDH by a suitable siderophile allowed stable suspensions of LDH in organic solvents and assured a better compatibility with the polymer matrix. Additionally, we systematically investigated the effect of specific surface area and aspect ratio of the filler on the fire properties of PS/LDH nanocomposites in an attempt to elucidate the mechanism of flame retardancy of LDHs.

Experimental Section

Materials

Polystyrene (PS 158K, melt index 3.00 g/10 min (200 °C/5kg, ASTM D1238), density 1.04 g/cm^3, ASTM D792, glass transition temperature 100 °C, ISO 11357) was supplied by BASF. For Mg/Al-LDH synthesis, urea and magnesium chloride hexahydrate were purchased from Grüssing GmbH, and aluminum chloride hexahydrate was purchased from Merck. LDH-syntal (density 2 g/cm^3, BET-surface 74 m^2/g) was provided from Süd-Chemie. The siderophilic ligand (3,4-dihydroxybenzophenone, DBP) used for the surface modification was purchased from Alfa-Aesar. The organic solvents (tetrahydrofuran and ethanol) used for solution blending and surface modification were purchased from Aldrich chemicals.

Instruments and Characterization

The powder X-ray diffraction (PXRD) patterns of the synthesized LDH and the surface modified LDH were obtained in reflection mode on a PANalytical Xpert Pro equipped with a X'Celerator Scientific RTMS detector and using Cu Kα radiation. The samples were measured on flat glass holders.

A 5 wt% aqueous suspension of LDH was milled in a stirred media mill, Netzsch Labstar LS 1 LMZ. Yttrium stabilized zirconia beads were used as grinding media (diameter of 0.6 – 0.8 mm). The volume fraction of the grinding media in the grinding chamber was 80 vol%.

The particle size distribution (PSD) was determined by static light scattering using a Retsch Horiba LA-950 SLS instrument.

The Brunauer, Emmett, and Teller (BET) method was used to calculate the specific surface areas of freeze-dried LDH. Measurements were carried out on a Quantachrome Nova 2000e analyzer. The specific surface area was determined using 5 points within the range of $0.05 < p/p_o < 0.3$ using N_2 as adsorption gas. All samples were degassed overnight at 110 °C under ultra high vacuum.

Scanning electron microscope (SEM) measurements were carried out on a Zeiss 1530 FESEM (acceleration voltage of 3 kV). The samples were freeze-dried then mounted on conductive sample holders and sputtered with carbon.

Transmission electron microscope (TEM) measurements were carried out on a Zeiss EM 922 EFTEM with an acceleration voltage of 200 kV. Specimens were microtomed to obtain 30-70 nm thick pieces, which were placed on a lacey carbon copper grid.

The suspension stability tests were carried out in a Lumifuge 114 stability analyzer. Suspensions of LDH and modified LDH (0.25 wt%) were centrifuged for 900 s with gradually increasing centrifuge velocities (300, 400, 500 rpm).

Solution blending was carried out in a three roll mill (Exakt-80E) at -23 °C. All samples were passed through the mill 7 times. The roller distance was gradually lowered from initially 25 µm in the first cycle to 5 µm in the final cycle.

The cone calorimeter experiments were carried out using an ULTRAMAT 6 instrument from FIRE (35 kW/m^2 heat flux with horizontal orientation of the samples) according to ASTM E 1354, on 100 x 100 mm^2 plaques (4 mm thickness) prepared by melt pressing at 190 °C for 8 min. All samples were tested in triplicate and the recorded cone data were reproducible to within ±5 %.

Synthesis of Magnesium Aluminum Carbonate Layered Double Hydroxides ($Mg/Al\text{-}CO_3\text{-}LDH$)

$Mg/Al\text{-}CO_3$-LDH was synthesized applying the urea hydrolysis method (*24*). An aqueous solution of a mixture of metal salts (1.3 l, 0.5 M total metal concentration, Mg:Al-ratio; 2:1) of $MgCl_2.6H_2O$ (88.1 g, 0.43 mol) and $AlCl_3.6H_2O$ (52.3 g, 0.22 mol) was refluxed in the presence of urea (128.9 g, 2.1 mol) for 36 h. The suspension was then centrifuged and washed with deionized water. The obtained slurry was next re-suspended in a solution of sodium bicarbonate (1 l, 0.4 mol) and aged at 60 °C over night. The resulting white precipitate was centrifuged and repeatedly washed with deionized water until a test for chloride with $AgNO_3$ was negative. Please note that the obtained LDH was not dried but was rather stored as aqueous suspension.

Surface Modification and Suspension Stability of LDH

For surface modification, the aqueous LDH-suspension was centrifuged and then re-suspended (5 wt%) in ethanol which contained the siderophilic ligand 3,4-dihydroxybenzophenone (0.5×10^{-3} mol). To complete surface modification, the suspension was ultrasonified for 3 min and was then shaken for 30 min in a rotary shaker. Finally, the suspension was centrifuged and washed with ethanol and tetrahydrofuran (THF). At last, the surface modified LDH-DBP was re-suspended in THF at a solid content of 5 wt%.

To compare suspension stability, suspensions of 0.25 wt% of the LDH and the surface modified LDH-DBP were prepared in THF. The measurement was carried out using the Lumifuge with increasing centrifuge velocities (300, 400, 500 rpm).

Preparation of PS/LDH Nanocomposites by Solution Blending

PS/LDH nanocomposites were prepared by adding appropriate amounts of the 5 wt% suspension of LDH-DBP in THF to a solution of 25 wt% of PS in THF to achieve loadings of 5, 10, and 15 wt% in the final nanocomposites. The dispersions were first mixed for 30 min using an overhead stirrer (500 rpm, RT). Afterwards, the dispersion was further homogenized applying a three roll mill. Despite cooling at -23 °C a good share of THF evaporated in the course of three roll milling (1 h) and highly viscous dispersions were obtained which were dried in a vacuum oven (80 °C, 600 mbar, 3 h). For better processability, all samples were ground into a powder in a planetary ball mill (5 min, 350 rpm) and dried again in a vacuum oven (110 °C, 300 mbar, 24 h) to remove remaining traces of THF. Moreover, a blank sample of the virgin polymer was prepared following the same described procedure. Finally, the dried powders were hot pressed for cone calorimetric analysis.

Results and Discussions

Synthesis, Morphology, and Stirred Media Milling of Mg/Al-CO_3 LDH

LDH was synthesized by the urea hydrolysis method with a Mg:Al ratio of 2:1. By raising the temperature to 100 °C, hydrolysis of urea was accelerated and pH rose to 9 - 10, which is a suitable pH to precipitate LDHs.

The urea hydrolysis method is also called the homogeneous precipitation method and produces well ordered, crystalline LDHs of high aspect ratio with carbonate (CO_3^{2-}) as charge balancing interlayer anions whereas the more frequently used co-precipitation method produces disordered, low crystalline LDHs of comparatively lower aspect ratio but more variable interlayer anions (in particular Cl- or NO_3^--LDH are also accessible). Due to the high charge density and the low hydration enthalpy of carbonate, CO_3^{2-}-LDHs, however, cannot be directly ion exchanged/intercalated with other organic/inorganic anions, in contrast to the nitrate or chloride containing LDHs obtained by the co-precipitation method.

Although the urea hydrolysis method in principal delivers platelets of larger aspect ratio, the product was obtained as tightly intergrown crystals of so-called rose-like aggregates (Figure 1).

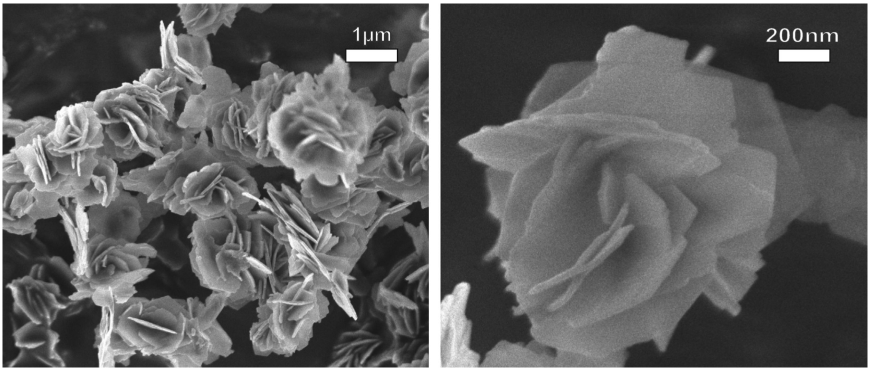

Figure 1. SEM images of LDH synthesized by the urea hydrolysis method showing the rose-like aggregate morphology at low (left) and high (right) magnification.

Disaggregation of rose-like morphologies required strong shearing forces as supplied e.g. by stirred media mills. By stirred media milling of the as-synthesized LDH in an aqueous medium, two crucial features could be significantly improved: i) the aspect ratio, which is the ratio between the diameter and the thickness of the particles, and ii) the interface area between the polymer matrix and the LDHs (filler) because the specific surface area of the LDH increased.

The influence of stirred media milling on the PSDs is presented in Figure 2. Please note that SLS measures the hydrodynamic diameter of the platelets which is closely related to the lateral extension. The thickness can only be determined by the Scherer broadening of basal reflections. However, due to the high layer charge density of LDHs and the low hydration enthalpy of carbonate anions, the electrostatic attraction between positively charged layer and negatively charged interlayer was found to be too strong as to allow for any exfoliation. Although stirred media mills provide considerable shearing forces and are for instance capable to exfoliate hectorite clays (*25*), we noticed no increase of the full widths of half maximum of the *003* basal reflections (Figure 3). The shearing forces produced in this mill were insufficient to induce any exfoliation.

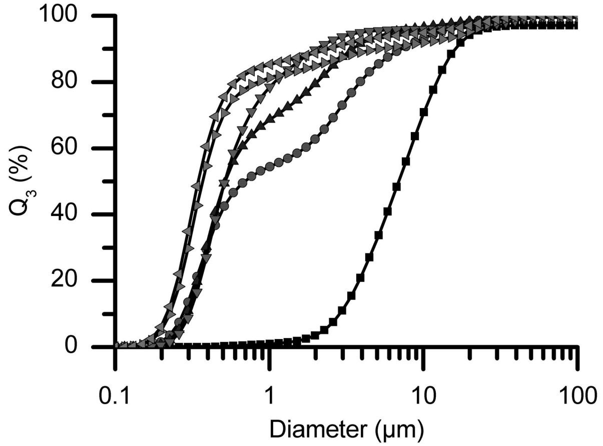

Figure 2. Particle size distributions of (■) LDH (●) LDH-SMM 5min (▲) LDH-SMM 10min (▼) LDH-SMM 20min (▶) LDH-SMM 30min, and (◀) LDH-SMM 60min. All measurements were done in an aqueous suspension.

The suspension of non-milled LDH (referred to as LDH) in water had a median particle diameter of 9 µm that was attributed to rose-like aggregates of singular platelets. Stirred media milling for 5 min (LDH-SMM 5min), disaggregated already most of the particles and a bimodal PSD with maxima at 1.2 and 0.4 µm, respectively, was observed. After 20 min (LDH-SMM 20min), all aggregates were destroyed and a median particle diameter of 0.4 µm was observed. At this point the monomodal size distribution suggested that all rose-like structures are disaggregated. Further stirred media milling partially breaks the disaggregated singular platelets as indicated by the gradual shift of median particle diameter to 0.3 µm for 60 min (LDH-SMM 60min). Breakage of particles was accompanied by an increase of specific surface area caused by additional edge surface produced. The calculated specific surface areas (BET method) for LDH, LDH-SMM 30min, and LDH-SMM 60min are 45, 64, and

84 m^2/g, respectively. Please note, that, since no exfoliation was observed, this increase of specific surface area was solely related to breakage of platelets and thus concomitantly the aspect ratio was significantly reduced.

These LDHs with different specific surface areas and aspect ratios were used for preparation of PS nanocomposite to evaluate the influence of these LDHs-features on the flame retardant properties.

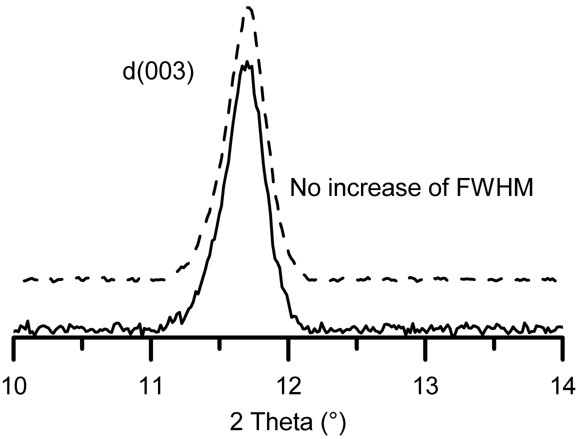

Figure 3. PXRD pattern of the LDH (—) and LDH-SMM 60min (---).

Surface Modification and Suspension Stability of LDHs

Because of strong selective adsorption of carbonate anions, LDH, in contrast to ordinary cationic clays, like MMT (zeta potential typically > -40 mV), have a small zeta potential (≈ +25 mV) which moreover is strongly dependant on CO_2 and CO_2^{3-} concentration. In 0.01 M Na_2CO_3 solution the surface was even "umgeladen" and the zeta potential then was -20 mV. Consequently, modification of LDHs by anion exchange at external basal planes was found not to be a particularly robust process. Therefore, based on previous work on kaolinite modification (*23*, *26*), we choose an unconventional modifier for LDHs, siderophilic ligands. These ligands form selectively very stable complexes with trivalent metal cations in solution or at heterogeneous external basal surfaces of LDHs. Since the complexation reaction is independent of Coulomb attraction, the charge status of the surface is irrelevant in a first approximation. The structure of the siderophilic ligand used here for surface modification, 3,4-dihydroxybenzo-pheneone, is shown in Figure 4.

Appropriate surface modification in the course of preparing PS/LDH nanocomposites via solution blending has to serve two main purposes: i) Stabilization of modified LDH in organic solvents, and ii) compatibilization of the filler with the hydrophobic polymer matrix, which prevents re-aggregation and thus fosters a homogenous dispersion of the filler.

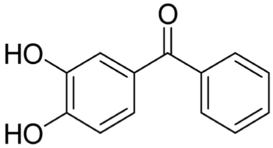

Figure 4. Structure of the organic siderophilic surface modifier; 3,4-dihydroxy-benzophenone (DBP).

PXRD patterns of LDH-DBP (Figure 5) did not indicate any shift in the d-spacing values and hence confirmed that the modifier is not intercalated but only modified the external basal surface of the octahedral layer by complexation. Success of the surface modification was indicated by the tainted yellow color of the surface modified LDH (Figure 7) inherited by the ligand.

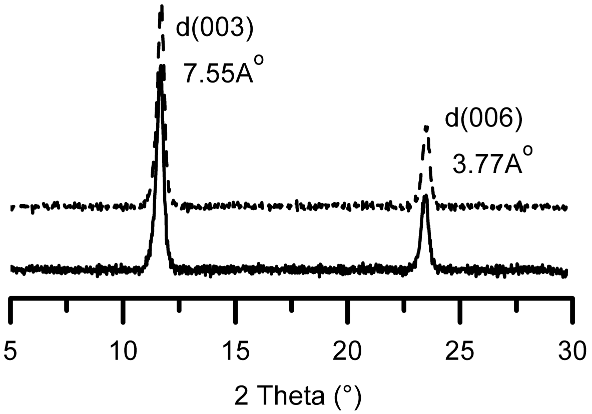

Figure 5. PXRD pattern of the LDH (—) and LDH-DBP (---).

The stability of the suspensions of LDH and LDH-DBP in an organic solvent, THF, was compared by using the Lumifuge. The transmission of light through a horizontal centrifuge cell was measured during centrifugation at different velocities providing important semi-quantitative information about the sedimentation kinetics of these suspensions at low solid concentration (in our case 0.25 wt%). For stable suspensions (LDH-DBP/THF), less transmission is recorded, due to absorption/scattering of light by particles kept in suspension. On the other hand, for unstable suspensions (LDH/THF), the particles sediment readily, and hence, more light was transmitted through the sample and a higher transmission is recorded as compared to the stable suspensions as shown in Figure 6.

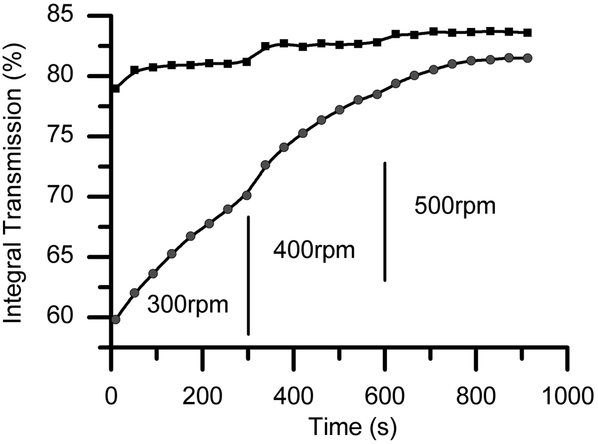

Figure 6. Sedimentation kinetics of LDH (■) and the surface modified LDH-DBP (●) in THF as determined by centrifugation forced sedimentation using a Lumifuge. Vertical lines indicate times when the centrifugation velocity was increased stepwise.

While the instable LDH/THF suspension clarified quickly, the LDH-DBP/THF suspension remained more stable even at high centrifugation velocities. At the beginning of the measurement, only 59 % of the light was transmitted through the LDH-DBP/THF suspension while for the LDH/THF suspension 78 % of the light was transmitted. By centrifugation at higher velocities, both suspensions clarify due to forced sedimentation but the stabilized LDH-DBP/THF did so at much reduced pace. The results of the Lumifuge experiment are confirmed by static sedimentation tests (Figure 7).

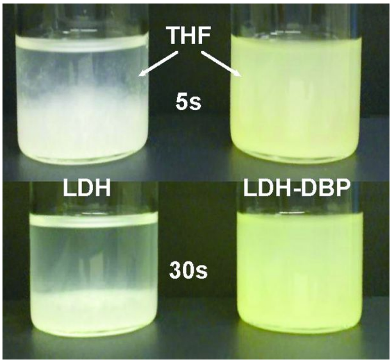

Figure 7. Photographs of THF suspensions of LDH (left) and LDH-DBP (right). (see color insert)

Compounding by Solution Blending

The specific interface area in a nanocomposite is crucially dependant on the specific surface area of the filler and the quality of the dispersion which defines the share of the surface area being active in the composite. Therefore, the quality of dispersion of fillers is always considered to have an essential effect on fire retardancy of nanocomposites (*15*). In order to optimize the dispersion and to take advantage of the full potential of the filler, special care was taken in handling the filler. For instance we avoided drying of LDH throughout all steps, this way electrosteric stabilization helped in minimizing agglomeration/aggregation of the LDH particles. Moreover, solution blending was carried out in two steps to achieve a homogenous dispersion: i) suspension of the surface modified LDH was first mixed with the polymer solution using an overhead stirrer. ii) Then homogenization and disaggregation was pushed by applying high shear forces by milling the dispersions in a three roll mill. Seven cycles were applied at different milling velocities and roller distances (from 25 µm down to 5 µm) at -23 °C. Despite the cooling, due to the energy input and the high surface nevertheless most of the solvent was removed during three roll milling and a highly viscous dispersion was obtained.

To evaluate the efficiency of solution blending and to check the dispersion quality, the resulting highly viscous dispersions were diluted with THF again and then the PSDs were determined by SLS. The results were compared to the PSDs of the pristine suspension of surface modified LDH in THF before solution blending (Figure 8).

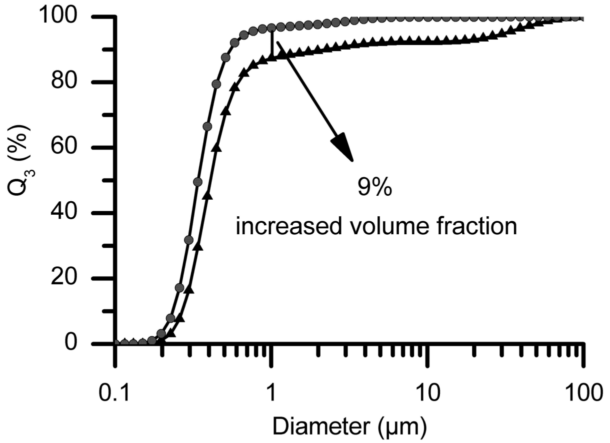

Figure 8. Particle size distributions of (▲) LDH-SMM 60min-DBP and (●) PS/LDH-SMM 60min-DBP-5wt% -7 cycles three roll mil.

Comparison of the PSDs underlines the quality of compatibilization applying the siderophilic ligand and dispersion by three roll milling. The applied shear forces even increased the volume fraction of non-aggregated particles < 1 µm by 9 %, suggesting the solution blending did not induce any aggregation and that the maximum potential interface area could be assured by this type of solution blending affording a three roll mill. This will allow probing the full potential of the different fillers since the specific surface area of the filler was fully converted to specific interface area in the PS/LDH nanocomposites produced by solution blending.

Figure 9 shows TEM images of the PS/LDH-SMM 30min-DBP-5wt% nanocomposite. LDH particles appeared well dispersed and no rose-like aggregates could be observed. Please note that no exfoliation has occurred either by stirred media milling or by solution blending in a three roll mill.

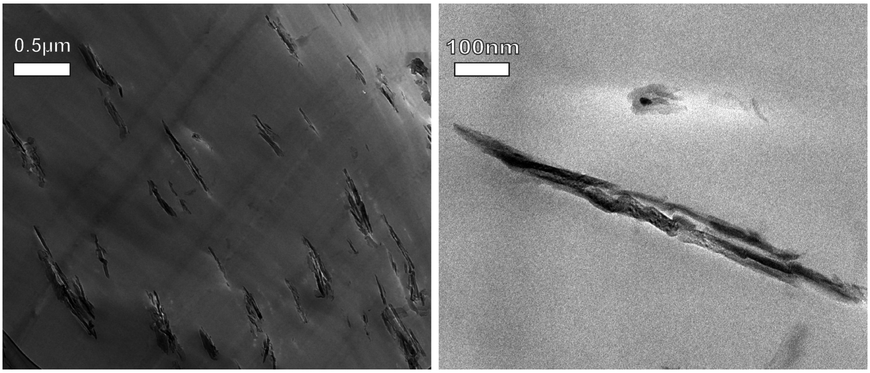

Figure 9. TEM images of PS/LDH-SMM 30min-DBP-5wt% at low (left) and high (right) magnification.

Thermal Decomposition of LDHs

The flame retardancy effect of inorganic fillers, like ATH and LDHs, is related to heat consumption and release of inert gases (H_2O, CO_2) produced by decomposition of the inorganic filler during combustion of nanocomposites. To quantitatively evaluate the heat consumption by LDH as compared to conventional ATH additives, differential scanning calorimetric (DSC) analysis was applied (Figure 10). Although structurally closely related, the decomposition of ATH and LDH is quite different. As known from literature, the endothermic decomposition of LDH occurred in three separate steps: i) dehydration, ii) dehydroxylation, and iii) decarbonation, whereas the decomposition of ATH occurred in one step.

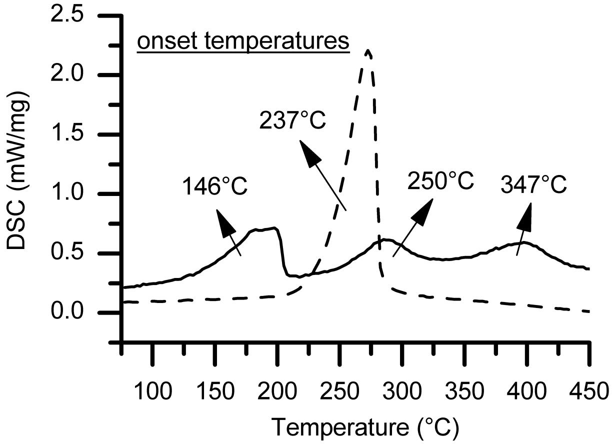

Figure 10. Differential scanning calorimetry curves (DSC) for LDH (—) and ATH (---) measured at a heating rate of 1 °C/1 min.

Please note that the exact temperatures at which the individual steps are observed vary a great deal with the type of octahedral cations and the layer charge of the LDH. In principle these decomposition steps could even be tailored to best fit the particular matrix and its decomposition kinetics. For the particular composition chosen here, the onset temperature for the dehydration of interlayer water of LDH is as low as 146 °C. This implies that dehydration will at least partially have occurred during processing. Remaining interlayer water will, however, induce an early cooling effect that spreads over a wider temperature range as compared to ATH. The heat consumption of ATH is solely related to dehydroxylation which represents a much sharper endothermic event. The heat consumption by ATH (931 J/g) is, however, 47% higher than the total heat consumption by LDH (490 J/g).

Cone Calorimeter Data

In a systematic effort to evaluate the effect of the specific surface area versus the aspect ratio of LDH on the flame retardant properties of PS/LDH nanocomposites, LDH with different specific surface areas obtained with different synthesis routes were prepared. The specific surface area of large aspect ratio LDH obtained by urea hydrolysis was increased to different levels by means of stirred media milling as described before. Furthermore, a commercially available LDH (LDH-syntal supplied by Süd-Chemie) produced by co-precipitation and thus showing low aspect ratio but a high specific surface area of 74 m^2/g was included. The LDH as obtained from the urea hydrolysis method has a specific surface are of 45 m^2/g. After stirred media milling for 30 and 60 min, the specific surface areas increased to 64 and 84 m^2/g, respectively. The different LDHs

In Fire and Polymers VI: New Advances in Flame Retardant Chemistry and Science; Morgan, A., et al.;
ACS Symposium Series; American Chemical Society: Washington, DC, 2012.

were surface modified in the same way and PS/LDH nanocomposites with a constant loading of 5 wt% were produced by solution blending while dispersion was assisted by three roll milling. Finally, their flame retardant properties were investigated by cone calorimeter.

Cone calorimetry analysis is an essential analysis to determine the fire properties of polymer nanocomposites. Information is collected about the time to ignition (t_{ign}), the heat release rate (HRR), the peak of heat release rate (PHRR), the total heat release (THR), and burn out time. For perfect flame retardants, as known from literature, it is favorable to increase t_{ign}, decrease PHRR and THR, and increase the burn out time.

Table I. Cone calorimeter data for PS/LDH nanocomposites

Formulation	*PHRR (kW/m^2)*	*PHRR Reduct. (%)*	*THR (MJ/m^2)*	*T_{ign} (s)*	*specific surface area (m^2/g)*
PS	813 ± 29	-	138 ± 2	88 ± 3	-
PS/LDH-DBP -5wt%	616 ± 13	24	133 ± 3	72 ± 2	45
PS/LDH-SMM 30min-DBP-5wt%	517 ± 17	36	133 ± 3	65 ± 3	64
PS/LDH-SMM 60min-DBP -5wt%	621 ± 25	23	131 ± 4	66 ± 1	84
PS/LDH-syntal DBP -5wt%	627 ± 8	22	129 ± 1	59 ± 2	74

Table I summarizes the cone data for LDHs with different surface areas and aspect ratios, while the heat release rate curves obtained at a heat flux of 35 kW/m^2 are shown in Figure 11. A maximum reduction in the peak of heat release rate of 36 % was obtained by PS/LDH nanocomposite using LDH-SMM 30min. As suggested by the PSD (Figure 2) at this point of stirred media milling, rose aggregates were already destroyed while little breakage of singular platelets had occurred. This filler thus represents the material with the largest aspect ratio. Prolonged stirred media milling further increased the specific surface area but on the cost of reducing the aspect ratio. For these samples, despite the increase of the specific surface areas (Table I), the flame retardancy deteriorated suggesting that the aspect ratio is more important than specific interface area. It is however not clear at this point, whether the main role of the aspect ratio is reduction of gas permeability or reinforcement of the char.

In Fire and Polymers VI: New Advances in Flame Retardant Chemistry and Science; Morgan, A., et al.;
ACS Symposium Series; American Chemical Society: Washington, DC, 2012.

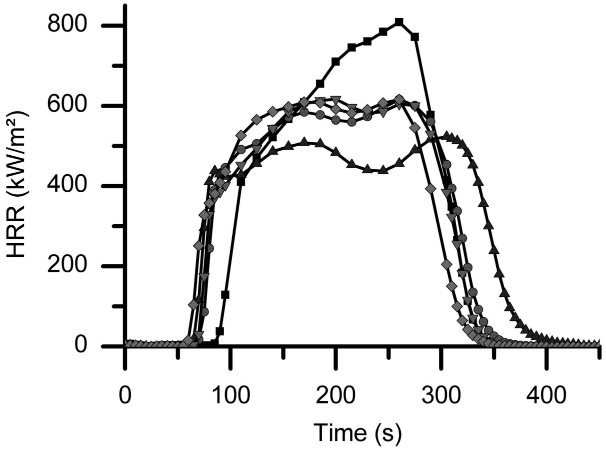

Figure 11. Heat release rate curves for PS/LDH nanocomposites at different surface areas: (■) PS (●) PS/LDH-DBP-5wt% (▼) PS/LDH- syntal-DBP-5wt% (▲) PS/LDH-SMM 30min-DBP-5wt% (♦) PS/LDH-SMM 60min-DBP-5wt%.

The time to ignition (ease of ignition) is reduced for all PS/LDH nanocomposites. This reduction ranges between 16 and 33 % for PS nano-composites with LDH and LDH-syntal, respectively. Reduction of t_{ign} commonly is attributed to the content of the easily flammable organic modifier, since most of the organic modifiers have lower onset temperature than the virgin polymer. Alternatively, the filler might act as heterogeneous catalyst in the degradation of the virgin polymer. With our samples, the surface modification being restricted to outer basal planes considerably reduces the organic content as compared to intercalated LDHs commonly used. Please note that for intercalated LDH, the organic content could reach 30 - 40 wt% of the modified LDHs and reductions of t_{ign} up to 80 % may be observed (*4*).

The increase of viscosity of nanocomposites as compared to neat polymers is closely related to specific interface area which limits the maximum filler content that can still be processed. If the specific surface, however, plays a minor role in the retardancy mechanism, the lower values of LDH (45 m^2/g) as offers the advantage that much higher filler contents (more than 10 wt%) can be explored.

Table II and Figure 12 present the cone calorimeter data and the heat release rate curves for PS nanocomposites with LDH at increasing loadings (5, 10, and 15 wt%) measured at a heat flux of 35 kW/m^2. For the nanocomposites with higher LDH loadings, the PHRR is significantly decreased which could be the result of the endothermic decomposition of LDH (thermal quenching) that releases water and CO_2 and, hence, cools the surface of the burning polymer and dilutes the combustible gases (inert gas dilution).

Table II. Cone calorimeter data for PS/LDH nanocomposites

Formulation	*PHRR (kW/m²)*	*PHRR Reduct. (%)*	*THR (MJ/ m²)*	*T_{ign} (s)*
PS	813 ± 29	-	138 ± 2	88 ± 3
PS/LDH-DBP-5wt%	616 ± 13	24	133 ± 3	72 ± 2
PS/LDH- DBP-10wt%	444 ± 12	45	127 ± 2	74 ± 2
PS/LDH- DBP-15wt%	402 ± 15	51	125 ± 2	95 ± 2

A maximum reduction of PHRR of 51 % was achieved at 15 wt% loading. At this loading, the HRR curve was spread over a wide range of time and shifted towards a higher burn out time value (from 370 to 960 s), which indicates a slower transfer of mass and heat during the combustion of the polymer (longer burning time at lower HRR). This spread, which only sets in at higher loadings, may be related by the formation of a thin layer of char and residues of metal oxides that insulate the polymer from heat radiation.

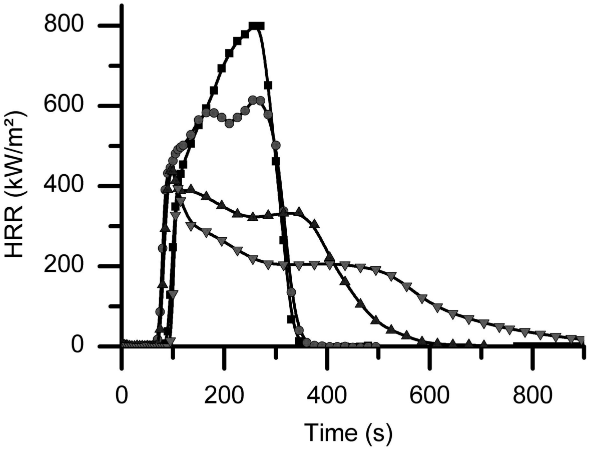

Figure 12. Heat release rate curves for PS/LDH nanocomposites at different loadings; (■) virgin PS (●) 5wt% (▲) 10wt%, and (▼) 15wt%.

Surprisingly, contrary to the usual decrease of t_{ign} observed for all lower loadings, for 15 wt% loading instead an increase of 8 % of t_{ign} was observed. We suggest that the PS/LDH nanocomposite at 15 wt% loading released more water during early stages of decomposition and therefore diluted the combustible gases sufficiently to delay the ignition.

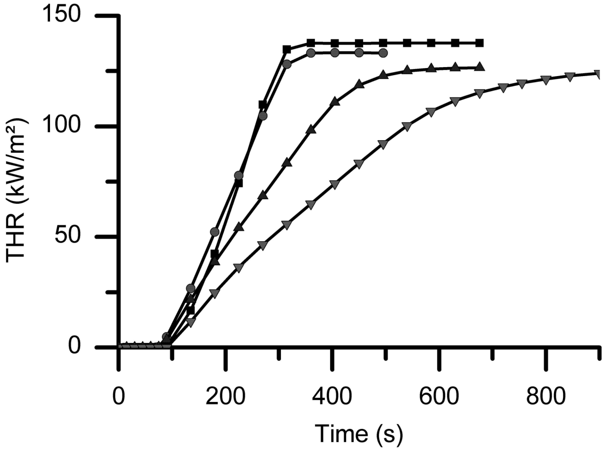

Figure 13. Total heat release curves for PS/LDH nanocomposites at different loadings; (■) virgin PS (●) 5wt% (▲) 10wt%, and (▼) 15wt%.

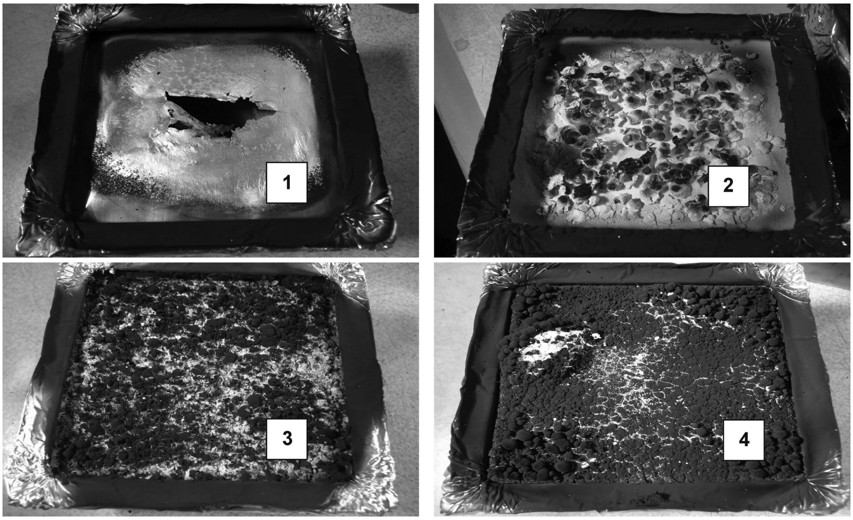

Figure 14. Photographs represent a comparison between the residues of the cone test (1) PS (2) PS/LDH-DBP-5wt% (3) PS/LDH-DBP-10wt% and (4) PS/LDH-DBP-15wt%.

Figure 13 shows the total heat release of PS/LDH nanocomposite at different loadings. The total heat release was consistently decreased with increasing LDH loadings (from 138 MJ/m^2 for virgin PS to 125 MJ/m^2 for PS/LDH at 15 wt% loading) while at the same time the final value was achieved at increasing time lags. The reduction of total heat release may be explained by first the reduction of the mass of combustible polymer when more LDH is added (reduction of the fuel content) and second the thermal dissipation effect due to the endothermic nature of the decomposition of LDH. This effect is comparable to MDH and ATH flame retardants. For intercalated types of LDH-fillers, no appreciable reduction of total heat release was observed (*4*, *27*) which might be attributed to the high organic content which increases the fire load, and consequently counterbalances the cooling effect of the filler on total heat release.

The combustion residues of different PS/LDH nanocomposites at different loadings are shown in Figure 14 . With increasing LDH loadings more carbonaceous char was formed suggesting that LDHs promoted char formation. Nevertheless, the char surfaces were not continuous but rather had a lot of cracks.

Conclusions

We present a new approach for surface modification of LDH selective to external basal surfaces using a siderophilic ligand (3,4-dihydroxybenzophenone). LDHs were synthesized by urea hydrolysis method. This modification provides a stable suspension in organic solvents and a good compatibility with the polystyrene matrix. We systematically investigated the influence of specific surface area and aspect ratio of LDH on flame retardancy of PS nanocomposites prepared by solution blending in a three roll mill. The specific surface area and aspect ratio of LDH were varied by means of stirred media milling. Flame retardant properties were determined by cone calorimeter analysis. Cone calorimeter data suggest that aspect ratio is more important than specific surface area of the fillers investigated. A maximum reduction of PHRR of 51% could be achieved at a loading of 15wt%. Interestingly, at this loading an unusual increase of t_{ign} could be observed. The data underline the potential of large aspect ratio LDH which certainly can be further optimized by applying more sophisticated surface modifiers.

Acknowledgments

The authors thank Prof. Dr. V. Altstädt, Department of Polymer Engineering, University of Bayreuth, for his assistance for the hot pressing of the cone samples. B. D-B. also acknowledges the German Academic Exchange Service (DAAD) for financial support. This work was further supported by the Deutsche Forschungsgemeinschaft (DFG) within the Collaborative Research Center (SFB) 840.

References

1. Law, R. J.; Herzke, D.; Harrad, S.; Morris, S.; Bersuder, P.; Allchin, C. R. *Chemosphere* **2008**, *73*, 223–241.
2. Birnbaum, L. S.; Staskal, D. F. *Environ. Health Perspect.* **2003**, *112*, 9–17.
3. Nyambo, C.; Chen, D.; Su, S.; Wilkie, C. A. *Polym. Degrad. Stab.* **2009**, *94*, 1298–1306.
4. Nyambo, C.; Songtipya, P.; Manias, E.; Jimenez-Gasco, M. M.; Wilkie, C. A. *J. Mater. Chem.* **2008**, *18*, 4827–4838.
5. Nyambo, C.; Kandare, E.; Wang, D.; Wilkie, C. A. *Polym. Degrad. Stab.* **2008**, *93*, 1656–1663.
6. Costa, F. R.; Wagenknecht, U.; Heinrich, G. *Polym. Degrad. Stab.* **2007**, *92*, 1813–1823.
7. Chen, W.; Qu, B. *J. Mater. Chem.* **2004**, *14*, 1705–1710.
8. Ramaraj, B.; Nayak, S. K.; Yoon, K. R. *J. Appl. Polym. Sci.* **2010**, *116*, 1671–1677.
9. Pereira, C. M. C.; Herrero, M.; Labajos, F. M.; Marques, A. T.; Rives, V. *Polym. Degrad. Stab.* **2009**, *94*, 939–946.
10. Sahu, B.; Pugazhenthi, G. *J. Appl. Polym. Sci.* **2011**, *120*, 2485–2495.
11. Nogueira, T.; Botan, R.; Wypych, F.; Lona, L. *Composites, Part A* **2011**, *42*, 1025–1030.
12. Ding, P.; Qu, B. *J. Colloid Interface Sci.* **2005**, *291*, 13–18.
13. Evans, D.; Slade, R. Layered Double Hydroxides. In *Structure and Bonding*; Duan, X. E, Evans, D., Eds.; Springer: Berlin/Heidelberg, 2005; Vol. 119, pp. 1−87.
14. Schutz, M. R.; Kalo, H.; Lunkenbein, T.; Breu, J.; Wilkie, C. A. *Polymer* **2011**, *52*, 3288–3294.
15. Schutz, M. R.; Kalo, H.; Lunkenbein, T.; Groschel, A. H.; Muller, A. H. E.; Wilkie, C. A.; Breu, J. *J. Mater. Chem.* **2011**, *21*, 12110–12116.
16. Greenwell, H. C.; Jones, W.; Rugen-Hankey, S. L.; Holliman, P. J.; Thompson, R. L. *Green Chem.* **2010**, *12*, 688–695.
17. Wypych, F.; Satyanarayana, K. G. *J. Colloid Interface Sci.* **2005**, *285*, 532–543.
18. Oh, J. M.; Biswick, T. T.; Choy, J. H. *J. Mater. Chem.* **2009**, *19*, 2553–2563.
19. Costa, F. R.; Leuteritz, A.; Meinl, J.; Wagenknecht, U.; Heinrich, G. *Macromol. Symp.* **2011**, *301*, 46–54.
20. Newman, P.; Jones, W. *New J. Chem.* **1998**, *22*, 105–115.
21. Sancho, M. I.; Jubert, A. H.; Blanco, S. E.; Ferretti, F. H.; Castro, E. A. *Spectrochim. Acta, Part A* **2007**, *68*, 387–393.
22. Golounin, A. V.; Shchedrin, Y.; Fedorov, V. A. *Russ. J. Org. Chem.* **2001**, *37*, 1266–1269.
23. Hirsemann, D.; Shylesh, S.; De Souza, R. A.; Diar-Bakerly, B.; Biersack, B.; Mueller, D. N.; Martin, M.; Schobert, R.; Breu, J. *Angew. Chem., Int. Ed.* **2012**, *51*, 1348–1352.
24. Costantino, U.; Marmottini, F.; Nocchetti, M.; Vivani, R. *Eur. J. Inorg. Chem.* **1998**, *1998*, 1439–1446.

25. Ziadeh, M.; Chwalka, B.; Kalo, H.; Schuetz, M. R.; Breu, J. *Clay Miner.* **2012** in press.
26. Hirsemann, D.; Koester, T. K. J.; Wack, J.; van Wuellen, L.; Breu, J.; Senker, J. *Chem. Mater.* **2011**, *23*, 3152–3158.
27. Manzi-Nshuti, C.; Chen, D.; Su, S.; Wilkie, C. A. *Polym. Degrad. Stab.* **2009**, *94*, 1290–1297.

Chapter 27

A Review of Engineering Biodegradable Polymer Blends: Morphology, Mechanical Property, and Flame Retardancy

Seongchan Pack,*,[1] Menahem Lewin,[#] and Miriam H. Rafailovich[1]

**[1]Department of Materials Science and Engineering,
State University of New York at Stony Brook,
Stony Brook, New York 11794-2275
[#]Deceased
*E-mail: parkarrow@hotmail.com**

We first review recent flame retardant formulations on biodegradable polymer blends, such as either starch/poly(butylene adipate-co-terephthalate) (PBAT) or poly(lactic acid)/poly(butylene adipate-co-terephthalate) (PLA/PBAT), where interfacial tensions of the biodegradable polymer blends can play an important role on mechanical and flame retardant properties. The improved material properties are also mainly influenced by morphology of the blends. In addition, a novel approach to increase not only compatibility but also flame retardancy of the biodegradable polymer blends is reviewed. In this method, an aryl phosphate flame retardant, resorcinol di(phenyl phosphate) (RDP), is adsorbed onto the added particles. This is shown to have the following advantages; (a) it can act as a surfactant on either starch or clays, leading to better dispersion in the polymer matrices, (b) enhance compatibilization of PLA and ECOFLEX by localizing the particles at the blend interfaces, and (c) segregated to the blend surface when heated, and reacted with both polymer and starch. These factors allowed for the formulation of self-extinguishing PLA/ECOFLEX blends, with unusual properties that distinguished them from other blends using standard flame retardant halogen formulations. The reactive properties allowed the formation of a shell like layer whose

In Fire and Polymers VI: New Advances in Flame Retardant Chemistry and Science; Morgan, A., et al.;
ACS Symposium Series; American Chemical Society: Washington, DC, 2012.

modulus was much higher than the interior polymer, and which dissipated the heat of the approaching front. Analysis of the chars formed after combustion in a cone calorimeter, indicated that addition of the RDP soaked clays did not affect the ductility of the chars or their ability to encase the combustion products which sustained internal pressures from the decomposition gases allowing the release at a steady rate.

Introduction

The rapid accumulation of polymer wastes in landfills has raised significant concern regarding their use, and slowed their rapid growth as replacements for other structural materials, such as wood, metals, and glass (*1*). Furthermore, studies on environmental impact of the traditional halogenated flame retardant formulations have shown that they made their way into regional water supply causing them to be banned in some locations (*2–4*). These events have led to a rise in interest for developing biodegradable polymers, as well as environmentally benign flame retardant formulations, as replacements for the traditional petroleum polymers. This has poses several challenges for the industry, which have to overcome before a sustainable substitute is produced on an industrial scale.

Unlike the conventional polymers, biodegradable polymers tend to be more polar, absorb water more easily, and have higher reactivity in ambient conditions. This makes them more difficult to thermally process, control their mechanical properties, form blends, and find appropriate flame retardant agents which combine with their decomposition products. In this chapter we review the basic properties of some of the common biodegradable polymers currently in use, the flame retardant formulations that have been developed, and the synergy which the materials properties, such as surface tension and compatibility, can play in enhancing their flame retardant response.

Review of Common Biodegradable Polymers: Morphology and Mechanical Properties

Poly(lactic acid) (PLA) is a transparent linear aliphatic polyester, which derived from renewable sources such as sugarcane and starch. (*5*). PLA also belongs to the class of Polyhydroxyalikanoates (PHAs) (*6*). PLA biodegrades to carbon oxide, water and humus since the synthesis of lactic acid is a process of bioconversion to ring-opening polymerization (*7–9*). The tensile properties of PLA, are listed below; the polymer has a very high modulus and strength, which can be comparable to oil-based thermoplastic polymers (*10*). However, since PLA has a low glass transition temperature and is semicystalline, it does not have good processability and toughness. Furthermore, it is not a good char former and is not flame retardant according to most standard testing protocols, which restrict its applications to electronics, construction, and automobile parts. (*11*, *12*). The thermal properties of biodegradable polymers are shown in Table 1.

Table 1. The material properties and chemical structures of common biodegradable polymers

Material and Chemical Structure	Tg (°C)	Tm(°C)	Company
Poly (lactic acid) (PLA) 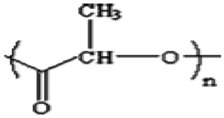	50-60	160-170	Amco Plastics
Poly (butylene adipate-co-terephthalate) **(Trade Name: Ecoflex)** 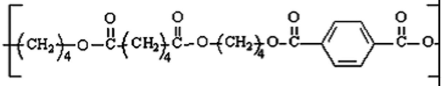 (CH2)4 O C (CH2)4 C O (CH2)4 O C C O	-30	110-115	BASF Corporation
Starch (Trade Name: Melojel) 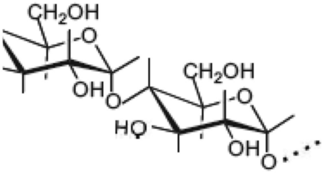	60-67	160	National Starch Food Innovation

Poly (butylene adipate-co-terephthalate) (PBAT), commercialized as Ecoflex, is another popular biodegradable polymer which is digested by enzymes, to produce (*13*). PBAT is amorphous and can be characterized as an elastomeric polymer, with low modulus, but high elongation at break similar to the properties of butylene rubber. Hence PBAT is frequently blended with the PHA group of polymers to engineer biodegradable blends with improved mechanical strength and impact toughness (*14*, *15*). For example, Pack et al. (*15*) investigated a biodegradable blend of PLA/Ecoflex with different nanofillers, and showed that PLA was well dispersed within the Ecoflex matrix (Figure 1a) and that the Ecoflex forms a fibrillar structure which further imparts strength and impact resistance to the material (Figure 1b). Other mechanical properties of the two materials are listed in Table 2.

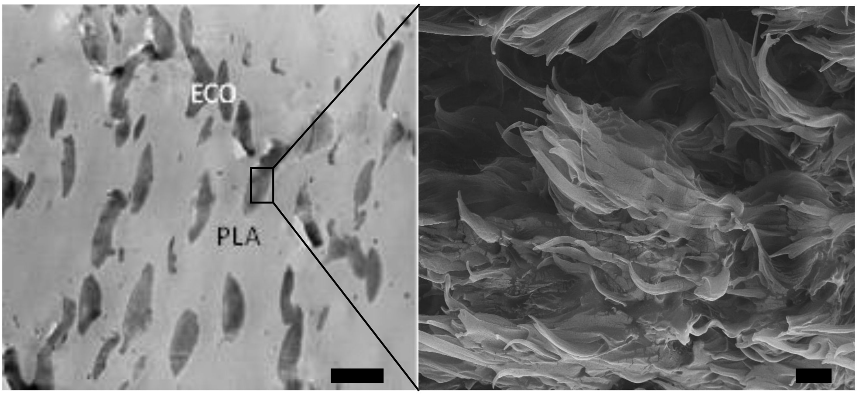

Figure 1. TEM/SEM of a blend of PLA/Ecoflex (80/20 wt%) (the scale bar is 2 μm).

Table 2. Mechanical properties of neat ecoflex, PLA, and a blend of 80% PLA to 20% Ecoflex

Polymer	*Elongation at break (%)*	*Toughness (MPa)*	*Tensile Strength (MPa)*	*Young's Modulus (MPa)*	*Storage Modulus (Pa)*
PLA	6.5	1.9	53.4	1205.5	1.51E+09
Ecoflex	*	*	12.5	59.5	-
PLA/Ecoflex (80/20%)	270.8	82.3	36.6	916.7	1.17E+09

* Pure Ecoflex did not rupture.

Review of Flame Retardant of Biodegradable Polymers

PLA is not known for its flame retardant properties. In fact the polymer has a poor LOI compared to aromatic polymers, such as polycarbonate (*16*, *17*). Reti et al. demonstrated that addition of both ammonium polyphosphate (APP) and either starch or lignin to PLA could achieve the vertical flammable designation (*18*). Zhan et al. also showed that the addition of bisphosphorate diphosphoryl melamine had an impact on reducing flammability of PLA (*19*). Metal oxides were also being used to decrease flammability of the biodegradable polymer (*16*, *20*, *21*). Moreover, they developed a synthesis process of being attached a phosphours oligomers to the back bone of PLA (*16*). As a result of that, good flame retardant properties were obtained. However, these processes produced significant amounts of hazardous chemical waste and involved complicated multiple step synthesis procedures.

Starch is well known to have good flame retardant properties, due to the carbonization process of the starch occurs at exposed surface from heat fronts (*15*, *22*). However, crystallization of starch is a major drawback for melt-blending and extruding it together with other polymers (*23*). Owing to the fact that PLA is derived from starch, it is one of the few polymers which can be melt-blended with PLA, especially when the starch is treated with glycerol (*24*, *25*). Wang et al reported adding 10% starch to PLA slightly increased the LOI of neat PLA from 20 to 23 (*26*). They also investigated that a combination of melamine with ammonium polyphosphate (APP) could render the starch/PLA be self-extinguished, which was rated as UL-94-V0. The improvement though occurred at a relatively large loading of the flame retardants. So it might reduce in the impact toughness from the pure PLA polymer.

Table 3. Properties of thermal stability of Resorcinol bis (diphenyl phosphate) (RDP)

Material and Chemical Structure	**T_{onset} (°C)**	**Tm (°C)**	**Company**
Resorcinol bis (diphenyl phosphate) (RDP) 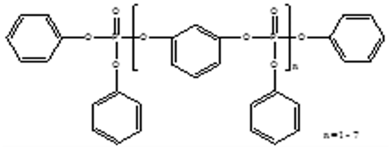 	370	-	ICL-Supresta Inc

Recently, Park et al. have succeeded that when starch can be soaked with the RDP, a common flame retardant compound (see Table 3), it is also possible to blend it with PBAT to produce a flame retardant compound. In this case though, they showed that the addition of a third component, namely Halloysite tubes, This compound was achieved with acceptable impact toughness, and was also able to pass the UL-94-V0, which is shown in Figure 2. In order to understand the process, the samples were cross sectioned and analyzed with STXM, a technique which allows one to identity the different chemical components and map their distribution within the blend. The STXM spectra are shown in Figure 3a, where the distinct abortion peaks corresponding to the components are shown. From Figure 3b-d we can see that the distribution of the starch within the PBAT improved when the starch is soaked in RDP, but a major improvement in the distribution is achieved when the Halloysite tubes are added. The ability of large aspect ratio nanoparticles to compabiltize polymer blends had been shown previously (*27*, *28*).

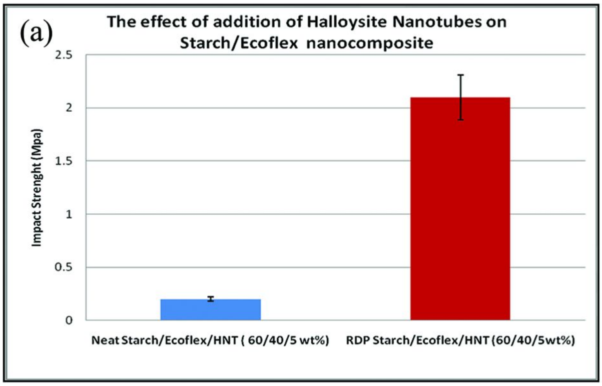

(b) Sample	Weight %	UL-94V0	Dripping
Neat Starch /Ecoflex®/ HNT	60/40/5	NG*	NO
Starch RDP/Ecoflex®/HNT	60/40/5	V0	NO

* note: Burnt to the clamp

Figure 2. (a) Results of Impact Strength and (b) UL94-V0 flammable test of RDP starch/Ecoflex with HNTs. Reproduced with permission from reference (1). Copyright 2012 Elsevier.

Recent Work on PLA/PBAT Blends: Common "Environmental" FR Formulations and Flammability

In order to achieve better mechanical properties, as well as flame retardance, it is important to greatly reduce the amount of additives. This is usually achieved by blending polymers to achieve a new material with desirable properties. Here we discuss blends of PLA and PBAT, where we vary the mechanical and impact toughness. This variation is essential if biodegradable materials are produced as effective replacements for the petroleum based polymers. In this section we show that either the RDP coated starch or RDP coated nanoparticles can be very effective as flame retardant agents and compatibilizers in biodegradable polymers. The synthesis of the RDP-coated starch, montmorillontie clay, and Halloysite nanotubes (HNTs) is straightforward and no harmful chemical wastes are generated. The process consists of pouring 20 wt % of RDP into a beaker containing clays or starch and then the beaker is mixed in a high shear mixer at 60°C. A typical SEM image of the RDP-coated particles is shown at Figure 4. From the figure we can see that Halloysites tubes are completely coated with RDP, which is confirmed by the EDAX spectra obtained from the corresponding the SEM image.

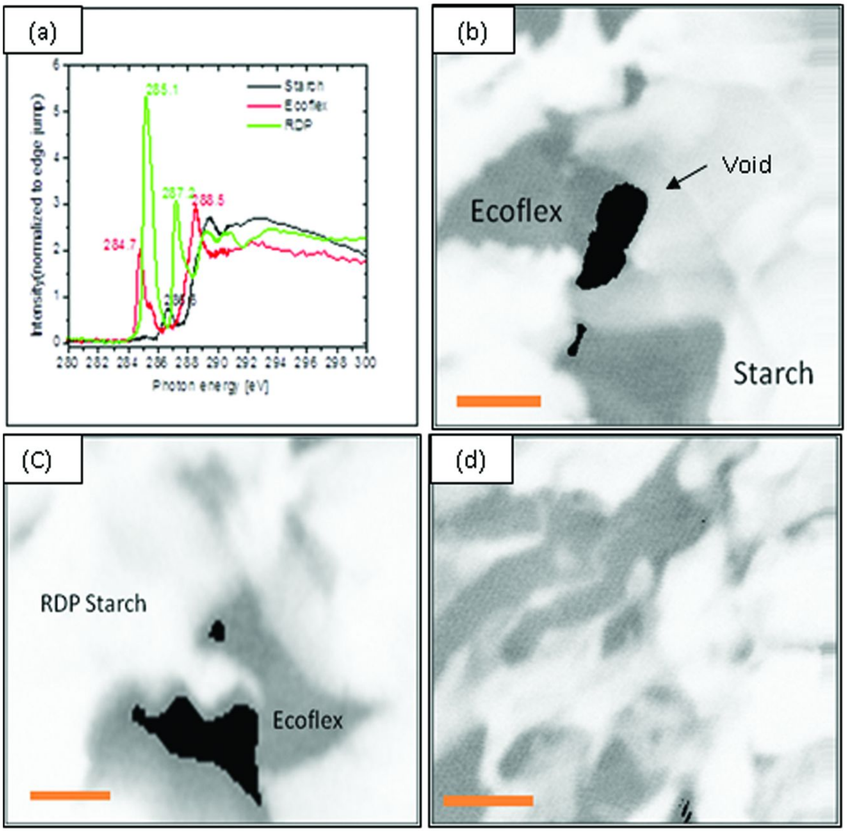

Figure 3. (a) The NEXAFS spectra of Starch, Ecoflex, and RDP and STXM images: (b) Starch/Ecoflex (50/50 wt%) (c) RDP Starch/Ecoflex (50/50 wt%), (d) RDP Starch/Ecoflex/Halloysites (60/40/5 wt%) (the scale bar is 3 µm and the image was taken at 284.7 eV). Reproduced with permission from reference (15). Copyright 2012 Elsevier.

In previous section, Pack et al. showed that the addition of HNTs could make the blends of RDP starch/Ecoflex(60/40 wt%) self-extinguishing, whereas the same ratio of neat starch/Ecoflex blend was not. They also showed that the addition of RDP starch could have same impact on flame retardant properties of the blend of PLA/Ecoflex, where the addition of the RDP starch can increase the degree of dispersion of the Ecoflex domains, which is shown in Figures 5 and 6.

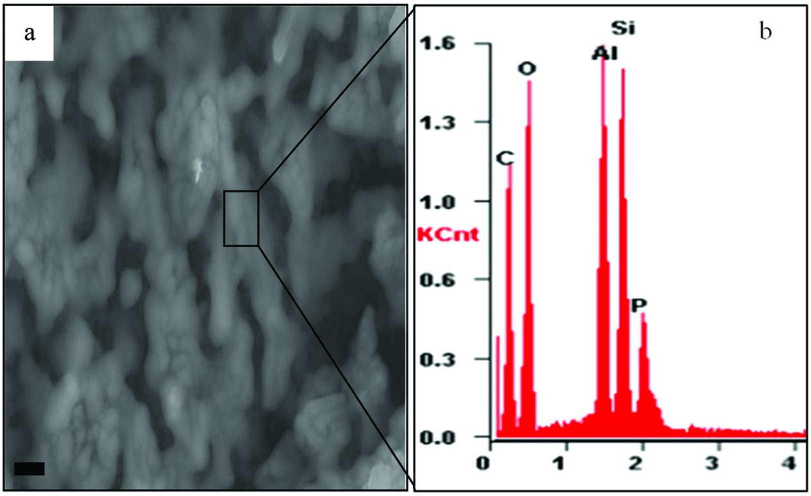

Figure 4. SEM images: (a) RDP-coated HNTs (b) EDAX of the square box (the scale bar is 0.3 μm).

From the figures we can see that dark phases are Ecoflex, which are aligned in the direction of extrusion and fairly dispersed in PLA matrix. These morphology dramatically changes when 5 % RDP starch is introduced to the blend. As a result, the fiber-like domains become spherical ones. It can lead to changing tensile properties. Pack et al. reported that the absorption of RDP to starch surfaces could increase compatibility of the PLA/Ecoflex blend, which led to an increase of strength and toughness. They also showed that surface energy of RDP starch could play a significant role on flame retardant properties, where the surface tension of RDP (~48 mN/m) is relatively higher than that of starch (35~45 mN/m) thereby the strong RDP absorption occurs at the starch surfaces. The surface tensions of the polymers are shown in Table 4. Moreover, from the table, we can see that the surface energy of PBAT is much higher than that of PLA, which may cause RDP starch be segregated at the interfaces between Ecoflex and PLA. This may be confirmed in the TEM image of the PLA/Ecoflex blends in Figure 5b.

Table 4. The surface tensions of polymers are obtained from contact angle measurement at a room temperature (at 25°C)

Polymer	*PLA*	*PBAT*	*Starch*	*RDP*
Surface Tension (mN/m)	37	53	35-42	48

In Fire and Polymers VI: New Advances in Flame Retardant Chemistry and Science; Morgan, A., et al.;
ACS Symposium Series; American Chemical Society: Washington, DC, 2012.

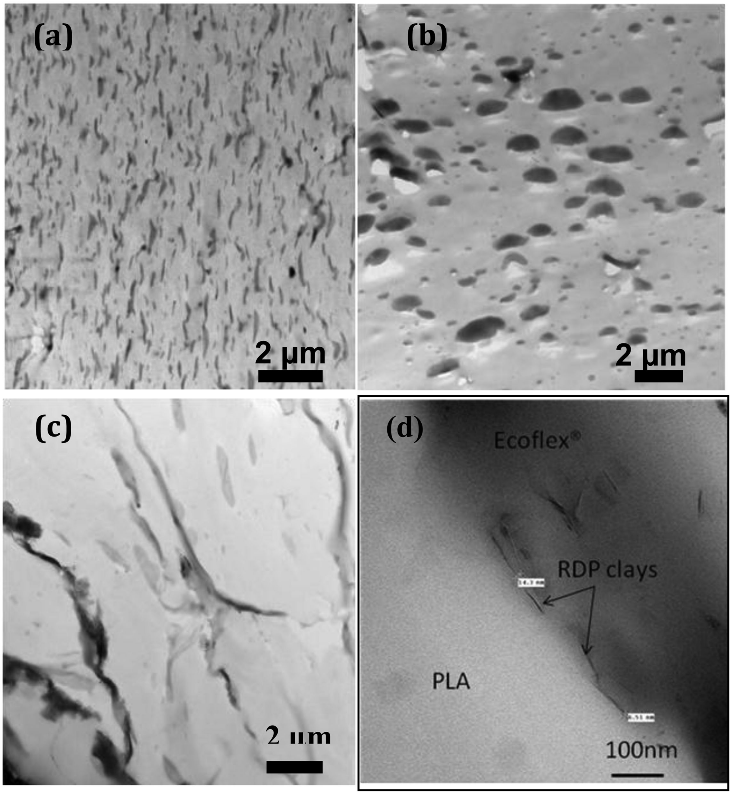

Figure 5. TEM images at PLA/Ecoflex blends with different RDP coated particles: dark phases are Ecoflex domains; (a) PLA/Ecoflex (80/20 wt%), (b) PLA/Ecoflex/RDP Starch (80/20/5 wt%), and (c) PLA/Ecoflex/RDP clays (80/20/5 wt%) (d) A high magnification of PLA/Ecoflex/RDP clays(80/20/5 wt%). (Reproduced with permission from reference (15). Copyright 2012 Elsevier).

On the other hand, the addition of RDP clay can change the Ecoflex domain in morphology. In Figure 6 we show the STXM data obtained from PLA/Ecoflex blends (wt percent 79/19) comparing the morphology when 5% starch or 5% RDP impregnated starch is added. In each case we can clearly see that the domains of the minority phase(Ecoflex), are significantly smaller in the samples where the starch was first impregnated with RDP. From Figure 5c-d we can also see that as the long fibers is aligned in the shear direction, the sharp interfaces between the blends become opaque. It can be indicated that the blend is more compatible since the RDP clays are localized at the interfaces. The localization of RDP clays may be predicted by a balance of surface energy between PLA/RDP and PBAT/RDP clays, where interfacial energy can be reduced by the inclusion of RDP clays in the blend.

As an expectation by the interfacial energy between RDP particles, a combination RDP-coated starch with RDP-coated clay could be given to more improvement on toughness and flame retardant properties of the biodegradable blends, which was reported in ref. (*15*). Moreover, In their previous report, a combination of two different particles might lead to a synergistic effect at interfacial area (*29*). Since the RDP starch particles were more likely to be segregated at interfaces between PLA and Ecoflex, RDP clays could be segregated into Ecoflex domains. As a result of that, more exfoliated RDP clays are observed, which is shown in Figure 5d. Thus, the ability of segregation of RDP-coated particles to either polymers or interfaces is mainly contributed to surface energy of each particle.

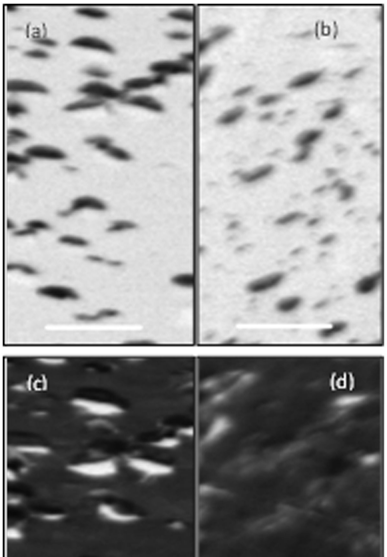

Figure 6. STXM images: (a) PLA/Ecoflex/starch (b) PLA/Ecoflex/RDP starch, taken at 284.7 eV; (c) PLA/Ecoflex/starch (d) PLA/Ecoflex/RDP starch, taken at 288.5 eV (the scale bar is 5 μm).

In Figure 7, we show that a series of SEM images of chars surfaces is examined in terms of microstructure. It is indicated that the different chars morphology can be confirmed by EDAX from each of chars surface. From the figure we can see that, in the case of neat starch/Ecoflex blend (60/40 wt%), the char surfaces seem to consist of strand-like bundles with many small holes. about a few micro sizes in diameter. However, when the HNTs are added, the small holes looks covered with the nanotubes, where the peak intensity of Si/Al is relatively higher than that of C/O in the EDAX. Moreover, when RDP clays are added in the blend, a network-like structures is observed at on the surface of the chars, as shown in Figure 8i. The structures become segregated when 2% HNTs/3% RDP clays is replaced with the 5% RDP clays. Later, the segregated network-like structures appears little at the char surface when 3% C20A is introduced in the blend, instead of the 3% RDP-coated clays. These morphology evolutions may be contributed to a competition of the surface tensions of either RDP-coated clays/HNTs or C20A/HNTs. Since we have reported that the surface tension of RDP is relatively higher than that of the di-tallow on the C20A (*28*), in the case of RDP clays/HNTs, RDP clays are more segregated to HNT clays, which can interrupt the network-like structures. The relatively lower surface energy of HNTs becomes a relatively high surface energy when C20A is added in the blends. As a result of that, there are no network-like structures at the exposed surface. Therefore, the two nanoparticles may compete with each other at interfaces. This competition of surface energy can determine the morphology of chars surface. The morphology is further confirmed by the EDAX spectra of the chars which are shown adjacent to the SEM images.

In Figure 7b we see that for the unfilled polymer, we see a large carbon peak and no Si or Al peaks are present. In Figures 7d we see that when neat HNT are added the carbon peak is reduced, while two peaks of similar amplitude are present corresponding to Si and Al. The spectra in Figure 7f corresponding to the addition of Closite 20A clay is similar, except that the Aluminum content relative to the silicate content is reduce in the clays. The reduced carbon peak in both spectra indicates that the HNT and the Cloisite 20A particles are enriched in the char at the expense of the polymer. In Figure 7h and 7j we show the spectra corresponding to the char formed when RDP impregnated clay is added. Here we find similar Aluminum to Si ratio, but the carbon peak is much larger and comparable to that found in the polymer sample, indicating that the near surface layer was mostly composed of the polymer matrix and the RDP clays were further into the interior of the char. Hence, even though biodegradable polymers have higher surface energies than most non-biodegradable polymers, the surface energy of RDP is still higher, addition of RDP clay causes enrichment of the polymer to the air surface when heated, and the larger carbon content in the char. Conversely, the high surface energy of the polymers allows enrichment of the surface with the relatively low surface energy neat HNT and Cloiste 20A particles, reducing the carbon component in the char.

It is well established that the char formation occurs at a nearly exposed surface from heat, which could prevent melt polymers underneath the chars (*30–32*). Both the rate of heat release and the rate of mass loss from cone calorimety have been typically used to interpret thermal behavior of polymers. In particular, charring polymers are well investigated since the mass loss rate dramatically reduces when chars are formed at an exposed surface against heat fronts (*28*, *33*). Recently, Pack et al. reported that the combination carbon nanotubes with clays could reduce the flammability since the carbon nanotubes were entangled with clay platelets, which may increase heat capacity of the system (*29*).

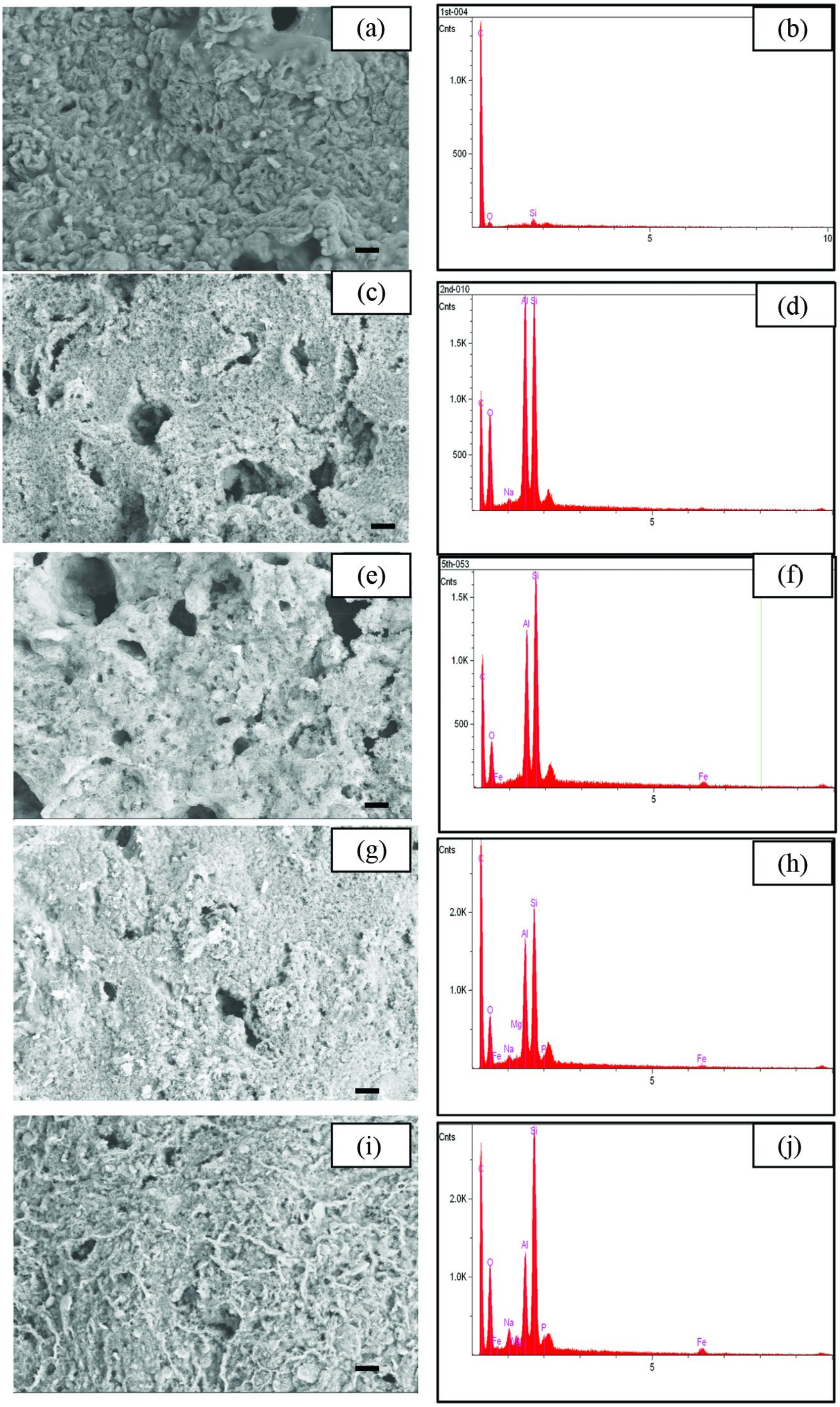
(a)
(b)
1st-004
Cnts
1.0K
500
C
O
Si
5
10
(c)
(d)
2nd-010
Cnts
1.5K
1.0K
500
C
O
Na
Al
Si
5
(e)
(f)
5th-053
Cnts
1.5K
1.0K
500
C
O
Fe
Al
Si
Fe
5
(g)
(h)
Cnts
2.0K
1.0K
C
O
Fe
Na
Mg
Al
Si
P
Fe
5
(i)
(j)
Cnts
2.0K
1.0K
C
O
Fe
Na
Mg
Al
Si
P
Fe
5

Figure 7. SEM images of the Residues: (a-b) Starch/Ecoflex (60/40 wt%), (c-d) Starch/Ecoflex/HNTs (60/40/5 wt%), (e-f) Starch/Ecoflex/C20A/HNTs (60/40/3/2 wt%) , (g-h) Starch/Ecoflex/RDP-coated clays/HNTs (60/40/3/2 wt%), and (i-j) Starch/Ecoflex/ RDP-coated clays (60/40/5 wt%), the scale bar is 20 micrometers.

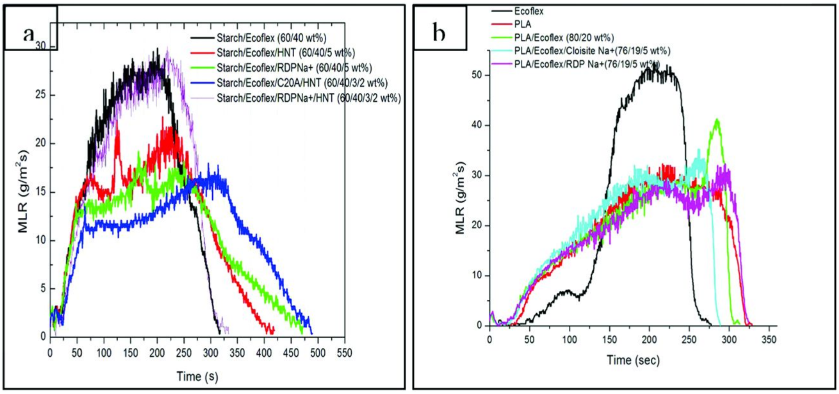

Figure 8. (a) The MLR of starch/Ecoflex with different nanoparticles in gasification at 50kW/m2 under N$_2$*. (Reproduced with permission from reference (15). Copyright 2012 Elsevier). (b) The MLR of PLA/Ecoflex with RDP starch in gasification at 50kW/m2 under N*$_2$*.*

A combination of two different nanoparticles can be also applied to biodegradable polymers in order to obtain the synergy in flammability. The MLR of the 60% starch/40% Ecoflex blends with different nanoparticles is shown in Figure 8a, where the addition of Cloisite 20A (C20A) leads to a greater reduction of the MLR trace of the blend with HNTs, which is about 12g/m^{2}s. Since the surface energy of C20A is relatively lower than the other components in the blend the C20A could segregate to the exposed surfaces, forming a char layers with the HNTs as a heat barrier, which may cause to lowering mass loss rate at the beginning in the burning process. However, the addition of RDP-coated MMT (RDP Na$^+$) does not reduce the initial mass loss rate of the starch/Ecoflex blend since the surface energy of the RDP nanoparticles is higher than that of the blend, and hence the RDP clay would not segregate to the surface. Rather, the MLR is similar to that of the starch homopolymer. Furthermore, in the case of the blend with RDP Na+ and HNTs, no steady plateau is obtained at the MLR, which may be attributed to formation of a softer char.

This kind of thermal response also occurs in blends of PLA/Ecoflex with nanoparticles. Since the surface energy of PLA is much lower than that of Ecoflex, it is reasonable to assume that the surface of the blend is enriched in the PLA component. Hence the MLR of all the compounds is determined by the component at the surface, or the one having the lower surface energy, which is shown in Figure 8b. from the figure we can see that the peak of MLR of the neat Ecoflex is dramatically reduced to about 30g/m^{2}s when PLA is added, which is similar to that of the neat PLA. However, when 5% Cloistie Na$^+$ is added in PLA/Ecoflex blend, the MLR trace of the blend is slightly increased, and the whole burning process is finished at an earlier time, about 275 sec. This may be attributed to a fact that Cloisite Na$^+$ clays could be regarded as an agglomerate in the blend, where local temperature/pressure gradient along the interfaces between the clays and polymers may be high enough to vaporize the polymer matrix. Since RDP is well known as a phosphours-based flame retardant and mainly retards combustion process of polymers in condense phases as a charring agent, the addition of RDP Na+ clays somewhat could reduce the MLR trace of the blend. It may be contributed to an excess of RDP on the clays. On the other hand, the addtition of RDP-coated starch can affect the rate of heat release(RHR) of the PLA/Ecoflex blend in cone calarimetry. In particular, the peak RHR of the blend is greately reduced when the RDP starch is added, which is shown in Figure 9. Thus, the addition of RDP coated particles could not only increase the compatibility but also improve the flammability of the blend.

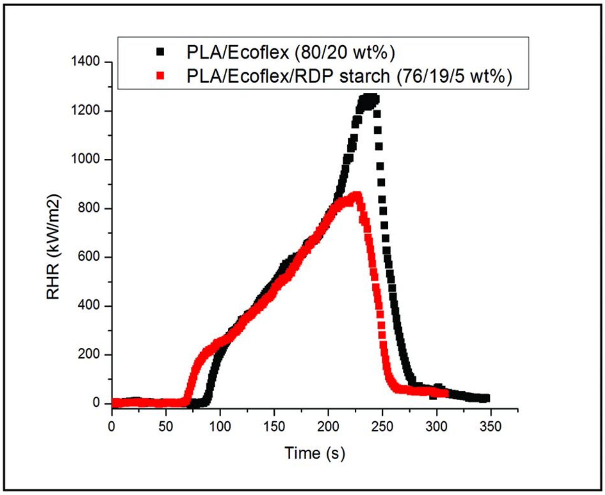

Figure 9. The RHR of starch/Ecoflex with RDP starch at 35kW/m^2 under air.

In previous paragraph , we discuss that surface energy of biodegradable polymers can be altered by the addition of nanoparticles, which also leads to different chars formation in microstructure. Pack et al. (*28*, *29*) reported that the flexibility of the chars layers might be important in reducing the MLR since the chars are most effective when they keep the hot gases from diffusing throughout the matrix, accelerating the decomposition process. The char formed by the unfilled polymer blend is usually the most ductile and free of holes. From Figure 7 above we showed that the morphology of the chars can be very different depending on the type of nanoparticle filler used. We showed that it was possible to quantify the hardness and modulus of the chars using nanoidentation (*15*). The results are tabulated in Table 5, where we see that soft char also produced the best MLR spectra. On the other hand, when the chars became too soft, and could not contain the gases, i.e. the results for the formulation with 5%HNT, the MLR we not reduced. Hence the best results were obtained with chars of intermediate rigidity, where had both, good mechanical integrity as well as ductility. The malfunctioned expandability of chars layers could decrease flame retardant properties, which was reported in ref (*15*). Therefore, measuring elastic modulus and hardness of chars surface is to understand a mechanism of stretching chars.

Table 5. The Elastic Modulus and Hardness of Starch/Ecoflex blends with different nanoparticles

Sample (wt%)	*Reduced Elastic Modulus (GPa)*	*Hardness (GPa)*
Starch/Ecoflex (60/40 wt%)	0.2	0.5
Starch/Ecoflex/HNTs (60/40/5 wt%)	5.3	0.78
Starch/Ecoflex/RDP clay (60/40/5 wt%)	2.5	0.43
Starch/Ecoflex/C20A/HNTs (60/40/3/2 wt%)	3.2	0.37
Starch/Ecoflex/RDP Na+/HNTs (60/40/3/2 wt%)	0.2	0.03

From the table we can see that when HNTs are added, the elastic modulus and hardness are 5.3 GPa and 2.5 GPa, respectively. However, when RDP clays are added to the blend, both E’ and H are reduced to 2.5 GPa and 0.43GPa, respectively, which may be explained with the morphology of chars formation in the previous paragraph, where the HNTs are uniformly segregated onto the char surface, whereas the RDP clays are well dispersed in the matrix. Therefore, the transformation of a ductile chars layer when the RDP clays are introduced can explain the mechanism of expanding chars formation, which ultimately lead to an improvement of flame retardant properties, such as MLR and RHR. Moreover, when 3% C20A is added in the blend, the char layers become more plastic deformed, which may indicate that a maximum capacity of expansible chars increases against heat fronts. This can be contributed to a balance of surface energy of between polymers/particles, where the HNTs may have highest surface tension against the polymer blend, Therefore, the mechanical properties of chars layers may be taken into consideration in order to reduce the flammability of polymer blends.

Conclusion

We first review recent flame retardant formulations on biodegradable polymer blends, such as either starch/ poly(butylene adipate-co-terephthalate) (PBAT) or poly(lactic acid)/poly(butylene adipate-co-terephthalate) (PLA/PBAT), where interfacial tensions of the biodegradable polymer blends can play an important role on mechanical and flame retardant properties. The improved material properties are also mainly influenced by morphology of the blends. In addition, a novel approach to increase not only compatibility but also flame retardancy of the biodegradable polymer blends is reviewed. In this method, an aryl phosphate flame retardant, resorcinol di(phenyl phosphate) (RDP), can act as a surfactant on either starch or clays. The strong absorption of RDP to the particles leads to segregation of the Ecoflex domains in the PLA matrix. Therefore, the addition of RDP-coated particles could render the biodegradable polymer blends self-extinguishing since rigid shell-like chars are formed on the exposed surface which act as a barrier against the heat front. In addition, the shell also changes the effective viscosity and prevents dripping of polymer melts.

We also found that the surface energy f\of the components in the polymer blend can determine the flame retardant characteristics. We found that the surface energy determines which component will segregate to the blend surface when the material is heated. The nature of this component then determines the time to ignition, as well as the mechanical properties of the char which forms during combustion Hence the char properties, as well as the time to ignition can be controlled by judicious choice of the lower surface energy component.

Nanidentation measurements of the chars showed that the best results were obtained when the char was ductile and could sustain the large internal pressures from the decomposing gases. Containment of the gases resulted in steady state release, and lower MLR values.

Acknowledgments

Support from the NSF MRSEC and CBET divisions is gratefully acknowledged. We would like to thank Prof. Chad Korach for performing the nanodientation measurements and discussion regarding their interpretation. The help of Neil Muir and Ezra Bobo was invaluable in sample preparation in the early part of this work.

References

1. United States Environmental Protection Agency-Office of Solid Waste (5306P), EPA530-R-06-011, 2006; www.epa.gov.
2. Soderstrom, G.; Sellstrom, U.; De Witt, C. A.; Tyskind, M. *Environ. Sci. Technol.* **2004**, *38*, 127–32.
3. Anh, M. Y.; Filley, T. R.; Jafver, C. T.; Nies, L. *Environ. Sci. Technol.* **2006**, *40*, 215–20.
4. Viberg, H.; Fredriksson, A.; Jakobson, E. *Toxicol. Sci.* **2003**, *76*, 112–20.
5. Ray, S. S. *Progr. Mater. Sci.* **2005**, *50*, 962–1079.

6. Vroman, I.; Tighzert, L. *Materials* **2009**, *2*, 307–304.
7. Gross, R. A.; Bhau, K. *Science* **2002**, *97*, 803–807.
8. Lipinsky, E.; Sinclair, R. *Chem. Eng. Prog.* **1986**, *82*, 26.
9. Jiang, L.; Wolcott, M.; Zhang, J. *Biomacromolecules* **2006**, *7*, 199–207.
10. Zhang, N.; Wang, Q.; Ren, J.; Wang, L. *J. Mater. Sci.* **2009**, *44*, 250–256.
11. Wei, L.; Wang, D.; Chen, H.; Chen, L.; Wang, X.; Wang, Y. *Polym. Degrad. Stab.* **2011**, *96*, 1557–15610.
12. Volker Frenz, D. S. *ANTEC* **2008**, 1682–1684.
13. Witt, U.; Eining, T.; Kleeberg, Y. M.; Deckwer, W.; Muller, R. *Chemosphere* **2001**, *44* (2), 289–99.
14. Gallo, E.; Schartel, B.; Acierno, D.; Russo, P. *Eur. Polym. J.* **2011**, *47*, 1390–1401.
15. Pack, S.; Bobo, E.; Muir, N.; Yang, K; Swaraj, S.; Ade, H.; Cao, C.; Korach, C. S.; Kashiwagi, T.; Rafailovich, M. H. *Polymer* **2012**, *53*, 4787–4799.
16. Wang, D.; Song, Y.; Wang, L. X.; Yang, Y. *Polymer* **2011**, *94*, 233–238.
17. Hu, Z.; Chen, L.; Zhao, B.; Luo, Y.; Wang, D.; Wang, Y. *Polym. Degrad. Stab.* **2011**, *96*, 320–327.
18. Reti, C.; Casetta, M.; Duquesne, S.; Bourbigot, S.; Delobel, R. *Polym. Adv. Technol.* **2008**, *19*, 628–635.
19. Zhan, J.; Song, L.; Nie, S.; Hu, Y. *Polym. Degrad. Stab.* **2009**, *94*, 291–296.
20. Wang, D.; Leuteritz, A.; Wang, Y.; Wagenknecht, U.; Heinrich, G. *Polym. Degrad. Stab.* **2010**, *95*, 2474–2480.
21. Song, L.; Nie, S.; Hu, Y. *Polym. Degrad. Stab.* **2009**, *94*, 291–296.
22. Ma, X. F.; Yu, J. G.; Wan, J. J. *Carbohydr. Polym.* **2006**, *64*, 267–273.
23. Walenta, E.; Fink, H.; Weigel, P.; Ganster, J.; Schaaf, E. *Macromol. Mater. Eng.* **2001**, *286*, 462–471.
24. Altskar, A.; Andersson, R.; Boldizar, A.; Koch, K.; Stading, M.; Rigdahl, M.; Thunwall, M. *Carbohydr. Polym.* **2008**, *71*, 591–597.
25. Averous, L.; Martin, O. *Polymer* **2001**, *42*, 6209–6219.
26. Wang, X.; Hu, Y.; Song, L.; Xuan, S.; Xing, W.; Bai, Z.; Lu, H. *Ind. Eng. Chem. Res.* **2011**, *50*, 713–720.
27. Si, M.; Araki, T.; Ade, H.; Kilcoyne, A.; Fisher, R.; Sokolov, J. C.; Rafailovich, M. H. *Macromolecules* **2006**, *36*, 4793–4801.
28. Pack, S.; Kashiwagi, T.; Cao, C.; Korach, C.; Rafailovich, M. *Macromolecules* **2010**, *43*, 5338–5351.
29. Pack, S.; Kashiwagi, T.; Stemp, D.; Koo, J.; Si, M.; Sokolov, J. C.; Rafailovich, M. H. *Macromolecules* **2009**, *42*, 6698–6707.
30. Kashiwagi, T.; Mu, M.; Winey, K. I.; Cipriano, B.; Raghavan, S.; Pack, S.; Rafailovich, M.; Yang, Y.; Grulke, E.; Shields, J.; Harris, R.; Douglas, J. *Polymer* **2008**, *49*, 4358–4368.
31. Tang, T.; Lewin, M.; Pearce, E. M. *Macromol. Rapid Commun.* **2006**, *18*, 1545–1549.
32. Lewin, M.; Pearce, E. M.; Levon, K.; May-Marom, A.; Zammarano, M.; Willkie, C. A.; Jang, B. N. *Polym. Adv. Technol.* **2006**, *17*, 226–234.
33. Pack, S.; Si, M.; Koo, J.; Sokolov, J. C.; Koga, T.; Kashiwagi, T.; Rafailovich, M. H. *Polym. Degrad. Stab.* **2009**, *93*, 306–326.

Chapter 28

Milligram Scale Flammability Testing of Flame Retardant Polyurethane Foams

Alexander B. Morgan*

**University of Dayton Research Institute, 300 College Park,
Dayton, OH 45469-0160
*E-mail: alexander.morgan@udri.udayton.edu**

To speed up the development of new flame-retardant chemistries for polyurethane foam, there is a strong need for small-scale flammability tests, especially those which work at the milligram scale. In this paper we discuss current results using the only standard milligram heat release test (Pyrolysis combustion flow calorimetry – ASTM D7309) to study how some commercial flame retardants work in flexible polyurethane. Flexible polyurethane foams formulated to pass small flame ignition regulatory tests showed only small reductions in measured heat release when compared to non-flame retardant foams. This suggests that reductions in heat release are not the primary mechanism by which these additives pass these regulatory tests (FMVSS 302, TB-117) and additional testing in combination with ASTM D7309 may be needed to understand performance and further develop this technique for future flame retardant polyurethane chemistries.

Introduction

Flexible polyurethane foams present a significant risk of catastrophic fire loss in the home, should items that contain them (bedding / furniture) catch fire and not be extinguished within 5 minutes of ignition (*1–4*). The reason for this high chance of fire loss due to flashover type events is that polyurethane foam, when it burns, drips and flows to form a pool-type fire which leads to rapid increases

In Fire and Polymers VI: New Advances in Flame Retardant Chemistry and Science; Morgan, A., et al.;
ACS Symposium Series; American Chemical Society: Washington, DC, 2012.

in heat release (*5*, *6*). While flame retardants do exist for polyurethane foams, most of them are optimized against small ignition sources (cigarettes, small open flames) (*7*, *8*) and do not address the dripping and fuel pool fire should larger ignition sources be present. However, there are robust flame retardant systems that address this dripping behavior when foams are used in aircraft (*9*) or in the United Kingdom (*10*), but for most commercial goods in the US containing flexible polyurethane foam, the dripping upon burning that leads to faster flame growth remains an unsolved problem. To that end, there is a need for new reactive flame retardants which can co-polymerize with the polyurethane backbone during foam synthesis so that they present no environmental concerns later (*11–13*), and also have a flame retardant mechanism that causes the polyurethane to char rather than drip and flow. While there are some new potential flame retardants which show potential for reactivity and char formation in polyurethanes (*14–16*), there is much more work to do before they can be considered for commercial flame retardant solutions. Specifically, these additives need to be scaled up, tested for commercial viability, and have their environmental, health, and safety (EH&S) issues tested *before* they can be used. This research must be done in addition to regulatory scale fire testing to confirm that the new flame retardant provides satisfactory fire safety, and all of this testing results in significant costs to the researcher, whether they be academic or industrial. Before such resources can be committed, there needs to be some confidence that the lab-scale evaluation of new flame retardants has a high chance of success at larger scale. Therefore, there is need for a small-scale test which can screen through lots of different chemical structures using commercial, EH&S, and flammability criteria **before** resources are consumed scaling up the flame retardant additive. Some commercial and EH&S screening models exist which work regardless of scale, but a small-scale screening test for definite flammability screening criteria does not exist today. However, one particular small-scale test which measures heat release may be appropriate in this role, and that is the pyrolysis combustion flow calorimeter, or PCFC, also known as the microcone calorimeter, MCC.

PCFC is a 5-50 mg scale heat release test which uses oxygen consumption calorimetry to determine the inherent heat release of a material (*17*). This small-scale test is an ASTM method (ASTM D7309-07) and has been used successfully as a screening tool for several polymeric materials (*18–21*), but has yet to be used for polyurethane foam flame retardant development. Because of the prior success with this technique for developing flame retardant materials, and because it has been used to quantify heat release as an effect of chemical structure (*22*), PCFC seems as if it could be a potent screening tool for future flexible polyurethane foam development with new flame retardant chemistries. With this in mind, research was undertaken to see if the PCFC could be used to understand how commercial flame retardants work in polyurethane foam to pass existing regulatory small-scale flame tests. Specifically, do these flame retardant (FR) additives yield significant reductions in heat release which leads to the passing of the test, or do the FR additives provide a passing result via another mechanism?

In light of the discussion about the need of a technique that can screen for flame retardant performance before scale-up of the new flame retardant chemical, it is important to say what this work is meant to accomplish and what it does not do. This work is meant as a starting point to take a look at what commercial flame retardants achieve in flexible polyurethane foam from a small scale heat release test. To date, no one has published what the heat release of commercial flame retardant polyurethane materials is when measured by PCFC, and so just obtaining that measurement and sharing it with the broader community has value. By measuring how these flame retardants affect heat release in flexible polyurethane foam, we have some starting information to begin building a model of flame retardant screening for polyurethane foams. So the work in this chapter is an initial observation that hopefully this researcher and other groups can build upon. This work is not intended to validate what amount of heat release is required to achieve a passing result in regulatory tests. Nor is this work giving any indication that the measurements within are the definitive explanation for how the flame retardants work to enable polyurethane to pass the test. Again, it is an initial investigation and the hope is that this paper will inspire others to publish their own data on flexible polyurethane foams that pass regulatory tests with the PCFC so we can see and share the wider range of heat release behavior provided by different flame retardants and flame retardant approaches.

In this paper the results of such a study are presented by measuring the heat release of two sets of commercial flame retardant flexible polyurethane foams. The first set of foam studied was optimized to pass a small flame ignition, horizontal orientation, flame spread test (FMVSS 302) used to rate the fire performance of foams in automobile seating. The second set of foam studied was optimized to pass a small flame ignition, vertical orientation, flame spread test (California Technical Bulletin TB-117) used for foams sold in US-made upholstered furniture. Details on these specific regulatory tests can be found in reference #3. Since no flame spread or specific flame test data for these two regulatory tests was provided for the foams tested in this report, no attempt will be made to correlate the results of PCFC to these two tests.

Experimental Section

Flame retardant polyurethane foams containing commercial flame retardants were provided by Israeli Chemical Ltd. (ICL) and Clariant GmbH, and were used as received. The exact composition of the flame retardant foams was not provided by the manufacturers, other than the general flame retardant present in the foam. PCFC testing was conducted via ASTM D7309-07, in triplicate, using Method A (pyrolysis under N_2, 1 °C/sec heating rate) with the use of a MCC-1 instrument (Govmark, NJ, USA). Typical results from the PCFC, including char yield, heat release rate (HRR) peak values (in W/g) and HRR peak temperatures, were recorded.

Results and Discussion

The samples for the FMVSS 302-rated foams utilized reactive (will react into the polymer backbone during foam synthesis) phosphate-based flame retardants. These flame retardants, Exolit OP550 and Exolit OP560, are phosphate polyols, and while the exact chemical structure was unknown, some general details were provided by the manufacturer (Figure 1). The samples for the TB-117-rated foams had non-reactive flame retardants, namely an organochloro phosphate (Fyrol FR2) and a polymeric organophosphate (Fyrol PNX), which are shown in Figure 1.

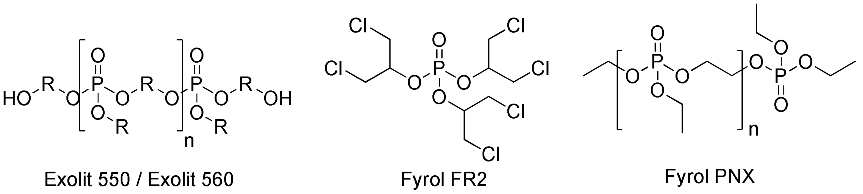

Figure 1. Chemical Structures of Flexible Polyurethane Foam Flame Retardants.

With each set of foams optimized for a particular regulatory test, a set of control foams (no flame retardant) was provided for each set. First we will discuss the FMVSS 302 foams and then the TB-117 foams.

For the FMVSS302 foams, there is not a great deal of difference in the measured heat release rates for these materials, as can be seen in Figures 2 and 3, when comparing the flame retardant sample to the control sample. Indeed, the only major difference noted is that the first peak of heat release is reduced in the flame retardant samples when compared to the control sample. Even the temperatures at which the peak HRR occurs are mostly the same, although they do seem to occur about 10-15 °C lower when compared to the control sample. OP550 yields a slight reduction in the second peak of HRR as well, while OP560 seems to increase the second peak of HRR slightly. Total HR is reduced though with the use of flame retardant, and char yields are slightly increased as well.

While there is no definitive chemical analysis data available to comment exactly on the chemical flame retardant mechanism provided by these additives, the data suggests that the flame retardants do not seem to change the known polyurethane thermal decomposition chemistry. Flexible polyurethanes typically decompose in two steps (*1*, *14*). The first, (lower temperature,) event is the decomposition of the urethane groups which leads to pyrolysis of the chemical structures associated with the starting isocyanate monomers used to produce the foam. The second, (higher temperature,) event is where the polyols decompose and pyrolyze. This two-step phenomena is seen in the FMVSS 302-rated samples (Figures 2 and 3), and other than some minor reductions in heat release, there is very little difference between the samples (Table 1). While the % error and uncertainty have not been officially published in the ASTM D7309, these differences in heat release, while reproducibly measured, are likely not statistically significant and therefore cannot be used to differentiate the samples. Therefore, some other sort of mechanism is likely occurring with these polyphosphate additives that allow the foams containing them to pass the FMVSS 302 test. Since we do not have actual FMVSS 302 test data for these samples, nor any physical observations on how these samples passed the test, we cannot make any further commentary on the results.

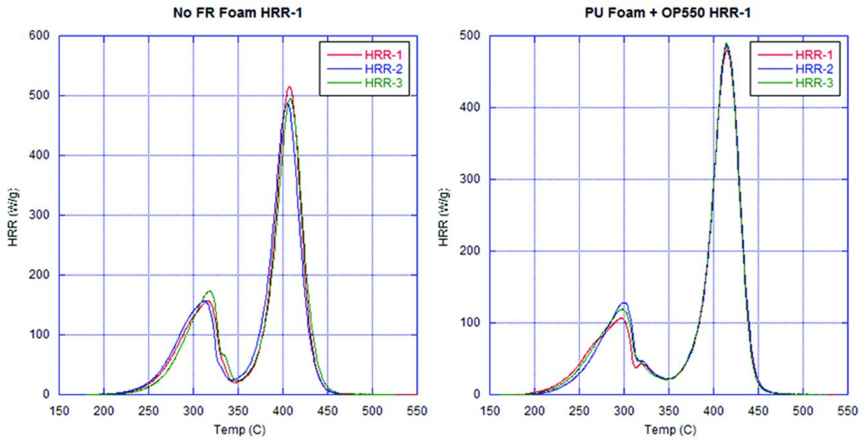

Figure 2. HRR for FMVSS 302 Control foam (left) and Flame Retardant Foam with OP550 (right).

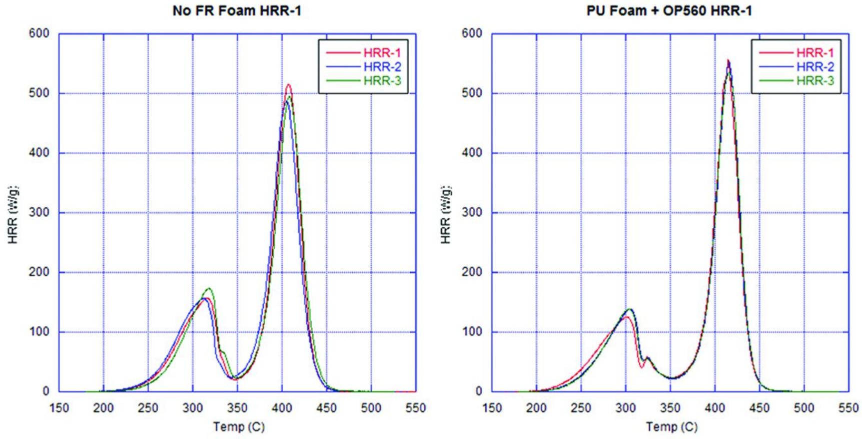

Figure 3. HRR for FMVSS 302 Control foam (left) and Flame Retardant Foam with OP560 (right).

Table 1. Heat Release Data for FMVSS 302-Rated Foams

Sample	*Char Yield (wt%)*	*HRR Peak(s) Value (W/g)*	*1st peak HRR % Reduction*	*2nd peak HRR % Reduction*	*Peak Temps (°C)*	*Total HR (kJ/g)*	*Total HR % Reduction*
Non FR	0.21	157, 514	n/a	n/a	316, 408	27.0	n/a
Flex PU Foam	0.37	156, 486	n/a	n/a	312, 405	27.0	n/a
	0.51	173, 496	n/a	n/a	319, 409	27.1	n/a
OP 550	1.93	107, 479	34	4	298, 415	25.7	4.9
Flex PU Foam	1.99	129, 488	20	2	300, 416	25.8	4.6
	1.91	118, 490	27	2	299, 415	25.7	4.9
OP 560	0.49	125, 552	23	-11	300, 415	26.3	2.7
Flex PU Foam	0.87	139, 554	14	-11	306, 416	26.3	2.7
	0.74	138, 535	15	-7	304, 416	26.3	2.7

In Table 1 the measured heat release and % reductions in peak HRR and total HRR for the FMVSS 302 samples are shown. OP550 shows a 20-34% reduction in first peak HRR, only a 2-4% reduction in second peak HRR, and 4.6-4.9% reduction in total HR. OP560, on the other hand, shows a 14-23% reduction in first peak HRR, a 7-11% increase in second peak of HRR, and a 2.7% reduction in total HR. So assuming the loading of flame retardant was the same in both foams, OP550 is the superior flame retardant in regards to passing the test and reducing heat release. However, since the official % uncertainty and error for the ASTM D7309 technique has not yet been published by ASTM, no definite error bars can be given for the data. Discussions with other experts who have used the PCFC as well as the reviewer of this paper suggest that the differences are not significant. So what can be said about the results? While the differences may be within assumed % error of the technique, it is worth noting that the data is quite reproducibly different. Clearly the flame retardants have some effect on heat release, even if it is minor. So if the heat release reduction is small, and more of an effect is noted on the first peak of HRR than the second, one can conclude that these flame retardants inhibit thermal decomposition of the urethane groups in the polymer structure and subsequently delay pyrolysis of the isocyanate monomer groups. This suggests that the flame retardants slow initial thermal decomposition and mass loss of the flammable isocyanate-based monomers, which may in turn slow flame spread in the FMVSS 302 test. Admittedly this is speculation, and two things are needed to verify this point further: 1) a larger sample set of more flame retardant foams which pass FMVSS 302 with different flame retardant chemistries, and 2) chemical analysis confirming vapor-phase or condensed-phase activity, plus physical property analysis looking at polymer viscosity during burning (dripping away from flame to slow flame spread). Existing literature suggests that these polyphosphates likely have both vapor- and condensed-phase chemistry (*23*), so with that information, more work is needed before the PCFC data can be interpreted further.

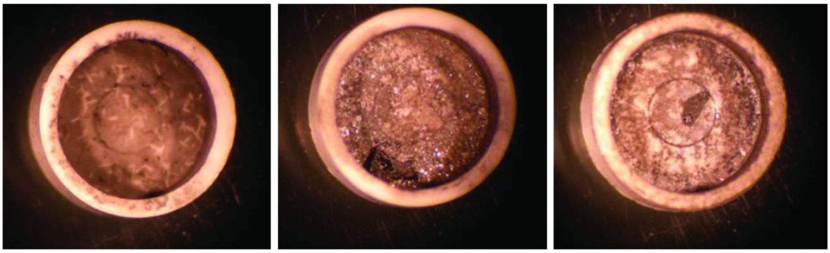

Figure 4. Final chars for FMVSS control foam (left), Flame Retardant Foam with OP550 (center), and Flame Retardant Foam with OP560 (right).

Also of note when discussing the FMVSS 302 samples, the chars for these samples collected at the end of the PCFC test are shown in Figure 4. As can be seen, all of the samples showed very little residual char remaining, indicating that none of these materials generate a lot of char when they thermally decompose, and that they likely flow during burning (*2*), which is indicated by the presence of black residue all over the PCFC test crucible by the end of the test (Figure 4). Some small "chunks" of char do remain with the OP550 and OP560 containing samples though.

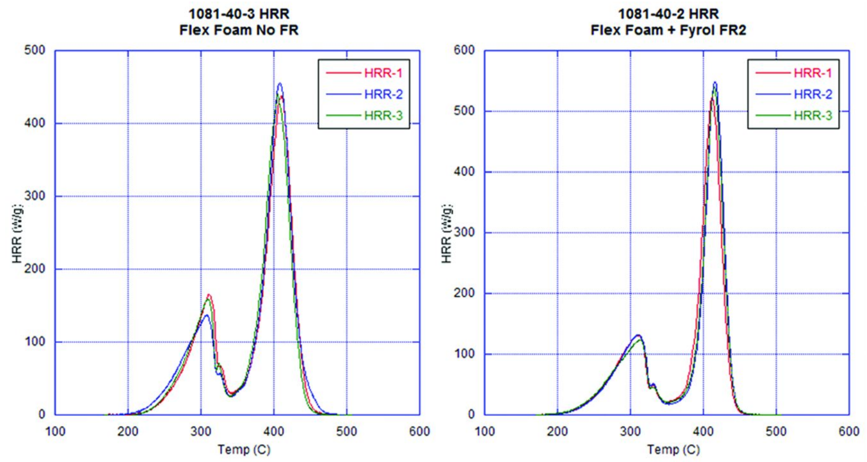

Figure 5. HRR for TB-117 Control foam (left) and Flame Retardant Foam with Fyrol FR2 (right).

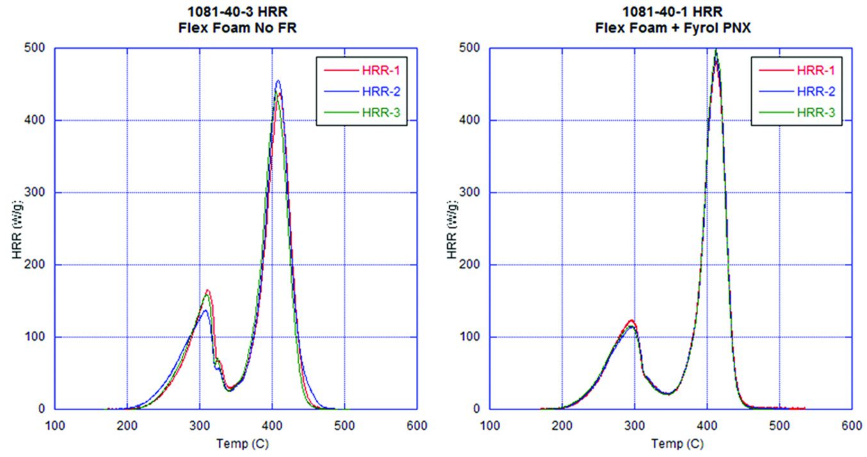

Figure 6. HRR for TB-117 Control foam (left) and Flame Retardant Foam with Fyrol PNX (right).

For the TB-117-rated foams, as with the FMVSS 302 samples, the differences in heat release are minor. The use of flame retardant results in a reduction of the first peak of HRR, but a slight increase in the second peak of HRR is noted as well. The temperatures of the first peak of heat release are either slightly decreased by

10-15 °C (Fyrol FR2) or unchanged (Fyrol PNX). Total HR is always reduced with the TB-117-rated flame retardant samples, although char yields are not always increased with Fyrol FR2 generating considerably more char than Fyrol PNX. This is worth noting on since normally decreases in total HR are accompanied by increases in measured char yield (*18*, *20*). Otherwise, the shapes of HRR for the flame retardant and control samples are very similar, as can be seen in Figures 5 and 6. Again, a two-peak HRR is observed, with the first peak corresponding to the thermal decomposition of the isocyanate-based monomer and the second peak to the decomposition and pyrolysis of the polyol.

The measured heat release reductions are shown in Table 2, and as with the FMVSS 302 samples, reductions in peak HRR and total HR are observed for the samples that pass this test. For Fyrol PNX, there is a 19-25% reduction in first peak HRR and a 4.9-5.7 % reduction in total HR. The second peak of HRR increases, however, by about 6-10%. Fyrol FR2 shows a 14-20% reduction in first peak of HRR and a 6.8-7.1% decrease in Total HR, but second peak of HRR increases by 15-21%. Since the two flame retardants are not at equal loading, one cannot make an exact comparison of performance, but when looking at this data, Fyrol PNX is more effective at reducing the first peak of HRR, and almost as effective at reducing Total HR, at half the loading of flame retardant. The increase in second peak of HRR for these materials likely is related to the chemical mechanism of flame retardancy that these two flame retardants bring to polyurethane, but it is counterintuitive that the flame retardant reduces one aspect of heat release while increasing another. Specifically, the flame retardants seem capable of reducing the mass loss and heat release caused by the thermal decomposition of the urethane groups, but appear to accelerate the pyrolysis or decomposition of the polyol. As with the FMVSS 302 discussion, it can be argued that these results are not statistically significant, although they are reproducible measurements. Therefore, the following comments can be made about the TB-117-rated foam data:

- The flame retardants seem to inhibit initial decomposition and pyrolysis of the urethane groups, and slowing this initial heat release may slow flame spread.
- Definite chemical and physical analysis of the thermally decomposed foams is needed to verify the mechanism of “passing” the TB-117 test. The data only suggests, and does not prove, that a reduction in urethane decomposition and pyrolysis occurs, but it also suggests an increase in polyol decomposition which may yield a dripping effect in the TB-117 test where the foam drips away from the flame source, thus limiting flame spread.
- More flame retardant foams rated to pass TB-117 with different flame retardant chemistries are needed to determine whether the measured results here are flame retardant specific, or something always required for any TB-117 foam to pass the test.

Table 2. Heat Release Data for TB-117-Rated Foams

Sample	*Char Yield (wt%)*	*HRR Peak(s) Value (W/g)*	*1st peak HRR % Reduction*	*2nd peak HRR % Reduction*	*HRR Peak Temp (°C)*	*Total HR (kJ/g)*	*Total HR % Reduction*
1081-40-3	0.52	165, 438	n/a	n/a	312, 411	27.2	n/a
Flex - no FR	0.51	137, 456	n/a	n/a	308, 408	27.6	n/a
	0.55	159, 469	n/a	n/a	309, 405	26.6	n/a
1081-40-1	1.72	124, 483	19	-6	295, 412	25.8	4.9
Flex - 6 parts	1.78	114, 497	26	-9	297, 413	25.6	5.7
Fyrol PNX	1.54	115, 498	25	-10	293, 412	25.6	5.7
1081-40-2	0.24	131, 523	15	-15	311, 412	25.3	6.8
Flex - 12 parts	0.28	132, 549	14	-21	310, 416	25.3	6.8
Fyrol FR2	0.24	123, 540	20	-19	313, 415	25.2	7.1

Final chars for the TB-117-rated foams are shown in Figure 7. These foams flowed during thermal decomposition, but did form some fragments of char, as can be seen in the crucibles. However, these fragments are quite small, and as can be seen from the data in Table 2, these foams are not robust char formers.

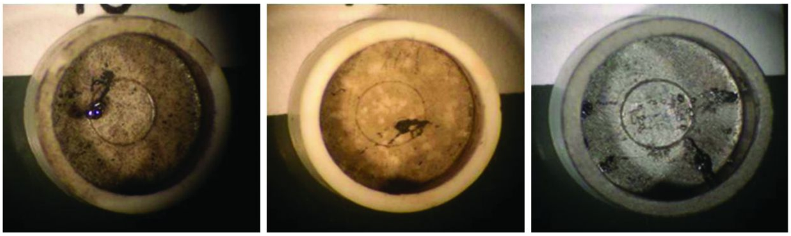

Figure 7. Final chars for TB-117 control foam (left), Flame Retardant Foam with Fyrol FR2 (center), and Flame Retardant Foam with Fyrol PNX (right).

Conclusions

Using PCFC with flame retardant flexible foams rated for regulatory tests gives some information about how the flame retardants may be working to provide a passing result, but the results are not definitive. Flexible polyurethane foams have a two-step decomposition, the first step being caused by the decomposition of the urethane groups in the polymer, and the second step being caused by polyol decomposition. This was measured with the PCFC as a two peak heat release, with the first peak coming from urethane decomposition/pyrolysis and the second peak coming from polyol decomposition and pyrolysis. In the case of the FMVSS 302 foams, which used reactive polyphosphate flame retardants (phosphates that react into the polymer backbone), there is a reduction in the first peak of heat release, but little to no reduction in the second peak of heat release. This suggests, but does not prove, that these flame retardants help the foam pass the horizontal flame spread test by slowing urethane decomposition chemistry and pyrolysis. However, since the residue in the PCFC crucibles at the end of the test suggests that the polymer flowed during decomposition, one cannot rule out that the polymer dripping away from the flame may also play a role in achieving a passing result in the FMVSS 302 test. Similar behavior of first and second peak of heat release is also seen for the TB-117 foams, which are rated to pass a vertical flame spread test. Specifically, the first peak of heat release is reduced while the second peak of heat release either is unchanged or increases. So again, the flame retardants (a chloroalkyl phosphate and a polymeric non-reactive phosphate) used to provide passing results in TB-117, suggest that they help slow down urethane group decomposition and pyrolysis, but have little effect on polyol decomposition and pyrolysis. Also similar to the FMVSS 302 samples, final residues from the PCFC crucibles suggests that the foams may flow during decomposition, and so a combination of slowing of urethane decomposition plus dripping away from the flame cannot be ruled out as the mechanism of passing TB-117 for these foams.

Admittedly these conclusions are speculative and not definitive, especially in light of the fact that the % error and uncertainty for the PCFC measurements are still not officially known, and therefore the differences in the samples are believed not to be greatly significant. Therefore one can ask, “Why bother using PCFC at all for these materials?” or “Why have you wasted our time publishing this if there are no definitive results?” The answer to these questions is simply this: There is no other small-scale milligram test available to measure heat release of materials, which is a fundamental aspect of material flammability and flame retardancy; and therefore, this technique is a good starting point because there is no other milligram scale test available. Based upon the data in this paper, to advance PCFC as a tool for polyurethane development further, the following is needed:

- A larger sample set of flexible polyurethane foams in which the chemical composition is known, so chemical structure of the flame retardant and its effect on heat release (if important) can be used to predict % chance of passing a specific regulatory test.
- Known flame spread / fire phenomena for the samples tested in FMVSS 302 and TB-117 (or other relevant polyurethane tests) so that physical effects of flame retardant mechanism can be captured.
- Additional measurements to confirm which flame retardant chemistries are appropriate to evaluate with the PCFC, and which ones are not.

Returning to the introduction, if new flame retardant chemistries are to be developed, one needs to develop small-scale tests to minimize the risks and costs of synthesizing, registering, and developing new chemicals. So far, only the PCFC continues to show this potential, and indeed, the PCFC has been used with some success to predict % likelihood of passing the 12-second flame exposure, vertical orientation, Federal Aviation Administration test based upon the measured heat release of flame retardant flexible polyurethane foams used in aircraft seating (*24*). So with that potential being reported, it still makes sense to use the PCFC for future flame retardant polyurethane foam development. Before that potential can be fully achieved, though, more samples must be tested and a wider range of chemistries must be studied to develop a database that can predict % chance of passing larger scale regulatory tests. It is the author’s belief that the data in this paper is a starting point, and he hopes that others will build upon this data to enable the potential of the PCFC to be fully reached.

Acknowledgments

The author wishes to thank Kathleen Beljan, Mary Galaska, and Kathy Schenck for their assistance in collecting the PCFC data shown in this report. Thanks also goes to Israeli Chemical Ltd. (Sergei Levchik for technical discussions, Barbara Williams and Emanuel Pinzone for foam sample fabrication) and Clariant GmbH (Timothy Reilly for project coordination, Elke Huthmacher and Frank Osterod for PU foam sample fabrication) for the kind donation of commercial flame retardants and flame retardant polyurethane foams. The author also wishes to thank numerous reviewers of this paper (and previous versions) who have greatly improved the concept of using PCFC for flame retardant material development. Funding for this work was provided by the US taxpayer through the National Institute of Standards and Technology Fire Research Grant # 70NANB9H9183.

References

1. Lefebvre, J.; Le Bras, M.; Bastin, B.; Paleja, R.; Delobel, R. Flexible Polyurethane Foams: Flammability. *J. Fire Sci.* **2003**, *21*, 343–367.
2. http://www.nist.gov/el/fire_research/charleston_102810.cfm (accessed 06/07/12).
3. http://fire.nist.gov/fire/fires/sofa/sofa.html (accessed 06/07/12).
4. Hirschler, M. M. Polyurethane foam and fire safety. *Polym. Adv. Technol.* **2008**, *19*, 521–529.
5. Kramer, R. H.; Zammarano, M.; Linteris, G. T.; Gedde, U. W.; Gilman, J. W. Heat release and structural collapse of flexible polyurethane foam. *Polym. Degrad. Stab.* **2010**, *95*, 1115–1122.
6. Denecker, C.; Liggat, J. J.; Snape, C. E. Relationship Between the Thermal Degradation Chemistry and Flammability of Commercial Flexible Polyurethane Foams. *J. Appl. Polym. Sci.* **2006**, *100*, 3024–3033.
7. *Technical Bulletin 117 – Requirements, Test Procedure and Apparatus for Testing the Flame Retardance of Resilient Filling Materials Used in Upholstered Furniture*; State of California Department of Consumer Affairs; March 2000.
8. Federal Motor Vehicle Safety Standard No. 302. *Flammability of Interior Materials - Passenger Cars, Multipurpose Passenger Vehicles, Trucks, and Buses*; http://www.nhtsa.gov/cars/rules/import/fmvss/index.html#SN302 (accessed 06/07/12).
9. Federal Aviation Regulations 25.853-1. *Flammability Requirements for Aircraft Seat Cushions*; http://www.fire.tc.faa.gov/pdf/25-853.pdf (accessed 06/07/12).
10. British Standard (BS) 5852:2006. *Methods of test for assessment of the ignitability of upholstered seating by smouldering and flaming ignition sources*.
11. Stapleton, H. M.; Dodder, N. G.; Offenberg, J. H.; Schantz, M. M.; Wise, S. A. Polybrominated Diphenyl Ethers in House Dust and Clothes Dryer Lint. *Environ. Sci. Technol.* **2005**, *39*, 925–931.
12. Betts, K. S. Unwelcome Guest: PBDEs in Indoor Dust. *Environ. Health Perspect.* **2008**, *116*, A202–209.
13. Betts, K. S. New Thinking on Flame Retardants. *Environ. Health Perspect.* **2008**, *116*, A210–213.
14. Levchik, S. V.; Weil, E. D. Thermal decomposition, combustion and fire-retardancy of polyurethanes – a review of the recent literature. *Polym. Int.* **2004**, *53*, 1585–1610.

15. Singh, H.; Jain, A. K. Ignition, Combustion, Toxicity, and Fire Retardancy of Polyurethane Foams: A Comprehensive Review. *J. Appl. Polym. Sci.* **2009**, *111*, 1115–1143.
16. Benin, V.; Durganala, S.; Morgan, A. B. Synthesis and flame retardant testing of new boronated and phosphonated aromatic compounds. *J. Mater. Chem.* **2012**, *22*, 1180–1190.
17. Lyon, R. E.; Walters, R. N. *J. Anal. Appl. Pyrolysis* **2004**, *71*, 27–46.
18. Stoliarov, S. I.; Crowley, S.; Walters, R. N.; Lyon, R. E. *Combust. Flame* **2010**, *157*, 2024–2034.
19. Cogen, J. M.; Lin, T. S.; Lyon, R. E. *Fire Mater.* **2009**, *33*, 33–50.
20. Lyon, R. E.; Takemori, M. T.; Safronava, N.; Stoliarov, S. I.; Walters, R. N. *Polymer* **2009**, *50*, 2608–2617.
21. Lyon, R. E.; Walters, R. N.; Stoliarov, S. I. *Polym. Eng. Sci.* **2007**, 1501–1510.
22. Walters, R. N.; Lyon, R. E. *J. Appl. Polym. Sci.* **2002**, *87*, 548–563.
23. Modesti, M.; Lorenzetti, A. FR Design for Foam Materials. In *Fire Retardancy of Polymeric Materials*, 2nd ed.; Wilkie, C. A., Morgan, A. B., Eds.; Taylor and Francis: Boca Raton, FL, 2010; ISBN 978-1-4200-8399-6.
24. Davis, R. D.; Lyon, R. E.; Takemori, M. T.; Eidelman, N. High Throughput Techniques for Fire Resistant Materials Development. In *Fire Retardancy of Polymeric Materials*, 2nd ed.; Wilkie, C. A., Morgan, A. B., Eds.; Taylor and Francis: Boca Raton, FL, 2010; ISBN 978-1-4200-8399-6.

Chapter 29

Smoldering in Flexible Polyurethane Foams: The Effect of Foam Morphology

**Mauro Zammarano,*,[1] Szabolcs Matko,[1] Roland H. Krämer,[1]
Rick D. Davis,[1] Jeffrey W. Gilman,[2] Li Piin Sung,[3]
Douglas M. Fox,[1] and Shivani Mehta[4]**

**[1]Fire Research Division, Engineering Laboratory, National Institute of Standards and Technology (NIST), Gaithersburg, Maryland 20899
[2]Polymers Division, Material Measurement Laboratory, and Engineering Laboratory, National Institute of Standards and Technology (NIST), Gaithersburg, Maryland 20899
[3]Materials and Structural Systems Division, Engineering Laboratory, National Institute of Standards and Technology (NIST), Gaithersburg, Maryland 20899
[4]Directorate for Engineering Sciences, U.S. Consumer Product Safety Commission, Rockville, Maryland 20850
*E-mail: mauro.zammarano@nist.gov**

Flexible polyurethane foams with different cell morphology (cell size and fraction of open cells) were prepared. The effect of foam morphology on smoldering was assessed. Cell-size, in combination with air permeability, appeared to be a good indicator for smoldering propensity in the range of formulations investigated here.

Introduction

Smoldering is a self-sustaining heterogeneous oxidation reaction that induces a slow, low temperature, flameless combustion. Flexible polyurethane foams (PUF) are prone to smoldering due to their high air permeability, low density and high specific surface area. Smoldering of PUF poses a serious fire hazard because

Not subject to U.S. Copyright. Published 2012 by American Chemical Society
In Fire and Polymers VI: New Advances in Flame Retardant Chemistry and Science; Morgan, A., et al.;
ACS Symposium Series; American Chemical Society: Washington, DC, 2012.

it typically yields a substantially higher yield of toxic carbon monoxide (CO) per unit mass of fuel than does flaming (though at a lower rate), and because it can initiate flaming (by transition from smoldering to flaming) with heat sources otherwise too weak (*1*).

Smoldering of upholstered furniture and bedding remains a threat to life and property, despite the promising introduction of Reduced Ignition Propensity cigarettes in all 50 states (*2*). Upholstered furniture and bedding remain the most frequent “first items to ignite” that result in residential fire deaths in the United States (*3*). According to estimates by the U.S. Consumer Product Safety Commission (CPSC), a large number of these fire deaths can be attributed to smoldering materials commonly found in upholstered furniture and bedding.

Smoldering in PUF has been studied extensively; however, an experimental assessment of the key parameters affecting smoldering propensity of such materials has been limited by the difficulties in obtaining foam samples with consistent and homogeneous properties (*4*, *5*).

Numerical simulation of smoldering combustion of PUF indicated the significance of oxygen supply on the rate of smolder propagation (*6–10*). Thermal analysis of the foams has been performed in great detail in order to obtain multi-step models of foam pyrolysis and char oxidation that provided input data for models (*8*). However, morphological description of the PUF has been limited to the simplest terms.

In this study we characterize the morphology of conventional PUF (cell size, strut thickness, and open versus closed cell structure) by direct morphological indicator (*e.g.*, cell size) or indirect morphological indicators (*e.g.*, apparent density, air permeability and specific surface area) that are related to the foam morphology. Custom made batches of PUF were prepared according to the National Institute of Standards and Technology (NIST) specifications and were obtained from a commercial manufacturer (foamer). Each foam was characterized in terms of smoldering (assessed by cigarette-mockup test, see below for a description of the method) and morphology. Finally, the potential correlation between smoldering and the aforementioned morphological indicators is discussed.

Our results show that PUF foam with a largely closed-cell structure and low permeability does not smolder in the mockup test. This is in agreement with the common perception that, for natural convection smoldering, air permeability (*i.e.*, oxygen supply) is the key parameter and that smoldering always increases with air permeability (*11*, *12*). However, for conventional foams with a largely open-cell structure and air permeability above a threshold value, smoldering appeared to be surprisingly independent of air permeability and dominated by other properties of PUF. This unexpected result shows a need for a better morphological description of the foam structure. For open-cell foams with relatively high permeability and given chemical composition, smoldering appeared to be controlled by the average cell size rather than air permeability. As a corollary, smoldering-resistant PUF can be prepared by promoting a large cell structure independently of the air permeability of the foam.

Experimental (*13*)

Materials

All materials were used as-received unless otherwise indicated. Commercial-grade polyether triols with a molar mass between (3000 and 3200) g·mol^{-1} and OH number between (50.5 and 57.5) mg KOH·g^{-1} (data provided by the manufacturer, uncertainties not available), were used. Similarly, commercial-grade organo/silicone surfactants for PUF were selected. As discussed elsewhere (*14*), the specific polyol and surfactant did not show any systematic significant effect on smoldering and, for sake of conciseness, are not further specified here. The other reagents used were toluene diisocyanate (TDI) (mass ratio mixture of 2,4- (80%) and 2,6-isomers (20%)), water, an amine based catalyst (DABCO **33LV**, Airproducts), a polyether based catalyst (Niax **C323**, Momentive), a tin-catalyst (Kosmos 29, **K29**, Evonik) and a fatty ester emulsifier (Addotovate **D1092**, RheinChemie).

Sample Preparation

Foam samples were prepared in a small pilot plant or in a production line by the foamer. In both cases, all reagents were pumped at a controlled rate into a fixed mixing chamber (mixing head). The pressure in the mixing head was adjusted by controlling a valve at the outlet in a range between (35 to 124) kPa. In the pilot plant, the material was transferred from the mixing head to a foaming box through a feeding tube. After 15 min at room temperature, the foams were cured in an oven at 110 °C for 1hour and post-cured at room temperature for an additional 24 hours. In the production line, the ingredients of the foam formulation were discharged through the nozzle of the mixing head and deposited onto the front of a conveyor belt. The temperature of the foam typically reached about (150 to 170) °C in water-blown foams. Curing was completed in air, and no post-curing was required. Samples were cut with an automatic laser system. All samples were conditioned at a temperature of (21 ± 3) °C and between 50 % and 66 % relative humidity for at least 24 hours prior to testing.

Sample Characterization

Mass loss due to **smoldering** in PUFs **(ML$_{\text{Mockup}}$)** was measured by the upholstery cover fabric smoldering ignition resistance test (*Mockup Test*), described in the CPSC's proposed flammability standard for upholstered furniture (*15*), which aims to mimic a realistic ignition scenario for upholstered furniture. Briefly, two pieces of PUF are placed at right angles to one another, simulating the seat and back of a chair. The surface of the foam to be tested is covered by an upholstery fabric. A lit cigarette (Standard Cigarette for Ignition Resistance Testing, NIST SRM 1196) (*16*) is placed in the crevice formed by the two foam pieces, and is then covered by a piece of a standard lightweight fabric, a 100 %

cotton, white plain weave of (19 to 33) threads/cm^2, and areal density of (115 ± 1) g·m^{-2}. The test result is the mass loss of the foam specimens (after removing the charred material) during the 45 min duration of the test. A cotton upholstery fabric with consistent high smoldering (100 % cotton, indigo twill weave and an average aerial density of 445 g·m^{-2} ± 3 g·m^{-2}) was selected for this study and used with all foams for assessing the smoldering propensity of the foam.

The openness or porosity of PUF was described by measuring the **air permeability (Φ)**. Briefly, the volume of air flowing per unit of time through a PUF sample with a given thickness and area at a given differential pressure is measured. An electronic high differential pressure air permeability measuring instrument (FAP 5352 F2, Frazier Precision Instrument Co. Inc., Hagerstown, MD) was used in this study. Foam was cut into samples (90 x 90 x 13) mm^3 and placed in a circular clamp, exposing a surface of 38.5 cm^2 to perpendicular air flow. The target pressure-drop through the 13 mm thick foam slice was set to 127 Pa (13 mm of water). Nozzles with orifice diameters of 1.0 mm, 1.4 mm, 2.0 mm, 3.0 mm, 4.0 mm, 6.0 mm, 8.0 mm, or 11.0 mm were used in order to reach the target pressure drop. The tests were conducted at room temperature. The values of air permeability (Φ) are expressed in terms of volumetric air flow as cubic meters per square meter of sample per min (or simply meters per min) at a temperature of 0 °C and a pressure of 100 kPa. Air permeability was measured by the foamer for all the buns (replicate foams poured per each formulation) on a foam slice collected near the center point between pour start and pour end, and at a depth of about 2.5 cm from the top surface of the foam. The foam slice was cut parallel to the bottom surface of the bun. For selected buns, multiple air permeability measurements were performed to evaluate the variation of air permeability throughout the bun.

The surface area of PUF was calculated by Brunauer-Emmett-Teller (BET) measurements (*17*) carried out by Micromeritics, US. The BET values of surface per unit mass of sample are then converted into mass per unit volume (specific surface area) dividing the BET values by the apparent density of the sample (ρ). The **specific surface area (SSA)** is defined here as surface per unit volume and it is expressed in inverse meters. The samples used for BET measurements were about (1 x 1 x 23) cm^3.

The cell size is expressed in terms of average cross-sectional cell area measured in two-dimensional images with an area of (11.9 x11.9) mm^2 and scanned by a confocal microscope (Zeiss LSM 510) with an optical thickness of 19.75 µm. For each foam location, three confocal images were acquired from orthogonal planes to account for possible anisotropy in the foam. The cross-sectional cell area in a specific foam location is calculated as the average value of cell area calculated for these three orthogonal planes. The **cell size (Σ)** for a PUF is calculated by averaging the values of cross-sectional cell area in at least three specific foam locations. Similarly, the standard deviation for Σ is calculated using the cross-sectional cell areas in multiple locations (at least three).

Image analysis of confocal images was carried out by an ImageJ plug-in (*18*) capable to directly segment a gray-level image using a local-maxima algorithm. A Gaussian filter blurring with a diameter of 20 pixels was applied to remove noise and prevent over-segmentation before applying the local-maxima algorithm (noise tolerance: 2, output type: segmented particles). Finally, the ImageJ macro "analyze particle" was used for calculating the area of each segmented particle (*i.e.*, cell) that is not on the edge of the image and has a combination of area above 0.02 mm^2 and circularity (*19*) equal or above 0.75 (to remove small artifacts and minimize over-segmentation).

Table 1. Formulation identification names, number of replicates per formulation and processing conditions (uncertainties for the dosing units and pressure were not determined by the foamer)

	Replicate Foams	*K29[‡] (php)*	*H_2O (php)*	*P (kPa)*
F1	4	0.21	3.04	34.5
F1R	4	0.21	3.04	34.5
F2	4	0.13	3.04	34.5
F3	4	0.16	3.04	34.5
F4	8	0.16	2.95	34.5
F5	4	0.16	2.95	55.2
F6	4	0.16	2.60	34.5
F7	4	0.19	2.7	55.2
F8	4	0.16	2.7	55.2
F9	4	0.16	2.7	34.5
F10	4	0.19	2.7	34.5
F11	4	0.19	2.95	34.5
F12	4	0.19	2.95	55.2
F13	16	0.16	2.95	34.5
F14	14	0.15	2.95	48.3
F15	12	0.15	2.95	48.3
F16[*]	1	0.16	2.95	104
F17[*]	1	0.16	2.95	124
F18[*,†]	1	-	-	-

[‡] ***Tin Catalyst.*** [*] ***Foamed on a production line.*** [†] ***Commercial PUF (unknown composition).***

Formulations

The formulations, processing conditions and number of replicate foams (buns) poured per each formulation are described in Table 1.

The TDI index (percentage ratio between the actual amount of TDI used in a formulation and the theoretical stoichiometric amount of TDI required to react with any reactive additive, *e.g.*, water and polyols) was kept constant at a value of 105 for all formulations by adjusting the content of TDI. The amount of each component in a formulation is expressed in parts per hundred polyols (php) (*20*).

The uncertainty for the dosing units and pressure were not determined by the foamer. The surfactant and polyol loadings were equal to 1 php and 100 php, respectively. The two catalysts, 33LV and C-323, were used at a constant loading of 0.06 php each. Formulations F1 to F15 were prepared in a small pilot plant (approximate bun dimensions: 0.8 m x 0.5 m x 0.2 m), formulations F16 to F17 were prepared in an industrial production line (approximate bun dimensions: 1.1 m x 1.6 m x 13.0 m). Some formulations (F4 to F14) required 0.15 php of a processing aid (D1092), due to the relatively low ambient temperature during foaming. Formulation F18 is a standard high-smoldering commercial PUF of unknown formulation, used here as an arbitrary benchmark.

Results and Discussion

Foams are three-dimensional structures containing gas bubbles (cells). In PUF, cells are polyhedrons, most closely described as dodecahedrons with pentagonal faces, separated from each other by thin sections of polymer: the foam struts (polymer at the shared edge of the polyhedrons) and the foam membranes or windows (polymeric thin film connecting the struts on a face of the polyhedron). An open-cell is a cell with only open windows, *i.e.*, no residual membrane. A closed-cell is a cell completely separated from the adjacent ones by windows. PUFs typically contain closed and open cells, as well as partially open cells (cell with few residual membranes).

PUF morphology is strongly affected by the formulation and the **processing parameters** (*i.e.*, water content, tin catalyst content and head pressure) reported in Table 1. They are routinely adjusted during PUF manufacturing to compensate for morphological variations caused by climatic conditions (*i.e.*, variations in atmospheric temperature, humidity and pressure) in order to deliver a PUF with consistent specifications throughout the year. Water is essential for the blowing action by reacting with TDI and releasing CO_2, the tin catalyst accelerates the rate of the polyol/TDI reaction, and the head pressure affects nucleation and cell growth at the exit of the mixing head (*14*). The cell size increased with an increase in mixing pressure and water level, and a decrease in tin catalyst. The open-/closed-cell ratio, as well as air permeability, increased with an increase in water content, and a decrease in mixing pressure and tin catalyst content (*14*).

Table 2. Values of density (ρ), air permeability (Φ), specific surface area (SSA) and smoldering (ML_{Mockup}). Uncertainty is shown as one standard deviation

	ρ ($kg \cdot m^{-3}$)	Φ ($m \cdot min^{-1}$)	$SSA^{\dagger}$ ($10 \cdot m^{-1}$)	ML_{Mockup} (%)
F1	30.1±0.8	77.1±5.2	454±55	30.5±12.1
F1R	28.4±0.3	87.5±15.2	-	0.5±0.2
F2	29.1±0.3	81.7±5.7	-	32.0±2.3
F3	28.8±0.2	77.7±8.6	-	29.3±6.5
F4	30.1±0.6	74.2±8.4	-	8.1±3.4
F5	30.4±0.3	44.8±4.1	384±46	0.2±0.1
F6	33.8±0.8	33.4±5.5	-	0.5±0.2
F7	31.6±0.4	4.7±1.7	-	0.5±0.6
F8	33.6±0.5	16.6±4.1	-	0.7±0.2
F9	34.3±0.6	59.7±3.4	-	15.2±5.6
F10	30.7±0.7	3.1±0.4	-	1.2±0.5
F11	29.2±0.6	43.3±5.9	572±69	2.5±2.2
F12	28.4±0.6	12±12	517±62	0.3±0.3
F13	30.9±0.9	78.4±4.6	374±45	21.5±10.6
F14	30.1±0.8	70.9±10.7	300±36	10.0±2.5
F15	29.9±0.6	78.5±6.9	309±37	1.2±0.3
F16	26.9±0.5	83.9±13.3	345±43	19.6±5.5
F17	29.1±0.4	27.9±4.1	-	1.3±1.0
F18	28.1±0.4	-	-	28.9±4.0

† ***Typical uncertainty values measured for F16.***

In this study, the processing parameters were systematically varied in order to tune the properties of PUF in terms of air permeability (closed- vs. open-cell structure) and/or cell size. The density, the air permeability and the specific surface area of these PUFs are reported in Table 2. Variations for these foam properties were observed between different buns of the same formulation (bun-to-bun variability), due to intrinsic foaming repeatability limitations, and different locations in the same bun (in-bun variability), due to foam heterogeneity. The average and standard deviation for each property is reported in Table 2. Density and air permeability were measured in the same center location for each bun of formulation F1 to F15 (pilot plant foams), or in multiple locations (at least four) of the same large bun produced in the production line (formulation F16 to F18). Smoldering (ML_{Mockup}) was measured for each formulation over at least three replicate samples from one or two buns. The specific surface area was measured for each formulation over one or two replicate measurements. A relative standard deviation of 12 % for SSA, calculated over nine repeated measurements on formulation F16, is assumed as typical standard deviation for all formulations of Table 2.

The effect of these foam properties on smoldering propensity, measured in terms of mass loss in the mockup test, is evaluated in the following sections.

Effect of Apparent Density (ρ)

The apparent density controls the net fuel load and thermal inertia of PUFs. Numerical simulation of smoldering combustion of PUF indicated an inversely proportional relationship between ρ and propagation velocity in opposed smoldering (*12*).

Smoldering in terms of ML_{Mockup} is plotted vs. density in Figure 1 for all formulations of Table 2. There is no suggested trend, so density does not appear to be a critical parameter for smoldering in PUF at least in the scenario and range of densities investigated here.

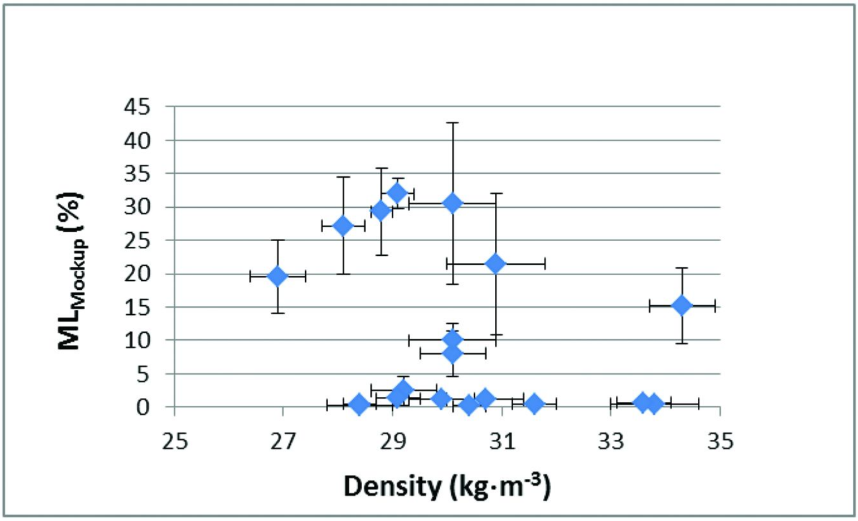

Figure 1. Values of density (ρ) vs. smoldering (ML_{Mockup}). Uncertainty is shown as one standard deviation.

Effect of Air Permeability (Φ)

Oxygen supply to the smoldering front is commonly described as the limiting factor that controls the amount of heat produced by thermal degradation of PUF. An increase in oxygen supply promotes the exothermic oxidation reaction of PUF to char (i.e., smoldering) and inhibits the endothermic pyrolytic tar formation (*21*). In general, oxygen transport inside a porous medium is accomplished by diffusion and convection. In natural-convection smoldering of PUF, unless the cell structure is completely closed, oxygen transport through the foam occurs mainly by convection and the determining factor in the generation of the buoyant flow is the pressure loss through the virgin foam (*11*, *12*). According to Darcy's law (*22*), the air permeability of the foam is inversely proportional to its pressure loss. These considerations suggest that, for a given PUF formulation, natural-convection smoldering increases with air permeability.

The experimental data of Figure 2, where ML_{Mockup} is plotted versus air permeability for all formulations of Table 2, show the perception that smoldering propensity increases with air permeability is too simplistic.

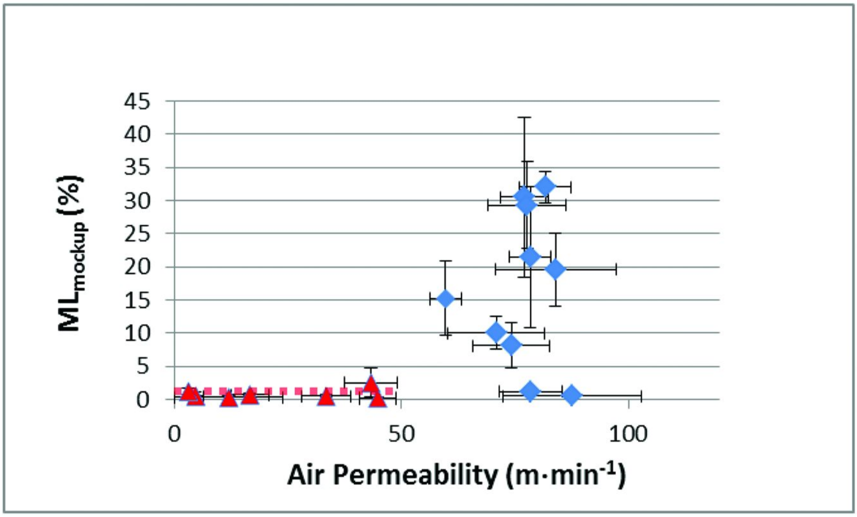

Figure 2. Smoldering versus air permeability for all formulations of Table 2. The data are split in two sets: the diamond-shaped data points (formulations with an air permeability below a threshold value $\Phi_{threshold} \approx 50$ m·min^{-1}) and the triangle-shaped data points (formulations with $\Phi > \Phi_{threshold}$). The dotted line is a least-squares regression fit to the triangle-shaped data points (uncertainty shown as one standard deviation).

Negligible smoldering (below 3 % mass loss) was observed for formulations with an air permeability below a threshold value ($\Phi_{threshold}$) of about 50 m·min^{-1} (triangle-shaped data points). Above this threshold value (diamond-shaped data points), there is no apparent correlation between the air permeability and smoldering. Thus, an air permeability above $\Phi_{threshold}$ is a necessary but not sufficient condition for achieving a high smoldering PUF. The data of Figure 2 are average values for a given formulation and, as previously discussed, are affected by both, in-bun variability and bun-to-bun variability.

In Figure 3, the average ML_{Mockup} measured for eight different buns of formulation F13 (at least three measurements per bun) is plotted as a function of the air permeability (one measurement per bun). Each data point is not affected by bun-to-bun variability but it is still affected by in-bun variability. The typical standard deviation due to in-bun variability for the air permeability of these buns was calculated as follow. Four buns with high air permeability ($\Phi > 70$ m·min^{-1}) were selected. For each bun, the air permeability was measured in three locations (center, pour start and pour end) and a relative standard deviation was calculated. The average value of these four relative standard deviations was used as typical standard deviation in the data of Figure 3.

Despite the large uncertainties, mainly due to the intrinsic variability of the foam properties throughout the bun, it appears that smoldering decreases when the air permeability increases. The dotted line in Figure 3 is a least-squares regression fit to the data points and has a coefficient of determination $R^2 = 0.49$. These data indicate that, at least for high values of air permeability (above 70 m·min^{-1}) and for the formulations and smoldering scenario investigated here, air permeability is not the dominating morphological factor, and that there are parameters other than air permeability that affect smoldering.

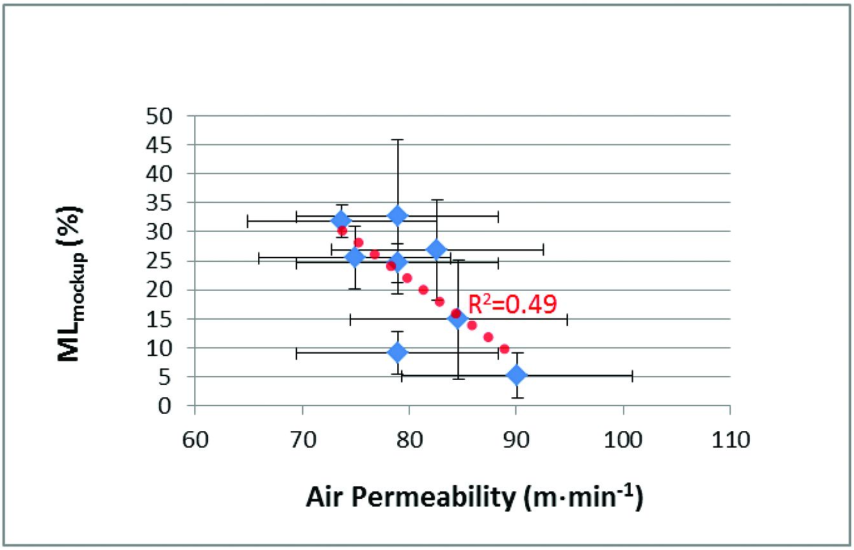

Figure 3. Average ML_{Mockup} versus air permeability for eight buns of formulation F13. The dotted line is a least-squares regression fit to the data points with a coefficient of determination $R^2 = 0.49$. Uncertainty is shown as one standard deviation.

In Fire and Polymers VI: New Advances in Flame Retardant Chemistry and Science; Morgan, A., et al.;
ACS Symposium Series; American Chemical Society: Washington, DC, 2012.

Effect of Specific Surface Area (SSA)

The effect of SSA on smoldering is two-fold. First, smoldering is a heterogeneous reaction and, as such, the smoldering rate is expected to increase with the surface area. Second, the thermochemistry of PUF degradation is affected by SSA (*23*). The volume fraction of material subject to smoldering (exothermic reaction) *vs.* the volume fraction of material subject to pyrolysis (endothermic reaction) increases with SSA; therefore, the heat of degradation of PUF is expected to increases with SSA.

The values of SSA were measured for eight formulations of Table 2. The relative ML_{Mockup} data are plotted in function of SSA in Figure 4.

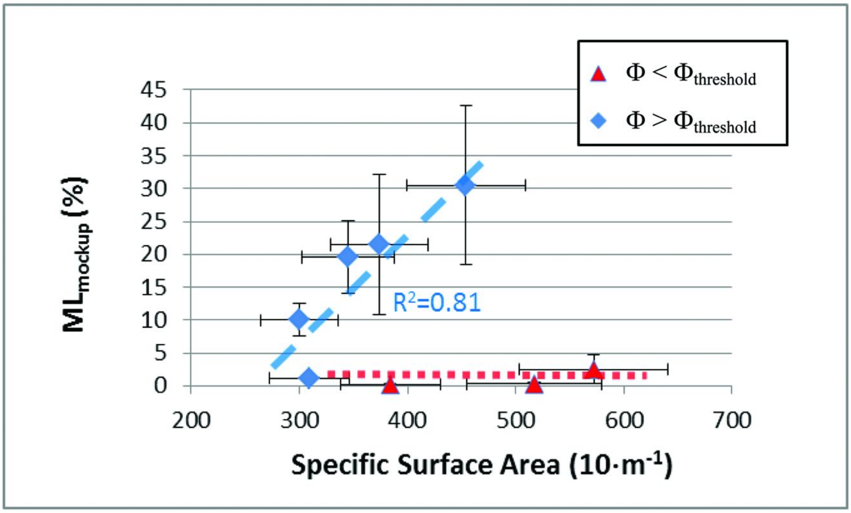

Figure 4. ML_{Mockup} versus specific surface area for eight formulations of Table 2. The dashed and dotted lines are least-squares regression fits to formulations with $\Phi < \Phi_{threshold}$ (triangle-shaped data points) and $\Phi > \Phi_{threshold}$ (diamond-shaped data points), respectively. The uncertainty is shown as one standard deviation.

The dashed and dotted lines are least-squares regression fits to the formulations with $\Phi < \Phi_{threshold}$ (triangle-shaped data points) and $\Phi > \Phi_{threshold}$ (diamond-shaped data points), respectively. The dashed line is a decent fit to the data (coefficient of determination R^2 = 0.81) considering the observed heterogeneity in foam properties.

These data indicate that:

- for $\Phi > \Phi_{threshold}$, SSA plays a key role in smoldering of PUF and ML_{Mockup} increases sharply with SSA (the linear fit indicates that, approximately, a 50 % increase in SSA generates a four-fold increase in smoldering);
- for $\Phi < \Phi_{threshold}$, smoldering is dominated by limited oxygen supply and $ML_{Mockup} \approx 0$ even for values of SSA > 500 m^{-1}.

In completely open-cell foams, SSA is generated only by struts but, in general, SSA accounts for the surface of both residual windows and struts. An increase in the number of residual windows causes a decrease in air permeability and convective buoyancy until the point where, in a completely closed cell, oxygen transport through the foam is controlled by diffusion rather than convection. Due to the limited oxygen-supply rate, the smoldering propensity at a given SSA value for a largely closed foam ($\Phi < \Phi_{threshold}$) is lower than a largely open foam ($\Phi > \Phi_{threshold}$).

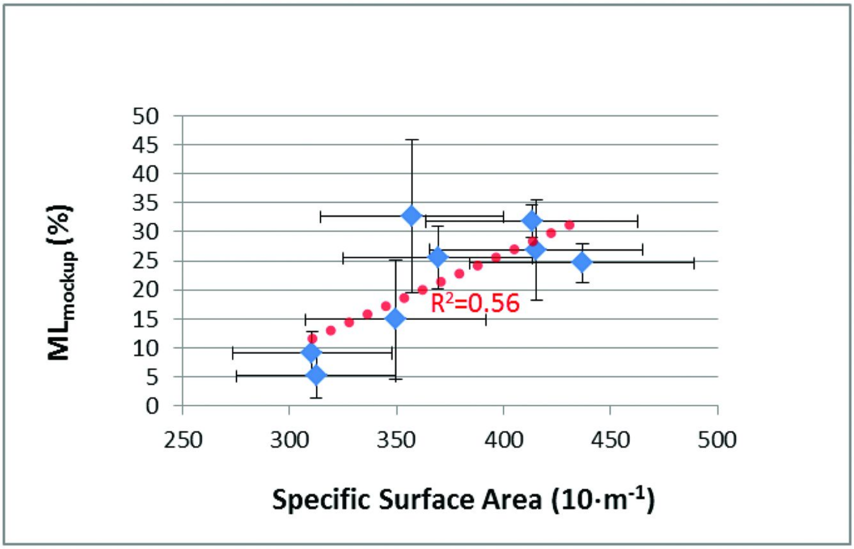

Figure 5. Smoldering (ML_{Mockup}) for eight buns of formulation F13 (same of Figure 3) as a function of the specific surface area. The dotted line is a least-squares regression fit to the data points with a coefficient of determination R^2=0.56 (uncertainty shown as one standard deviation).

To further support the role of SSA for $\Phi > \Phi_{threshold}$, the ML_{Mockup} data of the formulations in Figure 5 are plotted as a function of SSA (Figure 5). As already observed, there was a large scatter in these foams due to in-bun variability; however, the linear fit in Figure 5 (coefficient of determination R^2=0.56) indicates that smoldering increases when the specific surface area increases. Noticeably, data of ML_{Mockup} as a function of air permeability for the same buns (Figure 3), showed that smoldering increased when air permeability decreased. These data suggest that the increase in surface area override the decrease in air permeability at least to the extent observed here.

The possible morphological implications for these phenomena are discussed in the following section.

General Considerations on Foam Morphology

The parameters considered until now (density, air permeability and specific surface area) are indirect macroscopic indicators of the foam morphology, useful to quantify microscopic features of the foam otherwise almost impossible to measure directly (*e.g.*, air permeability is used as an indicator of the fraction of open cells). In this section, samples of PUFs were observed by confocal microscopy to directly investigate the foam morphology and its possible correlation with smoldering. As an example, in Figure 6, the micrographs of one specific bun from a smoldering formulation (F13 with ML_{Mockup} = 21.5 % ± 10.6 %, three replicates) and one bun from a non-smoldering formulation (F15 with $ML_{Mockup} \approx 1.2$ % ± 0.3 %, three replicates) are compared. Samples (about 0.1 g) were collected from the center of specific bun for each of the two formulations. The values of permeability and specific surface area were measured in close proximity to these locations in order to minimize the errors induced by in-bun variability ($SSA \approx 2.6\ 10^3\ m^{-1}$ and $\Phi \approx 79\ m^{-1}$ for F13; $SSA \approx 4.8 \cdot 10^3\ m^{-1}$ and $\Phi \approx 90\ m^{-1}$ for F15) (*24*). Noticeably, the two samples have comparable air permeabilities but substantially different specific surface area and smoldering propensity.

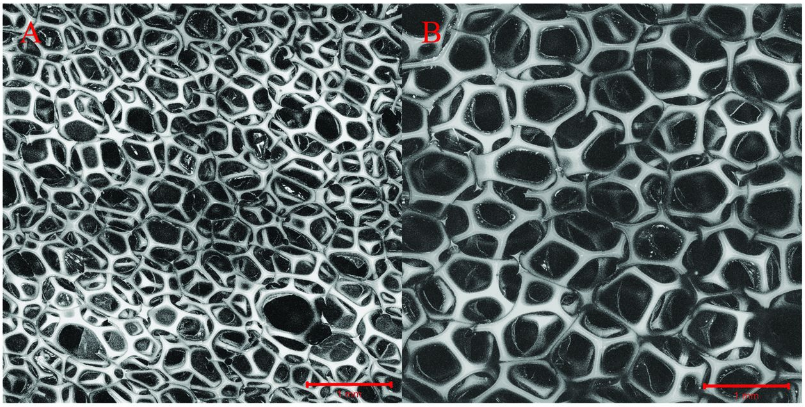

Figure 6. Confocal images for: (A) a smoldering foam ($ML_{Mockup} \approx 22$ %) and (B) a non-smoldering foam ($ML_{Mockup} \approx 1$ %). The smoldering foam had a smaller cell size, higher SSA and comparable air permeability ($SSA \approx 4.8 \cdot 10^3$ m^{-1}, $\Phi \approx 79\ m^{-1}$) as compared to the non-smoldering foam ($SSA \approx 2.6\ 10^3\ m^{-1}$, $\Phi \approx 90\ m^{-1}$). Bar size shown is 1 mm.

There is a large increase in cell size between the foam of Figure 6A and the foam of Figure 6B. This explains the observed increase in SSA, even though the presence of residual windows in Figure 6A might also play a role. As reported in Table 2, an increase in cell size was achieved by increasing the pressure in the mixing chamber (34.5 kPa for F15 and 48.3 kPa for F13) that controls nucleation and cell growth at the exit of the mixing head (*25*).

In predominantly closed-cell foams, an increase in air permeability is promoted by an increase in the fraction of open windows. In completely open-cell foams (*i.e.*, no residual closed windows), an increase in permeability can be achieved by increasing the cell size. This effect is dominant in a high permeability range where most of the cells are open. These principles are illustrated in the schematic drawing of Figure 7.

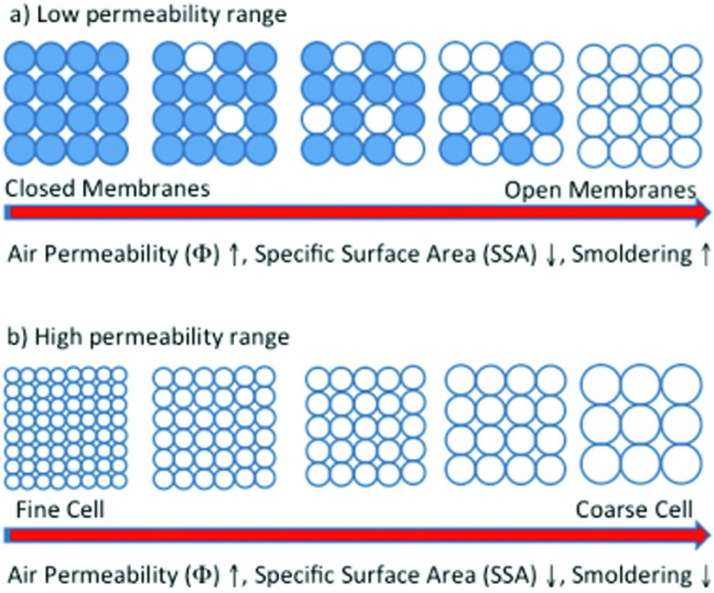
a) Low permeability range
Closed Membranes
Open Membranes
Air Permeability (Φ) ↑, Specific Surface Area (SSA) ↓, Smoldering ↑
b) High permeability range
Fine Cell
Coarse Cell
Air Permeability (Φ) ↑, Specific Surface Area (SSA) ↓, Smoldering ↓

Figure 7. Schematic drawing illustrating two possible mechanisms promoting an increase in air permeability (Φ): a) increase in fraction of open membranes; b) increase in cell size. Both mechanisms induce also a decrease in SSA but only a) promotes an increase in smoldering due to an increase in oxygen supply.

Either increasing the fraction of open membranes (case *a*) or increasing the cell size (case *b*) induces an increase in air permeability and a decrease in SSA. However, smoldering increases for case *a*, due to an increase in convective buoyance (*i.e.*, oxygen supply), and decreases for case *b*, due to a reduction in SSA. For a given formulation, the morphology of the foam that maximizes smoldering is characterized by a fine and largely open cell structure with a high value of air permeability (*i.e.*, $\Phi > 70$ m·min^{-1}). A high value of Φ is necessary to promote high oxygen supply through convective movements. In this high range of permeability a decrease in cell size promotes smoldering by increasing the amount of air/foam interface available for oxidation. This effect appears to prevail over the decrease in air permeability (*i.e.*, oxygen supply) also expected with a reduction in cell size. In general, in a typical PUF, where both open and closed cells coexist, there is no clear correlation between SSA and smoldering. This implies that SSA, by itself, is a good morphological descriptor for smoldering propensity only in fully open PUF, like reticulated PUF (*26*).

The cell size affects not only the specific surface area but also the heat transfer (the radiative heat transfer increase with the cell size) with possible effects on the thermochemistry of PUF degradation (*27*). Another potentially indirect effect of cell size on heat transfer is the reduction of strut thickness with decreasing cell size (Figure 6). The strut thickness affects the heat transfer in the foam (the ratio between conductive heat transfer over radiative and/or convective heat transfer increases with strut thickness). The contribution of each heat-transfer mode is strictly dependent on the smoldering scenario. In downward smoldering in reverse mode, for example, the convective heat flow is in the wrong direction to aid smoldering and the radiative heat transfer is equal or greater than the conductive heat transfer (*28*). In general, the heat transfer mode is extremely complex and dependent on the relative position to the smoldering front and smoldering scenario (*1*, *12*). This implies that the effect of cell size on heat transfer is position dependent and hardly quantifiable.

The Effect of Cell Size

In this section, cell size measurements are used as an alternative tool to SSA for smoldering propensity assessment. Due to the bun-to-bun and in-bun variability, multiple measurements are necessary for a statistically sound approach. This is often impractical for SSA measurements because they are extremely time-consuming (several hours per test) but it is feasible for cell-size measurements (about 15 min per test).

As discussed in the previous section, the surface area of a PUF is a combination of strut-generated and window-generated surfaces. The smoldering behavior of these two types of surfaces might be different due to variations in fuel-load per unit surface area (as the thickness of a strut is approximately two orders of magnitude higher than the thickness of a window) (*29*), variations in the thermochemistry of decomposition (oxidation dominates pyrolysis in thin membranes) and variations in heat transfer (the ratio between conductive to radiative and/or convective heat transfer is higher in a strut due to a lower specific surface area). Cell size measurements are not affected by the fraction of closed windows, so they can be used to calculate the strut-generated surface by geometrical considerations (*30*).

In this study, the average cell size was measured by means of image analysis; then the effect of cell size on smoldering was considered. In general, three-dimensional imaging is required for accurate cell-size measurements, whereas, two-dimensional imaging provides an "apparent" cell-size that is a function of the optical-slice thickness.

Here, for simplicity, the cell size is expressed in terms of an average cross-sectional area per cell calculated by image analysis of two-dimensional images. The optical thickness of these images was kept constant for a proper comparison by using a confocal microscope and taking advantage of the self-fluorescence of PUF (staining is usually required to increase imaging contrast but variations in the stain penetration potentially affect the apparent cell size) (*31*). Image analysis was then used to identify the contour of each cell and to measure the cell area. This type of image analysis is intrinsically subject to under/over segmentation. These artifacts were minimized by using circularity filters (*i.e.*, all cells with a circularity below 0.75 were rejected).

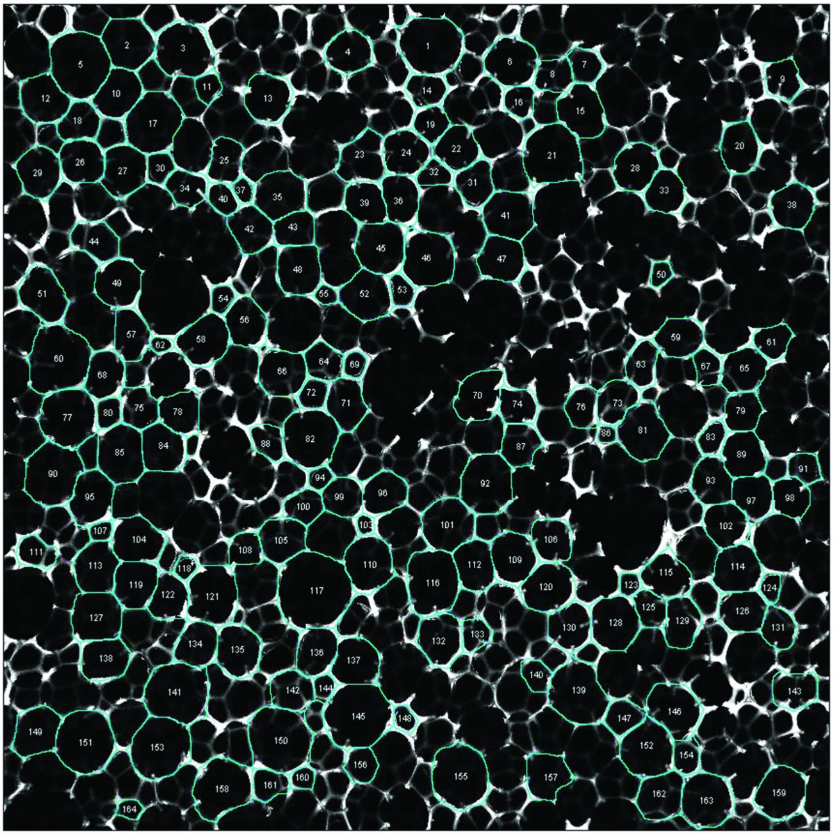
1
2
3
4
5
6
7
8
9
10
11
12
13
14
15
16
17
18
19
20
21
22
23
24
25
26
27
28
29
30
31
32
33
34
35
36
37
38
39
40
41
42
43
44
45
46
47
48
49
50
51
52
53
54
55
56
57
58
59
60
61
62
63
64
65
66
67
68
69
70
71
72
73
74
75
76
77
78
79
80
81
82
83
84
85
86
87
88
89
90
91
92
93
94
95
96
97
98
99
100
101
102
103
104
105
106
107
108
109
110
111
112
113
114
115
116
117
118
119
120
121
122
123
124
125
126
127
128
129
130
131
132
133
134
135
136
137
138
139
140
141
142
143
144
145
146
147
148
149
150
151
152
153
154
155
156
157
158
159
160
161
162
163
164

Figure 8. Confocal image for a sample of formulation F16 with highlighted contours (cyan line) for the cells identified by image analysis. (Image size: 11.9 mm x 11.9 mm).

Examples of a confocal image and image analysis are shown in Figure 8 and Figure 9. The total area of the cells identified by image analysis is only a fraction of the total area of the image (area fraction) due to the small optical thickness of the image (197.5 μm) and the circularity filter. For each foam location, three confocal images were acquired from three orthogonal planes to account for possible anisotropy in the foam. A cross-sectional cell area in a specific foam location is calculated as an average value for the three orthogonal planes. Finally, the **cell size (Σ)** is calculated by averaging the values of cross-sectional cell areas in at least three specific bun locations. For simplicity, Σ is used as a morphological indicator for smoldering propensity without accounting for possible effects of cell-size distribution. This is considered acceptable since the average strut-area is proportional to the average cell size at a given strut thickness, unless macroscopic imperfections are observed in the cell structure (e.g., visible pits or cracks in the foam). The effect of the strut thickness on specific surface area is not accounted for in cell size measurements; it is expected that in large cell foams the observed increase in strut thickness as compared to small cell foams (Figure 6) can further decrease the specific surface area.

The values of cell size (Σ) and smoldering (ML_{Mockup}) were measured for five custom-made buns and one commercial PUF with an air permeability $\Phi > \Phi_{threshold}$. These data are plotted in Figure 10. Clearly, smoldering increases when the cell size decreases. This is mainly due to a variation of SSA, even though an effect of cell size on heat transfer might also play a role. The dotted-line curve is a power-law least-squares regression fit to the diamond-shaped data points (custom made foams) with a coefficient of determination (R^2) equal to 0.74. The power-law regression appears to be a decent fit also for the commercial formulation F18 (triangle-shaped point). These results indicate that foam morphology has a paramount importance in smoldering behavior and cell size is a good indicator of smoldering propensity for conventional PUF with $\Phi > \Phi_{threshold}$, at least for the range of formulations investigated here (impurities, such as alkali metals, are capable of enhancing smoldering) (*32*). Noticeably, smoldering resistance of PUFs can be enhanced by promoting a large cell size (for example, by increasing the head pressure within the processing window).

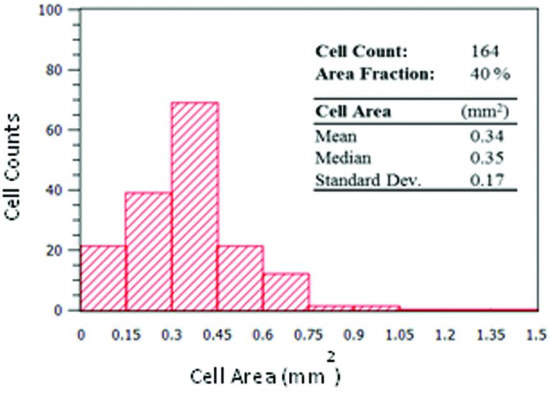

Figure 9. Histogram and basic statistical analysis for the confocal image of Figure 8.

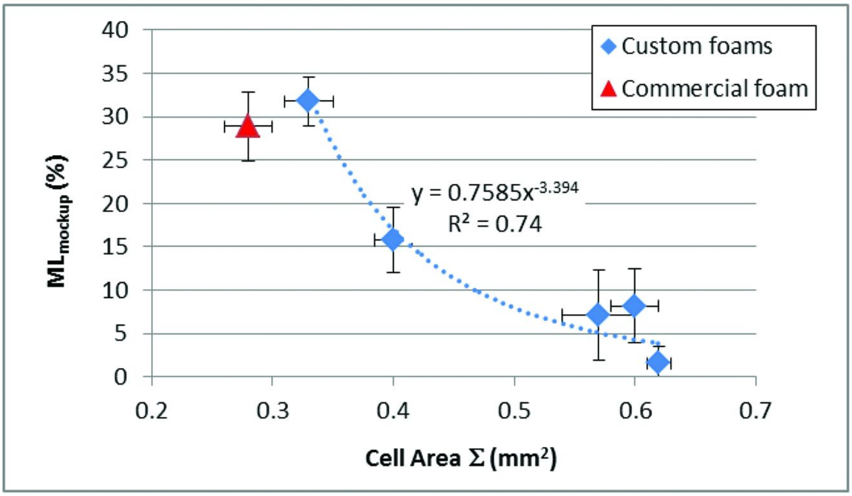

Figure 10. Smoldering propensity (ML_{Mockup}) versus cell size (Σ) for PUF with $\Phi > \Phi_{threshold}$.. The dotted-line curve is a power-law least-squares regression fit to the diamond-shaped data points (custom made foams); the fitting equation and relative coefficient of determination (R^2=0.74) are also shown. The triangle-shaped data point is a commercial foam (F18) with unknown formulation. The uncertainties are shown as one standard deviation.

Conclusions

Custom-made, conventional, flexible polyurethane foams with large variations in air permeability and cell size were prepared and their smoldering propensity was determined. Significant variations for these foam properties were observed between different buns of the same formulation (bun-to-bun variability), due to intrinsic foaming repeatability limitations, and between different locations in the same bun (in-bun variability), due to foam heterogeneity. Multiple measurements were necessary for a statistically sound approach.

Smoldering was investigated with the *Mockup Test* that aims to mimic a realistic combustion scenario for upholstered furniture. No apparent effect of foam density on smoldering was observed in the range investigated. Negligible smoldering was observed for formulations with air permeability below a threshold value of about 50 m·min^{-1}. Above this threshold, there was no apparent correlation between air permeability and smoldering. This is somewhat surprising because oxygen supply, that is typically the limiting factor in smoldering, increases with air permeability.

Above the permeability threshold, smoldering increased with the specific surface area. This is not surprising because smoldering is a heterogeneous oxidation reaction, and both heat and rate of reaction increases with the extent of air-foam interface. In addition, an increase in SSA promotes the exothermic oxidation reaction of PUF to char and inhibits the endothermic pyrolytic tar formation. Below the permeability threshold, there was no effect of specific surface area and smoldering was dominated by the reduced oxygen supply.

In predominantly open-cell foams and relatively narrow range of density, the larger the cell-size, the higher the air permeability and the lower the surface available for oxidation. In addition, the cell size might affect the heat transfer mode and the thermochemistry of PUF degradation. The experimental data indicate that when the cell size decreases smoldering increases; hence, the resulting increase in surface area dominates over the decrease in air permeability, even though an effect of cell size on heat transfer might also play a role. Cell-size, in combination with air permeability, appears to be a good indicator for smoldering propensity in the range of formulations investigated here.

In conclusion, these data show that smoldering resistance of PUFs can be enhanced by promoting a large cell size (reduced surface available for oxidation) and/or a low air permeability (reduced oxygen supply).

References

1. Ohlemiller, T. J. Smoldering combustion. In *SFPE Handbook of Fire Protection Engineering*, 3rd ed.; DiNenno, P. J., Drysdale, D., Beyler, C. L., Walton, W. D., Eds.; National Fire Protection Association: Quincy, MA, 2002; p 2.200–2.210.
2. *National Fire Protection Association, Coalition for Fire-Safe Cigarettes*; http://www.nfpa.org/categoryList.asp?categoryID=2254 or www.firesafecigarettes.org.
3. Ahrens, M. *U.S. fires in selected occupancies*; National Fire Protection Association: Quincy, MA, 2006; p 318.
4. Ohlemiller, T. J. Modeling of smoldering combustion propagation. *Progr. Energy Combust. Sci.* **1985**, *11* (4), 277–310.
5. Rogers, F. E.; Ohlemiller, T. J.; Kurtz, A.; Summerfield, M. Studies of the smoldering combustion of flexible polyurethane cushioning materials. *J. Fire Flammability* **1978**, *9*, 5–13.
6. Dodd, A. B.; Lautenberger, C.; Fernandez-Pello, C. Computational modeling of smolder combustion and spontaneous transition to flaming. *Combust. Flame* **2012**, *159* (1), 448–461.
7. Ortiz-Molina, M. G.; Toong, T-Y.; Moussa, N. A.; Tesoro, G. C. Smoldering combustion of flexible polyurethane foams and its transition to flaming or extinguishment. *Symp. (Int.) Combust.* **1979**, *17* (1), 1191–1200.
8. Rein, G.; Lautenberger, C.; Fernandez-Pello, A. C.; Torero, J. L.; Urban, D. L. Application of genetic algorithms and thermogravimetry to determine the kinetics of polyurethane foam in smoldering combustion. *Combust. Flame* **2006**, *146* (1-2), 95–108.
9. Torero, J. L.; Fernandez-Pello, A. C. Forward smolder of polyurethane foam in a forced air flow. *Combust. Flame* **1996**, *106* (1-2), 89–109.
10. Rein, G. Smouldering combustion phenomena in science and technology. *Int. Rev. Chem. Eng.* **2009**, 3–18.

In Fire and Polymers VI: New Advances in Flame Retardant Chemistry and Science; Morgan, A., et al.;
ACS Symposium Series; American Chemical Society: Washington, DC, 2012.

11. Torero, J. L.; Fernandez-Pello, A. C. Natural Convection Smolder of Polyurethane Foam, Upward Propagation. *Fire Saf. J.* **1995**, *24*, 35–52.
12. Bar-Ilan, A.; Rein, G.; Walther, D. C.; Fernandez-Pello, A. C. The Effect of Buoyancy on Opposed Smoldering. *Combust. Sci. Technol.* **2004**, *176*, 2027–2055.
13. The policy of the National Institute of Standards and Technology (NIST) is to use metric units of measurement in all its publications, and to provide statements of uncertainty for all original measurements. In this document however, data from organizations outside NIST are shown, which may include measurements in non-metric units or measurements without uncertainty statements. The identification of any commercial product or trade name does not imply endorsement or recommendation by NIST. Opinions, interpretations, conclusions, and recommendations are those of the authors and are not necessarily endorsed by NIST or CPSC.
14. Zammarano, M.; Krämer, R. H.; Matko, S.; Mehta, S.; Gilman, J. W.; Davis, R. D. *Factors Influencing the Smoldering Performance of Polyurethane Foam*; NISTTN 1747, http://dx.doi.org/10.6028/NIST.TN.1747.
15. *Proposed standard for the flammability of upholstered furniture*; 73 FR 11702 (March 4, 2008).
16. http://www.nist.gov/customcf/get_pdf.cfm?pub_id=902075.
17. Brunauer, S.; Emmett, P. H.; Teller, E. Adsorption of gases in multimolecular layers. *J. Am. Chem. Soc.* **1938**, *60* (2), 309–319.
18. http://rsbweb.nih.gov/ij/.
19. Circularity of a cell is defined as $4\pi(A/P^2)$, where A and P are the area and the perimeter of the cell, respectively.
20. Parts (by mass) per hundred parts of polyol for a specific component in a foam formulation (*e.g.*, 10 php of X means that 10 g of component X were used in combination with 100 g of polyol).
21. Rogers, F. E.; Ohlemiller, T. J. Smolder Characteristics of Flexible Polyurethane Foams. *J. Fire Flammability* **1980** (11), 32–44.
22. Darcy H. *Les Fontaines Publiques de la Ville de Dijon*; Dalmont: Paris, 1856.
23. Rogers, F. E.; Ohlemiller, T. J. Smolder Characteristics of Flexible Polyurethane Foams. *J. Fire Flammability* **1980** (11), 32–44.
24. Values based on a single measurement. The typical uncertainty for specific surface area and air permeability measurements is below 5 %.
25. Housel, T. Flexible polyurethane foam. In *Handbook of Polymer Foams*; Eaves, D., Ed.; Rapra Technology Limited: Shawbury, U.K., 2004; Chapter 5, p 85−122.
26. Reticulated foams are foams that are post-processed to remove all residual membranes by chemical etching or thermal treatment.
27. Rogers, F. E.; Ohlemiller, T. J. Smolder Characteristics of Flexible Polyurethane Foams. *J. Fire Flammability* **1980** (11), 32–44.
28. Ohlemiller, T. J.; Bellan, J.; Rogers, F. A model of smoldering combustion applied to flexible polyurethane foams. *Combust. Flame* **1979** (36), 197–215.

29. Zhang, X. D.; Macosko, C. W.; Davis, H. T.; Nikolov, A. D.; Wasan, D. T. Role of Silicone Surfactant in Flexible Polyurethane Foam. *J. Colloid Interface Sci.* **1999** (215), 270–279.
30. Gong, L.; Kyriakides, S.; Jang, W.-Y. Compressive response of open-cell foams. Part I: Morphology and elastic properties. *Int. J. Solids Struct.* **2005** (42), 1355–1379.
31. Landers, R.; Venzmer, J.; Boinowitz, T. Methods for Cell Structure Analysis of Polyurehtane Foams. *PU Magazine* **2006** (8), 110–121.
32. McCarter, R. Smoldering Combustion of Cotton and Rayon. *J. Consum. Prod. Flammability.* **1977** (4), 346–358.

Chapter 30

Comparison of Fiber-Reinforced Polymers in Global Fire Performance Tests

Michael Stevens* **and Philippe Coutelen**

Ashland Performance Materials 5200 Blazer Parkway, Dublin OH 43017
***E-mail: mgstevens@ashland.com**

Fiber-reinforced polymers (FRP) have been used widely in building, construction and mass transit applications in many parts of the world. Although some efforts towards the harmonization of fire performance standards are taking place (like EN45545 in the European train industry) most countries continue to have their own requirements to qualify materials for specific applications. As the economy becomes more global, it would be helpful for composite fabricators and end users to predict how materials perform in the different tests.

A study was undertaken to test 10 different materials from the United States and Europe to see how they perform in a range of North American and European fire performance tests. The tests studied were UL 94, ASTM E162, ASTM E84, ASTM E662, ASTM E1354, IMO A653, NFP 92501, NFP 16-101, and EN 13823. The results will be discussed. Although it was found that fire performance is generally dependant upon the resin system and the type of fire retardant used, the fire performance in a given test was seldom indicative of a material's performance in another procedure.

Introduction

The fire code requirements for building, construction and mass transit applications vary significantly across the world. Even fire performance requirements within the same country are different for these applications. Materials used in these areas may be similar, but must be tested to all of the different standards. Historically, there has been very little correlation between the

In Fire and Polymers VI: New Advances in Flame Retardant Chemistry and Science; Morgan, A., et al.;
ACS Symposium Series; American Chemical Society: Washington, DC, 2012.

various fire performance tests. This makes it difficult for a material supplier or a fabricator to determine what fire retardant system to use for each application. In the past, each European country had its own fire codes and employed its own fire test procedure. This required that materials meet different qualifications for the same application in each nation. The European Union has begun harmonizing the fire code tests. The new standard for building and construction applications has been issued and is starting to be adopted by various European nations. EN45545 is the proposed standard for the European rail industry. This will make it easier to have materials qualified for use all across Europe without having to tests to every country's individual specifications.

As companies continue to expand globally, there is a strong need to find economies of scale and to sell a uniform product across all geographies. It is of paramount importance to know how a particular FRP product will perform in the fire performance tests used for qualifying them for applications in different countries. This study was set up to look at how typical FRP systems from the United States will perform in the new EU standard tests and also how FRP systems designed for the European market will perform in the standard U.S. fire performance tests for buildings, mass transit and marine applications.

Experimental

A series of resins with various degrees of fire performance was chosen for this study. All of the resins are commercially available. The method for obtaining fire retardancy was also varied. This was done to see if the method of obtaining fire retardancy would give different results in the various tests. The resins evaluated include brominated resins, a combination of brominated resins filled with aluminum trihydrate (ATH), and non-brominated resins filled with ATH.

The test laminates were made using three layers of chopped strand glass mat to achieve 20-30% glass fiber content. The panels were made in the laboratory using a hand lay-up process. The thickness of each panel measured approximately 3 mm. All panels were made the same in order to remove this variable from the comparison. The panels were cured at room temperature and then post cured for six hours at 80 °C. The resin systems tested are listed in Table 1.

The fire tests that were evaluated covered the most common tests used in building applications, mass transit rolling stock, and the marine industry. The tests used in the study were ASTM E84 (*1*), ASTM E162 (*2*), ASTM E662 (*3*), ASTM E1354 (*4*), NFP92501 (*5*), NFP16-101 (*6*), EN 13823 (*7*) and IMO A653 (*8*). The descriptions of these tests can be found in the standards. Each of these tests uses different sample configurations and heat fluxes. Some of the tests (e.g. ASTM E84) also have a set air flow through the test apparatus.

A description of the requirements as well as guidance on how to test FRP for the new European Union requirements for building and construction applications is described in the Draft International Standard ISO/DIS 25762 (*9*). This also compares how different FRP materials perform in these tests.

Table 1. Resins used in test program

Resin Number	*Halogen*	*ATH Filler*
A	Yes	Yes
B	Yes	Yes
C	Yes	Yes
D	Yes	Yes
E	Yes	No
F	Yes	No
H	No	Yes
I	No	Yes
K	No	Yes

Results and Discussions

Tables 2, 3 and 4 gives the flame spread data for all of the tests, Tables 5, 6 and 7 gives the smoke test data for all of the tests. The discussion of these results are below.

The most common test used in the United States for building and construction applications is ASTM E84; commonly referred to as the Steiner Tunnel Test. The Flame Spread Index (FSI) results of these tests are shown in Figure 1. The Smoke Developed Index (SDI) is shown in Table 2. The resin systems containing halogens performed well in this test. The level of halogen in the resin tends to determine the flame spread index. Bromine synergists like antimony can also be employed to obtain a lower flame spread index with a given amount of bromine or the same FSI with lower bromine content. The systems utilizing ATH as the sole fire retardant (FR) additive do not do as well in this test. It requires very high loadings of ATH to obtain a flame spread index of <25. A combination of ATH and bromine does very well in this test. The ASTM E84 test also generates a smoke index value. Interior building applications in the U.S. require a smoke index of <450 according to US building codes. This can only be obtained through the exclusive use of ATH. Even a combination of halogen and ATH will not meet the low smoke requirement for the building codes if the panels are tested with the normal thickness at which they are used, which is 2 to 5 mm.

Table 2. Flame Spread Tests for Filled Halogenated Resin Systems

Resin	*A*	*B*	*C*	*D*
ASTM E84				
FSI	20	20	20	20
ASTM E162				
FSI	15	5	10	5
ASTM E1354				
Tig	60	99	63	55
PHRR	159	146	148	170
THR	31.5	51.1	13.5	13.2
EHC	10.6	11.5	6.2	5.6
IMO A653				
CFE	25.6	36.3	39.1	37.7
Qsb	3.9	6.7	5.2	4.6
Qt	0.7	0.7	0.2	0.6
Qp	3.1	3.3	2.4	2.9
IMO Part 5	Pass	Pass	Pass	Pass
EN 13823				
FIGRA 0.2	102.8	45	47.6	49.9
FIGRA 0.4	111.7	61	56.2	41.9
THR600	8.1	8	2.5	1.8
EN Class	C	C	B	B
NFP92501				
Class	M2	M1	M1	M1

Table 3. Flame Spread Tests for Halogenated Resins

Resin	*E*	*F*
ASTM E84		
FSI	20	30
ASTM E162		
FSI		40
ASTM E1354		
Tig	39	41
PHRR	193	219
THR	64	39.5
EHC	10.2	10.2
IMO A653		
CFE	17.8	15.7
Qsb	2.6	3
Qt	0.8	0.9
Qp	3.5	3.7
IMO Part 5	Fail	Fail
EN 13823		
FIGRA 0.2	284	140
FIGRA 0.4	370	203
THR600	17.6	16.4
EN Class	D	D
NFP92501		
Class	M2	M2

Table 4. Flame Spread tests for Halogen Free Resins

Resin	*H*	*I*	*K*
ASTM E84			
FSI	30	35	30
ASTM E162			
FSI	10	10	15
ASTM E1354			
Tig	73	104	82
PHRR	200	152	164
THR	55	61.7	45.2
EHC	19.7	13.9	16.7
IMO A653			
CFE	18.9	24.8	17.1
Qsb	7.9	7	9.3
Qt	1.3	0.8	1.1
Qp	4.3	3.5	2.4
IMO Part 5	Fail	Fail	Fail
EN 13823			
FIGRA 0.2	36.9	53	77
FIGRA 0.4	48.5	54.8	77
THR600	7.2	2.7	9.8
EN Class	B	B	C
NFP92501			
Class	M2	M1	M2

Table 5. Smoke Tests for Filled Halogenated Resin Systems

Resin	*A*	*B*	*C*	*D*
ASTM E84				
SDI	850	700	700	900
ASTM E1354				
Sa	3353	3328	1362	2240
SEA	1120	741	627	941
ASTM E662				
Flaming				
D1.5	26	1.9	7.6	9.7
D4.0	420	170	230	580
Dmax	590	550	530	660
Non-Flaming				
D1.5	0.29	0.36	0.29	1
D4.0	8.5	11	10	49
Dmax	350	300	210	320
EN 13823				
SMOGRA	90.3	18.56	40.2	114
TSP600	769	394	419	876
EN Class	S3	S3	S3	S3
NFP16-101				
Class	F2		F2	F3

Table 6. **Smoke Tests for Halogenated Resin Systems**

Resin	*E*	*F*
ASTM E84		
SDI	690	900
ASTM E1354		
Sa	7654	5526
SEA	1216	1428
ASTM E662		
Flaming		
D1.5		230
D4.0		710
Dmax		750
Non-Flaming		
D1.5		0.89
D4.0		20
Dmax		440
EN 13823		
SMO GRA	90.3	18.56
TSP600	769	394
EN Class	S3	S3

Table 7. Smoke Tests for Halogen Free Resin Systems

Resin	*H*	*I*	*K*
ASTM E84			
SDI	57	95	300
ASTM E1354			
Sa		517	1085
SEA	169	103	398
ASTM E662			
Flaming			
D1.5	0	0.73	2
D4.0	1.5	24	58
Dmax	180	210	210
Non-Flaming			
D1.5	0	0.05	0.27
D4.0	6	2.5	11
Dmax	150	130	170
EN 13823			
SMOGRA	1.47	2.81	16.9
TSP600	3.9	49	105.1
EN Class	S1	S1	S2
NFP16-101			
Class	F0	F0	F0

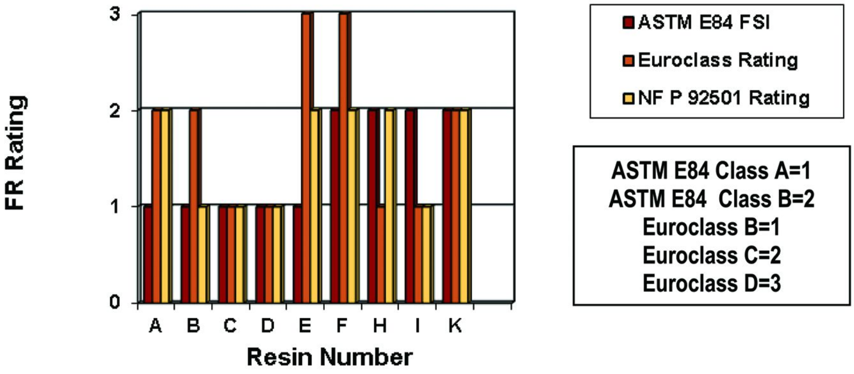

Figure 1. Comparison of ASTM E84 Flame Spread Rating. Euroclass Rating and French Rating. Reproduced with permission from Ashland Inc.

The results in the ASTM E162 test show that lower flame spread index values can be obtained with ATH or a combination of bromine and ATH. Unfortunately, this test does not appear to correlate well with the ASTM E84 test. Resin I has an ASTM E84 flame spread index of 35 and ASTM E162 flame spread index of 10 while Resin F had an E-84 flame spread index of 30 and an E162 flame spread index of 40. So one cannot assume that a good flame spread index in ASTM E84 test will predict a low flame spread index in the ASTM E162 test (Figure 2). The value required for the mass transit industry in the US is <35 flame spread index in the ASTM E162 test. This difference in performance is probably because of the different configuration of the samples. The ASTM E162 test has the sample at a 30 degree angle with the flame source at the top of the panel. ASTM E84 has the panel placed horizonitally above the flame source. There is also a set air flow going through the ASTM E84 test apparatus.

The ASTM E662 test only measures smoke density. This test is used in the mass transit industry to set the smoke requirements for materials used. The mass transit industry has a maximum smoke density of <100 at 90 seconds and <200 at 4 minutes. The mass transit requirement can be met with a combination of bromine and ATH if sufficient ATH is used to depress the generation of smoke in the first 4 minutes of the test. There does seem to be some general correlation between the ASTM E662 maximum smoke density values and the ASTM E84 smoke development index. The ASTM E662 test could possibly be used as a rough screening test for predicting the smoke index in the ASTM E84 test (Figure 3). A resin system that has a maximum smoke density below 200 will probably generate an E84 smoke index below 450. This system will also have a good chance of meeting the S1 smoke rating in the EN 13823 SBI test.

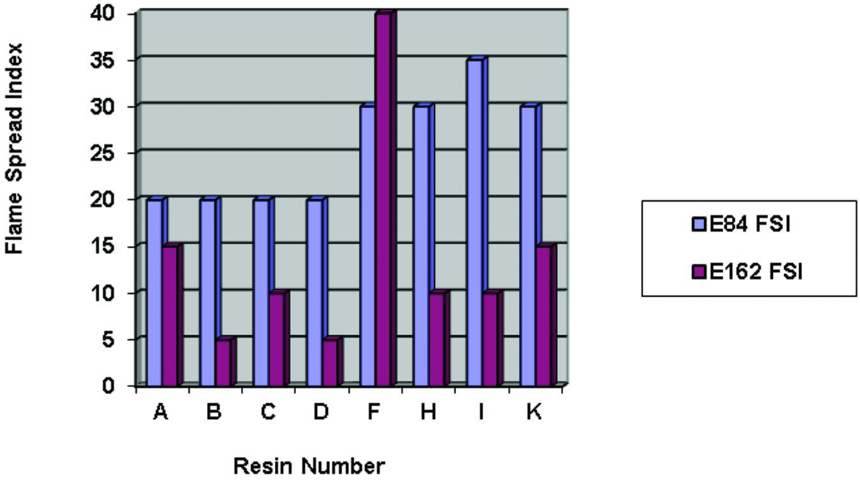

Figure 2. Comparison of ASTM E84 and E162 Flame Spread Index Values. Reproduced with permission from Ashland Inc.

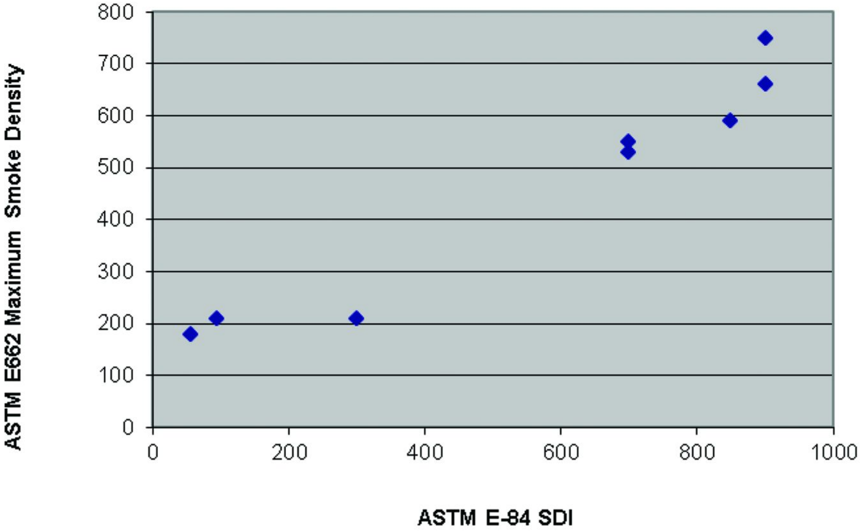

Figure 3. Comparison of Maximum smoke density in ASTM E662 to E84 smoke density. Reproduced with permission from Ashland Inc.

The ASTM E1354 cone calorimeter test is not currently required to meet any application standards. It is a very good research tool, however, for screening systems before running larger scale tests. Work by Stevens (*10*) showed that this test can be used to screen materials and predict how they will perform in the ASTM E84 test. Work at the SP Swedish National Testing and Research Institute fire testing laboratory has been done using the cone calorimeter test to screen materials for the EN 13823 SBI test and the ISO 9705 room corner burn test. Janssens et al (*11*) has also published work on the use of the cone calorimeter to predict performance of FRP materials in the ISO 9705 room corner burn tests.

The International Maritime Organization (IMO) sets the standards for all vessels going into international waters. The requirements for reaction to fire for wall, ceiling and bulkhead lining materials is based on the IMO A653 fire performance test which is described in the FTP code book (Figure 4). Of the systems tested, only the resin systems containing both ATH and bromine passed the flame spread requirements for IMO part 5. Unfortunately, the resin systems that passed the Part 5 requirements for flame spread will not meet the <200 smoke density requirement.

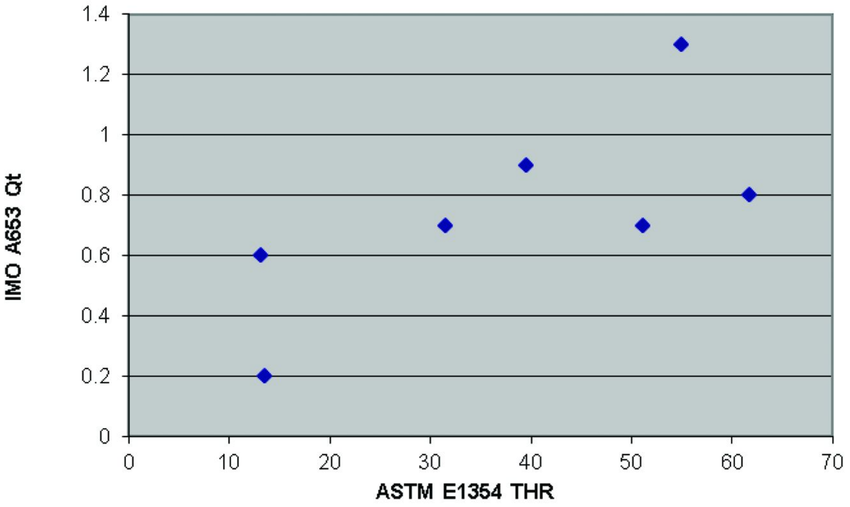

Figure 4. Comparison of total heat release from ASTM E1354 and A653. Reproduced with permission from Ashland Inc.

It was also noted that the resins that did well in the IMO A653 fire performance test may not perform as well in the SBI test. Two of the systems in this evaluation that met the IMO A653 flame spread requirement, could only be rated a Class C in the new Euro classification for building materials. Moreover, resins that had a flame spread index <25 in the ASTM E84 test do not necessarily meet the IMO A653 requirements.

The NFP 92501 Epiradiateur test has been used in Europe for many years to rate the flame spread tendency of materials. A rating of M1 is the lowest flame spread rating. In most cases the combination of ATH and bromine performed the best by this fire performance test method. The results from the ASTM E84 fire performance test do not effectively predict the fire performance in the NFP 92501 Epiradiateur test, however. Some materials that generated a M1 rating in the NFP 92501 test delivered an E84 flame spread index of 35 and some materials that had an E84 flame spread index of 20 generated an NFP 92501 rating of M2.

The new unified European classification for building and construction applications uses the EN 13823 Single Burning Item test (SBI) for determining fire performance classifications. This classification contains three parts. The first is based on heat release and relates to flame spread. Class A is the rating for non-combustible materials. Class B is the best classification for combustible materials. Class E is the lowest classification for combustible materials. The second part of the EN 13823 SBI test is the smoke rating. S1 is the lowest achievable rating with S3 being the highest rating. The third part of the EN 13823 SBI test is a determination of material drip performance as it burns / melts. None of the FRP materials tested in this evaluation demonstrated any dripping. It was found that the brominated systems which met the E84 flame spread requirement of <25, might not be able to obtain a Class B rating by the EN 13823 SBI test. Resin system G (with a very high bromine content) did obtain a Class B rating on this test. The resins systems containing both bromine and ATH did better than those containing bromine alone. In all cases where bromine was present in the system a smoke rating of S3 was obtained. The system that performed the best in this test was resin filled with high levels of ATH. The two resin systems that contained 150 phr (parts per hundred weight resin) ATH and no bromine, resin systems H and I, gave a Class B, S1 rating which is the best rating in this test. No good correlations were seen between the other tests and this test. Some have indicated that the cone calorimeter can be used to screen materials for this test.

Conclusion

There are wide variety of fire performance tests used in the world today for qualifying FRP material in building and construction, mass transit and marine applications. The tests requirements differ greatly from country to country. There is no good correlation between these fire performance tests. A material may meet the ASTM E84 Class 1 fire performance requirement for U.S. building and construction applications, but not meet the requirements for the Euro Class B fire performance test. Each resin system needs to be tested and qualified for each respective application. The type of fire retardant system has a direct impact on how the product will perform in each test. Bromine seems to be the best way to meet flame spread index requirements such as ASTM E84. A high loading of ATH without the use of bromine appears to deliver optimum smoke performance such as what is required to meet the new Euro class B, S1 requirements.

Additional work will be required to further understand the differences on how the different FR systems perform in these global tests.

References

1. ASTM E84, Standard Test Method for Surface Burning Characteristics of Building Materials. *Annual Book of ASTM Standards*; 2008.
2. ASTM E162, Test for surface flammability of materials using radiant heat energy source. *Annual Book of ASTM standards*; 2008.
3. ASTM E662, Standard test method for specific optical density of smoke generated from solid materials. *Annual Book of ASTM Standards*; 2008.
4. ASTM E1354, Standard Test Method for Heat and Visible Smoke Release Rates for Materials and Products using an Oxygen Consumption Calorimeter. *Annual Book of ASTM Standards*; 2008.
5. NFP 92501, Epiradiator Test.
6. NFP 16-101, Rolling stock –Fire behavior materials selection.
7. EN 13823, Reaction to fire tests for building products – Building products excluding flooring exposed to the thermal attack of a single burning item.
8. IMO Resolution, A653, Recommendation on improved fire test procedures for surface flammability of bulkhead, ceiling and deck finish materials. *FTP Code book, International Maritime Organization*; 1998.
9. ISO/DIS 25762. *Plastics – Guidance on the assessment of fire characteristics and fire performance of fiber-reinforced composites*; 2008.
10. Stevens, M. G. Cone Calorimeter as a Screening Test for ASTM E-84 Tunnel Test. *Proceedings of Composites 2000, Annual conference of Composites Fabricators Association*, October 2000.
11. Janssens, M. Modeling of the Performance of GRP Panels in the ISO 9705 Room/Corner Test. *Conference proceedings from ACMA Composites 2009*, January 2009.

Chapter 31

Fire Testing Requirements for Interior Finish in United States Codes

Timothy T. Earl and Marcelo M. Hirschler[*]

GBH International, 2 Friars Lane, Mill Valley, California 94941, U.S.A.
[*]E-mail: gbhint@aol.com

The most important code requirements on reaction-to-fire safety for building products involve interior finish testing. In terms of interior wall and ceiling interior finish, traditionally this testing was conducted in the U.S. with the Steiner tunnel fire test (ASTM E84). In recent years there has been abundant work designed to revise and improve the ASTM E84 standard, because it did not describe how materials or products need to be mounted for testing in enough detail. Thus misleading tests are often conducted, and some corresponding materials or products are being approved without the proper associated fire safety. In order to improve the fire safety of materials or products tested in the Steiner tunnel for interior finish applications, two strategies are being employed: (a) modification of the wording in the standard and (b) issuance of standard practices for specimen preparation and mounting of specific materials and products, which are then referenced in the base standard. Standard practices have been issued for specimen preparation and mounting of wall/ceiling coverings, pipe and duct insulation, wood products, site-fabricated stretch systems, reflective insulation materials, radiant barrier materials, vinyl stretch systems, tapes and caulks and sealants. Key changes to the ASTM E84 test address details of specimen width and thickness, incorporation of requirements to use the standard practices and special clarifications.

However, increasingly regulatory and research testing is conducted to assess heat and smoke release rate with room-corner tests and now the de-facto default test for interior wall and ceiling finish is the NFPA 286 room-corner test. In both Steiner

In Fire and Polymers VI: New Advances in Flame Retardant Chemistry and Science; Morgan, A., et al.;
ACS Symposium Series; American Chemical Society: Washington, DC, 2012.

tunnel testing and room-corner testing, significant differences in fire test results can be obtained by variations in specimen preparation techniques and mounting methods. For interior floor finish, this testing has, and continues to be, done principally by means of the flooring radiant panel (ASTM E648 or NFPA 253). This work will present an update and indicate areas where additional work is still needed.

Introduction

Any building material that causes a fire that would otherwise stay small to become large has undesirable fire properties. Interior finish materials can greatly increase the fire hazard in a compartment by providing a large, unbroken surface over which flame spreads. As the flame spreads to involve greater surface area, a fire's rate of heat release, and, therefore, the fire size will increase significantly. Flames from interior finish with poor fire performance may release sufficient energy to cause the formation of a dangerous hot gas layer.

Codes in the United States tend to define interior finish with concepts such as: the exposed surfaces of walls, ceilings, and floors within buildings, often with added explanations that clarify that interior finish is not intended to apply to: (a) surfaces within spaces, such as those that are concealed or inaccessible or (b) furnishings that are secured in place for functional reasons. Thus, interior finish materials are those materials or assemblies of materials that form the exposed interior surfaces of walls and ceilings in a building. Interior wall finishes usually also include the interior finish of columns, fixed or movable walls, and fixed or movable partitions. Interior finish materials include traditional materials and more modern materials, such as plastics (including light-transmitting plastics). Interior finish materials also include interior floor finishes, which tend to be a less severe fire problem, because heat and smoke rise in a fire. Interior floor finishes are the exposed floor surfaces of buildings and include floor coverings, e.g. carpets or floor tiles, which may be applied over, or instead of, a finished floor. Outside of the United States, the term interior finish is often replaced by the term interior lining or lining material.

A parallel concept that needs to be considered in conjunction with that of interior finish is "interior trim". Interior trim represents the picture moldings, baseboards, handrails, door and window frames and similar decorative or protective materials used in fixed applications. Interior trim is ordinarily regulated by U.S. codes as interior finish. However, the requirements for interior trim are normally more lenient than those for the remainder of the wall and ceiling interior finish, but only when the interior trim occupies less than 10% of the wall or of the ceiling area. The leniency is intended to apply to trim distributed uniformly so that no significant surface area would allow flames to spread throughout the trim; however codes are often not explicit on this.

The fire hazard of partitions, which led to them usually being regulated as interior finish, was demonstrated by full-scale tests at the National Institute of Standards and Technology (NIST) involving office work stations consisting of computer terminals, partitions of textile covering over fiberglass on metal frames, wood desks, and typical office contents. The tests showed that fires involving such work stations may reach several megawatts and do so in as short as 300 to 600 s.

For that reason, the use of interior finish with superior fire performance is a way to passively protect building occupants from the dangers of fire. Once a fire has progressed so that the upper layer temperature approaches 600°C and that layer becomes thick, descending toward the lower portion of the room, all combustible furnishings and combustible room contents may be ignited, leading to flashover or full room fire involvement. Although some fires involve extended periods of slow, undetected fire development, fires that cause large loss of life or such high property loss nearly always grow rapidly to large size. Such fires typically reach flashover, or full room involvement, within minutes of having been small and easy to control. Therefore, prevention of flashover by controlling the fire performance of interior finish is a key strategy for lowering fire hazard.

Codes and Standards Containing Interior Finish Fire Requirements

Three key terms are of interest regarding U.S. requirements for fire safety: regulations, codes and standards.

(a) Regulations are documents with the force of law which list general objectives and act as a framework for more detailed requirements.
(b) Codes are documents connected with regulations, but which comprise more specific requirements and are valid for particular cases such as hospitals or schools.
(c) Standards are documents referred to either in regulations or in codes and which put forward special techniques to quantify results, with typical examples being test methods.

In the United States building interior finishes are regulated by the adoption of model codes (or of key standards, in some instances), which contain the fire safety requirements. Model codes are issued by code development organizations, typically the International Code Council (ICC) and the National Fire Protection Association (NFPA) and then adopted, sometimes after some modifications, by states, counties and/or municipalities. Both ICC and NFPA are private companies which develop multiple codes and standards.

ICC develops a full family of codes, including the following, related to interior finish: International Building Code (IBC), International Fire Code (IFC), International Mechanical Code (IMC), International Residential Code (IRC) and International Existing Building Code (IEBC), which have been adopted widely throughout the country. Until the mid-1990s, the U.S. had three regional code development companies: (1) ICBO (International Conference of Building Officials), which issued the Uniform Building Code or UBC, primarily used in the 25 states West of the Mississippi, (2) BOCA (Building Officials and Code Administrators), which issued the National Building Code or NBC, primarily used in the Northeast and Midwest and (3) SBCCI (Southern Building Code Conference International), which issued the Standard Building Code or SBC, primarily used in the Southeast. The three organizations joined up to form ICC, at which point updates of the old regional model codes ceased and they were mostly discontinued. However, but some old codes may still be in use in some jurisdictions. This will not be addressed in the present work, which will focus on the most recent editions, those dated 2012, and the proposed changes to them.

NFPA also develops a full family of codes and standards which relate to interior finish, and they include the following: NFPA 5000 (Building Construction and Safety Code, equivalent to IBC), NFPA 101 (Life Safety Code, intended for protection of life safety of occupants from fire and focusing heavily on egress), NFPA 1 (Fire Code, equivalent to the IFC), UMC (Uniform Mechanical Code, equivalent to the IMC), NFPA 501 (Standard on Manufactured Housing, which handles mobile homes), NFPA 90A (Standard for the Installation of Air-Conditioning and Ventilating Systems, which handles interior finish in plenums), NFPA 130 (Standard for Fixed Guideway Transit and Passenger Rail Systems), NFPA 909 (Code for the Protection of Cultural Resource Properties - Museums, Libraries, and Places of Worship) and NFPA 914 (Code for Fire Protection of Historic Structures).

Building codes normally apply to the construction, alteration, movement, enlargement, replacement, repair, equipment, use and occupancy, location, maintenance, removal and demolition of every building or structure or any appurtenances connected or attached to such buildings or structures. However, the IBC does not apply to "detached one- and two-family dwellings and multiple single-family dwellings (townhouses) not more than three stories above grade plane in height with a separate means of egress and their accessory structures", to which the IRC applies. On the other hand NFPA 5000 does apply to one- and two-family dwellings. Fire codes apply to structures, facilities and conditions arising after the adoption of the fire code edition, as well as to existing structures, facilities and conditions, particularly those which, in the opinion of the regulatory official, constitute a distinct hazard to life or property. Fire codes do not allow any change to be made in the use or occupancy of any structure that would place the structure in a different division of the same group or occupancy or in a different group of occupancies, unless such structure is made to comply with the requirements of both the fire code and the building code. NFPA 101 applies to both new construction and existing buildings and existing structures. It addresses those construction, protection, and occupancy features necessary to minimize danger to life from the effects of fire, including smoke, heat, and toxic gases created during a fire. It establishes minimum criteria for the designs of egress facilities so as to allow prompt escape of occupants from buildings or, where desirable, into safe areas within buildings. NFPA 101 does not address the following: (a) general fire prevention or building construction features that are normally a function of fire prevention codes and building codes, (b) prevention of injury incurred by an individual due to that individual's failure to use reasonable care or (c) preservation of property from loss by fire. The NFPA Fire Code (NFPA

1) is, to a significant extent, a document extracted from NFPA 101, including in terms of interior finish requirements. NFPA 90A, NFPA 130 and NFPA 501 have limited applications (as clear from their titles) but are of key importance; NFPA 130 also addresses all rail stations, above ground and underground.

Development of ICC and NFPA Codes and Standards

ICC codes are updated periodically (on a 3-year cycle beginning with the 2012 editions) by proposals submitted by the public, which are considered by specialized committees at code development hearings. The committees vote on their decisions following testimony by proponents and opponents to explain the pros and cons of each proposal. Once the committees have voted, the attendees may propose alternatives to the committee recommendations. The results of the committee actions and of the public votes are published and comments from the public are sought. These comments are discussed at “Final Action Hearings” where proponents and opponents of the comments discuss the pros and cons. The final decision on these comments is reached by a vote of code officials present. At the conclusion of this process a revised code is published, with the most recent editions being dated 2012.

The key NFPA codes and standards discussed above are all updated every 3 years. The process differs from the ICC process in that the public makes proposals (called “public input” after the 2012 editions) and a technical committee makes decisions on them. The public then comments on the decisions and the committees make adjustments to their original recommendations. An important distinction between the ICC and NFPA processes is that the ICC committees are discouraged from doing anything other than minor “tinkering” with the public proposals while NFPA committees are encouraged to make all the changes needed to get the best possible document issued. Once the NFPA committees have completed their work and NFPA has published it, motions can be made to make further changes (within very limiting rules) which are discussed at the NFPA Annual Meeting and those decisions are then approved (or not) by the NFPA Standards Council.

As explained earlier, jurisdictions are entitled to adopt the codes as published or to modify them. Often, adoption into regulations does not follow publication directly, but there is a lag of 1 or more years.

Where Are Interior Finish Fire Requirements Found?

The key locations for interior finish fire safety requirements in the documents listed above where interior finish fire safety requirements are Chapters 8 of the IBC and IFC and Chapters 10 of NFPA 101 and NFPA 5000. Efforts are always made to ensure that the partner codes are consistent with one another, i.e. IBC with IFC and both NFPA 101 and NFPA 1 with NFPA 5000.

In the NFPA Fire Code, the requirements are primarily found in section 12.5, but they are “extracted” from NFPA 101, meaning that the language is identical. In NFPA 501 requirements have been placed in Chapter 5 (on fire safety), in NFPA 909 they can be found in section 9.12 on the prescriptive fire safety option for new constructions or additions and in NFPA 914 they can be found in section 12.8 (alterations). In NFPA 130, interior finish is addressed in Chapter 5, on stations and in NFPA 90a in section 4.3.11 on plenums, with specific emphasis on foam plastic insulation. The IMC and UMC each have a specific chapter on ducts and plenums and all combustible materials contained therein are discussed in that chapter, including interior finish; plenum materials are in section 602 in both codes.

The IEBC contains references to interior finish in the sections addressing alterations and change of occupancy (chapters 8 to 10, directing the user to the IBC) and in the section on historic buildings (where it says that they can stay as is if they are historic except that, when there is a change of occupancy the requirements must be met by using coatings).

Fire Tests for Interior Wall and Ceiling Finish Materials

The traditional test for interior finish fire performance is ASTM E84, Standard Test Method for Surface Burning Characteristics of Building Materials (Steiner tunnel test, which also has an equivalent designation in UL 723), and it is still widely used in the U.S. However, in recent versions of codes, the default test (used for alternative testing of interior finish materials) is the room-corner test: NFPA 286, Standard Methods of Fire Tests for Evaluating Contribution of Wall and Ceiling Interior Finish to Room Fire Growth. The major reason for the use of the room-corner test is that it assesses interior finish in a realistic room scenario and measures the key fire property, heat release, and therefore results of room-corner tests are more reliable than results of tunnel tests. The Steiner tunnel test has been found to be an adequate fire test for traditional building materials and for materials that are not very thin and that remain in place during the test. However, many modern interior finish materials and systems are more complex than that and may not be suitably assessed by the Steiner tunnel fire test.

Steiner Tunnel Test Details

The 25-ft (7.62-m) Steiner tunnel test, also known as ASTM E84, NFPA 255, and UL 723, was developed in the 1940s by A. J. Steiner at Underwriters Laboratories, Inc. After a series of fatal fires, the need for a method of controlling interior finishes was recognized and the use of the tunnel test proposed. The method was adopted by the American Society for Testing and Materials (ASTM, now ASTM International) as a tentative standard in 1950 and as an official standard in 1958 (as ASTM E84). NFPA adopted the test method tentatively in 1953 and officially in 1958 as NFPA 255 and withdrew it in 2009. ASTM E84 and UL 723 are still revised periodically.

A detailed description of the Steiner tunnel test apparatus can be found in ASTM E84. The tunnel chamber is a rectangular horizontal duct with a removable lid. The inside dimensions are as follows: 7.62 m (25 ft.) length, 450 mm (17.7 in.) width and 305 mm (12 in.) depth. The sides and base of the chamber are lined with an insulating firebrick. One of the sides of the tunnel chamber has double-paned windows with the inside pane flush mounted, for observation of the flame spread. The windows are placed so that not less than 305 mm (12 in.) of the test specimen width can be viewed. The side of the chamber has ledges at a height of 305 mm (12 in.) from the tunnel floor, for placing the test specimen. The ledges are level with respect to the length and width of the chamber and each other. The removable and insulated lid is constructed of a noncombustible metal and mineral composite structure and completely covers the test chamber and the test specimen. During the test a dual gas burner projects a 1.4 m (4½ ft.) long flame (corresponding to an intensity of 89 kW) upwards onto the underside of a test specimen while air flows through the tunnel at a controlled linear air velocity of 73 m/min (240 ft. /min). The test specimen must be either one continuous length of material or a series of sections joined or butted end-to-end. The test specimen is 508-610 mm (20-24 in.) wide by 7.3 m (24 ft.) long and is placed face down on a ledge at the top of the tunnel furnace to form the ceiling of the tunnel test chamber. The ASTM E84 test apparatus is not designed for testing materials or products in specimens of thicknesses greater than 101 mm (4 in.), but has the ability to be modified to do so (to a limited extent) if required. This is done either by changing the lid to maintain an airtight seal with thicker samples or, more commonly, by introducing sample/lid supports above the test apparatus ledges.

Flame spread in the ASTM E84 test is reported as a flame spread index (FSI). Flame spread over the face of the test specimen is observed through windows in the side of the tunnel. Flame propagation is recorded as a function of time over the 10 min test duration. The record of flame propagation versus time is used to calculate the FSI, by comparison with two standard reference materials. Red oak flooring is arbitrarily assigned an FSI of 100 and a cementitious board material is assigned an FSI of 0. According to the test standard, red oak flooring spreads flame 7.3 m (24 ft.) to the end of the test specimen in 5½ min ± 15 s. FSI values for products are calculated on the basis of a graph of flame spread versus time. The lower the FSI value the better the presumed performance. However, it is often the case that there is no correlation between the FSI measured in the Steiner tunnel test and product behavior in actual fires, particularly for non-traditional materials. The Steiner tunnel test simply provides a basis for comparing one product with another under a standardized set of test conditions.

Smoke release in the ASTM E84 test is reported as a smoke developed index (SDI). The attenuation of the light transmitted across the tunnel exhaust caused by the material burning in the test is measured photometrically using a lamp and a photo cell. The reduction in light transmission by the flow of smoke and gases is used to calculate the SDI. The SDI for a test specimen is determined by comparing the results for the test specimen of the material tested with those for red oak flooring. This is done by comparing the curve of the area under the photoelectric cell readings versus time. Red oak flooring has been arbitrarily assigned an SDI value of 100 and the cementitious board material (the other calibration material) has been assigned an SDI of 0. Therefore, when a test result shows an SDI of 450, this means that the area under the photoelectric cell readings curve is 4.5 times the area under the red oak flooring curve. It is thus assumed that a product exhibiting an SDI of 450 produces some 4.5 times as much smoke as red oak flooring during the 10 min tunnel test.

Application Practices for Steiner Tunnel Test

There are many issues associated with the way in which materials or products are mounted in the tunnel, and they are addressed via guidance in a non-mandatory appendix. Since 2002, however, several standard practices were developed to address mounting and testing of some specific materials or products in a mandatory way. Those practices have all been incorporated into section 6.8 of ASTM E84 so that testing for the corresponding materials or products in accordance with those standard practices has become mandatory. Each standard practice describes, in detail, how to prepare test specimens and how to mount them in the tunnel. There are three types of issues being addressed by these standard practices. The first issue is to ensure that materials are tested in such a way that there is consistency between labs. ASTM E2579, for wood materials, specifically addresses that issue. The second, and most common, issue is to ensure that products, particularly composite products, are tested by exposing all components of the product in a standard way and preventing some of the combustible components from being hidden (e.g. by placing them on the ledges where the flame does not reach them). This applies to most of the standard practices: ASTM E2231, ASTM E2404, ASTM E2573 and ASTM E2599, which will be discussed in more detail. The third issue is to ensure that products that are tested at less than full width are tested appropriately. This applies to the two newest practices, namely ASTM E2688, for tapes, and ASTM E2690, for caulks and sealants.

Section 6.8 of ASTM E84 specifically requires that the 7 standard practices discussed in this chapter be used for specimen preparation and mounting if the relevant test materials. It also sends the user to Appendix X1 for guidance on mounting methods for all other products.

ASTM E2231 ensures that pipe and duct insulation systems that have multiple components are tested as a system, with the jacket, the adhesive and the insulation in the test specimen. It also addresses those cases where the insulation is a single component. The practice contains mounting instructions for five cases: (a) self-supporting multi-component systems, not intended to be bonded to a pipe or duct substrate, (b) non self-supporting, multi-component systems not intended to be bonded to a pipe or duct substrate, (c) self-supporting, single-component systems, not intended to be bonded to a pipe or duct substrate, (d) non self-supporting, single-component systems, not intended to be bonded to a pipe or duct substrate and (e) systems intended to be bonded to a pipe or duct substrate. The practice addresses different types of noncombustible materials to which the system can be bonded and it excludes all testing of systems that use chicken wire. This was the first standard practice associated with ASTM E84 to be issued and it addressed the critical problem that some manufacturers were testing the individual components of an insulation system independently of the others, leading to the approval and use of systems which would be considered unsafe if tested as a complete system. It is particularly important for plenums but not normally for interior finish materials.

ASTM E2404 applies to all types of wall and ceiling coverings and requires that all such wall or ceiling coverings be tested exactly as they are intended to be used, with the substrate and adhesive to be employed in the field. It discusses the following three substrates: noncombustible surface, gypsum board and wood. The key issue here is that wall or ceiling coverings not be allowed to be tested by simply adhering them with a heavily fire retarded adhesive to a noncombustible substrate unless that is the system to be used in actual installations. This misuse of the test method was common. Originally the standard had a vague section that stated that wall or ceiling coverings not intended to be adhered directly to a wall or ceiling surface, but intended to be otherwise supported by a framing or a track system should be tested in a manner that is representative of its installation. Once ASTM E2573 was issued (see below) it was understood that this last mounting method really describes site-fabricated stretch systems and the committee has changed the ASTM E2404 practice to refer in this section to ASTM E2573. Most recently it was discussed that facings or wood veneers intended to be applied on-site over a wood substrate (and not factory-produced) need to be tested in accordance with this practice, when mounted over a standard plywood substrate (just like other wall coverings intended to be applied over a wood substrate). This was changed in the standard and the title was amended to ensure that all wall or ceiling coverings are addressed by this standard practice. This practice is widely used in codes.

ASTM E2573 applies to site-fabricated stretch systems. They are systems, fabricated on site and intended for acoustical, tackable or aesthetic purposes, that are comprised of three elements: (a) a frame (constructed of plastic, wood, metal or other material) used to hold fabric in place, (b) a core material (infill, with the correct properties for the application), and (c) an outside layer, comprised of a textile, fabric or vinyl, that is stretched taut and held in place by tension or mechanical fasteners via the frame. The key concern regarding these systems is that both the fabric and the frame must be properly exposed to the flame, so as to avoid the use of individual components with poor fire performance. Before the development of ASTM E2573 these systems were usually tested in the tunnel but using highly combustible frames and "hiding" them on the ledges of the tunnel while testing the fabric independently with the vertical fabric test in NFPA 701, Standard Methods of Fire Tests for Flame Propagation of Textiles and Films, which is a much milder test than ASTM E84. As discussed above, ASTM E2573 also applies to "Wall or Ceiling Coverings Not Intended to be Adhered Directly to a Wall or Ceiling Surface, but Intended to be Otherwise Supported by Framing or a Track System" and does not apply to vinyl stretch ceiling materials, which are covered by ASTM E2599. This practice is specifically referenced in codes.

ASTM E2579 applies to a variety of wood products, virtually all of which are used as interior finish. This practice was developed primarily to ensure consistency within labs, but it introduces little that is not already contained within ASTM E84. This practice is not specifically referenced in codes, at least up to 2012 editions, but is used by the reference to ASTM E84. The most recent debate relates to facings or wood veneers factory-produced into panels where the facing is applied over a wood substrate. The consensus appears to be that they need to be tested in accordance with this practice. However, they should probably not be tested mounted over a standard plywood substrate, but rather they should be tested as they are produced commercially. This has not yet been adopted into the standard.

ASTM E2599 was originally developed to address a problem area: reflective insulation materials and radiant barrier materials intended for mechanical fastening to substrates or building structural members, or intended to be mounted to a substrate with an adhesive. Reflective insulation is thermal insulation which has a low emittance surface on one or more sides, bounding enclosed air spaces; radiant barriers are examples of the low emittance surfaces. These systems typically consist of very thin metallic surfaces covering a layer of insulating material. The internal insulating material is often polyethylene (made into bubble wrap), but it can also be a foam plastic or another type of thermal insulation material. These materials were normally tested in the Steiner tunnel by mounting the specimen on chicken wire for all applications. Tested in this manner, the materials usually obtained FSI values < 25, but full scale tests (or even room-corner tests) showed that the test results did not represent the real fire hazard. The ASTM E2599 practice requires that reflective insulation materials be tested with an air gap; this produces consistent results that correlate with realistic tests. If these materials are to be used as pipe or duct insulation they need to comply with ASTM E2231 (which does not allow the use of chicken wire). The applicability of ASTM E2599 was later expanded to encompass other materials that are also applied in practice with an air gap: vinyl stretch ceiling materials. Vinyl stretch ceiling materials are vinyl materials stretched and mechanically fastened to a noncombustible frame and intended to be used as a suspended ceiling without associated backing material. It is important to understand that these materials are different from site-fabricated stretch systems in that they are two-component systems without a core material, they have noncombustible (typically metallic) frames and they are not installed against a wall or ceiling but with an air gap. This practice is specifically referenced in codes for use with reflective insulation materials.

ASTM E2688 addresses testing tapes intended for use at up to and including 203 mm (8 in.) widths and which are not able to be supported by their own structural characteristics during the test. If the tapes are intended for uses in excess of 200 mm (actually 8 in.) they must be tested in full coverage as applied to fiber cement board as described in the normal ASTM E84 method. The standard practice has separate requirements for tapes up to 51 mm (2 in.) and between 51 mm and 203 mm (2 in. to 8 in.). The slimmer tapes are tested with two 51 mm (2 in.) strips running along the tunnel length and the other ones with two 203 mm (8 in.) strips. In both cases the tapes are adhered to fiber cement board with an adhesive such as the one to be used in actual practice. This practice is implicitly used in codes for interior finish regulation by the application of the requirement to test to ASTM E84.

ASTM E2690 addresses testing caulks and sealants intended for use at up to and including 203 mm (8 in.) widths and which are not able to be supported by their own structural characteristics during the test. If the caulks and sealants are intended for uses in excess of 200 mm (actually 8 in.) they must be tested in full coverage as applied to fiber cement board as described in the normal ASTM E84 method. The test specimens consist of two 7.47 m (24.5 ft.) long beads or strips of sealant or caulk installed 203 mm (8 in.) on center down the center of the tunnel. The beads or strips are at the maximum width or diameter recommended for use by the manufacturer, but not less than 9.5 mm (3/8 in.). The test specimens are centered so that they align on the center line of the tunnel burner nozzles. The caulks or sealants are cured per manufacturer instructions and then applied to fiber cement board. The intent of this practice is to address exposed caulks and sealants applied on top of existing interior finish materials, which would require testing. Note that caulks and sealants are different from adhesives, in that an adhesive is a layer joining two materials to be adhered to each other, while a caulk or sealant is often the exposed surface. Caulks or sealants intended to be applied at widths of over 203 mm (8 in.) must be tested at full width in the ASTM E84 tunnel and must be cured and applied in accordance with the manufacturer's instructions. This practice is implicitly used in codes for interior finish regulation by the application of the requirement to test to ASTM E84.

Fire retardant treated wood has always been required to meet what came to be known as the "extended ASTM E84" test. In this modification to ASTM E84, testing must continue for a total of 30 min (as opposed to 10 min for normal tests) and the material must exhibit a Class A flame spread index, show no evidence of significant progressive combustion, and have a flame front that does not progress more than 3.2 m (10.5 ft.) beyond the centerline of the burners at any time during the test. In 2011, a new standard test method (and not a practice) was developed, ASTM E2768, Standard Test Method for Extended Duration Surface Burning Characteristics of Building Materials (30 min Tunnel Test). In order to meet the requirements of ASTM E2768, a material (not necessarily wood) must exhibit an FSI of no more than 25 (over a 30 min test) and must have a flame front that does not progress more than 3.2 m (10.5 ft.) beyond the centerline of the burners at any time during the 30 min test. It needs to be pointed out that ASTM E2768 does not include a specific requirement for showing "no evidence of significant progressive combustion" because the practice by all laboratories has been that when the flame front ceases progressing (and it is not allowed to go beyond the 3.2 m) that lack of progress indicates "no significant progressive combustion". This is still somewhat controversial. Another controversial issue is the applicability of ASTM E2768, which is neither limited to wood nor limited to materials that are impregnated throughout with additives, so that it can be "passed" by plastic materials (and the International Wildland Urban Interface Code (IWUIC) allows any material that passes this test to be used for decks in wildland areas) or by coated wood. However, coated wood would fail the concept of fire retardant treated wood, which must be "impregnated with chemicals" and not just coated. The "extended ASTM E84" is a test method used in the codes for regulating interior finish, but ASTM E2768 has not yet been incorporated as of the 2012 editions.

It is essential to understand that 5 standard test methods exist which use variations of the Steiner tunnel test, in which several changes have been implemented in both the equipment and the test procedure as opposed to simply in the test specimen and mounting method. ULC S102.2 applies to some floor coverings and to some melting materials (including ones potentially used as interior finish); it tests materials on the floor and has some other minor test equipment differences from ASTM E84.The other four test methods have several things in common: the test specimen is not mounted on the ledges of the tunnel but on a support tray, and measurements involve flame spread and optical density. The inlet section of the test apparatus has also been modified substantially, to develop tighter requirements. Any test apparatus that is suitable for conducting these alternate tests is also suitable for conducting ASTM E84 tests. However the opposite is not the case: test apparatuses used for ASTM E84 testing are unsuitable without modification for use in the other tests. The tests are:

1. ULC S101.2, used for cellulose loose-fill insulation materials and some floor coverings or melting materials.
2. NFPA 262, used for wires and cables in plenums.
3. UL 1820, used for pneumatic tubing for control systems.
4. UL 1887, used for combustible sprinkler piping.
5. UL 2024, used for raceways and cable routing assemblies.

Smoke Measurements

The smoke developed index limit of 450 originated from research conducted by UL with products burned in the ASTM E84 "tunnel test" and the smoke discharged into a 5000 ft^3 (141.5 m^3) room equipped with illuminated exit signs. Based on the time required for exit signs to be obscured, the UL report stated that materials with SDI values above 325 tended to show good to marginal visibility. The 450 SDI limit has now been used for many years and is thought to set a "reasonable" limit for smoke developed index values. This limit of 450 takes into account both the time required to produce the smoke and the effect of the smoke on vision distance. There is no direct relationship between flame spread index and smoke developed index. In the UL work for example, one material exhibited an FSI of 490 and an SDI of 57, while another one had an FSI of 44 and an SDI of 1387.

Note that the ASTM E84 SDI is determined based on light obscuration only. No physiological effects of smoke are evaluated by the 450 SDI limit.

Effects on Steiner Tunnel Results

Products should be tested as proposed for use. For example, the use of high-temperature mortar cement to mount a thin wall covering to an inorganic reinforced cement board substrate may result in artificially good test performance, but such an assembly is not likely to simulate actual installation practices. A product installed in a manner different from that used in testing may perform differently and, in some cases, unsatisfactorily. To illustrate, products that are to be installed over gypsum board with adhesives, such as vinyl wall covering, must be tested over gypsum board, because the paper facing on the gypsum board can affect fire behavior. (This is something addressed by ASTM E2404).

The significance of adhesives is a key issue. Products should be tested with fastening details that are representative of conditions of actual use and codes require that. For example, paragraph 10.2.1.1 of NFPA 101 states: "Classification of interior finish materials shall be in accordance with tests made under conditions simulating actual installations …" This idea is reinforced in the test method itself, since ASTM E84 states in 6.1: "Specimens shall be representative of the materials which the test is intended to examine."

Specimen thickness can also affect flame spread. Thinner sections of the same material often will spread flame more rapidly than thicker sections. For example, data show that the flame spread rate remains constant for an acrylic sheet (poly (methyl methacrylate) or PMMA) with a thickness greater than approximately 9.5 mm (3/8 in.). If the thickness decreases below that value, this tends to increase the rate of flame spread for that acrylic sheet. These findings indicate that products to be used in varying thicknesses must be tested at the thickness at which they are to be used. Similarly, products that are offered in different densities should be tested in a range of densities. The ASTM E84 test standard explains that test results obtained at a thickness greater than 101 mm (4 in.), which require changes in the lid or the addition of supports, are likely to be different from results of a test on the same material tested at a thickness of 101 mm (4 in.) or less.

Other mounting details can be important too. Thermally thin products, such as wood paneling with thickness of 6.4 mm (¼ in.) or less, that are tested when directly applied to an inorganic-reinforced cement board may behave differently if they were installed over furring strips with air space. The installation of paneling with air space will likely result in a greater tendency for surface flame spread. Similarly, where a product is to be applied in multiple layers, it should be tested in the maximum thickness intended for use. For example, a wall covering tested on its own may perform satisfactorily, but multiple layers of the same product applied to a wall covering may spread flame and, in recent years, multiple layers of wall coverings applied to gypsum board have been shown to contribute to flame propagation in a number of fires where multiple lives were lost.

As discussed above, the tunnel test is not able to adequately evaluate certain types of materials. Some materials, such as foam plastic insulation, can achieve a low flame spread index and still spread flames readily in actual fires. A research program involving textile wall coverings was conducted in the 1980s, and it demonstrated that ASTM E84 is often unable to evaluate textile wall coverings properly.

One should be suspicious of tunnel results for lightweight materials with low thermal inertia.

The Steiner tunnel test can also produce misleading results for some materials when they are tested using chicken wire (officially known as poultry netting) as support, since the steel will absorb much of the heat generated by the test specimen and produce lower FSI values. This is of particular interest in the case of loose fill insulation, which, when tested, uses a steel mesh with very small openings, thus maximizing the effect of the screen.

A critical issue in Steiner tunnel testing involves the use of thermoplastic materials that drip to the floor of the tunnel during testing. ASTM E84 explains (in the scope) the following three concepts.

1. *"The material, product, or assembly shall be capable of being mounted in the test position during the test. Thus, the specimen shall either be self-supporting by its own structural quality, held in place by added supports along the test surface, or secured from the back side."*
2. *"The use of supporting materials on the underside of the test specimen has the ability to lower the flame spread index from those which might be*

obtained if the specimen could be tested without such support. These test results do not necessarily relate to indices obtained by testing materials without such support."

3. *"Testing of materials that melt, drip, or delaminate to such a degree that the continuity of the flame front is destroyed, results in low flame spread indices that do not relate directly to indices obtained by testing materials that remain in place."*

Another problem area involves plastic piping. It has been common practice for some companies to test pipes in the ASTM E84 test full of water, either by placing stoppers on either end of the pipes during the test or by having water flowing through the pipes continuously. Testing pipes full of water will allow them to attain lower FSI values in the test, and that means that they would pass the requirements for use in plenums. This is not permitted in ASTM E84 (see next paragraph) because pipes are not products exempted from being required to be tested at full width. However, there is no specific language in the standard disallowing this practice.

An important issue is the testing of materials at full tunnel width. This has been very controversial but clarity now exists in the ASTM E84 verbiage. The standard states, in section 6.3, that test specimen width shall be 508-610 mm (20-24 in.), which ensures that the test specimen reaches the ledges. This section is followed by sections describing the permitted exceptions. The only exceptions are: (a) those materials for which a specific standard practice has been issued (and they were all discussed earlier), (b) "listed" adhesives and trim when the listing requires them to be tested at less than full width and (c) the products that are tested to variations of the ASTM E84 tunnel, namely the products covered by NFPA 262, UL 1820, UL 1887 and UL 2024. The language in the standard is as follows:

6.3.1 *The test specimen shall not be required to conform to the test specimen length and width described in 6.3 when the material complies with 6.3.1.1-6.3.1.3.*

NOTE 2 - When tests are conducted with materials installed at less than full width, representing the end-use width, any resulting flame spread and smoke developed indices will not relate to indices obtained with the calibration material, which is tested using the specimen width described in 6.3.

6.3.1.1 Materials for which there is a standard practice to address specimen preparation and mounting with this test method shall be tested as described in the appropriate standard practice (see 6.8).

6.3.1.2 Adhesives and trim shall be permitted to be tested in the width or length, or both, specified in their listings, or as part of their conditions for being labeled, by a nationally recognized testing laboratory.

6.3.1.3 Materials and products for which there is a specific test method or application standard requiring the use of the apparatus described in Section 5 shall be permitted to be tested in accordance with that specific test method or application standard (see Appendix X5).

When questions arise about the fire performance of a material or product, the product should be evaluated on a full-scale basis, using an ignition source simulating the type of fire likely to be encountered in actual use. Products should be mounted in a manner that is representative of the conditions of actual use, as it has been shown that often each component of a system may "pass" a certain set of fire test criteria, but the entire system will perform much worse.

Room Corner Tests

Seeking a more realistic means of assessment of the hazard of interior finishes than the Steiner tunnel, several laboratories started conducting room-corner tests around 1970. These originally comprised a 2.44 m (8 ft.) high corner construction with 0.6 to 1.2 m (2-4 ft.) wing walls. A simulated ceiling of the same material was provided. A wood crib placed in the corner at floor level was used for ignition. The degree of flame spread and the rate and amount of smoke developed were the primary observations. Interest in the rapidity of flame spread across the surface of what was considered low-flame-spread cellular plastics in actual fires reinforced the use of the corner test. Large-scale corner tests conducted by Factory Mutual Research (now FM Global) and UL (Underwriters Laboratories) have used corners up to 7.6 m (25 ft.) high with wing walls up to 15.4 m (50 ft.) long to determine the burning characteristics of cellular plastics, and the effectiveness of protective measures, such as automatic sprinkler protection or thermal barriers. Results have reinforced the premise that fire hazard cannot be fully judged on the basis of a traditional fire test method and have led to the development of the modern room-corner tests.

Three room-corner tests are particularly important: NFPA 286, Standard Methods of Fire Tests for Evaluating Contribution of Wall and Ceiling Interior Finish to Room Fire Growth; NFPA 265, Standard Methods of Fire Tests for Evaluating Room Fire Growth Contribution of Textile Wall Coverings on Full Height Panels and Walls; and ISO 9705, International Standard Fire Tests - Full Scale Room Test for Surface Products. They all use the same room and the same gas burner. The room is 2.4 m x 3.7 m x 2.4 m high (8 ft. x 12 ft. x 8 ft. high), with a door centered on one of the smaller walls. The fuel source is a propane gas burner producing a diffusion flame to expose walls (and/or ceilings) in the corner of the room opposite the door (see some details in Table 1). The ISO 9705 test is used for interior finish materials in ships but not for regulation of interior finish in buildings in the U.S.

In the NFPA 265 test method products are mounted on three walls, opposite the room door. A diffusion burner is positioned near the corner of the room and provides the required fire exposure. The smoke from the room is collected in a hood and duct exhaust system where instrumentation is used to determine heat release rate (through oxygen depletion) and smoke release (as optical density). Heat flux and temperature measurements are also, optionally, made within the room. Key visual observations are the extent of flame spread and the occurrence of flashover. In NFPA 265, the burner (placed 2 inches away from each wall, near a corner) provides 5 min 40 kW fire exposure (which simulates a "waste basket" sized fire exposure) followed by a 10 min 150 kW fire exposure. A total heat flux gauge is mounted 26 mm above the floor, facing upward, in the geometric center of the test room. A flow rate is established through the duct. Within 10 s of the initial exposure, the gas flow is increased to the final heat release rate. The ignition burner is shut off 15 or 20 min after start of the test and the test is terminated. A key issue is the burner flame height: the 150 kW burner flame does not reach the ceiling when placed as the test requires. The test method is, therefore, not applicable to ceiling coverings. Thus, while the NFPA 265 fire exposure is appropriate for some wall coverings, ceiling coverings are not adequately evaluated by this procedure because of the flame itself not reaching the ceiling and the specimens mounted on walls only.

For ceiling coverings and for all other interior finish materials, the codes use a different burner placement and output, as detailed in NFPA 286. The NFPA 286 test places the test specimen on the three walls of the room (just like the NFPA 265 test) but also covering the entire ceiling. The test uses a 5 min, 40 kW initial fire exposure, followed by a 10 min, 160 kW fire exposure, with the burner flush against both walls in the corner. The 160 kW fire exposure (even absent any contribution by the products undergoing test) will result in burner flames hitting the ceiling and turning to expose the underside of the ceiling for 457–610 mm (18-24 in.). This direct flame exposure to the ceiling is considered necessary to adequately evaluate ceiling finish.

For both NFPA 265 and NFPA 286 all measurements are made in the exhaust duct using the principle of oxygen depletion calorimetry (for heat release) and using white light technology (for smoke release).

Table 1. Room-corner Test Gas Burner: Location and Exposure

Standard	*Product exposed*	*Burner power*	*Exposure time*	*Burner location*
NFPA 265	3 walls	40 kW & 150 kW	5 min & 10 min	51 mm from walls
NFPA 286	3 walls & ceiling	40 kW & 160 kW	5 min & 10 min	Flush against two walls
ISO 9705	3 walls & ceiling	100 kW & 300 kW	10 min & 10 min	Flush against two walls

Code Requirements in the U.S.

The ASTM E84 test standard simply reports a flame spread index and a smoke developed index; it does not report classes. However, in North America these results are used to determine a classification, which determines the potential use of the material/product in practice. Table 2 shows the standard “Classes” used: Classes A, B, and C (or Classes I, II, and III) and the requirements for materials that can be used in plenums. For virtually all U.S. codes a reference to ASTM E84 is accompanied by a parallel reference to its equivalent test from UL, namely UL 723, Standard Test for Surface Burning Characteristics of Building Materials.

Table 2. Code Classification for Materials or Products Tested Using ASTM E84

	Flame Spread Index	*Smoke Developed Index*
Class A (Class I)	FSI ≤ 25	SDI ≤ 450
Class B (Class II)	26 ≤ FSI ≤ 75	SDI ≤ 450
Class C (Class III)	76 ≤ FSI ≤ 200	SDI ≤ 450
Plenum Materials	FSI ≤ 25	SDI ≤ 50

U.S. regulations classify interior finish materials using the Classes shown above, based on a combination of both FSI and SDI. It is now well recognized that considerable variability exists in tunnel test data, and precise values are not likely to be obtained in replicate tests. Further, small differences in indices (10–20 points, for example) are unlikely to be discernible in terms of actual fire behavior. Accordingly, FSI values are usually rounded to the nearest whole number divisible by 5 and SDI values are usually rounded to the nearest whole number divisible by 5 for low SDI values and to the nearest whole number divisible by 50 for SDI values of 200 or more.

In fact, the way the codes must be interpreted is that the default test is NFPA 286 (although they are not always written that way) since all wall or ceiling interior finish materials are allowed to be tested to NFPA 286 but not all of them are allowed to be tested to ASTM E84. The pass/fail criteria used in all U.S. codes for NFPA 286 (which has no criteria of its own) are as follows: there can be no flashover at any time during the test, the heat release rate cannot exceed 800 kW, the total smoke released cannot exceed 1,000 m^2, and the flame cannot spread to the edges of the test specimen (with the same pass/fail criteria also used by the codes for NFPA 265). It is important to note that any material that causes flashover in the test automatically fails. In practice, most materials are tested in accordance with the Steiner tunnel test, ASTM E84, but, as noted above, some materials are not allowed to be tested to ASTM E84 or not required to be tested at all. The “exception” materials are: very thin materials, exposed portions of structural (wood) members, foam plastic insulation, textile and expanded vinyl wall and ceiling coverings, polypropylene and high density polyethylene, plastic lockers, reflective insulation materials, site-fabricated stretch systems, fire-retardant treated wood, fire retardant coatings and interior trim (see Table 3). Two added materials have special requirements: wall base and coated wall or ceiling panels. There is a rationale for each one of the exceptions.

The exception allowing very thin materials (< 1/28 inch or < 0.9 mm) not to be fire tested is based on the concept that the paper cover for gypsum board does not constitute a serious fire hazard. Unfortunately, some wall coverings can also fall under this exception. This is a potential problem in view of the work that showed the misleading results with thin wall coverings. More important is the fact that this has, in recent times, been assumed to mean that it is acceptable to put thin veneers onto wood substrates and not test the system, in spite of the fact that it has been shown that adding a veneer onto a wood substrate will negatively affect its fire performance, whether the wood substrate is plain wood or fire-retardant treated wood. This is an item under discussion for the 2015 codes.

The exception allowing exposed portions of "structural members" (or "building elements") not to be fire tested is a very reasonable one as it addresses solid wood beams and joists, which are in general much more difficult to ignite than most interior finish materials.

Foam plastic insulation is not allowed to be used as interior finish when tested to the ASTM E84 test because experience has shown that the results are misleading, especially for thermoplastic foam insulation materials, which melt and drip in advance of the passage of the flame. This is a result of practical fire loss experience, going back to the 1970s, and the past tendency to ascribe excessive implications to Steiner tunnel results. The four tests that can be used to assess the fire performance of exposed foam plastic insulation (NFPA 286, UL 1040, Standard Fire Test of Insulated Wall Construction, UL 1715, Standard Fire Test of Interior Finish Material, and FM 4880, Approval Standard for Class 1 Fire Rating of Insulated Wall or Wall and Roof/Ceiling Panels, Interior Finish Materials or Coatings and Exterior Wall Systems) are all severe full scale tests that can adequately predict real-scale fire behavior. NFPA 286 is the only one of the four tests to quantitatively assess smoke obscuration and is both the most modern of the tests and the most widely used. Foam plastic insulation is allowed to be used when it becomes concealed (as opposed to exposed) insulation. In that case the foam plastic must be covered by a thermal barrier (which is a material that complies with the NFPA 275, Standard Method of Fire Tests for the Evaluation of Thermal Barriers Used Over Foam Plastic Insulation, set of tests. In NFPA 275 the foam plastic insulation is covered by the material to be assessed as a thermal barrier and the system is tested in two ways: (a) by means of a small-scale fire resistance test (for 15 min, but with the same pass/fail criteria as other fire resistance tests) and (b) a reaction-to-fire test. The reaction-to-fire test could be NFPA 286 (with the pass-fail criteria described above for the use of that test to approve interior finish materials) or one of the three other tests permitted for foam plastic insulation (UL 1040, UL 1715 and FM 4880). As an alternate to conducting NFPA 275, 13 mm (½ in.) thick gypsum board is automatically classified as a thermal barrier. If a foam plastic insulation material is installed behind a thermal barrier, the foam plastic insulation material must also be tested to ASTM E84 and it must comply with a Class B classification.

Textile wall and ceiling coverings have low mass and can produce misleading results when tested in the ASTM E84 test, and NFPA 265 is unsuitable for testing any ceiling coverings. Expanded vinyl wall and ceiling coverings are similar to textile coverings but they are also foam plastics, although they do not melt and drip in the tunnel and are not likely to cause the problems that foam plastic insulation materials cause. Therefore, textile wall coverings and expanded vinyl wall coverings are allowed to be tested in the NFPA 265 test as well as in the ASTM E84 test (but in the latter case they must be a Class A and the compartment must be sprinklered). Textile ceiling coverings and expanded vinyl ceiling coverings must be tested in the NFPA 286 test. The IFC allows also “existing” textile wall coverings and expanded vinyl wall coverings to continue to be used based on prior approval via a screening test version of NFPA 265, namely the so-called Method B protocol, which is now a nonmandatory part of the standard.

Polypropylene and high density polyethylene are thermoplastic materials that usually melt and drip and often used for toilet partitions. They are not allowed to be tested with the ASTM E84 tunnel because they are known to produce misleading results and they must be tested to NFPA 286.

Lockers have traditionally been constructed of steel and often line an entire wall (or even more than one) in high school corridors or in gymnasiums. In recent years lockers have been increasingly constructed of plastic materials or of wood. Codes are now requiring plastic lockers to be treated as interior finish materials and, therefore, to be tested to NFPA 286 if they are made of polypropylene or high density polyethylene. However, wood lockers are exempt from added testing if the requirement in the application is for a Class C material.

Reflective insulation materials must be tested in accordance with ASTM E84, with the mounting protocol in ASTM E2599, but are also allowed to be tested to NFPA 286.

Site-fabricated stretch system materials must be tested in accordance with ASTM E84, with the mounting protocol in ASTM E2573, but are also allowed to be tested to NFPA 286. A mounting method for these materials was added to NFPA 286.

Interior trim is allowed to exhibit a lesser level of fire performance because it covers such a small fraction of the surface; in the case of foam plastic trim, there is also a requirement for very high density, which minimizes the problems with tunnel testing. It is interesting to note that trim gets a double benefit, because it is one of the few materials/products that the standard allows to be tested at less than full width, as shown in section 6.3.1.2 of ASTM E84, described above.

Fire-retardant treated wood must meet the “extended ASTM E84” test, which means that testing must continue for a total of 30 min (as opposed to 10 min for normal tests) and the material must exhibit a Class A flame spread index, show no evidence of significant progressive combustion, and have a flame front that does not progress more than 3.2 m (10.5 ft.) beyond the centerline of the burners at any time during the test.

Fire retardant coatings are not allowed to be used for new construction (although an exception for listed factory-applied fire-retardant coated assemblies has been added to the Life Safety Code) because there is concern that it is very difficult to regulate the thickness of the coating applied in the field.

Table 3. Requirements for Interior Wall and Ceiling Finish in U.S. Codes (General)

Very thin materials (< 1/28 inch, < 0.9 mm)	*No testing required*
Exposed portions of structural members	No testing required
Foam plastic insulation	NFPA 286 (and UL 1040, UL 715, FM 4880)*
Textile wall coverings	NFPA 265, NFPA 286 or ASTM E84 **
Expanded vinyl wall coverings	NFPA 265, NFPA 286 or ASTM E84 **
Textile wall coverings (existing, IFC)	NFPA 265 (A or B), NFPA 286 or ASTM E84 **
Expanded vinyl wall coverings (existing, IFC)	NFPA 265 (A or B), NFPA 286 or ASTM E84 **
Textile ceiling coverings	NFPA 286 or ASTM E84 **
Expanded vinyl ceiling coverings	NFPA 286 or ASTM E84 **
Polypropylene	NFPA 286
High density polyethylene	NFPA 286
Plastic lockers (polypropylene or high density polyethylene)	NFPA 286
Reflective Insulation materials	ASTM E84 with ASTM E2599 or NFPA 286
Site-fabricated stretch system materials	ASTM E84 with ASTM E2573 or NFPA 286
Interior trim (not foam plastic)	ASTM E84 Class C (no smoke) or NFPA 286 ***
Interior trim (foam plastic)	ASTM E84 Class B (no smoke) or NFPA 286 ***
Fire-retardant-treated wood (FRTW)	NFPA 286 or ASTM E84 extended
Fire retardant coatings	Only for existing construction
Factory-applied listed fire-retardant coated assemblies (NFPA 101)	NFPA 286 or ASTM E84 extended (as FRTW)
Wall base	NFPA 253 ****
Metal ceiling/wall panels (NFPA 101/5000)	If listed as Class A, a coat of paint is allowed

* UL 1040, UL 1715 and FM 4880 are large scale tests suitable for comparison to NFPA 286. ** Unless NFPA 286 is used, the compartment must be sprinklered. *** Trim must cover < 10% of wall or ceiling associated. Foam plastic trim must have a minimum density of 320 kg/m^3 (20 lb./ft^3), a maximum thickness of 13 mm (½ in.) and a maximum width of 205 mm (8 in.). **** Floor trim material used at the junction of the wall and the floor to provide a functional or decorative border, and not exceeding 150 mm (6 in.) in height.

Floor trim material used at the junction of the wall and the floor to provide a functional or decorative border, and not exceeding 150 mm (6 in.) in height, which is basically an extension of the floor finish, is allowed to be tested like interior floor finish, to the flooring radiant panel test, NFPA 253, Standard Method of Test for Critical Radiant Flux of Floor Covering Systems Using a Radiant Heat Energy Source. NFPA 253 is equivalent to the better known ASTM E648, Standard Test Method for Critical Radiant Flux of Floor-Covering Systems Using a Radiant Heat Energy Source.

In the NFPA codes, listed factory-finished metal ceiling and wall panels meeting the requirements of Class A when tested in accordance with ASTM E84 are permitted to be finished with one additional application of paint of a paint thickness that does not exceed 0.9 mm (1⁄28 in.).

Plenums are defined as "compartments or chambers to which one or more air ducts are connected and that form part of the air distribution system" and they are fairly unusual outside of North America. They are primarily regulated via mechanical codes (IMC or UMC), but also via a standard for air conditioning, NFPA 90A. Interestingly, NFPA Standards Council has established that all NFPA codes must be subservient to the fire safety requirements of NFPA 90A for plenum materials. All materials contained within plenums, including interior wall and ceiling finish, must comply with a more severe classification, because they must comply with a flame spread index of ≤ 25 and a smoke developed index ≤ 50. In the case of foam plastic insulation used as wall or ceiling interior finish in plenums, it must comply with one of the following 3 options:

1. The foam plastic insulation exhibits ASTM E84 Class B fire performance and a thermal barrier separates it from the plenum.
2. The foam plastic insulation has a flame spread index of 25 or less and a smoke developed index of 50 or less when tested in accordance with ASTM E84 and meets one of the following criteria: (a) the foam plastic is separated from the plenum by a thermal barrier or (b) the foam plastic is approved based on NFPA 286, UL 1040, UL 1715 or FM 4880.
3. The foam plastic insulation exhibits ASTM E84 Class B fire performance, is covered by corrosion-resistant steel having a base metal thickness of not less than 0.016 in. (0.4 mm) and meets one of the following criteria: (a) a thermal barrier separates the foam plastic from the plenum or (b) the foam plastic is approved based on NFPA 286, UL 1040, UL 1715 or FM 4880.

Interior Floor Finish Materials

Several studies have investigated the use of the Steiner tunnel to assess the fire performance of flooring materials (especially carpets). It was determined that, among other issues, the geometry of exposure (from underneath) is not appropriate. This is of interest since red oak flooring is one of the calibration materials for the tunnel. There is, thus, no U.S. regulation of interior floor finish using ASTM E84.

In Fire and Polymers VI: New Advances in Flame Retardant Chemistry and Science; Morgan, A., et al.;
ACS Symposium Series; American Chemical Society: Washington, DC, 2012.

The traditional test used to assess interior floor finish fire performance is the flooring radiant panel test (ASTM E648 or NFPA 253). The flooring radiant panel test was designed in the early 1970's to solve the problem of carpets spreading fire outside the room of fire origin. The maximum incident flux to this test is adequate to assess flame spread but is too small (10 kW/m^2) for it to adequately address the flooring product contribution to fire hazard if the fire reaches significant intensity. The test method involves a gas-fired radiant panel which exposes a horizontal test specimen to heat from a radiant panel at a 30 degree angle to the horizontal, so the incident radiant heat flux to the test specimen varies with the distance from the specimen edge. The test assesses the critical radiant flux, which is the minimum heat flux needed for materials to propagate flame, and is assessed as the distance from the specimen edge at which flame spread ceases. Thus, the higher the value of critical radiant flux the better the fire performance of the flooring material, because it means that the minimum heat flux required to cause flame propagation of the interior floor finish tested is higher. Neither the standard ASTM nor the standard NFPA tests include smoke measurements but the ISO standard (ISO 9239-1, Reaction to Fire Tests for Floorings – Part 1: Determination of the Burning Behaviour Using a Radiant Heat Source, with a virtually identical apparatus otherwise) does, and smoke is measured in the exhaust duct; this test is not used in the U.S.

An additional interior floor finish test is the carpet ignitability test to ASTM D2859, Standard Test Method for Ignition Characteristics of Finished Textile Floor Covering Materials, also known as the methenamine pill test. In the U.S. there is a federal mandatory requirement that carpets and rugs comply with 16 CFR 1630 (Standard for the Surface Flammability of Carpets and Rugs, FF 1-70) and 16 CFR 1631 (Standard for the Surface Flammability of Small Carpets and Rugs, FF 2-70), which are technically equivalent to ASTM D2859. This is one of the very few products that is regulated at "point of sale", meaning that it is not legal to sell carpets or rugs that do not comply with the methenamine pill test. The test involves placing a lit methenamine pill on the floor covering (typically carpet) and observing whether the flame, or glow, progresses 152 mm (6 in.) from the center of the pill; if it does the product fails.

Codes require interior floor finish to meet requirements based on NFPA 253 (or ASTM E648), with minimum critical radiant flux values of 0.22 W/cm^2 (Class II) or 0.45 W/cm^2 (Class I), depending on the application. Codes usually recognize that traditional finish floors and floor coverings, such as wood flooring and resilient floor coverings, have not proved to present an unusual hazard and are not required to be tested. U.S. codes do not require smoke obscuration for interior floor finish, but smoke limits are often required for carpets in many specifications and in some transport environments.

Plenums do not have interior floor finish; it simply is the floor of the plenum itself.

Discussion

In terms of interior wall and ceiling finish, clearly the room-corner test is a much more suitable way of assessing fire performance than the ASTM E84 tunnel test. However, the codes admit the NFPA 286 room-corner test results based on the premise that materials that don't cause flashover (or high smoke release) in the room-corner test are known to also have flame spread indices of < 200 and smoke developed indices of less than 450 in the Steiner tunnel test. This is excellent as far as it goes, but needs refinement. The Steiner tunnel test is very likely to give falsely favorable results (in fact that happens often with materials that melt and drip and with materials that are thin films) but it rarely gives falsely unfavorable results (meaning that a high flame spread index, or FSI, is almost always indicative of a material with mediocre or poor fire performance). The room-corner test results are potentially much more suitable to classification of materials, because the heat release rate is obtained in the test. However, the fact that the full heat release rate data is not used for code classification purposes results in some inconsistencies occurring when comparing results from both tests. Therefore, it would be important to use the full heat release rate data in the room-corner test and not just whether flashover does or does not occur, and the codes have started in that direction by requiring a peak heat release rate not exceeding 800 kW and not just the absence of flashover. Work based on a survey of published data analyzed the comparative fire performance of 25 materials tested in the Steiner tunnel and in the room-corner and illustrates the problem:

- 5 materials exhibited an FSI of 200 or less (i.e. Class A, B, or C) in ASTM E84 and yet led to flashover in the room corner test. The Steiner tunnel test classifies them as acceptable and the room-corner test as unacceptable.
- 14 materials exhibited an FSI of 25 or less (i.e. Class A) in ASTM E84 and released less than 400 kW in the room corner test. Both tests consider them satisfactory materials.
- 2 materials exhibited an FSI of > 25 and 75 (i.e. Class B) in ASTM E84 and also released less than 400 kW in the room corner test. The Steiner tunnel test classifies them as Class B and yet, the codes would allow such materials to be used instead of Class A materials.
- 2 materials exhibited an FSI of 25 or less (i.e. Class A) in ASTM E84 and released more than 400 kW but less than flashover in the room corner test. The codes classify the materials as Class A but these materials are clearly less fire safe than those that release less than 400 kW.
- 2 materials exhibited an FSI of 200 or less (i.e. Class C) in ASTM E84 and released heat release very close to flashover (but less than flashover) in the room corner test. The Steiner tunnel test classifies them as Class C and the codes consider them equivalent to Class A materials.

In terms of smoke release by interior wall and ceiling finish, the question has been posed: is it necessary to test for smoke release if a material shows excellent fire performance in the room corner test, or is it enough to just develop low heat release products? Recent work has shown that of five series of tests conducted in room-corner tests (2 of them in Europe and 3 in the U.S.), with a total of 84 materials tested, systematically some 10% of the materials (in fact 10 of the 84) give low heat release but very high smoke release. Therefore, it is important to also assess smoke release of interior wall and ceiling finish, in a large scale test. Thus, a smoke release criterion is included in the codes for use with the NFPA 286 room-corner test. The code requirements, total smoke release (TSR) of 1,000 m^2 in the NFPA 286 room corner test, is roughly equivalent to the 450 smoke developed index (SDI) criterion used for the Steiner tunnel test.

The use of bench-scale test data to predict product behavior through the use of models has been under study for many years, but there is no agreement yet in the U.S. on using such tests for regulatory purposes. Use of data from bench-scale tests, such as the cone calorimeter (ASTM E1354, Standard Test Method for Heat and Visible Smoke Release Rates for Materials and Products Using an Oxygen Consumption Calorimeter) or the lateral ignition and flame spread test (ASTM E1321, Standard Test Method for Determining Material Ignition and Flame Spread Properties, LIFT apparatus) to predict product behavior under a variety of circumstances, may result in improved regulation of interior finish materials in the future. The models are fairly adequate in linking the actual fire hazard associated with the use of a product in a specific situation to regulatory limits. It is of interest to contrast such a future form of regulation with the current regulation of interior finishes using the traditional standardized procedure (ASTM E84) or the more modern heat release tests (such as NFPA 286) in which the behavior of one product is simply compared with another. However, it needs to be recognized that the prescriptive approach is still a practical approach for building regulation.

Referenced Codes and Standards

ICC Codes (International Code Council, Washington, DC)

- IBC: International Building Code
- IEBC: International Existing Building Code
- IFC: International Fire Code
- IMC: International Mechanical Code
- IRC: International Residential Code for One- and Two-family Dwellings
- IWUIC: International Wildland Urban Interface Code

NFPA Codes and Standards (National Fire Protection Association, Quincy, MA)

- NFPA 1: Fire Code
- NFPA 70: National Electrical Code (NEC)
- NFPA 90a: Standard for the Installation of Air-Conditioning and Ventilating Systems
- NFPA 101: Life Safety Code
- NFPA 130: Standard for Fixed Guideway Transit and Passenger Rail Systems
- NFPA 253: Standard Method of Test for Critical Radiant Flux of Floor Covering Systems Using a Radiant Heat Energy Source
- NFPA 255: Standard Method of Test of Surface Burning Characteristics of Building Materials (withdrawn 2009)
- NFPA 262: Standard Method of Test for Flame Travel and Smoke of Wires and Cables for Use in Air-Handling Spaces
- NFPA 265: Standard Methods of Fire Tests for Evaluating Room Fire Growth Contribution of Textile Wall Coverings on Full Height Panels and Walls
- NFPA 286: Standard Methods of Fire Tests for Evaluating Contribution of Wall and Ceiling Interior Finish to Room Fire Growth
- NFPA 501: Standard on Manufactured Housing
- NFPA 701: Standard Methods of Fire Tests for Flame Propagation of Textiles and Films
- NFPA 909: Code for the Protection of Cultural Resource Properties - Museums, Libraries, and Places of Worship
- NFPA 914: Code for Fire Protection of Historic Structures
- NFPA 5000: Building Construction and Safety Code
- UMC: Uniform Mechanical Code

ASTM Standards (ASTM International, West Conshohocken, PA)

- ASTM D2859: Standard Test Method for Ignition Characteristics of Finished Textile Floor Covering Materials
- ASTM E84: Standard Test Method for Surface Burning Characteristics of Building Materials
- ASTM E162: Standard Test Method for Surface Flammability of Materials Using a Radiant Heat Energy Source)
- ASTM E648: Standard Test Method for Critical Radiant Flux of Floor-Covering Systems Using a Radiant Heat Energy Source
- ASTM E1321: Standard Test Method for Determining Material Ignition and Flame Spread Properties
- ASTM E2231: Standard Practice for Specimen Preparation and Mounting of Pipe and Duct Insulation Materials to Assess Surface Burning Characteristics

- ASTM E2404: Standard Practice for Specimen Preparation and Mounting of Wall or Ceiling Coverings to Assess Surface Burning Characteristics
- ASTM E2573: Standard Practice for Specimen Preparation and Mounting of Site-Fabricated Stretch Systems to Assess Surface Burning Characteristics
- ASTM E2579: Standard Practice for Specimen Preparation and Mounting of Wood Products to Assess Surface Burning Characteristics
- ASTM E2599: Standard Practice for Specimen Preparation and Mounting of Reflective Insulation, Radiant Barrier and Vinyl Stretch Ceiling Materials for Building Applications to Assess Surface Burning Characteristics
- ASTM E2688: Standard Practice for Specimen Preparation and Mounting of Tapes to Assess Surface Burning Characteristics
- ASTM E2690: Standard Practice for Specimen Preparation and Mounting of Caulks and Sealants to Assess Surface Burning Characteristics
- ASTM E2768: Standard Test Method for Extended Duration Surface Burning Characteristics of Building Materials (30 min Tunnel Test

UL Standards (Underwriters Laboratories, Northbrook, IL)

- UL 723: Standard for Test for Surface Burning Characteristics of Building Materials
- UL 1040: Standard Fire Test of Insulated Wall Construction
- UL 1715: Standard Fire Test of Interior Finish Material
- UL 1820, Standard for Safety Fire Test of Pneumatic Tubing for Flame and Smoke Characteristics
- UL 1887: Standard for Safety Fire Test of Plastic Sprinkler Pipe for Visible Flame and Smoke Characteristics
- UL 2024: Standard for Signaling, Optical-Fiber and Communications Cable Raceways and Cable Routing Assemblies
- ULC S102.2: Standard Method of Test for Surface Burning Characteristics of Flooring, Floor Coverings, and Miscellaneous Materials and Assemblies

Other Standards

U.S. Consumer Product Safety Commission (Washington, DC)

- 16 CFR 1630 (Standard for the Surface Flammability of Carpets and Rugs, FF 1-70)
- 16 CFR 1631 (Standard for the Surface Flammability of Small Carpets and Rugs, FF 2-70)

FM Global (Norwood, MA)

- FM 4880: Approval Standard for Class 1 Fire Rating of Insulated Wall or Wall and Roof/Ceiling Panels, Interior Finish Materials or Coatings and Exterior Wall Systems

International Organization for Standardization (ISO, Geneva, Switzerland)

- ISO 9239-1: Reaction to Fire Tests for Floorings – Part 1: Determination of the Burning Behaviour Using a Radiant Heat Source
- ISO 9705: International Standard Fire Tests - Full Scale Room Test for Surface Products

Chapter 32

Flame Retardants - Regulatory Issues and Sustainability

Susan D. Landry[*]

**Albemarle Corporation, 451 Florida Street,
Baton Rouge, Louisiana, 70820 U.S.A.
[*]E-mail: susan.landry@albemarle.com**

A global shift in chemical regulations and regulatory programs has been actively underway over the past two decades. It impacts many different materials, including flame retardants. Emerging chemical regulations are focusing on characterizing the environmental and human health impacts of all substances. Industry is responding to market driven and regulatory challenges to ensure that flame retardants are safe, effective, sustainable, and meet evolving marketplace demands. A crucial aspect of sustainability is to understand the life-cycle implications of chemicals and even polymer formulations. Life-Cycle Assessments can determine if the substitution of one flame retardant or technology for another can result in unforeseen consequences that can impact society or the ecosystem. Programs are in place to drive all members of the supply chain to reduce or eliminate chemical emissions to the environment, understand human health and environmental characteristics, and make transitions to more environmentally preferred products that are sustainable. This Chapter reflects the state of activity as of July 2012.

In Fire and Polymers VI: New Advances in Flame Retardant Chemistry and Science; Morgan, A., et al.;
ACS Symposium Series; American Chemical Society: Washington, DC, 2012.

Background

The need for flame retardancy has been well known throughout our history. Around 450 BC, Egyptians used alum to reduce the flammability of wood (*1*). Romans also used a mixture of alum and vinegar to also reduce the combustibility of wood around 200 BC. About 24 BC, Roman Emperor Augustus began the first fire-fighting vigils (*2*). He also instituted fire prevention laws that impacted building regulations around 18 BC (*3*).

In the U.S. in 1938, records showed that every year fire caused the loss of 15,000 human lives (*4*). President Hoover went on record saying, *"Fire losses are in effect a tax on every man, woman, and child in the United States. This is one case where the 'tax payers' entirely by their own efforts, can reduce the rate. I hope we shall have no slackers in this campaign."* President Hoover's message and the efforts of many over the years reduced the number of fire deaths in the U.S. by a large amount. However, even with our best efforts, fire continues to be a problem and an ever-present threat in our society. In 2009, there were 1,348,500 fires reported in the United States. While the fires reported in 2009 have decreased (7% since 2008), these fires caused 3,010 civilian deaths, 17,050 civilian injuries, and $12.5 billion in property damage (*5*). On average during the period from 2005-2009, seven people died in U.S. home structure fires every day (*6*). The risk of fire is a worldwide problem, and the costs of fires and accidents are enormous throughout the world. In the 2006, the Center of Fire Statistics reported a total of 3,302,055 reported fires in 2004 in 33 countries (3.2 fires per 1,000 inhabitants) (*7*). The results were 30,170 fire deaths. A reduction in the number and consequences of fires is important for our society.

Flame Retardant Introduction

The use of flame retardants has had a positive impact on overall safety of homes, hotels, hospitals, nursing homes, offices, automobiles, and public transportation. Many lives have been and continue to be saved by the use of flame retardants (*8*). Flame retardants are used to delay the spread of fires or delay the time of flashover to enable people time to escape.

In addition to saving lives and property, the use of flame retardants prevents the formation of pollutants to air and water that are generally caused by fires. Typically, a complex mixture of materials is involved in fires (furniture, electronics, building materials, household cleaners, etc…). Combustion gases and pollutants are generated regardless of whether or not flame retardants are present. "Clearly, fire gases are dangerous to fire fighters and other citizens who could be exposed, independent of the presence or absence of flame retardants (*9*)." "Combustion gases contain very high concentrations of acutely toxic substances (*10*)." Combustion gases generated during fires that contribute to acute toxicity include CO, HCN, HCl, and acrolein (*11*).

The acute toxicity of fire gases is controlled by carbon monoxide (CO) – responsible for over 90% of fire deaths. In two studies in the U.S. involving >5,000 fatalities during 1938-1979 and the early 1990's, there was an excellent correlation between fire fatalities and levels of CO absorbed in the blood (*12*, *13*). This was the most extensive study ever put together, and the conclusion was that fire fatalities are overwhelmingly associated with the CO generated when a fire becomes large. Other causes of fire deaths are of minor importance.

Polycyclic Aromatic Hydrocarbons (PAHs) and polyhalogenated dibenzodioxins and furans (PHDDs/PHDFs) are the most important pollutants generated in fires. Compared to PAHs, the impact of PHDDs/PHDFs on our health is negligible (*11*). In the Lengerich fire (Germany in 1992), measurements and their respective cancer risk and relationship showed that the PAHs have an up to 500 times higher cancer risk than the PHDDs/PHDFs. PAHs are generated in all fires

- There are several hundred different substances in the PAH family
- Many PAHs generated in fires are carcinogenic compounds, including benzo[a]pyrene (BaP)
- PAHs are found in high quantities in the soot after fires.

There are many different flame retardants used in a wide range of applications. The flame retardant chemistries range from minerals, bromine, chlorine, phosphorus, and others. They vary in use based on the polymer used and the flame retardant standards required. Flame retardant chemistries work differently in various polymer types that are used in different applications. Selection of a specific flame retardant in a polymer will depend on required properties, such as desired loadings, physical properties, thermal stability, chemical resistance, UV stability, and reliability, to name a few. Each flame retardant has a unique set of properties and must be evaluated for each specific application.

Regulations

Over the last two decades, there has been a considerable amount of scrutiny and review over the use of a wide variety of chemicals. This has led to an ever-changing patchwork of worldwide chemical regulations. In order to ensure that the products we are using are sustainable and will be available for continued use in the future, regulatory decisions need to be based on sound science. The regulatory systems in place also need to be adhered to and accepted by everyone to ensure that we operate effectively and efficiently. While the European Union (EU) appears to have taken the lead on chemical reform, many other countries have been actively working in this area to either create similar, somewhat different, or very different chemical regulations.

EU

In the EU, the primary regulatory driver for chemicals is the REACH regulation (Registration, Evaluation, Authorization, and Restriction of Chemical substances). The RoHS Directive (European Parliament and of the Council 2002/95/EC on the Restriction of the Use of certain Hazardous Substances in Electrical and Electronic Equipment) is important for electrical goods.

The REACH Regulation entered into force on June 1, 2007 (*14*). It replaced the Council Regulation (EEC) 793/93 on Existing Substances (EU Risk Assessment Regulation). REACH was adopted to improve the protection of human health and the environment from the risks that can be posed by certain substances of very high concern (*15*). The principle of REACH is "no data, no market." This approach is welcomed, as it is important to ensure that all chemicals, including flame retardants, are safe for use now and in the future.

Pre-registration of phase-in substances under REACH was completed in (or by) December 2008. REACH indeed created a special transition regime for substances which, under certain circumstances, were already being manufactured or placed on the market before its entry into force and were notified according to Directive 67/548/EEC. Those substances are called 'phase-in substances' because they are being subject to the registration system in different phases over time, rather than all at once. The transitional arrangements set for the registration of phase-in substances introduce different deadlines based on tonnage manufactured or imported, as well as hazard profile of the said substances. The first round of substance Registration (Art. 23) was completed on 1 December 2010. This was for existing substances of the following volumes (per year/substance/any manufacturer or importer):

- 1,000 tonnes or more,
- 1 tonne or more carcinogenic, mutagenic, or toxic for reproduction substances (CMR) substances, or
- 100 tonnes or more of very toxic & R50/53 substances.

The timeline for additional existing substances to go through Registration is as follows (per year/substance/any manufacturer or importer):

- 100 tonnes or more per year by 1 June, 2013 and
- 1 tonne or more per year by 1 June, 2018.

Starting in November 2012, the European Chemicals Agency (ECHA) will make more information from registration dossiers available on its website (*16*).

The purpose of the authorization process is to ensure that risks from a Substance of Very High Concern (SVHC) are properly controlled and that the SVHC is ultimately replaced by suitable alternatives or technologies, where economically and technically feasible. Authorization is a multi-step process. The identification of a substance as a SVHC and its inclusion in the SVHC Candidate List is the first step of this process. Substances qualify as SVHC where they have either of the following properties:

- CMR (Carcinogenic, Mutagenic, Reprotoxic) cat. 1A and 1B,
- PBT (Persistent, Bioaccumulative, and Toxic),
- vPvB (very Persistent and very Bioaccumulative), or
- Substances of equivalent concern (e.g. endocrine disruptors).

The first SVHC Candidate List was published by the European Chemicals Agency on October 28, 2008, and has since been updated several times to include 84 substances. There are 14 substances on the SVHC authorization list (*updated on 18 June 2012*) (*17*). Inclusion in the list generates immediate new legal obligations for communication in the supply chain. These obligations are linked to the listed substances themselves, in preparations and articles. The second step of the authorization process is the decision of which substances from the candidate list are included in Annex XIV (substances subject to authorization). The flame retardants included in the SVHC Candidate List and Annex XIV (subject to Authorization) are hexabromocyclododecane (HBCD) and all major diastereoisomers and tris (2-chloroethyl) phosphate (TCEP) (*17*). The third step of the authorization process is the submission of an application for authorization by the manufacturers, importers, or downstream users within the deadline. After the sunset date set in Annex XIV, the substance may not be used or placed on the EU market without authorization. The authorization process differs from the restriction process in that it does not directly affect the manufacturing of a substance in the EU, only the placing of it on the market or its use. The restriction process aims at limiting or banning the manufacture, ability to place on the market (including in articles), or use of any substances that pose an unacceptable risk to human health or the environment.

In July of 2012, an updated harmonized classification and labeling for HBCD was published in the Official Journal of the EU (*18*). It has been classified as a category 2 for reproductive toxicity; the classification will be accompanied by the following labeling requirements (H361) “Suspected of damaging fertility or the unborn child” and (H362) “May cause harm to breast-fed children.” This is based on the amended Annex VI of the EU Regulation on the Classification, Labeling and Packaging (CLP) of substances and mixtures. This new classification will enter into force on 30 July 2012 and must be used as of 1 December 2013, allowing for an 18 month transition period. The CLP Regulation ensures that the hazards presented by chemicals are clearly communicated to workers and consumers in the EU through classification and labeling of chemicals (*15*).

For electrical and electronic equipment (EEE) applications, the RoHS directive was put into effect on 1 July 2006 and was recently recast (*19*). It states that Member States shall ensure that new EEE put on the market shall not contain Pb, Hg, Cd, Cr (VI), polybrominated biphenyls (PBBs) and polybrominated diphenyl ethers (PBDEs) above de-minimus levels. The RoHS recast went into effect 1 July 2011. It promotes science-based legislation, underlines the importance of coherence of RoHS with other chemicals legislation (REACH Regulation), and includes a methodology for possible future restrictions of substances in EEE (*20*). The recast RoHS will gradually open the scope of application to all EEE over an 8-year period, from 2011 to 2019.

North American Activity

North America has a wide variety of chemical regulations that are typically not overseen by a primary government agency. In addition to Federal regulations that are overseen by the U.S. Environmental Protection Agency (EPA), each U.S.

states can (and often do) have their own differing state laws and programs that regulate chemicals.

The U.S. EPA has several activities in progress for chemicals. One of their goals is the reform of the Toxic Substances Control Act (TSCA). The EPA's goal should align with their Principle #1 for TSCA reform stated on their website: to establish safety standards that are based on scientific risk assessments (*21*). They feel that sound science should be the basis for the assessment of chemical risks, while recognizing the need to assess and manage risk.

Deca-BDE

The three major producers of decabromodiphenyl ether (Deca-BDE) entered into a "partnership" with the U.S. EPA to voluntarily phase out production and importation of Deca-BDE (*22*). For many applications, including electrical & electronic equipment (except transportation and military), the target is to have Deca-BDE phased out of use by the end of 2012. Completion of the phase out for all applications, including transportation and military, is targeted for the end of 2013. Annual progress reports will be submitted to the EPA. Effective and environmentally sound alternatives for Deca-BDE are available today.

After the Deca-BDE production phase-out period, the EPA will seek to amend the Toxic Substances Control Act (TSCA) section 5(a) SNUR for certain polybrominated diphenylethers (PBDEs) by imposing a "significant new use rule" (SNUR) and a test rule under TSCA section 4(a)(1)(A) on Deca-BDE and articles containing Deca-BDE. "EPA's focus in this proposed rule is on the phase-out of the manufacture and import of PDBEs for all uses, including in articles."

The proposed SNUR includes a proposal to eliminate the article exemption. Importers of articles containing commercial Deca-BDE would be considered manufacturers of these mixtures and subject to the proposed test rule, along with persons who domestically manufacture these chemicals in bulk or as part of a mixture. You would be subject to this rule if you:

- Manufacture (includes import and for U.S. export) or process (includes for U.S. export) Deca-BDE (as well as pentaBDE and OctaBDE)
- Import articles containing commercial Deca-BDE (as well as pentaBDE and OctaBDE).

The proposed SNUR and Test Rule have been published in the U.S. Federal Register, and were open for comments until July 31, 2012.

Additional EPA Activity

In late 2009, the EPA announced a chemical action plan which is intended to identify chemicals that pose a concern to the public, move quickly to evaluate them and determine what actions need to be taken to address the risks they may pose, and initiate appropriate action. Currently, there are 10 chemicals or groups of chemicals included in the action plan. Two of those are flame retardants or flame retardant groups: PBDEs and HBCD. Recently, the EPA identified a work plan of 83 chemicals for further assessment and identified seven of these chemicals for risk assessment in 2012 (*23*). EPA intends to use the TSCA Work Plan Chemicals to help focus and direct the activities of the Existing Chemicals Program over the next several years. Antimony and antimony compounds, as well as TCEP are included in the list of 83 chemicals.

Another EPA program that has included several evaluations of alternative chemicals in various applications is the Design for Environment (DfE) program (*24*). This program is a partnership with a broad range of stakeholders. Several DfE programs that include flame retardants are currently in progress.

Other

The “Green Chemistry Initiative” was signed into law in California in October 2008 to examine the regulatory process under which chemicals should be evaluated and regulated (*25*). The plan is to develop a regulatory framework, which will encourage the development of “green chemistry” solutions to environmental and human health issues arising from currently used chemicals. In January 2012, a formal agreement was signed by the California Department of Toxic Substances Control (DTSC) and the U.S. EPA. The announcement notes that this will allow them to cooperate to minimize duplication of effort and promote consistency in methodology. Also noted in the announcement was that this creates a partnership between the two agencies and sets up a framework to collaborate on Green Chemistry issues so that California’s innovative “Green Chemistry” program can grow.

In December 2006, the Canadian federal government announced a new Chemical Substances Plan (CSP) to prioritize chemicals targeted for risk assessment and risk management (*26*). Canadians understand that they depend on “chemical substances each and every day for hundreds of things, from medicines to computers to fabrics to fuels (*27*).” Also, that “some chemical substances are made deliberately and are used in manufacturing. Others are byproducts of chemical processes. Still others occur naturally in the environment (*27*).” The Canadian CSP seeks to understand:

- How, where, and if chemicals are getting into our air, water and food
- At what levels they are found
- What is the exposure level for given chemicals
- What happens at End-of-Life
- What could short or long term exposure mean
- Advancements in research.

The Canadian Environmental Protection Act (CEPA) 1999 required the Government of Canada to examine ~23,000 "existing substances" on the Domestic Substances List by September 2006. Health Canada and Environment Canada completed a systematic categorization of these approximately 23,000 chemicals on this Domestic Substances List to determine which substances pose a risk to human health and/or the environment. Of these 23,000 substances screened, ~19,000 substances did not meet the criteria used for the categorization (persistence, bioaccumulation, inherently toxic, or greatest potential for exposure to Canadians). The remaining 4,000 substances are those that will be the subject of further attention under the Chemicals Management Plan. The Government of Canada will focus on 500 high priority substances.

Sustainable Flame Retardant Landscape

Sustainable solutions must meet the needs of the present without compromising the ability of future generations to meet their own needs (*28*). Awareness and understanding of best practices to protect the environment, human health, and safety have evolved considerably over the last several decades and grown to sustainable development. It is required that sustainable development has environmental, society, and economic concerns reconciled. Sustainable chemistry is a concept that encompasses all factors that contribute to avoiding and reducing risks for human health and the environment posed by dangerous chemicals and pollutants. Included are contributions to a decrease of resource consumption including energy and incentives to organizations or businesses that come up with innovation. Sustainable chemicals need to be functional, cost effective, and safe. The selection of a flame retardant for a specific application should be based on *"Informed Selection"* and must include the following considerations:

- Appropriate human health and environmental profile for their intended use
    - Evaluation for potential impact on human health and the environment in intended use
        - Risks during manufacturing, use, and end-of-life
        - CMR, PBT, and endocrine disruption properties

- Effectiveness in use
    - Must provide fire safety performance and address property requirements
    - Properties (physical/chemical) during manufacturing and use (including service life, reliability)
    - Maintain properties after recycle
    - Pass necessary qualification testing (including testing in use)

- Innovative Technologies
  - Keep pace with changing technologies to meet future product performance needs
  - Seek opportunities to improve environmental footprints for new and existing flame retardants
    - Life Cycle Assessment (LCA)
    - Carbon footprint, global warming, energy consumption, ozone depletion, air acidification, etc…
    - Cradle to Gate, or better yet, Cradle to Cradle
  - Demonstrate recyclability in end-use or other End-of-Life options
  - Reduce or eliminate emissions
  - Must be cost competitive.

By following these *"Informed Selection"* considerations, flame retardants are carefully selected to help avoid human health and environmental risks, failure in use, unintended consequences, and to improve the environmental footprint. Selection should be based on sound science. The quality of science has to be factored in, and there must be data transparency. Selection should be based on risk, not simply hazard. It is important to remember that Detection ≠ Risk.

End-of-Life is another issue that is important for flame retardants. For flame retardant plastics used in EEE applications a considerable amount of flame retardant plastics are used in many different parts. It has been well documented that mechanical recycle and waste-to-energy recovery are they typical options. Mechanical recycle of plastics from EEE applications is currently practiced to a limited extent due to the infrastructure and technology needed to collect and separate these materials into acceptable streams. It can result in materials for use in the original application or in downgraded applications, depending on the thoroughness of sorting, dismantling, identification, and shredding of large parts.

Several studies have looked into the recyclability of flame retardant plastics used in EEE applications (*29–33*). Studies have demonstrated that the excellent thermal stability of brominated flame retardants in formulations help to maintain the mechanical properties after recycle to what they were prior to recycle (*29*). One recycle study performed in the state of Minnesota (U.S.A.) reported in July 2001 looked into the recycle of 8,649 televisions along with other electronic equipment collected for recycle (*30*). From the televisions, 53,152 lbs of High Impact Polystyrene (HIPS) resin containing a brominated flame retardant, was collected and sent to a recycler for evaluation and comparison with commercial flame retardant HIPS containing a brominated flame retardant. The evaluation demonstrated that recycled flame retardant HIPS from the televisions met critical specification standards and could readily be reused in new products. Many other multi-pass recycle evaluations of commercial formulations again showed the excellent recyclability of various brominated flame retardant resins. Some of these were extended heat and humidity recycle evaluations. This was intended to simulate the potential exposure of EEE to heat and humidity via outdoor storage at end-of-life.

Many different EEE applications, such as large TV's and laptop computers, use polycarbonate/ acrylonitrile-butadiene-styrene (PC/ABS) resins in combination with phosphorus-based flame retardants. Several recyclability studies have looked at the mechanical recyclability of flame retardant PC/ABS formulations that are typically used in these EEE applications (*34*, *35*). These studies showed severe reduction in impact strength of these formulations after either multi-pass or humid aging recycle studies at different levels of recyclate.

LCA is an approach to assess the environmental aspects and potential impacts connected with a product, process, or service. This approach typically looks for an inventory of relevant energy and material inputs and environmental releases, evaluates the potential environmental impacts associated with inputs and releases that have been identified, and interprets the results to help a producer or user make a more knowledgeable decision. More efforts to develop LCAs for flame retardants are underway. This will help to determine environmental footprint differences from the production of various flame retardants (carbon footprint, global warming, energy consumption, ozone depletion, and air acidification.

Flame retardants should be developed using the principles of "Green Chemistry." This includes the development of chemicals and chemical processes designed to reduce or eliminate negative environmental and human health impacts. Green chemistry focuses on the design of chemical products and processes. An example of this is the development of products that are more efficient (fewer reaction steps, fewer resources required, less waste), are simpler to use (stable in air, at normal temperatures and pressures), and contain safer solvents and less waste products that are not reusable.

Voluntary Emissions Control Action Program (VECAP™)

Advances made in industrial operations, improved performance, and improvements to society (by the use of flame retardants) all help to improve the standard of living and the environment. Reducing or eliminating emissions of chemicals to air and water further minimize exposure of chemicals to humans.

VECAP stands for Voluntary – implemented by producers and users, Emissions – identify sources of product emissions, Control – develop procedures to better manage chemicals and minimize emissions, Action – dynamic continuous improvement, Program – focus on best practices (*36*).

It is an innovative environmental management tool for handling chemicals down through the supply chain, based on ISO 14001 principles. It demonstrates the proactive involvement of companies, many of whom are small and medium-sized enterprises, to adopt practices both for reasons of environmental best practice and economic efficiency.

VECAP was developed and first implemented in 2004 by three producers of flame retardants in partnership with user industries (*37*). VECAP is a program for reducing emissions to the environment by increasing an understanding of chemicals management in the value chain over and above existing legislation; promoting and facilitating open and constructive dialogue with industry, regulators and other stakeholders; raising awareness among all those involved in the process, from site personnel to top management; and implementing and disseminating best practices identified through the program.

VECAP has seen significant successes and has been implemented in European Member States, North America, Japan, and other parts of Asia. In the VECAP *EUROPEAN ANNUAL PROGRESS REPORT 2011*, it was noted that the potential emissions of one particular flame retardant (tetrabromobisphenol A - TBBPA) to land "were reduced to zero since the VECAP program began" and to air and water "were reduced to the lowest achievable level (*38*)" There has been a significant reduction in total potential emissions for three commercially available flame retardants (Deca-BDE, HBCD, TBBPA). VECAP is not only a flame retardant program; it is a model program for all plastics additives. VECAP provides both a practical and a cost-effective means of controlling emissions and will help to ensure a sustainable future for plastic additives, including flame retardants.

Fire Safety Solutions

The use of particular flame retardant chemistries depends on many factors. Each specific flame retardant has its own unique set of properties (chemical, physical, human health, environmental) and must be evaluated individually for each application. Flame retardants within particular "classes" or "families" differ greatly in properties and must be evaluated individually for specific applications.

- In a recent study published in April of 2011, commissioned by the European Commission (DG Health and Consumers / Consumer Affairs), and performed by Arcadis Belgium, 42 different flame retardants in consumer products in domestic environments were evaluated (*39*). The results had flame retardants classified in categories as follows:
- "*No Need For Immediate Risk Management*" - 6 flame retardants identified (had no risks identified): 2 Brominated Flame Retardants (decabromodiphenylethane and Tetrabromobisphenol A), 2 Chlorophosphate Flame Retardants [Bis(chloromethyl)trimethylene bis(bis(2-chloroethyl)phosphate) and Tris (2-chloro-1-methylethyl)phosphate], Diethylphosphinate aluminium salt and Chloroparaffin (MCCP).
- "*Inconclusive*" - 10 flame retardants identified: 9 Phosphorus Flame Retardants [Tricresylphosphate, Isopropylphenyl diphenyl phosphate –IPP, Resorcinol bis-diphenylphosphate – RDP, triphenylphosphate, Tris (2-chloroethyl)phosphate, 2-Ethylhexyldiphenyl phosphate, cresyl diphenyl phosphate, Tris-(isopropylphenyl)phosphate, tert-Butylphenyl diphenyl phosphate (BDP)] and 1 Brominated Flame Retardant [tetrabromobisphenol A bis (2,3-dibromopropyl ether)]

- “*Data Gaps*” - 22 flame retardants identified: 14 Phosphorus Flame Retardants [(triethyl phosphate, Tris (2-chloro-1-(chloromethyl)ethyl)phosphate, trixylyl phosphate, tris-(tert-Butylphenyl)phosphate (TBDP), guanidine phosphate, bisphenol A-bis(diphenylphosphate), bis-(tert-Butylphenyl)phenylphosphate (BBDP), melamine phosphate, tris(tribromoneopentyl)phosphate, bis-(Isopropylphenyl) phenylphosphate (BIPP), Isodecylphosphate (IDP), Hypophosphite, Hypophosphite, diethyl ethylphosphonate], 4 Brominated Flame Retardants [ethylene bis(tetrabromophtalimide), 1,2-bis(2,4,6-tribromophenoxy)ethane, tris(2,4,6 tribromophenoxy)triazine, bis(2-ethylhexyl) tetrabromophthalatedimethyl propane phosphonate], and 5 Mineral Flame Retardants [ethylene bis(tetrabromophtalimide), 1,2-bis(2,4,6-tribromophenoxy)ethane, tris(2,4,6 tribromophenoxy)triazine, bis(2-ethylhexyl) tetrabromophthalatedimethyl propane phosphonate]
- “*Risk*” - 1 flame retardant identified: Isodecyldiphenylphosphate

Some of the major significant points of this study are:

- Substituting one particular flame retardant “class” or “family” is not a method to eliminate Environmental or Human Health risks
- Some of the alternative flame retardants being promoted today will fit in the “Inconclusive,” “Data Gaps,” or “Risk” categories
- Each specific flame retardant has its own unique set of properties (chemical, physical, human health, environmental, etc…) and must be evaluated individually.

There are many different flame retardants that have been commercially available for a number of years and have undergone a considerable amount of human health and environmental tests and are not considered a CMR cat. 1A and 1B, PBT, or vPvB. One of these flame retardants is ethane-1, 2-bis (pentabromophenyl), or EBP, (also referred to as decabromodiphenyl ethane), commercially available from Albemarle Corporation as SAYTEX® 8010 Flame Retardant (8010). It is one of the most widely applicable alternatives to Deca-BDE. It is non-blooming, has very good thermal stability, very good UV stability for color applications, and excellent recyclability. In 2007, the UK Risk Evaluation found no need for risk reduction measures to be taken (*40*). EBP (8010) was one of those six flame retardants that had no risks identified in the recent DG Health and Consumers / Consumer Affairs study performed by Arcadis Belgium (*39*). It was recently announced that EBP (along with 89 other substances) would be evaluated under the EU Community Rolling Action Plan (CoRAP), part of the REACH process. For EBP, the CoRAP will be led by the United Kingdom. Positive evaluation under CoRAP should provide further confidence for the sustainable use of EBP. Over the past several years, EBP has been included in the VECAP program in order to minimize or eliminate product emissions from production and downstream supply chain use. This includes working with EBP users to encourage their understanding of the best available practices developed to reduce product emissions (*36*).

Another flame retardant that is not considered a CMR cat. 1A and 1B, PBT, or vPvB is ethylene bis-tetrabromophthalimide (EBTBP), commercially available from Albemarle Corporation as SAYTEX® BT-93 Flame Retardant (BT-93).

It is also an alternative to Deca-BDE. It has, outstanding electrical properties, is non-blooming, and has superior UV light stability. Due to its excellent thermal stability and chemical resistance, as well as insolubility, BT-93 is use in many higher temperature polymers. It is also included in the VECAP program to minimize or eliminate emissions from production and use.

In recent years, polymeric products have been the focus of many new research and development projects. This is the case for flame retardants. Polymeric materials are usually too large to be absorbed by the body or animal life. This in turn leads to products that should not be toxic or bioaccumulative. An environmentally-preferred portfolio of products called Earthwise™ , launched by Albemarle Corporation include a family of materials with a more rigorous focus on sustainability and eco-friendliness, above and beyond criteria set for existing commercial products (*41*). These criteria include bioaccumulation, toxicity, recycle capability, carbon footprint, and other critical environmental metrics. Products included in this family are GreenArmor™ and GreenCrest™. GreenArmor™ is a proprietary product, designed to be an environmentally sustainable flame retardant that maintains premium performance attributes (*42*). It is a highly stable polymeric flame retardant that lends itself to efficient recycling of plastics. It exists in a pelletized form rather than in powder to minimize emissions to the environment. When combined with the good practices driven through such programs as VECAP, emissions to the environment can truly be minimized. GreenCrest™ is a proprietary highly stable polymeric flame retardant designed to replace HBCD for use in extruded (XPS) and expanded (EPS) polystyrene applications (*43*). The VECAP program will also be used with this product to help minimize emissions to the environment.

Conclusions

The use of flame retardants provides a valuable service in our society. Flame retardants not only save lives, they help to reduce injuries, destruction of property, and reduce local pollutants that result from fires. Chemical regulations throughout the world are developing or changing to address public concern about a variety of chemicals. REACH, in particular, is setting a standard that will influence many of these developments. However, it is most important that there is consistency in approach and methodology.

Regulatory action should be risk-based and be built on a sound foundation of science. The use of particular flame retardants should be made by decisions based on *"Informed Selection."* This approach should allow sound science-based decisions to be made about existing chemicals, their use, and, where necessary, substitution strategies. For the producers and down-stream users of chemicals, there will be new opportunities for innovation, but within a more stable business environment than in the recent past. This should be positive for flame retardants as well as for other chemicals.

Sustainable flame retardant solutions should include the management of resources and stewardship of the environment. Minimizing or eliminating environmental emissions is of the utmost importance. The adoption of programs such as VECAP can result in every member of the supply chain playing its part in protecting humans and the environment from potential harm.

Flame retardants that are preferable should have acceptable environmental profiles, human health profiles, and risk management practices in place. Currently, many safe and effective flame retardants that meet these requirements are available, and Albemarle Corporation markets many of these solutions. Four of these are: SAYTEX® 8010 Flame Retardant, BT-93 Flame Retardant, GreenArmor™, and GreenCrest™.

References

1. Hindersinn, R. Historical Aspects of Polymer Fire Retardance. In *Fire and Polymers Hazard Identification and Prevention*; ACS Symposium Series 415; American Chemical Society: New York, 1990.
2. www.toadspad.net/toad-history.html, History of Fire Fighting, 9-12-12.
3. http://www.miamiokla.net/Fire/FirePrevention.html, City of Miami, Fire Department, 9-12-12.
4. Van Buskirk, E. F.; Smith, E. L.; Nourse, W. L. *The Science of Everyday Life*; Houghton Mifflin Company: Boston, MA, 1938.
5. Karter, M. J., Jr. *Fire Loss in the United States During 2009*; August 2010, www.nfpa.org.
6. Ahrens, M. *Home Structure Fires*; May 2011, www.nfpa.org.
7. *Fire Statistics*; Center of Fire Statistics, June 2006, http://ctif.org/IMG/pdf/CTIF_report11_world_fire_statistics_2006.pdf.
8. *Proven simple actions could save up to 850 lives each year from fires in Europe*; June 1, 2005, http://portal.surrey.ac.uk/portal/page?_pageid=799,434945&_dad=portal&_schema=PORTAL.
9. *Review of Fire Emissions from Products with and without BFRs and the Hazard of Exposure for Fire Fighters and Clean-up Crews*; SP Report, 2007:74.
10. Rechenbach, P.; Troitzsch, J. Smoke Toxicity and Pollutants from Fires. *Kunststoffe* **1999**, *89* (9), 132–134.
11. Troitzsch, J. *Fire Gas Toxicity and Pollutants in Fires – The Role of Flame Retardants*; FR2000 Conference, London, 8th-9th February 2000.
12. Debanne, S. M.; Hirschler, M. M.; Nelson, G. L. The importance of carbon monoxide in the toxicity of fire atmospheres. In *Fire Hazard and Fire Risk Assessment*, ASTM STP 1150; Hirschler, M. M., Ed.; American Society Testing and Materials: Philadelphia, PA, 1992;, pp 9−23.

In Fire and Polymers VI: New Advances in Flame Retardant Chemistry and Science; Morgan, A., et al.;
ACS Symposium Series; American Chemical Society: Washington, DC, 2012.

13. *Carbon Monoxide and Human Lethality - Fire and Non-Fire Studies*; Hirschler, M. M., Debanne, S. M., Larsen, J. B., Nelson, G. L., Eds.; Elsevier: London, U.K., 1993.
14. http://ec.europa.eu/environment/chemicals/reach/reach_intro.htm, European Commission, REACH, 9-12-12.
15. http://echa.europa.eu/regulations;jsessionid=FEBFE6A2B58D47C59848C02E2537D0EF.live2, European Chemicals Agency, 9-12-12.
16. http://echa.europa.eu/web/guest/view-article/-/journal_content/acde6540-cfbc-420c-b0cf-0b58485c7da9, European Chemicals Agency, 9-12-12.
17. www.echa.europa.eu/web/guest/candidate-list-table, European Chemicals Agency, Candidate List Table, 9-12-12.
18. http://www.cefic-efra.com/images/stories/Position_Paper /efra_statement_on_new_hazard_classification_2012-07-24.pdf, EFRA, 9-12-12.
19. http://ec.europa.eu/environment/waste/weee/index_en.htm, European Commission, 9-12-12.
20. http://earthwisefiresafety.com/wp-content/uploads/2011/07/EFRA_Factsheet_RoHS_20111.pdf, EFRA, 9-12-12.
21. http://www.epa.gov/oppt/existingchemicals/pubs/principles.html, U.S. EPA, Existing Chemicals, 9-12-12.
22. https://www.federalregister.gov/articles/2012/04/02/2012-7195/certain-polybrominated-diphenylethers-significant-new-use-rule-and-test-rule#p-3, The Federal Register, 9-12-12.
23. http://www.epa.gov/oppt/existingchemicals/pubs/ecactionpln.html, U.S. EPA, Existing Chemicals, 9-12-12.
24. http://www.epa.gov/dfe/pubs/about/index.htm, U.S. EPA, Design for the Environment, 9-12-12.
25. www.dtsc.ca.gov/PollutionPrevention/GreenChemistryInitiative/index.cfm, CA.gov, Green Chemistry, 9-12-12.
26. http://www.chemicalsubstanceschimiques.gc.ca/index-eng.php, Government of Canada, Chemical Substances, 9-12-12.
27. www.chemicalsubstanceschimiques.gc.ca/about-apropos/canada-eng.php, Government of Canada, Chemical Substances, 9-12-12.
28. http://epa.gov/sustainability/basicinfo.htm, U.S. EPA, Sustainability, 9-12-12.
29. www.bsef.com/uploads/Documents/documents/BSEF_factsheet_End-of-Life.pdf, bsef.com, FACTsheet, 9-12-12.
30. http://archive.leg.state.mn.us/docs/pre2003/other/010468.pdf, Minnesota Office of Environmental Assistance, Recycling Used Electronics - Report on Minnesota's Demonstration Project, 9-12-12.
31. Dawson, R. B.; Landry, S. D. *Electrical and Electronic Equipment: Are Plastics Housings and Parts Containing Flame Retardants Recyclable?* GPEC 2005, Atlanta, GA, Feb 2005.
32. TV case study, a life cycle analysis; SP TV LCA data; Simonson, M., Blomqvist, P., Boldizar, A., Moeller, K., Rosell, L., Tullin, C., Stripple, H., Sundqvist, J. O., Eds.; *Fire-LCA model*, 2000. Interscience Communication Ltd., London, ISBN 91-7848-811-7.

33. http://www.bsef.com/uploads/MediaRoom/documents/main_studies_assessing_deca-bde_end_of_life_studies.pdf, BSEF, 9-12-12.
34. Imai, T. *Comparative Recyclability of Flame Retarded Plastics*; FRCJ Proceedings, Asia Pacific Seminar, Tokyo, November 17, 2000.
35. Dawson, R. B.; Landry, S. D. *Recyclability of Flame Retardant HIPS, PC/ABS, and PPO/HIPS used in Electrical and Electronic Equipment*; IEEE 2005, New Orleans, LA, May 2005.
36. www.vecap.info, BSEF, ERFA, 9-12-12.
37. The Textile Finishers Association initiated a Code of Good Practice calling on the textile industry to audit their processes and take action to reduce Deca-BDE emissions, BSEF, 9-12-12.
38. http://www.vecap.info/uploads/VECAP_report_light.pdf, BSEF, ERFA, 9-12-12.
39. http://ec.europa.eu/consumers/safety/news/index_en.htm, European Commission, 9-12-12.
40. United Kingdom. 2007b. *Environmental risk evaluation report: 1,1'-(Ethane-1,2-diyl)bis[penta-bromobenzene]* CAS: 84852-53-9. May 2007. United Kingdom on behalf of the European Union.
41. http://earthwiseinside.com/sustainability/sustainability-with-green-chemistry.html, Earthwise, 9-12-12.
42. http://www.albemarle.com/Products-and-Markets/Polymer-Solutions/Fire-Safety-Solutions/Brominated-Flame-Retardants-183.html, Albemarle.com, 9-12-12.
43. http://investors.albemarle.com/phoenix.zhtml?c=117031&p=irol-newsArticle&ID=1697942&highlight=, Albemarle.com, 9-12-12.

Subject Index

A

ABS. *See* acrylonitrile-butadiene-styrene (ABS)
Acid-base titrations, 226
Acrylic polymers, 43
  acrylonitrile (AN), 43
  methyl methacrylate (MMA), 43
  polyacrylonitrile (PAN), 43
  poly(methyl methacrylate) (PMMA), 43
  structures of comonomers, 43*f*
Acrylonitrile (AN), 43
Acrylonitrile-butadiene-styrene (ABS), 151
Additive
  anti-oxidant, UV stabilizer, flame retardant, 3
  metal-based compounds, 83
  retard spread of flame, 3
ADP. *See* ammonium phosphate dibasic (ADP)
AIBN. *See* 2,2′-Azobis(isobutyronitrile) (AIBN)
Alkyl side-groups elimination from phosphonate unit, 46*f*
Aluminium trihydroxide (ATH), 142, 252
Aluminum hypophosphite (AP), 167
  weak Lewis acid-base, 170
AMLR. *See* average mass loss rate (AMLR)
Ammonium phosphate dibasic (ADP), 153
Ammonium polyphosphate (APP), 52, 151, 223, 335
AN. *See* acrylonitrile (AN)
Anti-dripping agents, 23
AP. *See* aluminum hypophosphite (AP)
APP. *See* ammonium polyphosphate (APP)
APP-based coatings, multistep adsorption, 335
Aromatic back bond carbons, 127
Arrhenius pre-exponential factor, 380
Aryl phosphates, 120
  flame retardancy mechanisms, 16
ASEA. *See* average specific extinction area (ASEA)
ASTM E1354 cone calorimeter test, 492
ASTM E84 test, 483
ATH. *See* aluminium trihydroxide (ATH)
ATH and another mineral filler FR, production methods, 99
Av-EHC. *See* average effective heat of combustion (Av-EHC)
Average effective heat of combustion (Av-EHC), 173
Average heat release rate (Avg.HRR), 196
Average mass loss rate (AMLR), 86
Average mass loss rate (Avg.MLR), 196
Average specific extinction area (ASEA), 86
Avg.HRR. *See* average heat release rate (Avg.HRR)
Avg.MLR. *See* average mass loss rate (Avg.MLR)
α-zirconium phosphate-based LbL coatings, multistep adsorption, 333
2,2′-Azobis(isobutyronitrile) (AIBN), 236

B

Battenfeld injection molding machine, 153
BBA. *See* tetrabromobisphenol A (BBA)
BDBA. *See* tetrabromodiglycidylether of bisphenol A (BDBA)
BDP. *See* bisphenol A bis(diphenyl phosphate) (BDP)
  flame retardancy mechanisms, 33
  gas-phase activity, 33
Bifunctional phenolic hardeners, 298
Bilayered (BL), 331
Bisphenol A bis(diphenyl phosphate) (BDP), 15, 114
  halogen-free flame retardants, 16
  investigated materials, composition in wt.%, 17*t*
Bisphenol A bis-diphenyl phosphate (BPADP), 153
Bisphenol A polycarbonate/ acrylonitrilebutadiene-styrene (PC/ABS), 15
  engineering polymer blend, 16
BKZ vertical burning test, 261, 264
BL. *See* bilayered (BL)
BL + BL deposited architecture, 338
Block copolymer synthesis
  general reaction, 274*s*
Block copolymers
  char formation and char decomposition processes, 289
  oxygen index measurements, 289
Block copolymers and reference materials, oxygen index (OI) values, 284*t*

Downloaded by BROWN UNIV on December 19, 2012 | http://pubs.acs.org
Publication Date (Web): December 18, 2012 | doi: 10.1021/bk-2012-1118.ix002

In Fire and Polymers VI: New Advances in Flame Retardant Chemistry and Science; Morgan, A., et al.;
ACS Symposium Series; American Chemical Society: Washington, DC, 2012.

Block copolymers structure, phosphate ester moiety, 289
Block copolymers synthesis
  examples, 279*t*
  general reaction, 274*s*
Block copolymers synthesized based on OI results, 290*t*
Boltzmann radiation constant (σ), 386
BPADP. *See* bisphenol A bis-diphenyl phosphate (BPADP)
Brominated epoxies, analysis of combustibility, 193
  average molar rate of decomposition, 202
  Avg.HRR and molar THR trends, discrepancies, 202
  bromine as gas-phase combustion suppressant, CC dependencies, 198
  calculated heats of complete combustion, 198*t*
  conclusions, 202
  cone calorimetry, flammability test, 198
  cone calorimetry THR, reductions, 200*f*
  experimental, 194
    analysis, 197
    BBA, efficient flame-retardant than BDBA, 196
    cone calorimetry data, summary, 196*t*
    gas-phase combustion processes, 197
    oxygen consumption technique, 195
    results, 195
  gas-phase combustion efficiencies, 199*f*
  heats of combustion, 193
  introduction, 194
  pyrolysis-flaming-combustion calorimeter, 193
  pyrolysis-flaming-combustion calorimetry apparatus, 195*f*
  relative Avg.HRR and relative molar THR, comparison, 201*f*
Brominated fire-suppressing agents, 194
Bunsen burner test, 3

C

Cage-shaped solid phosphate, tris(1-oxo-2,6,7-trioxa-1-phosphobicyclo[2,2,2]octane methylene-4) (trimer), 115*s*
  flexural modulus, 116
Canadian Environmental Protection Act (CEPA), 530
Carbon nanofibers (CNF), 344
Carbonaceous char, 25
CB[6]. *See* Cucurbit[6]uril (CB[6])
CB[6]/20A–MMT, preparation, 71
CB[n] family, ability to bind amines, 70
CC. *See* cone calorimetry (CC)
Cellulose and wood flour
  cellulose-based flame retardant systems, 156
  effect of feed location, 156
    flexural modulus, 158*f*
    flexural strength, 158*f*
    TG and DTG curves, 159*f*
  glass transition temperature, 159
    ABS blends, glass transition data, 160*t*
    plasticization flow improvements, 161*t*
  mechanical properties, 157
  morphology, 160
  thermogravimetric analysis, 157
  wood-based flame retardant systems, 155
Cellulose phosphate, thermal stabilities, 227
CEP. *See* charring efficiency of phosphorus (CEP)
CEPA. *See* Canadian Environmental Protection Act (CEPA)
Cetyltrimethyl ammonium bromide (CTAB), 391
Chain growth polymers, reactive modification, 38
Char promoter, phosphorous, 40
Charring efficiency of phosphorus (CEP), 373
Chemical substances plan (CSP), 529
Chi. *See* chitosan (Chi)
Chitosan (Chi), 335
Chloro-phosphate esters, 251
Classic IFR systems, 52
CloNa. *See* sodium montmorillonite (CloNa)
CNF. *See* carbon nanofibers (CNF)
CNF additives, 350
Combined usage of phosphonates and ZS, 143
Combined useage of organo-ferrocene and Fyrol RDP, 144
Complex of CB[6]/20A, preparation, 71
Cone calorimetry (CC), 194
Cone test of PMP and PMPN, 65*f*
Conventional halogen-free flame retardants and nanocomposites technology, synergy, 119
  phosphorus-containing compounds, 114
  siloxanes, 117
  sulfur-containing compounds, 118
COP. *See* CO production (COP)

Downloaded by BROWN UNIV on December 19, 2012 | http://pubs.acs.org
Publication Date (Web): December 18, 2012 | doi: 10.1021/bk-2012-1118.ix002

Downloaded by BROWN UNIV on December 19, 2012 | http://pubs.acs.org
Publication Date (Web): December 18, 2012 | doi: 10.1021/bk-2012-1118.ix002

Copolyester (PES), 183
Copolymer of MMA, condensed phase mechanism, 46*f*
CO production (COP), 176
Core-shell structure latex, 117
Cost-effective flame retardants, 328
CSP. *See* chemical substances plan (CSP)
CTAB. *See* cetyltrimethyl ammonium bromide (CTAB)
Cucurbit[6]uril (CB[6]), 69
  compression-molded surfaces, X-ray diffraction patterns, 74
  conclusion, 81
  cone calorimetry, 78
  cone calorimetry results, 75
  experimental, instrumentation, 71
  experimental materials, 70
  fire retardant material, 69
  introduction, 69
  melt blended PMMA and PS, heat release rate curves, 76*f*
  PMMA and PS, cone calorimetry, 75*t*
  PMMA and PS series
    char morphology, 77*f*
    TGA plots, 74*f*
  polyurea composites with CB[6], 76
  preparation, 71
  PS- and PMMA composites with CB[6], 73
    1H NMR spectra, comparison, 73*f*
  robust cage structure, 72
  robust macrocyclic host molecule, 69
  structure, 72*f*
  thermal properties of FR filled PU, 79*t*
  thermal properties of polyurea, 78*t*
  thermal stability, 74, 76
Cu Kα radiation, 409
Curable silicone-based coatings, fire performance, 205
  changes of $\rho.c_p$, 216
  convective/radiative heating test, 207
  cross-linked elastomers, 211
  D $[SiO_2(CH_3)_2]$ and T $[CH_3Si(O_{1/2})_3]$ structures, 205
  discussion and conclusion, 220
  experimental
    D, T^i silicone structures, schematics presentation, 208*f*
    fire performance, 208
    materials, 207
    solid state NMR, 207
    thermal properties, 209
    Torch test, schematic representation, 209*f*
  fire performance, 212
  heat diffusivity, 216
  Hotdisk method, 207
  introduction, 206
  poly-addition reaction, 206*f*
  poly-condensation reaction, 206*f*
  resin characterization, 210
  resin cross-linking, chemical pathway, 210*f*
  S1/GCC and S2/GCC, TG curve, 216
  Si-O-Si bond, 218
  spectra, deconvolution, 211
  TGA-FTIR experiment, 216
  thermal diffusivity α, 215
  thermal properties, 213
  thermal stability of S1/GCC compared to S2/GCC, 216
  virgin steel plate and silicone coatings plate, 212*f*
Cyanuric chloride, 125
Cyanuric ring, 128

D

DBA. *See* diglycidylether of bisphenol A (DBA)
Deca-BDE. *See* decabromodiphenyl ether (Deca-BDE)
Decabromodiphenyl ether (Deca-BDE), 528
DGEBA. *See* diglycidyl ether of bisphenol A (DGEBA)
DGEBA based epoxy system, 306
DGEBA resins flame retardant, 301
DICY. *See* dicyandiamide (DICY)
Dicyandiamide (DICY), 295
Differential scanning calorimeter (DSC), 237
Differential scanning calorimetry (DSC), 154, 271
Differential termogravimetric (DTG), 157
Diglycidyl ether of bisphenol A (DGEBA), 295
Diglycidylether of bisphenol A (DBA), 194
9,10-dihydro-9-oxa-10-phosphaphenanthrene-10-oxide (DOPO), 83, 120, 236
Dimethyl 2-(methacryloyloxyethyl) phosphate (DMMEP), 363
Diphenyl decyl phosphate (DPDP), 153
DMA. *See* dynamic mechanical analysis (DMA)
DMMEP. *See* dimethyl 2-(methacryloyloxyethyl) phosphate (DMMEP)
DMP-RDP. *See* tetra-2,6-dimethyl resorcinol diphosphate (DMP-RDP)

Downloaded by BROWN UNIV on December 19, 2012 | http://pubs.acs.org
Publication Date (Web): December 18, 2012 | doi: 10.1021/bk-2012-1118.ix002

DOPO. *See* 9,10-dihydro-9-oxa-10-phosphaphenanthrene 10-oxide (DOPO)
DPDP. *See* diphenyl decyl phosphate (DPDP)
DSC. *See* differential scanning calorimeter (DSC); differential scanning calorimetry (DSC)
DTG. *See* differential termogravimetric (DTG)
3D TG/FTIR spectrum, 61*f*
Dynamic mechanical analysis (DMA), 225, 343

E

EBS. *See* ethylene bis-stearamide (EBS)
Eco-friendly FR-ABS, 165
EDX. *See* electron dispersive X-ray spectroscopy (EDX)
EEE. *See* electrical and electronic equipment (EEE)
Effective heat of combustion (EHC), 175
Efficiency of phosphorus in vapor phase (EPV), 373
EG. *See* expandable graphite (EG)
EHC. *See* effective heat of combustion (EHC)
Electrical and electronic equipment (EEE), 527
Electron dispersive X-ray spectroscopy (EDX), 271
Electron scanning microscopy (ESM), 271
Engineering biodegradable polymer blends
  biodegradable polymers, flame retardant, 430
  common biodegradable polymers, 428
    material properties and chemical structures, 429*t*
    neat ecoflex, PLA, PLA-Ecoflex blend, mechanical properties, 430*t*
    PLA/ecoflex, biodegradable blend, 429
    TEM/SEM of blend of PLA/ecoflex, 430*f*
  common environmental FR formulations and flammability, 432
    blends of RDP starch/ecoflex(60/40 wt%) self-extinguishing, 433
    contact angle measurement, 434*t*
    HNT and Cloiste 20A particles, 437
    MLR of starch/ecoflex with different nanoparticles, 439*f*
    NEXAFS spectra of starch, ecoflex, and RDP and STXM images, 433*f*
    PLA/ecoflex blends, SEM images, 435*f*
    PLA/ecoflex/starch and PLA/ecoflex/RDP starch, STXM images, 436*f*
    PLA/RDP and PBAT/RDP clays, 435
    RDP-coated HNTs and EDAX of squire box, 434*f*
    RHR of starch/ecoflex with RDP starch, 440*f*
    SEM images of residues, 438*f*
    starch/ecoflex blends, elastic modulus and hardness, 441*t*
  conclusion, 442
  introduction, 428
  morphology, mechanical property, and flame retardancy, 427
  resorcinol bis (diphenyl phosphate) (RDP), properties of thermal stability, 431*t*
    impact strength and UL94-V0 flammable test, 432*f*
Epoxy/amine systems containing ZnAc, cone data summary, 89*t*
Epoxy-amine thermoset
  fire-retardant additives, 83
    cobalt-aluminum dodecanoate LDH (CoAl), 86
    conclusions, 94
    EPON 826, 85
    experimental, 85
    hydrated metal salts, 90
    metal salt hydrates of zinc acetate and cobalt acetate, 94
    studied compositions, 86*t*
  introduction, 83
Epoxy materials, additive flame retardants, 304
Epoxy-novolac based resin, 299
  DOPO, its derivatives, DPPO and Ph_2PO, efficient flame retardants, 299
Epoxy resin formulations, 297*f*
Epoxy resins, synergistic flame retardant mixtures, 295
  combining gas-phase and condensed-phase active flame retardants, 305
  crystalline boehmite and DOPO, synergistic combinations, 303
  DDPO and its derivatives, poor flame retardant efficiencies, 299
  ecologically-friendly and cost-efficient, 309
  epoxy-novolac, 297
  fusion process (so-called preformulation), 296

In Fire and Polymers VI: New Advances in Flame Retardant Chemistry and Science; Morgan, A., et al.;
ACS Symposium Series; American Chemical Society: Washington, DC, 2012.

Downloaded by BROWN UNIV on December 19, 2012 | http://pubs.acs.org
Publication Date (Web): December 18, 2012 | doi: 10.1021/bk-2012-1118.ix002

  inert fillers, insoluble, 302
  introduction, 296
  non-reinforced epoxy samples, 298
  novel melaminium or guanidinium salts, 309
  organic cations and anions containing nitrogen and phosphorus, chemical structures, 305*f*
  polyepoxide-based resin system, 297
  PWB epoxy materials, reactive flame retardants, 298
  summary and conclusions, 308
  synergistic flame-retardant systems, 304
EPV. *See* efficiency of phosphorus in vapor phase (EPV)
ESM. *See* electron scanning microscopy (ESM)
Ethylene bis-stearamide (EBS), 153
Ethylene-vinyl acetate (EVA), 99
EU. *See* European Union (EU)
European Union (EU), 392, 525
EVA. *See* ethylene-vinyl acetate (EVA)
EVA copolymers
  mineral filler fire retardants, 97
    aluminium hydroxide ($Al(OH)_3$), 98
    calculated FR contributions and measured LOI values, comparison, 104*f*
    conclusions, 110
    effect of huntite/hydromagnesite ratio, limiting oxygen index, 104*t*
    EVA-huntite-hydromagesite mixtures, 107
    experimental, materials, 102
    group II or III carbonates or hydroxides, 98
    heat absorbed, determined from heat capacity, 100
    HRR at varying heat fluxes of diferent samples of FR EVA, 105*f*
    huntite and hydromagnesite, mixtures, 102
    individual energy contributions to FR effect, 108*f*
    peak heat release rate and endothermic decomposition of filler, 109*f*
    polymer flammability reduction, non-combustible filler, 97
    pyrolysis GC-MS traces, 109*f*
    summary of cone calorimeter data, 107*t*
Expandable graphite (EG), 253

F

FESEM. *See* field emission scanning electron microscope (FESEM)
Fiber reinforced polymers (FRP), 481
  fiber reinforced polymers, comparison
    ASTM E662 test only measures smoke density, 490
    conclusion, 493
    degrees of fire performance, 482
    experimental, 482
    filled halogenated resin systems, flame spread tests, 484*t*
    flame spread tests, 486*t*
    resins used in test program, 483*t*
    smoke tests, 488*t*
  perform in fire performance tests, 481
Field emission scanning electron microscope (FESEM), 154
FIGRA. *See* fire growth rate (FIGRA)
Fire behavior, 8
Fire death rates per million population, comparison, 3*f*
Fire growth rate (FIGRA), 375
Fire performance index (FPI), 330
Fire propagation index (FPI), 56
Fire risk and fire safety, 8
Flame retardancy
  synergistic use of talc, 15
    conclusion, 33
    introduction, 16
    investigating materials with different talc content, 33
Flame retardancy chemistry, the golden age (1950-80 period), 328
Flame retardant chemicals, 3
  undergone extensive risk assessment, 5
Flame retardant chemistry
  conclusion, 12
  fire death rate, 2
    high rate, factors, 3
  flame retardant value example, 2
  introduction, 1
  polymers, enabling technology, 7
  toxic fire emissions
    prime toxic product, carbon monoxide (CO), 5
Flame retardant polyurethane foams, 140
  advance PCFC as tool for polyurethane development, 456
  chemical structures, 448
  conclusions, 455
  FMVSS foam samples, final chars, 451*f*
  FMVSS 302-rated foams, heat release data, 450*t*
  milligram scale flammability testing, 445

Downloaded by BROWN UNIV on December 19, 2012 | http://pubs.acs.org
Publication Date (Web): December 18, 2012 | doi: 10.1021/bk-2012-1118.ix002

        ASTM method, 446
        dripping behavior, 445
        environmental, health, and safety (EH&S) issues, 445
        experimental section, 447
        flame ignition, horizontal orientation, flame spread test, 447
        FMVSS 302-rated foams, 448
        introduction, 445
        synthesizing, registering, and developing new chemicals, risks and costs minimization, 456
    risk of catastrophic fire loss, 445
    TB-117-rated foam data, 453
    TB-117-rated foams, heat release data, 453
    two-step decomposition, 455
Flame retardant PUR foams, smoke generation, 146*f*
Flame retardants
    conclusions, 535
    fire safety solutions, 533
        alternative to Deca-BDE, 535
        data gaps, 534
        EU Community Rolling Action Plan (CoRAP), 534
        GreenArmor™ and GreenCrest™, 535
        research and development projects, 535
        risk, 534
    introduction, 524
    regulation
        additional EPA activity, 528
        Canadian Environmental Protection Act (CEPA), 530
        chemical substances plan (CSP), 529
        green chemistry initiative, 529
        significant new use rule (SNUR), 528
    regulations
        certain hazardous substances in electrical and electronic equipment, restriction of use, 525
        decabromodiphenyl ether (Deca-BDE), 528
        EU, 525
        EU risk assessment regulation, 526
        North American activity, 527
        pre-registration of phase-in substances under REACH, 526
        SVHC authorization list, 527
        U.S. Environmental Protection Agency (EPA), 527
    regulatory issues and sustainability, 407
        background, 524
        global shift in chemical regulations and regulatory programs, 407
        life-cycle assessments, 407
    sustainable flame retardant landscape
        appropriate human health and environmental profile, 530
        EEE applications, 532
        effectiveness in use, 530
        informed selection considerations, 531
        innovative technologies, 531
        principles of green chemistry, 532
    sustainable flame retardant solutions, 536
    use of particular flame retardant, 533
    voluntary emissions control action program (VECAP™), 532
Flame retardant toxicity, 4
Flame retardation by phosphorus compounds
    acrylic polymers, 43
    active in condensed or vapor phase, 39
    conclusion, 48
    general considerations, 39
    highly effective flame retardants, 39
    polyolefins and some related polymers, 41
Flame retarded polypropylene nanocomposites, melt dripping behavior characterization
    complex viscosity of flame retarded PP samples, 321*f*
    complex viscosity of polymers and their molten drops, 321*t*
    conclusions, 324
    experimental
        effect of nanoclay and flame retardants, 315
        mass percentages of various components in formulations, 313*t*
        melt dripping testing, 313
        rheology, 315
        sample, 312
    flammability of polymers, 311
    furnace and UL-94 equivalent test, 316*f*
    introduction, 311
    mass loss as function of time, 320*f*
    melt dripping during UL94 vertical burning test, 317
    melt dripping in furnace, 315
    melt viscosity, 312
    melt-processed polymeric materials, 312
    molten drops
        characterization, 321
        complex viscosities, 322
    NH 1197 and FR 372, furnace tests, 316*f*

In Fire and Polymers VI: New Advances in Flame Retardant Chemistry and Science; Morgan, A., et al.;
ACS Symposium Series; American Chemical Society: Washington, DC, 2012.

  - PP, PP containing clay and FRs, thermal analysis results, 323*t*
  - PP, PP-NH 1197 and PP-E-NH 1197 drops, digital images, 317*f*
  - real-time melt-dripping behavior, 311
  - rheology, 320
  - summary of melt dripping results for PP, 318*t*
  - summary of melt/burn dripping results, 319*t*
  - themogravimetric curves of polymer samples and their molten drops, 322*f*
- Flaming and non-flaming combustion, 194
- Flammability of ABS with cellulose fibers, 156*t*
- Flammability of ABS with wood fibers, 155*t*
- Flammable Fabrics Act, 6
- Flexible polyurethane foam (FPUF), 251
- Flexible polyurethane foams, flame retardancy
  - allyl-substituted compound, 258
  - boron- and phosphorus-containing aromatic compounds, 256
  - boronated and phosphonated terephtalic acid derivatives, 256
  - cellulose treated PU foam, 254
  - conclusion, 268
  - effect of PAED and melamine as flame retardants, 262*t*
  - effect of PAPD and melamine as flame retardants, 263*t*
  - EG and Fyrol PNX, 255
  - foam manufacturing process, 268
  - introduction, 251
  - linear flammability test, 255
  - melamine (co-additive to PAED), 262
  - melamine and TCPP, synergistic effect, 261
  - methyl-DOPO, 256*f*
  - non-phosphorus additives, 252
    - exothermic oxidation, 253
    - slabstock flexible polyurethane foams, 253
    - sol-gel process, 252
  - phosphoramidates and melamine, synergism/antagonism
    - acid catalyzed polyurethane bond scission, 267
    - antagonistic effect of melamine, 266
    - BKZ flammability test, 260*t*
    - complex multistep degradation, 266
    - flame retardancy of TCPP containing foams, effect of melamine, 262*t*
    - flame retardant action in FPUF, 267*s*
    - flame retardants compounds, 259*f*
    - flammability results TCPP treated FPUF, 261*t*
    - Foam E, thermal decomposition, 265*f*
    - heat release rates of foams with and without any FR, 264*f*
    - PAED and PAPD, synthesis, 259*s*
    - PAPD + melamine treated foams, 266
    - PAPD and PAPD + melamine treated foams, PCFC analysis
    - PCFC data for foams, 265*t*
    - PFUF manufacturing, formulation, 260*t*
  - phosphorus FRs, general structure, 258*f*
  - phosphorus-based flame retardants, 256
  - reactivity, mechanical and fire properties, 253
  - smoke density and toxicity test, 255
  - solid flame retardants, application, 254
- Flexible polyurethane foams, preparation, 140
- Flexible PUR foams, inorganic flame retardant additives approach, 142
- Foams, three-dimensional structures containing gas bubbles, 464
- Forced-flaming behavior, 19
- Fourier transformed infrared (FTIR), 209
- FPI. *See* fire performance index (FPI); fire propagation index (FPI)
- FPUF. *See* flexible polyurethane foam (FPUF)
- FR natural fiber blends, property improvements
  - base color improvements, 163
  - color improvements, 163
  - improved ductility, 164
  - improved ductility with added NBR, 164*t*
- FRP. *See* fiber reinforced polymers (FRP)
- FTIR. *See* fourier transformed infrared (FTIR)
- FT-IR of organo-modified sepiolite, 396
- FTIR spectra of PMP and PMPN at different temperatures, 64*f*
- Fyrol PNX, 452
- Fyrolflex® RDP, 147

G

- GCC. *See* ground calcium carbonate (GCC)
- Gel permeation chromatography (GPC), 237, 271
- GFPA6. *See* Glass fiber reinforced polyamide 6 (GFPA6)

Downloaded by BROWN UNIV on December 19, 2012 | http://pubs.acs.org
Publication Date (Web): December 18, 2012 | doi: 10.1021/bk-2012-1118.ix002

Downloaded by BROWN UNIV on December 19, 2012 | http://pubs.acs.org
Publication Date (Web): December 18, 2012 | doi: 10.1021/bk-2012-1118.ix002

GFPA6-AP-MCA composites, TG and DTG curves, 171*f*
GFPA6-AP-MPyP composites, TG and DTG curves, 172*f*
GFPA6 composites
  AP/MCA could reduce CO production, 176
  conclusions, 179
  cone calorimetric analysis, 173
  cone calorimetric data, 174*t*
  COP and TSP curves, 176*f*
  degradation, 171
  degradation products and residue analysis, 178
    char residues, digital photographs, 178*f*
    SEM images of residues, 179*f*
    small lumps char layer, 179
  fire safety degree, 179
  flame retardance, 173
  gas fuel-dilution effect, 179
  HRR curves, 174*f*
  thermogravimetry results, 170*t*
  UL-94 and LOI tests for composites, results, 173*t*
Glass fiber reinforced materials, 175
Glass fiber reinforced PA6 flame, 167
Glass fiber reinforced polyamide 6 (GFPA6), 167
  candlewick effect, 168
  engineering plastic composite, 168
  experimental
    materials, 169
    measurements, 169
    sample preparation, 169
  introduction, 168
  thermal degradation behavior, 170
Glass transition temperature values, 85
Global fire performance tests, introduction, 481
Global market of flame retardants, 9
Glycidyltrimethylammonium ions, 228
GPC. *See* gel permeation chromatography (GPC)
Ground calcium carbonate (GCC), 205

H

Halogenated polyurethanes, gas phase and char retardation, 291
Halogen free fire retardants, 392
Halogen-free flame retardant flexible polyurethane foams, 139
  average smoke extinction area, 147
  conclusion, 148
  flame retardant additives list, 141*t*
  flammability evaluation, 141
  introduction, 140
  mechanism, 140
  synergistic flame retardant effects, 148
HCC. *See* heats of complete combustion (HCC)
HDT. *See* high heat distortion temperature (HDT)
Heat release capacity (HRC), 57
Heat release rate (HRR), 254
Heats of complete combustion (HCC), 197
High heat distortion temperature (HDT), 113
High impact polystyrene (HIPS), 531
HIPS. *See* high impact polystyrene (HIPS)
Hot disk technology, 213
HRC. *See* heat release capacity (HRC)
HRR. *See* heat release rate (HRR)
HT. *See* hydrotalcite (HT)
Huggett's relation, 362
Huntite and hydromagnesite, decomposition, 99
Hybrid organic-inorganic APP based LbL complex architectures, 337
Hydrated metal salts
  composites of ZnAc, PHRR and AMLR values, 92*f*
  enhance fire retardant properties of polymers, 90
  epoxy/amine composites of ZnAc, 90
    do not produce extra smoke, 92
    heat release rate curves, 91*f*
  zinc acetate dihydrate (ZnAc), 90
    fire retardant action, 92
Hydromagnesite, endothermic decomposition, 99
Hydrophilicity and hygroscopicity, 114
Hydrophobic polymer matrices, 408
Hydrotalcite (HT), 329
Hydroxyl terminated phosphate ester oligomers, 288
Hydroxy terminated oligomers
  condensation of phenyl phosphonic dichloride, diol, diphenol or diamine in excess, 288
  molecular weight, GPC, 288

I

IBC. *See* International Building Code (IBC)
ICC. *See* International Code Council (ICC)

Downloaded by BROWN UNIV on December 19, 2012 | http://pubs.acs.org
Publication Date (Web): December 18, 2012 | doi: 10.1021/bk-2012-1118.ix002

- ICP-OES technique, 226
- IEBC. *See* International Existing Building Code (IEBC)
- IFC. *See* International Fire Code (IFC)
- IFR. *See* intumescent flame retardant (IFR)
- IFRs. *See* intumescing flame retardants (IFRs)
- IMC. *See* International Mechanical Code (IMC)
- IMO. *See* International Maritime Organization (IMO)
- Incandescent melt-dripping phenomenon, 332
- Inter-chain cyclizations, 43
- Interior finish fire requirements, codes and standards, 497
  - NFPA 1 (fire code), 498
  - NFPA 101 (life safety code), 498
  - NFPA 501 (standard on manufactured housing), 498
  - NFPA 5000 (building construction and safety code), 498
  - NFPA 90A (standard for the installation of air-conditioning and ventilating systems), 498
  - UMC (Uniform Mechanical Code), 498
- Interior finish in United States Codes
  - building material, undesirable fire properties, 496
  - fire testing requirements, 495
  - ICC and NFPA codes and standards, development, 499
  - interior finish fire safety requirements, key locations, 499
  - interior trim, 496
  - interior wall and ceiling finish materials, fire tests, 500
    - ASTM E2573, site-fabricated stretch systems, 503
    - ASTM E2579, variety of wood products, 503
    - ASTM E2690 addresses testing caulks and sealants, 504
    - ASTM E2688 addresses testing tapes, 504
    - ASTM E84 test, 501
    - ASTM E84 test standard, 507
    - code classification purpose, 517
    - code requirements in U.S., 510
    - different burner placement and output, 510
    - discussion, 517
    - effects on Steiner tunnel results, 506
    - exception materials, 511
    - extended ASTM E84 test, 505
    - factory-finished metal ceiling and wall panels, 514
    - fire-retardant treated wood, extended ASTM E84 test, 513
    - foam plastic insulation used as wall or ceiling interior finish, 514
    - inorganic-reinforced cement, 507
    - insulated wall construction, standard fire test, 512
    - interior floor finish fire performance, traditional test, 516
    - interior floor finish materials, 514
    - interior wall and ceiling finish in US codes, requirements, 514*t*
    - materials or products tested using ASTM E84, code classification, 511*t*
    - minimum critical radiant flux values, 516
    - mounting instructions, 502
    - NFPA 265 test method, 509
    - plastic piping, 508
    - polypropylene and high density polyethylene, thermoplastic materials, 513
    - progressive combustion, 505
    - real-scale fire behavior, 512
    - referenced codes and standards, 518
    - room corner test, 509
    - smoke measurements, 506
    - standard practices, ASTM E2231, ASTM E2404, ASTM E2573 and ASTM E2599, 502
    - standard test methods, 505
    - Steiner tunnel test, 500
    - surface burning characteristics of building materials, standard test, 511
    - testing of materials at full tunnel width, 508
    - textile wall coverings, 507
  - introduction, 496
  - NFPA 286 room-corner test, 495
- International Building Code (IBC), 497
- International Code Council (ICC), 497
- International Existing Building Code (IEBC), 497
- International Fire Code (IFC), 497
- International fire death rates per million population, 2*f*
- International Maritime Organization (IMO), 492
- International Mechanical Code (IMC), 497
- International Residential Code (IRC), 497
- Intra-molecular cyclization interruption, radical mechanism, 45*f*

Downloaded by BROWN UNIV on December 19, 2012 | http://pubs.acs.org
Publication Date (Web): December 18, 2012 | doi: 10.1021/bk-2012-1118.ix002

Intumescent char characterization, 64
Intumescent flame retardant (IFR), 52, 183
Intumescent flame retardant copolyester hot melt adhesive
  conclusion, 191
  experimental
    carbonaceous residue, 190
    cone calorimeter, 186*f*
    flame retardancy, 185
    materials, 184
    performance test, 184
    PES/IFR and PES/IFR/3%4A, 190*t*
    sample preparation, 184
    thermal degradation and charring behavior, 188
  introduction, 183
  polybasic acids and polyatomic alcohols, 183
Intumescent flame-retarded polypropylene composites
  Ni^{2+}-Fe^{3+} layered double hydroxide, synergistic effects, 51
    conclusion, 67
    crystallization behavior, 59
    experimental, 53
    flame retardancy, 55
    introduction, 52
    MP/PEPA IFR system, 52
    results and discussions, 55
    thermal stability, 58
Intumescing flame retardants (IFRs), 224
IRC. *See* International Residential Code (IRC)
Isocyanate-based monomer, 452

L

Layered double hydroxide and metal oxide, 86
  heterogeneous dispersion state, 86
  thermal degradation studies, 87
Layered double hydroxide flame retardants, 407
  Brunauer, Emmett, and Teller (BET) method, 409
  cone calorimeter data, 418
    comparison between residues, 422*f*
    conclusions, 423
  d-spacing values, 414
  exfoliate hectorite clays, 412
  experimental section
    instruments and characterization, 409
    materials, 409
    PS/LDH nanocomposites by solution blending, preparation, 410
    results and discussions, 411
    surface modification and suspension stability of LDH, 410
    synthesis of magnesium aluminum carbonate layered double hydroxides (Mg/Al-CO_3-LDH), 410
  high efficiency allowing for low loadings, 408
  hydrophobic polymer matrix, 413
  introduction, 408
  LDH and ATH, differential scanning calorimetry curves (DSC), 418*f*
  LDH and LDH-DBP
    photographs of THF suspensions, 415*f*
    PXRD pattern, 414*f*
  LDH and LDH-SMM, 60min PXRD pattern, 413*f*
  LDH and surface modified LDH-DBP, sedimentation kinetics, 415*f*
  LDH synthesized by urea hydrolysis method, 411*f*
  LDHs
    surface modification and suspension stability, 413
    thermal decomposition, 417
  Mg/Al-CO_3 LDH, organic modification, 408
  nanocomposites, increase of viscosity, 420
  organic siderophilic surface modifier, structure, 414*f*
  particle size distributions, 412*f*
  PS/LDH nanocomposites
    cone calorimeter data, 419*t*
    heat release rate curves, 420*f*
  PS/LDH-SMM 30min-DBP-5wt%, TEM images, 417*f*
  rose-like morphologies, disaggregation, 411
  solution blending, compounding, 416
  synthesis, morphology, and stirred media milling of Mg/Al-CO_3 LDH, 411
  time to ignition (ease of ignition), 420
Layered double hydroxides (LDHs), 407
LCA. *See* life cycle analysis (LCA)
LDHs. *See* layered double hydroxides (LDHs)
Lead-free soldering, 296
Life cycle analysis (LCA), 4
Limiting oxygen index (LOI), 41
Linear low density polyethylene (LLDPE), 152
List of oligomers synthesized, 275*t*

In Fire and Polymers VI: New Advances in Flame Retardant Chemistry and Science; Morgan, A., et al.;
ACS Symposium Series; American Chemical Society: Washington, DC, 2012.

Downloaded by BROWN UNIV on December 19, 2012 | http://pubs.acs.org
Publication Date (Web): December 18, 2012 | doi: 10.1021/bk-2012-1118.ix002

LLDPE. *See* linear low density polyethylene (LLDPE)
Loaded epoxy resins preparation, 308
LOI. *See* limiting oxygen index (LOI)
Low surface crystalline boehmite, 308

M

Magic angle spinning (MAS), 208
Magnesium dihydroxide (MDO), 302
Magnesium hydroxide (MDH), 142
MAS. *See* magic angle spinning (MAS)
Mass loss capacity (MLC), 372
Mass loss rate (MLR), 175
Matrix
  mechanical and thermal properties, 117
  toughness and rigidity, 118
Maximum heat release rate (MHRR), 264
MCA. *See* melamine cyanurate (MCA)
MCC. *See* microscale combustion calorimeter (MCC)
MDH. *See* magnesium hydroxide (MDH)
MDO. *See* magnesium dihydroxide (MDO)
Mechanistic aspects of flame retardation
  combustion begining condition, 38
  elemental phosphorus and various
    compounds, used to retard flame, 37
  introduction, 37
MEL. *See* melamine (MEL)
Melamine (MEL), 183
Melamine cyanurate (MCA), 167
Melamine polyphosphate (MPP), 295
Melamine pyrophosphate (MPyP), 167
Metal-based additives, 84
Methyl methacrylate (MMA), 43
Methyl-DOPO
  gas-phase efficiency, 257
  incomplete combustion, 256
  proposed gas-phase mechanism, 256
  ring-opened analogue, 257
Methylphenoxyphenyl-phosphinate (MPPP), 257*f*
Methyltrimethoxysilane (MTM), 207
MHRR. *See* maximum heat release rate (MHRR)
Michaelis-Arbrusov reaction, 127
Microscale combustion calorimeter (MCC), 362
Microscale combustion calorimetry testing, HRR curves of sample PMP and PMPN, 58*f*
MLC. *See* mass loss capacity (MLC)
MMA. *See* methyl methacrylate (MMA)
MMT. *See* montmorillonite (MMT)
Modified clays, Cloisite family, 81
Mono- and di-substituted diethyl phosphonate, 124
Montmorillonite (MMT), 69
Montmorillonite-type clays, 80
MPP. *See* melamine polyphosphate (MPP)
MPPP. *See* methylphenoxyphenyl-phosphinate (MPPP)
MPyP. *See* melamine pyrophosphate (MPyP)
MSiS. *See* polysiloxane rubbery core (MSiS)
MTM. *See* methyltrimethoxysilane (MTM)
Multi-wall carbon nanotubes (MWCNT), 374
MWCNT. *See* multi-wall carbon nanotubes (MWCNT)
MWNT-based nanocomposite, 348

N

Nanocomposite technology, 119, 120
Nanocomposites, self-extinguishing properties, 113
Nano-dispersed boehmite, 16
Nanofibrillated cellulose fibers (NFC), 224
Nano-filler
  clays, 120
  nano-dispersion, 120
National Electrical Manufacturers Association (NEMA), 296
National Fire Protection Association (NFPA), 497
Neat PET and PET coated by single-step adsorption of CloNa after cold plasma pre-activation, cone calorimetry data, 331
NEMA. *See* National Electrical Manufacturers Association (NEMA)
NFC. *See* nanofibrillated cellulose fibers (NFC)
NFC-PO4Q. *See* quaternized cellulose phosphate (NFC-PO4Q)
NFP 92501 Epiradiateur test, 493
NFPA. *See* National Fire Protection Association (NFPA)
Ni^{2+}-Fe^{3+} LDH, PMP and PMPN, TG and DTG data, 59*t*
NMR. *See* Nuclear magnetic resonance (NMR); nuclear magnetic resonance (NMR)
Non-halogen additive modified polyurethane foams, fire performance, 142*t*

Downloaded by BROWN UNIV on December 19, 2012 | http://pubs.acs.org
Publication Date (Web): December 18, 2012 | doi: 10.1021/bk-2012-1118.ix002

Non-phosphorus and phosphorus-based FRs, synergistic interaction, 255
Nonreactive salt-like additives, 297
Novel biomass-based non-halogenated FR styrenic blends, 151. *See* Cellulose and wood flour
  cellulose and wood flour, 155
  conclusions, 165
  experimental details
    flammability, color, and mechanical characterization, 154
    materials used, 153
    morphology characterization, 154
    sample preparation, 153
    thermal characterization, 154
  introduction, 152
  starch, flammability, 162
  starch vs cellulose, 162*t*
  UL-94 test, 152
4N-RDP. *See* resorcinol bis(*N,N′*-diarylphosphoramidate) (4N-RDP)
Nuclear magnetic resonance (NMR), 123, 237
Nucleophilic species, cyclization initiated, 45*f*

O

OBDPO. *See* octabromodiphenyl oxide (OBDPO)
Octabromodiphenyl oxide (OBDPO), 152
Oligomer synthesis, general method, 274*s*
Oligomeric hexafluoroisopropyl 4,4′-bisphenol-A-benzyl, 273
Openness or porosity of PUF, air permeability, 462
Organic phosphate, 114
Organic polymers, heat capacity, 98
Organohalogens, organobromides, organochlorine compounds, flame retardants, 5
Organo-MMT, 120
Organophosphorus compounds, used as flame retardants, 235
Organophosphorus moieties, classes, 258
Organo-sepiolite, 397
Oxyacetylene torch, 345

P

Pad-bake phosphorylating method, 224
PAN. *See* polyacrylonitrile (PAN)
Particle size distribution (PSD), 409
PBAT. *See* poly(butylene adipate-co-terephthalate) (PBAT)
PBB. *See* polybrominated biphenyls (PBB)
PBDE. *See* polybrominated diphenyl ethers (PBDE)
PBDPO. *See* pentabromodiphenyl oxide (PBDPO)
PC. *See* polycarbonate (PC)
PC/ABS, PC/ABS + BDP, PC/ABS + 10 wt.% talc and PC/ABS + BDP + 10 wt.%
  cone calorimeter residues, 27*f*
    deformation characteristic, 27
    intumescent behavior, 27
  fire behavior, 24
  fire behavior, pHRR, THR/ML, 26*t*
  fire properties, 27
  forced-flaming behavior, 25
    cone calorimeter, 19
  gas-phase mechanism, 27
  gravimetric gas sorption measurements, diffusion coefficients for oxygen, 18
  HRR and THR, 25*f*
  melt rheology, 19
  morphologies, 17
  phosphorus analysis, 27
  TEM bright field image, 18*f*
  thermal decomposition, 19, 21*t*
    activation energy (EA) *versus* conversion and pyrolysis product release rates, 21*f*
    decomposition scheme of PC, 23*f*
    mass loss and mass loss rates, 20*f*
    melt viscosity, characteristics, 24*f*
    styrene as main decomposition product, 21
    TG-FTIR measurements, 22
    volatile pyrolysis products, 22
  thermogravimetry (TG), thermal decomposition investigation, 18
PC/ABS + BDP + talc with various talc concentrations, 28
  carbonaceous charring or flame inhibition, 32
  cone calorimeter results, 33*f*
  diffusion coefficients, 29*t*
    linear dependency, 29
    non-linear dependency, 29
  fire behavior, 31*t*
  LOI plotted against talc content, 32*f*
  mass loss and mass loss rate, 28*f*
  maximum mass loss rate and mass loss, increased talc content, 28
  melt viscosity, characteristics, 30*f*
  rheological properties, 30
  talc acts as inert filler, 32
  thermal decomposition, 29*t*

Downloaded by BROWN UNIV on December 19, 2012 | http://pubs.acs.org
Publication Date (Web): December 18, 2012 | doi: 10.1021/bk-2012-1118.ix002

- PCBMPP. *See* phloroglucinol tris(cyclic 2,2-dimethyl-1,3-propanediol phosphate) (PCBMPP)
- PCFC. *See* pyrolysis combustion flow calorimeter (PCFC); pyrolysis combustion flow calorimetry (PCFC)
- PC-PDMS. *See* PC-polydimethylsiloxane (PC-PDMS)
- PC-polydimethylsiloxane (PC-PDMS), 119
- PCPP. *See* phloroglucinol tris(cyclic 1,3-propanediol phosphate) (PCPP)
- PDMS. *See* polydimethylsiloxane (PDMS)
- PE. *See* polyethylene (PE)
- Peak heat release rate, 15, 86, 330
- Peak smoke production rate (PSPR), 187
- Pentabromodiphenyl oxide (PBDPO), 152
- Pentaerythritol (PER), 183
- PER. *See* pentaerythritol (PER)
- Performance of ZHS, dual phase mechanism, 145
- PES. *See* copolyester (PES)
- PET. *See* poly(ethylene terephthalate) (PET)
- PET fabrics coated by 10 BL silica, SEM micrographs, 332*f*
- PET fabrics coated by 10BL POSS/ZrP and 10BL SiO$_2$/ZrP, SEM micrographs, 333*f*
- PET fabrics coated by single step adsorption of HT, SiO$_2$, CloNa, SEM micrographs, 329*f*
- PET-CO. *See* polyester-cotton blends (PET-CO)
- PET-CO fabrics coated by 10 QL and 10 BL + BL, SEM micrographs performed, 338*f*
- PET-CO fabrics coated by 20BL Chi/APP
  - cone combustion residue, 337*f*
  - SEM micrographs, 335*f*
- PFCC. *See* pyrolysis-flaming-combustion calorimetry (PFCC)
- Phloroglucinol tris(cyclic 2,2-dimethyl-1,3-propanediol phosphate) (PCBMPP), 115*s*
- Phloroglucinol tris(cyclic 1,3-propanediol phosphate) (PCPP), 115*s*
- Phosphate-urethane block copolymers synthesis, 271
  - characterization
    - block copolymers, DSC characteristics, 282*t*
    - block copolymers in nitrogen and (air), thermal analysis, 283*t*
    - FT-IR analysis, 274
    - gel perameation chromatograhy (GPC), 281
    - GPC of example block copolymers by GPC, 282*t*
    - ^{1}HNMR and ^{13}CNMR, 274
    - oxygen index, 284
    - scanning electron microscopy (SEM) and energy dispersive spectroscopy (EDS), 281
    - thermal analysis, 281
  - experimental materials
    - oligomeric hexafluoroisopropyl 4,4′-bisphenol-A-benzyl phosphate synthesis, 273
    - phosphate urethane block copolymer synthesis, 273
  - experimental results, 288
  - introduction, 272
- Phosphinate, flame-retardant mechanism, 168
- Phosphonates, chelating agent characteristics, 143
- Phosphorus moiety, 131
- Phosphorus-containing flame retardants, 116
  - self-extinguishing property, 120
- Phosphorus-nitrogen-containing triazine derivatives
  - antiflammable properties, 123
  - conclusions, 135
  - experimental
    - diethyl 4,6-dichloro-1,3,5-triazin-2-ylphosphonate (TPN1), synthesis, 124
    - dimethyl (4,6-dichloro-1,3,5-triazin-2-yloxy)methyl Phosphonate (TPN3), synthesis, 124
    - fabric treatment, 126
    - limiting oxygen index (LOI) and flammability test (vertical and 45° angle), 127
    - materials and measurements, 124
    - tetraethyl 6-chloro-1,3,5-triazin-2,4-diyldiphosphonate (TPN2), synthesis, 124
    - tetramethyl (6-chloro-1,3,5-triazine-2,4-diyl)bis(oxy)bis(methylene) diphosphonate (TPN4), synthesis, 125
  - fabric treatment and phosphorus and nitrogen contents, 129
  - flame retardant treated fabric, thermal properties, 131
  - flame retardants (TPN1-TPN4), synthesis and characterization, 127
  - promising flame retardants, 136
  - treated fabric of TPN1 and TPN2, 131*f*

Phosphorylated and non-phosphorylated polyurethane block copolymer, percent char residue, 291*f*
Phosphorylating agents, 224
Phosphorylation of cellulose, 224
PLA. *See* poly(lactic acid) or polylactide (PLA)
PLA/PBAT. *See* poly(lactic acid)/ poly(butylene adipate-co-terephthalate) (PLA/PBAT)
PLA/PBAT blends, 432
Plasma-etched fabrics, 330
PMMA. *See* poly(methyl methacrylate) (PMMA)
PMMA and PS combined with CB[6], XRD traces, 73
PMP and PMPN, SEM micrographs of inter char layer, 65*f*
Poly-addition and poly-condensation, silicone rubber cross-linking, 206
Poly(3-aminopropyl methylsiloxane bis(3-hydroxyphenyl spirocyclic pentaerythritol bisphosphate)) (PSBPBP), 116*s*
Polybrominated biphenyls (PBB), 392
Polybrominated diphenyl ethers (PBDE), 392
Poly(butylene adipate-co-terephthalate) (PBAT), 427
Polycarbonate and its blends
  halogen-free flame retardancy
    conclusion, 121
    introduction, 113
    nanocomposite technology, 119
Polycarbonate (PC), 113
Polydimethylsiloxane (PDMS), 205
Polyelectrolyte multilayers, 328
Polyene cross-links, 99
Polyester-cotton blends (PET-CO), 335
Polyethylene (PE), 41
Poly(ethylene terephthalate) (PET), 329
Polyhedral oilgomeric silesquioxane (POSS), 344
Poly(lactic acid) composites
  bio-derived and biodegradable polymers, 224
  conclusions, 232
  degree of quaternization in cellulose, 226
  dynamic mechanical analysis, 231
  dynamic mechanical analysis of composites, 232
  experimental
    instrumentation, 226
    materials, 225
  fiber characterization, 226
  flame-retarded using cellulose-based intumescing flame retardants, 223
  horizontal and vertical burn tests, 231
  introduction, 224
  PLA composite properties, 229
  potentiometric Cl^- concentrations, 227
  thermal and burning properties, 223
  thermal stability of PLA composites using APP-based IFRs, 230*f*
  thermal stability of PLA composites using cellulose phosphate fibers, 230*f*
  UL-94 rests of PLA composites, 231*t*
Poly(lactic acid) or polylactide (PLA), 224
Poly(lactic acid)/poly(butylene adipate-co-terephthalate) (PLA/PBAT), 427
Polymer structures, fire stability approaches, 11
Polymer/CB[6]/20A-MMT, preparation, 71
Polymer-clay nanocomposite, 74
Polymeric materials, phosphorus containing compounds as backbone, 272
Polyolefins and related polymers, 41
Polyphenylsilsesquioxane (PPSQ), 118*s*
Polyphosphate polyurethane block copolymers, 290
  conclusions, 292
  hydrogen bonds, mechanical integrity, 290
  microphase segregation, 290
  olefinic alcohol as chain extender, 292
Polypropylene (PP), 41
Polypropylene/sepiolite composite
  thermal stability and fire retardancy, 391
    composites thermal stability analysis, 399
    conclusion, 405
    cone calorimetric characterization, 401
    dynamic mechanical analysis, 398
    introduction, 392
    LOI and UL94 testing, 400
    materials and experimental, 393
    mechanical properties, 398
    modification of sepiolite, 395
    morphology of (nano)composite, 396
    polymer-clay nanocomposites, 402
    PP, PP/sepolite and PP/organo-sepiolite composites, HRR curves, 402*f*
    PP and its composites, 398
    PP and its organic composites, 400*t*
    PP/sepiolite and PP/organo-sepiolite, TEM images, 397*f*
    PP/sepiolite and PP/organo-sepiolite composites, 395*f*, 396*f*

Downloaded by BROWN UNIV on December 19, 2012 | http://pubs.acs.org
Publication Date (Web): December 18, 2012 | doi: 10.1021/bk-2012-1118.ix002

        - primitive sepiolite, acidic sepiolite, organo-sepiolite, FT-IR spectrum, 396*f*
        - pristine sepiolite, acidic sepiolite and organo-sepiolite, x-ray diffraction patterns, 395*f*
- Polysiloxane rubbery core (MSiS), 117
- Polytetrafluoroethylene (PTFE), 17
- Polyurethane (PU), 251
- Polyurethane foams (PUF), 459
- POSS. *See* polyhedral oilgomeric silesquioxane (POSS)
- Potential FR mineral fillers, heat absorbed, 101*f*
- Powder X-ray diffraction (PXRD), 409
- PP. *See* polypropylene (PP)
- PPSQ. *See* polyphenylsilsesquioxane (PPSQ)
- Printed wired boards (PWB), 295
- Pristine epoxy/amine thermoset
    - external irradiation of 50 kW/m^2, 93*f*
    - heat release rate curves, 87*f*
- Pristine polymer, 84
- PSBPBP. *See* poly(3-aminopropyl methylsiloxane bis(3-hydroxyphenyl spirocyclic pentaerythritol bisphosphate)) (PSBPBP)
- PSD. *See* particle size distribution (PSD)
- PSPR. *See* peak smoke production rate (PSPR)
- PTFE. *See* polytetrafluoroethylene (PTFE)
- PU. *See* polyurethane (PU)
- PUF. *See* polyurethane foams (PUF)
- PUF morphology, formulation and processing parameters, 464
- PUR foams
    - flame retardants and inorganic flame retardant additives combination, 144
    - flame retardants and reactive silicone combination, 147
    - phosphorus flame retardants, 143
        - phosphorus and halogen-phosphorus based additives modified polyurethane foams, 143*t*
- PWB. *See* printed wired boards (PWB)
- PXRD. *See* powder X-ray diffraction (PXRD)
- Pyrolysis-combustion flow calorimetry (PCFC)
    - apparent cone calorimeter temperature versus combustion efficiency, 379*f*
    - and calorimeter, modes-of-action, 377
    - characterize flammability, 370
    - combining PCFC and TGA, 371
    - combustion efficiency, 377
    - conclusions and propositions of future work, 387
    - evaluate flame retardancy of polymers, 361
    - FTIR-PCFC and FTIR-TGA couplings, 388
    - halogen-free polyolefin compounds, 387
    - heat of combustion, discrepancy, 384
    - heat of combustion in PCFC and in oxygen bomb calorimeter, 384*f*
    - important aspects
        - activation energy, 366
        - activation energy of pyrolysis, 365
        - anaerobic versus aerobic pyrolysis, 364
        - combustion, 366
        - critical temperature and oxygen rate, 366
        - FTIR spectra of gases, 369*f*
        - FTIR-PCFC coupling, 368
        - heat release capacity (HRC), 363
        - heterogeneous materials, 363
        - PE and filled PE under anaerobic pyrolysis and aerobic pyrolysis, HRR curves, 365*f*
        - phosphorus containing molecules, measured versus calculated THR, 371*f*
        - polymers, combustion efficiency profiles, 368*f*
        - Van Krevelen approach, predicting flammability, 370
        - various modified polystyrenes, combustion efficiency, 367*f*
        - well-known Kissinger method, 365
    - introduction, 361
    - mass loss rate, 374
    - one-dimensional pyrolysis model, 380
    - and other calorimetry methods, correlations, 374
    - and other flammability tests, correlations
        - flame spread tests for wires, 387
        - heat of gasification, 386
        - limiting oxygen index, 385
        - UL94, 385
    - other physical effects, 382
    - PA11 and PA11 filled with nanoboehmites, surface temperature, 382*f*
    - PA11 decomposition, 372
    - PA11 pure and filled, 372
    - peak of heat release rate in cone calorimeter of mineral fillers, 380
    - pHRR in cone calorimeter and first pHRR in PCFC, comparison, 376*f*
    - pHRR of PBT, 376

Downloaded by BROWN UNIV on December 19, 2012 | http://pubs.acs.org
Publication Date (Web): December 18, 2012 | doi: 10.1021/bk-2012-1118.ix002

Downloaded by BROWN UNIV on December 19, 2012 | http://pubs.acs.org
Publication Date (Web): December 18, 2012 | doi: 10.1021/bk-2012-1118.ix002

  R1 versus R2 graph for EVA28-MDH formulations, 378*f*
  R1 versus R2 graph for more than 60 formulations, 378*f*
  technique to understand fire behavior of material, 387
  thermal barrier effect, 375, 377
    cone calorimeter test, 376
  thermal stability, 380
  thermo-physical properties, 381
  total heat release, discrepancy, 387
Pyrolysis-flaming-combustion calorimetry (PFCC), 194
Pyro-/ultra- or poly-phosphoric acid, 175

Q

QL. *See* quad-layer (QL)
QNFC. *See* quaternized cellulose (QNFC)
Quad-layer (QL), 337
Quaternized cellulose (QNFC), 225
Quaternized cellulose phosphate (NFC-PO4Q), 225

R

Radical induced grafting of maleic anhydride on to PP, 41*f*
RDP. *See* resorcinol bis(diphenyl phosphate) (RDP)
Reactive organophosphorus compounds and synergistic additives, flame retardant mixtures, 302
Red phosphorus, 114
Reduced ignition propensity, 460
Resorcinol bis(diphenyl phosphate) (RDP), 114, 153
  low volatility and high heat stability characteristics, 147
Resorcinol bis(*N,N′*-diarylphosphoramidate) (4N-RDP), 116*s*
  intermolecular transesterification reactions, 116
  P–N rich residue, 116
Restriction of hazardous substances (RoHS), 183
RHF. *See* rice hull flour (RHF)
Rice hull flour (RHF), 225
RoHS. *See* restriction of hazardous substances (RoHS)
Rose-like morphologies, disaggregation, 411
RT-FTIR spectra of PMP and PMPN, different pyrolysis temperatures, 63*f*

S

Sample PMP and PMPN
  DSC exotherms, 61*f*
  fitted Raman curves of outer residual char, 67*f*
  HRR curves, 56*f*
  LOI values and UL-94 testing results, 55*t*
  microscale combustion calorimetry data, 58*t*
  onset temperature, peak temperature and enthalpy of crystallization, 60*t*
  Raman curves of outer residual char, 66*f*
  total intensity of pyrolysis product, 62*f*
Sample PMP and PMPN at 35 kW/m^2
  cone calorimetry data, 56*t*
  total heat release curves, 57*f*
SAN. *See* styrene-co-acrylonitrile (SAN)
Scanning electron microscopy (SEM), 329
Scheme of PCFC apparatus, 362*f*
SEA. *See* specific extinction area (SEA)
Selected reactive flame retardants for epoxies, 299*f*
Self-extinguishing PLA/ECOFLEX blends, 427
SEM. *See* scanning electron microscopy (SEM)
Significant new use rule (SNUR), 528
Silica (SiO_2), 329
Silica-based coatings, multistep adsorption, 331
Siliconated polyurethane block copolymers, 271
Siloxanes, 117
SiO_2. *See* silica (SiO_2)
Smoke production rate (SPR), 187, 391
Smoldering in flexible polyurethane foams
  average ML_{Mockup} versus air permeability, 468*f*
  bun-to-bun variability and in-bun variability, 468
  cell size decreases smoldering increases, 477
  completely open-cell foams, 470
  conclusion, 476
  confocal image
    histogram and basic statistical analysis, 475*f*
    image analysis, 462
  conventional PUF, morphology, 460

Downloaded by BROWN UNIV on December 19, 2012 | http://pubs.acs.org
Publication Date (Web): December 18, 2012 | doi: 10.1021/bk-2012-1118.ix002

  - decrease in cell size promotes smoldering, 472
  - effect of air permeability (φ), 466
  - effect of apparent density (ρ), 466
  - effect of cell size, 473
  - effect of specific surface area (SSA), 469
  - experimental
    - formulation identification names, 463*t*
    - formulations, 464
    - macro analyze particle, 462
    - materials, 461
    - results and discussion, 464
    - sample characterization, 461
    - sample preparation, 461
  - foam morphology, general considerations, 471
  - higher yield of toxic carbon monoxide, 459
  - introduction, 459
  - limited oxygen-supply rate, smoldering propensity, 470
  - mechanisms promoting increase in air permeability, schematic drawing, 472*f*
  - $\mathrm{ML}_{\mathrm{Mockup}}$ versus specific surface area, 469
  - mockup test, 460
  - numerical simulation, 466
  - PUF, combination of strut-generated and window-generated surfaces, 473
  - PUF degradation, affected by SSA, 469
  - PUF formulation, naturalconvection smoldering increases with air permeability, 466
  - rate of polyol/TDI reaction, tin catalyst, 464
  - sample of formulation F16, confocal image, 474*f*
  - smoldering foam and non-smoldering foam, confocal images, 471*f*
  - smoldering ($\mathrm{ML}_{\mathrm{Mockup}}$) for eight buns of formulation F13, 470
  - smoldering versus air permeability, 467*f*
  - specific surface area, strut thickness, 473
  - upholstery cover fabric smoldering ignition resistance test, 461
  - values of density (ρ), air permeability (φ), specific surface area (SSA) and smoldering ($\mathrm{ML}_{\mathrm{Mockup}}$), 465*t*
  - values of density (ρ) *vs.* smoldering ($\mathrm{ML}_{\mathrm{Mockup}}$), 466

- SNUR. *See* significant new use rule (SNUR)
- Sodium montmorillonite (CloNa), 329
- Sol-gel process, 252
- Specific extinction area (SEA), 352
- Specific surface area (SSA), 462
- SPR. *See* smoke production rate (SPR)
- SSA. *See* specific surface area (SSA)
- Standard for the Flammability of Clothing Textiles, 133
- Steiner tunnel fire test (ASTM E84), 495
- Strategies to reduce flammability of polymeric material, 38
- Structural fire deaths, 1
- Structural fires, 1
- Styrene-co-acrylonitrile (SAN), 120
- Styrenic oligomers flammability
  - experimental
    - analytical techniques, 237
    - materials, 236
  - impact of phosphorus and phosphorus/nitrogen, 235
    - combustion, heat release rate, 246*f*
    - conclusions, 247
    - experimental, 238
    - glass transition temperatures, 243*t*
    - heat release rate, 245*f*
    - homopolymers combustion, heat release (HR) values, 246*t*
    - infrared spectra, 241*f*
    - phosphoramidate series, 243
    - standard radical techniques, 242
    - styrene monomers containing flame-retarding moieties, polymerization, 241*s*
    - styrene polymers bearing phosphorus-containing pendants, thermal degradation, 244*f*
    - styrenic polymers, proton NMR spectra, 242*f*
    - synthesis of styrene monomers containing flame-retarding moieties, 240*s*
    - thermal degradation, 243*f*
    - thermal degradation data, 245*t*
    - unsubstituted poly(styrene), 244
- Styrenic polymers, 47
  - char formation and flame retardance, 47
  - conclusion, 48
- Substance of very high concern (SVHC), 526
- Surface area of PUF, Brunauer-Emmett-Teller (BET) measurements, 462
- SVHC. *See* substance of very high concern (SVHC)

T

- Tailor-made synthetic procedures, 69
- Talc

Downloaded by BROWN UNIV on December 19, 2012 | http://pubs.acs.org
Publication Date (Web): December 18, 2012 | doi: 10.1021/bk-2012-1118.ix002

  hydrated magnesium silicate, 16
  used as inert filler in plastics, 16
TB-117 foams, 448
TBBA. *See* tetrabromo bisphenol A (TBBA)
TBC. *See* 4-tert-butylcatechol (TBC)
TCPP. *See* tris-(chloropropyl) phosphate (TCPP)
TDI. *See* toluene diisocyanate (TDI)
TEM. *See* transmission electron microscope (TEM)
4-Tert-butylcatechol (TBC), 236
Testing material ignitability, 202
Tetrabromo bisphenol A (BBA), 194, 295
Tetrabromodiglycidylether of bisphenol A (BDBA), 194
Tetra-2,6-dimethyl resorcinol diphosphate (DMP-RDP), 152
Tetramethylsilane (TMS), 208, 237
Textile flame retardancy
  introduction, 327
  surface adsorption techniques, 328
  surface-assembled nanoarchitectures, 327
    cold plasma pre-treatment, 339
    complex LbL architectures, 339
    conclusions, 339
    novel and non-conventional procedures, 328
    PET fabrics, silica coating, 331
    PET textiles, cold plasma surface treatment, 330
    PET thermal degradation, 331
    silica-based coatings, multistep adsorption, 331
    single-step adsorption, 329
Textiles and textile products, classes of flammability performance, 133
TG. *See* thermogravimetry (TG)
TG and DTG curves of Ni^{2+}-Fe^{3+} LDH, PMP and PMPN in air, 59*f*
TGA. *See* thermogravimetric analysis (TGA)
Thermal decomposition mechanism of polypropylene, 316*s*
Thermal oxidative degradation, 63
Thermal/base catalyzed cracking of phosphonate ester group and formation of acidic nucleophilic species, 44*f*
Thermogravimetric analysis (TGA), 72, 76, 116, 123, 225, 264
Thermogravimetry residues, 22
Thermoplastic polyurethane (TPU), 256, 343
Thermoplastic polyurethane nanocomposites
  high-temperature flammability and mechanical properties, 343
    burn tests, 350
    effect of nanoparticle loading on onset of storage modulus depression, 357*f*
    experimental, 346
    flammability studies, 347
    high resolution SEM images of virgin and burnt TPU/MWNT/10 after UL 94 test, 349*f*
    mass loss of neat and 5% PNC cone calorimeter test at 50 kW/m², 350*f*
    summary and conclusions, 359
    TPU and TPU/CNF/15 nanocomposites, storage modulus and loss modulus, 358*f*
    TPU nanocomposites, dynamic mechanical analysis, 354
    TPU/Cl nanocomposites, variation of storage modulus versus temperature, 354*f*
    TPU/CNF nanocomposites, variation of storage modulus versus temperature, 356*f*
    TPU/MWNT nanocomposites, variation of storage modulus versus temperature, 355*f*
  introduction, 344
  storage modulus, loss modulus and tan delta, 345
Thermoplastic resin sales by major market 2011, 8*t*
THR. *See* total heat released (THR)
THR, mass-based value, 200
THR/mass loss (THR/ML), 25
THR/ML. *See* THR/mass loss (THR/ML)
Time to ignition (TTI), 56, 330
TLC. *See* thin layer chromatography (TLC)
TMS. *See* tetramethylsilane (TMS)
Toluene diisocyanate (TDI), 461
Torch test fire testing method, 205
Total heat release (THR), 254
Total heat released (THR), 15
Total smoke production (TSP), 176
Toxic Substances Control Act (TSCA), 528
TPOSS. *See* trisilanolphenyl polyhedral oligomeric silsesquioxane (TPOSS)
TPP. *See* triphenyl phosphate (TPP)
TPU. *See* thermoplastic polyurethane (TPU)
TPU nanocomposites
  dynamic mechanical analysis, 353
  flame retardant properties, 344
Trans-esterification reactions, 43
Transmission electron microscope (TEM), 409

Downloaded by BROWN UNIV on December 19, 2012 | http://pubs.acs.org
Publication Date (Web): December 18, 2012 | doi: 10.1021/bk-2012-1118.ix002

Triarylphosphate, flame retardant filler, 272
Triazine and its derivatives, 124
Triphenyl phosphate (TPP), 114, 153
Tris-(chloropropyl) phosphate (TCPP), 252
Trisilanolphenyl polyhedral oligomeric silsesquioxane (TPOSS), 119
TSCA. *See* Toxic Substances Control Act (TSCA)
TSP. *See* total smoke production (TSP)
TTI. *See* time to ignition (TTI)
Typical wire and cable formulation, 103*t*

U

UL-94 test (vertical burning test), 43, 51, 84, 114, 151, 167, 173, 223
Uncontrolled combustion, 38
Unexpected FR performance of micro and nano-boehmites, 102
Unmodified variants, 38
Unzipping reaction, schematic illustration, 218*f*
Upholstery cover fabric smoldering ignition resistance test, 461
Urethane bond, acid catalyzed decomposition, 265
Urethane bond scission, 268
U.S. production, sales and captive use, 7*t*

V

Van Krevelen approach, predicting flammability, 370
Vapor phase flame retardation, elementary steps, 40*f*
Various nanoscopic additives, increasing use, 49
Vertical flammability test, 123
Vertical UL 94 test, 346
Volatilized products analysis, 60
  FTIR spectrums, 62*f*
Voluminous carbonaceous char layer, 253

W

Well-known flame inhibition effect of halogens, 366
Well-known Kissinger method, 365

X

X-ray diffraction (XRD), 71
XRD. *See* X-ray diffraction (XRD)

Z

Zeolite 4A, 183
  synergistic agent, 184
ZHS. *See* zinc hydorxystannate (ZHS)
Zinc hydorxystannate (ZHS), 139
Zinc stannate (ZS), 139
ZS. *See* zinc stannate (ZS)